

**MOLECULAR SIEVING ON DENDRITIC POLYMER-PROTEIN
CONJUGATES**

by

BILLY DENG, M.Sc.

A THESIS SUBMITTED TO THE SCHOOL OF GRADUATE STUDIES OF
MCMASTER UNIVERSITY
IN PARTIAL FULFILMENT OF THE REQUIREMENTS FOR THE DEGREE OF
DOCTOR OF PHILOSOPHY IN CHEMISTRY

McMaster University

Hamilton, Ontario, Canada

Copyright © Billy Deng, 2025

All Rights Reserved

Title: MOLECULAR SIEVING ON DENDRITIC POLYMER-PROTEIN
CONJUGATES

Doctor of Philosophy (PhD, Chemistry)

Author: Billy Deng, H.BSc. (University of Toronto), MSc. (Queen's University)

Supervisor: Professor Alex Adronov

McMaster University, Hamilton, Ontario, Canada

Number of Pages: xvii, 319

Abstract

Polymer-protein conjugates are hybrid biomaterials that combine the unique biological functions of proteins with the tunable properties of synthetic polymers. Conjugates often exhibit unique properties that set them apart from their native counterparts, including higher stability towards environmental stressors, altered interactions with their substrates, and lowered immunogenicity in therapeutic applications. Such qualities have made them excellent candidates for therapeutics, and the development of polymer-protein is an intense area of ongoing research. In recent years, increasing attention is being paid to controlling conjugate interaction with their substrates solely based on size – an effect known as molecular sieving. The grafting polymer forms a porous layer which blocks macromolecules above a certain size threshold from approaching the protein surface, while smaller substrates can diffuse through and interact with the protein.

The objective of this work is to present approaches to regulating protein-ligand binding stoichiometry and specificity without making genetic modification to the protein itself. We first describe the development of a series of dendrimers with a highly stable backbone and modular click functionalities. The chemistry of which is then incorporated to dendritic architectures in the second portion of our work, where we explore dendritic-linear architectures as grafting polymers for introducing molecular sieving to chymotrypsin conjugates. Lastly, we systematically investigate how size-dependent sieving on avidin is controlled by dendron generation on both the protein surface and on its biotin ligands. We demonstrate throughout this thesis that dendrimers are a viable platform for tuning binding in protein hybrids.

Acknowledgements

The impact that Professor Alex Adronov has had on my Ph.D., and on me as a scientist, is immeasurable. I am forever thankful for his guidance and mentorship. He inspired me to be curious, to be systematic, and most importantly, to not be afraid to fail. For all the times I hit a brick wall, and you encouraged me to keep going – thank you.

I would like to thank my committee members, Professors Harald Stöver and Ryan Wylie, for providing their time and valuable feedback throughout my Ph.D., and for introducing me to new realms within chemistry. I would like to thank Bob and Hilary at the McMaster NMR facility for our wonderful chats about science and beyond. I am grateful to my friend, Dr. Stuart McNelles, for his advice and mentorship. Thank you for paving the landscape for my thesis work, and I am sure you will be as wonderful of a father as you have been a mentor to me – congratulations.

To my friends at McMaster and in the Adronov Group – especially Dan, Dusan, Ben, Alex, Heather, Emma, Mokha, Anjilee, Sara, Kyle, and Annika, thank you all for the laughs, and for enduring the hell that is graduate school with me. I now truly understand the meaning of trauma bonding. I'm privileged to have worked with all of you, and I'm looking forward to our friendship beyond school – see you on the other side.

To Rashida and Aleem Jeeva. I cannot express how grateful I am for everything you have done for Fiona and me throughout the years. You are both incredible individuals, and you taught me – through example – what family is, and what it means to be selfless, and to have dignity and self-respect. Thank you.

To my mother, thank you for granting me resilience, and the grit to fight through the hardest times. I am so proud of everything you have achieved, and I hope that you can say the same for me. You have been through so, so much for us, and I know that you will gladly do it all over again if it means that we'll make it in life. I hope you no longer need the incredible strength you have – I made it, mom.

Finally, to my love, Fiona. You have been a pillar in my life, and nothing is ever as bad as it seems when I have you by my side. You have been with me through the lowest lows, and I hope that you'll be here with me for the highest highs. These chapters are one of many in our story, and I hope that I'll have the rest of my life to tell you every day just how much you mean to me.

List of Abbreviations

α -CT	α -Chymotrypsin
ACN	Acetonitrile
ANOVA	Analysis of variance
ATRP	Atom Transfer Radical Polymerization
BCA	Bicinchoninic Acid
Bis-MPA	2,2-Bis(hydroxymethyl)propionic Acid
Boc	tert-Butyloxycarbamate
BOP	Benzotriazol-1-yloxytris(dimethylamino)phosphonium Hexafluorophosphate
BSA	Bovine Serum Albumin
Cbz	Carboxybenzyl carbamate
CD	Circular Dichroism
CDI	<i>N,N'</i> -carbonyldiimidazole
CDM	Carboxy Dimethyl Maleic Anhydride
DBCO	Dibenzocyclooctyne
D _h	Hydrodynamic Diameter
DHB	2,5-Dihydroxybenzoic acid
DLS	Dynamic Light Scattering
DMF	Dimethylformamide
DMSO	Dimethylsulfoxide
DNA	Deoxyribonucleic Acid
DP	Degree of Polymerization
DRIFTS-IR	Diffuse Reflectance Infrared Fourier Transform Spectroscopy
EDC	1-Ethyl-3-(3-dimethylaminopropyl)carbodiimide
EM	Electron Microscopy
ESI-MS	Electrospray Ionization Mass Spectrometry
EtOAc	Ethyl Acetate
FDA	Food and Drug Administration
FPE	Fluoride-Promoted Esterification
FTIR	Fourier Transform Infrared Spectroscopy
GSH	Glutathione
HABA	4'-hydroxyazobenzene-2-carboxylic acid
HATU	Hexafluorophosphate Azabenzotriazole Tetramethyl Uronium
HBTU	Hexafluorophosphate Benzotriazole Tetramethyl Uronium
HPMA	<i>N</i> -(2-Hydroxypropyl) methacrylamide
ITC	Isothermal Titration Calorimetry
KLH	Keyhole Limpet Hemocyanin
LDA	Lithium diisopropylamide
MALDI-TOF	Matrix-assisted Laser Desorption/Ionization Time-of-Flight
MeOH	Methanol

MW	Molecular Weight
MWCO	Molecular Weight Cut-Off
NHS	<i>N</i> -hydroxysuccinimide
NIPAM	Poly(<i>N</i> -isopropylacrylamide)
NMI	<i>N</i> -methylimidazole
NMR	Nuclear Magnetic Resonance
PAGE	Polyacrylamide Gel Electrophoresis
PAMAM	Poly(amidoamine)
PBS	Phosphate Buffered Saline
PCBMA	poly(carboxybetaine methacrylate)
PDI	Polydispersity Index
PEG	Poly(ethylene glycol)
PMA	Phosphomolybdic Acid
POEGMA	Poly(oligoethyleneglycol) methyl ether methacrylate
PPC	Polymer-Protein Conjugate
PPI	Poly(propylene imine)
PTFE	Polytetrafluoroethylene
PTGG	Poly(thioglycidyl glycerol)
RAFT	Reversible Addition-Fragmentation Chain-Transfer Polymerization
ROMP	Ring-Opening Metathesis Polymerization
ROP	Ring-Opening Polymerization
ROS	Reactive Oxygen Species
SD	Standard Deviation
SEC	Size-Exclusion Chromatography
SPAAC	Strain Promoted Azide-Alkyne Cycloaddition
TCFH	Chloro- <i>N,N,N',N'</i> -tetramethylformamidinium Hexafluorophosphate
TCO	Transcyclooctene
TEA	Triethylamine
TEG	Tri(ethylene Glycol)
TFA	Trifluoroacetic acid
THF	Tetrahydrofuran
TLC	Thin Layer Chromatography
UDEFT	Uniform Driven Equilibrium Fourier Transform
UV-VIS	Ultraviolet-Visible Light
ZBP	Zwitterionic Bottle Brush

List of Tables

Table 1.1. Main classes of dendrimers used in biological applications. Reproduced with permission. Copyright © 2021 Taylor and Francis.	11
Table 3.1. Calculated vs. experimentally measured dendron mass fractions.	159
Table 4.1. Intensity weighted hydrodynamic diameter (<i>Z</i> -avg <i>d</i>) of avidin-dendron conjugates.	247
Table 4.2. Tabulated ITC titration data for binding of dendronized biotin (BGx) to native avidin.	252
Table 4.3. Binding and thermodynamic parameters for binding of BGx by Av-Gx	256
Table 4.4. Molecular weight and hydrodynamic diameters of hydroxyl (OH)-periphery dendrons.	261

List of Supplementary Tables

Table S2.1. Tracking ¹ H NMR of BnO-G5-(Lin-NH₃⁺TFA⁻)₃₂ in 0.1 M pH 5.8 potassium phosphate buffer, trial 1.	91
Table S2.2. Tracking ¹ H NMR of BnO-G5-(Lin-NH₃⁺TFA⁻)₃₂ in 0.1 M pH 5.8 potassium phosphate buffer, trial 2.	92
Table S2.3. Tracking ¹ H NMR of BnO-G5-(Lin-NH₃⁺TFA⁻)₃₂ in 0.1 M pH 5.8 potassium phosphate buffer, trial 3.	92
Table S2.4. Tracking ¹ H NMR of BnO-G5-(Neo-NH₃⁺TFA⁻)₃₂ in 0.1 M pH 5.8 potassium phosphate buffer, trial 1.	93
Table S2.5. Tracking ¹ H NMR of BnO-G5-(Neo-NH₃⁺TFA⁻)₃₂ in 0.1 M pH 5.8 potassium phosphate buffer, trial 2.	93
Table S 2.6. Tracking ¹ H NMR of BnO-G5-(Neo-NH₃⁺TFA⁻)₃₂ in 0.1 M pH 5.8 potassium phosphate buffer, trial 3.	94
Table S2.7. Tracking ¹ H NMR of BnO-G5-(Lin-NH₃⁺TFA⁻)₃₂ in 0.1 M pH 7.4 potassium phosphate buffer, trial 1.	94
Table S2.8. Tracking ¹ H NMR of BnO-G5-(Lin-NH₃⁺TFA⁻)₃₂ in 0.1 M pH 7.4 potassium phosphate buffer, trial 2.	95
Table S2.9. Tracking ¹ H NMR of BnO-G5-(Lin-NH₃⁺TFA⁻)₃₂ in 0.1 M pH 7.4 potassium phosphate buffer, trial 3.	95
Table S2.10. Tracking ¹ H NMR of BnO-G5-(Neo-NH₃⁺TFA⁻)₃₂ in 0.1 M pH 7.4 potassium phosphate buffer, trial 1.	96
Table S2.11. Tracking ¹ H NMR of BnO-G5-(Neo-NH₃⁺TFA⁻)₃₂ in 0.1 M pH 7.4 potassium phosphate buffer, trial 2.	96
Table S2.12. Tracking ¹ H NMR of BnO-G5-(Neo-NH₃⁺TFA⁻)₃₂ in 0.1 M pH 7.4 potassium phosphate buffer, trial 3.	97

Table S2.13. Tracking ^1H NMR of BnO-G5-(Lin-NH₃⁺TFA⁻)₃₂ in 0.1 M pH 8 potassium phosphate buffer, trial 1	97
Table S2.14. Tracking ^1H NMR of BnO-G5-(Lin-NH₃⁺TFA⁻)₃₂ in 0.1 M pH 8 potassium phosphate buffer, trial 2	98
Table S2.15. Tracking ^1H NMR of BnO-G5-(Lin-NH₃⁺TFA⁻)₃₂ in 0.1 M pH 8 potassium phosphate buffer, trial 3	98
Table S2.16. Tracking ^1H NMR of BnO-G5-(Neo-NH₃⁺TFA⁻)₃₂ in 0.1 M pH 8 potassium phosphate buffer, trial 1	99
Table S2.17. Tracking ^1H NMR of BnO-G5-(Neo-NH₃⁺TFA⁻)₃₂ in 0.1 M pH 8 potassium phosphate buffer, trial 2	100
Table S2.18. Tracking ^1H NMR of BnO-G5-(Neo-NH₃⁺TFA⁻)₃₂ in 0.1 M pH 8 potassium phosphate buffer, trial 3	100
Table S2.19. Tracking ^1H NMR of BnO-G5-(Lin-NH₃⁺TFA⁻)₃₂ in 20% esterase in 0.1 M pH 7.4 potassium phosphate buffer, trial 1	102
Table S2.20. Tracking ^1H NMR of BnO-G5-(Lin-NH₃⁺TFA⁻)₃₂ in 20% esterase in 0.1 M pH 7.4 potassium phosphate buffer, trial 2	103
Table S2.21. Tracking ^1H NMR of BnO-G5-(Lin-NH₃⁺TFA⁻)₃₂ in 20% esterase in 0.1 M pH 7.4 potassium phosphate buffer, trial 3	103
Table S2.22. Tracking ^1H NMR of BnO-G5-(Neo-NH₃⁺TFA⁻)₃₂ in 20% esterase in 0.1 M pH 7.4 potassium phosphate buffer, trial 1	104
Table S2.23. Tracking ^1H NMR of BnO-G5-(Neo-NH₃⁺TFA⁻)₃₂ in 20% esterase in 0.1 M pH 7.4 potassium phosphate buffer, trial 2	104
Table S2.24. Tracking ^1H NMR of BnO-G5-(Neo-NH₃⁺TFA⁻)₃₂ in 20% esterase in 0.1 M pH 7.4 potassium phosphate buffer, trial 3	105
Table S3.1. Mass fraction of dendron-protein conjugates.....	206
Table S3.2. Concentration of protein-dendrimer conjugates for preparing digestion assays.....	226
Table S3.3. Summarized data for BTpNA assay.....	227
Table S3.4. Summarized data for casein digestion assay.....	228
Table S3.5. Summarized data for BSA digestion assay.....	229
Table S4.1. Hydrodynamic diameters (D_h) of biotin and hydroxyl periphery dendrimers.....	294
Table S4.2. Expected weight percent (Wt. %) of avidin (Av) in Av-G3 conjugate with increasing degrees of dendrimer conjugation.....	299
Table S4.3. Expected weight percent (Wt. %) of avidin (Av) in Av-G4 conjugate with increasing degrees of conjugation.....	299
Table S4.4. Expected weight percent (Wt. %) of avidin (Av) in Av-G5 conjugate with increasing degrees of dendrimer conjugation.....	300
Table S4.5. Expected weight percent (Wt. %) of avidin (Av) in Av-G6 conjugate with increasing degrees of dendrimer conjugation.....	300

Table S4.6. Expected weight percent (Wt. %) of avidin (Av) in Av-G7 conjugate with increasing degrees of dendrimer conjugation.	301
Table S4.7. ITC Binding and thermodynamic parameters of DSPE-PEG ₃₄₀₀ -biotin : avidin and Av-G4	304
Table S4.8. ITC Binding and thermodynamic parameters of BSA-biotin (8-16 average biotin group per protein) : avidin and Av-G6	304
Table S4.9. ITC Binding and thermodynamic parameters of Aprotinin-biotin (4.2 average biotins per protein) : avidin, Av-N₃ , and Av-G4 to Av-G6	304
Table S4.10. Competitive binding of biotin and BG_x (x = 3-7) to native avidin-HABA measured by ITC, tabulated data.	304
Table S4.11. Tabulated data of competitive binding of Biotin, BG5 and BG6 to Av-G6-HABA.	305
Table S4.12. Titration of BG6 to Av-G4 at 37 °C, tabulated data.	307

List of Figures

Figure 1.1. Schematic of a dendrimer. Successive generations (G1-4) are indicated by a deepening green colour. Starting at a bifunctional core (purple), the number of bifunctional monomers at each generation is represented by 2^n , where n = generation number.....	1
Figure 1.2. Divergent and convergent synthesis of dendrimers.	3
Figure 1.3. Synthesis of PAMAM "starburst" dendrimers by Tomalia et al. Reused with permission. ¹⁷ Copyright © 1985, The Society of Polymer Science, Japan.....	4
Figure 1.4. Convergent synthesis of poly(aryl ether) dendrimers reported by Hawker and Fréchet. Reproduced with permission. ¹⁹ Copyright © 1990, American Chemical Society.	5
Figure 1.5. Poly(alkyl ester) dendrimers synthesized by a convergent approach. Reused with permission. ¹⁸ Copyright © 1998, American Chemical Society.	6
Figure 1.6. Dendrimer-based drug delivery systems. Reproduced with permission. ⁵ Copyright © 2022, The Authors. (Licensed under CC-BY 4.0). Published by Springer Nature.....	10
Figure 1.7. Protein conjugated with redox-active poly(thioglycidyl glycerol). Reused with permission. ¹⁰¹ Copyright © 2022 The Authors. Published by American Chemical Society.....	14
Figure 1.8. Uricase oxidase-zwitterionic bottlebrush (ZBP) polymers developed by Chung et al. Reused with permission. ⁹⁶ Copyright © 2024 American Chemical Society.	16
Figure 1.9. An avidin-based molecular sieve used to scavenge small biotin tags in a protein purification process, reported by Minden et al. Reused with permission. ¹¹⁹ Copyright © 2019 American Chemical Society.....	20
Figure 1.10. To-scale 3D models of chymotrypsin grafted with G7 bis-MPA dendrimers, showing the structure from the side and from the top, looking directly at the active site (coloured red). Reproduced with permission. ²⁶ Copyright © 2019 John Wiley & Sons.	21
Figure 1.11. Molecular dynamics simulations of chymotrypsin grafted with different pCBMA architectures. (a) Linear pCBMA, 3 chains of DP ~200, (b) linear pCBMA, 7 chains of DP ~200, (c) Comb-shaped pCBMA, 3 primary chains with 15 pendant chains, and (d) Comb-shaped pCBMA, 7 primary chains with 35 pendant chains. Reproduced with permission. ¹¹⁵ Copyright © 2021 The Authors. Published by American Chemical Society. Licensed under CC-BY-NC-ND 4.0	22
Figure 1.12. Stepwise grafting-to approach developed by Maynard and co-workers to produce a PEG-lysozyme PPC with water-labile handles. Reproduced with permission. ¹³⁰ Copyright © 2022 American Chemical Society.....	25
Figure 1.13. Poly(pyridine)-RNase conjugates reported by Buchwald et al. The monomers bearing boronate esters were polymerized onto an RNase macroinitiator. Reproduced with permission. ¹⁴¹ Copyright © 2022, American Chemical Society	29

Figure 1.14. (A) Aminolysis-induced self-immolative RAFT polymers. (B) Reduction of disulfide linkages by glutathione releases the corresponding thiol-terminated polymer from the protein. Reproduced with permission. ¹⁴³ Copyright © 2023 The Authors. Published by American Chemical Society. Licensed under CC-BY 4.0	30
Figure 2.1. MALDI-TOF mass spectra of neopentyl alkene dendrons of generation 1-5.	50
Figure 2.2. Top: structures of BnO-G5-(Neo-NH₃⁺TFA⁻)₃₂ and BnO-G5-(Lin-NH₃⁺TFA⁻)₃₂ , TFA anions have been omitted for clarity. Bottom left: tracking ¹ H NMR showing BnO-G5-(Neo-NH₃⁺TFA⁻)₃₂ (pink) and BnO-G5-(Lin-NH₃⁺TFA⁻)₃₂ (blue) in pH 8 phosphate buffer at 37 °C. Boxed signals indicate evolution of the degradation peaks. Bottom right: graphical summary of <i>hydrolysis</i> ¹ H NMR data, the neopentyl species did not undergo visible hydrolysis, and so all the datapoints are superimposed..	52
Figure 2.3. Stacked NMR spectra of 1 mM BnO-G5-(Lin-NH₃⁺TFA⁻)₃₂ in 0.1M phosphate buffer across three different pH over 1 month. α-CH ₂ of dendron-bound amine, free amine, and lactam are colour-coded.	54
Figure 2.4. Degradation of BnO-G5-(Neo-NH₃⁺TFA⁻)₃₂ and BnO-G5-(Lin-NH₃⁺TFA⁻)₃₂ in 20% porcine esterase solution in pH 7.4 phosphate buffer at 37 °C, as monitored <i>via</i> ¹ H NMR.	54
Figure 3.1. Dendritic architectures used for grafting onto proteins for molecular sieving.	153
Figure 3.2. Schematic representation depicting the preparation of PEGylated α-CT-dendron conjugates, where the dendron is varied from G3 to G5, and the PEG chain lengths were 350, 1000, and 2000 Da at each dendron generation (a total of 9 different conjugates).	158
Figure 3.3. DRIFTS IR spectra of α-CT-(N ₃) ₁₄ (black), and a fully conjugated α-CT-G3-PEG ₃₅₀ (red). The azide peak at 2100 cm ⁻¹ completely disappears after SPAAC coupling.	159
Figure 3.4. Cryo-electron microscopy of CT-G3-PEG ₂₀₀₀ (273 kDa) and CT-G5-PEG ₂₀₀₀ (1023 kDa). The top three panels show representative cryo-EM images from CT-G3-PEG ₂₀₀₀ . The inset in the top right picture shows a zoomed view of the area included in the white frame. The arrowheads point to individual CT-G3-PEG ₂₀₀₀ dendrons. The bottom panels display three representative cryo-EM images from the CT-G5-PEG ₂₀₀₀ sample. In this case, the images on the left and middle panels were taken inside the grid holes. The left panel shows a zoomed view of the two dendrons shown in the image. The right panel shows an image of the carbon area between holes. Given the higher affinity of CT-G3-PEG ₂₀₀₀ dendrons towards carbon, this area shows a higher density of dendrons than images inside the holes, but with higher background caused by the continuous carbon layer. Arrowheads point to individual CT-G5-PEG ₂₀₀₀ dendrons. The 50 nm scale bar in the top left panel applies to all panels as all images were taken at 80,000× magnification.	161

Figure 3.5. Relative activity of the PEGylated α -CT conjugates (G3-G5) toward BTPNA versus native chymotrypsin. As well, control data for native α -CT in the presence of un-conjugated G3-G5 PEGylated dendrons is provided. Error bars indicate standard error (n=3). One-way ANOVA was performed to determine significance of PEG length and dendron generation on relative activity (p < 0.001 (***) , p < 0.01 (**), p < 0.05 (*), NS = not significant).	163
Figure 3.6. (A) Relative activity of the G3-G5 PEGylated conjugates toward casein and BSA. One-way ANOVA was performed to determine significance of PEG length and dendron generation on relative activity (p < 0.001 (***) , p < 0.01 (**), p < 0.05 (*), NS = not significant). (B) Sieving ratios for the G3-G5 PEGylated conjugates, expressed as a ratio of activity toward BTPNA and the respective proteins (casein and BSA). For both (A) and (B) , control data from mixtures of the native α -CT in the presence of un-conjugated G3-G5 PEGylated dendrons are provided.	166
Figure 4.1. Schematic representation of dendron generation-controlled sieving processes involving avidin-dendron conjugates interacting with biotin, dendronized biotin, and biotinylated proteins. Structures are not drawn to scale – size discrepancy between ligands are illustrated by differently sized cartoons.....	240
Figure 4.2. A) Stacked FT-IR spectra of azidoacetic acid NHS ester, avidin-N ₃ , and Av-Gx conjugates showing complete consumption of azides post SPAAC. Inset shows highlighted azide signal centered at ~2110 cm ⁻¹ . B) Native PAGE (6%) of avidin-dendron conjugates. From left to right: Ladder (NativeMark), avidin, avidin azide (Av-N₃) and avidin-dendron conjugates (Av-Gx , x = 3-7; lanes 4-8). PAGE was run in pH 8.3 tris-glycine buffer and stained with Coomassie R250. Native avidin was immobile under these conditions.....	245
Figure 4.3. Circular Dichroism spectra of avidin-dendron conjugates (0.2 mg/mL) in 10 mM PBS.....	246
Figure 4.4. Z-average diameter versus molecular weight of avidin-dendron conjugates. Error bars represent standard deviation.	247
Figure 4.5. Cryo-EM analysis of Av-G4 , Av-G5 , Av-G6 , and Av-G7 . Panels (A) to (D) show representative cryo-electron micrographs obtained for the Av-G4 , G5 , G6 and G7 samples. (E) Zoomed-in view of the framed area in panel (D) shows the small particles in the G7 sample. (F)) Zoomed-in view of the vesicle-like particle in panel (D) indicated with a white arrow as a representative example of the vesicles also observed in the G7 sample. (G) Single particle analysis of the G6 sample. About half a million particles were selected and extracted from the electron micrographs (left panel) and subjected to 2D classification and averaging. The right panel shows a few selected 2D class averages for the G6 sample.	249
Figure 4.6. Binding of biotin and BGx (x = 3-7) to native avidin measured by ITC. (A) Biotin, (B) BG3 , (C) BG4 , (D) BG5 , (E) BG6 , (F) BG7 . From the top: Row 1: Raw heats evolved from binding for titrants A-C; Row 2: Corresponding enthalpy derived	

from integrated heats. Rows 3-4: Raw heat evolved and corresponding enthalpy, respectively, for titrants D-F.....	251
Figure 4.7. Equilibrium dissociation constants (K_d) of BGx binding to Av-Gx as measured by ITC.....	253
Figure 4.8. Left: Binding stoichiometry between biotin, BGx and avidin and Av-Gx . Right: schematic representation of BGx : Av-Gx complexes. Illustrations of conjugates are not to scale.	255
Figure 4.9. A comparison of size-exclusion effects (left) and negatively cooperative effects (right) in avidin-dendron conjugates. A. Grafted dendrons (light blue spheres) on Av-G4 exclude the access of BG6 (dark blue spheres) to the binding sites. B. Av-G4 preferentially binds two molecules of BG5 at opposing binding sites, which then act as an additional steric barrier to exclude BG5 from further binding. C. BG4 binds three subunits of Av-G6 and distorts the remaining site, inhibiting further binding. D. BG5 binds an already compromised Av-G7 , further distorts the vacant subunits, preventing further binding. Structures are not drawn to scale – size discrepancy between ligands are illustrated by differently sized cartoons.	259
Figure 4.10. Top: Schematic representation of interstitial space between grafted dendrons in Av-Gx and sieving of various biotinylated ligands. Structures are not drawn to scale. Bottom: Binding of two small biotinylated ligands, aprotinin and PEG ₃₄₀₀ , to avidin and Av-G4 measured by ITC. A. native avidin : PEG ₃₄₀₀ . B. Av-G4 : PEG ₃₄₀₀ . C. native avidin : aprotinin. D. Av-G4 : aprotinin.....	262

List of Schemes

Scheme 2.1. General method for preparing neopentyl carboxylic acids 1-3 and representative synthesis of a generation 5 neopentyl periphery bis-MPA dendron.	48
Scheme 2.2. An example of using FPE to prepare BnO-G5-ene	49
Scheme 2.3. Example thiol-ene click reaction between thioglycerol and BnO-G5-ene using DMPA as the photo-initiator.	51
Scheme 3.1. Synthesis of the benzyl carbamate protected G3 dendron CBz-G3-(OH)₈	154
Scheme 3.2. Synthesis of the SPAAC-reactive PEGylated dendrons, DBCO-G3-(PEG_x)₈ (x = 350, 1000, 2000).	154
Scheme 3.3. Synthesis of the G4 and G5 dendrons (DBCO-G4-(PEG_x)₁₆ and DBCO-G5-(PEG_x)₃₂ , respectively, x = 350, 1000, or 2000) by convergent SPAAC reaction of G1 and G2 azide-terminated dendrons with DBCO-G3-(PEG_x)₈ , followed by installation of DBCO at the core.	157
Scheme 4.1. Iterative synthesis of benzyl carbamate-protected polyester dendrons up to the 7 th generation, CBz-G7-(OH)₁₂₈ . Structures of G4, 5, 6 dendrons bearing 16, 32, and 64 hydroxyl groups at the periphery, respectively, are omitted for clarity.....	241
Scheme 4.2. Core functionalization of bis-MPA-based polyester dendrons.	242
Scheme 4.3. Synthesis of avidin azide (Av-N ₃) and Avidin-dendron conjugates (Av-G_x) from native avidin.	243

Contents

ABSTRACT.....	III
ACKNOWLEDGEMENTS.....	IV
LIST OF ABBREVIATIONS.....	VI
LIST OF TABLES.....	VIII
LIST OF SUPPLEMENTARY TABLES.....	VIII
LIST OF FIGURES.....	XI
LIST OF SCHEMES.....	XV
CONTENTS.....	XVI
CHAPTER 1. INTRODUCTION.....	1
1.1 Overview of Dendrimers.....	1
1.2 Synthesis of Dendrimers.....	2
1.3 Dendrimers for Biological Applications.....	8
1.4 Amine versus Alcohol-Periphery Dendrons.....	10
1.5 Polymer-Protein Conjugates and the “Stealth” Effect.....	12
1.6 Molecular Sieving PPCs.....	17
1.7 Conjugation <i>via</i> Grafting-to Method.....	23
1.8 Conjugation <i>via</i> Grafting-from Method.....	25
1.9 Scope of Thesis.....	30
1.10 References.....	32
CHAPTER 2. NEOPENTYL DENDRIMERS AS ROBUST LINKERS FOR INTRODUCING FUNCTIONALITY TO BIS-MPA DENDRIMERS.....	45

2.1	Abstract	45
2.2	Introduction	46
2.3	Results and Discussion	49
2.4	Conclusion.....	55
2.5	Supporting Information	56
2.6	References	144
CHAPTER 3. MOLECULAR SIEVING WITH PEGYLATED DENDRON-PROTEIN CONJUGATES		148
3.1	Abstract	148
3.2	Introduction	149
3.3	Results and Discussion	153
3.4	Conclusion.....	167
3.5	Supporting Information	167
3.6	References	231
CHAPTER 4. DENDRIMER-MEDIATED MOLECULAR SIEVING ON AVIDIN		236
4.1	Abstract	237
4.2	Introduction	237
4.3	Results and Discussion	240
4.4	Conclusion.....	263
4.5	Supporting Information	264
4.6	References	310
CHAPTER 5. CONCLUSIONS AND FUTURE WORK		316
5.1	Conclusion.....	316
5.2	Future Work.....	318

Chapter 1. Introduction

1.1 Overview of Dendrimers

Dendrimers, derived from the Greek word ‘dendron’ meaning tree and ‘meros’ meaning part, are a class of polymers with successive layers of monomers radially branching from a central core. Dendrimers are uniform, structurally perfect macromolecules – each dendrimer can be defined exactly by its molecular formula and have a dispersity of unity. Dendrimers have narrow, homogeneous particle size distributions even at high molecular weights.¹ A dendrimer structure is divided into layers or *generations* of monomers, and with each generation the number of monomers at the periphery increases exponentially, depending on the number of terminal functionalities on monomers of the previous generation (Figure 1.1).

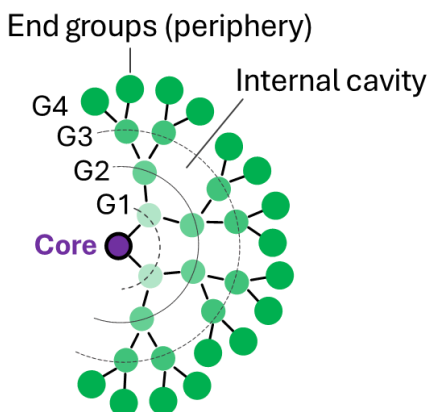


Figure 1.1. Schematic of a dendrimer. Successive generations (G1-4) are indicated by a deepening green colour. Starting at a bifunctional core (purple), the number of bifunctional monomers at each generation is represented by 2^n , where n = generation number.

As the dendrimer grows, monomers constituting the lower generations form the internal branches within the dendrimer. The type of monomer reflects the synthetic approach that is used to prepare its dendrimer (e.g., polyester vs. polyamidoamine dendrimers), while the generations create internal cavities that can encapsulate small molecules at high generations.²⁻⁶ The outermost layer from the core, also known as the periphery of the dendrimer, is terminated by a discrete number of surface functionalities that primarily dictate the overall reactivity, solubility, and valency of the dendrimer. Dendrimers have distinct molecular and bulk characteristics from their linear polymer counterparts owing to their unique architecture.¹ Since dendritic monomers branch concentrically from the core moiety instead of as linear chains, dendrimers will adopt an increasingly globular conformation with increasing generation and form tightly packed spheres with lower hydrodynamic radii (typically 1-10 nm) than their linear counterparts in solution. Unlike high MW linear polymers such as poly(ethylene glycol) or polystyrene, high generation dendrimers do not undergo chain entanglement and, as such, exhibit lower viscosity and higher solubility compared to linear polymers of the same composition and molecular weight. Most applications of dendrimers revolve around their unique structural features, exploiting reactivity at the core,⁷ internal cavity,^{3,8} or periphery,^{7,9} as well as physicochemical interactions arising from the spatial separation between core and peripheral moieties created by inner generations of monomers.¹⁰⁻¹⁵

1.2 Synthesis of Dendrimers

Dendrimers are built by repetitive growth, either 1) outwards i.e., divergently from the core, one generation at a time, or 2) inwards from the periphery in a convergent manner to

produce dendrons, which are fractional branches of the total dendrimer structure and contain a focal point. The archetypical divergent method is an iterative two-step process, where the first step is monomer coupling to the core, and the second step is modification of the periphery – typically by deprotection – to expose reactive functionalities for further growth (Figure 1.2).

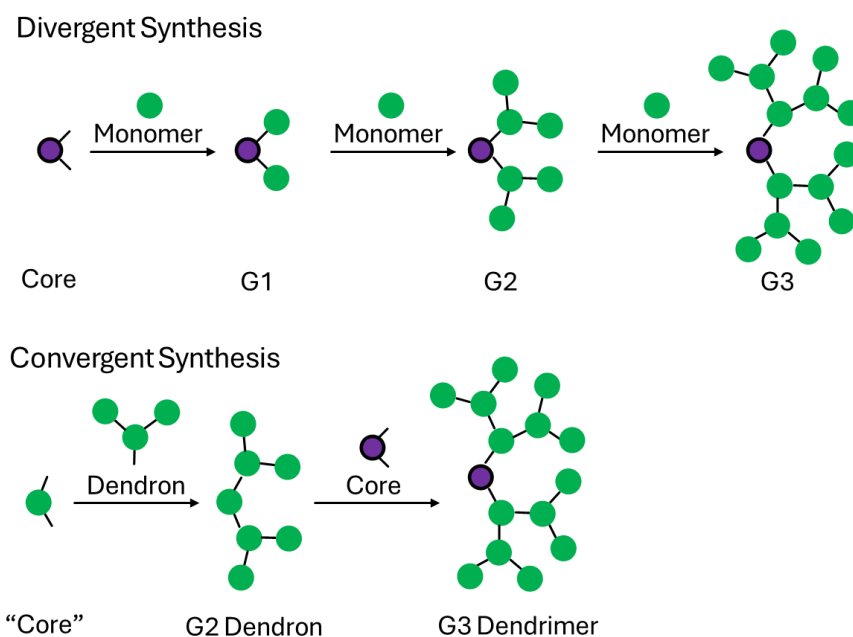


Figure 1.2. Divergent and convergent synthesis of dendrimers.

Each two-step iteration increases the generation number by one and necessitates purification of the dendrimer from excess coupling agents, monomer, and/or side-products. As such, this method can be inefficient due to product loss from multistep synthesis, incomplete functionalization of the periphery, and long reaction times. The divergent method was first realized by Vögtle in 1978 by sequential Michael addition of an amine core initiator to acrylonitrile, followed by Co(II)-catalyzed reduction to yield poly(propylene imine) (PPI) dendrimers.¹⁶ In 1985, Tomalia and coworkers reported G1-

G5 polyamidoamine (PAMAM) dendrimers, which were termed “starburst dendrimers” owing to their concentric branching structure from a central core.¹⁷ Ammonia was exhaustively alkylated *via* Michael addition to methyl acrylate forming the tri-branched core. Subsequent amidation at peripheral ester groups then afforded the next generation amine-terminated dendrimer (Figure 1.3).

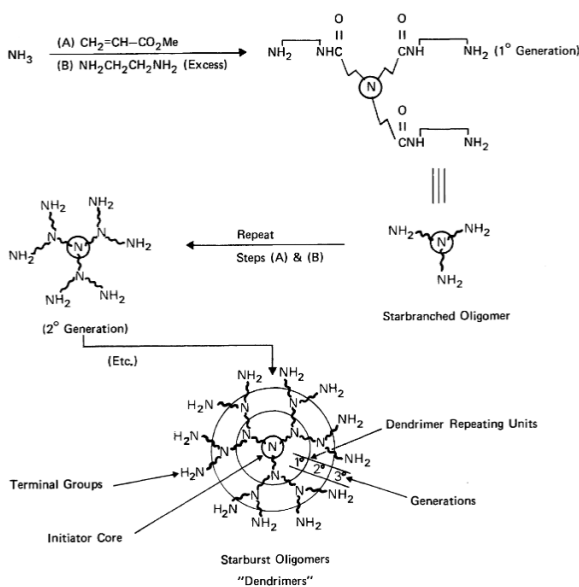


Figure 1.3. Synthesis of PAMAM "starburst" dendrimers by Tomalia et al. Reused with permission.¹⁷ Copyright © 1985, The Society of Polymer Science, Japan.

The convergent approach involves the prior synthesis of dendrons *i.e.*, parts or branches of a dendrimer, which are then coupled to the core to form the dendrimer.¹⁸ The periphery of the dendron forms the periphery of the dendrimer, and focal points of the dendron constitute junctions in the final structure.¹⁸ A single-stage convergence describes the coupling of peripheral dendrons to a non-dendronized core, whereas double-stage convergence describes the coupling of peripheral dendrons to core dendrons.⁴ Hawker and Fréchet reported the single-stage convergent synthesis of a poly(aryl ether) dendrimer by

coupling three G4 dendrons based on 3,5-dihydroxybenzyl alcohol to a 1,1,1-tris(4-hydroxyphenyl)ethane core (Figure 1.4).¹⁹

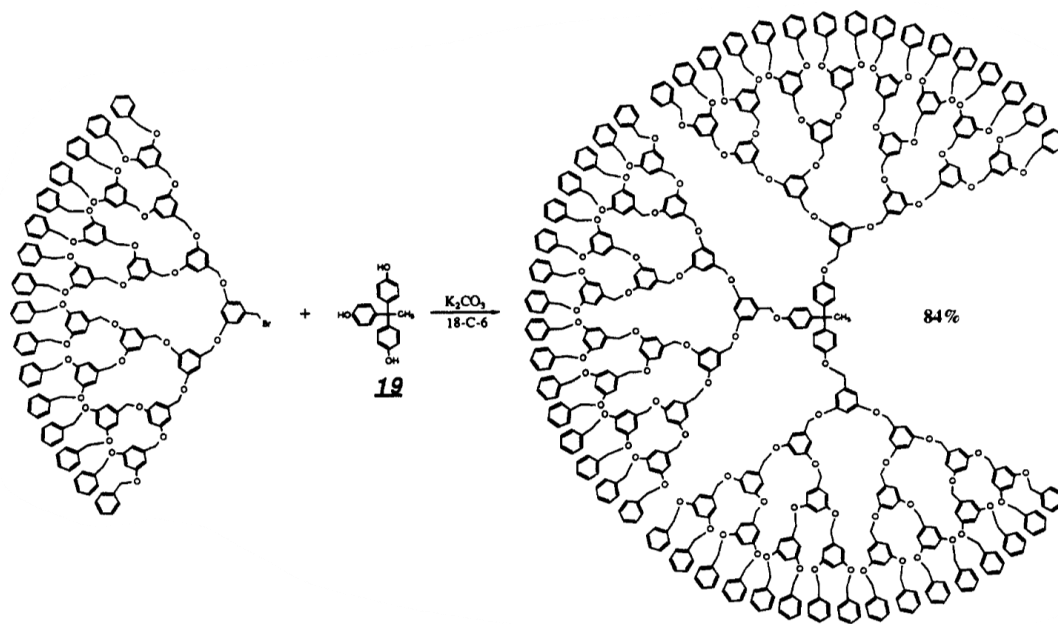


Figure 1.4. Convergent synthesis of poly(aryl ether) dendrimers reported by Hawker and Fréchet. Reproduced with permission.¹⁹ Copyright © 1990, American Chemical Society.

The same strategy was used by Hult and coworkers to synthesize G1-G4 poly(alkyl ester) dendrimers using 2,2-Bis(hydroxymethyl)propionic acid (Bis-MPA) as the monomer and tris(hydroxyphenyl)ethane as the core.²⁰ Sequential protection/deprotection steps at the periphery and focal points of the dendrons were achieved by *O*-acetylation of the alcohols by oxalyl chloride and hydrogenolysis for deacetylation, respectively. Hult et al. later reported a double-stage convergent synthesis of dendrimers based on Bis-MPA. In this manner, a G4 dendron was afforded by coupling four G2 dendrons divergently to (*i.e.*, at the periphery of) another G2 dendron with a deprotected alcohol periphery (Figure 1.5).¹⁸ Peripheral alcohol groups were protected by acetal formation with 2,2-dimethoxypropane which was easily reversible under mildly acidic conditions, which could be efficiently

achieved by exposing the acetonide-protected dendrons to sulfonic acid-bearing polymer resin (DOWEX) in methanol to regenerate the alcohol periphery.

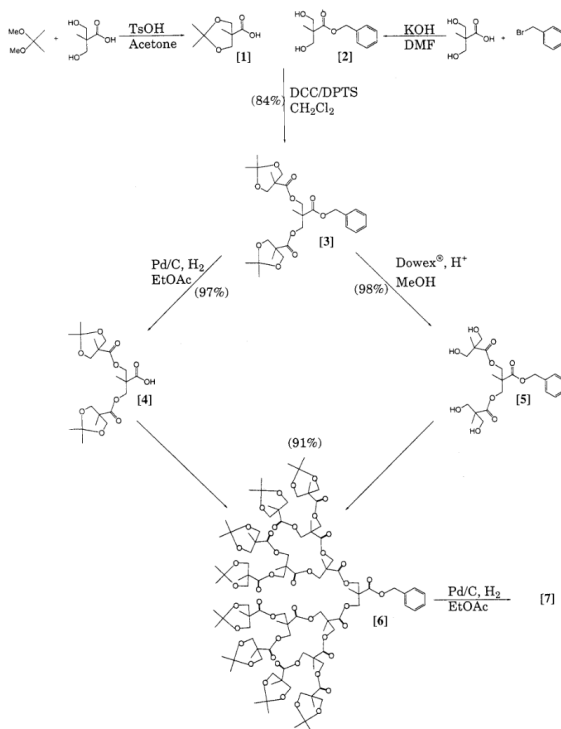


Figure 1.5. Poly(alkyl ester) dendrimers synthesized by a convergent approach. Reused with permission.¹⁸ Copyright © 1998, American Chemical Society.

As seen from these examples, both convergent and divergent methodologies rely on a systematic alternation in activating and deactivating orthogonal functional groups to selectively couple at either the core or periphery. While the number of synthetic steps to reach the dendrimer end-product may be identical between a divergent and convergent approach, the final coupling steps in the convergent approach *i.e.*, when dendrons culminate to form the dendrimer, generally comprise of fewer coupling steps between the *dendron* focal point(s) and the core moiety (Figure 1.2). However, high-generation dendrons may be difficult to synthesize convergently due to site-isolation of the focal points

or extreme steric hindrance when assembling large dendrons.^{10,21} This contrasts with the divergent method where the final growth step requires numerous coupling reactions to surface groups on a high-generation dendrimer, potentially resulting in surface defects or incomplete functionalization.^{1,22} It is worth noting that while site-isolation and steric hindrance limitations of the convergent methodology can be addressed through molecular design, for example by introducing spacers to extend the point of attachment away from the dendron backbone or by coupling dendrons at lower generation,²³ the limitations of divergent synthesis can be overcome by efficient coupling reactions.^{22,24,25} Originally developed for small molecule coupling, a number of esterification and amidation reactions based on activated imidazolium or imidazole-activated esters have been adapted for dendron growth (*vide infra*).^{22,24,26} As such, the divergent strategy is as viable and widely used as its convergent counterpart in contemporary dendrimer synthesis.

Since the pioneering work by Bertozzi, Sharpless, and Meldal on the development of click chemistry in the early 2000s,²⁷⁻³¹ the chemical toolbox available for dendrimer synthesis has vastly expanded, as have the menu of surface functionalities and the complexity of dendritic architectures.³² Owing to their favourable reaction kinetics, regio/stereospecificity, high yields and high atom economy, click reactions are used to address synthetic shortcomings that plague dendrimers at high generations, such as sluggish coupling steps or incomplete reactions at the periphery. Several types of click chemistry, including thiol-ene,³³ aza- and thiol-maleimide Michael addition,³⁴ strain-promoted alkyne-azide cycloaddition (SPAAC),^{31,35} copper-catalyzed alkyne-azide cycloaddition (CuAAC),^{29,36} and boronic acid/hydroxamate^{37,38} have been used to furnish

dendrimers in both convergent and divergent manners. Moreover, as they generally proceed well in both mild organic and aqueous conditions, and some can tolerate a wide range of pHs, click reactions have been heavily used to bridge polymers – including dendrimers – to biological interfaces such as peptides, proteins, and cells.^{26,39–42} In later chapters of this work, click-reactive functional groups are installed at dendron focal points or peripheries to enable dendron conjugation with small molecules (surface functionalization), other dendrons (convergent synthesis), as well as proteins to form polymer-protein conjugates.

1.3 Dendrimers for Biological Applications

Dendrimers are an attractive candidate for a myriad of biological applications, particularly as a carrier in gene transfection,⁴³ bioimaging,^{44–46} and small molecule drug delivery either by confinement within the dendron cavities or by surface conjugation.^{2–5,47–50} Since its inception in the 1970s, every structural domain of dendrimers has been subject to investigation for therapeutic or diagnostic use (Figure 1.6).⁵¹ Due to its controlled multivalency and orthogonality at the core and periphery, the dendrimer can bear a well-defined number of peripheral functional groups, allowing investigation of multivalent effects.^{52–54} Dendron-bound payloads may behave differently versus their unbound counterparts. Functional groups on a dendrimer may produce a response that is disproportionate to the number of functional groups available. This disproportionate response is termed the “dendritic effect”,^{55,56} and may present as a positive process, as was found by Ford and coworkers, where the rate of decarboxylation of 6-nitrobenzisoxazole-3-carboxylate catalyzed by *o*-iodosobenzoate was increased in the presence of a G3 dendrimer-bound ammonium counterion.⁵⁵ Alternatively, the effect can present as a

negative process where, for example, slowed enzymatic hydrolysis of a triazole nucleoside-functionalized periphery of G2 PAMAM dendrimers was observed.⁵⁷ As such, therapeutics exhibiting dendritic effects in the context of drug delivery can have longer drug half-lives, increased bioavailability, or more controllable release.⁵⁸ Dendrimers have been surface-decorated with biomolecules such as peptides,⁵⁹ lipids,⁶⁰ carbohydrates, and vitamins to target overexpressed receptors on cancer cells and virus-infected cells.^{50,61–63} The surface of the dendrimer allows conjugation with abundant targeting moieties to enhance local dendrimer concentration on or within the cell (*e.g.*, by inducing endocytosis), depending on payload. The payload can then induce a multitude of effects ranging from drug release within the cytosol, to immunostimulation (*e.g.*, by recruiting anti-hapten-antibodies).⁶⁰ Dendrimers also serve as grafts on proteins to modulate their binding,^{26,41} which is explored in Chapters 2 and 3 of this work.

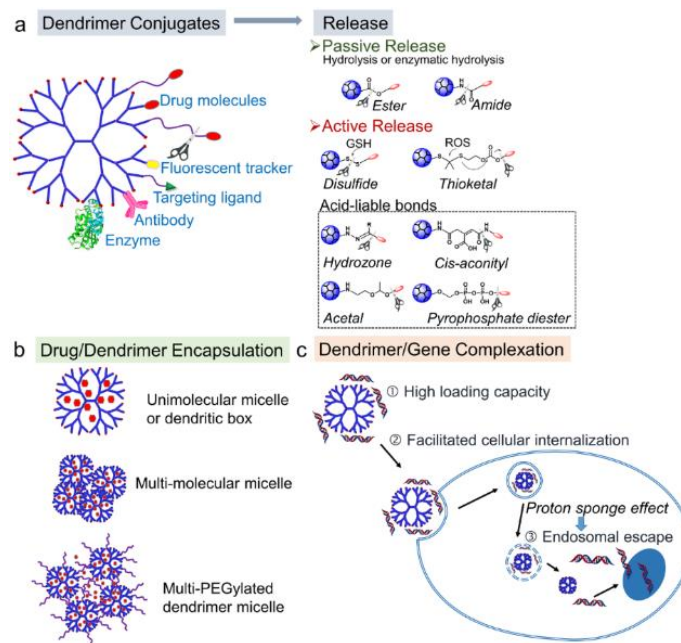


Figure 1.6. Dendrimer-based drug delivery systems. Reproduced with permission.⁵ Copyright © 2022, The Authors. (Licensed under [CC-BY 4.0](https://creativecommons.org/licenses/by/4.0/)). Published by Springer Nature.

1.4 Amine versus Alcohol-Periphery Dendrons

PAMAM, PPI, and polylysine dendrimers (Table 1.1) are most frequently encountered in the literature for biological use due to their amine-rich periphery, which allows them to complex anionic moieties (*e.g.*, siRNA, DNA) *via* electrostatic interactions.^{6,51,64,65} Surface amines are also frequently covalently functionalized with their payload *via* amide coupling (Figure 1.6).^{1,6,66,67}

Table 1.1. Main classes of dendrimers used in biological applications. Reproduced with permission.⁶ Copyright © 2021 Taylor and Francis.

Dendrimer Type	Cascade	PAMAM	PPI	Polylysine	Polyester	Phosphorus
Typical Chemical Structure						

However, there is a long-standing recognition of the *in vitro* toxicity associated with amine-terminated dendrimers due to their strong cationic character under physiological pHs. Dendrimer-bound ammonium ions impart high charge density which interacts with negatively charged phospholipids on cell membranes, disrupting them *via* hole formation leading to cell death.^{51,68} PAMAM dendrimers have been found to exhibit generation-dependent bactericidal properties, with larger dendrimers (G4 and above) inducing endocytosis in bacterial cells and subsequent localization at the mitochondrial membrane, leading to oxidative stress.⁶⁹ Recently, Malkoch and coworkers have also found that even lower generation (G2-G3) amino-functional dendrimers exhibit antibacterial effects when exposed to *E. coli* at micromolar concentrations, which is considered to be an unacceptably high concentration for *in vivo* use.⁷⁰ Conversely, alcohol peripheral groups, being neutral, do not form complexes with ionic moieties under physiological conditions, and are consequently less toxic than their amino-functionalized counterparts.^{64,71–73} In aqueous conditions, the alcohol periphery creates a hydration sphere around the dendrimer by hydrogen bonding to multiple water molecules, much akin to the effect achieved by PEGylation,⁷⁴ while the lack of electrostatic interactions deters protein corona formation

around the dendrimer.⁷⁵ Both of these effects lend strong support for the use of polyester alcohol-periphery dendrimers in biological applications in which limited interaction with the biomacromolecules in the bulk matrix is typically desired. Several studies have shown that polyester dendrimers, particularly those based on bis-MPA, are generally non-cytotoxic, biodegradable, and non-immunogenic,^{50,76,77} and that they are viable dendritic scaffolds for targeted delivery of therapeutics and protein conjugation.^{26,44,45}

1.5 Polymer-Protein Conjugates and the “Stealth” Effect.

As a fusion of biological and synthetic components that transcends the sum of their parts, polymer-protein conjugates (PPCs) represent one of the smallest and most intimate forms of partnerships between nature and human invention. While native proteins have unrivalled uniformity and specific functionality, their form and function can be further enhanced by conjugation to the massive and ever-growing arsenal of synthetic polymers. While native proteins often cannot be administered directly in part due to their instability and rapid clearance *in vivo*, the latter of which is generally due to recognition by the host immune system,⁷⁸⁻⁸⁰ polymers have long been recognized for their ability to sterically shield the bound protein from antibody recognition and unwanted binding.⁴⁰ The primary effect reported in the literature resulting from polymer conjugation has consistently been the protection of the grafted protein, which manifests as lowered protein immunogenicity (*i.e.*, stealth, *vida infra*) and increased protein stability under different stressors, such as heat, pH, and in organic solvents.^{74,81,82} PEGylation is the most influential and well-known form of polymer-protein conjugation. PEGylation protects the grafted protein by a combination of steric effects and forming a hydration sphere about the protein. Several

decades after their inception,⁸³ PEGylated proteins continue to see widespread therapeutic applications, with over a dozen FDA-approved PEGylated proteins currently on the market.⁸⁴ However, the issue remains with linear PEGylation that the conjugates can elicit an anti-PEG response *in vivo* and consequently suffer from diminished circulation time and increased elimination.^{85–88} Moreover, interactions between the grafted linear PEG and the protein scaffold can potentially hinder ligand binding,^{85,89–91} as well as protein folding.^{85,89,91} It has been found that the immunogenicity of PPCs is intricately tied to the immunogenic response stemming from the protein scaffold.⁸⁶ Moreover, the nature of the grafting polymers can also impact protein-polymer interaction, which stresses the importance of tailoring different polymers to proteins to achieve stealth properties instead of relying solely on PEGylation. Hence, recent work in the literature is trending away from linear PEGylation of proteins toward other polymers, such as amphiphilic and zwitterionic polymers,^{84,92–96} as well as other ethylene glycol (EG) bearing architectures such as poly(oligo(ethylene glycol) methyl ether methacrylate) (POEGMA) or PEG-substituted polynorbornenes for synthesizing “stealth” PPCs.^{74,87,92,97} The most common approach to imparting stealth properties is to form a hydration layer around the protein, which is accomplished by grafting highly hydrophilic polymers.⁹⁸ The hydration layer renders protein adsorption to the polymer coating entropically unfavourable, and the architecture of the grafting polymer is often designed to maximize the thickness of the polymer coat and, by extension, of the hydration layer.⁹⁹ For example, POEGMA selectively grafted *via* ATRP from the *N*-terminus of proteins has been found to exhibit favourable pharmacokinetics and longer circulation time *in vivo* versus native protein counterparts.¹⁰⁰

Thiol and sulfoxide-containing polymers have also been found to produce PPCs with desirable stealth properties. Tirelli and coworkers reported that a polymer containing both glycerol and thiol sidechains, poly(thioglycidyl glycerol) (PTGG) (Figure 1.7), achieved both passive and active protection of the grafted proteins.¹⁰¹

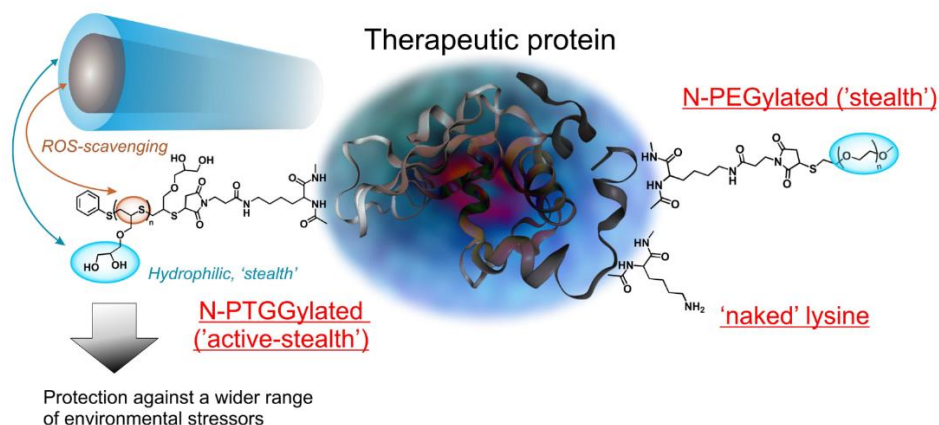


Figure 1.7. Protein conjugated with redox-active poly(thioglycidyl glycerol). Reused with permission.¹⁰¹ Copyright © 2022 The Authors. Published by American Chemical Society.

PTGG was found to exhibit low cytotoxicity, only nonspecific uptake by murine RAW 264.7 macrophages, and led to lower complement activation compared to PEG of similar MW.¹⁰¹ Passive stealth was afforded by the hydrophilic polyols, while the thiols act as a sacrificial quencher for reactive oxygen species (ROS) generated *via* an innate immune response. Remarkably, the lysozyme-PTGG PPC retained *in vitro* antibacterial activity, while mouse studies using ovalbumin-PTGG PPCs resulted in an absence of anti-polymer IgG/M response and accelerated blood clearance (ABC). The combination of active and passive stealth imparted by bifunctional monomers in this case serves as an important design guideline for next generation polymers used to construct PPCs.

The Chung group utilized several types of orthogonal click chemistry to afford densely grafted PPCs. Using a stepwise combination of RAFT followed by ATRP, the authors first constructed an azide-terminated, zwitterionic bottlebrush polymer (Figure 1.8). A bifunctional TEG linker with SPAAC and *trans*-cyclooctene (TCO) was then grafted onto urate oxidase bearing tetrazines by inverse electron-demand Diels-Alder (IEDDA) click reaction, which finally allowed SPAAC addition of the polymer to form the final PPC. The conjugates exhibited proteolytic resistance and reduced antibody binding while retaining their activity, which was postulated to originate from steric hindrance imparted by the grafting polymer.⁹⁶ Low-fouling polymers can also enable the “stealthy” delivery of a protein payload. Whittaker and Fu reported the conjugation of sulfoxide-containing polymer to transferrin.⁹⁸ Cellular uptake and cytotoxicity were similarly low compared to PEGylated transferrin, and the sulfoxide-containing PPC exhibited nearly a 3-fold increase in circulation time in mice compared to the native protein, which the authors attributed to the high hydrophilicity of the polymers. Interestingly, exposure to the presence of high ROS *in vivo* (i.e., inside tumor-bearing mice) induced polymer cleavage and led to the accumulation of transferrin within the tumor.⁹⁸

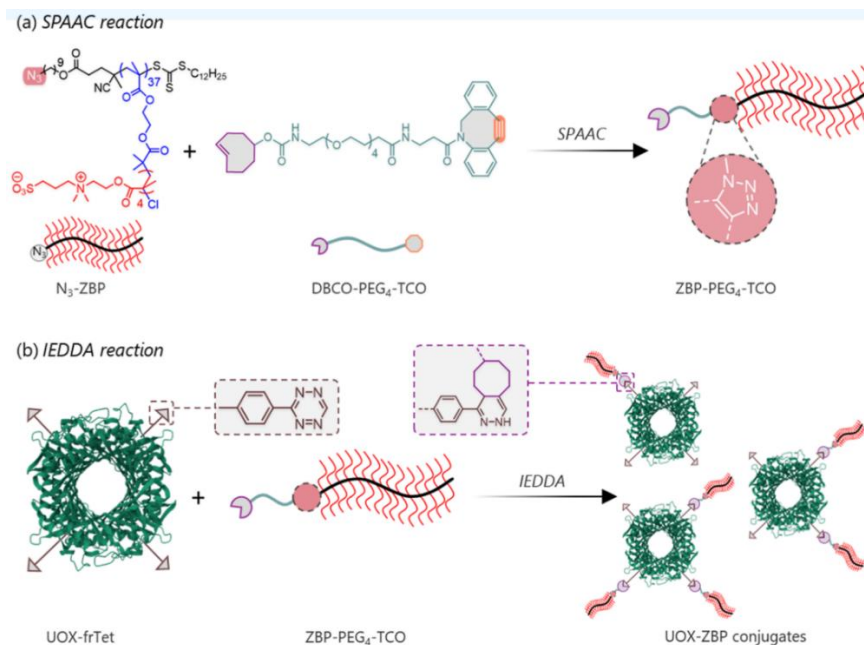


Figure 1.8. Uricase oxidase-zwitterionic bottlebrush (ZBP) polymers developed by Chung et al. Reused with permission.⁹⁶ Copyright © 2024 American Chemical Society.

Asparaginase, an enzyme commonly used to treat lymphoma (Oncaspar®), is a popular protein candidate for polymer modification.^{102–104} Lu et al. reported an “urchin”-like PPC using asparaginase and a polyglutamate grafted with tri(ethylene glycol) and carboxybetaine pedant groups. The work found lower IgG and IgM response elicited by experimental conjugates in mouse studies compared to the traditional PEGylated asparaginase.¹⁰²

The “hydrophilic” principle could be extended to other hydrophilic polymers. Indeed, zwitterionic polymers have emerged in recent years as promising non-fouling, biocompatible materials with several PPCs reported in the literature.^{84,93–95,105–107} Using alternating glutamic acid-lysine (EK) dimers, Jiang and coworkers disclosed an alternating (EK) polymer grafted onto keyhole limpet hemocyanin (KLH) and asparaginase.⁹⁴ After

initial conjugation of the first EK layer to the protein, one and two successive layers of EK dimers were respectively attached to lysine amines. Asparaginase PPCs with double and triple EK layers showed complete protein shielding against anti-asparaginase antibodies *in vitro*, and this lowered immunogenicity was mirrored in mouse models wherein the circulation half-time of the triple-layered PPC was 2.3-fold longer than that of native asparaginase, and negligible levels of anti-polymer IgG and IgM were detected. Interestingly, an extension of their work using an EKP (glutamic acid-lysine-proline) polymer grafted onto keyhole limpet hemocyanin (KLH), revealed that oligopeptides containing sequences EEEKKK and EEEEEKKKK elicited much higher levels of anti-peptide IgM and IgG response versus shorter EK counterparts. The higher immunogenicity stemmed from locally-charged domains and competitive charge pairing within the polymer chain, which decreased its hydrophilicity.⁹⁵ In contrast, proline incorporation into the monomeric triad resulted in a disordered polymer chain structure that exhibited increased radius of gyration and effective hydrodynamic volume versus the classical EK system, which helped to protect the protein scaffold. Through mouse models, EKP-fused interferon (IFN) exhibited prolonged circulation, low immunogenicity, and maintained circulation time even after multiple injections.⁹⁵

1.6 Molecular Sieving PPCs

Molecular sieving is the physical process of excluding ligands from binding to a protein based on the ligand's size and morphology.¹⁰⁸ Similar to some PPCs exhibiting stealth properties, the grafted polymers function as a coat, or *nano armor*,¹⁰⁹ to surround the grafted protein. Ligands below a molecular weight cut-off (MWCO) are allowed

passage through the cavities within the polymer coat to the binding site(s) while larger ligands are excluded. A seminal report by Gauthier and coworkers first reported molecular sieving in 2013 using pOEGMA grafted onto chymotrypsin,⁹⁷ and later onto asparaginase to similar effect.¹¹⁰ A PPC can exhibit the sieving effect provided that the grafted polymer layer is situated favourably around the binding pocket(s), such that it can directly influence the binding of ligands. While this can theoretically be fulfilled by conjugates that are partly grafted with linear polymers, experimentally, the published reports on molecular sieving are entirely composed of PPCs that have comb-shaped, branched, or dendronized polymers exhaustively conjugated to the surface of the protein.¹¹¹ Hydrophilic residues such as lysines are common sites for functionalization,^{26,41,97,109} while PPCs grafted at less abundant residues (*e.g.*, cysteine) have not been reported to show any explicit sieving due to the limited surface coverage in these structures. Coarse-grained simulations by Drossis et al. using chymotrypsin-POEGMA PPCs revealed that a grafting polymer backbone with a degree of polymerization above a minimum threshold ($DP \geq 5$), is required for molecular sieving.¹¹¹ Meanwhile, chemical shift perturbation studies have shown that comb-shaped polymers extended further from the protein surface compared to their linear analogues,¹¹² and also created a denser polymer coat that covered a larger portion of the protein surface, both of which were critical in excluding large ligands from the grafted protein.

In other work, it was found that polymer architectures containing a hydrophobic backbone and hydrophilic pendants/chain ends is conducive to molecular sieving (*i.e.*, the corresponding PPC exhibits considerably higher activity toward a small ligand than a macromolecular ligand). This increase in activity is attributed to a favourable

microenvironment established by the hydrophobic backbone closer to the protein surface, which may also promote ligand interactions with the protein.^{111,113,114} Meanwhile, the aqueous-facing region of the polymer coat consisting of hydrophilic groups restricts access of larger molecules to the inner microenvironment. The density of the polymer coat is critical as it dictates both the MWCO of the gaps through which large ligands can diffuse, as well as the availability of favourable microenvironments to host small molecules approaching the protein.¹¹⁵ Furthermore, the polymer coat acts to slow the diffusion of ligands to the active site, with larger molecules diffusing slower than smaller ones due to steric hindrance.¹⁰⁹ So while linear polymer grafts (e.g., PEG) are commonly used for stealth applications, they do not produce a sufficiently dense coverage on the surface of the protein for sieving, and elongating linear backbones may lead to self-association and entanglement. In fact, overall reduction of ligand binding or catalytic activity in linear PPCs is a well-documented phenomenon.^{85,89,91} Meanwhile, PPCs grafted with low MW branched or comb-shaped polymers generally exhibit poorer selectivity of ligand binding compared to their native forms.^{87,92,116} This is presumably caused by several factors, including but not limited to an unfavourable microenvironment, nonspecific adsorption of other biomacromolecules to the polymer or grafted protein surface,^{82,117} and incomplete exclusion of macromolecular inhibitors from the grafted protein.¹¹¹ Conversely, while high MW branched polymers are well-suited for sieving, in some instances, the conjugates also have lower catalytic efficiency compared to their native counterparts.^{115,118}

The sieving effect was used by Minden and coworkers to separate excess protein tag impurities from target proteins (Figure 1.9).¹¹⁹ Biotin carboxy dimethyl maleic

anhydride (biotin-CDM) was used to tag protein surfaces by acylation of surface amines, and excess tags were quenched by a poly(carboxybetaine methacrylate) (pCBMA)-avidin conjugate, dubbed a “caged avidin”.

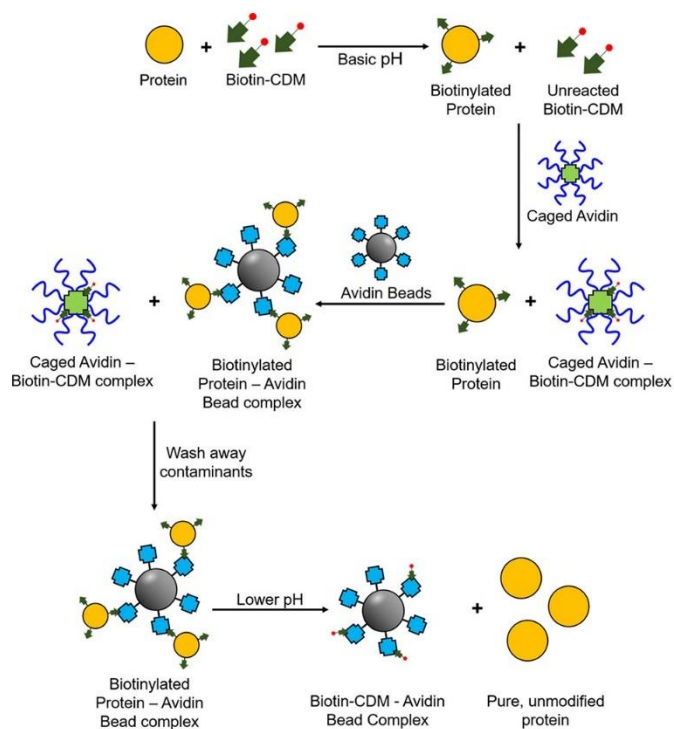


Figure 1.9. An avidin-based molecular sieve used to scavenge small biotin tags in a protein purification process, reported by Minden et al. Reused with permission.¹¹⁹ Copyright © 2019 American Chemical Society.

The tagged target proteins could then be immobilized by commercially available avidin-functionalized beads while the caged avidin-biotin-CDM complexes were washed away. Finally, the amide bond between biotin-CDM and the protein is hydrolyzed in mildly acidic (pH 4) conditions to recover the unmodified protein in high yields (>90%),¹¹⁹ which is crucially not achievable in traditional means of purification such as dialysis or spin

filtration. Most importantly, the authors demonstrated the utility of molecular sieving by integrating a sacrificial sieving protein into an affinity purification.

Our group previously reported the sieving effect in chymotrypsin-polymer conjugates by grafting dendrimers based on 2,2-bis(hydroxymethyl) propionic acid (bis-MPA).²⁶ The dendrimer-protein conjugate exhibited no significant change in activity (versus native chymotrypsin) toward BSA (66 kDa) from G2-6, while binding became negligible for G7 and G8 conjugates, indicating that the reduced spacing between dendrimers brought about by increasing dendrimer generations was critical for sieving efficiency (Figure 1.10). Meanwhile, conjugate activity toward a small ligand (Benzoyl-L-tyrosine *p*-nitroanilide, BTPNA) was >100% relative to native chymotrypsin for G2-G8 conjugates, which was attributed to the backbone of the dendrimer forming a favourable, hydrophobic microenvironment for substrate localization.²⁶

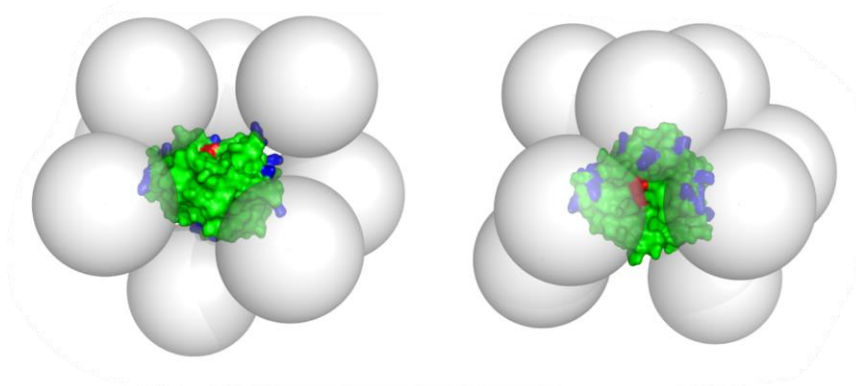


Figure 1.10. To-scale 3D models of chymotrypsin grafted with G7 bis-MPA dendrimers, showing the structure from the side and from the top, looking directly at the active site (coloured red). Reproduced with permission.²⁶ Copyright © 2019 John Wiley & Sons.

In 2021, Russell and coworkers investigated the effects of grafting density on molecular sieving using chymotrypsin-polymer conjugates.¹¹⁵ Linear, branched and comb-shaped pCBMA were grafted from lysine residues by ATRP. Through simulation studies, the authors found that free space around the CT active site (shown in green in Figure 1.11) decreased with increasing grafting density. The conjugates' catalytic efficiency toward a small peptide mimic (*N*-Succinyl-L-Ala-L-Ala-L-Pro-L-Phe-p-nitroanilide) were measured in the presence of various competitive inhibitors ranging from 6.5 (aprotinin) – 68 (α_1 anti-CT) kDa in size. Only the species with the densest polymer coats (see Figure 1.11d) retained their activity when exposed to a high concentration (10-fold to 100-fold eq.) of inhibitors.

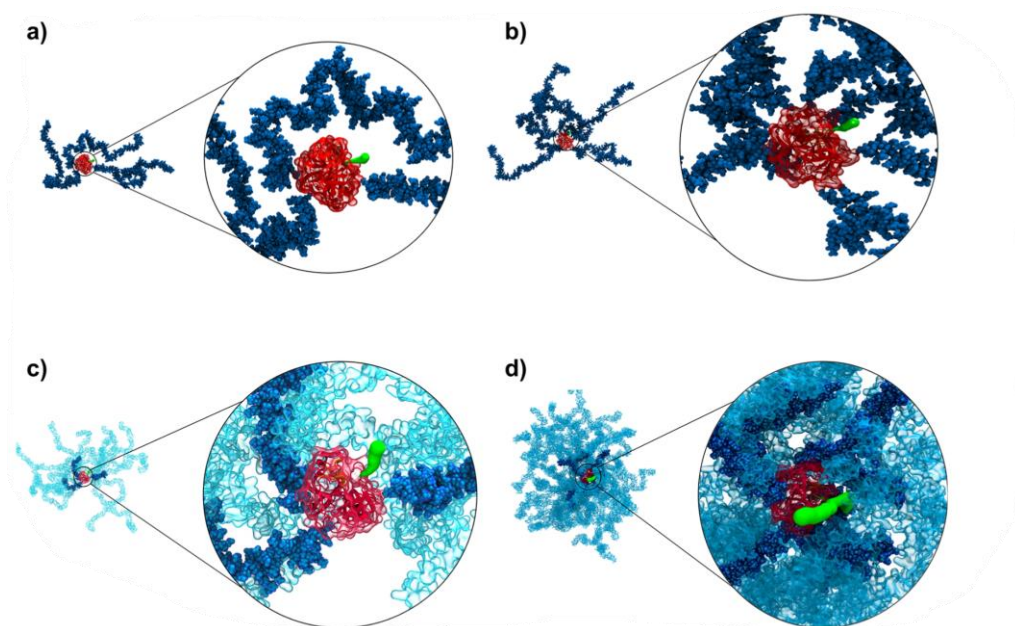


Figure 1.11. Molecular dynamics simulations of chymotrypsin grafted with different pCBMA architectures. (a) Linear pCBMA, 3 chains of DP ~200, (b) linear pCBMA, 7 chains of DP ~200, (c) Comb-shaped pCBMA, 3 primary chains with 15 pendant chains, and (d) Comb-shaped pCBMA, 7 primary chains with 35 pendant chains. Reproduced with

permission.¹¹⁵ Copyright © 2021 The Authors. Published by American Chemical Society. Licensed under [CC-BY-NC-ND 4.0](https://creativecommons.org/licenses/by-nc-nd/4.0/).

1.7 Conjugation *via* Grafting-to Method

There are two general methods to producing PPCs: grafting-to and grafting-from. Grafting-to is the method of conjugating preformed polymer chains onto reactive handles present on protein surfaces. Grafting-to exploits the accessibility and universal nature of its coupling chemistry. Nucleophilic amino acid residues, such as lysines, are abundant on protein surfaces and are often targets of conjugation by acylation. This is often mediated by coupling agents such as 1-Ethyl-3-(3-dimethylaminopropyl)carbodiimide (EDC)/*N*-hydroxysuccinimide (NHS) esters, phosphonium (*e.g.*, BOP, PyBOP) and uronium salts (*e.g.*, HATU, HBTU).¹²⁰ Alternatively, amines can also react directly *via* aza-Michael or imine-type chemistries.^{100,121} A drawback associated with amidation chemistry is often the incomplete functionalization and demand for a large excess of polymers relative to protein in order to promote product formation. The extent of lysine amidation is also strongly dependent on the isoelectric point (pI) of the protein,¹²² which requires optimization of the reaction conditions to balance between conjugation efficiency, stability of the protein, and/or cross-reactivity at other residues.^{122–125} Furthermore, incomplete amidation hinders elucidation of the structure-function relationship, especially when grafting density and/or conjugate size affect immunogenicity and clearance, respectively. Reactive groups on the polymer could be sterically hindered due to polymer chain size or morphology in aqueous media, diminishing their reactivity with the protein. To address this diminished reactivity, surface residues can be furnished with click-reactive handles to allow rapid and quantitative conjugation to allow for more efficient conjugation. Yao and co-workers reported aqueous-

soluble 3-acyl-4-pyranones with azide- and oligoethylene glycol- functionalities that were amenable to aza-Michael addition specifically to lysine residues, while other nucleophilic residues were unaffected.¹²⁶ Williams and coworkers reported a squaramide-mediated conjugation to 528mAB, a clinically-relevant antibody.¹²⁷ Squaric acid diesters are susceptible to stepwise amidation under neutral to alkaline pH and product formation is favourable due to aromatic effects.^{128,129} The authors performed poly(HPMA) and poly(HPMA-co-NIPAM) *via* reversible addition-fragmentation chain-transfer (RAFT) polymerization using a squaramide-functionalized chain-transfer agent (CTA). Following lysine conjugation, it was possible to obtain monofunctionalized (1:1) PPCs as the major product while using as little as a 1:1.2 ratio of antibody:polymer. Maynard and coworkers modified lysines with acid labile handles to enable traceless polymer cleavage from its protein scaffold (Figure 1.12).¹³⁰ A library of phenol linkers was mono-conjugated to lysozyme lysine *via* reductive amination, followed by PEGylation on the linker *via* copper-catalyzed azide-alkyne click cycloaddition (CuAAC). The resultant hydroxybenzylamine linkers on the PPC were susceptible to hydrolysis proceeding *via* a quinone methide intermediate, selectively liberating native lysozyme under neutral conditions with full activity retention.¹³⁰

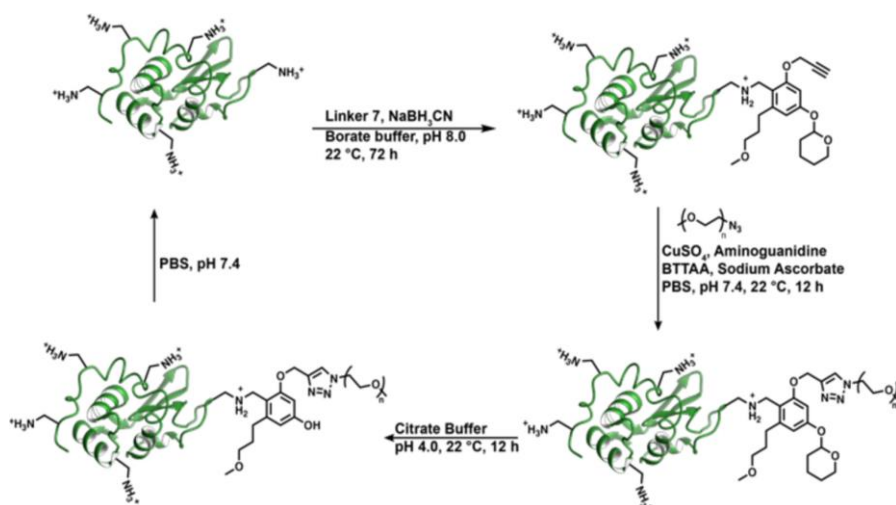


Figure 1.12. Stepwise grafting-to approach developed by Maynard and co-workers to produce a PEG-lysozyme PPC with water-labile handles. Reproduced with permission.¹³⁰ Copyright © 2022 American Chemical Society.

Grafting-to functionalization on cysteine residues has also been explored,³⁹ but the degree of functionalization is more localized due to the relative scarcity of cysteines compared to lysines. Cysteines form disulfide bridges with thiol-containing polymers and thioethers with maleimides and alkenes *via* thiol-ene click chemistry. The nitrogen on the maleimide is linked to the polymer chain typically *via* a hydroxyethyl, or as more recently reported by Konkolewicz,³⁹ amidoethyl end group which results in ester and amide bond formation, respectively. These linkages were selected for *in vivo* use based on a balance between hydrolytic stability and rapid biodegradation.³⁹

1.8 Conjugation *via* Grafting-from Method

The grafting-from approach furnishes the protein surface with small molecule initiators and the resulting construct subsequently acts as a macroinitiator for polymerization. This method has gained considerable popularity over the grafting-to method due to several

advantages.^{40,116,131,132} Grafting-from is generally less limited by steric effects imparted by competing large polymer chains for the reactive site(s), which could result in incomplete conjugation depending on the proximity of the reactive sites to each other.⁴⁰ In many cases grafting-from also benefits from more favourable reaction kinetics and thermodynamics compared to the grafting-to approach.¹³³ Purification is generally simpler compared to the grafting-to method due to the large differences in size between monomers and the PPC, which makes grafting-from mixtures more conducive to purification by size-exclusion chromatography (SEC). Conjugates made via the grafting-from method are subject to controlled radical polymerization methods such as reversible addition-fragmentation chain-transfer (RAFT) polymerization and atom transfer radical polymerization (ATRP). While a significant barrier traditionally facing ATRP and RAFT is that both require a rigorous exclusion of oxygen and highly controlled reaction conditions, several recent reports have addressed this issue.^{131,134} In 2018, Russell and Matyjaszewski first reported using ATRP for chain extension of oligo(ethylene oxide) methyl ether methacrylate (OEOMA) on a bovine serum albumin (BSA) macroinitiator.¹³⁵ In the presence of a glucose oxidase (GOx) and sacrificial glucose and sodium pyruvate, the authors were able to produce well-defined PPCs in reactions that were open to air.¹³⁵ In 2022, Matyjaszewski also reported PPC synthesis using photoinduced electron transfer-reversible addition-fragmentation chain transfer (PET-RAFT) in open air conditions using visible light as a catalyst.^{127,135} Inspired by their work, the same authors later demonstrated a dual photoredox/copper catalytic system that allowed open-air ATRP under green light irradiation, and yielded polymers with lower dispersity values when compared to PET-

RAFT.¹³⁶ Eosin Y was used as a photoinduced electron-transfer catalyst, which under irradiation is excited to a triplet state to subsequently reduce Cu(II) to Cu(I). The triplet state is reductively quenched by excess of sacrificial amine. In this manner, the authors conjugated poly oligo(ethylene glycol) methyl ether methacrylate (pOEOMA) to a BSA-iBBBr macroinitiator *via* a grafting-from method to yield a PPC with low dispersity ($D = 1.28$).¹³⁶ There have also been reports of oxygen-tolerant, UV-induced ATRP systems where the method of control included exclusion of oxygen from the headspace and by varying concentration of the monomer and/or copper catalyst; without explicitly deoxygenating the solvent, one could achieve complete consumption of the protein macroinitiator.^{116,137} Using this approach, Velonia and coworkers reported that a series of hydrophobic polymers ranging from styrene, (meth)acrylates, and acrylamides could be grown from a BSA-Br macroinitiator with quantitative consumption of the protein scaffold.¹³⁸ The same group later found that disproportionation of CuBr in the presence of a large amount of monomers and a protein initiator can graft various hydrophilic and hydrophobic polymers from proteins.¹³⁷ In 2024, Matyjaszewski and colleagues reported an aqueous, open-air photo-RAFT method to synthesize chymotrypsin PPCs using sodium pyruvate and pyruvate derivatives which were multifunctional as photoinitiators and oxygen scavengers and promoters during the growth step.¹³⁴ The authors demonstrated successful PPC synthesis using a typical CT macroinitiator and a range of monomers, including neutral (OEGMA), anionic (methacrylic acid), cationic, and zwitterionic, all with low dispersity ($D < 1.4$).¹³⁴ Pokorski and coworkers reported a grafting-from aqueous ring-opening metathesis polymerization (ROMP) with lysozyme and bacteriophage Q β as

model protein scaffolds.⁹² Lysozyme randomly amidated at lysine residues with norbornene initiators was subjected to ROMP conditions and the authors showed that polynorbornenes respectively derivatized with PEG and poly(sulfobetaine) pendants, as well as block copolymers of the two, successfully polymerized from the protein, though interestingly, oxanorbornene conversion was less successful. Lu and coworkers reported a cryo-ring-opening polymerization (cryo-ROP) of 1,2-dithiolanes directly from an EGFP bearing a cysteine near its *N*-terminus.¹³⁹ The authors proposed that polymerization is favoured at low temperatures (-30 °C) by minimizing the entropic penalty of polymer formation. The reaction is also accelerated in water by the increase in local monomer concentration as they are expelled from ice crystals. The polymerization was applicable to other model proteins and the chains were cleavable when treated with standard reducing agents to yield the original proteins retaining their native function. Similarly, Lu reported a one-step, grafting-from synthesis of PPCs with lipaic acids and their PEG-esters as the grafting polymers *via* an aggregate-induced ring-opening polymerization (AI-ROP).¹⁴⁰

Complementary to the many grafting-from living polymerization methods such as RAFT, ATRP and ROP discussed here, Buchwald and coworkers reported an unprecedented grafting-from method using catalyst-transfer polymerization (CTP) to grow polyarenes on protein macroinitiators (Figure 1.13).¹⁴¹ Buchwald reported an uncommon intersection between the biological interface (proteins) and conjugated polymers, where RNase A was amidated randomly at lysine residues with a preformed palladium oxidative addition complex to form a mixture of mono- and difunctionalized macroinitiators. Linear poly(pyridine) was then grown from the protein to yield a PPC that contained a terminal

pyridyl-Pd complex. It is interesting to note that the reaction was oxygen and water-tolerant, but self-terminating due to an unelucidated mechanism. The chain ends were also shown to be receptive to thioether formation with exogenous thiols, *i.e.*, cysteine residues of another protein.

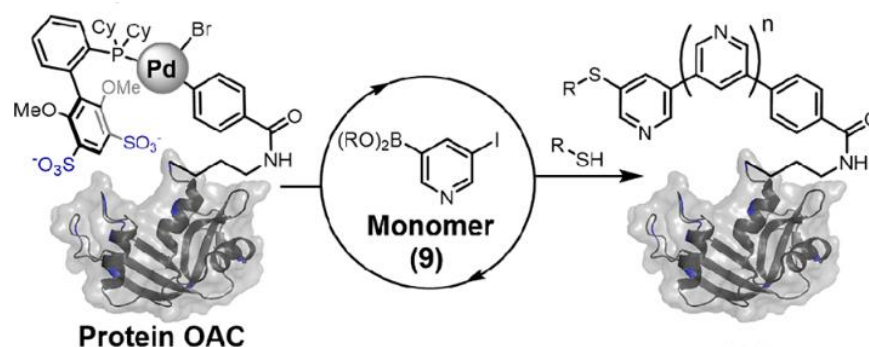


Figure 1.13. Poly(pyridine)-RNase conjugates reported by Buchwald et al. The monomers bearing boronate esters were polymerized onto an RNase macroinitiator. Reproduced with permission.¹⁴¹ Copyright © 2022, American Chemical Society

Both grafting-to and grafting-from methods are sometimes used together in the synthesis of PPCs with complex polymer architectures.⁹⁶ An interesting recent example is a PPC bearing self-immolative disulfide linkages present in the grafted polymer.^{142–144} Through a series of reports, Nuhn and co-workers showed that the trithiocarbonate end-group on RAFT-formed poly(dimethylacrylamide) (pDMA), a PEG alternative,¹⁴² underwent aminolysis in the presence of *n*-butylamine to yield the corresponding thiol-terminated pDMA (Figure 1.14).^{142–144} The thiols were then converted into disulfides by either (1) disulfide exchange with symmetrical disulfide carbonates, carbamates,¹⁴² or tosyl thiolates,¹⁴⁴ or (2) oxidative coupling with other thiol bearing desired functional group(s), such as an alcohol that was amenable to activation through CDI chemistry.¹⁴³ PPCs were

constructed in the second manner by exhaustive lysine conjugation to CDI-activated polymer chains (Figure 1.14), and both exhibited traceless release of the native proteins *in vitro* under reducing conditions (e.g., glutathione, (GSH)) by inducing a backbiting cascade to release 2-oxathiolone as the side-product.^{143,145}

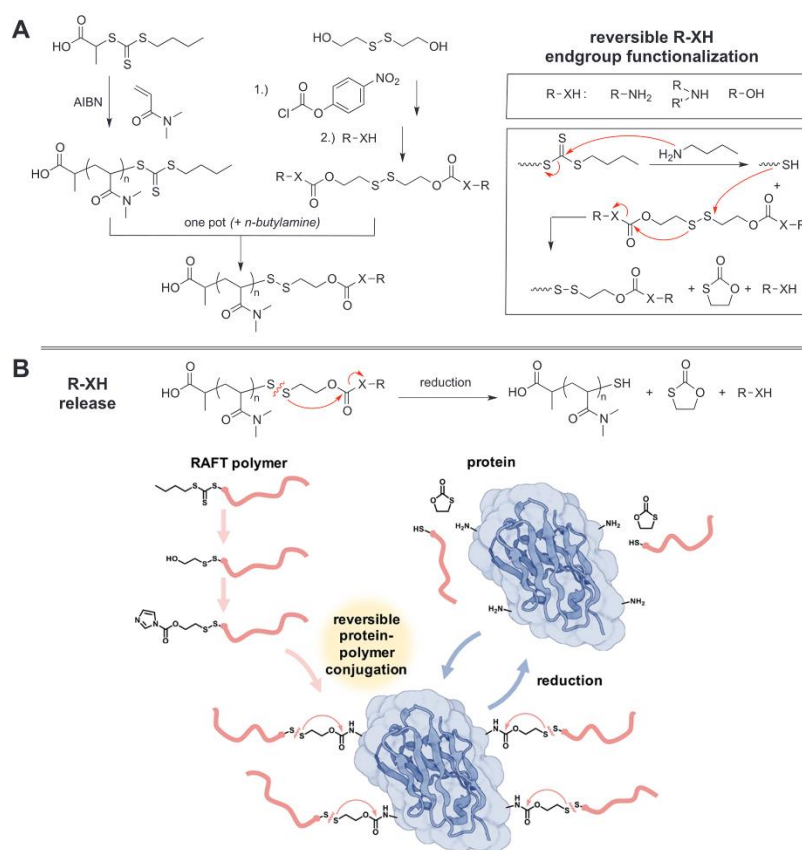


Figure 1.14. (A) Aminolysis-induced self-immolative RAFT polymers. (B) Reduction of disulfide linkages by glutathione releases the corresponding thiol-terminated polymer from the protein. Reproduced with permission.¹⁴³ Copyright © 2023 The Authors. Published by American Chemical Society. Licensed under [CC-BY 4.0](https://creativecommons.org/licenses/by/4.0/).

1.9 Scope of Thesis

The goal of this thesis is to investigate dendritic polymers – both dendrimers and dendritic-linear polymer hybrids – as a platform for introducing the molecular sieving

effect in protein conjugates. In chapter 2, G1-G5 bis-MPA dendrimers were surface-esterified with a series of neopentyl acids to afford a library of dendrons with modular surface functionalities. The neopentyl ester peripheries were fully conducive to downstream functionalization *via* different click-reactions at each dendron generation (*i.e.*, regardless of abundance of functional groups). A neopentyl dendron bearing an amine periphery was found to exhibit excellent hydrolytic and enzymatic stability compared to its linear counterpart, which, given the extensive biological utility of amine-terminated dendrons, could be useful for systems requiring prolonged dendrimer fidelity. Chapter 3 explores the convergent synthesis of a series of PEGylated bis-MPA dendrons. The terminal groups of the dendrons were furnished with neopentyl esters to provide a robust linkage between the outer dendrons and the inner core, and the latter was furnished with a dibenzocyclooctyne at the core to allow subsequent conjugation to chymotrypsin *via* the grafting-to methodology to produce the corresponding dendron-enzyme conjugates for molecular sieving. The exclusion of different sized substrates from the enzyme was evaluated using UV-VIS spectroscopy. In Chapter 4, bis-MPA dendrimers were conjugated to avidin to evaluate molecular sieving in a multivalent dendrimer-protein conjugate. G3 to G7 dendrimers were biotinylated at their core to produce a library of ligands of increasing size. The series of ligands were evaluated for their binding to G3-G7 dendrimer-avidin conjugates using isothermal titration calorimetry and UV-vis spectroscopy.

1.10 References

- (1) *Dendrimers in Nanomedicine Concept, Theory and Regulatory Perspectives*, First edition.; Mehra, N. K., Jain, K., Eds.; CRC Press: Boca Raton, 2021.
- (2) Gauro, R.; Nandave, M.; Jain, V. K.; Jain, K. Advances in Dendrimer-Mediated Targeted Drug Delivery to the Brain. *J. Nanoparticle Res.* **2021**, *23* (3), 76. <https://doi.org/10.1007/s11051-021-05175-8>.
- (3) Huang, D.; Wu, D. Biodegradable Dendrimers for Drug Delivery. *Mater. Sci. Eng. C* **2018**, *90* (March), 713–727. <https://doi.org/10.1016/j.msec.2018.03.002>.
- (4) Nikzamir, M.; Hanifehpour, Y.; Akbarzadeh, A.; Panahi, Y. Applications of Dendrimers in Nanomedicine and Drug Delivery: A Review. *J. Inorg. Organomet. Polym. Mater.* **2021**, *31* (6), 2246–2261. <https://doi.org/10.1007/s10904-021-01925-2>.
- (5) Wang, J.; Li, B.; Qiu, L.; Qiao, X.; Yang, H. Dendrimer-Based Drug Delivery Systems: History, Challenges, and Latest Developments. *J. Biol. Eng.* **2022**, *16* (1), 18. <https://doi.org/10.1186/s13036-022-00298-5>.
- (6) Zhang, J.; Liu, D.; Zhang, M.; Sun, Y.; Zhang, X.; Guan, G.; Zhao, X.; Qiao, M.; Chen, D.; Hu, H. The Cellular Uptake Mechanism, Intracellular Transportation, and Exocytosis of Polyamidoamine Dendrimers in Multidrug-Resistant Breast Cancer Cells. *Int. J. Nanomedicine* **2016**, *Volume 11*, 3677–3690. <https://doi.org/10.2147/IJN.S106418>.
- (7) Richers, M. T.; Passlick, S.; Agarwal, H.; Ellis-Davies, G. C. R. Dendrimer Conjugation Enables Multiphoton Chemical Neurophysiology Studies with an Extended π -Electron Caging Chromophore. *Angew. Chem. - Int. Ed.* **2019**, *58* (35), 12086–12090. <https://doi.org/10.1002/anie.201906067>.
- (8) Jansen, J. F. G. A.; de Brabander-van den Berg, E. M. M.; Meijer, E. W. Encapsulation of Guest Molecules into a Dendritic Box. *Science* **1994**, *266* (5188), 1226–1229. <https://doi.org/10.1126/science.266.5188.1226>.
- (9) Zhao, T.; Zhou, M.; Wu, R.; Wang, H.; Zouboulis, C. C.; Zhu, M.; Lee, M. Dendrimer-Conjugated Isotretinoin for Controlled Transdermal Drug Delivery. *J. Nanobiotechnology* **2023**, *21* (1), 285. <https://doi.org/10.1186/s12951-023-02052-5>.
- (10) Freeman, A. W.; Koene, S. C.; Malenfant, P. R. L.; Thompson, M. E.; Fréchet, J. M. J. Dendrimer-Containing Light-Emitting Diodes: Toward Site-Isolation of Chromophores. *J. Am. Chem. Soc.* **2000**, *122* (49), 12385–12386. <https://doi.org/10.1021/ja001356d>.
- (11) Abd-El-Aziz, A. S.; Abdelghani, A. A.; Wagner, B. D.; Bissessur, R. Advances in Light-Emitting Dendrimers. *Macromol. Rapid Commun.* **2019**, *40* (1), 58–61. <https://doi.org/10.1002/marc.201800711>.
- (12) Devadoss, C.; Bharathi, P.; Moore, J. S. Energy Transfer in Dendritic Macromolecules: Molecular Size Effects and the Role of an Energy Gradient. *J. Am. Chem. Soc.* **1996**, *118* (40), 9635–9644. <https://doi.org/10.1021/ja961418t>.
- (13) Aguilera, M. C.; Roitberg, A. E.; Kleiman, V. D.; Fernandez-Alberti, S.; Galindo, J. F. Unraveling Direct and Indirect Energy Transfer Pathways in a Light-Harvesting

- Dendrimer. *J. Phys. Chem. C* **2020**, *124* (41), 22383–22391.
<https://doi.org/10.1021/acs.jpcc.0c06539>.
- (14) Jiang, Y.; Lu, Y. X.; Cui, Y. X.; Zhou, Q. F.; Ma, Y.; Pei, J. Synthesis of Giant Rigid π -Conjugated Dendrimers. *Org. Lett.* **2007**, *9* (22), 4539–4542.
<https://doi.org/10.1021/ol702063e>.
- (15) Wang, J. L.; Yan, J.; Tang, Z. M.; Xiao, Q.; Ma, Y.; Pei, J. Gradient Shape-Persistent π -Conjugated Dendrimers for Light-Harvesting: Synthesis, Photophysical Properties, and Energy Funneling. *J. Am. Chem. Soc.* **2008**, *130* (30), 9952–9962. <https://doi.org/10.1021/ja803109r>.
- (16) Buhleier, E.; Wehner, W.; Vögtle, F. “Cascade”- and “Nonskid-Chain-like” Syntheses of Molecular Cavity Topologies. *Synthesis* **1978**, *1978* (02), 155–158.
<https://doi.org/10.1055/s-1978-24702>.
- (17) Tomalia, D. A.; Baker, H.; Dewald, J.; Hall, M.; Kallos, G.; Martin, S.; Roeck, J.; Ryder, J.; Smith, P. A New Class of Polymers: Starburst-Dendritic Macromolecules. *Polym. J.* **1985**, *17* (1), 117–132.
<https://doi.org/10.1295/polymj.17.117>.
- (18) Ihre, H.; Hult, A.; Fréchet, J. M. J.; Gitsov, I. Double-Stage Convergent Approach for the Synthesis of Functionalized Dendritic Aliphatic Polyesters Based on 2,2-Bis(Hydroxymethyl)Propionic Acid. *Macromolecules* **1998**, *31* (13), 4061–4068.
<https://doi.org/10.1021/ma9718762>.
- (19) Hawker, C. J.; Fréchet, J. M. J. Preparation of Polymers with Controlled Molecular Architecture. A New Convergent Approach to Dendritic Macromolecules. *J. Am. Chem. Soc.* **1990**, *112* (21), 7638–7647. <https://doi.org/10.1021/ja00177a027>.
- (20) Ihre, H.; Hult, A.; Söderlind, E. Synthesis, Characterization, and ¹H NMR Self-Diffusion Studies of Dendritic Aliphatic Polyesters Based on 2,2-Bis(Hydroxymethyl)Propionic Acid and 1,1,1-Tris(Hydroxyphenyl)Ethane. *J. Am. Chem. Soc.* **1996**, *118* (27), 6388–6395. <https://doi.org/10.1021/ja954171t>.
- (21) Hecht, S.; Fréchet, J. M. J. Dendritic Encapsulation of Function: Applying Nature’s Site Isolation Principle from Biomimetics to Materials Science. *Angew. Chem. Int. Ed.* **2001**, *40* (1), 74–91. [https://doi.org/10.1002/1521-3773\(20010105\)40:1<74::AID-ANIE74>3.0.CO;2-C](https://doi.org/10.1002/1521-3773(20010105)40:1<74::AID-ANIE74>3.0.CO;2-C).
- (22) García-Gallego, S.; Hult, D.; Olsson, J. V.; Malkoch, M. Fluoride-Promoted Esterification with Imidazolide-Activated Compounds: A Modular and Sustainable Approach to Dendrimers. *Angew. Chem. - Int. Ed.* **2015**, *54* (8), 2416–2419.
<https://doi.org/10.1002/anie.201411370>.
- (23) Malkoch, M.; Carlmark, A.; Woldegiorgis, A.; Hult, A.; Malmström, E. E. Dendronized Aliphatic Polymers by a Combination of ATRP and Divergent Growth. *Macromolecules* **2004**, *37* (2), 322–329.
<https://doi.org/10.1021/ma0347464>.
- (24) Beutner, G. L.; Young, I. S.; Davies, M. L.; Hickey, M. R.; Park, H.; Stevens, J. M.; Ye, Q. TCFH-NMI: Direct Access to N-Acyl Imidazoliums for Challenging Amide Bond Formations. *Org. Lett.* **2018**, *20* (14), 4218–4222.
<https://doi.org/10.1021/acs.orglett.8b01591>.

- (25) Luis, N. R.; Chung, K. K.; Hickey, M. R.; Lin, Z.; Beutner, G. L.; Vosburg, D. A. Beyond Amide Bond Formation: TCFH as a Reagent for Esterification. *Org. Lett.* **2024**, *26* (14), 2745–2750. <https://doi.org/10.1021/acs.orglett.3c01611>.
- (26) McNelles, S. A.; Marando, V. M.; Adronov, A. Globular Polymer Grafts Require a Critical Size for Efficient Molecular Sieving of Enzyme Substrates. *Angew. Chem. Int. Ed.* **2019**, *58* (25), 8448–8453. <https://doi.org/10.1002/anie.201902864>.
- (27) Meldal, M.; Tornøe, C. W. Cu-Catalyzed Azide–Alkyne Cycloaddition. *Chem. Rev.* **2008**, *108* (8), 2952–3015. <https://doi.org/10.1021/cr0783479>.
- (28) Tornøe, C. W.; Christensen, C.; Meldal, M. Peptidotriazoles on Solid Phase: [1,2,3]-Triazoles by Regiospecific Copper(I)-Catalyzed 1,3-Dipolar Cycloadditions of Terminal Alkynes to Azides. *J. Org. Chem.* **2002**, *67* (9), 3057–3064. <https://doi.org/10.1021/jo011148j>.
- (29) Wu, P.; Feldman, A. K.; Nugent, A. K.; Hawker, C. J.; Scheel, A.; Voit, B.; Pyun, J.; Fréchet, J. M. J.; Sharpless, K. B.; Fokin, V. V. Efficiency and Fidelity in a Click-Chemistry Route to Triazole Dendrimers by the Copper(I)-Catalyzed Ligation of Azides and Alkynes. *Angew. Chem. Int. Ed.* **2004**, *43* (30), 3928–3932. <https://doi.org/10.1002/anie.200454078>.
- (30) Wang, Q.; Chan, T. R.; Hilgraf, R.; Fokin, V. V.; Sharpless, K. B.; Finn, M. G. Bioconjugation by Copper(I)-Catalyzed Azide–Alkyne [3 + 2] Cycloaddition. *J. Am. Chem. Soc.* **2003**, *125* (11), 3192–3193. <https://doi.org/10.1021/ja021381e>.
- (31) Agard, N. J.; Prescher, J. A.; Bertozzi, C. R. A Strain-Promoted [3 + 2] Azide–Alkyne Cycloaddition for Covalent Modification of Biomolecules in Living Systems. *J. Am. Chem. Soc.* **2004**, *126* (46), 15046–15047. <https://doi.org/10.1021/ja044996f>.
- (32) Arseneault, M.; Wafer, C.; Morin, J.-F. Recent Advances in Click Chemistry Applied to Dendrimer Synthesis. *Molecules* **2015**, *20* (5), 9263–9294. <https://doi.org/10.3390/molecules20059263>.
- (33) Killops, K. L.; Campos, L. M.; Hawker, C. J. Robust, Efficient, and Orthogonal Synthesis of Dendrimers via Thiol–Ene “Click” Chemistry. *J. Am. Chem. Soc.* **2008**, *130* (15), 5062–5064. <https://doi.org/10.1021/ja8006325>.
- (34) Huang, Z.; Zhao, J.; Wang, Z.; Meng, F.; Ding, K.; Pan, X.; Zhou, N.; Li, X.; Zhang, Z.; Zhu, X. Combining Orthogonal Chain-End Deprotections and Thiol–Maleimide Michael Coupling: Engineering Discrete Oligomers by an Iterative Growth Strategy. *Angew. Chem. Int. Ed.* **2017**, *56* (44), 13612–13617. <https://doi.org/10.1002/anie.201706522>.
- (35) McNelles, S. A.; Adronov, A. Rapid Synthesis of Functionalized High-Generation Polyester Dendrimers via Strain-Promoted Alkyne–Azide Cycloaddition. *Macromolecules* **2017**, *50* (20), 7993–8001. <https://doi.org/10.1021/acs.macromol.7b01765>.
- (36) Joralemon, M. J.; O’Reilly, R. K.; Matson, J. B.; Nugent, A. K.; Hawker, C. J.; Wooley, K. L. Dendrimers Clicked Together Divergently. *Macromolecules* **2005**, *38* (13), 5436–5443. <https://doi.org/10.1021/ma050302r>.

- (37) Chatterjee, S.; V. Anslyn, E.; Bandyopadhyay, A. Boronic Acid Based Dynamic Click Chemistry: Recent Advances and Emergent Applications. *Chem. Sci.* **2021**, *12* (5), 1585–1599. <https://doi.org/10.1039/D0SC05009A>.
- (38) Ng, D. Y. W.; Arzt, M.; Wu, Y.; Kuan, S. L.; Lamla, M.; Weil, T. Constructing Hybrid Protein Zymogens through Protective Dendritic Assembly. *Angew. Chem. Int. Ed.* **2014**, *53* (1), 324–328. <https://doi.org/10.1002/anie.201308533>.
- (39) Wright, T. A.; Rahman, M. S.; Bennett, C.; Johnson, M. R.; Fischesser, H.; Ram, N.; Tyler, A.; Page, R. C.; Konkolewicz, D. Hydrolytically Stable Maleimide-End-Functionalized Polymers for Site-Specific Protein Conjugation. *Bioconjug. Chem.* **2021**, *32* (11), 2447–2456. <https://doi.org/10.1021/acs.bioconjchem.1c00487>.
- (40) Chen, C.; Ng, D. Y. W.; Weil, T. Polymer Bioconjugates: Modern Design Concepts toward Precision Hybrid Materials. *Prog. Polym. Sci.* **2020**, *105*, 101241. <https://doi.org/10.1016/j.progpolymsci.2020.101241>.
- (41) Deng, B.; Burns, E.; McNelles, S. A.; Sun, J.; Ortega, J.; Adronov, A. Molecular Sieving with PEGylated Dendron-Protein Conjugates. *Bioconjug. Chem.* **2023**, *34* (8), 1467–1476. <https://doi.org/10.1021/acs.bioconjchem.3c00237>.
- (42) Liu, B.; Ianosi-Irimie, M.; Thayumanavan, S. Reversible Click Chemistry for Ultrafast and Quantitative Formation of Protein–Polymer Nanoassembly and Intracellular Protein Delivery. *ACS Nano* **2019**, *13* (8), 9408–9420. [https://doi.org/10.1021/acsnano.9b04198](https://doi.org/10.1021/acs.nano.9b04198).
- (43) Li, S.; Chen, B.; Qu, Y.; Yan, X.; Wang, W.; Ma, X.; Wang, B.; Liu, S.; Yu, X. ROS-Response-Induced Zwitterionic Dendrimer for Gene Delivery. *Langmuir* **2019**, *35* (5), 1613–1620. <https://doi.org/10.1021/acs.langmuir.8b03758>.
- (44) McNelles, S. A.; Knight, S. D.; Janzen, N.; Valliant, J. F.; Adronov, A. Synthesis, Radiolabeling, and In Vivo Imaging of PEGylated High-Generation Polyester Dendrimers. *Biomacromolecules* **2015**, *16* (9), 3033–3041. <https://doi.org/10.1021/acs.biomac.5b00911>.
- (45) Parrott, M. C.; Rahima Benhabbour, S.; Saab, C.; Lemon, J. A.; Parker, S.; Valliant, J. F.; Adronov, A. Synthesis, Radiolabeling, and Bio-Imaging of High-Generation Polyester Dendrimers. *J. Am. Chem. Soc.* **2009**, *131* (8), 2906–2916. <https://doi.org/10.1021/ja8078175>.
- (46) Kim, J.-H.; Park, K.; Nam, H. Y.; Lee, S.; Kim, K.; Kwon, I. C. Polymers for Bioimaging. *Prog. Polym. Sci.* **2007**, *32* (8–9), 1031–1053. <https://doi.org/10.1016/j.progpolymsci.2007.05.016>.
- (47) Lee, C. C.; Gillies, E. R.; Fox, M. E.; Guillaudeu, S. J.; Fréchet, J. M. J.; Dy, E. E.; Szoka, F. C. A Single Dose of Doxorubicin-Functionalized Bow-Tie Dendrimer Cures Mice Bearing C-26 Colon Carcinomas. *Proc. Natl. Acad. Sci. U. S. A.* **2006**, *103* (45), 16649–16654. <https://doi.org/10.1073/pnas.0607705103>.
- (48) Medina, S. H.; El-Sayed, M. E. H. Dendrimers as Carriers for Delivery of Chemotherapeutic Agents. *Chem. Rev.* **2009**, *109* (7), 3141–3157. <https://doi.org/10.1021/cr900174j>.
- (49) Tian, W.; Ma, Y. Theoretical and Computational Studies of Dendrimers as Delivery Vectors. *Chem Soc Rev* **2013**, *42* (2), 705–727. <https://doi.org/10.1039/C2CS35306G>.

- (50) Gonçalves, M.; Kairys, V.; Rodrigues, J.; Tomás, H. Polyester Dendrimers Based on Bis-MPA for Doxorubicin Delivery. *Biomacromolecules* **2022**, *23* (1), 20–33. <https://doi.org/10.1021/acs.biomac.1c00455>.
- (51) Sorokina, S. A.; Shifrina, Z. B. Dendrimers as Anti-amyloid Agents. *Pharmaceutics* **2022**, *14* (4), 760. <https://doi.org/10.3390/pharmaceutics14040760>.
- (52) Menjoge, A. R.; Kannan, R. M.; Tomalia, D. A. Dendrimer-Based Drug and Imaging Conjugates: Design Considerations for Nanomedical Applications. *Drug Discov. Today* **2010**, *15* (5–6), 171–185. <https://doi.org/10.1016/j.drudis.2010.01.009>.
- (53) Ding, L.; Lyu, Z.; Tintaru, A.; Laurini, E.; Marson, D.; Louis, B.; Bouhlef, A.; Balasse, L.; Fernandez, S.; Garrigue, P.; Mas, E.; Giorgio, S.; Pricl, S.; Guillet, B.; Peng, L. A Self-Assembling Amphiphilic Dendrimer Nanotracer for SPECT Imaging. *Chem. Commun.* **2019**, *56* (2), 301–304. <https://doi.org/10.1039/C9CC07750B>.
- (54) Myung, J. H.; Gajjar, K. A.; Saric, J.; Eddington, D. T.; Hong, S. Dendrimer-Mediated Multivalent Binding for the Enhanced Capture of Tumor Cells. *Angew. Chem. Int. Ed.* **2011**, *50* (49), 11769–11772. <https://doi.org/10.1002/anie.201105508>.
- (55) Lee, J.-J.; Ford, W. T.; Moore, J. A.; Li, Y. Reactivity of Organic Anions Promoted by a Quaternary Ammonium Ion Dendrimer. *Macromolecules* **1994**, *27* (16), 4632–4634. <https://doi.org/10.1021/ma00094a033>.
- (56) Caminade, A. M.; Ouali, A.; Laurent, R.; Turrin, C. O.; Majoral, J. P. The Dendritic Effect Illustrated with Phosphorus Dendrimers. *Chem. Soc. Rev.* **2015**, *44* (12), 3890–3899. <https://doi.org/10.1039/c4cs00261j>.
- (57) Zhou, Z.; Cong, M.; Li, M.; Tintaru, A.; Li, J.; Yao, J.; Xia, Y.; Peng, L. Negative Dendritic Effect on Enzymatic Hydrolysis of Dendrimer Conjugates. *Chem. Commun.* **2018**, *54* (47), 5956–5959. <https://doi.org/10.1039/c8cc01221k>.
- (58) Qiu, L. Y.; Bae, Y. H. Polymer Architecture and Drug Delivery. *Pharm. Res.* **2006**, *23* (1), 1–30. <https://doi.org/10.1007/s11095-005-9046-2>.
- (59) Sapra, R.; Verma, R. P.; Maurya, G. P.; Dhawan, S.; Babu, J.; Haridas, V. Designer Peptide and Protein Dendrimers: A Cross-Sectional Analysis. *Chem. Rev.* **2019**, *119* (21), 11391–11441. <https://doi.org/10.1021/acs.chemrev.9b00153>.
- (60) Uvyn, A.; Vleugels, M. E. J.; De Waal, B.; Hamouda, A. E. I.; Dhiman, S.; Louage, B.; Albertazzi, L.; Laoui, D.; Meijer, E. W.; De Geest, B. G. Hapten/Myristoyl Functionalized Poly(Propyleneimine) Dendrimers as Potent Cell Surface Recruiters of Antibodies for Mediating Innate Immune Killing. *Adv. Mater.* **2023**, *35* (47), 2303909. <https://doi.org/10.1002/adma.202303909>.
- (61) Caminade, A. M. Phosphorus Dendrimers as Nanotools against Cancers. *Molecules* **2020**, *25* (15). <https://doi.org/10.3390/molecules25153333>.
- (62) Gao, Y.; Shen, M.; Shi, X. Interaction of Dendrimers with the Immune System: An Insight into Cancer Nanotheranostics. *View* **2021**, *2* (3), 20200120. <https://doi.org/10.1002/viw.20200120>.
- (63) Wang, Y.; Huang, D.; Wang, X.; Yang, F.; Shen, H.; Wu, D. Fabrication of Zwitterionic and pH-Responsive Polyacetal Dendrimers for Anticancer Drug

- Delivery. *Biomater. Sci.* **2019**, *7* (8), 3238–3248.
<https://doi.org/10.1039/c9bm00606k>.
- (64) Thiagarajan, G.; Greish, K.; Ghandehari, H. Charge Affects the Oral Toxicity of Poly(Amidoamine) Dendrimers. *Eur. J. Pharm. Biopharm.* **2013**, *84* (2), 330–334.
<https://doi.org/10.1016/j.ejpb.2013.01.019>.
- (65) Stenström, P.; Manzanares, D.; Zhang, Y.; Ceña, V.; Malkoch, M. Evaluation of Amino-Functional Polyester Dendrimers Based on Bis-MPA as Nonviral Vectors for siRNA Delivery. *Molecules* **2018**, *23* (8), 2028.
<https://doi.org/10.3390/molecules23082028>.
- (66) Wang, B.; Sun, Y.; Davis, T. P.; Ke, P. C.; Wu, Y.; Ding, F. Understanding Effects of PAMAM Dendrimer Size and Surface Chemistry on Serum Protein Binding with Discrete Molecular Dynamics Simulations. *ACS Sustain. Chem. Eng.* **2018**, *6* (9), 11704–11715. <https://doi.org/10.1021/acssuschemeng.8b01959>.
- (67) Taratula, O.; Garbuzenko, O. B.; Kirkpatrick, P.; Pandya, I.; Savla, R.; Pozharov, V. P.; He, H.; Minko, T. Surface-Engineered Targeted PPI Dendrimer for Efficient Intracellular and Intratumoral siRNA Delivery. *J. Controlled Release* **2009**, *140* (3), 284–293. <https://doi.org/10.1016/j.jconrel.2009.06.019>.
- (68) Chen, A.; Karanastasis, A.; Casey, K. R.; Necelis, M.; Carone, B. R.; Caputo, G. A.; Palermo, E. F. Cationic Molecular Umbrellas as Antibacterial Agents with Remarkable Cell-Type Selectivity. *ACS Appl. Mater. Interfaces* **2020**, *12* (19), 21270–21282. <https://doi.org/10.1021/acsaami.9b19076>.
- (69) Petit, A.-N.; Debenest, T.; Eullaffroy, P.; Gagné, F. Effects of a Cationic PAMAM Dendrimer on Photosynthesis and ROS Production of *Chlamydomonas Reinhardtii*. *Nanotoxicology* **2012**, *6* (3), 315–326.
<https://doi.org/10.3109/17435390.2011.579628>.
- (70) Stenström, P.; Hjorth, E.; Zhang, Y.; Andrén, O. C. J.; Guette-Marquet, S.; Schultzberg, M.; Malkoch, M. Synthesis and in Vitro Evaluation of Monodisperse Amino-Functional Polyester Dendrimers with Rapid Degradability and Antibacterial Properties. *Biomacromolecules* **2017**, *18* (12), 4323–4330.
<https://doi.org/10.1021/acs.biomac.7b01364>.
- (71) Aurelia Chis, A.; Dobrea, C.; Morgovan, C.; Arseniu, A. M.; Rus, L. L.; Butuca, A.; Juncan, A. M.; Totan, M.; Vonica-Tincu, A. L.; Cormos, G.; Muntean, A. C.; Muresan, M. L.; Gligor, F. G.; Frum, A. Applications and Limitations of Dendrimers in Biomedicine. *Molecules* **2020**, *25* (17).
<https://doi.org/10.3390/molecules25173982>.
- (72) Agashe, H. B.; Dutta, T.; Garg, M.; Jain, N. K. Investigations on the Toxicological Profile of Functionalized Fifth-Generation Poly(Propylene Imine) Dendrimer. *J. Pharm. Pharmacol.* **2006**, *58* (11), 1491–1498.
<https://doi.org/10.1211/jpp.58.11.0010>.
- (73) Janaszewska, A.; Lazniewska, J.; Trzepiński, P.; Marcinkowska, M.; Klajnert-Maculewicz, B. Cytotoxicity of Dendrimers. *Biomolecules* **2019**, *9* (8), 330.
<https://doi.org/10.3390/biom9080330>.
- (74) Ozer, I.; Tomak, A.; Zareie, H. M.; Baran, Y.; Bulmus, V. Effect of Molecular Architecture on Cell Interactions and Stealth Properties of PEG.

- Biomacromolecules* **2017**, *18* (9), 2699–2710.
<https://doi.org/10.1021/acs.biomac.7b00443>.
- (75) Douglas-Green, S. A.; Aleman, J. A.; Hammond, P. T. Electrophoresis-Based Approach for Characterizing Dendrimer–Protein Interactions: A Proof-of-Concept Study. *ACS Biomater. Sci. Eng.* **2024**, *10* (6), 3747–3758.
<https://doi.org/10.1021/acsbiomaterials.3c01579>.
- (76) Twibanire, J. D. amour K.; Grindley, T. B. Polyester Dendrimers. *Polymers* **2012**, *4* (1), 794–879. <https://doi.org/10.3390/polym4010794>.
- (77) Feliu, N.; Walter, M. V.; Montañez, M. I.; Kunzmann, A.; Hult, A.; Nyström, A.; Malkoch, M.; Fadeel, B. Stability and Biocompatibility of a Library of Polyester Dendrimers in Comparison to Polyamidoamine Dendrimers. *Biomaterials* **2012**, *33* (7), 1970–1981. <https://doi.org/10.1016/j.biomaterials.2011.11.054>.
- (78) Yasir, M.; Tripathi, A. S.; Shukla, P.; Maurya, R. K. Immunogenicity of Therapeutic Proteins. In *Protein-based Therapeutics*; Singh, D. B., Tripathi, T., Eds.; Springer Nature: Singapore, 2023; pp 251–273. https://doi.org/10.1007/978-981-19-8249-1_9.
- (79) Arends, M.; Biegstraaten, M.; Hughes, D. A.; Mehta, A.; Elliott, P. M.; Oder, D.; Watkinson, O. T.; Vaz, F. M.; Van Kuilenburg, A. B. P.; Wanner, C.; Hollak, C. E. M. Retrospective Study of Long-Term Outcomes of Enzyme Replacement Therapy in Fabry Disease: Analysis of Prognostic Factors. *PLoS ONE* **2017**, *12* (8), e0182379. <https://doi.org/10.1371/journal.pone.0182379>.
- (80) Zaghmi, A.; Greschner, A. A.; Gauthier, M. A. In Vivo Properties of Therapeutic Bioconjugates Composed of Proteins and Architecturally/Functionally Complex Polymers. In *Polymer-Protein Conjugates*; Elsevier, 2020; pp 389–406.
<https://doi.org/10.1016/B978-0-444-64081-9.00017-6>.
- (81) Panganiban, B.; Qiao, B.; Jiang, T.; DelRe, C.; Obadia, M. M.; Nguyen, T. D.; Smith, A. A. A.; Hall, A.; Sit, I.; Crosby, M. G.; Dennis, P. B.; Drockenmuller, E.; Olvera de la Cruz, M.; Xu, T. Random Heteropolymers Preserve Protein Function in Foreign Environments. *Science* **2018**, *359* (6381), 1239–1243.
<https://doi.org/10.1126/science.aao0335>.
- (82) Li, M.; Jiang, S.; Simon, J.; Paßlick, D.; Frey, M. L.; Wagner, M.; Mailander, V.; Crespy, D.; Landfester, K. Brush Conformation of Polyethylene Glycol Determines the Stealth Effect of Nanocarriers in the Low Protein Adsorption Regime. *Nano Lett.* **2021**, *21* (4), 1591–1598. <https://doi.org/10.1021/acs.nanolett.0c03756>.
- (83) Abuchowski, A.; van Es, T.; Palczuk, N. C.; Davis, F. F. Alteration of Immunological Properties of Bovine Serum Albumin by Covalent Attachment of Polyethylene Glycol. *J. Biol. Chem.* **1977**, *252* (11), 3578–3581.
[https://doi.org/10.1016/S0021-9258\(17\)40291-2](https://doi.org/10.1016/S0021-9258(17)40291-2).
- (84) Zeng, Z.; Chen, S.; Chen, Y. Zwitterionic Polymer: A New Paradigm for Protein Conjugation beyond PEG. *ChemMedChem* **2023**, *18* (20), e202300245.
<https://doi.org/10.1002/cmdc.202300245>.
- (85) Pelegri-Oday, E. M.; Lin, E. W.; Maynard, H. D. Therapeutic Protein-Polymer Conjugates: Advancing beyond Pegylation. *J. Am. Chem. Soc.* **2014**, *136* (41), 14323–14332. <https://doi.org/10.1021/ja504390x>.

- (86) Li, B.; Yuan, Z.; Hung, H.-C.; Ma, J.; Jain, P.; Tsao, C.; Xie, J.; Zhang, P.; Lin, X.; Wu, K.; Jiang, S. Revealing the Immunogenic Risk of Polymers. *Angew. Chem.* **2018**, *130* (42), 14069–14072. <https://doi.org/10.1002/ange.201808615>.
- (87) Davis, E.; Caparco, A. A.; Steinmetz, N. F.; Pokorski, J. K. Poly(Oxanorbornene)-Protein Conjugates Prepared by Grafting-to ROMP as Alternatives for PEG. *Macromol. Biosci.* **2024**, *24* (2), 2300255. <https://doi.org/10.1002/mabi.202300255>.
- (88) da Silva Freitas, D.; Spencer, P. J.; Vassão, R. C.; Abrahão-Neto, J. Biochemical and Biopharmaceutical Properties of PEGylated Uricase. *Int. J. Pharm.* **2010**, *387* (1), 215–222. <https://doi.org/10.1016/j.ijpharm.2009.11.034>.
- (89) Zaghmi, A.; Mendez-Villuendas, E.; Greschner, A. A.; Liu, J. Y.; Haan, H. W. de; Gauthier, M. A. Mechanisms of Activity Loss for a Multi-PEGylated Protein by Experiment and Simulation. *Mater. Today Chem.* **2019**, *12*, 121–131. <https://doi.org/10.1016/j.mtchem.2018.12.007>.
- (90) Ke, S.; Wright, J. C.; Kwon, G. S. Intermolecular Interaction of Avidin and PEGylated Biotin. *Bioconjug. Chem.* **2007**, *18* (6), 2109–2114. <https://doi.org/10.1021/bc700204k>.
- (91) Plesner, B.; Fee, C. J.; Westh, P.; Nielsen, A. D. Effects of PEG Size on Structure, Function and Stability of PEGylated BSA. *Eur. J. Pharm. Biopharm.* **2011**, *79* (2), 399–405. <https://doi.org/10.1016/j.ejpb.2011.05.003>.
- (92) Church, D. C.; Davis, E.; Caparco, A. A.; Takiguchi, L.; Chung, Y. H.; Steinmetz, N. F.; Pokorski, J. K. Polynorbornene-Based Bioconjugates by Aqueous Grafting-from Ring-Opening Metathesis Polymerization Reduce Protein Immunogenicity. *Cell Rep. Phys. Sci.* **2022**, *3* (10), 101067. <https://doi.org/10.1016/j.xcrp.2022.101067>.
- (93) Keefe, A. J.; Jiang, S. Poly(Zwitterionic)Protein Conjugates Offer Increased Stability without Sacrificing Binding Affinity or Bioactivity. *Nat. Chem.* **2012**, *4* (1), 59–63. <https://doi.org/10.1038/nchem.1213>.
- (94) Yuan, Z.; Li, B.; Niu, L.; Tang, C.; McMullen, P.; Jain, P.; He, Y.; Jiang, S. Zwitterionic Peptide Cloak Mimics Protein Surfaces for Protein Protection. *Angew. Chem. Int. Ed.* **2020**, *59* (50), 22378–22381. <https://doi.org/10.1002/anie.202004995>.
- (95) McMullen, P.; Luozhong, S.; Tsao, C.; Xu, H.; Fang, L.; Jiang, S. A Low-Immunogenic Genetically-Fusible Zwitterionic Polypeptide. *Nano Today* **2022**, *47*, 101674. <https://doi.org/10.1016/j.nantod.2022.101674>.
- (96) Saha, B.; Lee, J. H.; Kwon, I.; Chung, H. Site-Specific Conjugation of Bottlebrush Polymers to Therapeutic Protein via Bioorthogonal Chemistry. *Biomacromolecules* **2024**, *25* (5), 3200–3211. <https://doi.org/10.1021/acs.biomac.4c00359>.
- (97) Liu, M.; Tirino, P.; Radivojevic, M.; Phillips, D. J.; Gibson, M. I.; Leroux, J.-C.; Gauthier, M. A. Molecular Sieving on the Surface of a Protein Provides Protection Without Loss of Activity. *Adv. Funct. Mater.* **2013**, *23* (16), 2007–2015. <https://doi.org/10.1002/adfm.201202227>.
- (98) Ediriweera, G. R.; Chang, Y.; Wang, Q.; Gong, Y.; Akhter, D. T.; Pang, H.; Han, F. Y.; Chen, C.; Whittaker, A. K.; Fu, C. Stimuli-Responsive Sulfoxide Polymer–

- Protein Conjugates with Improved Pharmacokinetics and Tumor Delivery. *Chem. Mater.* **2023**, *35* (17), 7252–7265. <https://doi.org/10.1021/acs.chemmater.3c01566>.
- (99) Leitner, N. S.; Schroffenegger, M.; Reimhult, E. Polymer Brush-Grafted Nanoparticles Preferentially Interact with Opsonins and Albumin. *ACS Appl. Bio Mater.* **2021**, *4* (1), 795–806. <https://doi.org/10.1021/acsabm.0c01355>.
- (100) Sun, J.; Liu, X.; Guo, J.; Zhao, W.; Gao, W. Pyridine-2,6-Dicarboxaldehyde-Enabled N-Terminal In Situ Growth of Polymer–Interferon α Conjugates with Significantly Improved Pharmacokinetics and In Vivo Bioactivity. *ACS Appl. Mater. Interfaces* **2021**, *13* (1), 88–96. <https://doi.org/10.1021/acsami.0c15786>.
- (101) d’Arcy, R.; El Mohtadi, F.; Francini, N.; DeJulius, C. R.; Back, H.; Gennari, A.; Geven, M.; Lopez-Cavestany, M.; Turhan, Z. Y.; Yu, F.; Lee, J. B.; King, M. R.; Kagan, L.; Duvall, C. L.; Tirelli, N. A Reactive Oxygen Species-Scavenging ‘Stealth’ Polymer, Poly(Thioglycidyl Glycerol), Outperforms Poly(Ethylene Glycol) in Protein Conjugates and Nanocarriers and Enhances Protein Stability to Environmental and Biological Stressors. *J. Am. Chem. Soc.* **2022**, *144* (46), 21304–21317. <https://doi.org/10.1021/jacs.2c09232>.
- (102) Hu, Y.; Wang, D.; Wang, H.; Zhao, R.; Wang, Y.; Shi, Y.; Zhu, J.; Xie, Y.; Song, Y.-Q.; Lu, H. An Urchin-like Helical Polypeptide-Asparaginase Conjugate with Mitigated Immunogenicity. *Biomaterials* **2021**, *268*, 120606. <https://doi.org/10.1016/j.biomaterials.2020.120606>.
- (103) Kotzia, G. A.; Lappa, K.; Labrou, N. E. Tailoring Structure–Function Properties of L-Asparaginase: Engineering Resistance to Trypsin Cleavage. *Biochem. J.* **2007**, *404* (Pt 2), 337–343. <https://doi.org/10.1042/BJ20061708>.
- (104) Meneguetti, G. P.; Santos, J. H. P. M.; Obreque, K. M. T.; Barbosa, C. M. V.; Monteiro, G.; Farsky, S. H. P.; Marim de Oliveira, A.; Angeli, C. B.; Palmisano, G.; Ventura, S. P. M.; Pessoa-Junior, A.; de Oliveira Rangel-Yagui, C. Novel Site-Specific PEGylated L-Asparaginase. *PLoS ONE* **2019**, *14* (2), e0211951. <https://doi.org/10.1371/journal.pone.0211951>.
- (105) Mi, L.; Jiang, S. Integrated Antimicrobial and Nonfouling Zwitterionic Polymers. *Angew. Chem. - Int. Ed.* **2014**, *53* (7), 1746–1754. <https://doi.org/10.1002/anie.201304060>.
- (106) Paschke, S.; Lienkamp, K. Polyzwitterions: From Surface Properties and Bioactivity Profiles to Biomedical Applications. *ACS Appl. Polym. Mater.* **2020**, *2* (2), 129–151. <https://doi.org/10.1021/acsapm.9b00897>.
- (107) Zhang, P.; Jain, P.; Tsao, C.; Yuan, Z.; Li, W.; Li, B.; Wu, K.; Hung, H.-C.; Lin, X.; Jiang, S. Polypeptides with High Zwitterion Density for Safe and Effective Therapeutics. *Angew. Chem.* **2018**, *130* (26), 7869–7873. <https://doi.org/10.1002/ange.201802452>.
- (108) Kaupbayeva, B.; Russell, A. J. Polymer-Enhanced Biomacromolecules. *Prog. Polym. Sci.* **2020**, *101*, 101194. <https://doi.org/10.1016/j.progpolymsci.2019.101194>.
- (109) Kaupbayeva, B.; Murata, H.; Lucas, A.; Matyjaszewski, K.; Minden, J. S.; Russell, A. J. Molecular Sieving on the Surface of a Nano-Armored Protein.

- Biomacromolecules* **2019**, *20* (3), 1235–1245.
<https://doi.org/10.1021/acs.biomac.8b01651>.
- (110) Liu, M.; Johansen, P.; Zabel, F.; Leroux, J. C.; Gauthier, M. A. Semi-Permeable Coatings Fabricated from Comb-Polymers Efficiently Protect Proteins in Vivo. *Nat. Commun.* **2014**, *5* (May), 1–8. <https://doi.org/10.1038/ncomms6526>.
- (111) Drossis, N.; Gauthier, M. A.; Haan, H. W. de. Elucidating the Mechanisms of the Molecular Sieving Phenomenon Created by Comb-Shaped Polymers Grafted to a Protein – a Simulation Study. *Mater. Today Chem.* **2022**, *24*, 100861. <https://doi.org/10.1016/j.mtchem.2022.100861>.
- (112) Pritzlaff, A.; Ferré, G.; Dargassies, E.; Williams, C. O.; Gonzalez, D. D.; Eddy, M. T. Conserved Protein–Polymer Interactions across Structurally Diverse Polymers Underlie Alterations to Protein Thermal Unfolding. *ACS Cent. Sci.* **2023**, *9* (4), 685–695. <https://doi.org/10.1021/acscentsci.2c01522>.
- (113) Heredero, M.; Beloqui, A. Enzyme-Polymer Conjugates for Tuning, Enhancing, and Expanding Biocatalytic Activity. *ChemBioChem* **2023**, *24* (4), e202200611. <https://doi.org/10.1002/cbic.202200611>.
- (114) Beloqui, A.; Kobitski, A. Y.; Nienhaus, G. U.; Delaittre, G. A Simple Route to Highly Active Single-Enzyme Nanogels. *Chem. Sci.* **2018**, *9* (4), 1006–1013. <https://doi.org/10.1039/C7SC04438K>.
- (115) Kaupbayeva, B.; Boye, S.; Munasinghe, A.; Murata, H.; Matyjaszewski, K.; Lederer, A.; Colina, C. M.; Russell, A. J. Molecular Dynamics-Guided Design of a Functional Protein–ATRP Conjugate That Eliminates Protein–Protein Interactions. *Bioconjug. Chem.* **2021**. <https://doi.org/10.1021/acs.bioconjchem.1c00098>.
- (116) Velonia, K.; Voutyritsa, E.; Gryparis, C.; Theodorou, A. Synthesis of Multifunctional Protein-Polymer Conjugates via Oxygen-Tolerant, Aqueous Copper-Mediated Polymerization, and Bioorthogonal Click Chemistry. *Macromol. Rapid Commun.* **2023**. <https://doi.org/10.1002/marc.202200976>.
- (117) Luan, Y.; Li, D.; Wei, T.; Wang, M.; Tang, Z.; Brash, J. L.; Chen, H. “Hearing Loss” in QCM Measurement of Protein Adsorption to Protein Resistant Polymer Brush Layers. *Anal. Chem.* **2017**, *89* (7), 4184–4191. <https://doi.org/10.1021/acs.analchem.7b00198>.
- (118) Kapil, K.; Murata, H.; Szczepaniak, G.; Russell, A. J.; Matyjaszewski, K. Tailored Branched Polymer–Protein Bioconjugates for Tunable Sieving Performance. *ACS Macro Lett.* **2024**, *13* (4), 461–467. <https://doi.org/10.1021/acsmacrolett.4c00059>.
- (119) Wilson, A. L.; Kaupbayeva, B.; Murata, H.; Cummings, C.; Russell, A. J.; Minden, J. S. Utilization of the Polymer Sieving Effect for the Removal of the Small Molecule Biotin-CDM. *ACS Appl. Polym. Mater.* **2019**, *1* (11), 2897–2906. <https://doi.org/10.1021/acsapm.9b00611>.
- (120) Twibanire, J. K.; Grindley, T. B. Efficient and Controllably Selective Preparation of Esters Using Uronium-Based Coupling Agents. *Org. Lett.* **2011**, *13* (12), 2988–2991. <https://doi.org/10.1021/ol201005s>.
- (121) MacDonald, J. I.; Munch, H. K.; Moore, T.; Francis, M. B. One-Step Site-Specific Modification of Native Proteins with 2-Pyridinecarboxyaldehydes. *Nat. Chem. Biol.* **2015**, *11* (5), 326–331. <https://doi.org/10.1038/nchembio.1792>.

- (122) Vashist, S. K. Comparison of 1-Ethyl-3-(3-Dimethylaminopropyl) Carbodiimide Based Strategies to Crosslink Antibodies on Amine-Functionalized Platforms for Immunodiagnostic Applications. *Diagnostics* **2012**, *2* (3), 23–33. <https://doi.org/10.3390/diagnostics2030023>.
- (123) Wang, C.; Yan, Q.; Liu, H.-B.; Zhou, X.-H.; Xiao, S.-J. Different EDC/NHS Activation Mechanisms between PAA and PMAA Brushes and the Following Amidation Reactions. *Langmuir* **2011**, *27* (19), 12058–12068. <https://doi.org/10.1021/la202267p>.
- (124) Zhang, X.; Duan, F.; Zhang, F.; Deng, X.; Gao, W. Thermosensitive Polymer Conjugated Prodrug-Activating Enzyme with Enhanced Tumor Retention and Antitumor Efficacy. *Biomacromolecules* **2022**, *23* (11), 4834–4840. <https://doi.org/10.1021/acs.biomac.2c01006>.
- (125) Acosta-Guzmán, P.; Ojeda-Porras, A.; Gamba-Sánchez, D. Contemporary Approaches for Amide Bond Formation. *Adv. Synth. Catal.* **2023**, *365* (24), 4359–4391. <https://doi.org/10.1002/adsc.202301018>.
- (126) Nong, K.; Zhao, Y.-L.; Yi, S.; Zhang, X.; Wei, S.; Yao, Z.-J. 3-Acyl-4-Pyranone as a Lysine Residue-Selective Bioconjugation Reagent for Peptide and Protein Modification. *Bioconjug. Chem.* **2024**, *35* (3), 286–299. <https://doi.org/10.1021/acs.bioconjchem.3c00447>.
- (127) Ardana, A.; Ghosh, S.; Huda, P.; Fletcher, N. L.; Thurecht, K. J.; Williams, C. C. RAFT Polymer–Antibody Conjugation: Squaramide Ester Chemistry Leads to Conjugates with a Therapeutic Anti-EGFR Antibody with Full Retention of Activity and Increased Tumor Uptake In Vivo. *Mol. Pharm.* **2023**, *20* (6), 3073–3087. <https://doi.org/10.1021/acs.molpharmaceut.3c00085>.
- (128) Prohens, R.; Portell, A.; Font-Bardia, M.; Bauzá, A.; Frontera, A. Experimental and Theoretical Study of Aromaticity Effects in the Solid State Architecture on Squaric Acid Derivatives. *Cryst. Growth Des.* **2014**, *14* (5), 2578–2587. <https://doi.org/10.1021/cg500264k>.
- (129) Grus, T.; Lahnif, H.; Klasen, B.; Moon, E.-S.; Greifenstein, L.; Roesch, F. Squaric Acid-Based Radiopharmaceuticals for Tumor Imaging and Therapy. *Bioconjug. Chem.* **2021**, *32* (7), 1223–1231. <https://doi.org/10.1021/acs.bioconjchem.1c00305>.
- (130) Rose, D. A.; Treacy, J. W.; Yang, Z. J.; Ko, J. H.; Houk, K. N.; Maynard, H. D. Self-Immolative Hydroxybenzylamine Linkers for Traceless Protein Modification. *J. Am. Chem. Soc.* **2022**, *144* (13), 6050–6058. <https://doi.org/10.1021/jacs.2c01136>.
- (131) Lee, Y.; Boyer, C.; Sang Kwon, M. Photocontrolled RAFT Polymerization: Past, Present, and Future. *Chem. Soc. Rev.* **2023**, *52* (9), 3035–3097. <https://doi.org/10.1039/D1CS00069A>.
- (132) Miura, Y. Controlled Polymerization for the Development of Bioconjugate Polymers and Materials. *J. Mater. Chem. B* **2020**, *8* (10), 2010–2019. <https://doi.org/10.1039/C9TB02418B>.
- (133) Averick, S.; Simakova, A.; Park, S.; Konkolewicz, D.; Magenau, A. J. D.; Mehl, R. A.; Matyjaszewski, K. ATRP under Biologically Relevant Conditions: Grafting

- from a Protein. *ACS Macro Lett.* **2012**, *1* (1), 6–10.
<https://doi.org/10.1021/mz200020c>.
- (134) Jazani, A. M.; Murata, H.; Cvek, M.; Lewandowska-Andralojc, A.; Bernat, R.; Kapil, K.; Hu, X.; Bossa, F. D. L.; Szczepaniak, G.; Matyjaszewski, K. Aqueous Photo-RAFT Polymerization under Ambient Conditions: Synthesis of Protein–Polymer Hybrids in Open Air. *Chem. Sci.* **2024**.
<https://doi.org/10.1039/D4SC01409J>.
- (135) Enciso, A. E.; Fu, L.; Russell, A. J.; Matyjaszewski, K. A Breathing Atom-Transfer Radical Polymerization: Fully Oxygen-Tolerant Polymerization Inspired by Aerobic Respiration of Cells. *Angew. Chem. Int. Ed Engl.* **2018**, *57* (4), 933–936.
<https://doi.org/10.1002/anie.201711105>.
- (136) Szczepaniak, G.; Jeong, J.; Kapil, K.; Dadashi-Silab, S.; Yerneni, S. S.; Ratajczyk, P.; Lathwal, S.; Schild, D. J.; Das, S. R.; Matyjaszewski, K. Open-Air Green-Light-Driven ATRP Enabled by Dual Photoredox/Copper Catalysis. *Chem. Sci.* **2022**, *13* (39), 11540–11550. <https://doi.org/10.1039/D2SC04210J>.
- (137) Theodorou, A.; Gounaris, D.; Voutyritsa, E.; Andrikopoulos, N.; Baltzaki, C. I. M.; Anastasaki, A.; Velonia, K. Rapid Oxygen-Tolerant Synthesis of Protein-Polymer Bioconjugates via Aqueous Copper-Mediated Polymerization. *Biomacromolecules* **2022**, *23* (10), 4241–4253. <https://doi.org/10.1021/acs.biomac.2c00726>.
- (138) Theodorou, A.; Mandriotis, P.; Anastasaki, A.; Velonia, K. Oxygen Tolerant, Photoinduced Controlled Radical Polymerization Approach for the Synthesis of Giant Amphiphiles. *Polym. Chem.* **2021**, *12* (15), 2228–2235.
<https://doi.org/10.1039/D0PY01608J>.
- (139) Lu, J.; Wang, H.; Tian, Z.; Hou, Y.; Lu, H. Cryopolymerization of 1,2-Dithiolanes for the Facile and Reversible Grafting-from Synthesis of Protein–Polydisulfide Conjugates. *J. Am. Chem. Soc.* **2020**, *142* (3), 1217–1221.
<https://doi.org/10.1021/jacs.9b12937>.
- (140) Lu, J.; Xu, Z.; Fu, H.; Lin, Y.; Wang, H.; Lu, H. Room-Temperature Grafting from Synthesis of Protein–Polydisulfide Conjugates via Aggregation-Induced Polymerization. *J. Am. Chem. Soc.* **2022**, *144* (34), 15709–15717.
<https://doi.org/10.1021/jacs.2c05997>.
- (141) Rodriguez, J.; Dhanjee, H. H.; Pentelute, B. L.; Buchwald, S. L. Palladium Mediated Synthesis of Protein–Polyarene Conjugates. *J. Am. Chem. Soc.* **2022**, *144* (26), 11706–11712. <https://doi.org/10.1021/jacs.2c03492>.
- (142) Scherger, M.; Räder, H. J.; Nuhn, L. Self-Immolative RAFT-Polymer End Group Modification. *Macromol. Rapid Commun.* **2021**, *42* (8), 2000752.
<https://doi.org/10.1002/marc.202000752>.
- (143) Scherger, M.; Pilger, Y. A.; Komforth, P.; Räder, H.-J.; Nuhn, L. Reversible Polymer–Protein Functionalization by Stepwise Introduction of Amine-Reactive, Reductive-Responsive Self-Immolative End Groups onto RAFT-Derived Polymers. *ACS Biomater. Sci. Eng.* **2024**, *10* (1), 129–138.
<https://doi.org/10.1021/acsbiomaterials.2c01106>.
- (144) Scherger, M.; Pilger, Y. A.; Stickdorn, J.; Komforth, P.; Schmitt, S.; Koynov, K.; Räder, H. J.; Nuhn, L. Efficient Self-Immolative RAFT End Group Modification

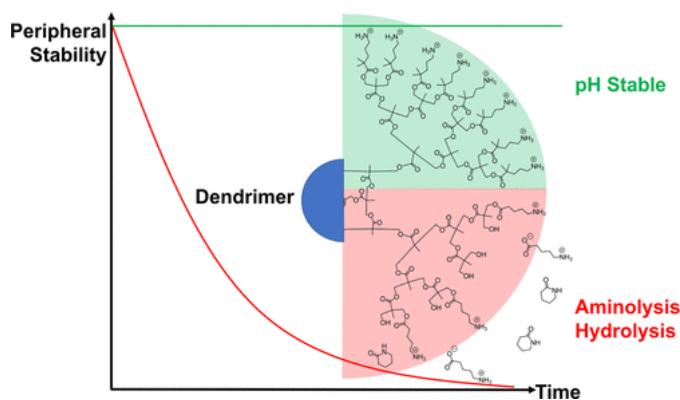
- for Macromolecular Immunodrug Delivery. *Biomacromolecules* **2023**, *24* (5), 2380–2391. <https://doi.org/10.1021/acs.biomac.3c00239>.
- (145) Scherger, M.; Pilger, Y. A.; Stickdorn, J.; Komforth, P.; Schmitt, S.; Arnouk, S. M.; Lebegge, E.; Koynov, K.; Räder, H.-J.; Van Ginderachter, J. A.; Nuhn, L. Self-Immolative Nanobody-Cysteine Residue Modification for Controlled Immunodrug Delivery. *Adv. Ther.* **2023**, *6* (11), 2300076. <https://doi.org/10.1002/adtp.202300076>.

Chapter 2. Neopentyl Dendrimers as Robust Linkers for Introducing Functionality to Bis-MPA Dendrimers

This chapter has been reproduced with permission from Deng, B.; McNelles, S. A.; Da-Ré, G.; Marando, V. M.; Ros, S.; Stöver, H. D. H.; Adronov, A. *Macromolecules* **2022**, *55* (1), 270–275. Copyright 2022, American Chemical Society.

This work detailed in this chapter was carried out in collaboration with Stuart McNelles, Giancarlo Da-Ré, Victoria Marando, and Samantha Ros. Billy Deng, Stuart McNelles, Giancarlo Da-Ré, and Victoria Marando synthesized and characterized the small molecules and polymers. Billy Deng and Samantha Ros performed and analyzed the quantitative NMR.

Graphical Abstract:



2.1 Abstract

A series of neopentyl carboxylic acids bearing functionality amenable to click chemistry were pre-pared, then appended to high generation bis-MPA dendrons via fluoride promoted esterification. The nucleophilic stability of the neopentyl and non-neopentyl

dendrons in acidic to basic phosphate buffers was compared by monitoring degradation via quantitative ^1H NMR. The neopentyl periphery dendrons were found to be highly resistant to hydrolysis under all experimental conditions. The neopentyl groups also did not impede click functionalization onto the dendrons.

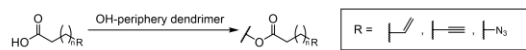
2.2 Introduction

Polymeric materials have been extensively used for a variety of biomedical applications, such as drug delivery,¹⁻⁷ gene delivery,⁸⁻¹⁰ and bioimaging.¹¹⁻¹⁴ While these polymeric systems exhibit desirable properties that cannot be found in small molecule systems, their performance¹⁵ and utility (especially *in vivo*) are generally limited by their dispersity. The use of dendrimers rather than traditional disperse polymers overcomes this issue, as they can be prepared with precise architectures,^{11,16-20} uniform size, and well-defined core and peripheral functionalization.^{19,21,22} While several dendrimer architectures have been used for biomedical applications such as poly(amidoamine) (PAMAM)¹⁸ and poly(propyleneimine) (PPI),²³ these are both limited by their intrinsic cytotoxicity stemming from the highly cationic periphery they exhibit at physiological pH.^{23,24} In contrast, polyester dendrimers based upon the poly(bis-2,2-(hydroxymethylpropionic acid)) (bis-MPA) scaffold have been shown to exhibit low cytotoxicity^{17,25} and are biodegradable,²⁵⁻²⁷ which alleviates the concerns of nanoparticle accumulation in tissues.^{6,22}

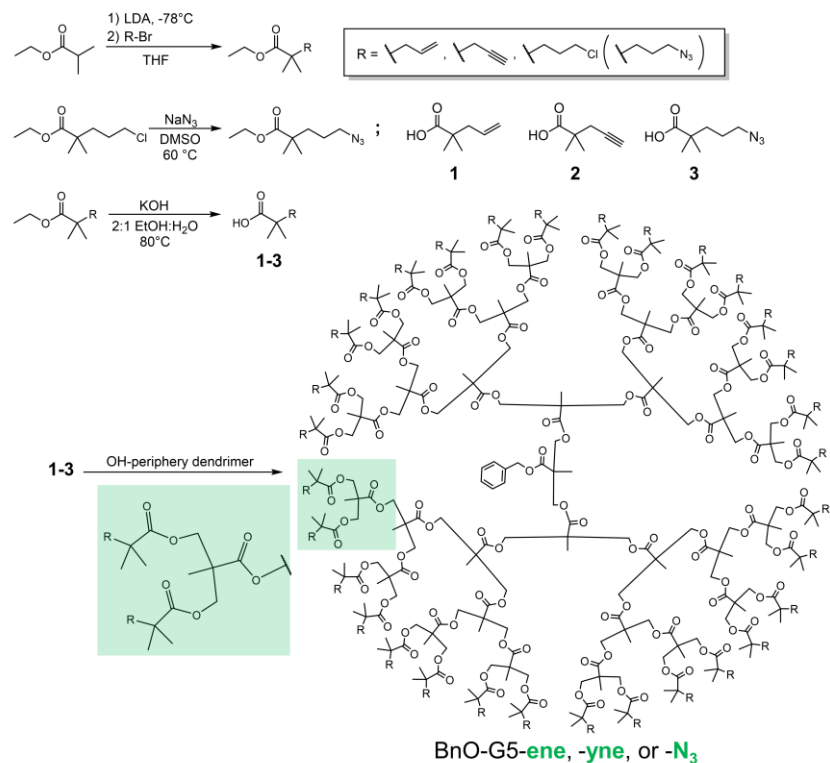
A major challenge associated with bis-MPA dendrimers is maintaining their uniform peripheral functionality under non-ambient conditions.^{18,28,29} Bis-MPA dendrimer

peripheries with hydroxyl groups are typically coupled with carboxylic acids,^{18,30} chloroformates²⁰, and carbonates,²⁷ which in turn can bear the desired reactive group for downstream applications. Alternatively, click chemistry *via* thiol-ene,^{19,21,31} strain-promoted alkyne-azide cycloaddition (SPAAC),³² and copper-catalyzed azide-alkyne cycloaddition (CuAAC) can also be used to modify the periphery.³¹ However, these approaches invariably introduce α -unsubstituted ester linkages at the periphery that are much more hydrolytically labile than the neopentyl esters constituting the dendrimer backbone.^{17,18} While rapid peripheral hydrolysis is desirable in certain situations,^{10,18,29,33} it precludes the use of these bis-MPA dendrimers for applications requiring a uniform architecture under extended circulation times, such as for anti-cancer drug delivery.²⁹ As a general solution to this dilemma, we have esterified a series of 2,2-dimethyl substituted (neopentyl) carboxylic acids onto high generation bis-MPA-based alcohol periphery dendrons (Scheme 2.1), which can still be modified *via* click chemistry to provide additional functionality. The synthesis of **1-3** is outlined in Scheme 1, in which alkylation of ethyl isobutyrate and subsequent ester hydrolysis produces the neopentyl carboxylic acids. The alkene and alkyne acids **1** and **2** were readily accessed in two steps, while the preparation of the azide first requires alkylation with 3-chloro-1-bromopropane and subsequent azidification with sodium azide, followed by ester hydrolysis to yield **3**. **1-3** can be considered as analogues of linear carboxylic acids previously used to introduce click functionality to the periphery of bis-MPA dendrimers,^{10,18,31} as seen in Scheme 2.1.

Previous work:



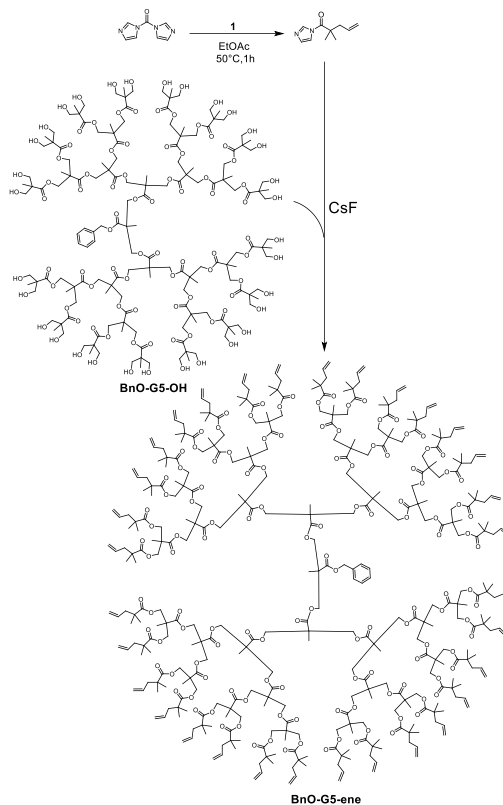
This work:



Scheme 2.1. General method for preparing neopentyl carboxylic acids 1-3 and representative synthesis of a generation 5 neopentyl periphery bis-MPA dendron.

In this work, we found that the neopentyl periphery dendrons easily underwent typical click reactions. Moreover, the water-soluble ammonium derivative of the 5th generation (G) azide dendron **BnO-G5-N₃** was found to be much more resilient toward hydrolysis at physiological temperature (37 °C) across different pH values, as well as in the presence of esterase versus its corresponding ammonium species furnished with α -unsubstituted esters.

2.3 Results and Discussion



Scheme 2.2. An example of using FPE to prepare **BnO-G5-ene**.

A series of benzyl-core (BnO) bis-MPA dendrons of generations 1-5 with peripheral esters **1-3** were prepared according to the procedures of Malkoch³⁰ and coworkers (Figure S2.1). Initial attempts to functionalize the dendrons with the anhydrides of compounds **1-3** were unsuccessful, likely due to extreme steric hindrance around the carbonyl groups with two neopentyl esters. Methods that activated the carboxylic acid without anhydride formation such as Steglich esterification and HOBt ester formation afforded some functionalization sluggishly, reaching only approximately 20% conversion over 24 hours. However, using the fluoride promoted esterification (FPE) chemistry developed by Malkoch and co-

workers³⁰ proved highly effective. As seen in Scheme 2.2, the neopentyl acid **1** was first activated with 1,1'-carbonyldiimidazole in ethyl acetate for 1 hour at 50°C, followed by addition of the alcohol periphery dendron and CsF. The reaction was monitored using ESI-MS until it reached full conversion, typically overnight. The compiled MALDI-TOF spectra for the alkene dendrons are shown in Figure 2.1 (see SI in Chapter 2.5 for additional spectra and synthetic details).

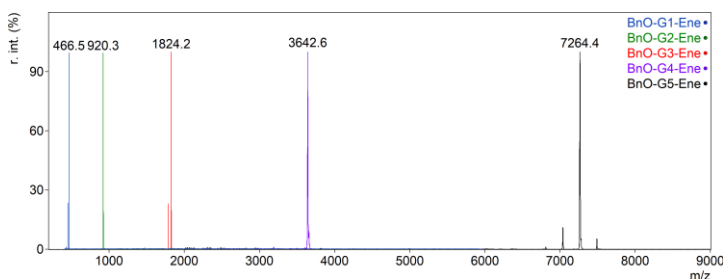
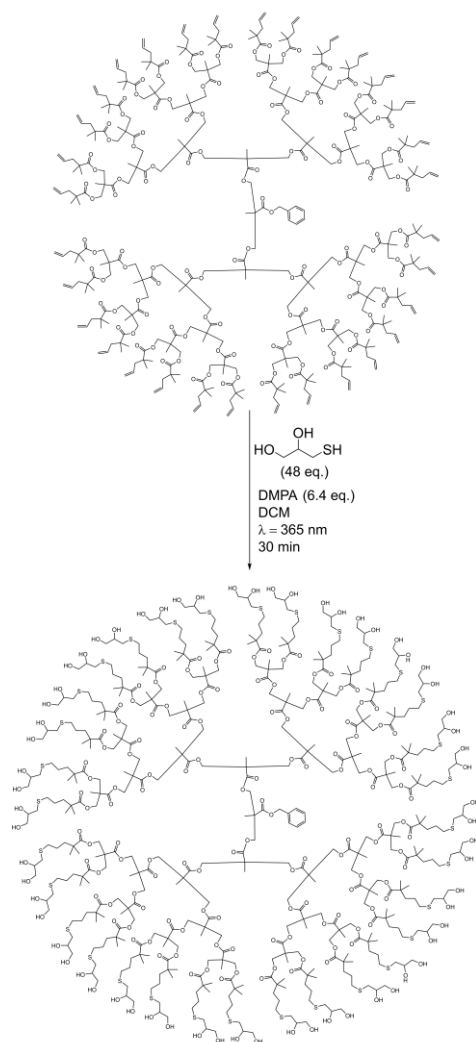


Figure 2.1. MALDI-TOF mass spectra of neopentyl alkene dendrons of generation 1-5.

We then investigated whether the relatively bulkier neopentyl ester groups affected higher generation dendrons' ability to functionalize the reactive peripheral groups by clicking on a model substrate for alkene (thioglycerol),²¹ alkyne (benzyl azide), and azide (DBCO-COOH) periphery dendrons.³⁴ As a proof of concept, the click reactions were performed on **BnO-G5-ene/yne/N₃** and monitored *via* ¹H NMR and confirmed for completion *via* MALDI-TOF. We were pleased to find that the coupling to each periphery was consistent with timeframes reported in literature for the linear analogues. The thiol-ene reaction with **BnO-G5-ene** was complete within 30 minutes (Scheme 3), while the SPAAC and CuAAC reactions were complete within 10 minutes and overnight, respectively (See SI in Chapter 2.5 for synthetic and characterization details).



Scheme 2.3. Example thiol-ene click reaction between thioglycerol and **BnO-G5-ene** using DMPA as the photo-initiator.

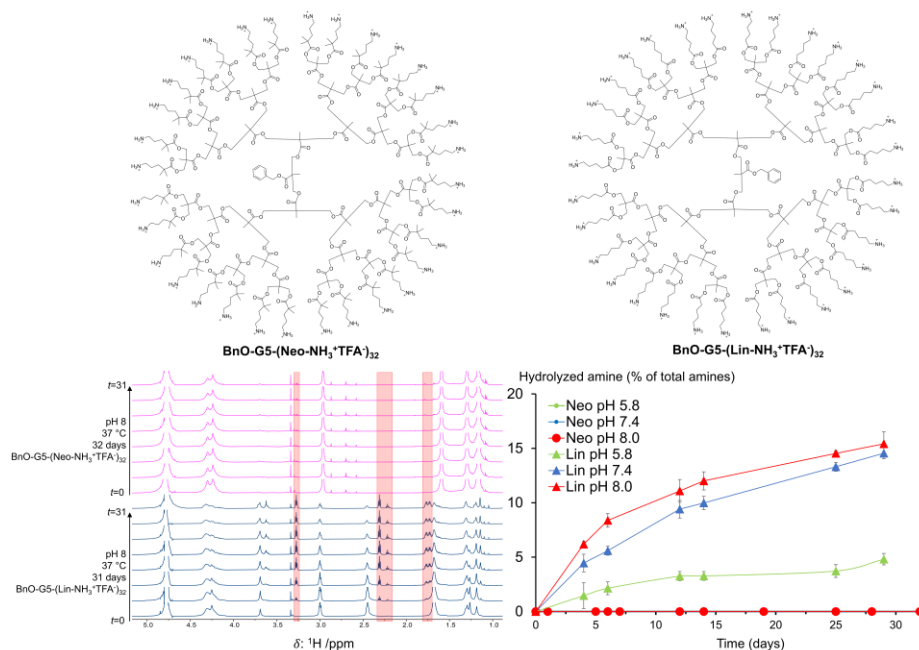


Figure 2.2. Top: structures of **BnO-G5-(Neo-NH₃⁺TFA⁻)₃₂** and **BnO-G5-(Lin-NH₃⁺TFA⁻)₃₂**, TFA anions have been omitted for clarity. Bottom left: tracking ¹H NMR showing **BnO-G5-(Neo-NH₃⁺TFA⁻)₃₂** (pink) and **BnO-G5-(Lin-NH₃⁺TFA⁻)₃₂** (blue) in pH 8 phosphate buffer at 37 °C. Boxed signals indicate evolution of the degradation peaks. Bottom right: graphical summary of *hydrolysis* ¹H NMR data, the neopentyl species did not undergo visible hydrolysis, and so all the datapoints are superimposed.

As mentioned previously, it is well-known that bis-MPA dendrimers are susceptible to peripheral degradation. To demonstrate the hydrolytic stability of the resulting dendrons relative to their non-neopentyl counterparts, two G5 amine-periphery dendrons, **BnO-G5-(Neo-NH₃⁺TFA⁻)₃₂** and **BnO-G5-(Lin-NH₃⁺TFA⁻)₃₂** were prepared. The former was accessed by catalytic hydrogenation of **BnO-G5-N₃** using Pd(OH)₂/C and in the presence of trifluoroacetic acid. The latter was prepared by esterifying **BnO-G5-OH** with 5-azidovaleric acid using FPE conditions, followed by reduction and acidification to the amine species under the same conditions. The resulting dendrons were isolated as the trifluoroacetate salts (Figure 2.2, see SI in Chapter 2.5 for MALDI spectra) and were

respectively dissolved in 0.1 M phosphate buffer in D₂O at pH 5.8, 7.4 and 8 and incubated at 37 °C. Hydrolysis of the periphery, as observed by growth of the free amine (*i.e.*, 5-aminovalerate) signals at 2.2 ppm, was monitored by ¹H NMR using sodium formate as an internal standard (see SI in Chapter 2.5 for additional qNMR spectra). In addition to hydrolysis, 2D TOCSY (Figure S2.9) of **BnO-G5-(Lin-NH₃⁺TFA⁻)₃₂** revealed aminolysis of the periphery due to intramolecular cyclization (*i.e.*, backbiting).^{18,35} In pH 8 and 7.4, formation of the cyclization product, δ-valerolactam (2.3 ppm), was favoured over hydrolysis to the linear amine, whereas in acidic pH hydrolysis was favoured due to most of the amines being protonated (Figure 2.3). The peak at 2.45 ppm is unique to the carbonyl α-CH₂ of the dendron-bound valerate ester, while the other methylene signals were superimposed with those from the free amine. Therefore, for **BnO-G5-(Lin-NH₃⁺TFA⁻)₃₂**, we derived the relative proportions of dendron-bound amine, hydrolyzed amine, and lactam from the NMR signal shifts mentioned above. Over the course of ~1 month, the neopentyl dendron exhibited markedly superior peripheral stability across all pH conditions compared to its non-neopentyl counterpart. The former retained all its 32 peripheral esters in acidic pH, 95% in neutral pH, and 87% of the esters in basic pH (where degradation was primarily due to aminolysis). While the latter lost 15% of its peripheral amines *via* hydrolysis and 32% *via* aminolysis in pH 7.4, and ~62% (47% to aminolysis, 15% to hydrolysis) at basic pH (see Figure 2.2 and Figure S2.8) after the same period. The degradation of **BnO-G5-(Lin-NH₃⁺TFA⁻)₃₂** was significantly slower at acidic pH than in other treatments (~5% hydrolyzed, 3% aminolyzed), which is consistent with previous findings.^{28,29}

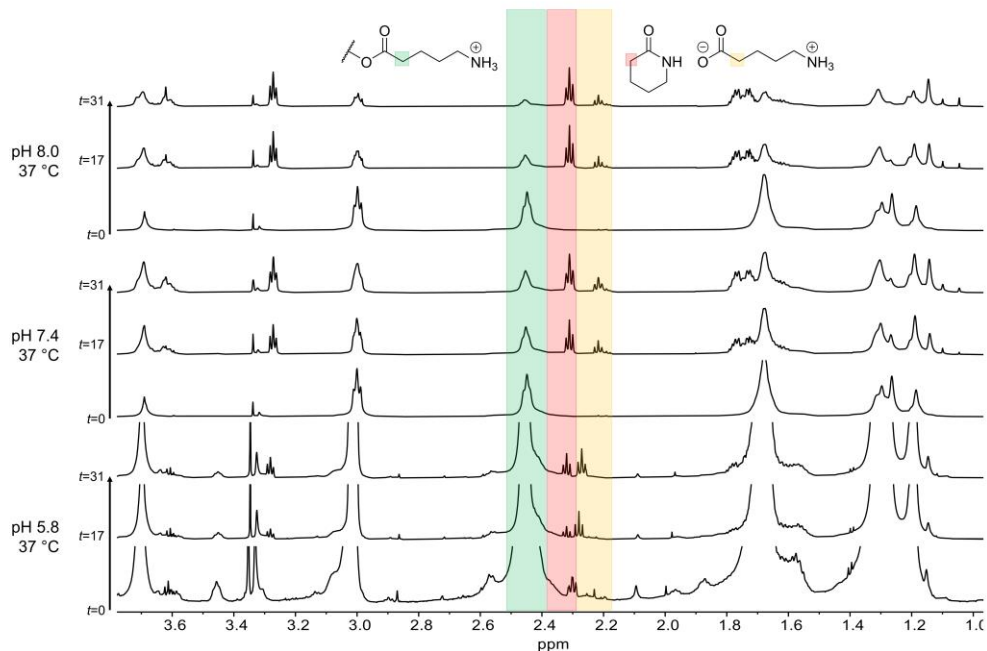


Figure 2.3. Stacked NMR spectra of $1\text{ mM BnO-G5-(Lin-NH}_3^+\text{TFA}^-)_{32}$ in 0.1M phosphate buffer across three different pH over 1 month. $\alpha\text{-CH}_2$ of dendron-bound amine, free amine, and lactam are colour-coded.

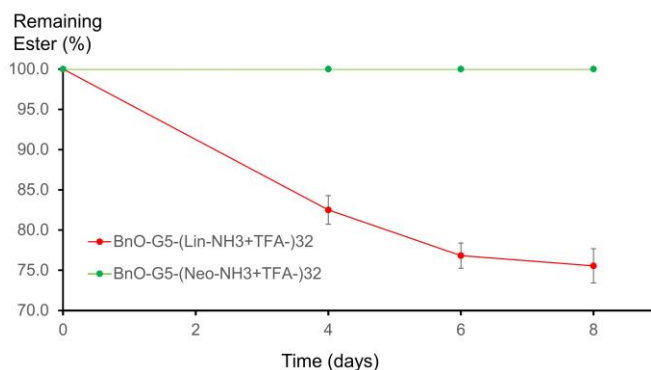


Figure 2.4. Degradation of $\text{BnO-G5-(Neo-NH}_3^+\text{TFA}^-)_{32}$ and $\text{BnO-G5-(Lin-NH}_3^+\text{TFA}^-)_{32}$ in 20% porcine esterase solution in $\text{pH } 7.4$ phosphate buffer at $37\text{ }^\circ\text{C}$, as monitored *via* ^1H NMR.

Polyester-based dendrimers also undergo peripheral ester cleavage catalyzed by esterases,^{29,36} which prompted us next to test the stability of both G5 ammonium species in a solution of porcine esterase. The dendrons were respectively incubated with 20% mol eq. esterase (vs. amine) in pH 7.4 phosphate buffer at 37 °C and monitored *via* ¹H NMR (Figure 2.4). Despite relatively high catalytic loading, we found only a minor difference in the amount of degraded **BnO-G5-(Lin-NH₃⁺TFA⁻)₃₂** between the esterase treatment (25%) and in just pH 7.4 buffer (18%, Figure S2.8) after 8 days, while **BnO-G5-(Neo-NH₃⁺TFA⁻)₃₂** remained stable after the same time. The minor difference afforded by the esterase treatment agrees with previous findings that higher generation dendrons better resist enzymatic cleavage of the periphery due to steric crowding.³⁶

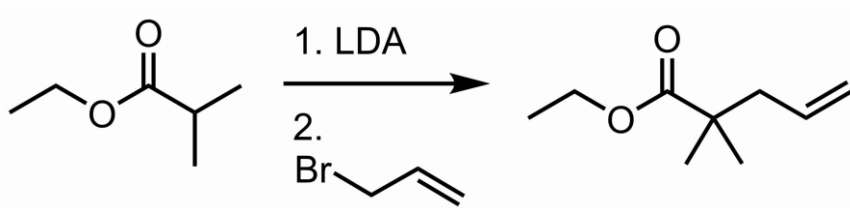
2.4 Conclusion

In conclusion, we have prepared a series of neopentyl carboxylic acids and appended these onto generation 1-5 bis-MPA dendrons. The resulting dendrons are markedly more resistant to degradation at various pH and under esterase treatment compared to the non-neopentyl dendrons, as a result of the increased steric bulk at the periphery. The same steric bulk did not noticeably affect click reactivity. We demonstrate that it is possible to tune the hydrolytic stability without changing critical surface functionality for these dendrons, which could make them relevant to previously unsuitable applications.

2.5 Supporting Information

Unless stated otherwise, all chemicals were purchased from Sigma-Aldrich and used without further purification. THF was dried through a column of activated neutral alumina. ¹H NMR spectroscopy was performed on a Bruker Avance AV600 at 600 MHz. ¹³C NMR spectroscopy was performed either on a Bruker Avance AV600 at 151 MHz or Bruker Avance AV700 at 176 MHz. All chemical shifts are reported in ppm. All MALDI mass spectra were collected on a Bruker UltraFlextreme spectrometer in positive ion mode using either dithranol or sinapic acid as matrix. Electrospray MS was performed using a Micromass Quattro triple quadrupole instrument in positive mode. Exact masses were collected on either an Agilent 6210 TOF or a Bruker Maxis II Q-TOF. Flash chromatography was performed using an AnaLogix Intelliflash 280 automated flash chromatography system, equipped with a variable wavelength (200-320 nm) UV detector. Sorbtech screwtop flash columns packed with Silicycle R60 20-45 μm silica gel were used as chromatography media.

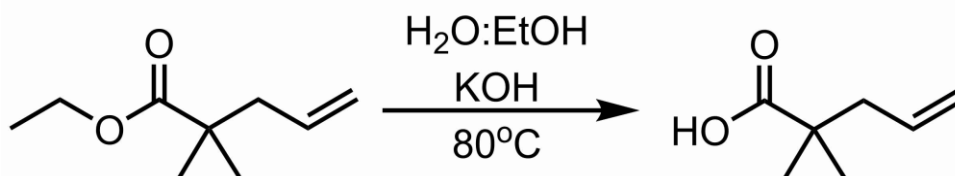
Ethyl 2,2-dimethylpent-4-enoate



To a flame dried 250 mL Schlenk flask equipped with a magnetic stir bar and placed under nitrogen, diisopropylamine (7.29 mL, 51.6 mmol) dissolved in 120 mL of dry THF was added. The solution was cooled to -78 °C and a solution of 2.5 M *n*-butyllithium in hexanes

(19.8 mL, 49.5 mmol) was then added dropwise *via* syringe over 2 minutes, resulting in a clear colourless solution. Separately, ethyl isobutyrate (5.00 g, 43.1 mmol) was dissolved in 25 mL of THF and cooled to -78 °C. This was then cannulated dropwise into the stirred solution of LDA and stirred for 30 minutes at -78 °C before allyl bromide (5.59 mL, 65.6 mmol) was added in one portion. The solution was left to stir at -78 °C for 2 hours, followed by addition of 100 mL of water to quench. The reaction mixture was diluted with 300 mL of diethyl ether, then washed with 3 × 100 mL 1 M HCl, 1 × 150 mL brine, and dried over MgSO₄. The solvent was removed by rotary evaporation to give the crude product as a yellow oil. The crude product was purified by flash chromatography using a 50-g silica gel silica gel column equilibrated in hexanes. The product was eluted with 100% hexanes followed by 5% ether in hexanes over 5 column volumes. The product fractions were then pooled and dried by rotary evaporation to give the product as a clear, colourless oil. (5.671 g, 83%) ¹H NMR (700 MHz; CDCl₃)³⁷: δ 5.76-5.70 (m, 1H), 5.05 (t, *J* = 0.9, 1H), 5.04-5.02 (m, 1H), 4.11 (q, *J* = 7.1, 2H), 2.27 (dt, *J* = 7.4, 1.1, 2H), 1.24 (t, *J* = 7.1, 3H), 1.16 (s, 6H).

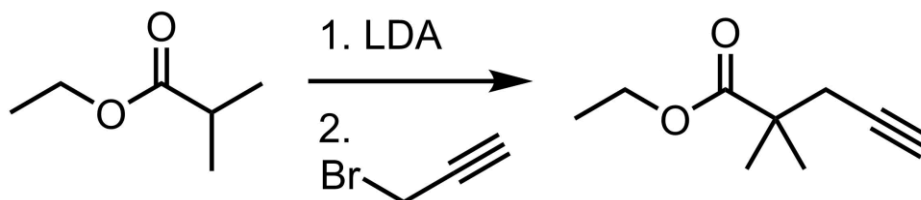
2,2-dimethylpent-4-enoic acid (1)



To a 100 mL round-bottomed flask equipped with a magnetic stir bar was added ethyl 2,2-dimethylpent-4-enoate (3.004 g, 19.3 mmol) and 50 mL of 2:1 EtOH:water, followed by potassium hydroxide (10.8 g, 192.6 mmol). The mixture was stirred at 80 °C for 2 hours

then left to cool to room temperature. The mixture was diluted with 100 mL of water, 100 mL of 1 M H₃PO₄, and extracted with 3 × 100 mL of ether. The combined organic layers were washed with 1 × 150 mL brine and dried over MgSO₄. The solvent was removed by rotary evaporation to give the product as a slightly yellow oil. (1.996 g, 81%) ¹H NMR (700 MHz; CDCl₃)³⁸: δ 5.80-5.74 (m, 1H), 5.09-5.07 (m, 2H), 2.30 (d, *J* = 7.4, 2H), 1.20 (s, 6H).

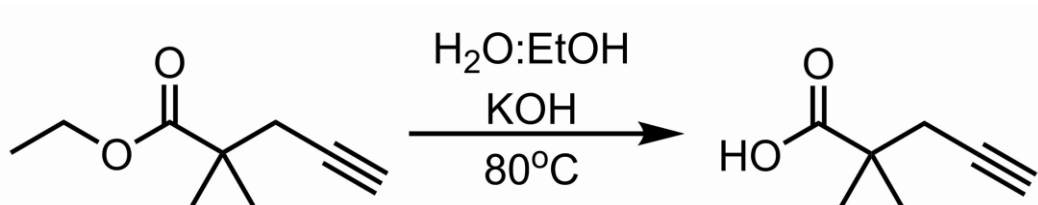
Ethyl 2,2-dimethylpent-4-ynoate



To a flame dried 250 mL Schlenk flask equipped with a magnetic stir-bar and placed under nitrogen was added diisopropylamine (7.29 mL, 51.6 mmol) dissolved in 120 mL of dry THF. The solution was cooled to -78 °C and left to stir for 10 minutes. To this, a solution of 2.5 M *n*-butyllithium in hexanes (19.8 mL, 49.5 mmol) was added dropwise *via* syringe over 2 minutes, resulting in a clear colourless solution. Separately, ethyl isobutyrate (5.00 g, 43.044 mmol) was dissolved in 25 mL of THF and cooled to -78 °C. This was then cannulated dropwise into the stirred solution of LDA and left for 30 minutes at -78 °C before an 80% solution of propargyl bromide in toluene (3.43 mL, 45.2 mmol) was added in one portion. This was stirred at -78 °C for 2 hours then quenched by adding 100 mL of water. The quenched reaction mixture was warmed to room temperature, then diluted with 300 mL hexanes and washed with 3 × 100 mL of 1 M H₃PO₄, 1 × 150 mL brine, then dried

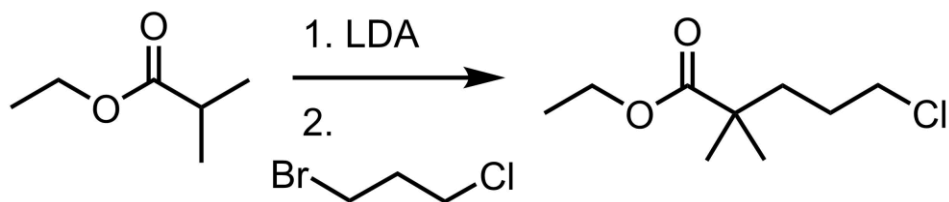
over MgSO₄. The solvent was removed by rotary evaporation to give the crude product as a yellow oil. This was purified by flash chromatography using a 50-gram silica gel column equilibrated in hexanes. The product was eluted with 100% hexanes followed by 5% ether in hexanes over 5 column volumes. The product-containing fractions were then pooled and dried by rotary evaporation to give the product as a clear, colourless oil. (5.78 g, 88%) ¹H NMR (600 MHz, CDCl₃)³⁹ δ 4.09 (q, *J* = 7.1, 2H), 2.38 (d, *J* = 2.7, 2H), 1.95 (t, *J* = 2.6, 1H), 1.23 – 1.17 (m, 5H).

2,2-dimethylpent-4-ynoic acid (2)



To a 100 mL round-bottomed flask equipped with a magnetic stir bar was added ethyl 2,2-dimethylpent-4-ynoate (2.503 g, 16.25 mmol) and 50 mL of 2:1 EtOH:water, followed by potassium hydroxide (9.107 g, 162.5 mmol). The mixture was stirred at 80 °C for 2 hours, then left to cool to room temperature. The mixture was diluted with 100 mL of water and 100 mL of 1 M H₃PO₄ and extracted with 3 × 100 mL of ether. The pooled organic layer was washed with 1 × 150 mL brine and dried over MgSO₄, and solvent was removed by rotary evaporation to give the product as a slightly yellow oil (1.984 g, 97%). ¹H NMR (500 MHz, CDCl₃)³⁹ δ 2.46 (d, *J* = 2.69, 2H) 2.03 (t, 1H), 1.31 (s, 6H).

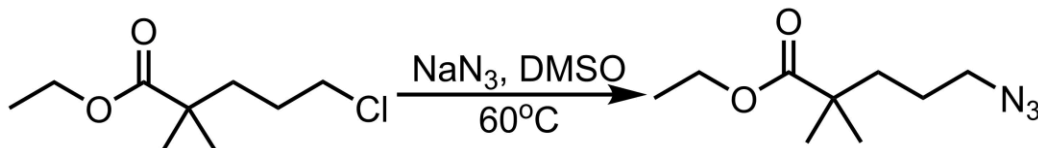
Ethyl 5-chloro-2,2-dimethylpentanoate



To a flame dried 250 mL Schlenk flask equipped with a magnetic stir bar and placed under nitrogen, diisopropylamine (7.29 mL, 51.6 mmol) was added *via* syringe, and 120 mL of dry THF was added *via* cannula. The solution was cooled to $-78\text{ }^{\circ}\text{C}$ in a dry ice/acetone bath and this was left to cool for 10 minutes with stirring. To this, a solution of 2.5 M *n*-butyllithium in hexanes (19.8 mL) was added *via* syringe over two minutes, resulting in a clear colourless solution of LDA in THF. Separately, ethyl isobutyrate (5.00 g, 43.1 mmol) was dissolved in 25 mL of THF and cooled to $-78\text{ }^{\circ}\text{C}$ in a dry ice/acetone bath. This was then cannulated dropwise into the stirred solution of LDA, then left for 30 minutes at $-78\text{ }^{\circ}\text{C}$ before 3-chloro-1-bromopropane (6.385 mL, 64.6 mmol) was added as a neat liquid *via* syringe. This was left to react at $-78\text{ }^{\circ}\text{C}$ for 30 minutes, then the reaction mixture was warmed to room temperature and left to stir for 3 hours. The reaction was then quenched by the addition of 50 mL of water, then diluted with 300 mL of diethyl ether and washed with $3 \times 100\text{ mL}$ 1 M HCl, $1 \times 150\text{ mL}$ brine, dried over MgSO_4 , filtered, and solvent was removed by rotary evaporation to give the crude product as a yellow oil. This was purified by flash chromatography using a 50 g silica gel column equilibrated in hexanes and elution with 5 column volumes of hexanes, then a gradient from 0% to 12% ether in hexanes over 20 column volumes. The fractions containing product were pooled and solvent was removed by rotary evaporation to give the product as a clear, colourless oil. (7.80 g, 94%).

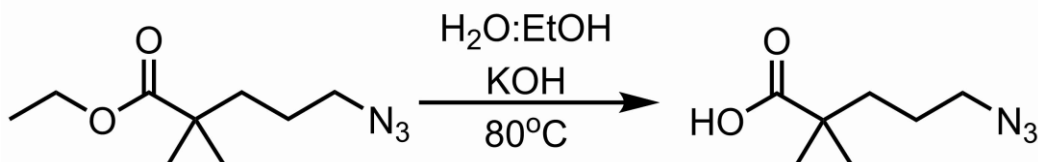
^1H NMR (700 MHz, CDCl_3)⁴⁰: δ 4.12 (q, $J = 7.1$, 2H), 3.50 (t, $J = 6.5$, 2H), 1.74-1.70 (m, 2H), 1.66-1.63 (m, 2H), 1.24 (t, $J = 7.1$, 3H), 1.18 (s, 6H).

Ethyl 5-azido-2,2-dimethylpentanoate



A 100 mL round-bottomed flask equipped with a magnetic stir bar was charged with a solution of sodium azide (3.373 g, 51.9 mmol) in 30 mL of DMSO, and to this ethyl 5-chloro-2,2-dimethylpentanoate (5.00 g, 25.95 mmol) was added. The solution was stirred and heated to 60°C in an oil bath overnight, and the following day the reaction mixture was cooled to room temperature and diluted with 80 mL of water. This reaction mixture was then extracted with 3×50 mL of ether, and the combined ether layers were washed with 1×50 mL water, 1×50 mL brine, dried over MgSO_4 , and solvent was removed by rotary evaporation to give the product as a clear, colourless oil. (5.16 g, 99%) ^1H NMR (700 MHz; CDCl_3): δ 4.12 (q, $J = 7.1$, 2H), 3.25 (t, $J = 6.5$, 2H), 1.60-1.52 (m, 4H), 1.25 (t, $J = 7.1$, 3H), 1.18 (s, 6H). ^{13}C NMR (176 MHz; CDCl_3): δ 177.6, 60.5, 51.9, 42.0, 37.7, 25.3, 24.7, 14.4.

5-azido-2,2-dimethylpentanoic acid (3)



A 100 mL round-bottomed flask equipped with a magnetic stir bar was charged with ethyl 5-azido-2,2-dimethylpentanoate (5.12 g, 25.7 mmol) dissolved in 50 mL of 2:1 EtOH:water, followed by addition of potassium hydroxide (7.20 g, 128.5 mmol). The reaction mixture was heated to 80 °C for 2 hours, then left to cool to room temperature. The reaction mixture was then diluted with 100 mL of water and 200 mL of H₃PO₄, then washed with 3 × 100 mL ether, and the combined ether layers were washed with 1 × 150 mL brine, dried over MgSO₄, filtered, and solvent was removed by rotary evaporation to give the product as a yellow-orange oil. (4.22 g, 96%). ¹H NMR (700 MHz; CDCl₃): δ 3.27 (t, *J* = 5.6, 2H), 1.63-1.58 (m, 4H), 1.22 (s, 6H) ¹³C NMR (176 MHz; CDCl₃): δ 184.5, 51.8, 42.0, 37.5, 25.1, 24.7.

The model alcohol periphery dendrons from generations 1-5 were prepared in a divergent methodology starting from bis-MPA. This carboxylic acid core was protected with benzyl bromide (“BnO”), and the dendrons were grown using fluoride promoted esterification using acetonide-protected bis-MPA according to procedures by Malkoch and co-workers (Figure S2.1).

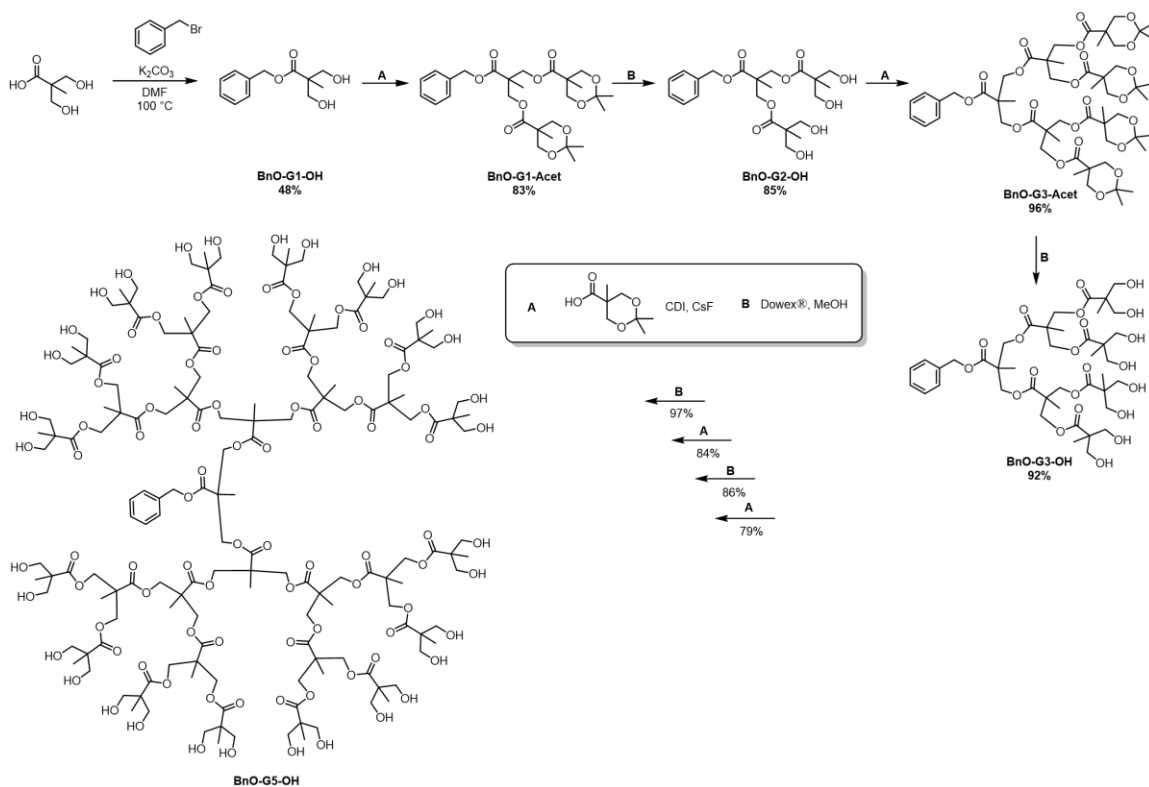


Figure S2.1. Preparation of G1-G5 benzyl core-protected hydroxyl periphery bis-MPA dendrons.

BnO-G1-OH¹⁶

A 100 mL round-bottomed flask equipped with a magnetic stir bar was charged with bis-MPA (9.00g, 67.11 mmol) dissolved in 50 mL of DMF, along with potassium hydroxide (4.300 g, 76.64 mmol), and this was stirred and heated to 100 °C for 1 hour. At this point, benzyl bromide (9.602 mL, 80.73 mmol) was added to the reaction mixture, which resulted in the formation of a white precipitate. This was left to heat for 16 hours, followed by removal of DMF *via* vacuum distillation. The resulting crude material was dissolved in 100 mL of DCM and washed with 3 × 50 mL of water, 1 × 50 mL brine, dried over MgSO₄, filtered, and solvent was removed by rotary evaporation. The crude material was then recrystallized from 2:1 hexanes:DCM to give the product as clear, colourless needles

(7.22g, 48 %). ^1H NMR (600 MHz; CDCl_3): δ 7.39-7.32 (m, 5H), 5.22 (s, 2H), 3.94 (dd, $J = 10.7, 6.8, 2\text{H}$), 3.74 (dd, $J = 11.4, 6.4, 2\text{H}$), 2.76 (t, $J = 6.7, 2\text{H}$), 1.08 (s, 3H).

BnO-G2-(Acet) $_4$ ¹⁶

A 100 mL round-bottomed flask equipped with a magnetic stir bar was charged with 1,1'-Carbonyldiimidazole (9.61 g, 59.27 mmol) dissolved in 30 mL of EtOAc. The mixture was stirred and heated to 50 °C. This solution was stirred rapidly while acetonide protected bis-MPA (10.34 g, 59.28 mmol) was added in small portions over 2 minutes, which resulted in the vigorous evolution of gas. This was left stirring at 50 °C for 1 hour, followed by addition of BnO-G1-OH (4.43 g, 19.76 mmol) and CsF (1.20 g, 8.90 mmol) in a single portion. After 4 hours the reaction was complete by TLC and was quenched with 5 mL of water for 1 hour, then diluted with 100 mL of EtOAc and washed with 3×100 mL of 10% NaHCO_3

and 1×100 mL brine, dried over MgSO_4 , filtered, and solvent was removed by rotary evaporation. The crude material was purified by chromatography using a 100-gram silica gel silica gel column equilibrated in 5% acetone:hexanes, and the material was purified using a gradient from 5% to 50% acetone:hexanes over 20 column volumes, with detection at 205 nm. The fractions containing product were pooled and solvent was removed by rotary evaporation and the resulting oil was dried *in vacuo* to give the product as a viscous, colourless oil (8.78 g, 83%). ^1H NMR (600 MHz; CDCl_3): δ 7.37-7.31 (m, 5H), 5.16 (s, 2H), 4.36-4.32 (m, 4H), 4.10 (d, $J = 11.8, 4\text{H}$), 3.58 (d, $J = 11.4, 4\text{H}$), 1.41 (s, 6H), 1.34 (s, 6H), 1.30 (s, 3H), 1.10 (s, 6H).

BnO-G2-(OH) $_4$ ¹⁶

A 100 mL round-bottomed flask equipped with a magnetic stir bar was charged with BnO-G2-Acet (2.15 g, 4.001 mmol) dissolved in 45 mL of EtOH, then 1 scoopula full of DOWEX beads was added and the solution was stirred for 3 hours at room temperature and monitored by ESI-MS. Once complete deprotection was observed, the solution was filtered through a glass frit to recover the DOWEX, and the filtrate was dried by rotary evaporation then *in vacuo* overnight to give the product as a sticky white powder (1.54 g, 85%) ¹H NMR (600 MHz; MeOD): δ 7.40-7.31 (m, 5H), 5.18 (s, 2H), 4.29 (q, *J* = 9.0, 4H), 3.63 (dd, *J* = 10.8, 5.6, 4H), 3.57 (d, *J* = 10.8, 4H), 1.30 (s, 3H), 1.09 (s, 6H)

BnO-G3-(Acet)₄¹⁶

A 100 mL round-bottomed flask equipped with a magnetic stir bar was charged with 1,1'-carbonyldiimidazole (4.26 g, 26.30 mmol) and 20 mL of EtOAc, and the mixture was stirred and heated to 50 °C. This suspension was stirred rapidly while acetonide protected bis-MPA (4.74 g, 27.16 mmol) was added in small portions over 2 minutes, which resulted in the vigorous evolution of gas. This was left stirring at 50 °C for 1 hour, followed by addition of BnO-G2-(OH)₄ (2.002 g, 4.381 mmol) and CsF (0.53 g, 3.51 mmol) in a single portion. After 4 hours the reaction was complete by TLC and was quenched with 5 mL of water for 1 hour, then diluted with 100 mL of EtOAc and washed with 3 × 100 mL of 10% NaHCO₃ and 1 × 100 mL brine, dried over MgSO₄, filtered, and solvent was removed by rotary evaporation. The crude material was purified by chromatography using a 100 g silica gel silica gel column equilibrated in 5% acetone:hexanes, and the material was purified using a gradient from 5% to 50% acetone:hexanes over 20 column volumes, with detection at 205 nm. The fractions containing product were pooled and solvent was removed by

rotary evaporation and the resulting oil was dried *in vacuo* to give the product as a viscous oil (4.570 g, 96%). ¹H NMR (600 MHz; CDCl₃): δ 7.37-7.30 (m, 5H), 5.16 (s, 2H), 4.30-4.23 (m, 12H), 4.14 (d, *J* = 11.8, 8H), 3.61 (d, *J* = 12.0, 8H), 1.40 (s, 12H), 1.34 (s, 12H), 1.27 (s, 3H), 1.19 (s, 6H), 1.13 (s, 12H).

BnO-G3-(OH)₈¹⁶

A 100 mL round-bottomed flask equipped with a magnetic stir bar was charged with a solution of BnO-G3-(Acet) (2.06 g, 1.91 mmol) in 45 mL of EtOH, then 1 scoopula full of DOWEX beads were added and the solution was stirred for 3 hours at room temperature, Once complete deprotection was observed by ESI-MS, This was filtered through a glass frit to recover the DOWEX, and the filtrate was dried by rotary evaporation then *in vacuo* overnight to give the product as a white powder. (1.62 g, 92%) ¹H NMR (700 MHz; MeOD): δ 7.35 (d, *J* = 7.1, 2H), 7.31 (t, *J* = 7.4, 2H), 7.27 (t, *J* = 7.2, 1H), 5.14 (s, 2H), 4.27 (d, *J* = 11.0, 2H), 4.22-4.19 (m, 6H), 4.13 (dd, *J* = 11.0, 6.6, 4H), 3.61 (dd, *J* = 10.9, 3.4, 8H), 3.53 (d, *J* = 10.8, 8H), 1.25 (s, 3H), 1.14 (s, 6H), 1.08 (s, 12H)

BnO-G4-(Acet)₈¹⁶

A 25 mL round-bottomed flask equipped with a magnetic stir bar was charged with a solution of 1,1'-Carbonyldiimidazole (2.11 g, 13.03 mmol) in 6.5 mL of EtOAc and heated to 50 °C. This suspension was stirred rapidly while acetonide protected bis-MPA (2.32 g, 13.29 mmol) was added in small portions over 2 minutes, which resulted in the vigorous evolution of gas. This was left to react for 1 hour, at which point BnO-G3-(OH)₈ (1.00 g, 1.086 mmol) was added, along with CsF (0.26 g, 1.74 mmol). After 6 hours the reaction was complete by ESI-MS and was quenched by the addition of 2 mL of water for 1 hour,

then diluted with 100 mL of EtOAc and washed with 3×100 mL of 10% NaHCO₃ and 1×100 mL brine, dried over MgSO₄, filtered, and solvent was removed by rotary evaporation. The crude material was purified by silica gel chromatography using a 25 g silica gel column equilibrated in 5% acetone:hexanes, and the material was purified using a gradient from 5% to 50% acetone:hexanes over 20 column volumes, with detection at 205 nm. The fractions containing product were pooled and solvent was removed by rotary evaporation. Solvent was removed *in vacuo* to give the product as a clear viscous oil. (1.86 g, 79%) ¹H NMR (600 MHz; CDCl₃): δ 7.36-7.31 (m, 5H), 5.15 (s, 2H), 4.32-4.27 (m, 18H), 4.22-4.18 (m, 10H), 4.13 (d, $J = 11.9$, 16H), 3.61 (dd, $J = 11.9, 2.3$, 16H), 1.40 (s, 24H), 1.34 (s, 24H), 1.29 (s, 3H), 1.26 (s, 12H), 1.17 (s, 6H), 1.13 (s, 24H)

BnO-G4-(OH)₁₆¹⁶

A 100 mL round-bottomed flask equipped with a magnetic stir bar was charged with BnO-G4-(acet)₈ (1.50 g, 0.95 mmol) dissolved in 45 mL of EtOH, followed by addition of 1 scoopula full of DOWEX beads and was left to stir for 6 hours and monitored by ESI-MS. This was filtered through a glass frit to recover the DOWEX, and the filtrate was dried by rotary evaporation then *in vacuo* overnight to give the product as a white powder. (1.11 g, 86%) ¹H NMR (600 MHz, MeOD) δ 7.47 – 7.30 (m, 5H), 5.22 (s, 2H), 4.46 – 4.15 (m, 28H), 3.67 (dd, $J = 10.9, 3.3$ Hz, 15H), 3.60 (d, $J = 10.9$ Hz, 15H), 1.35 (s, 3H), 1.29 (s, 12H), 1.22 (s, 6H), 1.15 (s, 24H).

BnO-G5-(Acet)₁₆¹⁶

A 25 mL round-bottomed flask equipped with a magnetic stir bar was charged with 1,1'-Carbonyldiimidazole (1.36 g, 13.03 mmol) added to 5 mL of EtOAc and heated to 50 °C.

This suspension was stirred rapidly while acetonide protected bis-MPA (1.99 g, 8.58 mmol) was added in small portions over 2 minutes, which resulted in the vigorous evolution of gas. This was left to react for 1 hour followed by addition of BnO-G4-(OH)₈ (640 mg, 0.346 mmol) and CsF (168.2 mg, 1.11 mmol) in a single portion. After 6 hours the reaction was complete by ESI-MS and was quenched with 2 mL of water for 1 hour, then diluted with 100 mL of EtOAc and washed with 3 × 100 mL of 10% NaHCO₃ and 1 × 100 mL brine, dried over MgSO₄, filtered, and solvent was removed by rotary evaporation. The crude material was purified by silica gel chromatography using a 25-gram silica gel column equilibrated in 5% acetone:hexanes, and the material was purified using a gradient from 5% to 50% acetone:hexanes over 20 column volumes, with detection at 205 nm. The fractions containing product were pooled and solvent was removed by rotary evaporation and the resulting oil was dried *in vacuo* to give the product as a white solid (1.26 g, 84%). ¹H NMR (600 MHz, CDCl₃) δ 7.39 – 7.29 (m, 5H), 5.16 (s, 2H), 4.07 – 4.42 (m, 90H), 3.74 – 3.53 (m, 32H), 1.41 (m, 45H), 1.34 (d, *J* = 1.7 Hz, 50H), 1.26 (m, 36H), 1.13 (d, *J* = 2.1 Hz, 60H).

BnO-G5-(OH)₃₂¹⁶

A 100 mL round-bottomed flask equipped with a magnetic stir bar was charged with BnO-G5-(acet)₁₆ (400 mg, 0.092 mmol) dissolved in 25 mL of EtOH, then 1 scoopula full of DOWEX beads was added and the mixture was stirred for overnight at room temperature. This was filtered through a glass frit to recover the DOWEX, and the filtrate was dried by rotary evaporation then *in vacuo* overnight to give the product as a white powder (329 mg, 97%). ¹H NMR (600 MHz, MeOD) δ 7.49 – 7.35 (m, 5H), 5.26 (s, 2H), 4.45 – 4.22 (m,

60H), 3.70 (dd, $J = 10.9, 2.9$ Hz, 32H), 3.63 (d, $J = 10.8$ Hz, 32H), 1.36 – 1.26 (m, 45H), 1.17 (s, 48H).

2,2-dimethylpent-4-enoic Acid Periphery Dendrons (BnO-G_x-ene)

BnO-G1-(ene)₂

A 25 mL round-bottomed flask equipped with a magnetic stir bar was charged with 1,1'-carbonyldiimidazole (0.108 g, 0.669 mmol) suspended in 0.33 mL of EtOAc and heated to 50 °C. Compound **1** (87 mg, 0.682 mmol) was added dropwise and stirred for 1 hour. BnO-G1-(OH)₂ (50 mg, 0.223 mmol) was added, along with CsF (14 mg, 0.089 mmol). The reaction progress was monitored by TLC (~4 hours) and quenched with 0.1 mL of water. The reaction mixture was extracted with, 3 × 30 mL of 10% Na₂CO₃, 3 × 30 mL of 1 M H₃PO₄, 1 × 50 mL brine, dried over MgSO₄, filtered, and solvent was removed by rotary evaporation to give the crude product as a slightly yellow oil. The resulting material was purified by silica gel chromatography using a 12-gram silica gel column equilibrated in 2% acetone:hexanes, then eluted using a gradient from 2% to 20% acetone:hexanes over 20 column volumes and monitored at 205 nm. The fractions containing product were pooled and solvent was removed by rotary evaporation and the resulting oil was dried *in vacuo* to give the product as a clear, colourless oil (73 mg, 74%). ¹H NMR (600 MHz; CDCl₃): δ 7.37-7.31 (m, 5H), 5.66 (ddt, $J = 17.0, 10.1, 7.2$, 2H), 5.15 (s, 2H), 5.04-4.99 (m, 4H), 4.24-4.20 (m, 4H), 2.21 (d, $J = 7.4$, 4H), 1.28 (s, 3H), 1.11 (d, $J = 1.5$, 12H). ¹³C NMR (176 MHz; CDCl₃): δ 176.9, 172.7, 135.6, 134.0, 128.8, 128.5, 128.3, 118.3, 67.0, 65.6, 46.7, 44.7, 42.6, 24.8, 18.1. MALDI: [M]_{calc}: 444.3 Da [M+Na]⁺_{found}: 466.5 Da.

BnO-G2-(ene)₄

A 25 mL round-bottomed flask equipped with a magnetic stir bar was charged with 1,1'-carbonyldiimidazole (0.108 g, 0.669 mmol) suspended in 0.33 mL of EtOAc and heated to 50 °C. Compound **1** (87 mg, 0.682 mmol) was added dropwise and stirred for 1 hour. BnO-G1-(OH)₂ (0.050 g, 0.223 mmol) and CsF (0.014 g, 0.089 mmol) was added in a single portion. The reaction progress was monitored by TLC (~5 hours) and then quenched by the addition of 0.1 mL of water. The reaction mixture was then extracted with, 3 × 30 mL of 10% Na₂CO₃, 3 × 30 mL of 1 M H₃PO₄, 1 × 50 mL brine, dried over MgSO₄, filtered, and solvent was removed by rotary evaporation to give the crude product as a slightly yellow oil. The resulting material was purified by silica gel chromatography using a 10-gram silica gel column equilibrated in 2% acetone:hexanes, then eluted using a gradient from 2% to 20% acetone:hexanes over 20 column volumes and monitored at 205 nm. The fractions containing product were pooled and solvent was removed by rotary evaporation and the resulting oil was dried *in vacuo* to give the product as a clear, colourless oil (73 mg, 74%). ¹H NMR (600 MHz; CDCl₃): δ 7.37-7.31 (m, 5H), 5.67 (ddt, *J* = 17.0, 10.0, 7.2, 4H), 5.16 (s, 2H), 5.04-5.01 (m, 8H), 4.30-4.22 (m, 4H), 4.17 (dd, *J* = 11.0, 8.7, 4H), 4.11 (dd, *J* = 11.1, 6.3, 4H), 2.24 (d, *J* = 7.3, 8H), 1.26 (s, 3H), 1.16 (s, 6H), 1.14 (s, 24H). ¹³C NMR (176 MHz; CDCl₃): δ 176.8, 172.1, 135.5, 134.0, 128.83, 128.66, 128.56, 118.3, 67.4, 66.2, 65.2, 46.85, 46.66, 44.7, 42.6, 24.9, 17.90, 17.75. MALDI: [M]_{calc}: 897.5 Da [M+Na]⁺_{found}: 920.3 Da.

BnO-G3-(ene)₈

A 25 mL round-bottomed flask equipped with a magnetic stir bar was charged with 1,1'-carbonyldiimidazole (0.106 g, 0.652 mmol) suspended in 0.33 mL of EtOAc and heated to

50 °C. Compound **1** (85 mg, 0.665 mmol) was added dropwise and stirred for 1 hour. BnO-G3-(OH)₁₆ (0.050 g, 0.0543 mmol) and CsF (0.013 g, 0.087 mmol) was added in a single portion. The reaction progress was monitored by MALDI (~6 hours) and then quenched by the addition of 1 mL of water. The reaction mixture was then extracted with 3 × 30 mL of 1 M H₃PO₄, 3 × 30 mL of 10% Na₂CO₃, 1 × 50 mL brine, dried over MgSO₄, filtered, and solvent was removed by rotary evaporation to give the product as a clear, colourless oil. (60 mg, 51 %). ¹H NMR (700 MHz; CDCl₃): δ 7.37-7.30 (m, 5H), 5.67 (ddt, *J* = 17.0, 10.1, 7.1, 8H), 5.15 (s, 2H), 5.04-5.01 (m, 16H), 4.31 (d, *J* = 11.0, 2H), 4.23-4.13 (m, 26H), 2.24 (d, *J* = 7.3, 16H), 1.29 (s, 3H), 1.23 (s, 12H), 1.16 (s, 6H), 1.14 (s, 48H). ¹³C NMR (176 MHz; CDCl₃): δ 176.7, 172.05, 171.89, 171.5, 135.5, 134.0, 128.82, 128.64, 128.49, 118.3, 67.3, 66.5, 65.6, 65.1, 46.90, 46.81, 46.66, 44.7, 42.6, 24.9, 18.0, 17.65, 17.55. [M]_{calc}: 1802.2 Da [M+Na]⁺_{found}: 1824.8 Da.

BnO-G4-(ene)₁₆

A 25 mL round-bottomed flask equipped with a magnetic stir bar was charged with 1,1'-carbonyldiimidazole (0.110 g, 0.681 mmol) dissolved in 0.3 mL of EtOAc and heated to 50 °C. Compound **1** (0.089 g, 0.694 mmol) was added dropwise and stirred for 1 hour. BnO-G4-(OH)₁₆ (0.050 g, 0.027 mmol) was added, along with CsF (0.013 g, 0.087 mmol). The reaction mixture was stirred for 12 hours, until MALDI showed complete conversion and then quenched by the addition of 0.1 mL of water. The reaction mixture was then extracted with 3 × 30 mL of 1 M H₃PO₄, 3 × 30 mL of 10% Na₂CO₃, 1 × 50 mL brine, dried over MgSO₄, filtered, and solvent was removed by rotary evaporation to give the crude product as a clear, colourless oil. This was then purified by flash chromatography in

a 12-gram silica gel column using a gradient of 5% to 30% acetone in hexanes over 20 column volumes, with UV monitoring at 205 nm. The fractions containing product were pooled and solvent was removed by rotary evaporation, then dried *in vacuo* overnight to give the product as a clear, colourless oil. (36 mg, 37%). ¹H NMR (600 MHz; CDCl₃): δ 7.35-7.34 (m, 4H), 7.33-7.31 (m, 1H), 5.70-5.63 (m, 16H), 5.15 (s, 2H), 5.04 (d, *J* = 1.1, 16H), 5.02-5.00 (m, 16H), 4.33 (d, *J* = 10.9, 2H), 4.26-4.13 (m, 58H), 2.24 (d, *J* = 7.3, 32H), 1.31 (s, 3H), 1.23 (s, 36H), 1.19 (s, 6H), 1.14 (s, 96H). ¹³C NMR (176 MHz; CDCl₃): δ 176.7, 172.05, 171.86, 171.44, 171.36, 135.6, 134.0, 128.8, 128.6, 128.4, 118.3, 67.3, 67.0, 65.8, 65.5, 65.0, 47.0, 46.80, 46.65, 18.0, 17.65, 17.52, 17.47. [M]_{calc}: 3609.9 Da [M+Na]⁺_{found}: 3635.2 Da.

BnO-G5-(ene)₃₂

A 25 mL round-bottomed flask equipped with a magnetic stir bar was charged with compound **1** (0.177 g, 1.381 mmol) dissolved in 0.5 mL of EtOAc at 50 °C, then 1,1'-carbonyldiimidazole (0.220 g, 1.359 mmol) was added and the reaction mixture vigorously bubbled off carbon dioxide. After 30 minutes, BnO-G5-(OH)₃₂ (0.050g, 0.0135 mmol) and CsF (0.013 g, 0.086 mmol) was added in a single portion. The reaction mixture was stirred overnight, at which point MALDI showed complete conversion, and the reaction was quenched by the addition of 1 mL of water. The reaction mixture was then extracted with 3 × 30 mL of 1 M H₃PO₄, 3 × 30 mL of 10% Na₂CO₃, 1 × 50 mL brine, dried over MgSO₄, filtered, and solvent was removed by rotary evaporation. The crude product was purified using a 10-gram silica gel column using a gradient from 5% to 30% acetone:hexanes over 20 column volumes, with monitoring at 205 nm. The fractions containing product were

pooled and solvent was removed by rotary evaporation and dried *in vacuo* overnight to give the product as a clear, colourless oil. (61 mg, 62%). ¹H NMR (600 MHz; CDCl₃): δ 7.35-7.31 (m, 5H), 5.67 (dq, *J* = 17.2, 8.6, 32H), 5.15 (d, *J* = 0.4, 2H), 5.03-5.00 (m, 64H), 4.36-4.13 (m, 124H), 2.24 (d, *J* = 7.2, 64H), 1.33 (s, 3H), 1.25 (s, 12H), 1.23 (s, 72H), 1.18 (s, 6H), 1.13 (s, 192H). ¹³C NMR (176 MHz; CDCl₃): δ 176.6, 172.0, 171.5, 134.0, 128.8, 128.4, 125.5, 121.9, 118.3, 65.3, 65.0, 46.79, 46.64, 44.7, 42.6, 24.9, 18.0, 17.69, 17.65, 17.4. [M]_{calc}: 7231.9 Da [M+CH₃OH]⁺_{found}: 7264.4 Da.

2,2-dimethylpent-4-ynoic Acid Periphery Dendrons (BnO-G_x-yne)

BnO-G1-(yne)₂

A 25 mL round-bottomed flask equipped with a magnetic stir bar was charged with 1,1'-carbonyldiimidazole (0.108 g, 0.669 mmol) suspended in 0.33 mL of EtOAc and heated to 50 °C. Compound **2** (86 mg, 0.682 mmol) was added dropwise and stirred for 1 hour. BnO-G1-(OH)₂ (0.050 g, 0.223 mmol) and CsF (0.014 g, 0.089 mmol) was added in a single portion. The reaction progress was monitored by MALDI (~1 hour) and then quenched by the addition of 1 mL of water. The reaction mixture was then extracted with 3 × 30 mL of 1 M H₃PO₄, 3 × 30 mL of 10% Na₂CO₃, 1 × 50 mL brine, dried over MgSO₄, filtered, and solvent was removed by rotary evaporation to give the crude product as a clear, colourless oil. This was then purified by flash chromatography in a 12-gram silica gel column using a gradient of 5% to 30% acetone in hexanes over 20 column volumes, with UV monitoring at 205 nm. The fractions containing product were pooled and solvent was removed by rotary evaporation, then dried *in vacuo* overnight to give the product as a clear, colourless oil (88 mg, 90%). ¹H NMR (600 MHz; CDCl₃): δ 7.37-7.31 (m, 5H), 5.16 (s, 2H), 4.29-

4.25 (m, 4H), 2.35 (d, $J = 2.6$, 4H), 1.29 (s, 3H), 1.21 (d, $J = 1.9$, 12H). ^{13}C NMR (176 MHz; CDCl_3): δ 175.9, 172.6, 135.6, 128.8, 128.6, 128.4, 80.9, 70.8, 67.1, 65.8, 46.7, 42.4, 29.6, 24.6, 18.0. $[\text{M}]_{\text{calc}}$: 440.2 Da $[\text{M}+\text{Na}]^+_{\text{found}}$: 462.4 Da.

BnO-G2-(yne)₄

A 25 mL round-bottomed flask equipped with a magnetic stir bar was charged with 1,1'-carbonyldiimidazole (0.213 g, 0.876 mmol) suspended in 0.66 mL of EtOAc and heated to 50 °C. Compound **2** (167 mg, 0.889 mmol) was added dropwise and stirred for 1 hour. BnO-G2-(OH)₄ (0.050 g, 0.223 mmol) and CsF (0.013 g, 0.087 mmol) was added in a single portion. The reaction progress was monitored by MALDI (~3 hours) and then quenched by the addition of 1 mL of water. The reaction mixture was then extracted with 3 × 30 mL of 1 M H₃PO₄, 3 × 30 mL of 10% Na₂CO₃, 1 × 50 mL brine, dried over MgSO₄, filtered, and solvent was removed by rotary evaporation to give the crude product as a clear, colourless oil. This was then purified by flash chromatography in a 12-gram silica gel column using a gradient of 5-30% acetone in hexanes over 20 column volumes, with UV monitoring at 205 nm. The fractions containing product were pooled and solvent was removed by rotary evaporation, then dried *in vacuo* overnight to give the product as a clear, colourless oil (38 mg, 40 %). ^1H NMR (600 MHz; CDCl_3): δ 7.38-7.32 (m, 5H), 5.17 (s, 2H), 4.30 (d, $J = 11.0$, 2H), 4.23 (dt, $J = 11.0$, 7.3, 6H), 4.17 (dd, $J = 11.1$, 5.0, 4H), 2.40 (d, $J = 2.3$, 8H), 1.99 (t, $J = 2.5$, 4H), 1.27 (s, 3H), 1.25 (s, 23H), 1.19 (s, 6H). ^{13}C NMR (151 MHz, CDCl_3) δ 175.84, 172.07, 128.86, 128.71, 128.60, 80.92, 70.92, 67.38, 66.15, 65.32, 46.84, 46.72, 42.44, 29.65, 24.67, 17.86, 17.77. $[\text{M}]_{\text{calc}}$: 888.4 Da $[\text{M}+\text{Na}]^+_{\text{found}}$: 912.1 Da.

BnO-G3-(yne)₈

A 25 mL round-bottomed flask equipped with a magnetic stir bar was charged with 1,1'-carbonyldiimidazole (0.106 g, 0.652 mmol) suspended in 0.33 mL of EtOAc and heated to 50 °C. Compound **2** (84 mg, 0.652 mmol) was added dropwise and stirred for 1 hour. BnO-G3-(OH)₁₆ (0.050 g, 0.0543 mmol) and CsF (0.013 g, 0.087 mmol) was added in a single portion. The reaction progress was monitored by MALDI (~6 hours) and then quenched by the addition of 1 mL of water. The reaction mixture was then extracted with 3 × 30 mL of 1 M H₃PO₄, 3 × 30 mL of 10% Na₂CO₃, 1 × 50 mL brine, dried over MgSO₄, filtered, and solvent was removed by rotary evaporation to give the crude product as a clear, colourless oil. This was purified by flash chromatography in a 12-gram silica gel column using a gradient of 5% to 30% acetone in hexanes over 20 column volumes, with UV monitoring at 205 nm. The fractions containing product were pooled and solvent was removed by rotary evaporation, then dried *in vacuo* overnight to give the product as a clear, colourless oil (74 mg, 63%). ¹H NMR (700 MHz; CDCl₃): δ 7.40-7.34 (m, 5H), 5.19 (s, 2H), 4.35-4.22 (m, 28H), 2.42 (d, *J* = 2.5, 16H), 2.03 (t, *J* = 2.3, 8H), 1.33 (s, 3H), 1.28 (s, 12H), 1.27 (s, 48H), 1.20 (s, 6H). ¹³C NMR (176 MHz; CDCl₃): δ 175.8, 171.99, 171.92, 135.5, 128.83, 128.68, 128.50, 80.9, 71.0, 67.3, 66.5, 65.7, 65.3, 46.89, 46.81, 46.76, 46.72, 42.4, 29.6, 24.7, 18.0, 17.68, 17.56, 14.4. [M]_{calc}: 1785.9 Da [M+Na]⁺_{found}: 1808.1 Da.

BnO-G4-(yne)₁₆

A 25 mL round-bottomed flask equipped with a magnetic stir bar was charged with 1,1'-carbonyldiimidazole (0.110 g, 0.681 mmol) dissolved in 0.3 mL of EtOAc and heated to 50 °C. Compound **2** (0.088 g, 0.694 mmol) was added dropwise and stirred for 1 hour.

BnO-G4-(OH)₈ (0.050 g, 0.027 mmol) and CsF (0.013 g, 0.087 mmol) was added in a single portion and stirred for 12 hours and monitored by MALDI and then quenched by the addition of 0.1 mL of water. The reaction mixture was then extracted with 3 × 30 mL of 1 M H₃PO₄, 3 × 30 mL of 10% Na₂CO₃, 1 × 50 mL brine, dried over MgSO₄, filtered, and solvent was removed by rotary evaporation to give the crude product as a clear, colourless oil. This was then purified by flash chromatography in a 12-gram silica gel column using a gradient of 5% to 40% acetone in hexanes over 20 column volumes, with UV monitoring at 205 nm. The fractions containing product were pooled and solvent was removed by rotary evaporation, then dried *in vacuo* overnight to give the product as a clear, colourless oil. (48 mg, 49%). ¹H NMR (600 MHz; CDCl₃): δ 7.39 (d, *J* = 4.4, 4H), 7.36 (dt, *J* = 8.6, 3.8, 1H), 5.19 (s, 2H), 4.38-4.22 (m, 60H), 2.43 (d, *J* = 2.6, 32H), 2.04 (t, *J* = 2.6, 16H), 1.35 (s, 3H), 1.29 (s, 24H), 1.28 (s, 96H), 1.23 (s, 6H). ¹³C NMR (176 MHz; CDCl₃): δ 175.8, 172.0, 171.50, 171.43, 135.6, 128.85, 128.65, 128.4, 81.0, 71.0, 67.3, 66.9, 65.8, 65.5, 65.2, 46.82, 46.72, 42.4, 29.6, 18.0, 17.67, 17.56, 17.51. [M]_{calc}: 3579.7 Da [M+Na]⁺_{found}: 3601.8 Da.

BnO-G5-(yne)₃₂

A 25 mL round-bottomed flask equipped with a magnetic stir bar was charged with 1,1'-carbonyldiimidazole (0.138 g, 0.850 mmol) dissolved in 0.3 mL of EtOAc and heated to 50 °C. Compound **2** (0.107 g, 0.850 mmol) was added dropwise and stirred for 1 hour. BnO-G5-(OH)₈ (0.050 g, 0.014 mmol) and CsF (6.2 mg, 0.041 mmol) was added in a single portion and stirred for 12 hours and monitored by MALDI and then quenched by the addition of 0.1 mL of water. The reaction mixture was then extracted with 3 × 30 mL of 1

M H₃PO₄, 3 × 30 mL of 10% Na₂CO₃, 1 × 50 mL brine, dried over MgSO₄, filtered, and solvent was removed by rotary evaporation to give the crude product as a clear, colourless oil. This was then purified by flash chromatography in a 12-gram silica gel column using a gradient of 5% to 40% acetone in hexanes over 20 column volumes, with UV monitoring at 205 nm. The fractions containing product were pooled and solvent was removed by rotary evaporation, then dried *in vacuo* overnight to give the product as a clear, colourless oil. (58 mg, 60%). ¹H NMR (600 MHz, CDCl₃) δ 7.42 – 7.30 (m, 5H), 5.17 (s, 2H), 4.41 – 4.09 (m, 124H), 2.40 (d, *J* = 2.7 Hz, 64H), 2.03 (t, *J* = 2.7 Hz, 32H), 1.25-1.27 (m, 285H). ¹³C NMR (151 MHz, CDCl₃) δ 175.60, 171.93, 171.89, 171.41, 171.32, 128.75, 128.30, 80.84, 80.81, 70.95, 65.27, 65.05, 46.67, 46.64, 46.60, 46.57, 42.27, 30.93, 29.48, 24.54, 17.86, 17.72, 17.56, 17.53, 17.29. [M]_{calc}: 7167.4 Da [M+Na]⁺_{found}: 7192.5 Da.

5-azido-2,2-dimethylpentanoic acid Periphery Dendrons (BnO-G_x-N₃)

BnO-G1-(N₃)₂

A 25 mL round-bottomed flask equipped with a magnetic stir bar was charged with 1,1'-carbonyldiimidazole (0.108 g, 0.669 mmol) suspended in 0.33 mL of EtOAc and heated to 50 °C. Compound **3** (117 mg, 0.682 mmol) was added dropwise and stirred for 1 hour. BnO-G3-(OH)₈ (0.050 g, 0.2230 mmol) and CsF (0.014 g, 0.0892 mmol) was added in a single portion. The reaction mixture was stirred until TLC showed complete conversion (~6 hours) and then quenched by the addition of 0.1 mL of water. The reaction mixture was then extracted with 3 × 30 mL of 10% Na₂CO₃, 3 × 30 mL of 1 M H₃PO₄, 1 × 50 mL brine, dried over MgSO₄, filtered, and solvent was removed by rotary evaporation to give the crude product as a clear, colourless oil. This was then purified by flash chromatography in

a 12-gram silica gel column using a gradient of 5% to 30% acetone in hexanes over 20 column volumes, with UV monitoring at 205 nm. The fractions containing product were pooled and solvent was removed by rotary evaporation, then dried *in vacuo* overnight to give the product as a clear, colourless oil (103 mg, 87%), ¹H NMR (600 MHz; CDCl₃): δ 7.37-7.33 (m, 5H), 5.16 (s, 2H), 4.25-4.20 (m, 4H), 3.22 (t, *J* = 6.5, 4H), 1.53 (dq, *J* = 10.8, 3.3, 4H), 1.50-1.46 (m, 4H), 1.29 (s, 3H), 1.12 (s, 12H). ¹³C NMR (176 MHz; CDCl₃): δ 176.9, 172.6, 135.6, 128.8, 128.6, 128.3, 67.1, 65.6, 51.8, 46.7, 42.3, 37.6, 25.2, 24.7, 18.0. [M]_{calc}: 530.3 Da [M+Na]⁺_{found}: 552.4 Da.

BnO-G2-(N₃)₄

A 25 mL round-bottomed flask equipped with a magnetic stir bar was charged with 1,1'-carbonyldiimidazole (0.107 g, 0.657 mmol) suspended in 0.33 mL of EtOAc and heated to 50 °C. Compound **3** (115 mg, 0.670 mmol) was added dropwise and stirred for 1 hour. BnO-G2-(OH)₄ (0.050 g, 0.223 mmol) and CsF (0.014 g, 0.0892 mmol) was added in a single portion. The reaction mixture was stirred until TLC showed complete conversion (~3 hours) and then quenched by the addition of 0.1 mL of water. The reaction mixture was then extracted with 3 × 30 mL of 10% Na₂CO₃, 3 × 30 mL of 1 M H₃PO₄, 1 × 50 mL brine, dried over MgSO₄, filtered, and solvent was removed by rotary evaporation to give the crude product as a clear, colourless oil. This was then purified by flash chromatography in a 12-gram silica gel column using a gradient of 5% to 30% acetone in hexanes over 20 column volumes, with UV monitoring at 205 nm. The fractions containing product were pooled and solvent was removed by rotary evaporation, then dried *in vacuo* overnight to

give the product as a clear, colourless oil (71 mg, 61%). ^1H NMR (600 MHz; CDCl_3): δ 7.41-7.36 (m, 5H), 5.19 (s, 2H), 4.33-4.25 (m, 4H), 4.21 (dd, $J = 11.0, 8.7$, 4H), 4.13 (dd, $J = 11.0, 6.8$, 4H), 3.28 (t, $J = 6.5$, 8H), 1.58 (q, $J = 3.8$, 9H), 1.55-1.50 (m, 8H), 1.31 (s, 3H), 1.20 (s, 6H), 1.19 (s, 24H). ^{13}C NMR (176 MHz; CDCl_3): δ 176.8, 172.0, 135.5, 128.84, 128.68, 128.54, 67.4, 66.2, 65.1, 51.8, 46.85, 46.71, 42.3, 37.6, 25.2, 24.7, 17.81, 17.74. $[\text{M}]_{\text{calc}}$: 1068.6 Da $[\text{M}+\text{Na}]^+_{\text{found}}$: 1043.7 Da.

BnO-G3-(N₃)₈

A 25 mL round-bottomed flask equipped with a magnetic stir bar was charged with 1,1'-carbonyldiimidazole (0.106 g, 0.652 mmol) suspended in 0.33 mL of EtOAc and heated to 50 °C. Compound **3** (114 mg, 0.664 mmol) was added dropwise and stirred for 1 hour. BnO-G3-(OH)₈ (0.050 g, 0.0543 mmol) and CsF (0.013 g, 0.087 mmol) was added in a single portion. The reaction mixture was stirred until MALDI showed complete conversion (~6 hours) and then quenched by the addition of 1 mL of water. The reaction mixture was then extracted with 3 × 30 mL of 1 M H_3PO_4 , 3 × 30 mL of 10% Na_2CO_3 , 1 × 50 mL brine, dried over MgSO_4 , filtered, and solvent was removed by rotary evaporation to give the crude product as a clear, colourless oil. This was then purified by flash chromatography in a 12-gram silica gel column using a gradient of 5% to 30% acetone in hexanes over 20 column volumes, with UV monitoring at 205 nm. The fractions containing product were pooled and solvent was removed by rotary evaporation, then dried *in vacuo* overnight to give the product as a clear, colourless oil (74 mg, 63%). ^1H NMR (700 MHz; CDCl_3): δ 7.38-7.32 (m, 5H), 5.16 (s, 2H), 4.32 (d, $J = 11.0$, 2H), 4.24-4.19 (m, 18H), 4.14 (dd, $J = 11.1, 4.3$, 8H), 3.25 (t, $J = 6.6$, 16H), 1.58-1.55 (m, 16H), 1.53-1.48 (m, 16H), 1.30 (s, 3H),

1.24 (s, 12H), 1.18 (s, 6H), 1.16 (s, 48H). ¹³C NMR (176 MHz; CDCl₃): δ 176.7, 171.96, 171.89, 171.5, 128.83, 128.66, 128.4, 67.3, 66.6, 65.7, 65.0, 51.8, 46.91, 46.81, 46.71, 42.3, 37.6, 24.7, 17.9, 17.62, 17.53. [M]_{calc}: 2146.1 Da [M+Na]⁺_{found}: 2167.6 Da.

BnO-G4-(N₃)₁₆

A 25 mL round-bottomed flask equipped with a magnetic stir bar was charged with 1,1'-carbonyldiimidazole (0.110 g, 0.681 mmol) dissolved in 0.3 mL of EtOAc and heated to 50 °C. Compound **2** (0.088 g, 0.694 mmol) was added dropwise and stirred for 1 hour. BnO-G4-(OH)₁₆ (0.050 g, 0.027 mmol) and CsF (0.013 g, 0.087 mmol) was added in a single portion. The reaction mixture was stirred for 12 hours, until MALDI showed complete conversion and then quenched with 0.1 mL of water. The reaction mixture was then extracted with 3 × 30 mL of 1 M H₃PO₄, 3 × 30 mL of 10% Na₂CO₃, 1 × 50 mL brine, dried over MgSO₄, filtered, and solvent was removed by rotary evaporation to give the crude product as a clear, colourless oil. This was then purified by flash chromatography in a 12-gram silica gel column using a gradient of 5% to 40% acetone in hexanes over 20 column volumes, with UV monitoring at 205 nm. The fractions containing product were pooled and solvent was removed by rotary evaporation, then dried *in vacuo* overnight to give the product as a clear, colourless oil. (93 mg, 80%). ¹H NMR (600 MHz; CDCl₃): δ 7.35 (d, *J* = 4.4, 4H), 7.32 (dt, *J* = 8.2, 4.1, 1H), 5.16 (s, 2H), 4.34 (d, *J* = 10.9, 2H), 4.27-4.20 (m, 42H), 4.13 (dd, *J* = 11.0, 5.6, 16H), 3.25 (t, *J* = 6.6, 32H), 1.58-1.54 (m, 32H), 1.52-1.47 (m, 32H), 1.31 (s, 3H), 1.24 (d, *J* = 3.3, 36H), 1.19 (s, 6H), 1.16 (s, 96H). ¹³C NMR (176 MHz; CDCl₃): δ 176.7, 171.97, 171.87, 171.43, 171.37, 135.6, 128.8, 128.6,

128.4, 67.3, 67.0, 65.8, 65.4, 65.0, 51.8, 46.79, 46.68, 42.3, 37.5, 25.2, 24.7, 17.9, 17.6, 17.4. $[M]_{\text{calc}}$: 4300.2 Da $[M+Na]^+$ found: 4273.9 Da.

BnO-G5-(N₃)₃₂

A 25 mL round-bottomed flask equipped with a magnetic stir bar was charged with 1,1'-carbonyldiimidazole (0.214 g, 1.32 mmol) dissolved in 0.6 mL of EtOAc and heated to 50 °C. Compound **2** (0.222 g, 1.29 mmol) was added dropwise and stirred for 1 hour. BnO-G5-(OH)₃₂ (0.100 g, 0.027 mmol) and CsF (0.026 g, 0.173 mmol) was added in a single portion. The reaction mixture was stirred overnight at which point MALDI showed complete conversion, and the reaction was quenched by the addition of 0.1 mL of water. The reaction mixture was then extracted with 3 × 30 mL of 1 M H₃PO₄, 3 × 30 mL of 10% Na₂CO₃, 1 × 50 mL brine, dried over MgSO₄, filtered, and solvent was removed by rotary evaporation to give the crude product as a clear, colourless oil. The crude was purified by flash chromatography in a 12-gram silica gel column using a gradient of 5% to 40% acetone in hexanes over 20 column volumes, with UV monitoring at 205 nm. The fractions containing product were pooled and solvent was removed by rotary evaporation, then dried *in vacuo* overnight to give the product as a clear, colourless oil. (165 mg, 71%). ¹H NMR (600 MHz, CDCl₃) δ 7.41 – 7.29 (m, 5H), 5.16 (s, 2H), 4.42 – 3.96 (m, 124H), 3.25 (t, *J* = 6.7, 64H), 1.64 – 1.45 (m, 137H), 1.25 (s, 84H), 1.16 (s, 192H). ¹³C NMR (151 MHz, CDCl₃) δ 176.71, 172.00, 171.47, 171.40, 128.83, 128.39, 67.04, 65.80, 65.47, 64.99, 51.79, 47.05, 46.81, 46.71, 42.31, 37.57, 25.22, 24.74, 17.92, 17.64, 17.44. $[M]_{\text{calc}}$: 8608.4 Da $[M+H]^+$ found: 8500.3 Da.

BnO-G5-Lin-(N₃)₃₂ Linear Azide

A 25 mL round-bottomed flask equipped with a magnetic stir bar was charged with 1,1'-carbonyldiimidazole (0.308 g, 1.90 mmol) dissolved in 2 mL of EtOAc and heated to 50 °C. 5-azidovaleric acid (0.335 g, 1.96 mmol) was added dropwise and stirred for 1 hour. BnO-G5-(OH)₃₂ (0.145 g, 0.039 mmol) was added, along with CsF (0.038 g, 0.250 mmol). The reaction mixture was stirred for overnight and monitored by MALDI and then quenched by the addition of 0.1 mL of water. The reaction mixture was extracted with 3 × 30 mL of 1 M H₃PO₄, 3 × 30 mL of 10% Na₂CO₃, 1 × 50 mL brine, dried over MgSO₄, filtered, and solvent was removed by rotary evaporation to give the crude product as a clear, colourless oil. This was then purified by flash chromatography in a 12-gram silica gel column using a gradient of 5% to 40% acetone in hexanes over 20 column volumes, with UV monitoring at 205 nm. The fractions containing product were pooled and solvent was removed by rotary evaporation, then dried *in vacuo* overnight to give the product as a clear, colourless oil. (128 mg, 43%). ¹H NMR (600 MHz, CDCl₃) δ 7.36 (d, *J* = 4.3 Hz, 4H), 7.33 (m, 1H), 5.16 (s, 1H), 4.43 – 3.94 (m, 124H), 3.30 (t, *J* = 6.7, 64H), 2.36 (t, *J* = 6.7, 64H), 1.66 (m, 135H), 1.32 (s, 6H) 1.28 – 1.22 (m, 80H). ¹³C NMR (151 MHz, CDCl₃) δ 172.72, 172.16, 129.03, 128.32, 65.57, 65.12, 51.14, 48.83, 46.78, 46.52, 33.57, 33.47, 28.39, 28.37, 22.19, 22.12, 17.93, 17.73, 17.44.

Preparation of Amine Periphery Dendrons

BnO-G5-(Neo-NH₃⁺TFA⁻)₃₂

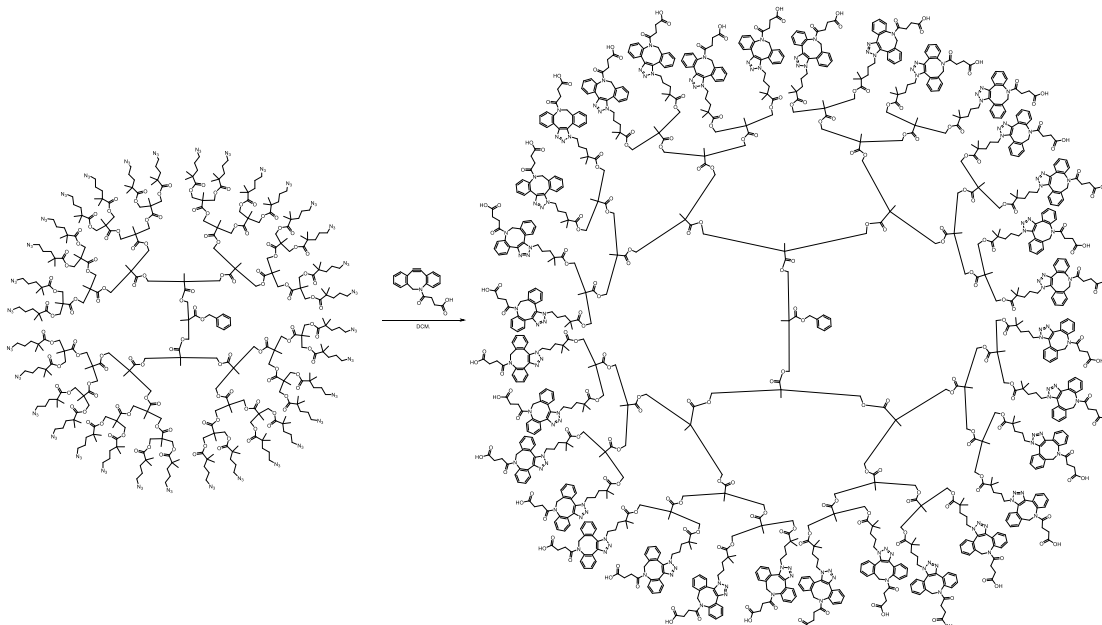
A 10 mL round-bottomed flask equipped with a magnetic stir bar was charged with BnO-G5-(N₃)₁₆ (13 mg, 1.5 μmol) dissolved in 1 mL of 1:1 DCM:MeOH, along with 40 μl of trifluoroacetic acid. Pd(OH)₂/C (12 mg) was added, and the reaction mixture was purged

and backfilled three times with hydrogen gas and was left to vigorously stir under a hydrogen atmosphere for overnight. The reaction mixture was then filtered through a 0.2 μm PTFE filter, solvent was removed by rotary evaporation and then dried *in vacuo* to give the product as a clear, colourless oil. (17 mg, 99%) ^1H NMR (600 MHz, D_2O , vs. NaHCOO^-) δ 4.27 (d, $J = 40.0$ Hz, 148H), 2.99 – 2.94 (m, 64H), 1.59 (s, 135H), 1.30 (s, 124H), 1.17 (s, 230H). ^{13}C NMR (151 MHz, D_2O , vs. NaHCOO^-) δ 179.19, 163.89, 163.66, 163.42, 163.19, 119.86, 117.93, 115.99, 114.06, 66.00, 47.25, 42.63, 40.16, 36.77, 24.96, 23.18, 17.83. $[\text{M}]_{\text{calc}}$: 7776.7 Da (neutral amine) $[\text{M}+\text{H}]_{\text{found}}$: 7702.5 Da.

BnO-G5-(Lin-NH₃⁺TFA⁻)₃₂

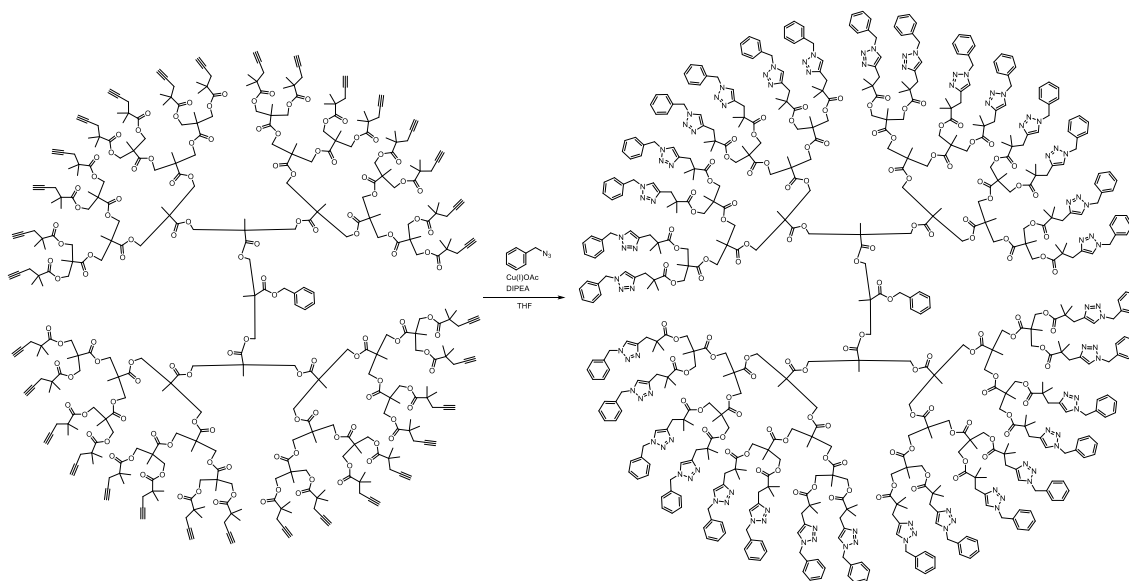
A 20 mL scintillation vial equipped with a magnetic stir bar was charged with BnO-G5-Lin-(N₃)₃₂ (22.5 mg, 2.92 μmol) dissolved 1 mL of 1:1 DCM:MeOH, along with 40 μL of trifluoroacetic acid. Pd(OH)₂/C (10 mg) was added, and the reaction mixture was purged and backfilled three times with hydrogen gas and was left to vigorously stir under a hydrogen atmosphere for overnight. The reaction mixture was then filtered through a 0.22 μm PTFE filter, solvent was removed by rotary evaporation and then dried *in vacuo* to give the product as a clear, colourless oil. (14.9 mg, 96%). ^1H NMR (600 MHz, D_2O) δ 4.27 (d, $J = 29.7$ Hz, 164H), 3.00 (t, $J = 7.1$ Hz, 64H), 2.45 (t, $J = 6.8$ Hz, 84H), 1.37 – 1.24 (m, 100H). ^{13}C NMR (151 MHz, D_2O) δ 174.78, 163.16, 162.92, 162.69, 162.45, 119.24, 117.31, 115.37, 113.43, 65.85, 65.35, 63.85, 57.73, 48.29, 46.58, 46.40, 39.03, 32.96, 32.90, 26.18, 21.12, 17.02, 16.65. $[\text{M}]_{\text{calc}}$: 10528.7 Da $[\text{M}+\text{H}]_{\text{found}}$: 11185.3 Da, $[\text{M}+2\text{H}]_{\text{found}}^{2+}$: 5626.5

Model Click Reactions



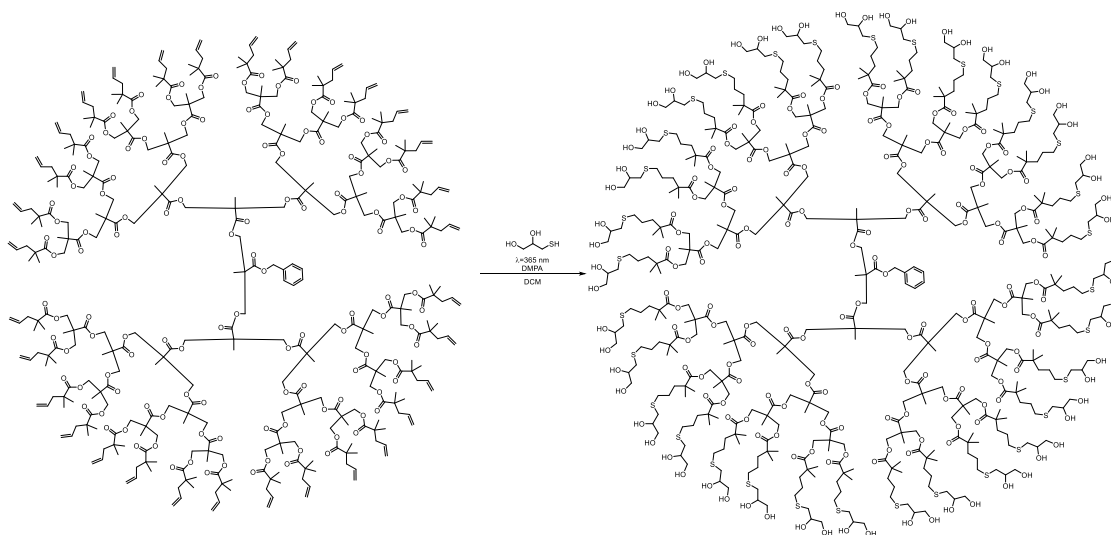
BnO-G5-(N₃)₃₂ SPAAC with DBCO-COOH (BnO-G5-(DBCO)₃₂)

In a 20 mL scintillation vial charged with a stir bar, BnO-G5-N₃ (13 mg, 1.51 μ mol) was dissolved in 1 mL DCM, DBCO-COOH (14.75 mg, 48.32 μ mol) was added in two portions between 2-minute intervals. The reaction was complete in 10 minutes by FTIR, and solvent was removed by rotary evaporator to yield BnO-G5-(DBCO)₃₂ as a white powder. (27 mg, 99%) ¹H NMR (600 MHz, CDCl₃) δ 7.74 – 7.33 (m, 166H), 7.24 – 6.93 (m, 116H), 4.30 (m, 223H), 2.51 – 0.96 (m, 605H). ¹³C NMR (151 MHz, CDCl₃) δ 177.08, 175.59, 172.15, 171.84, 170.72, 144.98, 142.61, 141.31, 140.18, 135.84, 134.61, 133.70, 132.62, 131.79, 131.49, 130.87, 129.89, 129.74, 129.58, 128.99, 128.49, 127.95, 127.55, 127.35, 124.48, 65.04, 53.04, 51.68, 49.69, 48.89, 46.78, 42.26, 42.20, 37.22, 36.52, 29.86, 29.58, 29.22, 28.55, 25.60, 25.02, 24.82, 17.91, 17.67, 17.37, 1.16. [M]_{calc}: 18374.0 Da [M+H]_{found}: 17534.8 Da, [M+2H]²⁺_{found}: 8889.1



BnO-G5-(yne)₃₂ CuAAC with Benzyl Azide (BnO-G5-(BzTr)₃₂)

In a 20 mL scintillation vial charged with a stir bar, BnO-G5-yne₃ (10 mg, 1.40 μ mol) was dissolved in 0.5 mL dry THF. Benzyl azide (7.3 μ l, 59 μ mol) and DIPEA (1.1 μ l, 5.8 μ mol) was added to the stirring mixture, followed by a 0.5 mL solution of Cu(I)OAc (274 μ g, 2.23 μ mol). The reaction was stirred vigorously at room temperature overnight. Solvent and excess benzyl azide was removed by rotary evaporator, and the crude was redissolved in 5 mL DCM and washed with 3 x 5 mL water. DCM was removed by rotary evaporator to yield BnO-G5-(BzTr)₃₂ as a greenish sticky solid (14.8 mg, 93%). ¹H NMR (600 MHz, CDCl₃) δ 7.43 – 7.27 (m, 76H), 7.16 (d, *J* = 7.0 Hz, 82H), 5.41 (s, 64H), 4.16 (m, 135H), 2.85 (s, 64H), 1.35 – 1.15 (m, 109H), 1.10 (s, 285H). ¹³C NMR (151 MHz, CDCl₃) δ 176.52, 172.10, 171.57, 144.38, 135.34, 129.11, 128.61, 127.98, 122.81, 65.07, 53.89, 46.69, 42.95, 35.86, 32.07, 30.25, 29.85, 25.01, 22.84, 17.81, 17.67, 14.27, 1.16. [M]_{calc}: 11426.4 Da [M+H]_{found}: 11418.1 Da.



BnO-G5-(ene)₃₂ thiol-ene click with 1-thioglycerol (BnO-G5-(SR)₃₂)

In a 1 mL tube, BnO-G5-yne₃ (10.6 mg, 1.47 μ mol), 1-thioglycerol (6.1 μ L, 70.35 μ mol) and DMPA (263 μ g, 1.03 μ mol) were dissolved in 0.1 mL acetonitrile. The mixture was irradiated with a handheld UV lamp at 365 nm for 30 minutes without stirring. The product partially precipitates out as an immiscible oil. Solvent and excess 1-thioglycerol was removed by rotary evaporator to yield a colourless oil (15.7 mg, 99%). [M]_{calc}: 10689.7 Da [M+H]_{found}: 10429.9 Da. ¹H NMR (600 MHz, MeOD) δ 7.63 – 7.24 (m, 5H), 5.25 (s, 2H), 4.37 – 4.17 (m, 128H), 3.74 (p, *J* = 5.8 Hz, 32H), 3.62 (dd, *J* = 11.2, 4.5 Hz, 32H), 3.54 (dd, *J* = 11.2, 5.9 Hz, 32H), 2.69 (dd, *J* = 13.5, 5.7 Hz, 32H), 2.60 – 2.54 (m, 90H), 1.67 – 1.61 (m, 64H), 1.57 – 1.48 (m, 64H), 1.33 (d, *J* = 7.4 Hz, 96H), 1.19 (s, 199H). ¹³C NMR (151 MHz, MeOD) δ 178.35, 173.55, 173.09, 72.87, 66.31, 66.09, 43.58, 43.52, 40.87, 36.47, 34.13, 26.49, 25.94, 18.72, 18.55. [M]_{calc}: 10689.7 Da [M+H]_{found}: 10429.9 Da.

Hydrolytic Stability Studies

pH Degradation Studies

Potassium phosphate buffers of pH 5.8, 7.4, and 8 were produced with D₂O as the solvent, and then individually spiked with sodium formate and then diluted with D₂O and pH adjusted with HCl/NaOH to produce a 0.1 M (as both buffer strength and standard) working solution. 500 μl of the corresponding solution was added to 7-10 mg of the dendron of interest in a glass NMR tube and incubated at 37 °C and monitored periodically by ¹H NMR. All qNMR spectra were obtained on a Bruker Avance AV600 at 600 MHz at room temperature. All hydrolysis NMR data were acquired with a 90° pulse, 30s relaxation delay (d1) and 20 spectral scans.

Tracking NMR Data

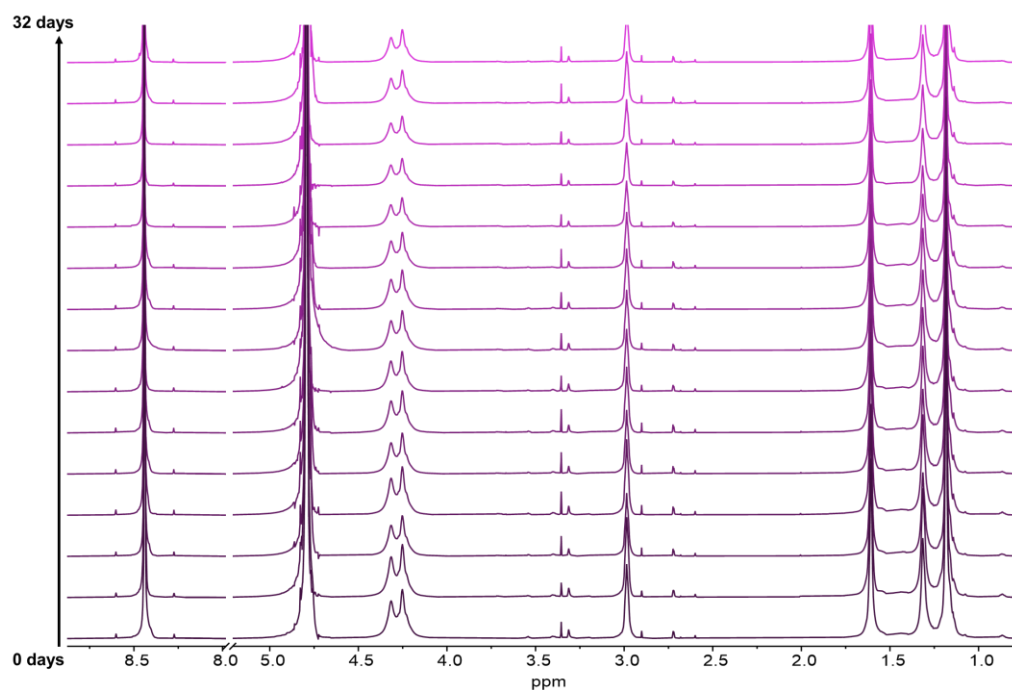


Figure S2.2. Tracking ¹H NMR of BnO-G5-(Neo-NH₃⁺TFA⁻)₃₂ in 0.1 M pH 5.8 potassium phosphate buffer.

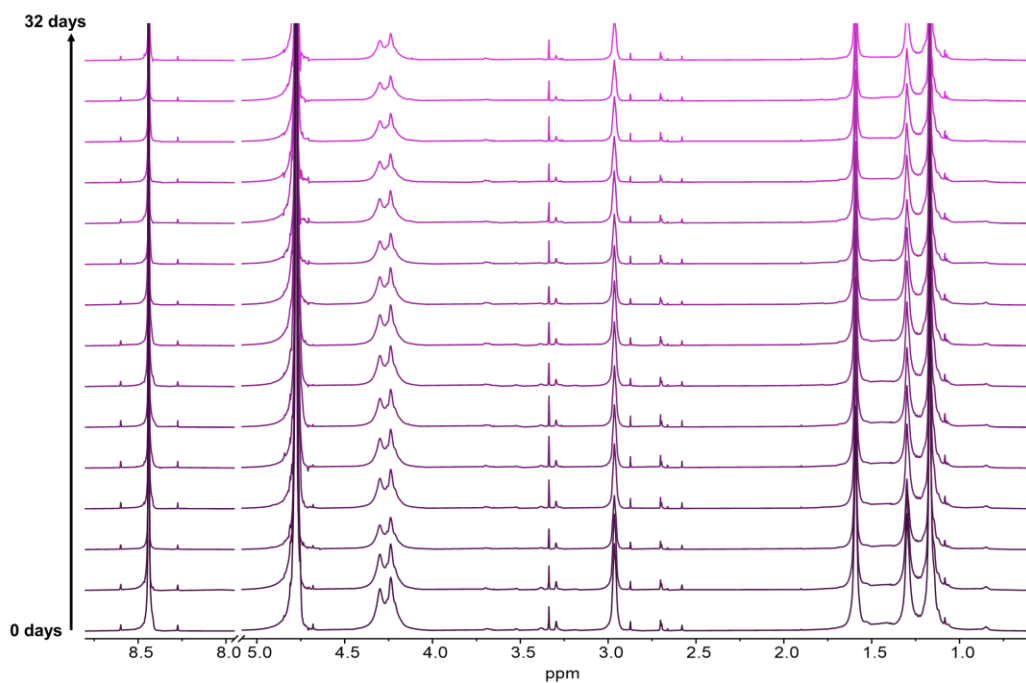


Figure S2.3. Tracking ¹H NMR of **BnO-G5-(Neo-NH₃⁺TFA⁻)₃₂** in 0.1 M pH 7.4 potassium phosphate buffer.

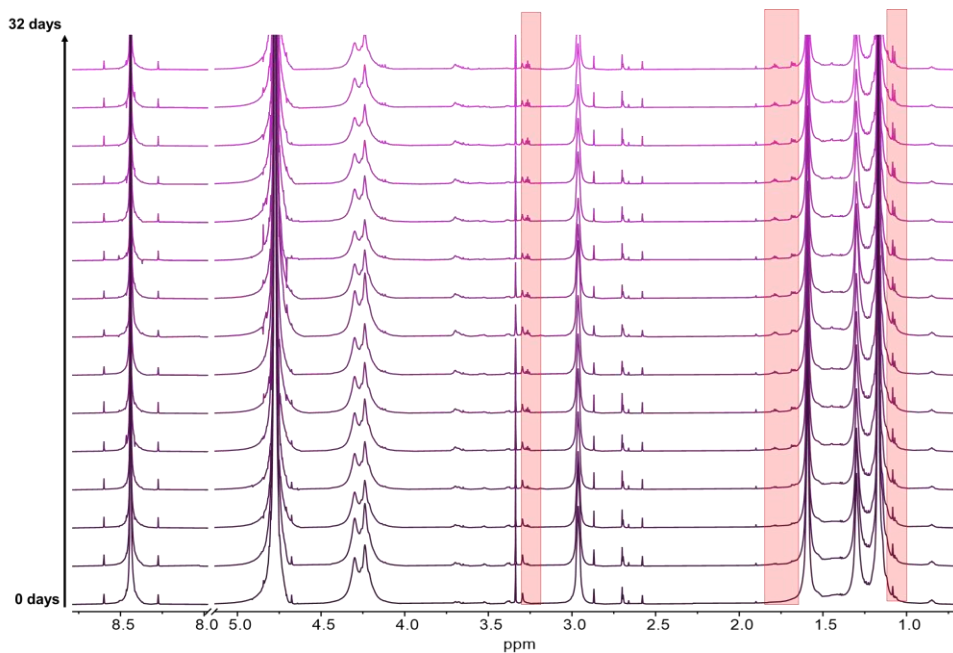


Figure S2.4. Tracking ¹H NMR of **BnO-G5-(Neo-NH₃⁺TFA⁻)₃₂** in 0.1 M pH 8 potassium phosphate buffer. Boxed signals are example degradation peaks from the amine and lactam.

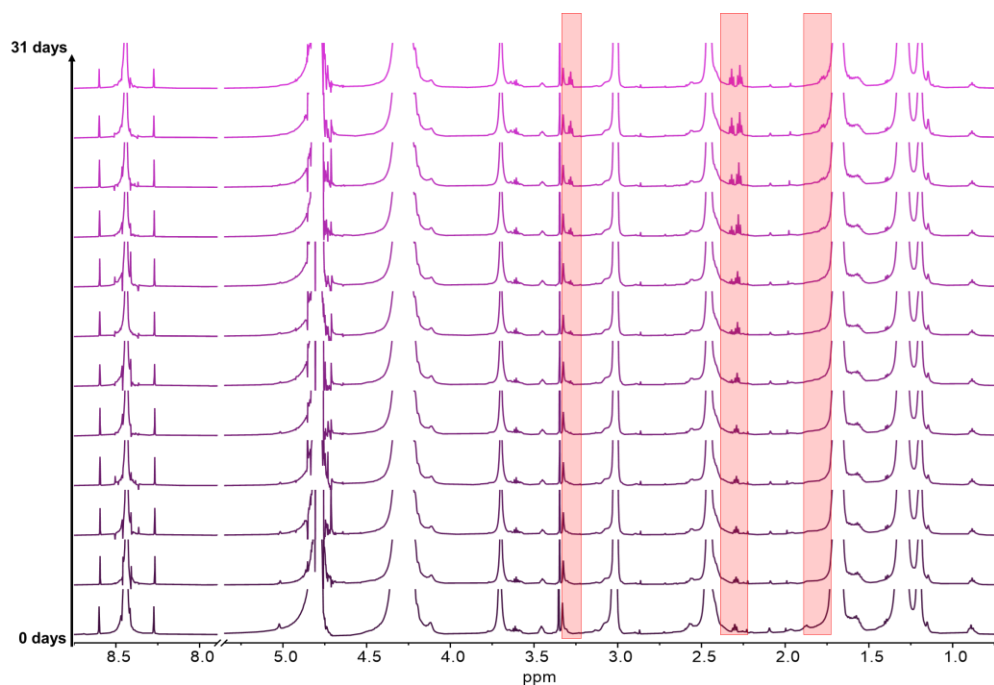


Figure S2.5. Tracking ^1H NMR of $\text{BnO-G5-(Lin-NH}_3^+\text{TFA}^-)_{32}$ in 0.1 M pH 5.8 potassium phosphate buffer. Boxed signals are example degradation peaks from the amine and lactam.

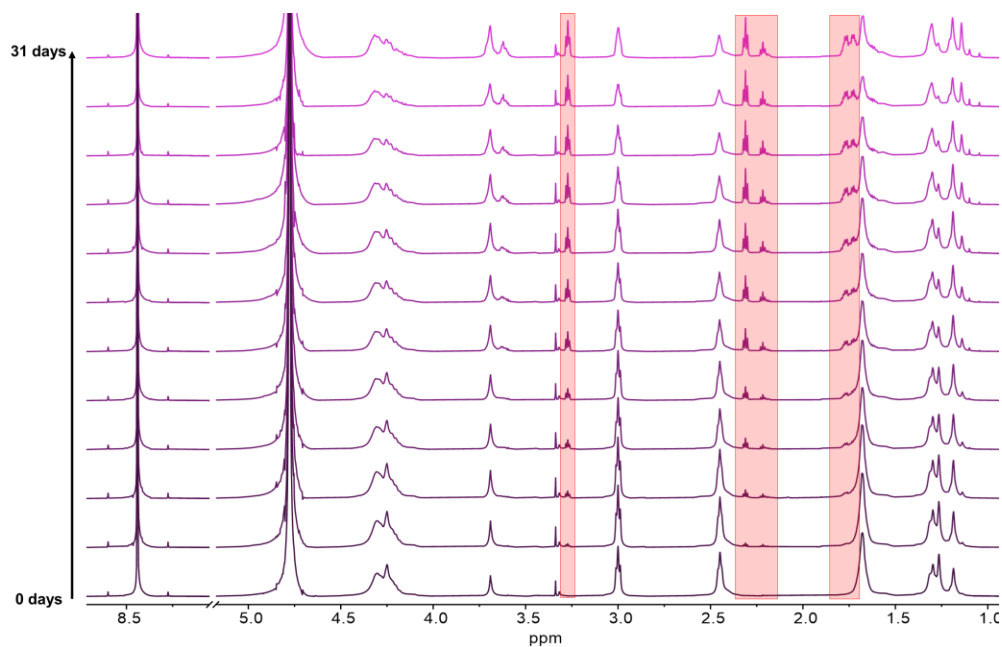


Figure S2.6. Tracking ^1H NMR of $\text{BnO-G5-(Lin-NH}_3^+\text{TFA}^-)_{32}$ in 0.1 M pH 7.4 potassium phosphate buffer. Boxed signals are example degradation peaks from the amine and lactam.

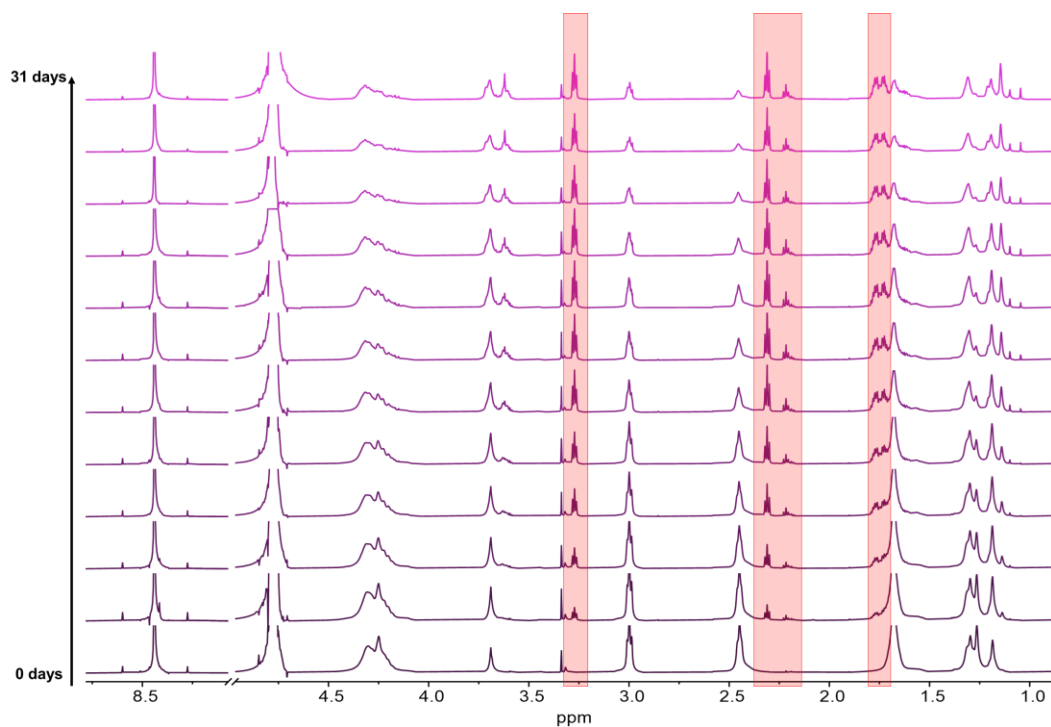


Figure S2.7. Tracking ¹H NMR of BnO-G5-(Lin-NH₃⁺TFA⁻)₃₂ in 0.1 M pH 8 potassium phosphate buffer. Boxed signals are example degradation peaks from the amine and lactam.

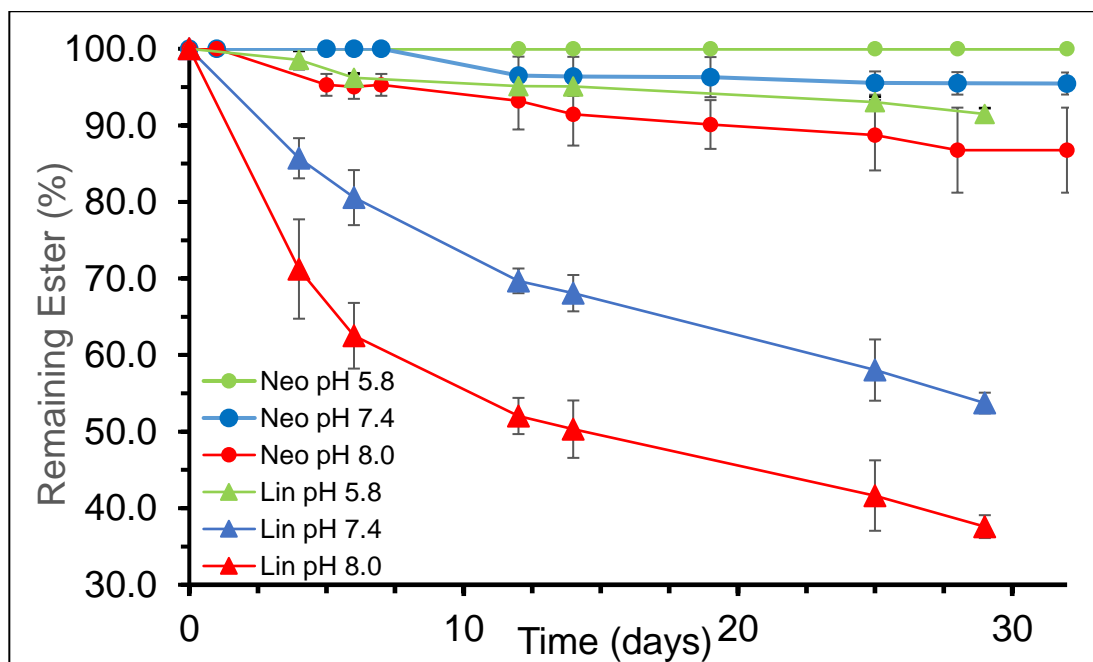


Figure S2.8. Compiled triplicate ¹H NMR measurements showing average % of intact dendrons over ~1 month.

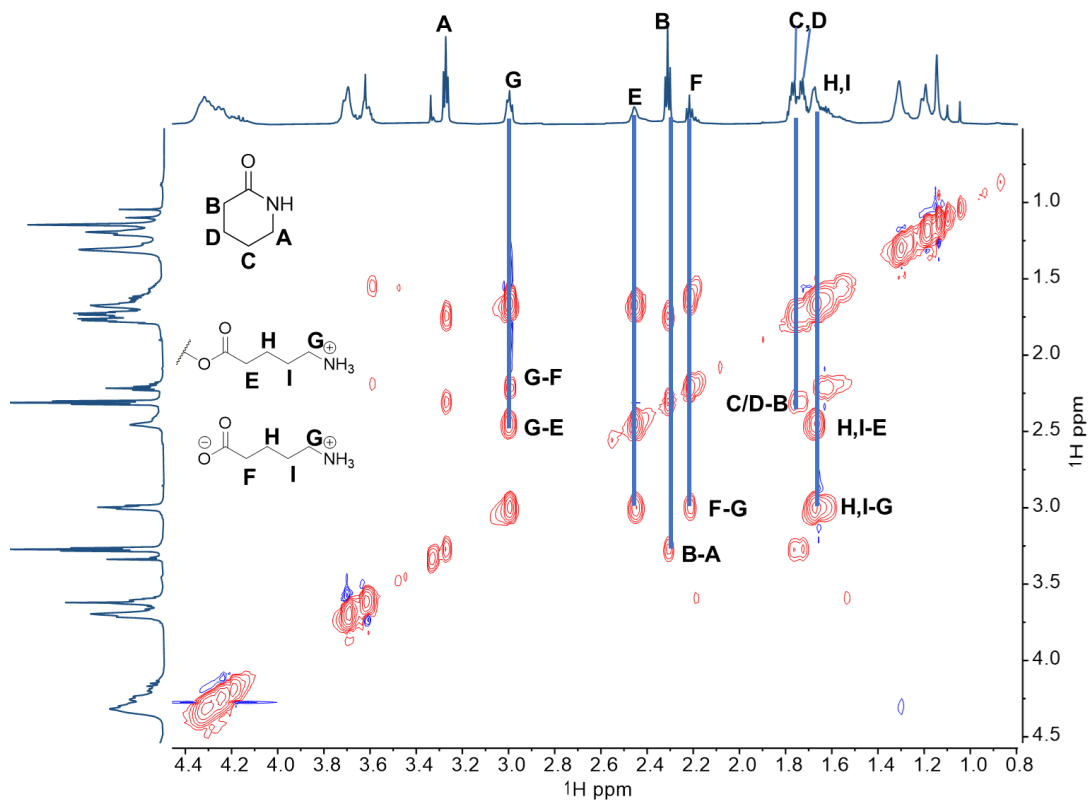


Figure S2.9. 2D TOCSY (D_2O) of **BnO-G5-(Lin-NH₃⁺TFA⁻)₃₂** in pH 8 buffer after 1 month.

Table S2.1. Tracking 1H NMR of **BnO-G5-(Lin-NH₃⁺TFA⁻)₃₂** in 0.1 M pH 5.8 potassium phosphate buffer, trial 1.

Linear Periphery, pH 5.8						
Time (days)	Dendron-bound amine (t, 2.45 ppm), (Int. vs. HCOONa)	Aminolysis; δ -valerolactam (t, 2.31 ppm; Int)	Hydrolysis; 5-aminovalerate (t, 2.2 ppm; Int)	5-aminovalerate as a (%) of total amines	Lactam as a (%) of total amines	Intact Amines (%)
0	0.48	0	0.00	0.0	0.0	100.0
4	0.48	0	0.00	0.0	0.0	100.0
6	0.49	0.01	0.01	2.0	2.0	96.1
12	0.49	0.01	0.02	3.8	1.9	94.2
14	0.49	0.01	0.02	3.8	1.9	94.2
25	0.49	0.02	0.02	3.8	3.8	92.5
29	0.49	0.02	0.03	5.6	3.7	90.7

Table S2.2. Tracking ^1H NMR of $\text{BnO-G5-(Lin-NH}_3^+\text{TFA}^-)_{32}$ in 0.1 M pH 5.8 potassium phosphate buffer, trial 2.

Linear Periphery, pH 5.8						
Time (days)	Dendron-bound amine (t, 2.45 ppm), (Int. vs. HCOONa)	Aminolysis; δ -valerolactam (t, 2.31 ppm; Int)	Hydrolysis; 5-aminovalerate (t, 2.2 ppm; Int)	5-aminovalerate as a (%) of total amines	Lactam as a (%) of total amines	Intact Amines (%)
0	0.62	0	0.00	0.0	0.0	100.0
4	0.66	0	0.01	1.5	0.0	98.5
6	0.64	0.01	0.01	1.5	1.5	97.0
12	0.65	0.01	0.02	2.9	1.5	95.6
14	0.64	0.01	0.02	3.0	1.5	95.5
25	0.63	0.02	0.02	3.0	3.0	94.0
29	0.62	0.03	0.03	4.4	4.4	91.2

Table S2.3. Tracking ^1H NMR of $\text{BnO-G5-(Lin-NH}_3^+\text{TFA}^-)_{32}$ in 0.1 M pH 5.8 potassium phosphate buffer, trial 3.

Linear Periphery, pH 5.8						
Time (days)	Dendron-bound amine (t, 2.45 ppm), (Int. vs. HCOONa)	Aminolysis; δ -valerolactam (t, 2.31 ppm; Int)	Hydrolysis; 5-aminovalerate (t, 2.2 ppm; Int)	5-aminovalerate as a (%) of total amines	Lactam as a (%) of total amines	Intact Amines (%)
0	0.66	0	0.00	0.0	0.0	100.0
4	0.67	0	0.02	2.9	0.0	97.1
6	0.65	0.01	0.02	2.9	1.5	95.6
12	0.64	0.01	0.02	3.0	1.5	95.5
14	0.64	0.01	0.02	3.0	1.5	95.5
25	0.63	0.02	0.03	4.4	2.9	92.6
29	0.62	0.02	0.03	4.5	3.0	92.5

Table S2.4. Tracking ^1H NMR of $\text{BnO-G5-(Neo-NH}_3^+\text{TFA}^-)_{32}$ in 0.1 M pH 5.8 potassium phosphate buffer, trial 1.

Neopentyl pH 5.8						
Time (days)	Dendron-bound amine (s, 2.96 ppm), (Int. vs. HCOONa)	Aminolysis; δ -valerolactam (t, 3.26 ppm; Int)	Hydrolysis; 5-aminovalerate (s, 1.6 ppm; Int)	5-aminovalerate as a (%) of total amines	Lactam as a (%) of total amines	Intact Amines (%)
0	0.34	0	0	0	0.0	100.0
1	0.35	0	0	0	0.0	100.0
5	0.35	0	0	0	0.0	100.0
6	0.35	0	0	0	0.0	100.0
7	0.35	0	0	0	0.0	100.0
12	0.35	0	0	0	0.0	100.0
14	0.36	0	0	0	0.0	100.0
19	0.35	0	0	0	0.0	100.0
25	0.35	0	0	0	0.0	100.0
28	0.35	0	0	0	0.0	100.0
32	0.35	0	0	0	0.0	100.0

Table S2.5. Tracking ^1H NMR of $\text{BnO-G5-(Neo-NH}_3^+\text{TFA}^-)_{32}$ in 0.1 M pH 5.8 potassium phosphate buffer, trial 2.

Neopentyl pH 5.8						
Time (days)	Dendron-bound amine (s, 2.96 ppm), (Int. vs. HCOONa)	Aminolysis; δ -valerolactam (t, 3.26 ppm; Int)	Hydrolysis; 5-aminovalerate (s, 1.6 ppm; Int)	5-aminovalerate as a (%) of total amines	Lactam as a (%) of total amines	Intact Amines (%)
0	0.17	0	0	0	0.0	100.0
1	0.18	0	0	0	0.0	100.0
5	0.18	0	0	0	0.0	100.0
6	0.17	0	0	0	0.0	100.0
7	0.17	0	0	0	0.0	100.0
12	0.17	0	0	0	0.0	100.0
14	0.18	0	0	0	0.0	100.0
19	0.17	0	0	0	0.0	100.0

25	0.18	0	0	0	0.0	100.0
28	0.17	0	0	0	0.0	100.0
32	0.18	0	0	0	0.0	100.0

Table S 2.6. Tracking ^1H NMR of **BnO-G5-(Neo-NH₃⁺TFA⁻)₃₂** in 0.1 M pH 5.8 potassium phosphate buffer, trial 3.

Neopentyl pH 5.8						
Time (days)	Dendron-bound amine (s, 2.96 ppm), (Int. vs. HCOONa)	Aminolysis; δ -valerolactam (t, 3.26 ppm; Int)	Hydrolysis; 5-aminovalerate (s, 1.6 ppm; Int)	5-aminovalerate as a (%) of total amines	Lactam as a (%) of total amines	Intact Amines (%)
0	0.18	0	0	0	0.0	100.0
1	0.19	0	0	0	0.0	100.0
5	0.2	0	0	0	0.0	100.0
6	0.19	0	0	0	0.0	100.0
7	0.2	0	0	0	0.0	100.0
12	0.2	0	0	0	0.0	100.0
14	0.19	0	0	0	0.0	100.0
19	0.19	0	0	0	0.0	100.0
25	0.2	0	0	0	0.0	100.0
28	0.2	0	0	0	0.0	100.0
32	0.2	0	0	0	0.0	100.0

Table S2.7. Tracking ^1H NMR of **BnO-G5-(Lin-NH₃⁺TFA⁻)₃₂** in 0.1 M pH 7.4 potassium phosphate buffer, trial 1.

Linear Periphery, pH 7.4						
Time (days)	Dendron-bound amine (t, 2.45 ppm), (Int. vs. HCOONa)	Aminolysis; δ -valerolactam (t, 2.31 ppm; Int)	Hydrolysis; 5-aminovalerate (t, 2.2 ppm; Int)	5-aminovalerate as a (%) of total amines	Lactam as a (%) of total amines	Intact Amines (%)
0	0.53	0	0.00	0.00	0.0	100
4	0.5	0.03	0.03	5.36	5.4	89.3

6	0.47	0.05	0.03	5.45	9.1	85.5
12	0.41	0.1	0.06	10.53	17.5	71.9
14	0.4	0.1	0.06	10.71	17.9	71.4
25	0.35	0.13	0.07	12.73	23.6	63.6
29	0.3	0.16	0.08	14.81	29.6	55.6

Table S2.8. Tracking ^1H NMR of **BnO-G5-(Lin-NH₃⁺TFA⁻)₃₂** in 0.1 M pH 7.4 potassium phosphate buffer, trial 2.

Linear Periphery, pH 7.4						
Time (days)	Dendron-bound amine (t, 2.45 ppm), (Int. vs. HCOONa)	Aminolysis; δ -valerolactam (t, 2.31 ppm; Int)	Hydrolysis; 5-aminovalerate (t, 2.2 ppm; Int)	5-aminovalerate as a (%) of total amines	Lactam as a (%) of total amines	Intact Amines (%)
0	0.63	0	0.00	0.00	0.0	100
4	0.54	0.08	0.03	4.62	12.3	83.1
6	0.5	0.11	0.04	6.15	16.9	76.9
12	0.45	0.15	0.06	9.09	22.7	68.2
14	0.43	0.16	0.06	9.23	24.6	66.2
25	0.36	0.21	0.09	13.64	31.8	54.5
29	0.34	0.22	0.09	13.85	33.8	52.3

Table S2.9. Tracking ^1H NMR of **BnO-G5-(Lin-NH₃⁺TFA⁻)₃₂** in 0.1 M pH 7.4 potassium phosphate buffer, trial 3

Linear Periphery, pH 7.4						
Time (days)	Dendron-bound amine (t, 2.45 ppm), (Int. vs. HCOONa)	Aminolysis; δ -valerolactam (t, 2.31 ppm; Int)	Hydrolysis; 5-aminovalerate (t, 2.2 ppm; Int)	5-aminovalerate as a (%) of total amines	Lactam as a (%) of total amines	Intact Amines (%)
0	0.61	0	0.00	0.00	0.0	100

4	0.5	0.07	0.02	3.39	11.9	84.7
6	0.46	0.09	0.03	5.17	15.5	79.3
12	0.4	0.13	0.05	8.62	22.4	69.0
14	0.4	0.14	0.06	10.00	23.3	66.7
25	0.33	0.18	0.08	13.56	30.5	55.9
29	0.32	0.19	0.09	15.00	31.7	53.3

Table S2.10. Tracking ^1H NMR of **BnO-G5-(Neo-NH₃⁺TFA⁻)₃₂** in 0.1 M pH 7.4 potassium phosphate buffer, trial 1

Neopentyl Periphery pH 7.4						
Time (days)	Dendron-bound amine (s, 2.96 ppm), (Int. vs. HCOONa)	Aminolysis; δ -valerolactam (t, 3.26 ppm; Int)	Hydrolysis; 5-aminovalerate (s, 1.67 ppm; Int)	5-aminovalerate as a (%) of total amines	Lactam as a (%) of total amines	Intact Amines (%)
0	0.42	0	0	0.00	0.0	100.0
1	0.41	0	0	0.00	0.0	100.0
5	0.41	0	0	0.00	0.0	100.0
6	0.4	0	0	0.00	0.0	100.0
7	0.41	0	0	0.00	0.0	100.0
12	0.41	0	0	0.00	0.0	100.0
14	0.4	0	0	0.00	0.0	100.0
19	0.42	0	0	0.00	0.0	100.0
25	0.42	0.01	0	0.00	2.3	97.7
28	0.4	0.01	0	0.00	2.4	97.6
32	0.39	0.01	0	0.00	2.5	97.5

Table S2.11. Tracking ^1H NMR of **BnO-G5-(Neo-NH₃⁺TFA⁻)₃₂** in 0.1 M pH 7.4 potassium phosphate buffer, trial 2

Neopentyl Periphery pH 7.4						
Time (days)	Dendron-bound amine (s, 2.96 ppm), (Int. vs. HCOONa)	Aminolysis; δ -valerolactam (t, 3.26 ppm; Int)	Hydrolysis; 5-aminovalerate (s, 1.6 ppm; Int)	5-aminovalerate as a (%) of total amines	Lactam as a (%) of total amines	Intact Amines (%)

0	0.16	0	0	0	0.0	100.0
1	0.18	0	0	0	0.0	100.0
5	0.17	0	0	0	0.0	100.0
6	0.17	0	0	0	0.0	100.0
7	0.18	0	0	0	0.0	100.0
12	0.18	0.01	0	0	5.3	94.7
14	0.18	0.01	0	0	5.3	94.7
19	0.17	0.01	0	0	5.6	94.4
25	0.17	0.01	0	0	5.6	94.4
28	0.17	0.01	0	0	5.6	94.4
32	0.17	0.01	0	0	5.6	94.4

Table S2.12. Tracking ^1H NMR of **BnO-G5-(Neo-NH₃⁺TFA⁻)₃₂** in 0.1 M pH 7.4 potassium phosphate buffer, trial 3

Neopentyl Periphery pH 7.4						
Time (days)	Dendron-bound amine (s, 2.96 ppm), (Int. vs. HCOONa)	Aminolysis; δ -valerolactam (t, 3.26 ppm; Int)	Hydrolysis; 5-aminovalerate (s, 1.6 ppm; Int)	5-aminovalerate as a (%) of total amines	Lactam as a (%) of total amines	Intact Amines (%)
0	0.18	0	0	0.0	0.0	100.0
1	0.18	0	0	0.0	0.0	100.0
5	0.18	0	0	0.0	0.0	100.0
6	0.18	0	0	0.0	0.0	100.0
7	0.18	0	0	0.0	0.0	100.0
12	0.18	0.01	0	0.0	5.3	94.7
14	0.17	0.01	0	0.0	5.6	94.4
19	0.17	0.01	0	0.0	5.6	94.4
25	0.17	0.01	0	0.0	5.6	94.4
28	0.17	0.01	0	0.0	5.6	94.4
32	0.17	0.01	0	0.0	5.6	94.4

Table S2.13. Tracking ^1H NMR of **BnO-G5-(Lin-NH₃⁺TFA⁻)₃₂** in 0.1 M pH 8 potassium phosphate buffer, trial 1

Linear Periphery, pH 8.0

Time (days)	Dendron-bound amine (t, 2.45 ppm), (Int. vs. HCOONa)	Aminolysis; δ -valerolactam (t, 2.31 ppm; Int)	Hydrolysis; 5-aminovalerate (s, 1.6 ppm; Int)	5-aminovalerate as a (%) of total amines	Lactam as a (%) of total amines	Intact Amines (%)
0	0.61	0	0.00	0.00	0.0	100
4	0.41	0.17	0.04	6.45	27.4	66.1
6	0.37	0.21	0.05	7.94	33.3	58.7
12	0.30	0.24	0.06	10.00	40.0	50.0
14	0.31	0.27	0.08	12.12	40.9	47.0
25	0.24	0.30	0.09	14.29	47.6	38.1
29	0.22	0.3	0.09	14.75	49.2	36.1

Table S2.14. Tracking ^1H NMR of **BnO-G5-(Lin-NH₃⁺TFA⁻)₃₂** in 0.1 M pH 8 potassium phosphate buffer, trial 2

Linear Periphery, pH 8.0						
Time (days)	Dendron-bound amine (t, 2.45 ppm), (Int. vs. HCOONa)	Aminolysis; δ -valerolactam (t, 2.31 ppm; Int)	Hydrolysis; 5-aminovalerate (s, 1.6 ppm; Int)	5-aminovalerate as a (%) of total amines	Lactam as a (%) of total amines	Intact Amines (%)
0	0.49	0	0.00	0.00	0.0	100
4	0.41	0.07	0.03	5.88	13.7	80.4
6	0.37	0.12	0.05	9.26	22.2	68.5
12	0.31	0.18	0.07	12.50	32.1	55.4
14	0.3	0.17	0.07	12.96	31.5	55.6
25	0.26	0.2	0.08	14.81	37.0	48.1
29	0.21	0.23	0.09	16.98	43.4	39.6

Table S2.15. Tracking ^1H NMR of **BnO-G5-(Lin-NH₃⁺TFA⁻)₃₂** in 0.1 M pH 8 potassium phosphate buffer, trial 3

Linear Periphery, pH 8.0

Time (days)	Dendron-bound amine (t, 2.45 ppm), (Int. vs. HCOONa)	Aminolysis; δ -valerolactam (t, 2.31 ppm; Int)	Hydrolysis; 5-aminovalerate (s, 1.6 ppm; Int)	5-aminovalerate as a (%) of total amines	Lactam as a (%) of total amines	Intact Amines (%)
0	0.6	0	0.00	0.00	0.0	100
4	0.43	0.17	0.04	6.25	26.6	67.2
6	0.38	0.2	0.05	7.94	31.7	60.3
12	0.33	0.25	0.07	10.77	38.5	50.8
14	0.31	0.26	0.07	10.94	40.6	48.4
25	0.24	0.29	0.09	14.52	46.8	38.7
29	0.23	0.3	0.09	14.52	48.4	37.1

Table S2.16. Tracking ^1H NMR of **BnO-G5-(Neo-NH₃⁺TFA⁻)₃₂** in 0.1 M pH 8 potassium phosphate buffer, trial 1

Neopentyl Periphery pH 8						
Time (days)	Dendron-bound amine (s, 2.96 ppm), (Int. vs. HCOONa)	Aminolysis; δ -valerolactam (t, 3.26 ppm; Int)	Hydrolysis; 5-aminovalerate (s, 1.6 ppm; Int)	5-aminovalerate as a (%) of total amines	Lactam as a (%) of total amines	Intact Amines (%)
0	0.37	0	0	0	0.0	100.0
1	0.36	0	0	0	0.0	100.0
5	0.36	0.01	0	0	2.7	97.3
6	0.36	0.01	0	0	2.7	97.3
7	0.36	0.01	0	0	2.7	97.3
12	0.36	0.01	0	0	2.7	97.3
14	0.35	0.01	0	0	2.8	97.2
19	0.35	0.02	0	0	5.4	94.6
25	0.35	0.02	0	0	5.4	94.6
28	0.35	0.02	0	0	5.4	94.6
32	0.35	0.02	0	0	5.4	94.6

Table S2.17. Tracking ^1H NMR of **BnO-G5-(Neo-NH₃⁺TFA⁻)₃₂** in 0.1 M pH 8 potassium phosphate buffer, trial 2

Neopentyl Periphery pH 8						
Time (days)	Dendron-bound amine (s, 2.96 ppm), (Int. vs. HCOONa)	Aminolysis; δ -valerolactam (t, 3.26 ppm; Int)	Hydrolysis; 5-aminovalerate (s, 1.6 ppm; Int)	5-aminovalerate as a (%) of total amines	Lactam as a (%) of total amines	Intact Amines (%)
0	0.16	0	0	0	0.0	100.0
1	0.16	0	0	0	0.0	100.0
5	0.16	0.01	0	0	5.9	94.1
6	0.15	0.01	0	0	6.3	93.8
7	0.16	0.01	0	0	5.9	94.1
12	0.15	0.02	0	0	11.8	88.2
14	0.15	0.02	0	0	11.8	88.2
19	0.14	0.02	0	0	12.5	87.5
25	0.15	0.03	0	0	16.7	83.3
28	0.14	0.03	0	0	17.6	82.4
32	0.14	0.03	0	0	17.6	82.4

Table S2.18. Tracking ^1H NMR of **BnO-G5-(Neo-NH₃⁺TFA⁻)₃₂** in 0.1 M pH 8 potassium phosphate buffer, trial 3

Neopentyl Periphery pH 8						
Time (days)	Dendron-bound amine (s, 2.96 ppm), (Int. vs. HCOONa)	Aminolysis; δ -valerolactam (t, 3.26 ppm; Int)	Hydrolysis; 5-aminovalerate (s, 1.6 ppm; Int)	5-aminovalerate as a (%) of total amines	Lactam as a (%) of total amines	Intact Amines (%)
0	0.17	0	0	0.0	0.0	100.0
1	0.17	0	0	0.0	0.0	100.0
5	0.17	0.01	0	0.0	5.6	94.4
6	0.16	0.01	0	0.0	5.9	94.1
7	0.17	0.01	0	0.0	5.6	94.4
12	0.16	0.01	0	0.0	5.9	94.1
14	0.16	0.02	0	0.0	11.1	88.9

19	0.15	0.02	0	0.0	11.8	88.2
25	0.15	0.02	0	0.0	11.8	88.2
28	0.15	0.03	0	0.0	16.7	83.3
32	0.15	0.03	0	0.0	16.7	83.3

Esterase Degradation Studies

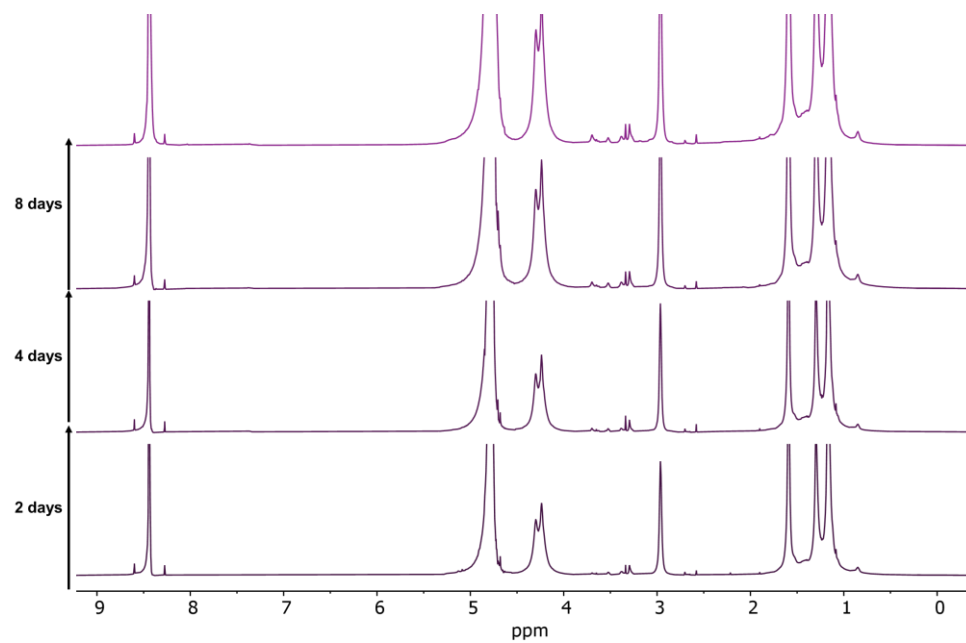


Figure S2.10. Tracking ¹H NMR of **BnO-G5-(Neo-NH₃⁺TFA⁻)₃₂** in 20% mol eq. (vs. amine group) esterase in 0.1 M pH 7.4 potassium phosphate buffer.

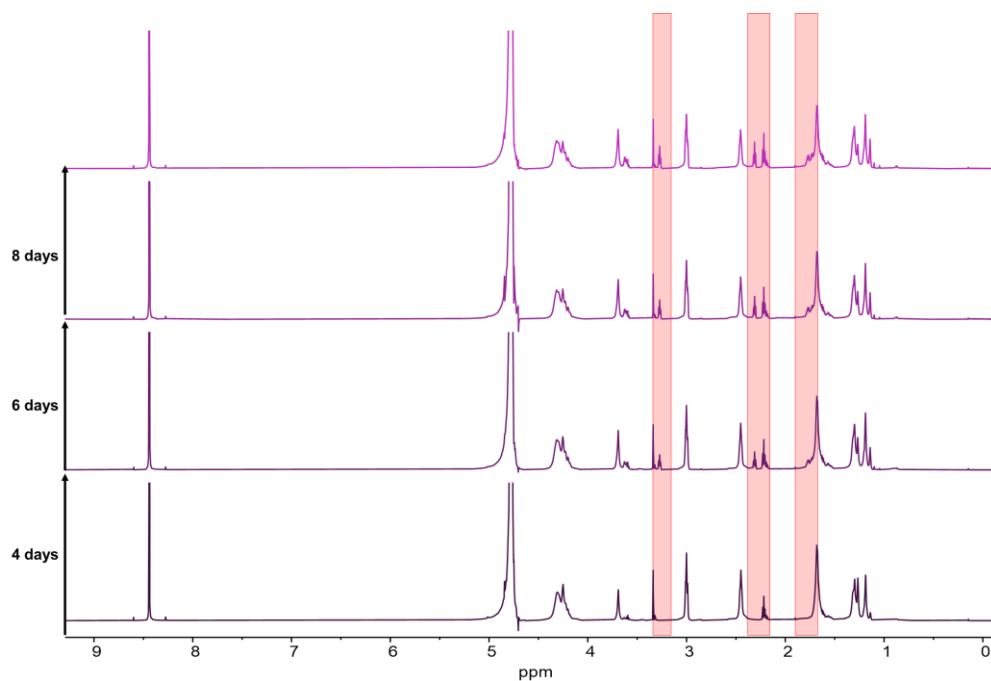


Figure S2.11. Tracking ^1H NMR of **BnO-G5-(Lin-NH₃⁺TFA⁻)₃₂** in 20% mol eq. (vs. amine group) esterase in 0.1 M pH 7.4 potassium phosphate buffer. Boxed signals are of the hydrolyzed ammonium-containing valeric acid.

Table S2.19. Tracking ^1H NMR of **BnO-G5-(Lin-NH₃⁺TFA⁻)₃₂** in 20% esterase in 0.1 M pH 7.4 potassium phosphate buffer, trial 1

Linear Periphery, esterase						
Time (days)	Dendron-bound amine (t, 2.45 ppm), (Int. vs. HCOONa)	Aminolysis; δ -valerolactam (t, 2.31 ppm; Int)	Hydrolysis; 5-aminovalerate (t, 2.2 ppm; Int)	5-aminovalerate as a (%) of total amines	Lactam as a (%) of total amines	Intact Amines (%)
0	0.75	0	0.00	0.0	0.0	100.0
4	0.62	0.1	0.05	6.5	13.0	80.5
6	0.58	0.12	0.05	6.7	16.0	77.3
8	0.54	0.14	0.05	6.8	19.2	74.0

Table S2.20. Tracking ^1H NMR of **BnO-G5-(Lin-NH₃⁺TFA⁻)₃₂** in 20% esterase in 0.1 M pH 7.4 potassium phosphate buffer, trial 2

Linear Periphery, esterase 2						
Time (days)	Dendron-bound amine (t, 2.45 ppm), (Int. vs. HCOONa)	Aminolysis; δ-valerolactam (t, 2.31 ppm; Int)	Hydrolysis; 5-aminovalerate (t, 2.2 ppm; Int)	5-aminovalerate as a (%) of total amines	Lactam as a (%) of total amines	Intact Amines (%)
0	0.91	0	0.00	0.0	0.0	100.0
4	0.84	0.1	0.05	5.1	10.1	84.8
6	0.80	0.14	0.08	7.8	13.7	78.4
8	0.77	0.14	0.07	7.1	14.3	78.6

Table S2.21. Tracking ^1H NMR of **BnO-G5-(Lin-NH₃⁺TFA⁻)₃₂** in 20% esterase in 0.1 M pH 7.4 potassium phosphate buffer, trial 3

Linear Periphery, esterase 3						
Time (days)	Dendron-bound amine (t, 2.45 ppm), (Int. vs. HCOONa)	Aminolysis; δ-valerolactam (t, 2.31 ppm; Int)	Hydrolysis; 5-aminovalerate (t, 2.2 ppm; Int)	5-aminovalerate as a (%) of total amines	Lactam as a (%) of total amines	Intact Amines (%)
0	0.79	0	0.00	0.0	0.0	100.0
4	0.69	0.1	0.05	6.0	11.9	82.1
6	0.65	0.15	0.07	8.0	17.2	74.7
8	0.63	0.15	0.07	8.2	17.6	74.1

Table S2.22. Tracking ^1H NMR of **BnO-G5-(Neo-NH₃⁺TFA⁻)₃₂** in 20% esterase in 0.1 M pH 7.4 potassium phosphate buffer, trial 1

Neopentyl Periphery, esterase 1						
Time (days)	Dendron-bound amine (s, 2.96 ppm), (Int. vs. HCOONa)	Aminolysis; δ -valerolactam (t, 3.26 ppm; Int)	Hydrolysis; 5-aminovalerate (s, 1.6 ppm; Int)	5-aminovalerate as a (%) of total amines	Lactam as a (%) of total amines	Intact Amines (%)
0	0.37	0	0	0	0.0	100.0
4	0.38	0	0	0	0.0	100.0
6	0.38	0	0	0	0.0	100.0
8	0.38	0	0	0	0.0	100.0

Table S2.23. Tracking ^1H NMR of **BnO-G5-(Neo-NH₃⁺TFA⁻)₃₂** in 20% esterase in 0.1 M pH 7.4 potassium phosphate buffer, trial 2

Neopentyl Periphery, esterase 2						
Time (days)	Dendron-bound amine (s, 2.96 ppm), (Int. vs. HCOONa)	Aminolysis; δ -valerolactam (t, 3.26 ppm; Int)	Hydrolysis; 5-aminovalerate (s, 1.6 ppm; Int)	5-aminovalerate as a (%) of total amines	Lactam as a (%) of total amines	Intact Amines (%)
0	0.16	0	0	0	0.0	100.0
4	0.17	0	0	0	0.0	100.0
6	0.17	0	0	0	0.0	100.0
8	0.17	0	0	0	0.0	100.0

Table S2.24. Tracking ^1H NMR of $\text{BnO-G5-(Neo-NH}_3^+\text{TFA}^-)_{32}$ in 20% esterase in 0.1 M pH 7.4 potassium phosphate buffer, trial 3

Neopentyl Periphery, esterase 3						
Time (days)	Dendron-bound amine (s, 2.96 ppm), (Int. vs. HCOONa)	Aminolysis; δ -valerolactam (t, 3.26 ppm; Int)	Hydrolysis; 5-aminovalerate (s, 1.6 ppm; Int)	5-aminovalerate as a (%) of total amines	Lactam as a (%) of total amines	Intact Amines (%)
0	0.18	0	0	0	0.0	100.0
4	0.17	0	0	0	0.0	100.0
6	0.18	0	0	0	0.0	100.0
8	0.16	0	0	0	0.0	100.0

Product NMR Spectra

Small Molecule NMR Data

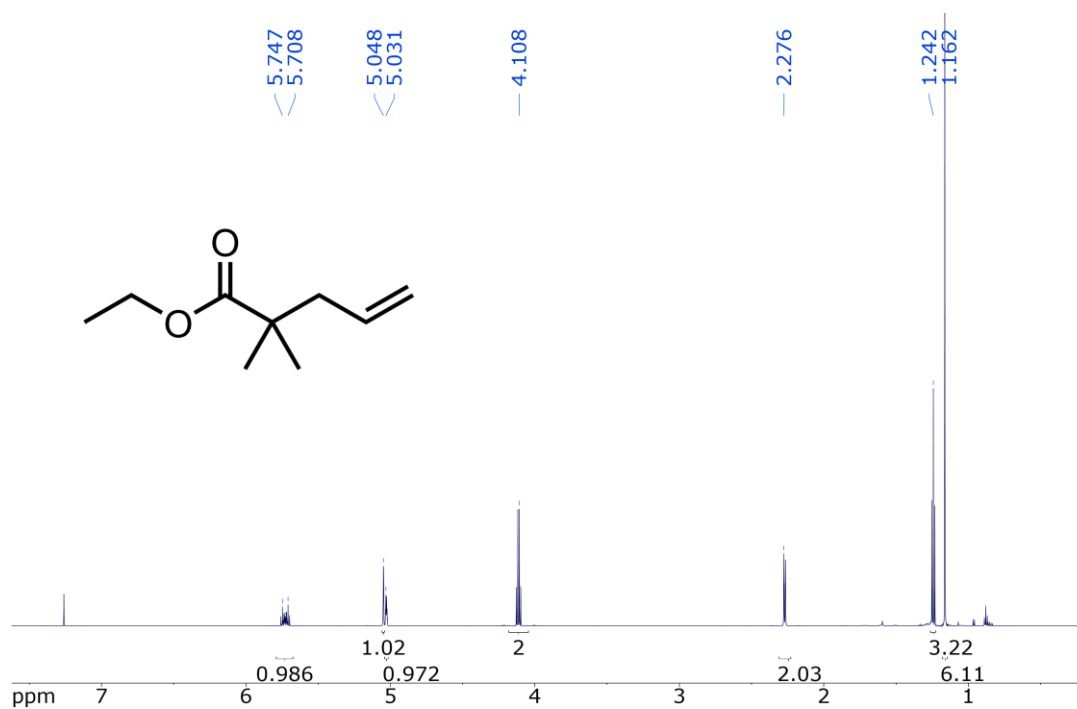


Figure S2.12. ^1H NMR spectrum of ethyl 2,2-dimethylpent-4-enoate in CDCl_3 .

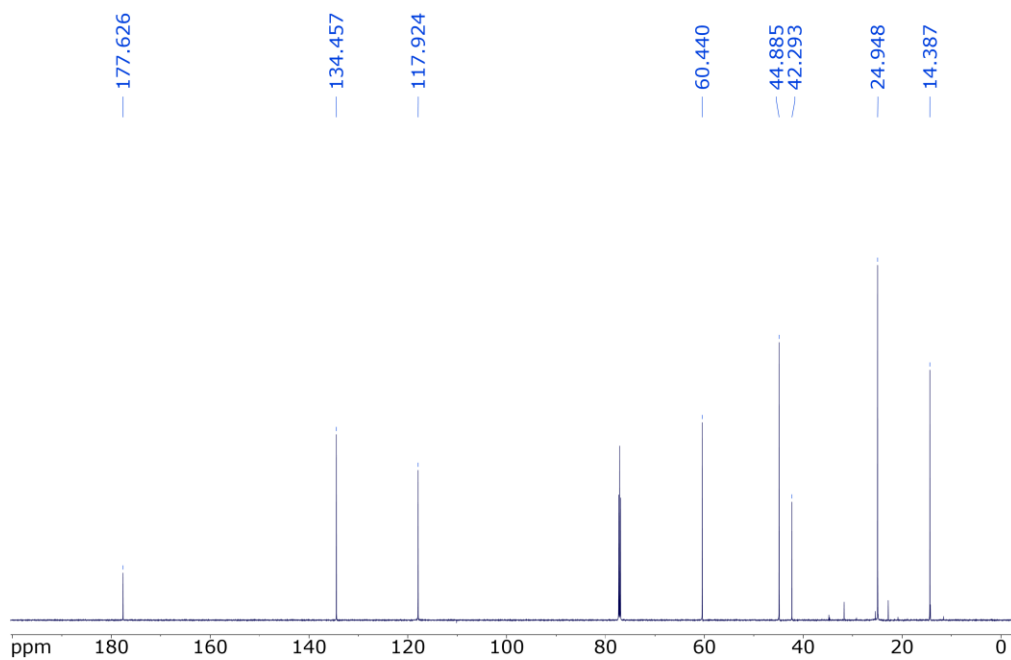


Figure S2.13. ^{13}C UDEFT NMR spectrum of ethyl 2,2-dimethylpent-4-enoate in CDCl_3 .

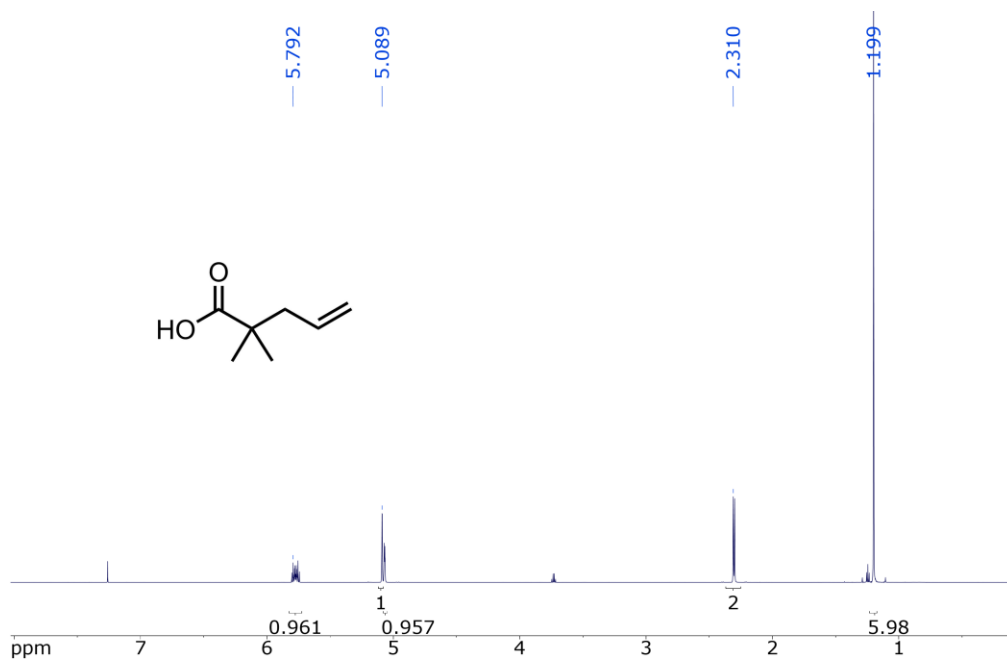


Figure S2.14. ^1H NMR spectrum of ethyl 2,2-dimethylpent-4-enoic acid in CDCl_3 .

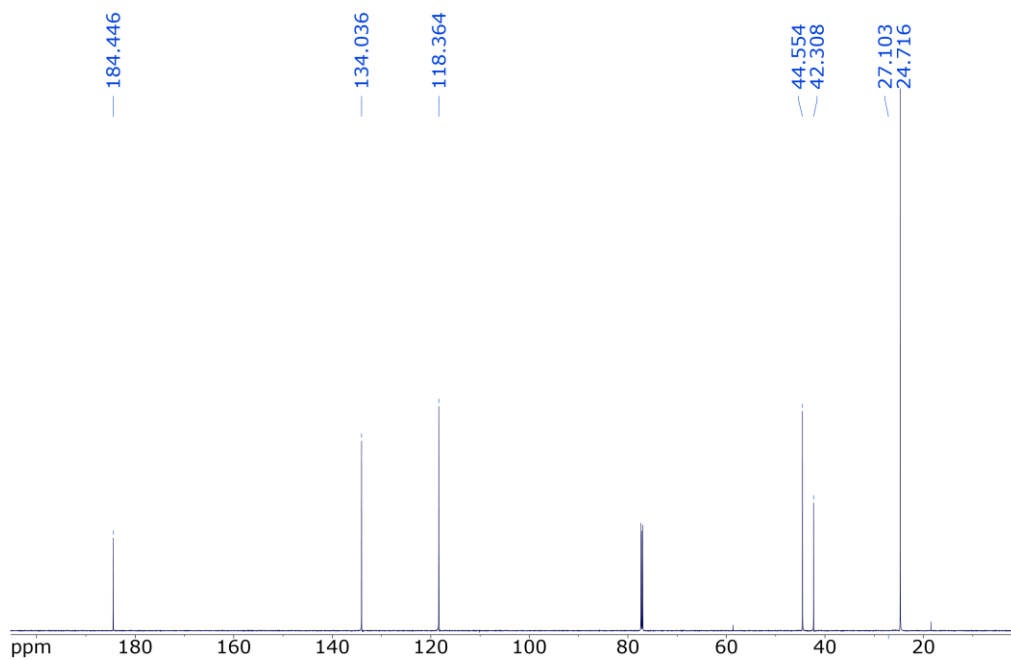


Figure S2.15. ^{13}C UDEFT NMR spectrum of ethyl 2,2-dimethylpent-4-enoic acid in CDCl_3 .

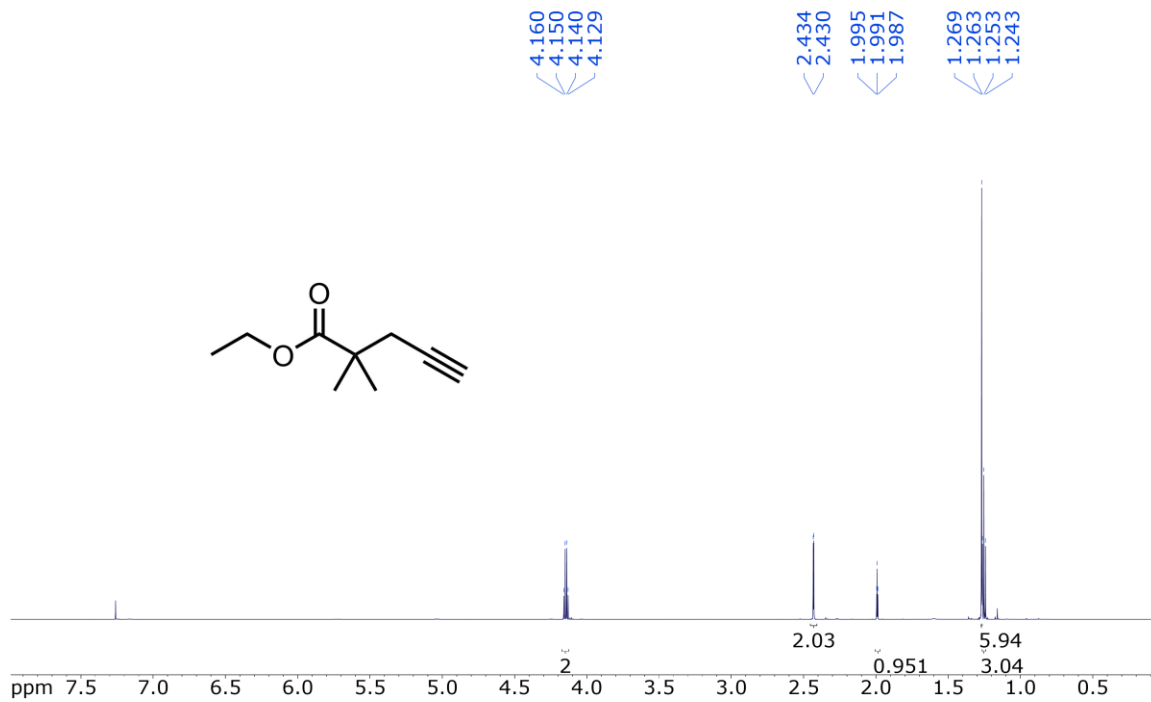


Figure S2.16. ^1H NMR spectrum of ethyl 2,2-dimethylpent-4-ynoate in CDCl_3 .

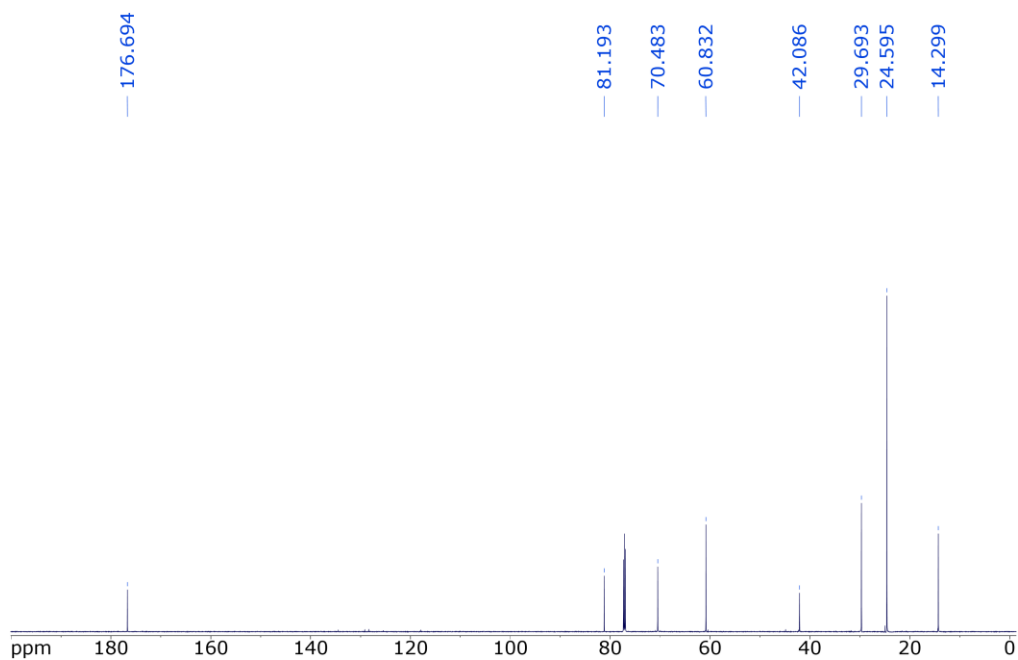


Figure S2.17. ^{13}C UDEFT NMR spectrum of ethyl 2,2-dimethylpent-4-ynoate in CDCl_3 .

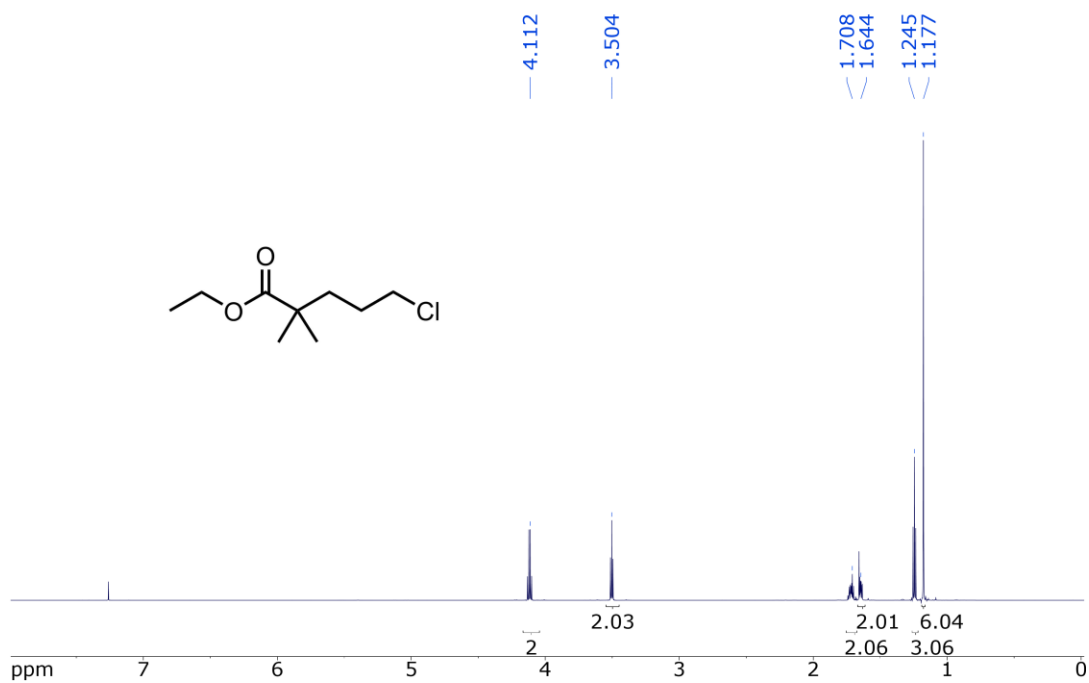


Figure S2.18. ^1H NMR of ethyl 5-chloro-2,2-dimethylpentanoate in CDCl_3 .

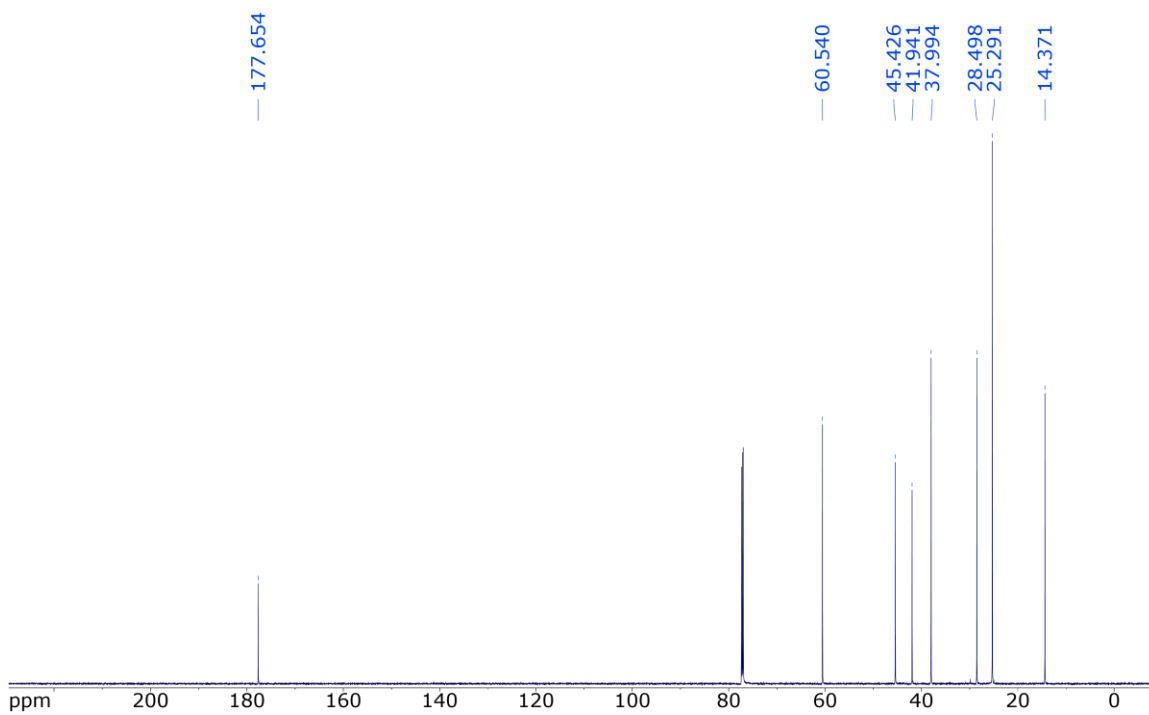


Figure S2.19. ¹³C UDEFT NMR of ethyl 5-chloro-2,2-dimethylpentanoate in CDCl₃.

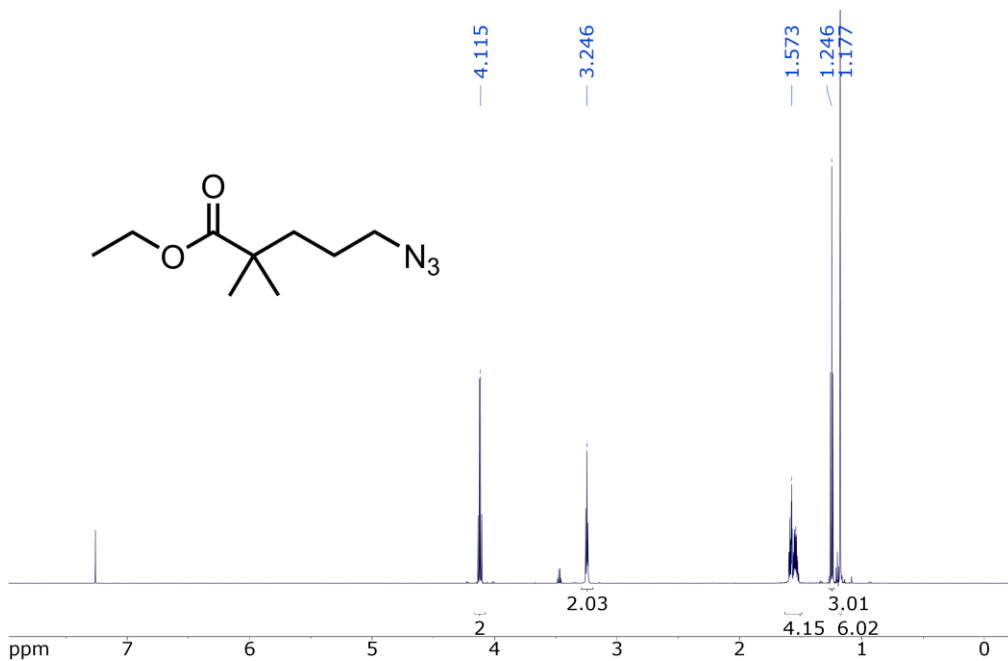


Figure S2.20. ¹H NMR of ethyl 5-azido-2,2-dimethylpentanoate in CDCl₃.

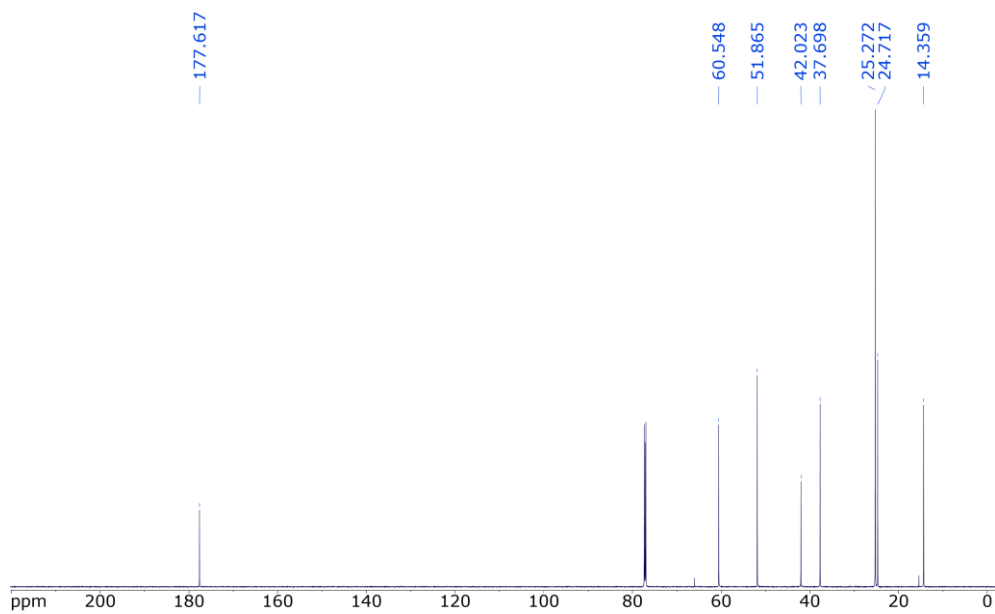


Figure S2.21. ¹³C UDEFT NMR of ethyl 5-azido-2,2-dimethylpentanoate in CDCl₃.

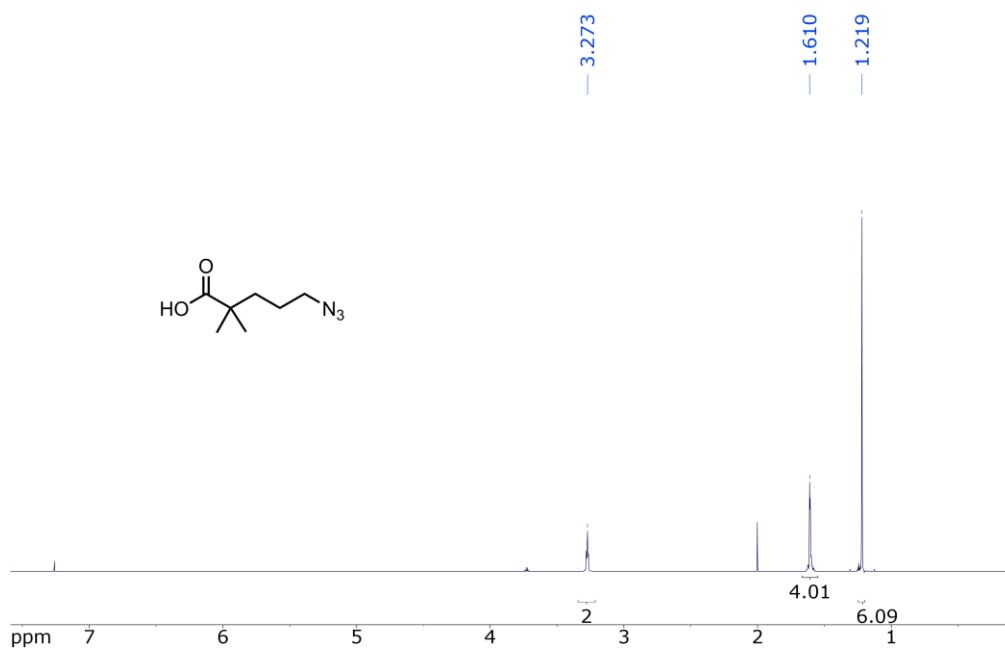


Figure S2.22. ¹H NMR of 5-azido-2,2-dimethylpentanoic acid in CDCl₃.

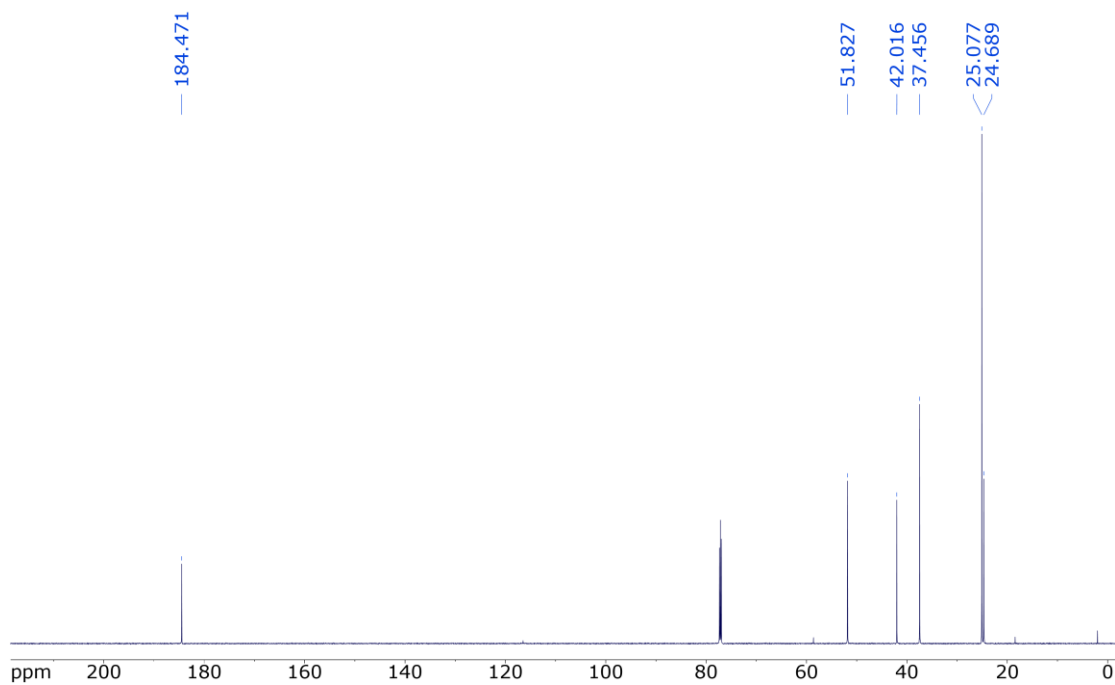


Figure S2.23. ^{13}C UDEFT NMR of 5-azido-2,2-dimethylpentanoic acid in CDCl_3 .

Dendron NMR Data

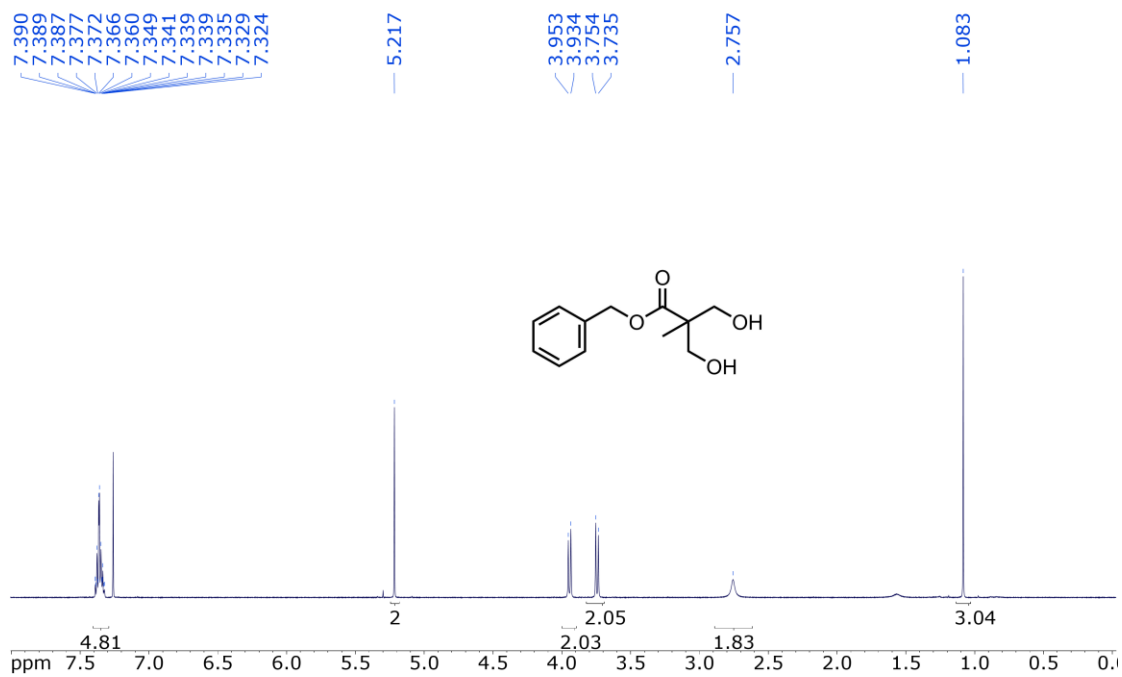


Figure S2.24. ^1H NMR of BnO-G1-(OH)_2 in CDCl_3 .

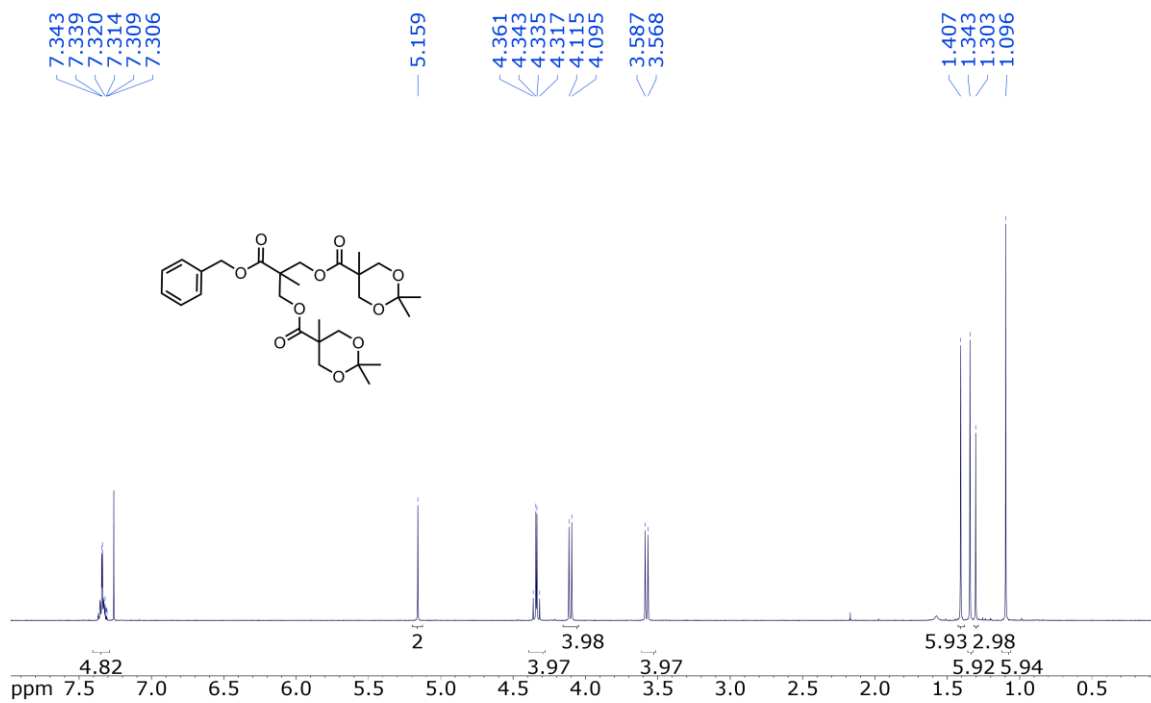


Figure S2.25. ¹H NMR of BnO-G2-(acet)₂ in CDCl₃.

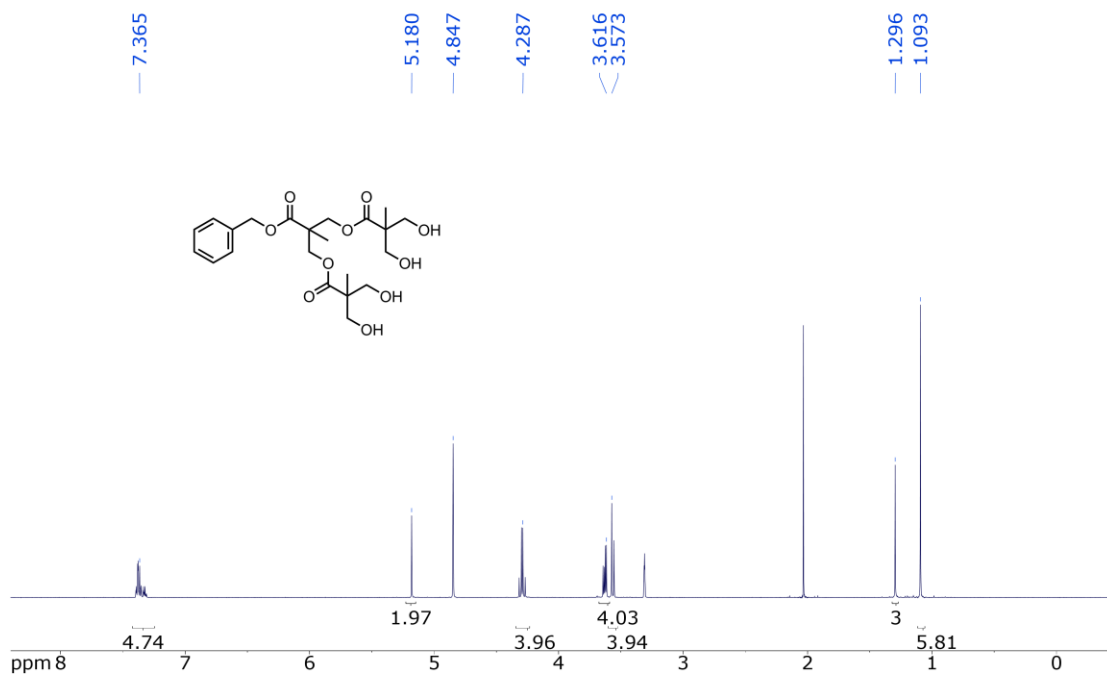


Figure S2.26. ¹H NMR of BnO-G2-(OH)₄ in MeOD.

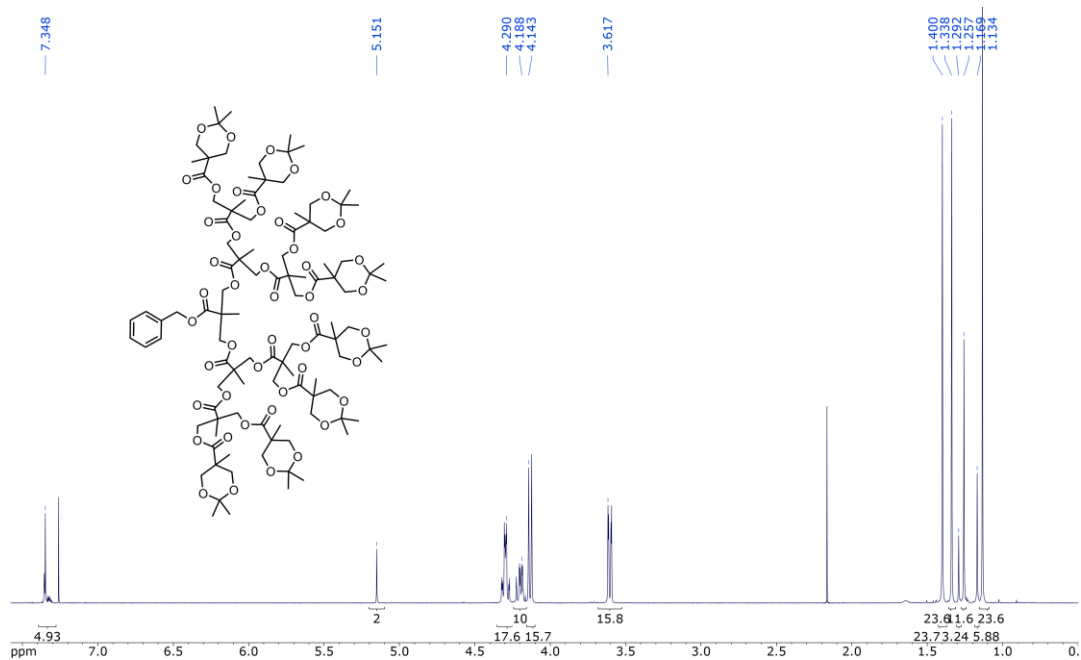


Figure S2.29. ¹H NMR of BnO-G4-(acet)₈ in CDCl₃.

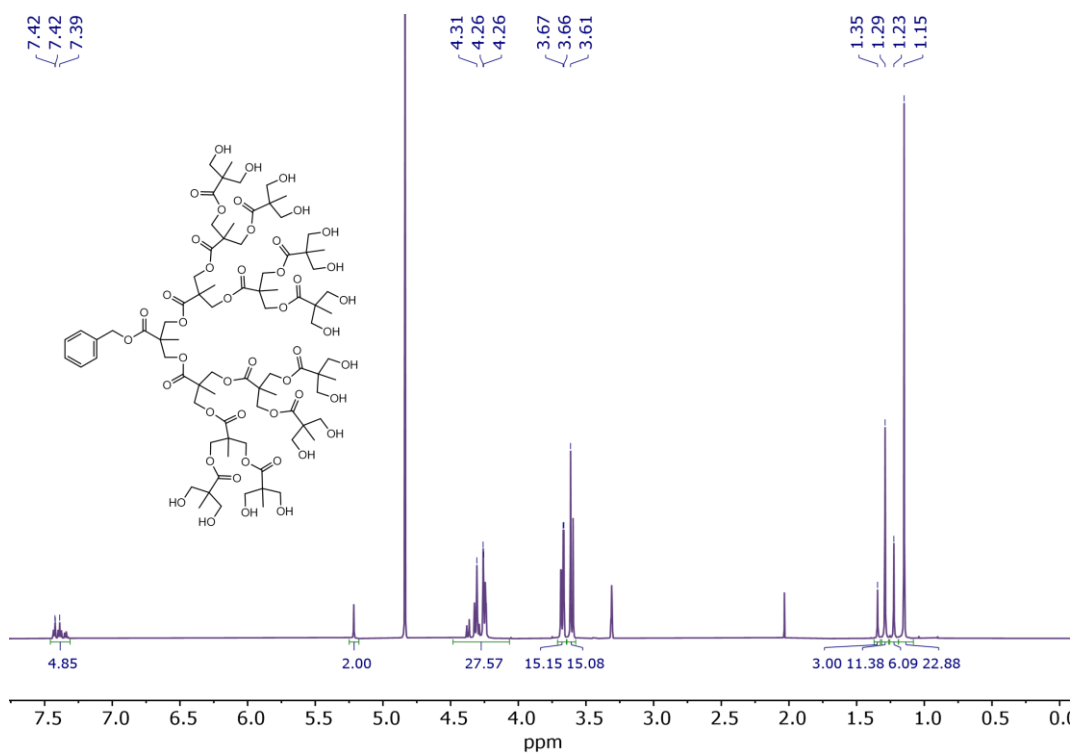


Figure S2.30. ¹H NMR of BnO-G4-(OH)₁₆ in MeOD.

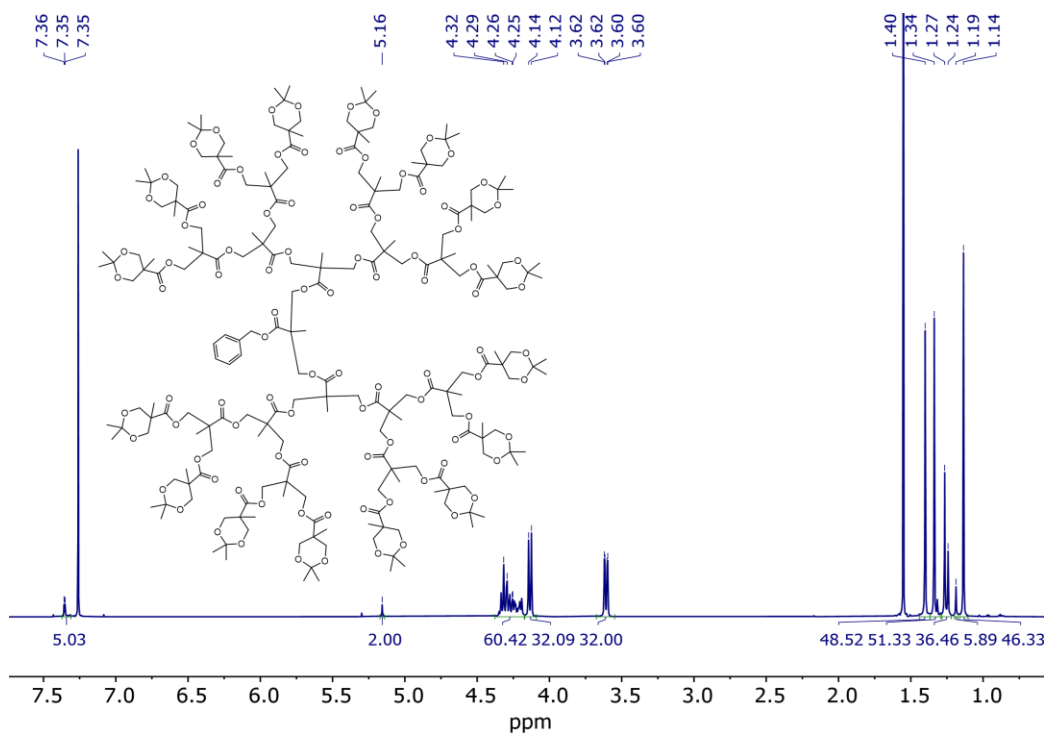


Figure S2.31. ^1H NMR of $\text{BnO-G5-(acet)}_{16}$ in CDCl_3 .

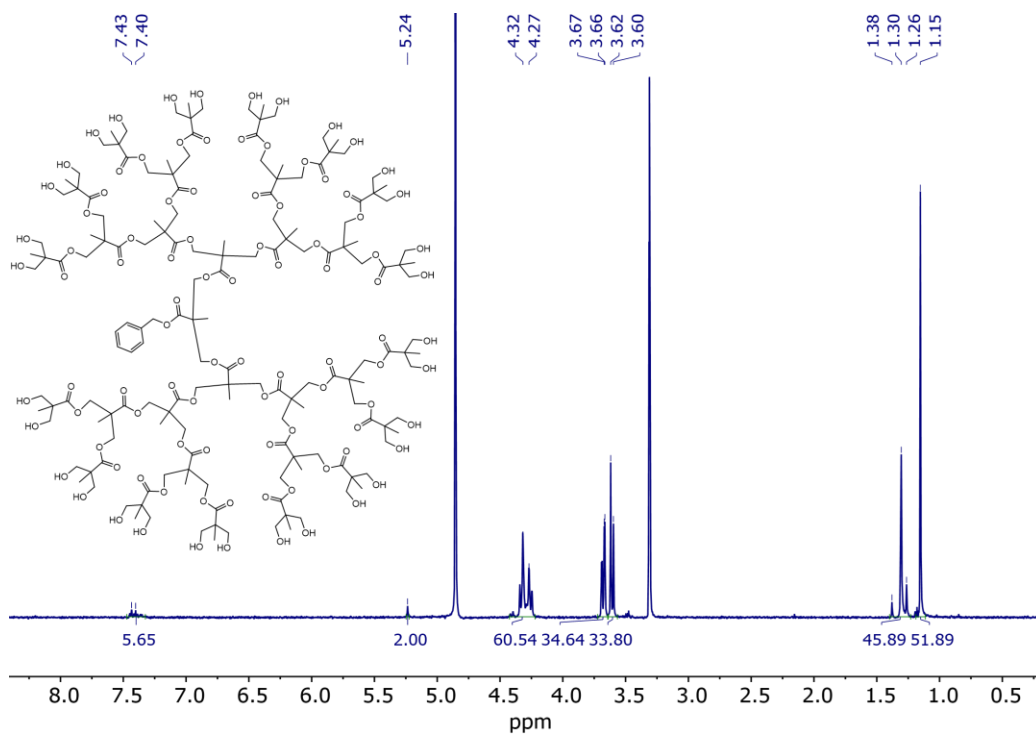


Figure S2.32. ^1H NMR of BnO-G5-(OH)_{32} in MeOD .

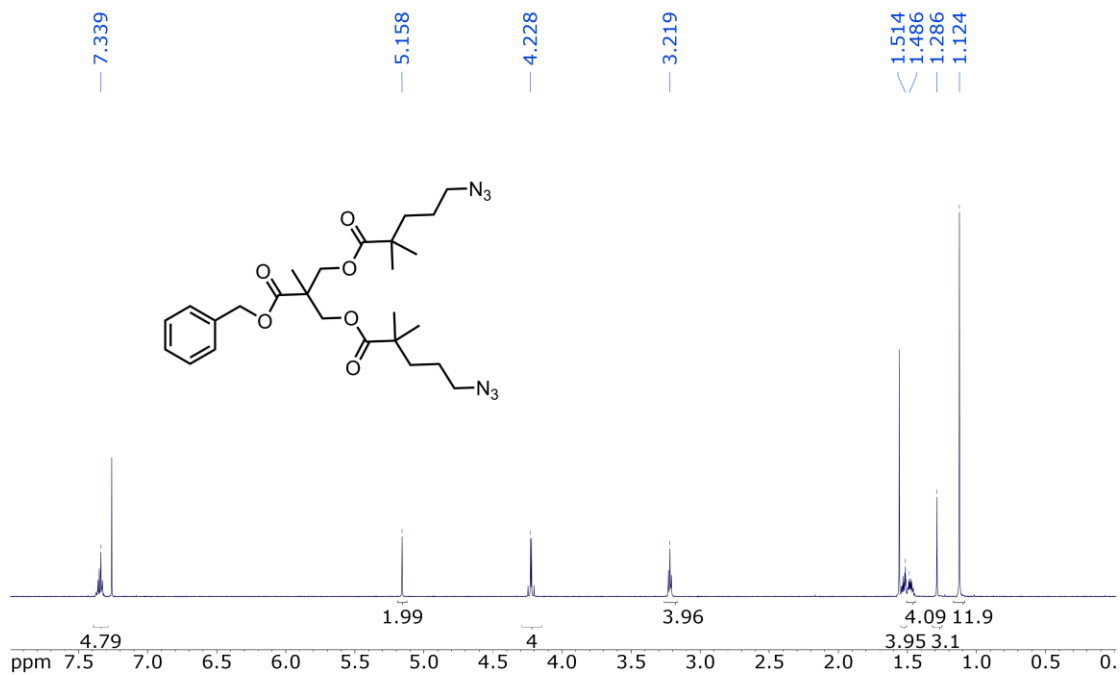


Figure S2.33. ¹H NMR of BnO-G1-(N₃)₂ in CDCl₃.

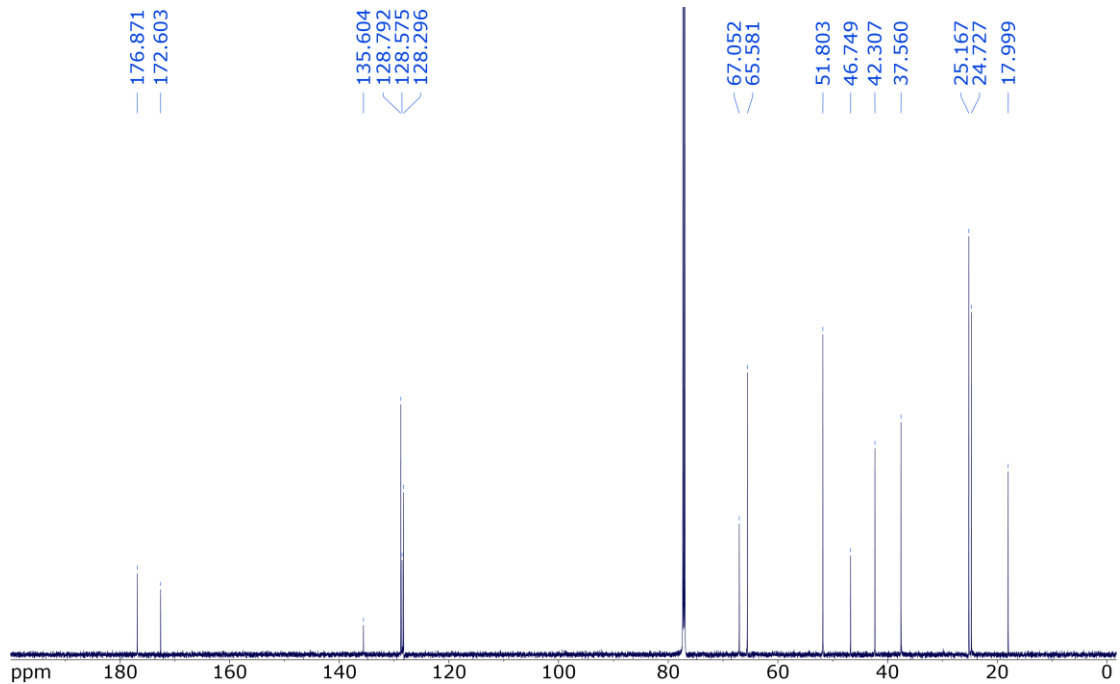


Figure S2.34. ¹³C NMR of BnO-G1-(N₃)₂ in CDCl₃.

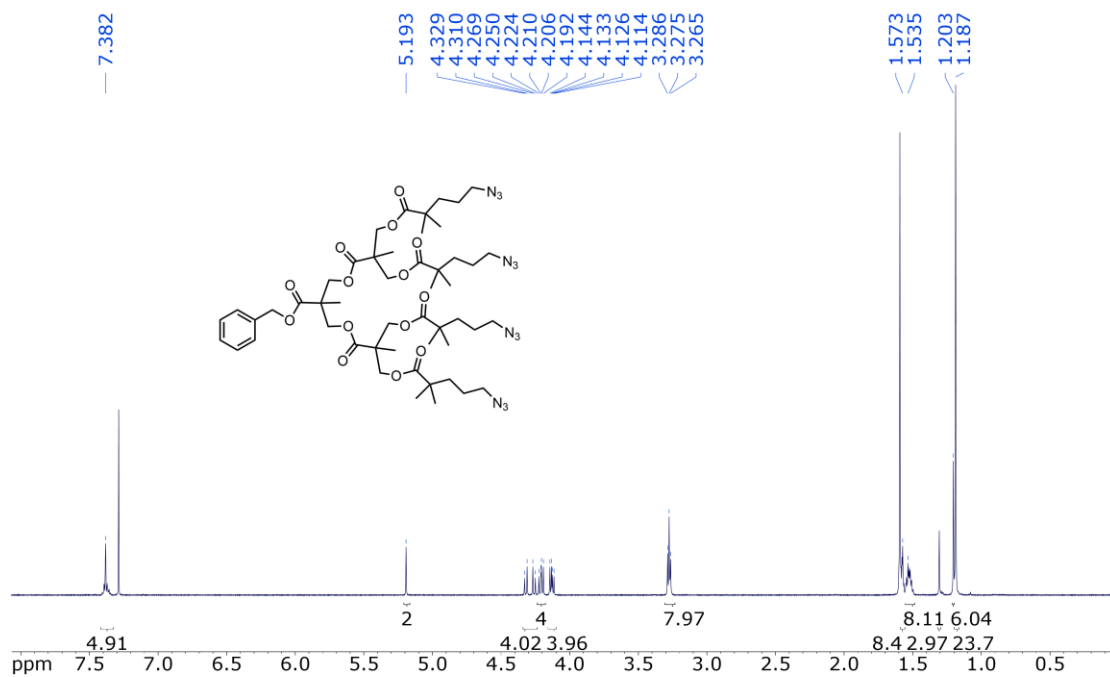


Figure S2.35. ¹H NMR of BnO-G2-(N₃)₄ in CDCl₃.

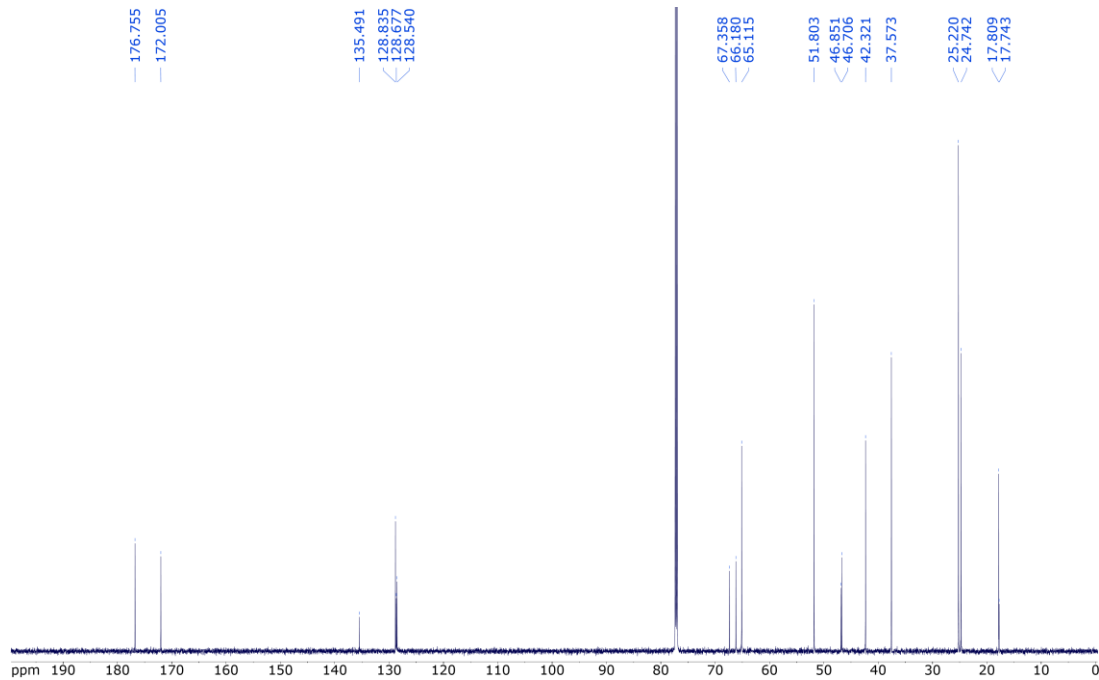


Figure S2.36. ¹³C NMR of BnO-G2-(N₃)₄ in CDCl₃.

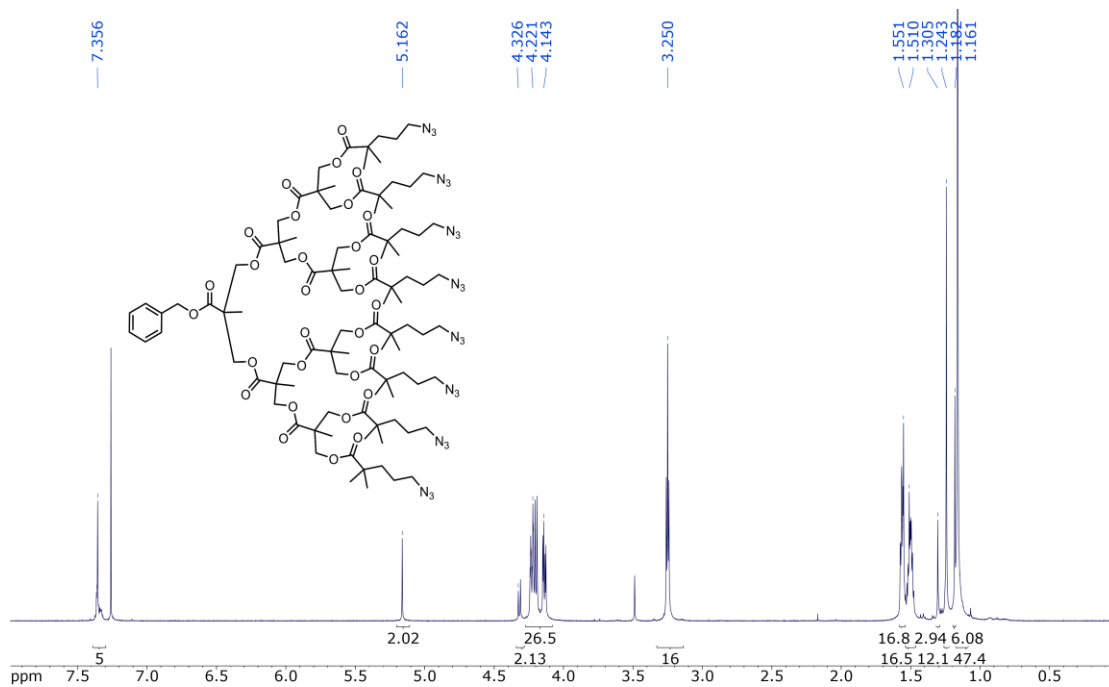


Figure S2.37. ¹H NMR of BnO-G3-(N₃)₈ in CDCl₃.

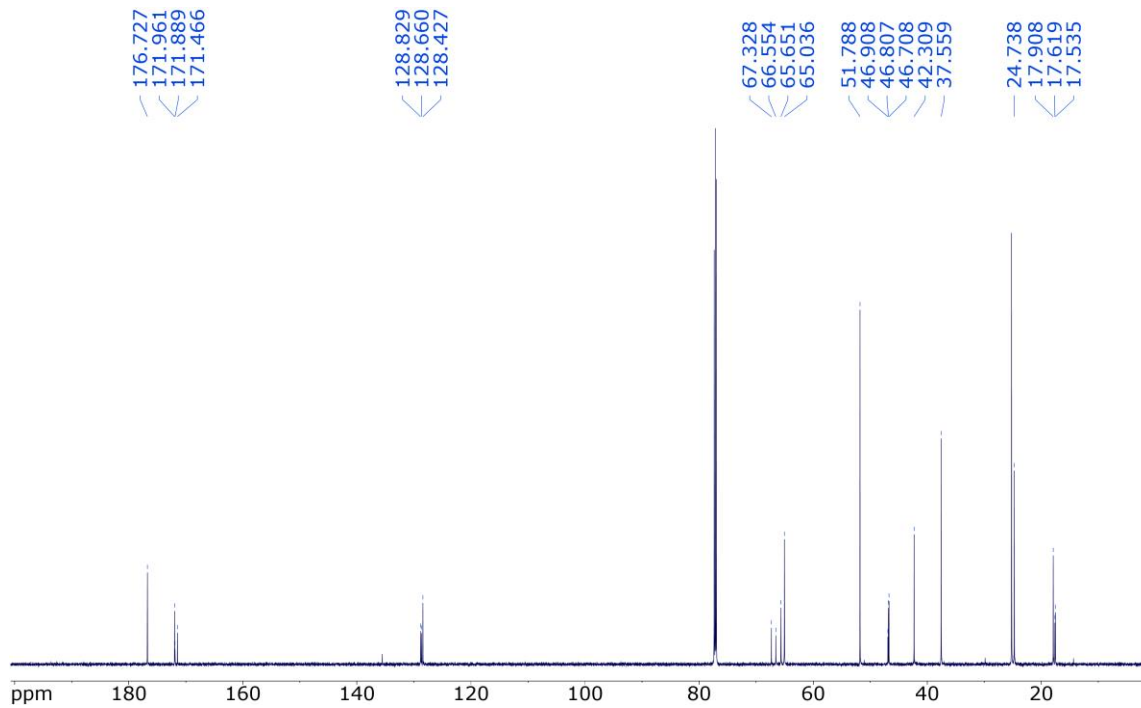


Figure S2.38. ¹³C NMR of BnO-G3-(N₃)₈ in CDCl₃.

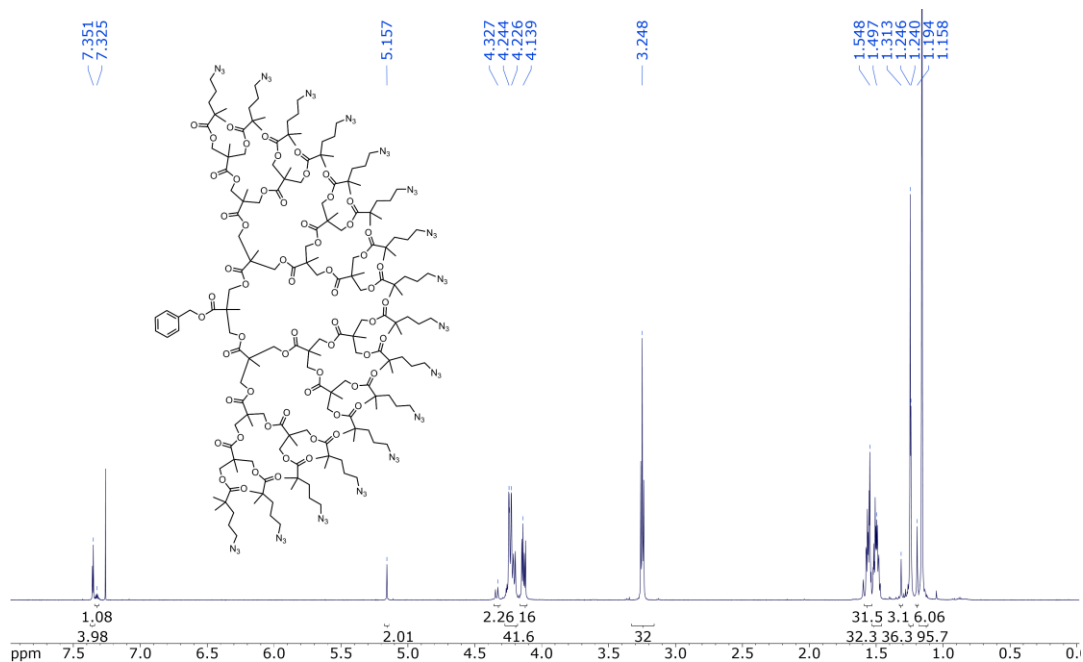


Figure S2.39. ¹H NMR of BnO-G4-(N₃)₁₆ in CDCl₃.

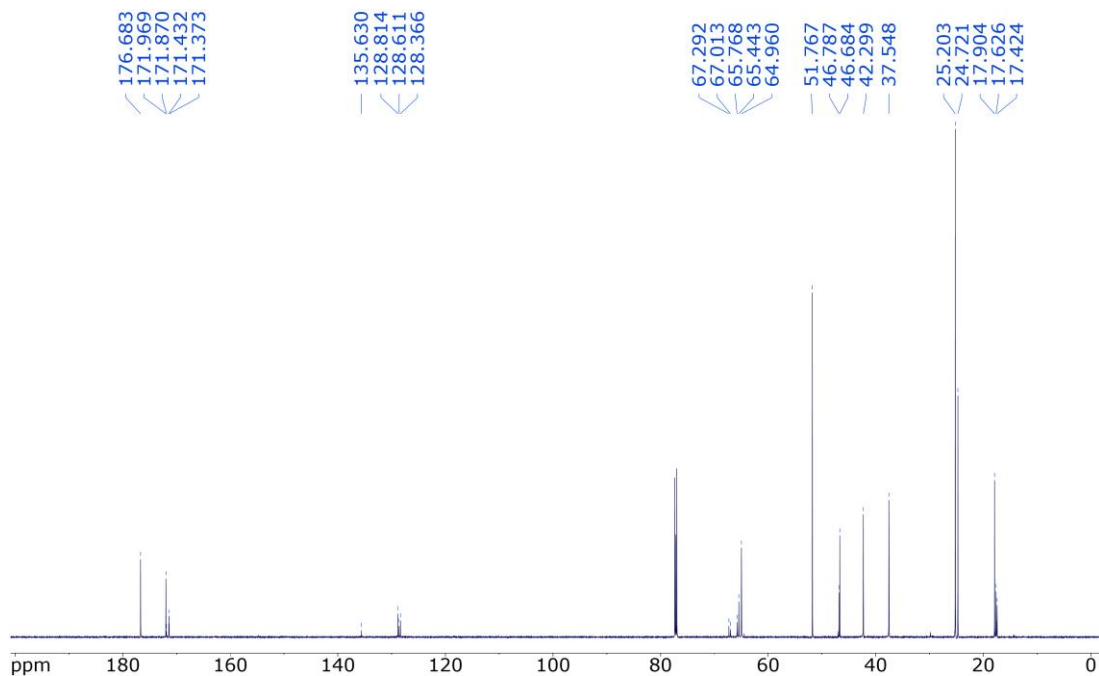


Figure S2.40. ¹³C NMR of BnO-G4-(N₃)₁₆ in CDCl₃.

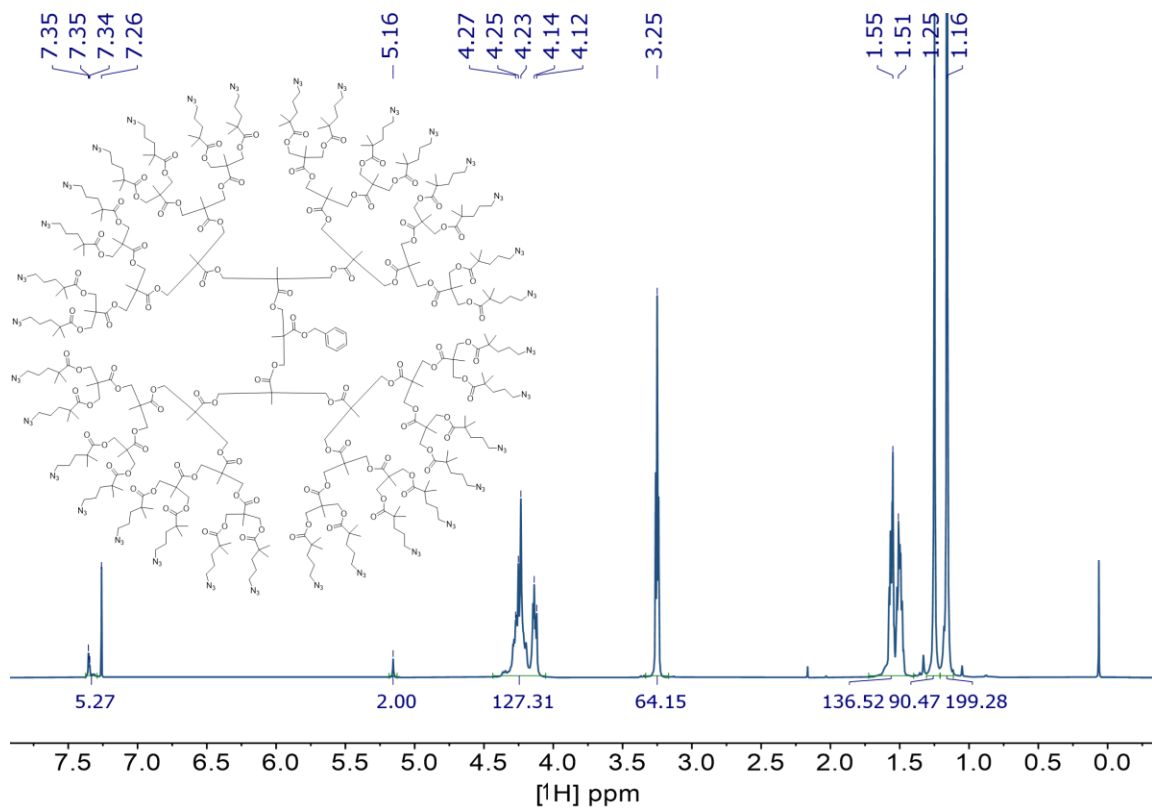


Figure S2.41. ^1H NMR of $\text{BnO-G5-(N}_3\text{)}_{32}$ in CDCl_3 .

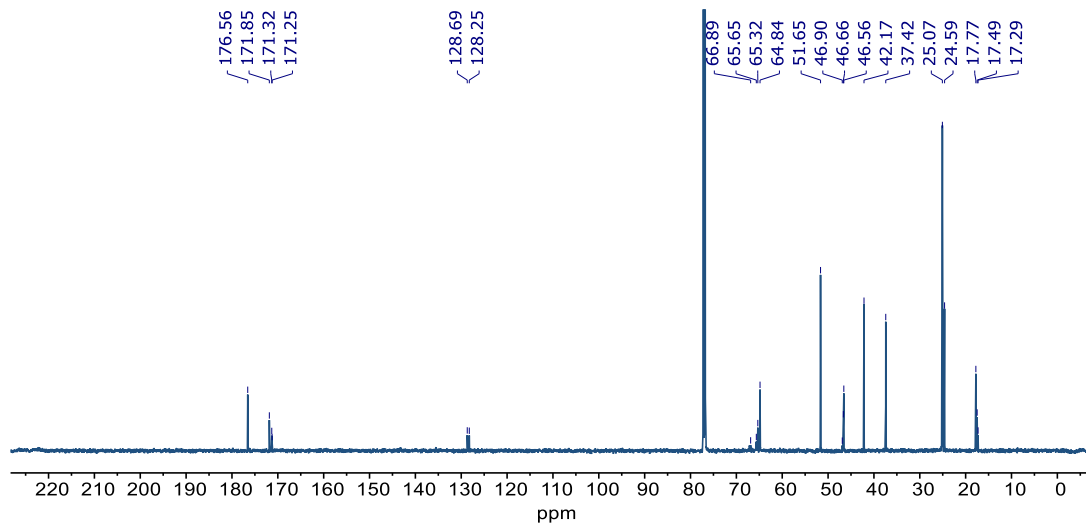


Figure S2.42. ^{13}C NMR of $\text{BnO-G5-(N}_3\text{)}_{32}$ in CDCl_3 .

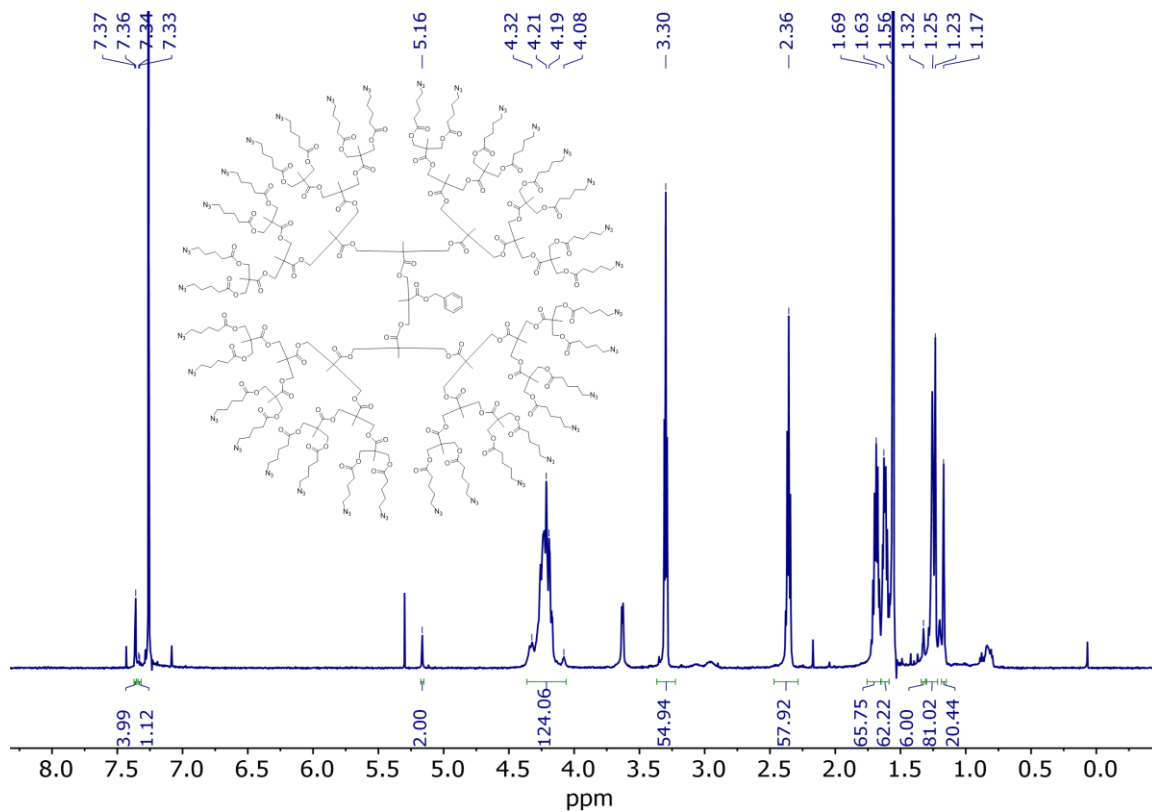


Figure S2.43. ¹H NMR of BnO-G5-Lin-N₃ in CDCl₃.

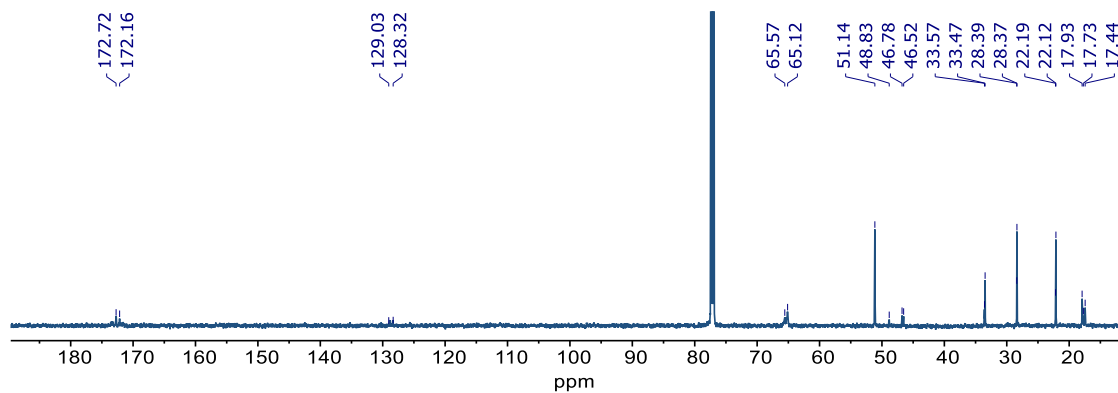


Figure S2.44. ¹³C NMR of BnO-G5-Lin-N₃ in CDCl₃.

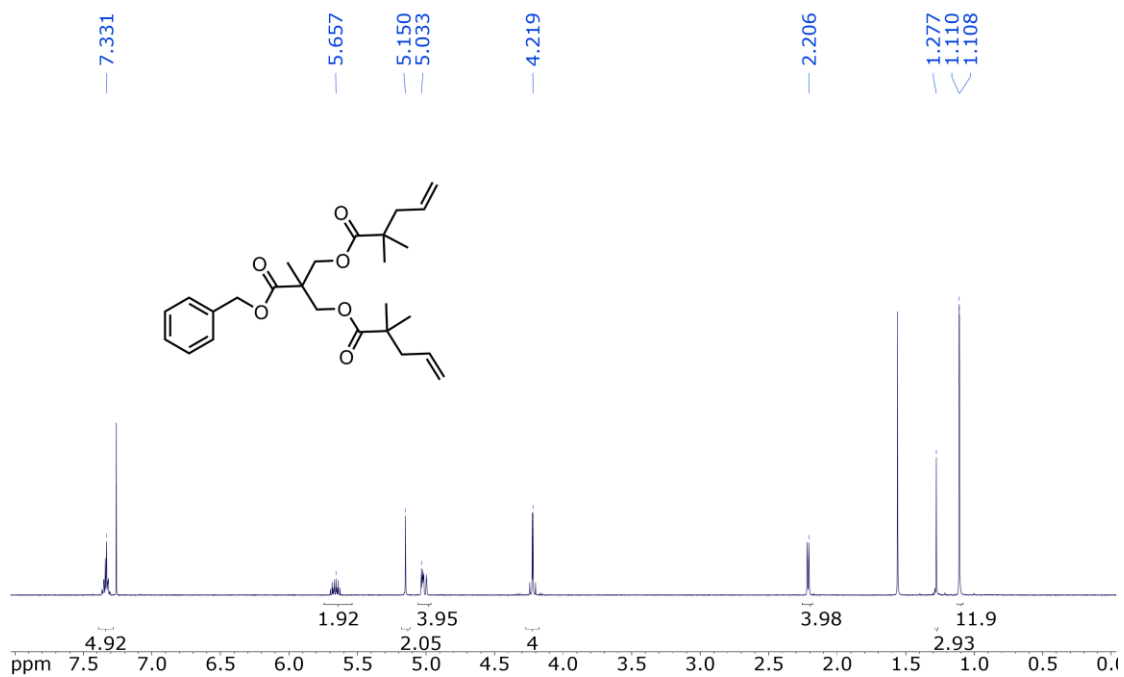


Figure S2.45. ¹H NMR of BnO-G1-(ene)₂ in CDCl₃.

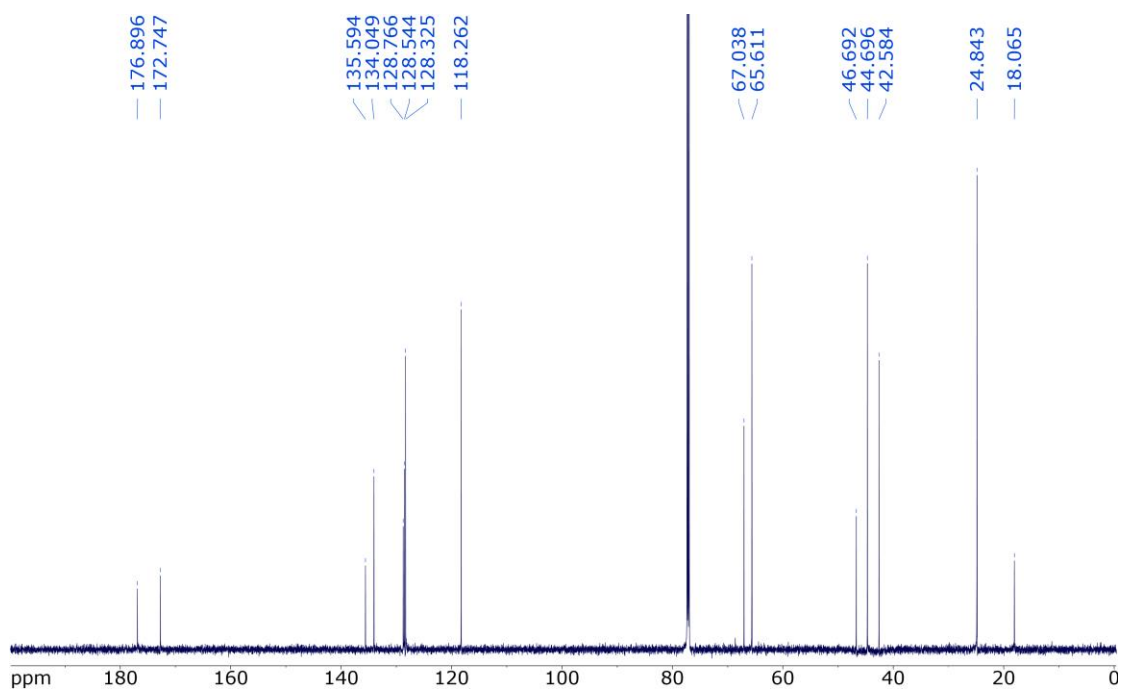


Figure S2.46. ¹³C NMR of BnO-G1-(ene)₂ in CDCl₃.

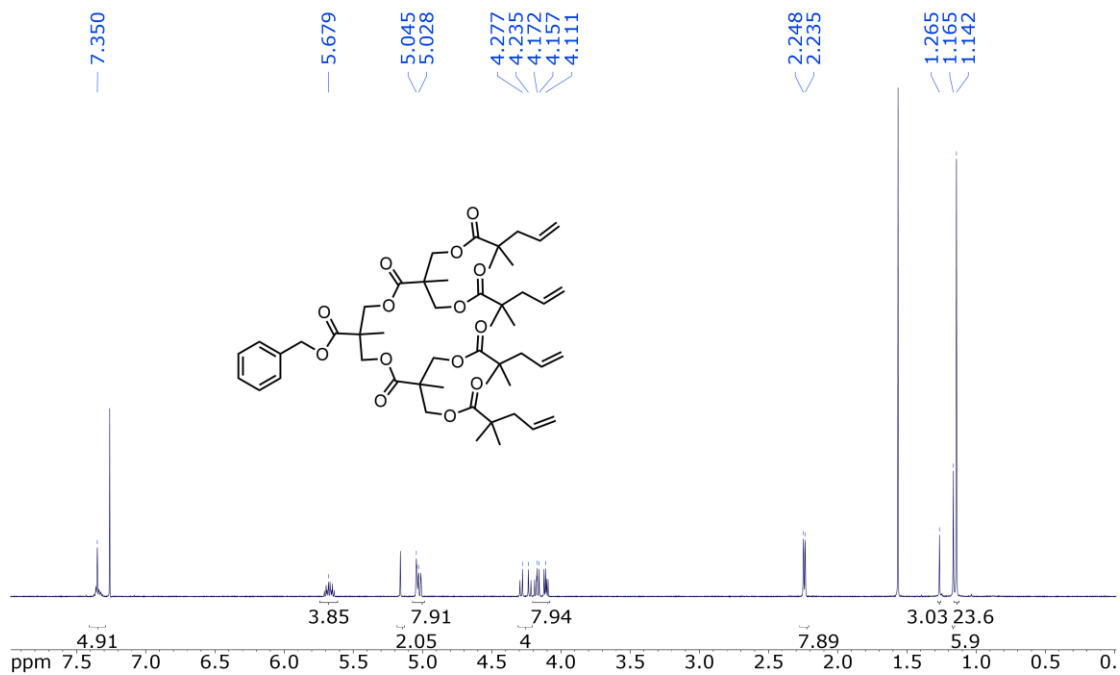


Figure S2.47. ¹H NMR of BnO-G2-(ene)₄ in CDCl₃.

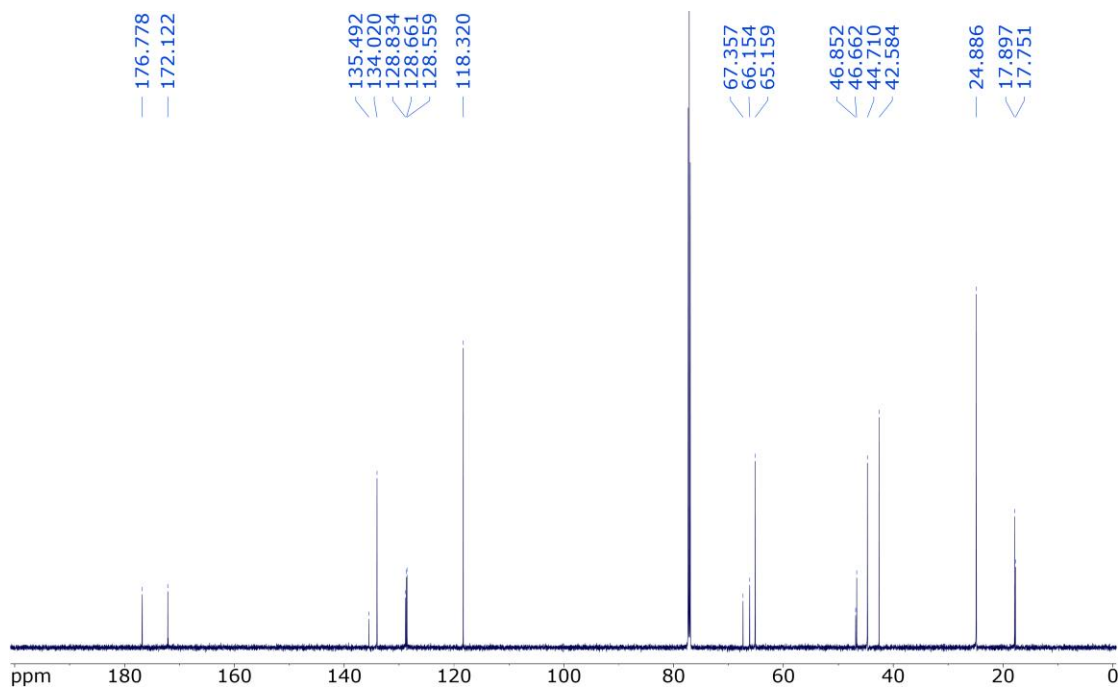


Figure S2.48. ¹³C NMR of BnO-G2-(ene)₄ in CDCl₃.

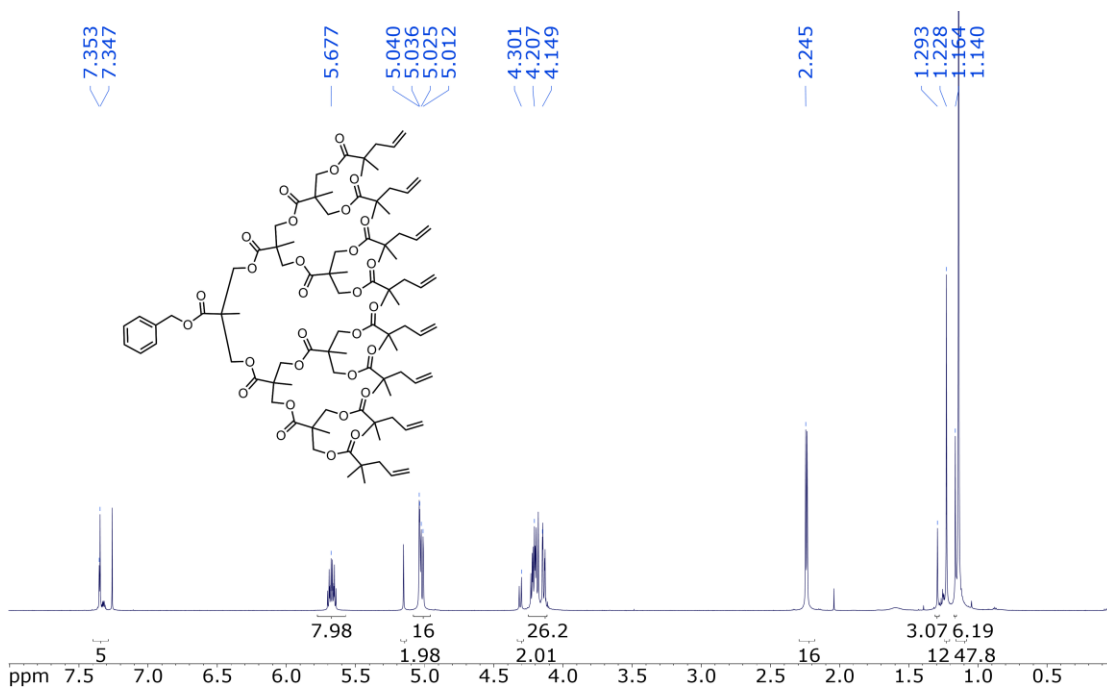


Figure S2.49. ¹H NMR of BnO-G3-(ene)₈ in CDCl₃.

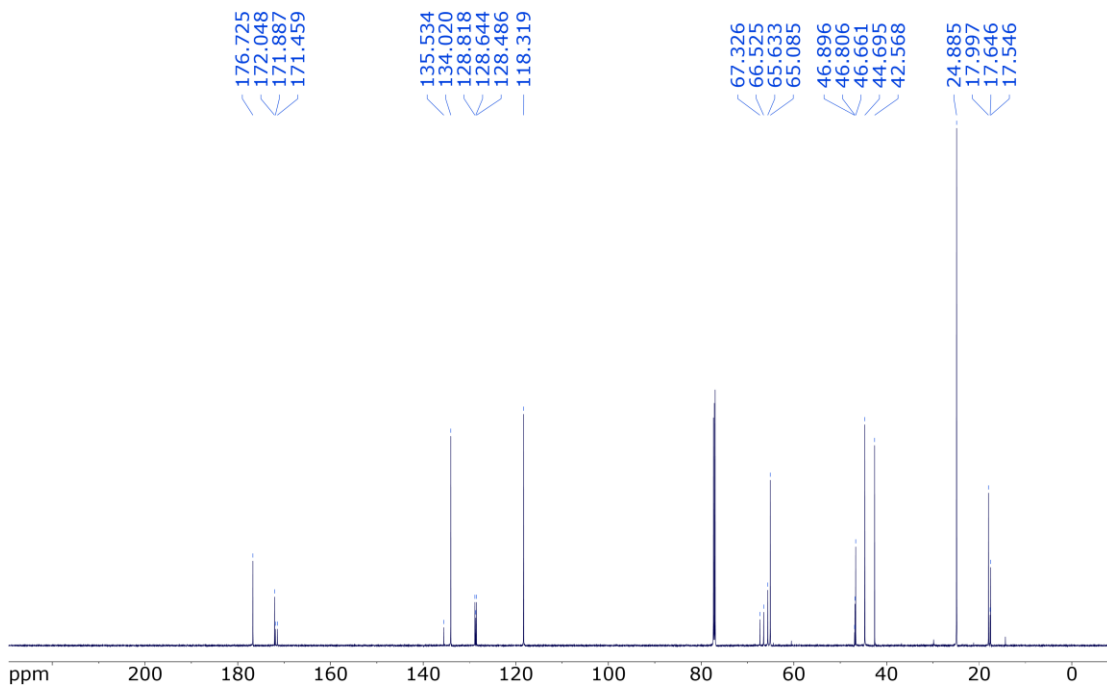


Figure S2.50. ¹³C NMR of BnO-G3-(ene)₈ in CDCl₃.

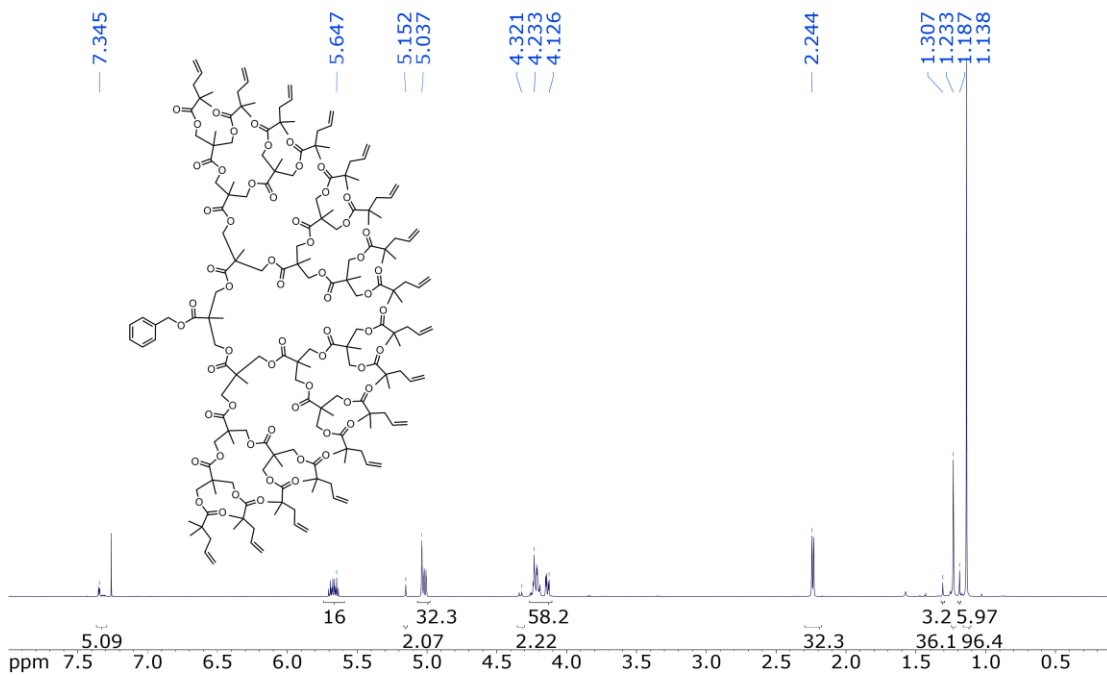


Figure S2.51. ¹H NMR of BnO-G4-(ene)₁₆ in CDCl₃.

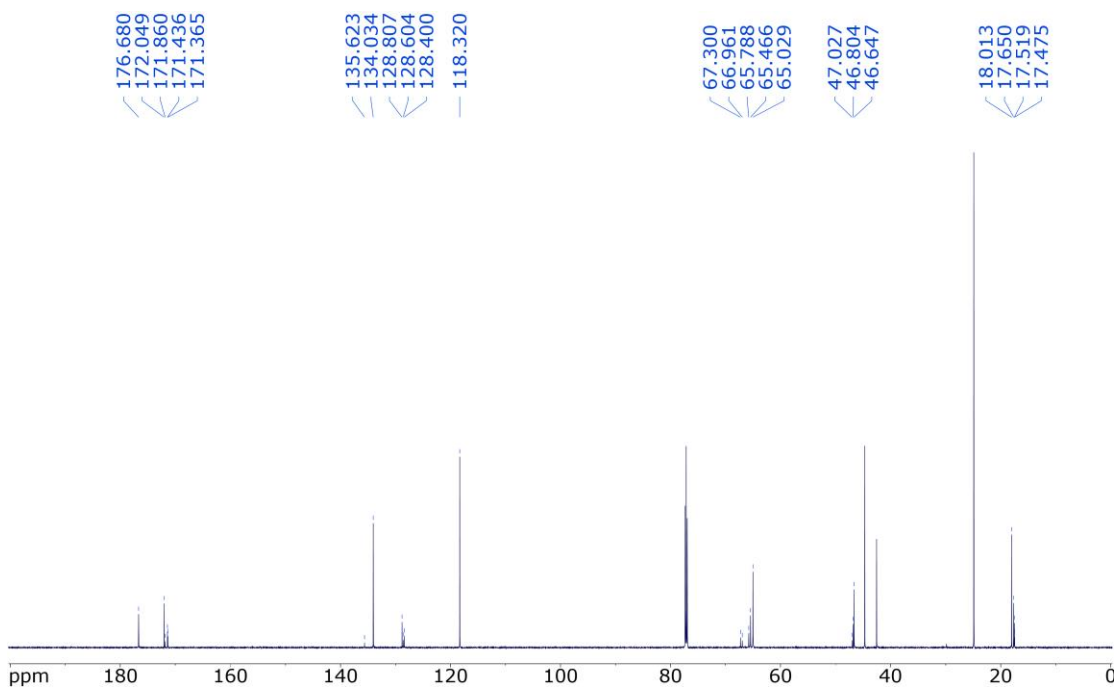
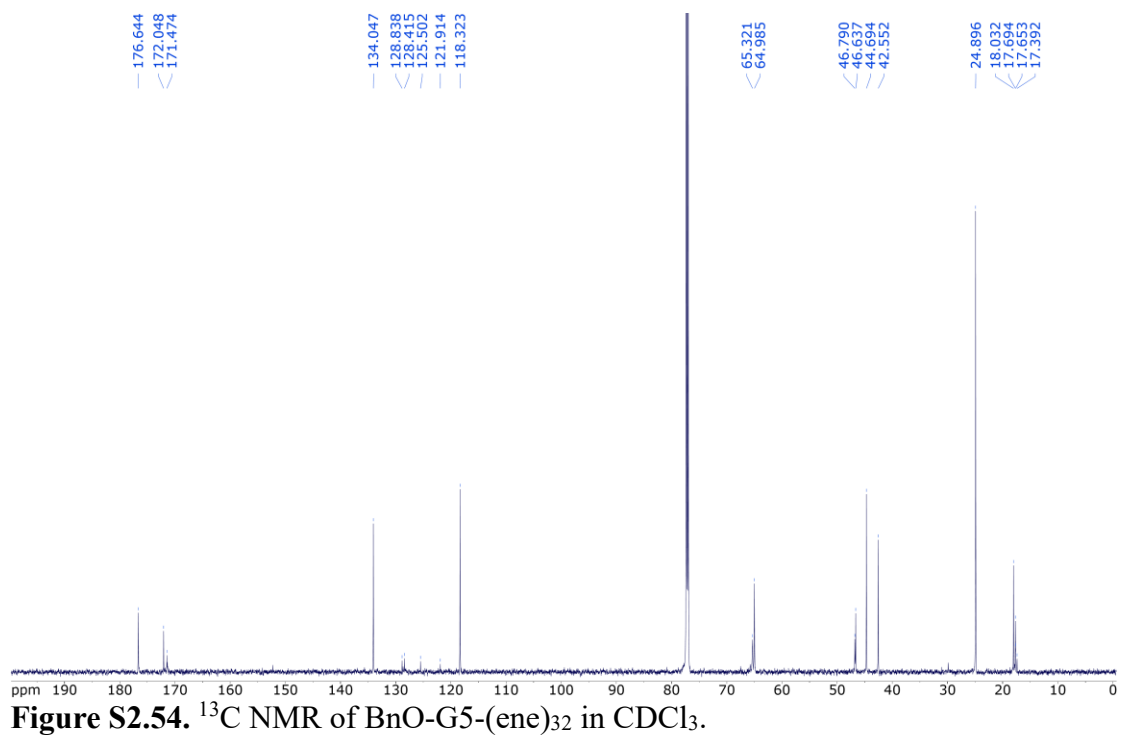
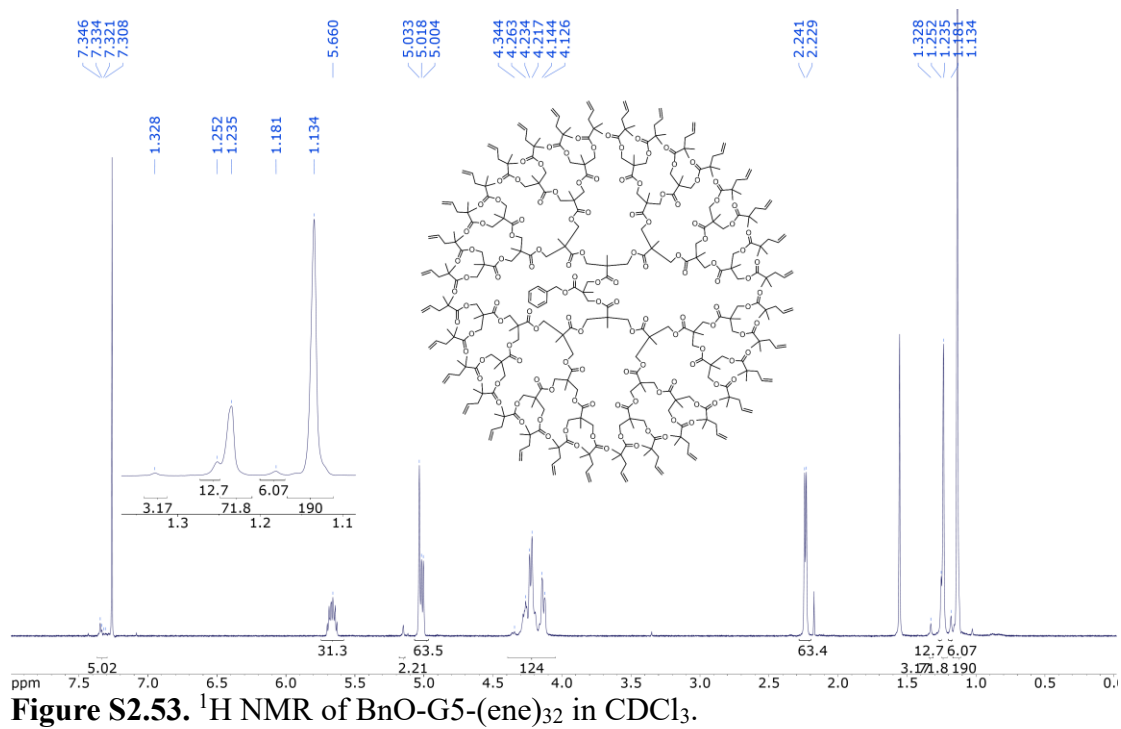


Figure S2.52. ¹³C NMR of BnO-G4-(ene)₁₆ in CDCl₃.



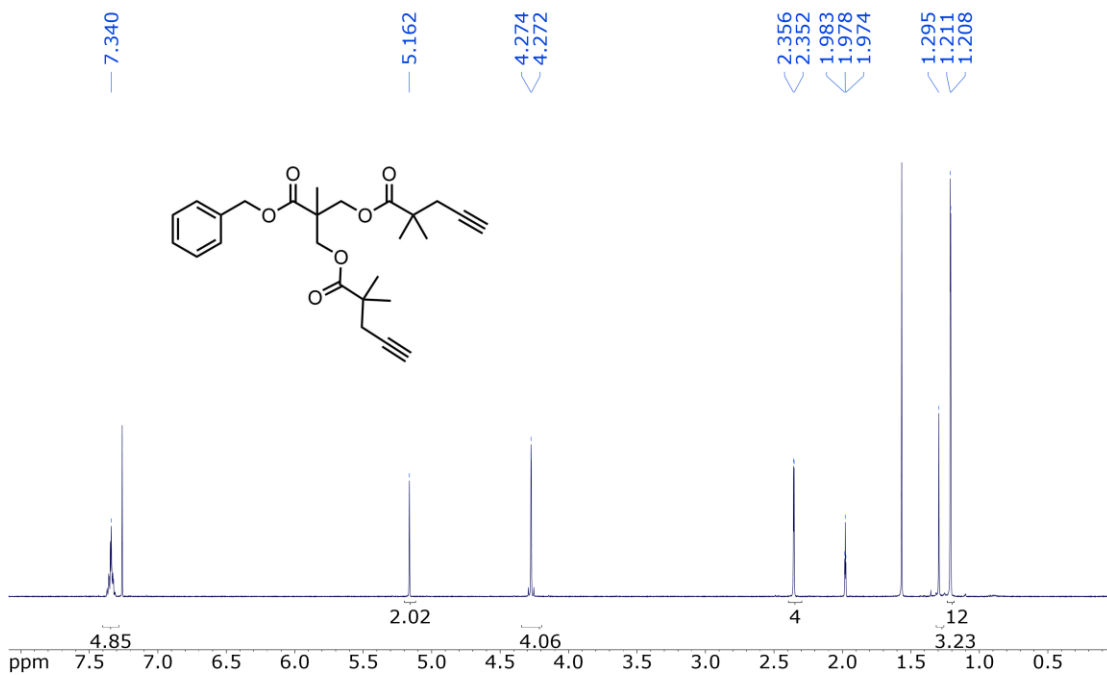


Figure S2.55. ¹H NMR of BnO-G1-(yne)₂ in CDCl₃.

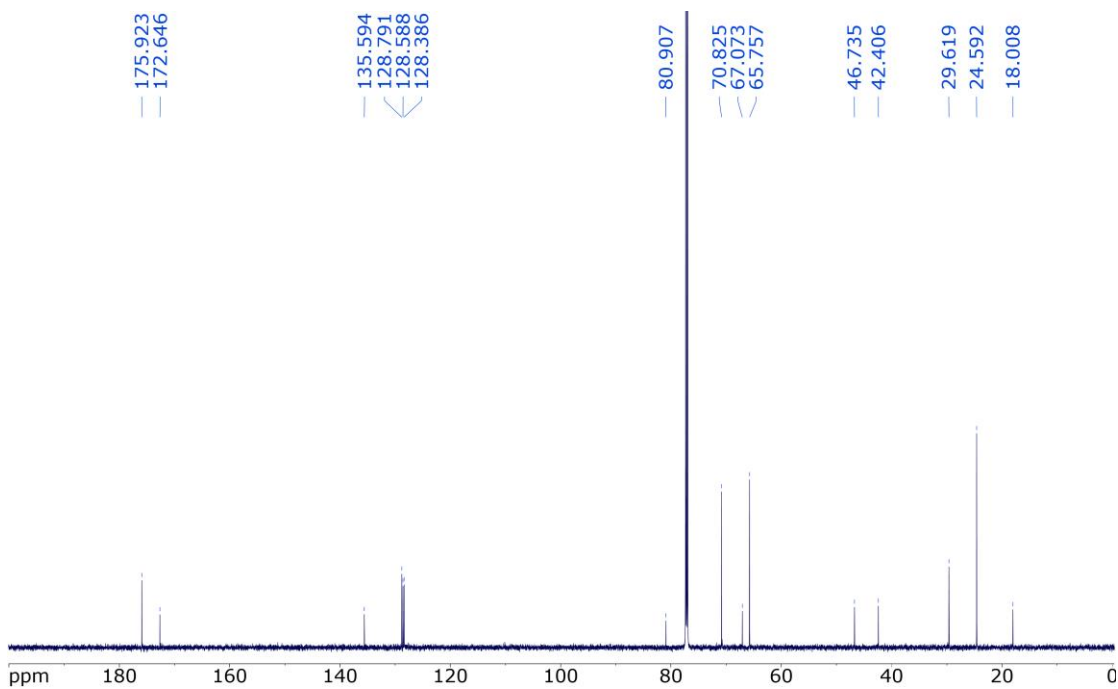


Figure S2.56. ¹³C NMR of BnO-G1-(yne)₂ in CDCl₃.

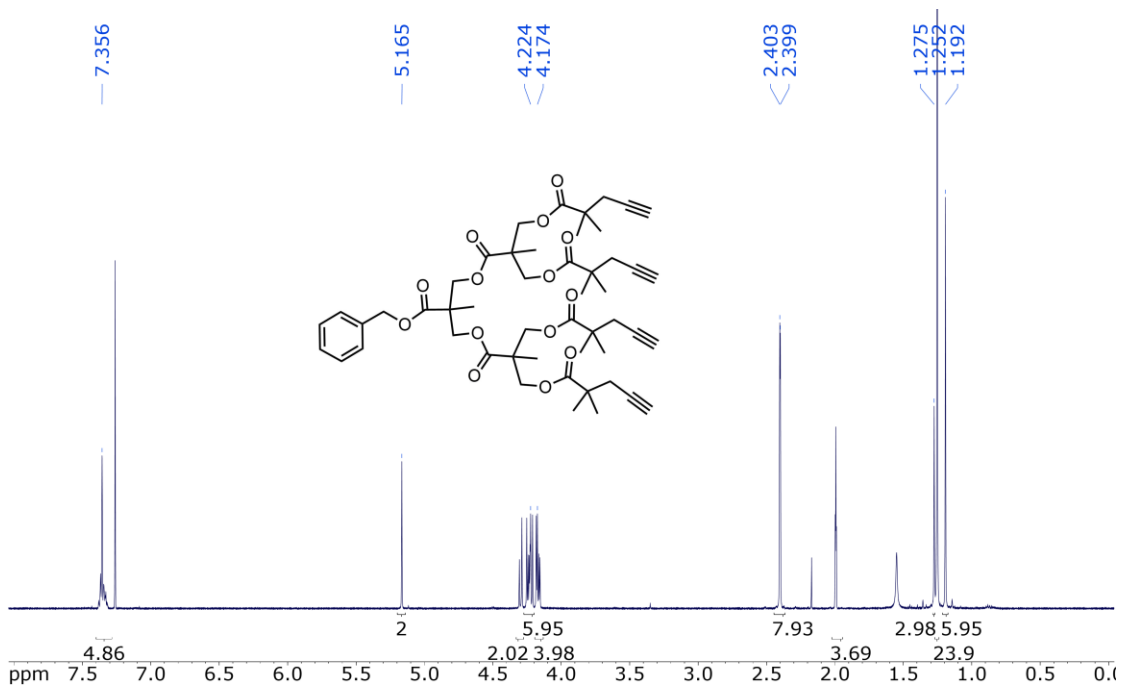


Figure S2.57. ¹H NMR of BnO-G2-(yne)₄ in CDCl₃.

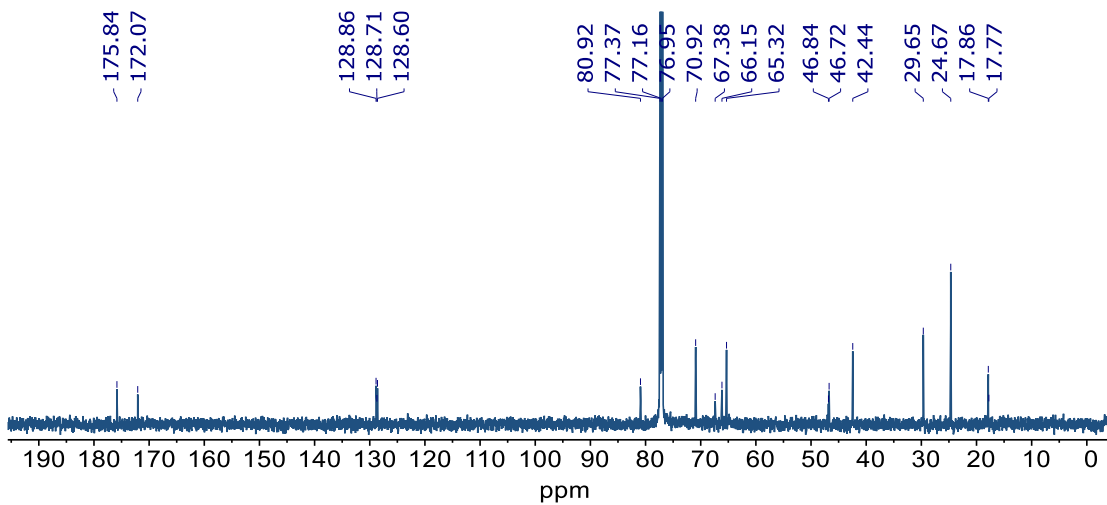


Figure S2.58. ¹³C NMR of BnO-G2-(yne)₄ in CDCl₃.

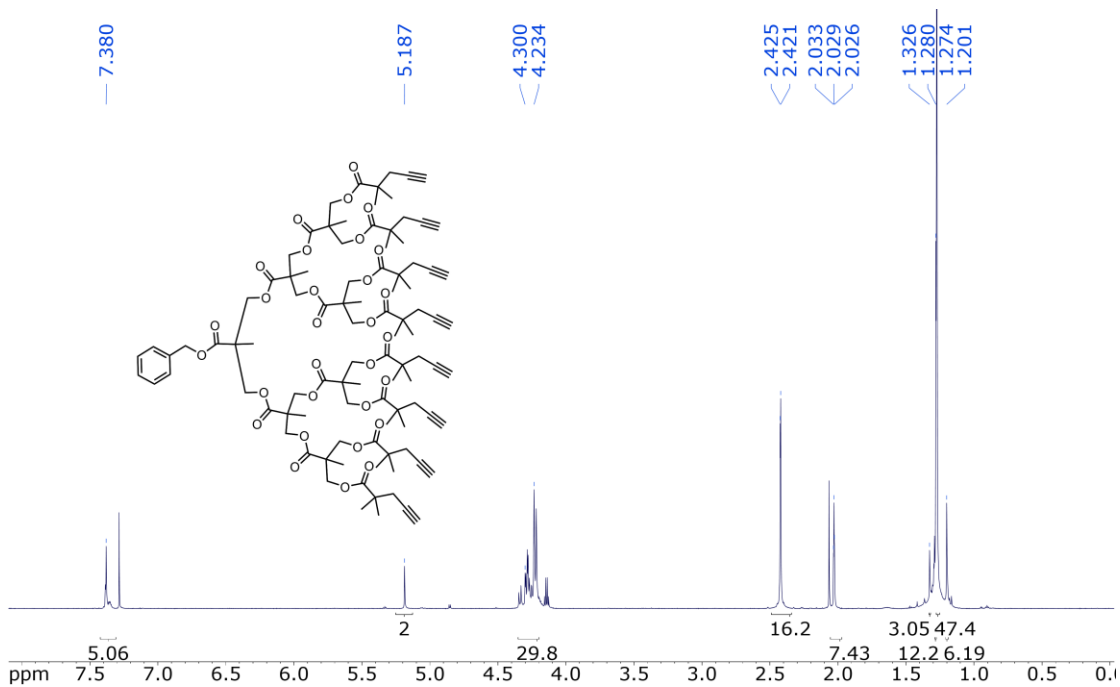


Figure S2.59. ¹H NMR of BnO-G3-(yne)₈ in CDCl₃.

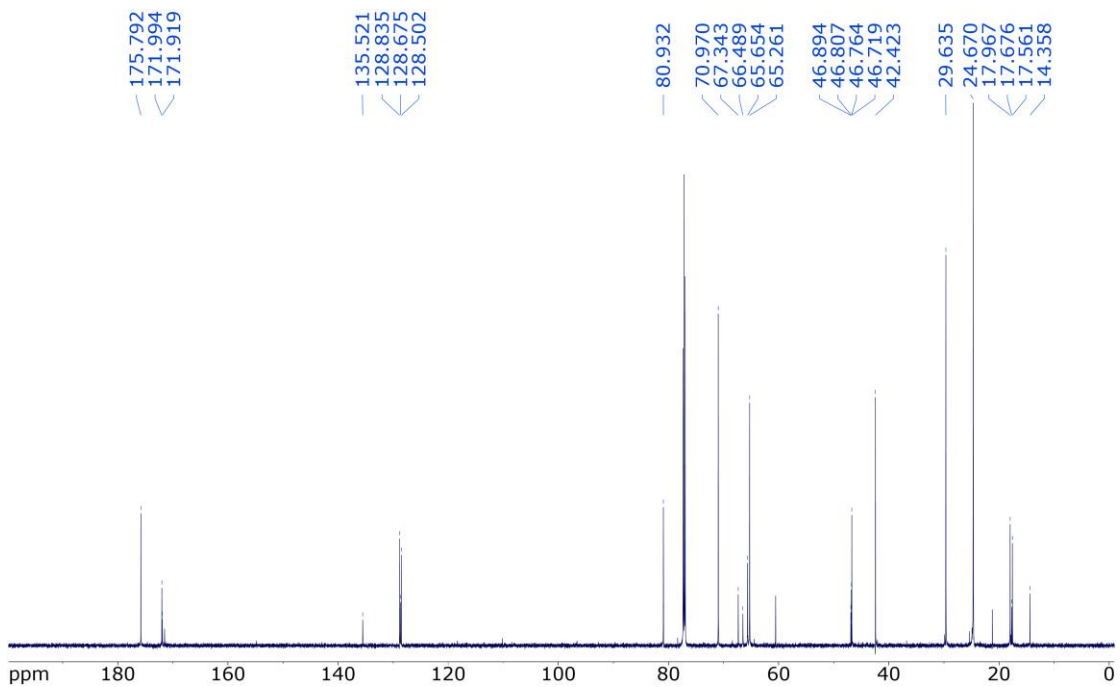


Figure S2.60. ¹³C NMR of BnO-G3-(yne)₈ in CDCl₃.

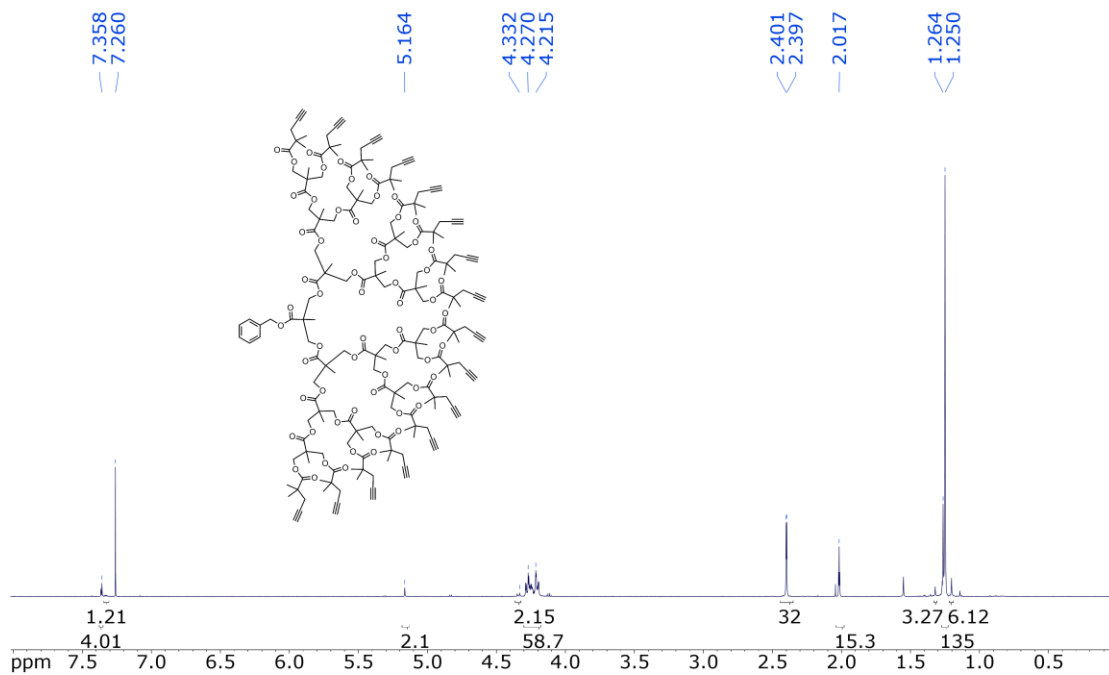


Figure S2.61. ¹H NMR of BnO-G4-(yne)₁₆ in CDCl₃.

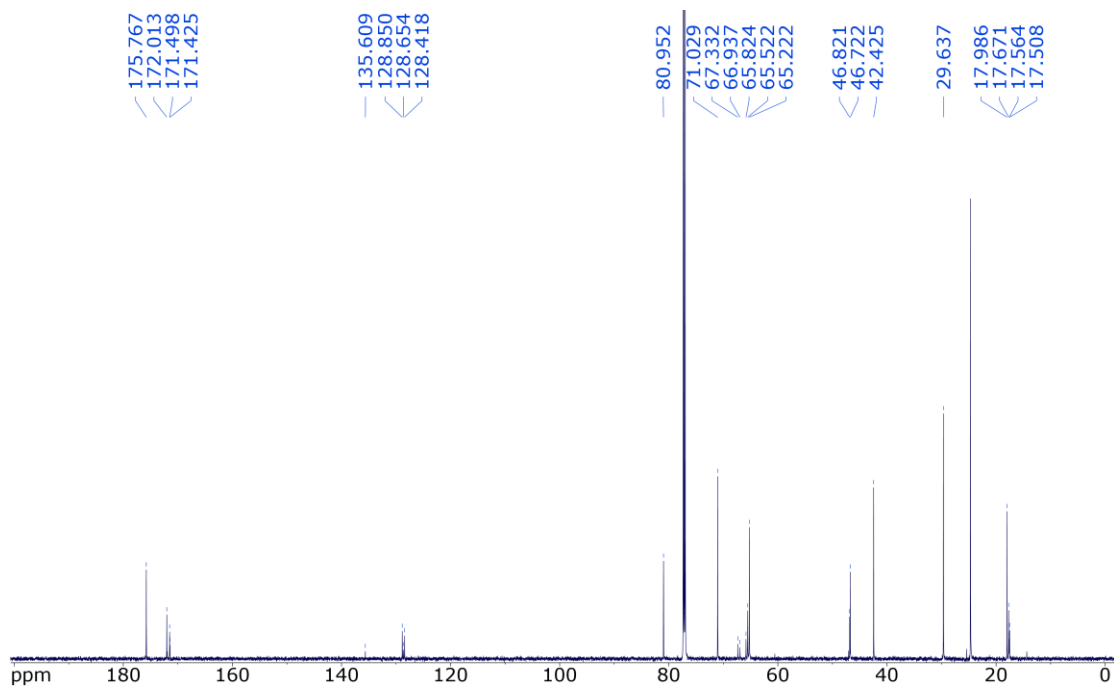


Figure S2.62. ¹³C NMR of BnO-G4-(yne)₁₆ in CDCl₃.

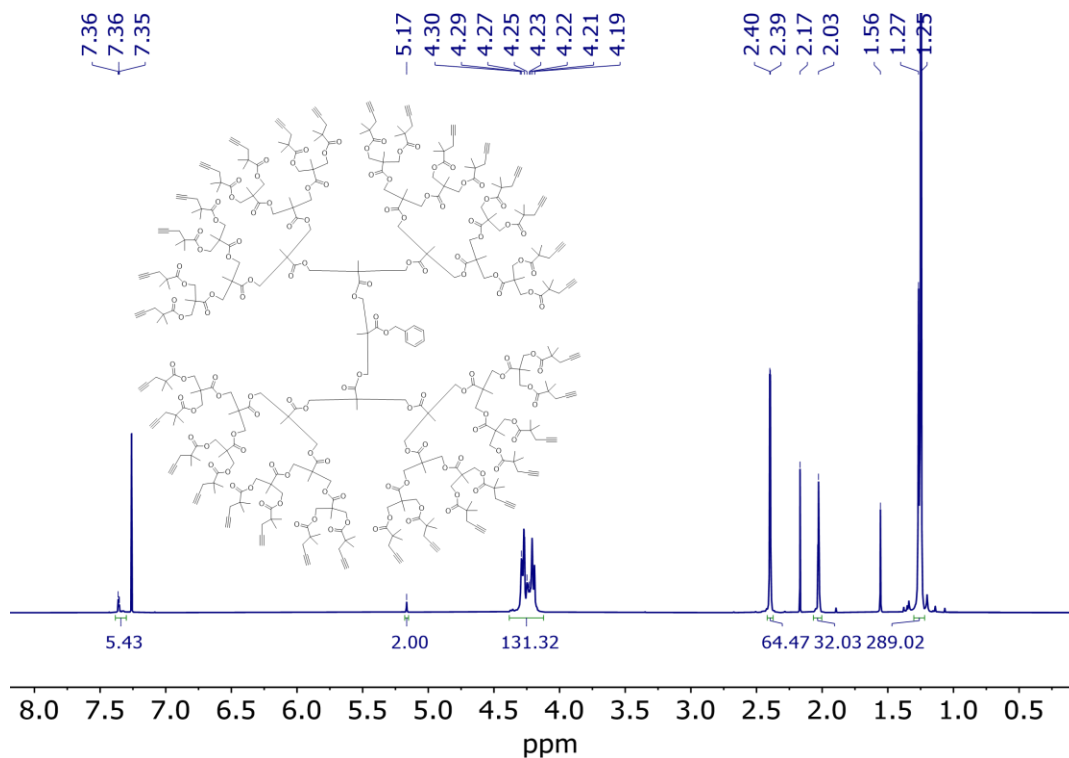


Figure S2.63. ¹H NMR of BnO-G5-(yne)₃₂ in CDCl₃.

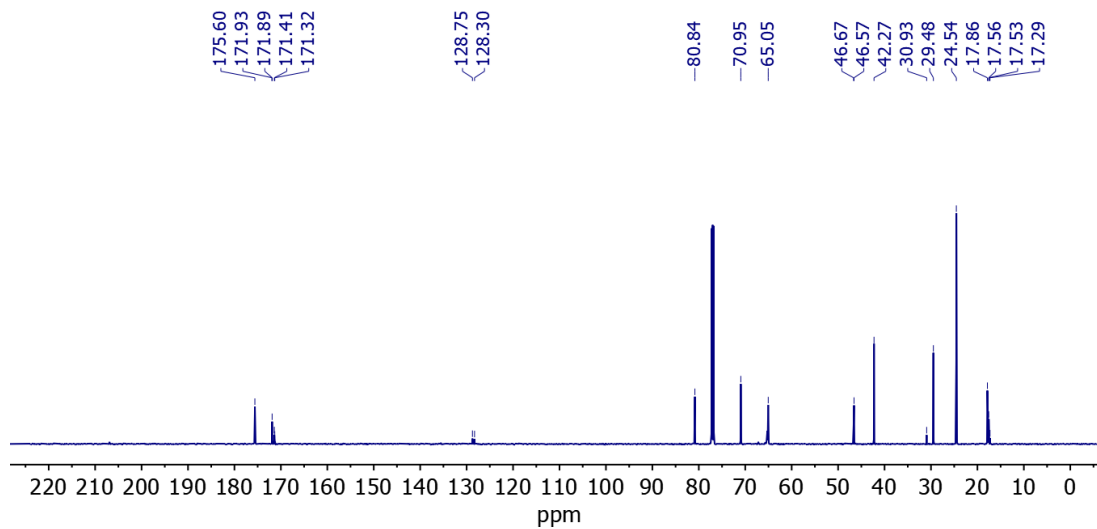


Figure S2.64. ¹³C NMR of BnO-G5-(yne)₃₂ in CDCl₃

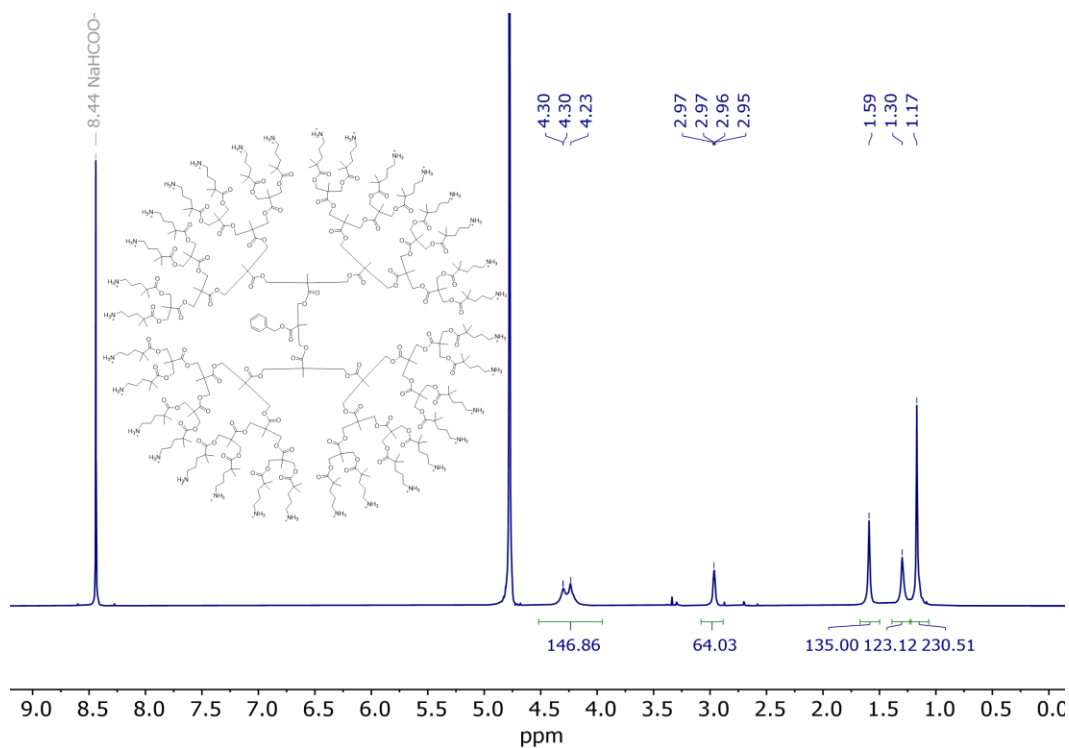


Figure S2.65. ¹H NMR of BnO-G5-(Neo-NH₃⁺TFA⁻)₃₂ in D₂O with NaHCOO⁻ as reference. TFA anions have been omitted from the structure.

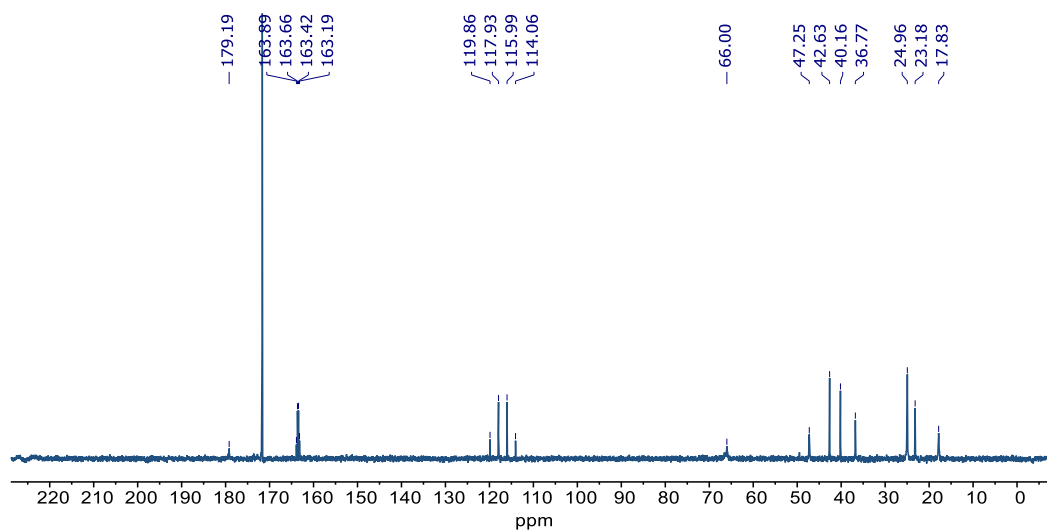


Figure S2.66. ¹³C NMR of BnO-G5-(Neo-NH₃⁺TFA⁻)₃₂ in D₂O with NaHCOO⁻ (δ = 171.67 ppm) as reference.

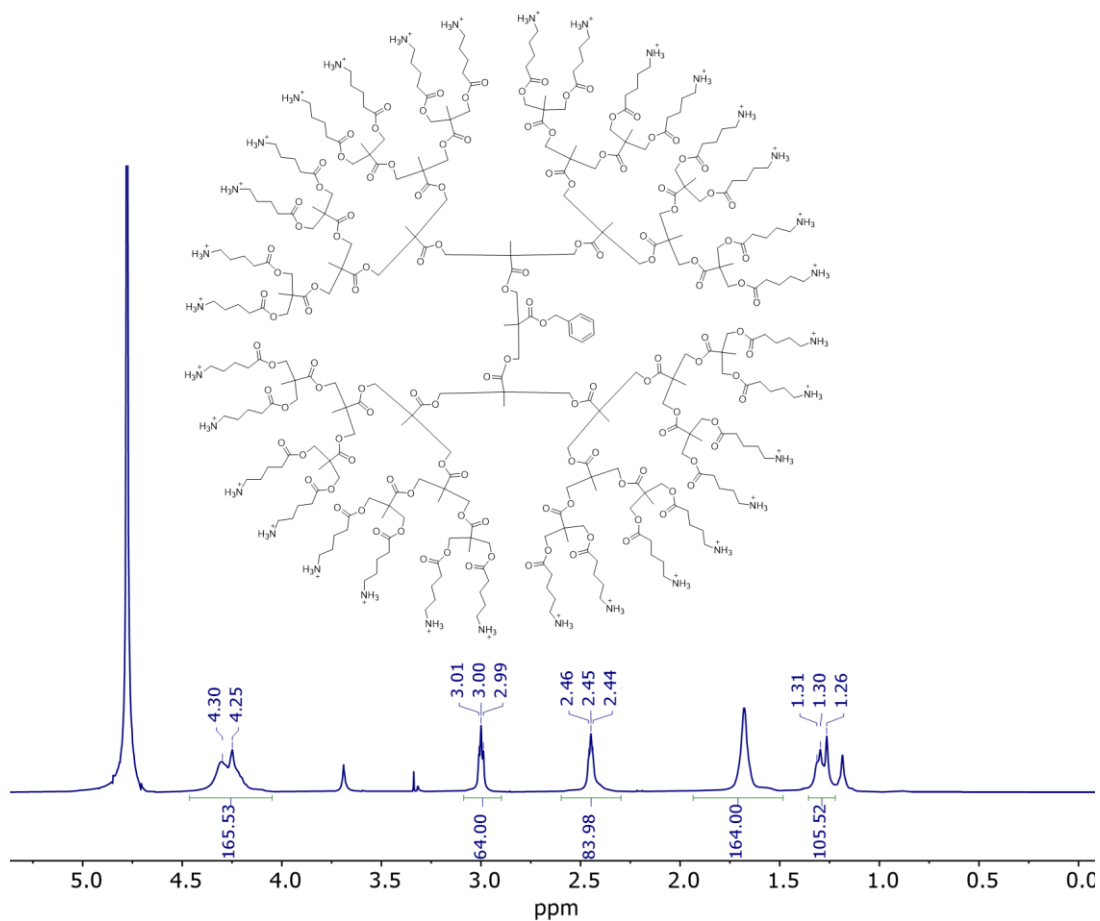


Figure S2.67. ¹H NMR of BnO-G5-(Lin-NH₃⁺TFA⁻)₃₂ in D₂O. TFA anions have been omitted from the structure.

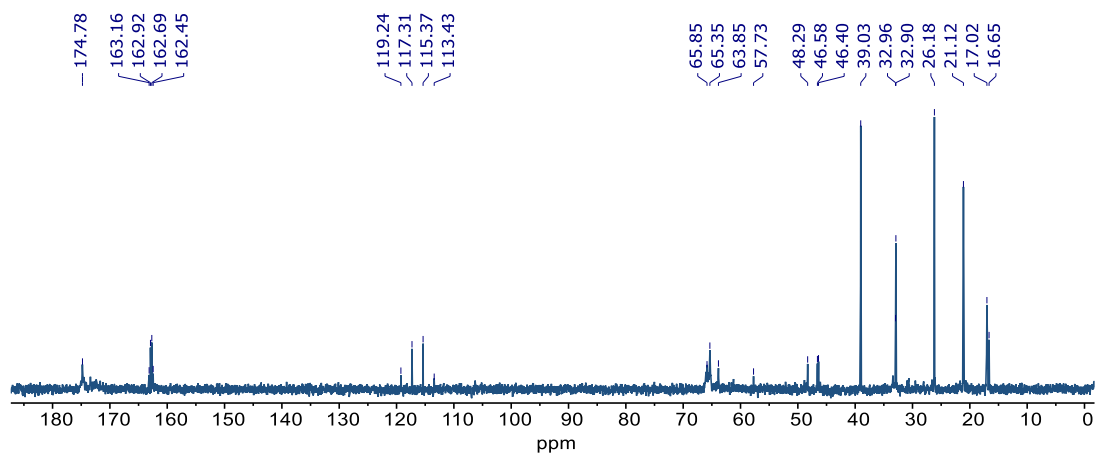


Figure S2.68. ¹³C NMR of BnO-G5-(Lin-NH₃⁺TFA⁻)₃₂ in D₂O.

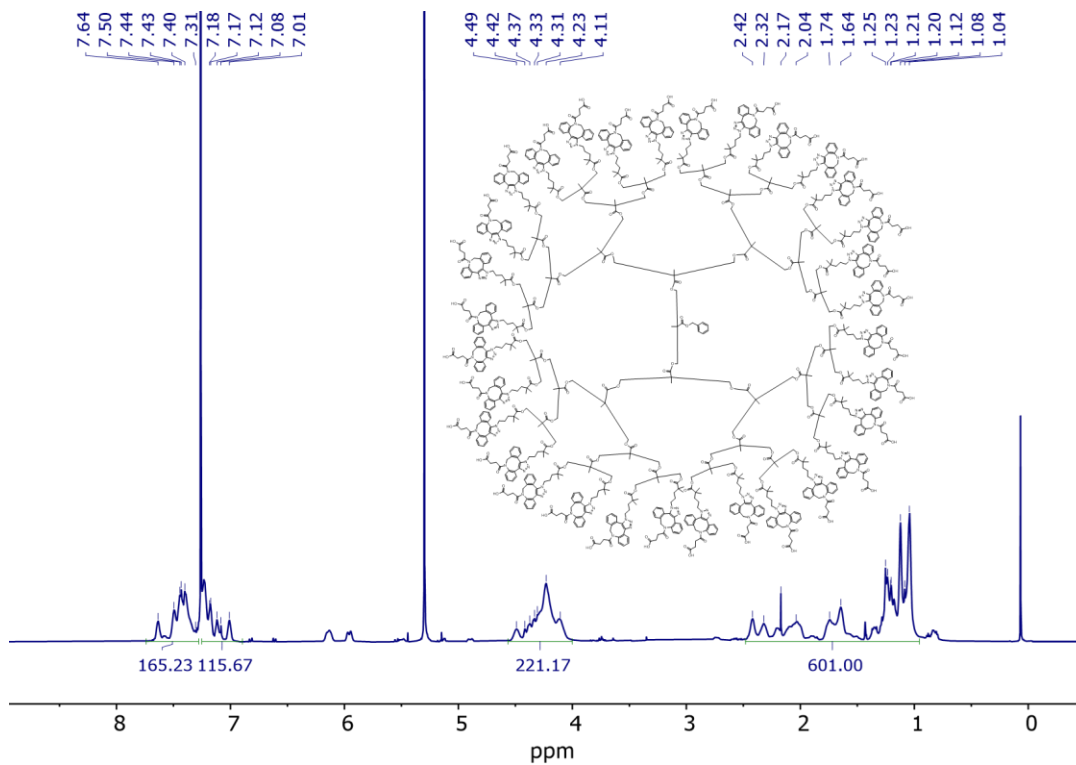


Figure S2.69. ^1H NMR of BnO-G5-(DBCO) $_{32}$ in CDCl_3 .

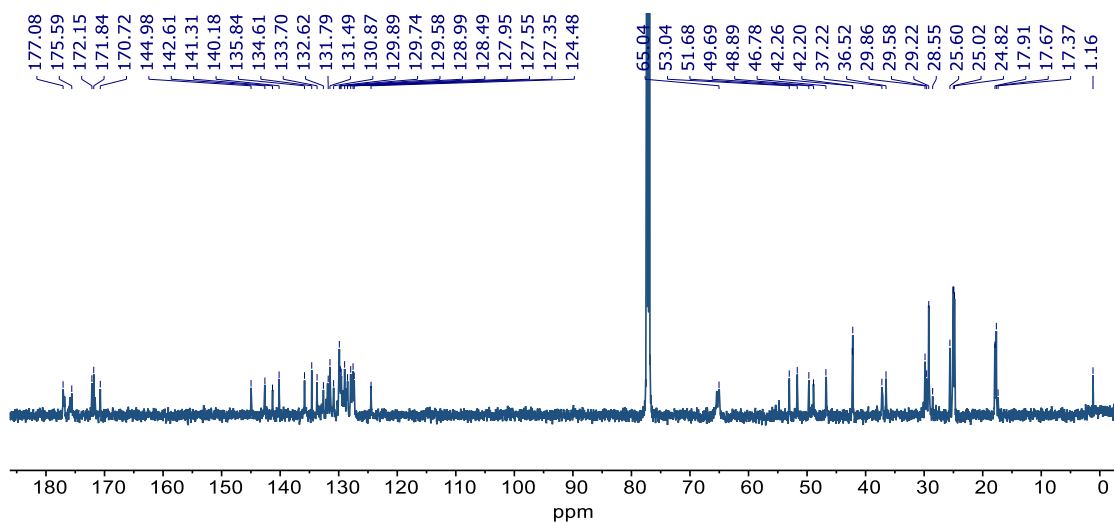


Figure S2.70. ^{13}C NMR of BnO-G5-(DBCO) $_{32}$ in CDCl_3 .

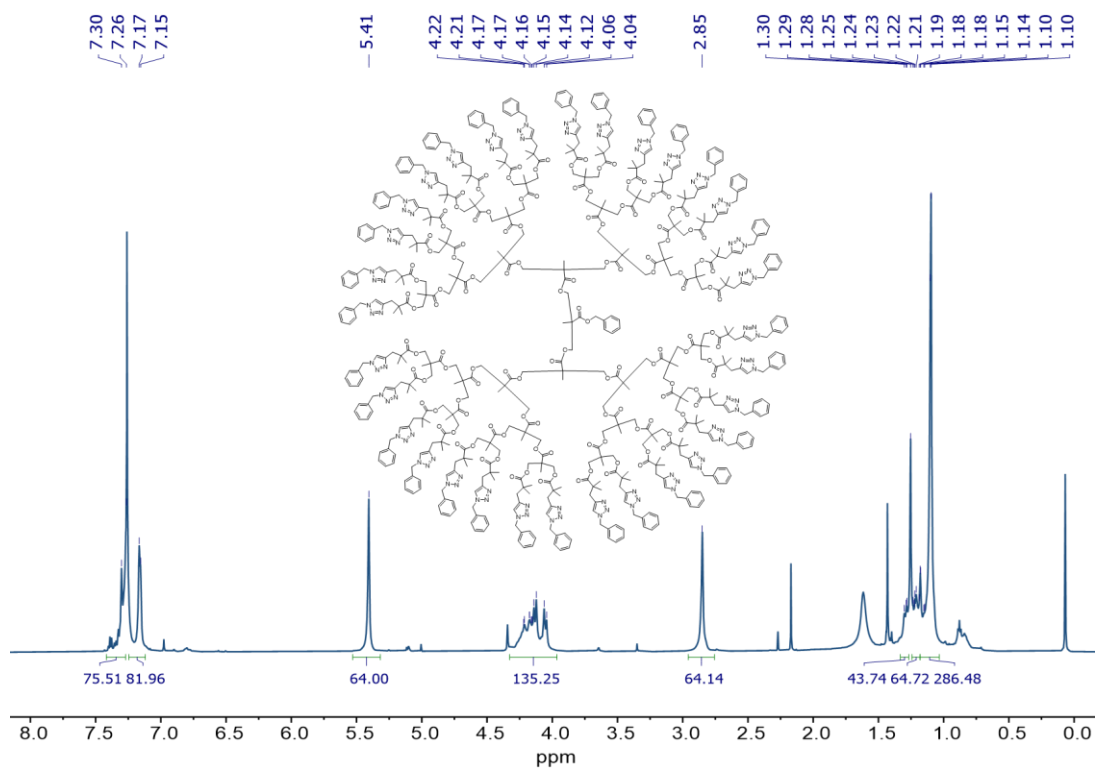


Figure S2.71. ¹H NMR of BnO-G5-(BzTr)₃₂ in CDCl₃.

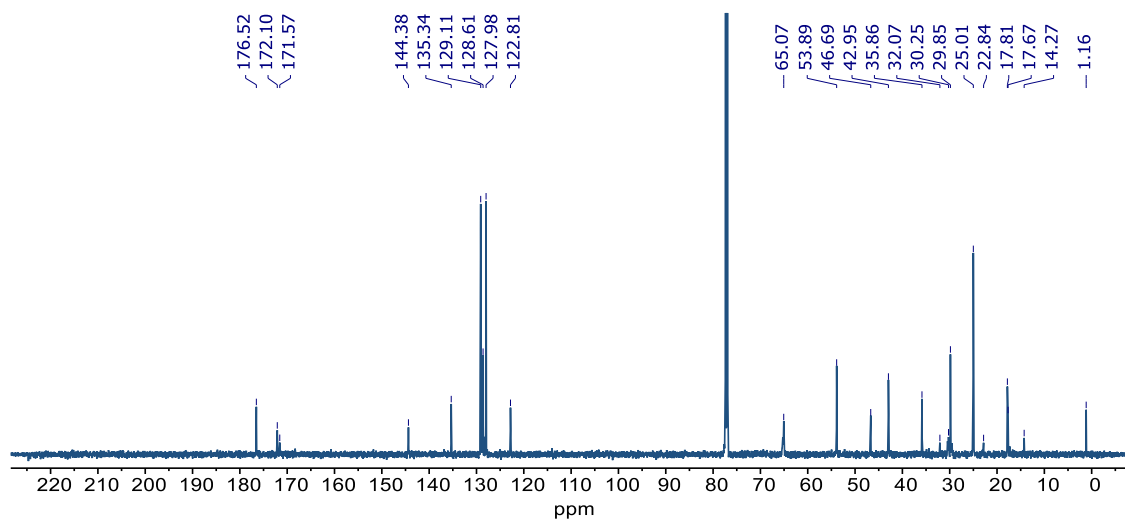


Figure S2.72. ¹³C NMR of BnO-G5-(BzTr)₃₂ in CDCl₃.

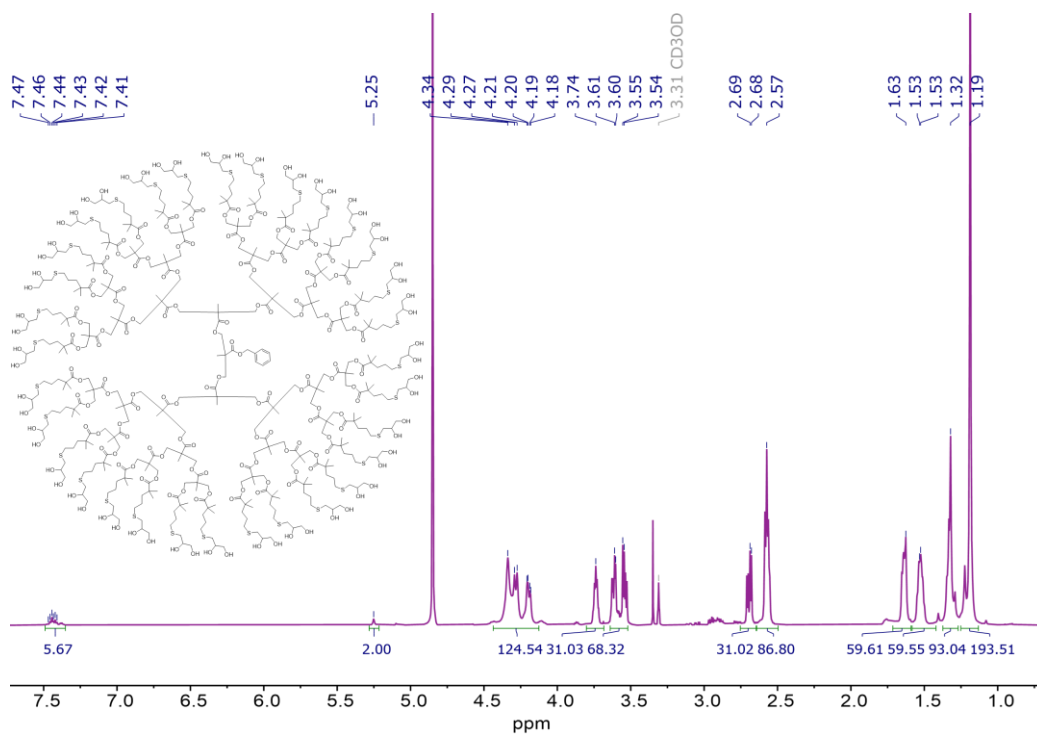


Figure S2.73. ^1H NMR of BnO-G5-(SR)₃₂ in MeOD.

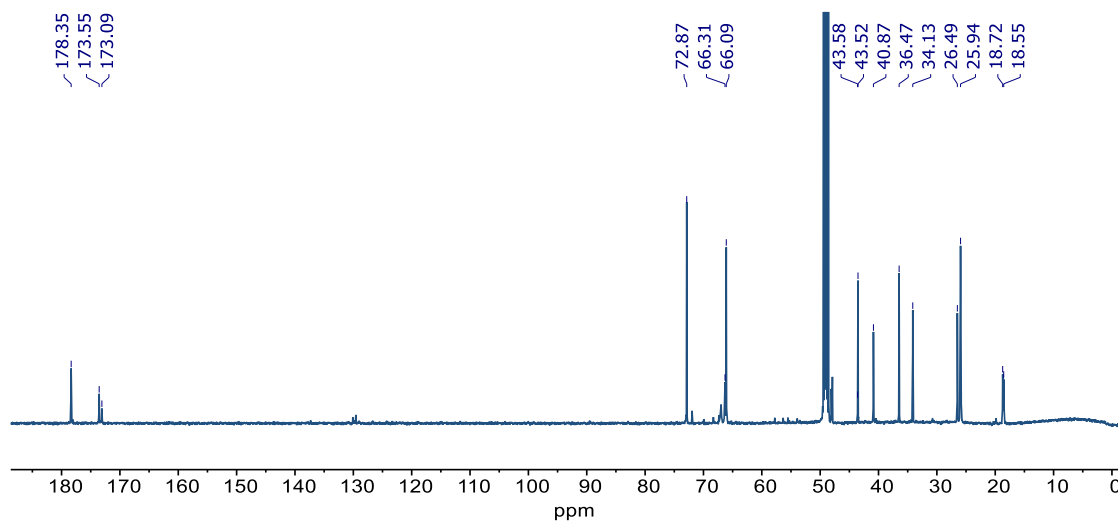


Figure S2.74. ^{13}C NMR of BnO-G5-(SR)₃₂ in MeOD.

Dendron MALDI Mass Spectra

Alkene Dendrons

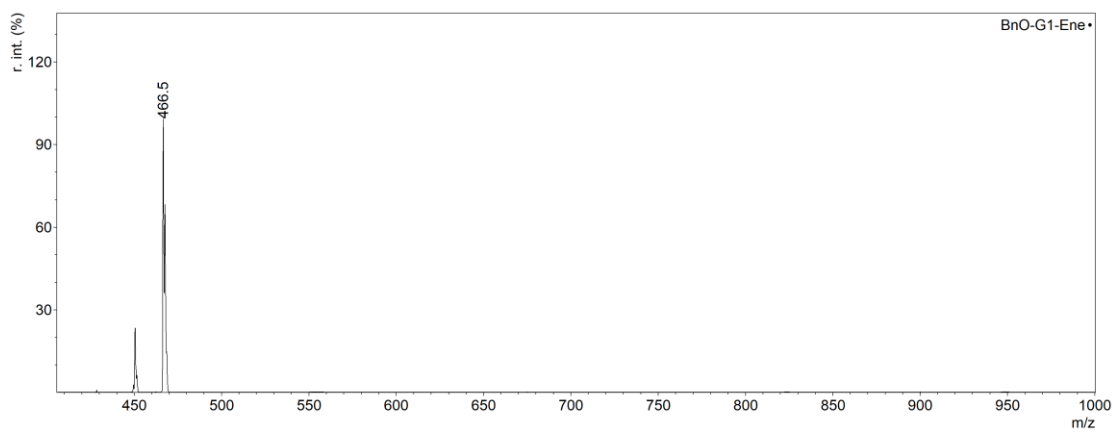


Figure S2.75. MALDI mass spectrum of BnO-G1-(ene)₂.

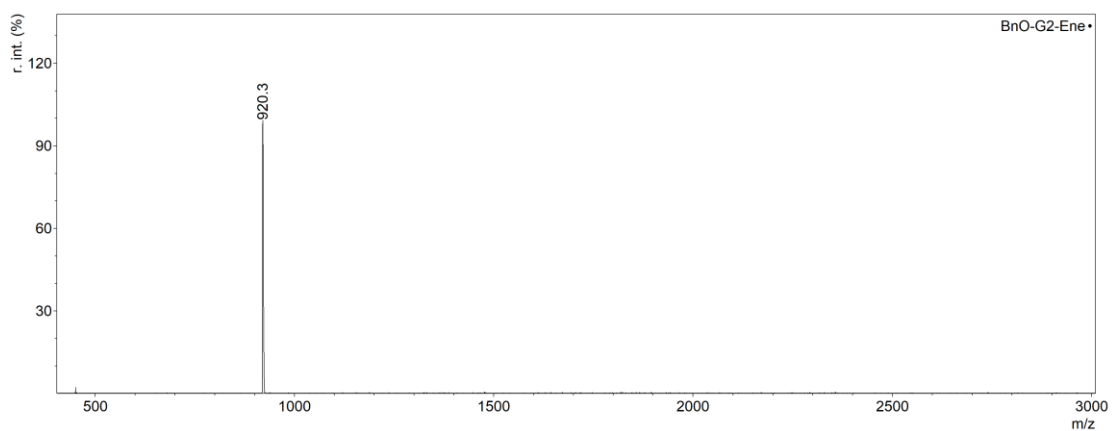


Figure S2.76. MALDI mass spectrum of BnO-G2-(ene)₄.

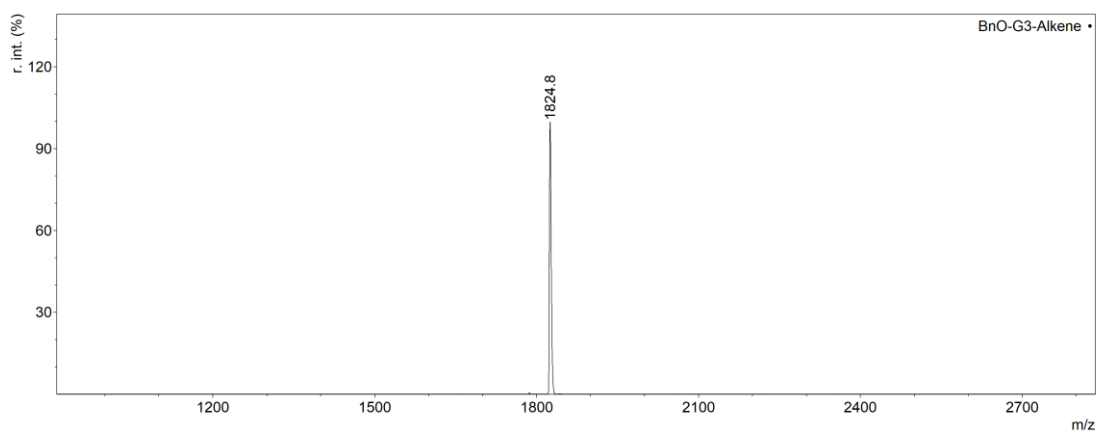


Figure S2.77. MALDI mass spectrum of BnO-G3-(ene)₈.

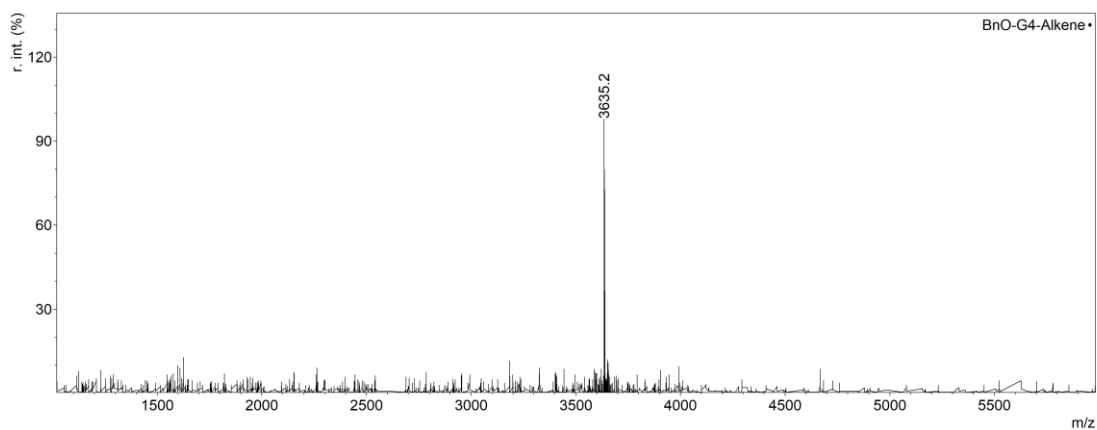


Figure S2.78. MALDI mass spectrum of BnO-G4-(ene)₁₆.

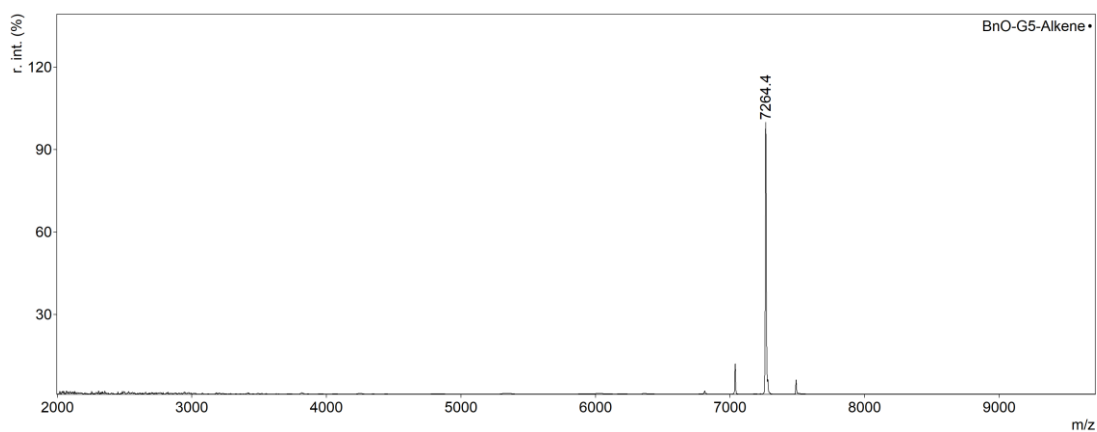


Figure S2.79. MALDI mass spectrum of BnO-G5-(ene)₃₂.

Alkyne Dendrons

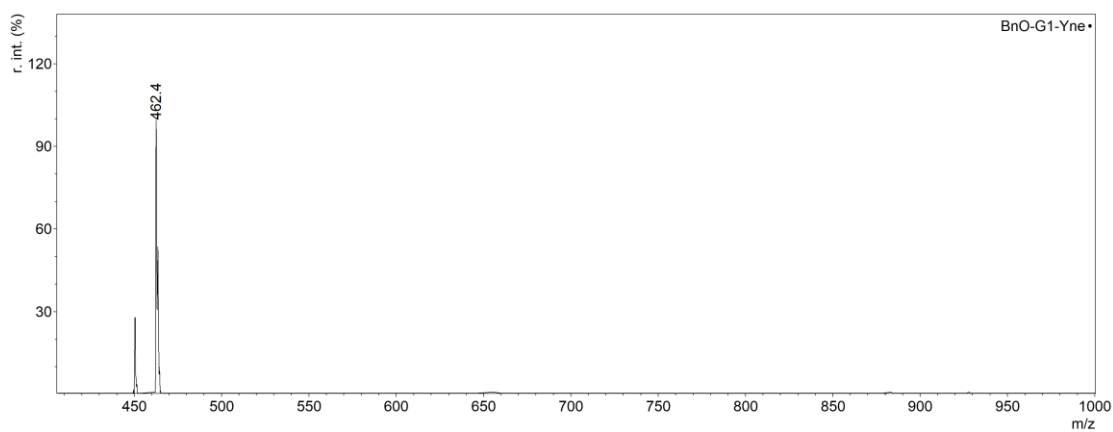


Figure S2.80. MALDI mass spectrum of BnO-G1-(yne)₂.

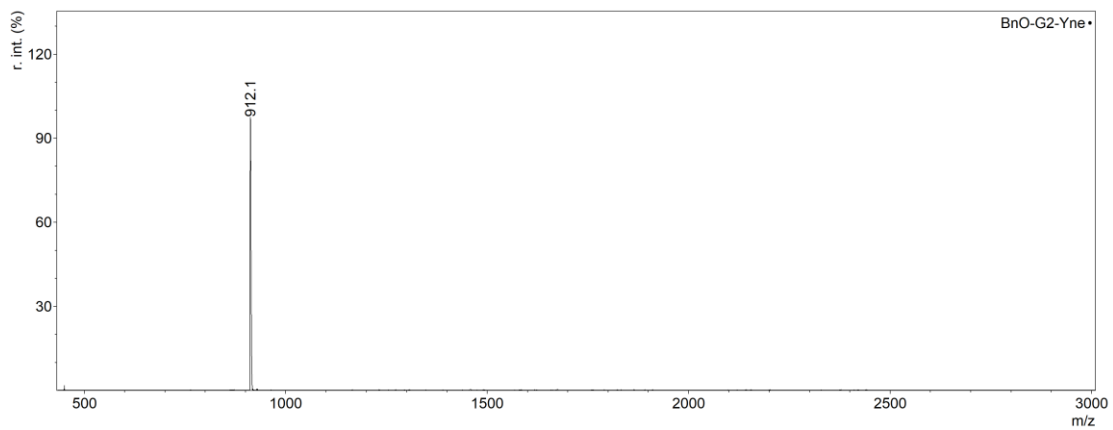


Figure S2.81. MALDI mass spectrum of BnO-G2-(yne)₄.

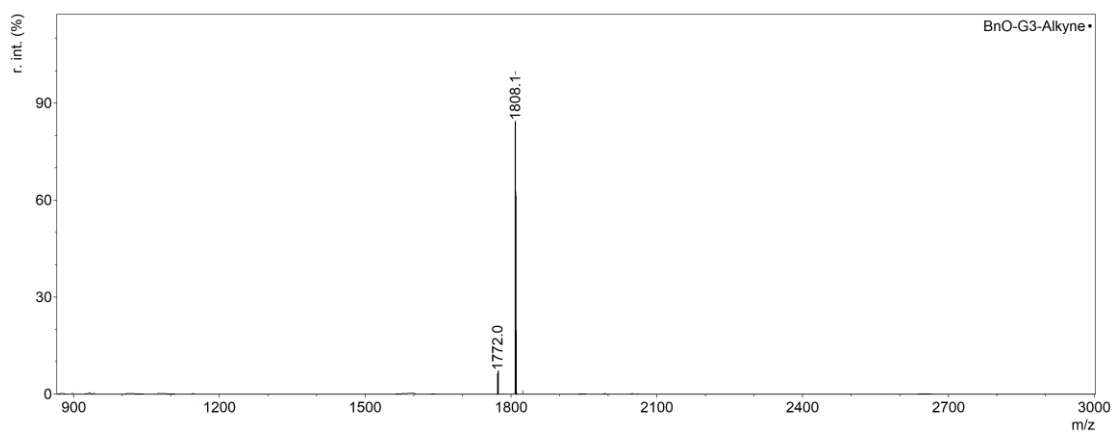


Figure S2.82. MALDI mass spectrum of BnO-G3-(yne)₈.

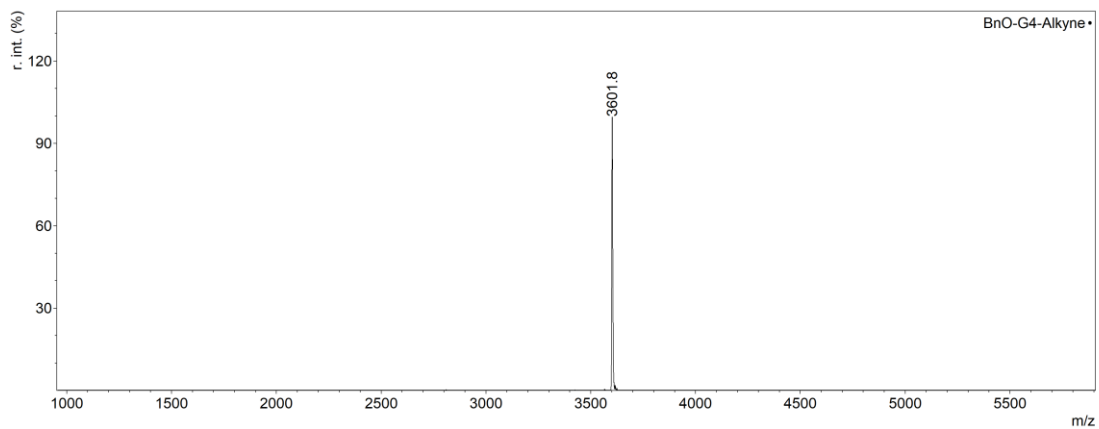


Figure S2.83. MALDI mass spectrum of BnO-G4-(yne)₁₆

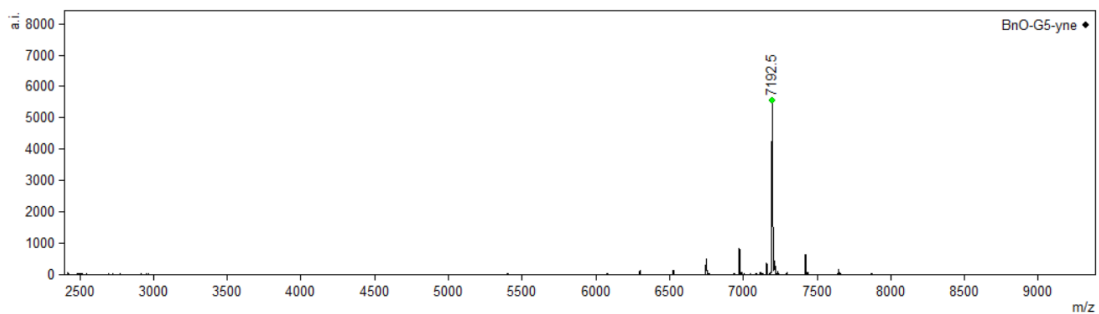


Figure S2.84. MALDI mass spectrum of BnO-G5-(yne)₃₂

Azide Dendrons

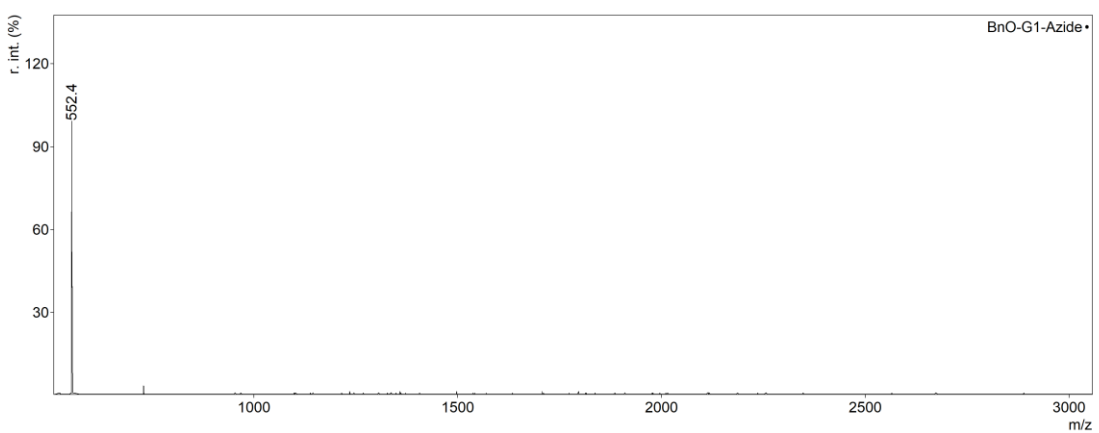


Figure S2.85. MALDI mass spectrum of BnO-G1-(N₃)₂.

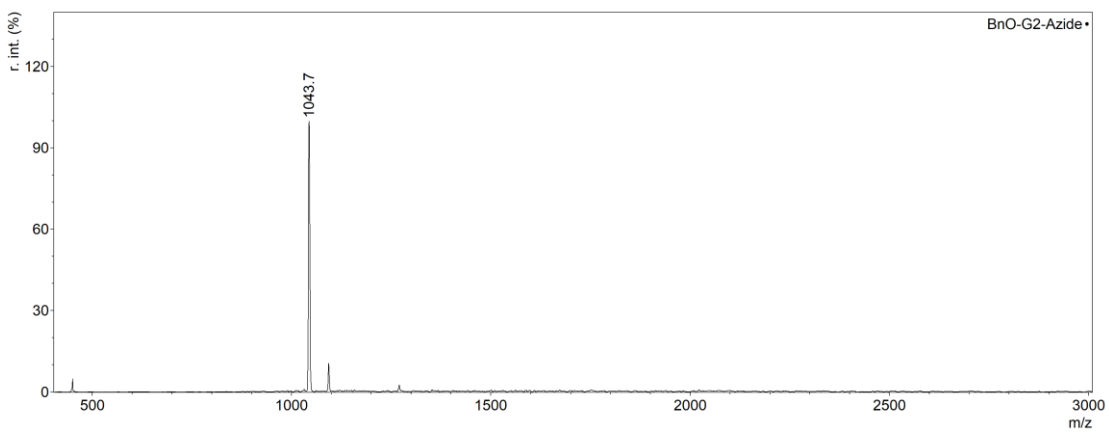


Figure S2.86. MALDI mass spectrum of BnO-G2-(N₃)₄.

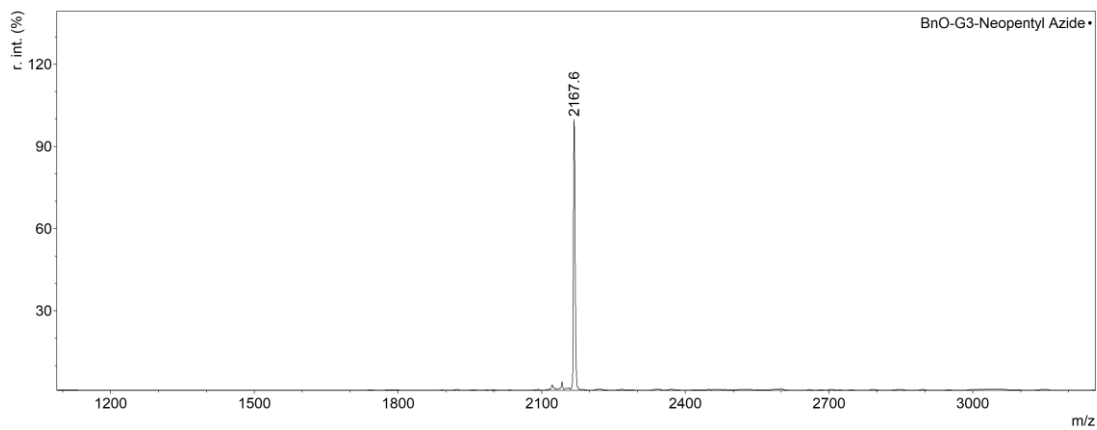


Figure S2.87. MALDI mass spectrum of BnO-G3-(N₃)₈.

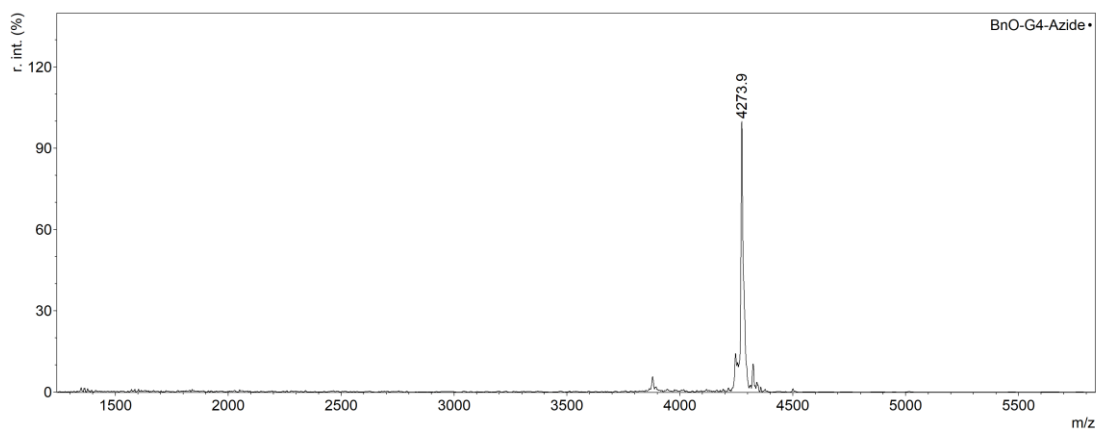


Figure S2.88. MALDI mass spectrum of BnO-G4-(N₃)₁₆.

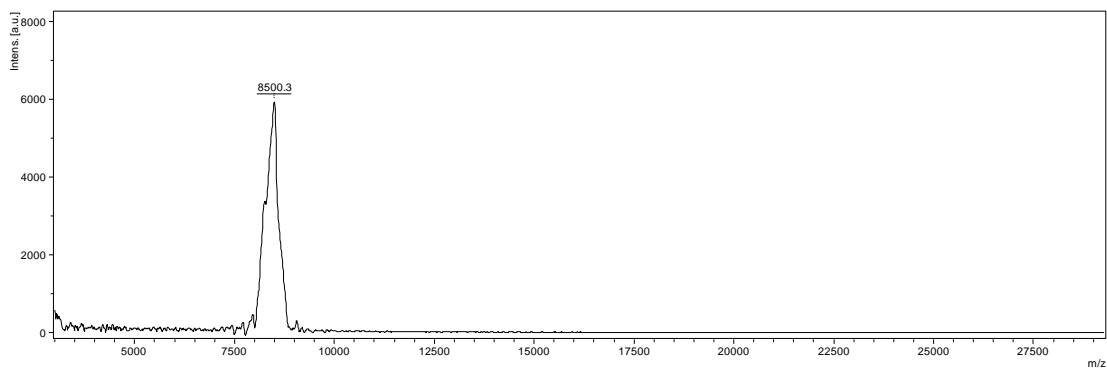


Figure S2.89. MALDI mass spectrum of BnO-G5-(N₃)₃₂.

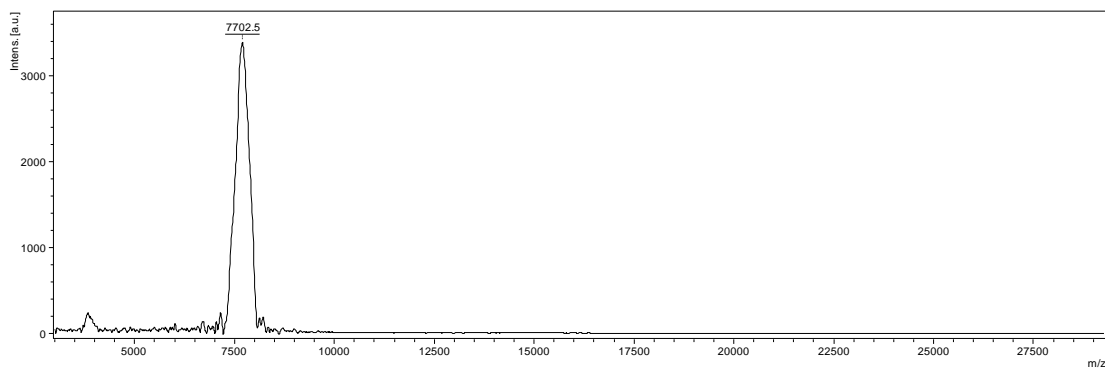


Figure S2.90. MALDI mass spectrum of BnO-G5-(Neo-NH₂)₃₂.

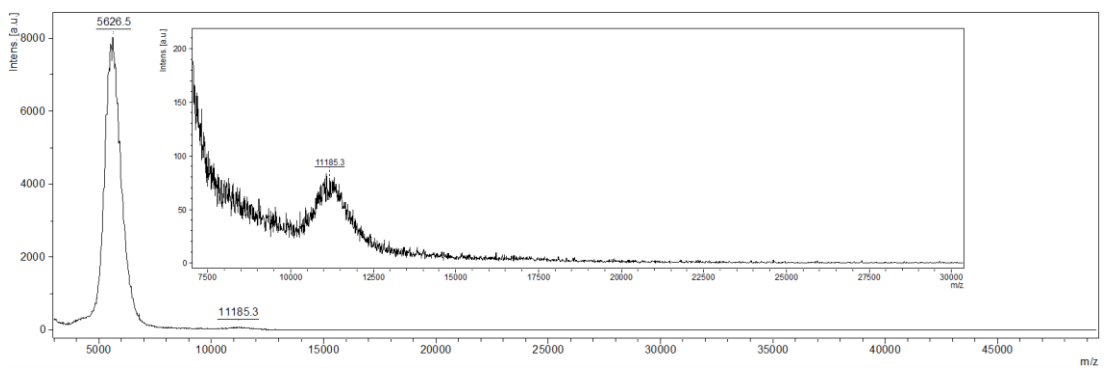


Figure S2.91. MALDI mass spectrum of BnO-G5-(Lin-NH₃⁺TFA⁻)₃₂ showing [m+H]⁺ and [m+2H]²⁺. Inset: magnification showing the [m+H]⁺ species.

Click-reacted Dendrons

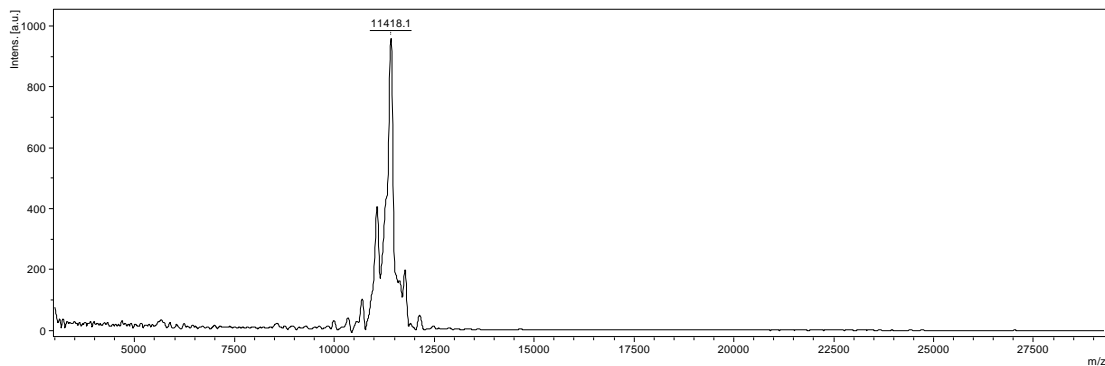


Figure S2.92. MALDI mass spectrum of BnO-G5-(BzTr)₃₂, the CuAAC product of BnO-G5-(yne)₃₂.

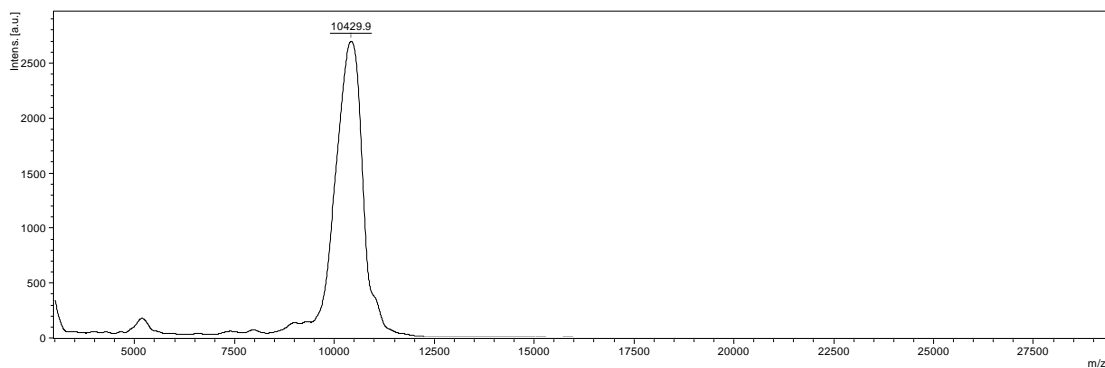


Figure S2.93. MALDI mass spectrum of BnO-G5-(SR)₃₂, the thiol-ene click product of BnO-G5-(ene)₃₂.

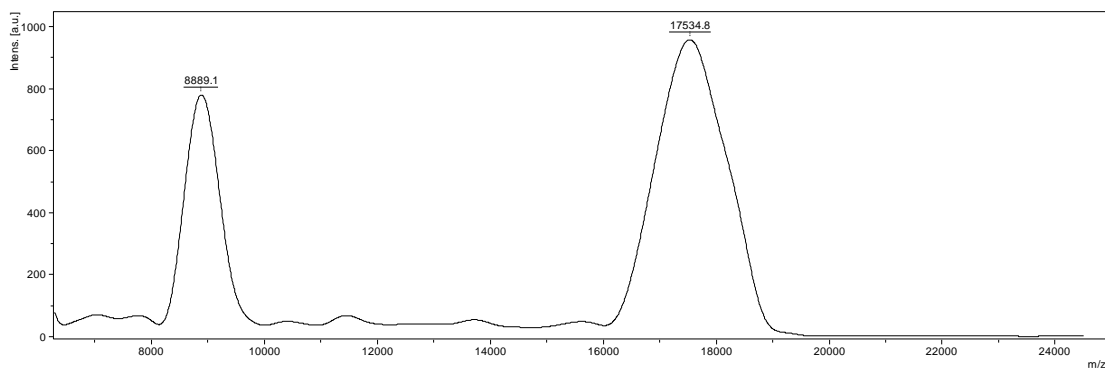


Figure S2.94. MALDI mass spectrum of BnO-G5-(DBCO)₃₂, the SPAAC click product of BnO-G5-(N₃)₃₂.

2.6 References

- (1) Lee, C. C.; Gillies, E. R.; Fox, M. E.; Guillaudeu, S. J.; Fréchet, J. M. J.; Dy, E. E.; Szoka, F. C. A Single Dose of Doxorubicin-Functionalized Bow-Tie Dendrimer Cures Mice Bearing C-26 Colon Carcinomas. *Proc. Natl. Acad. Sci. U. S. A.* **2006**, *103* (45), 16649–16654. <https://doi.org/10.1073/pnas.0607705103>.
- (2) Liechty, W. B.; Kryscio, D. R.; Slaughter, B. V.; Peppas, N. A. Polymers for Drug Delivery Systems. *Annu. Rev. Chem. Biomol. Eng.* **2010**, *1* (1), 149–173. <https://doi.org/10.1146/annurev-chembioeng-073009-100847>.
- (3) Qiu, L. Y.; Bae, Y. H. Polymer Architecture and Drug Delivery. *Pharm. Res.* **2006**, *23* (1), 1–30. <https://doi.org/10.1007/s11095-005-9046-2>.
- (4) Calori, I. R.; Braga, G.; de Jesus, P. da C. C.; Bi, H.; Tedesco, A. C. Polymer Scaffolds as Drug Delivery Systems. *Eur. Polym. J.* **2020**, *129*, 109621. <https://doi.org/10.1016/j.eurpolymj.2020.109621>.
- (5) Tong, X.; Pan, W.; Su, T.; Zhang, M.; Dong, W.; Qi, X. Recent Advances in Natural Polymer-Based Drug Delivery Systems. *React. Funct. Polym.* **2020**, *148*, 104501. <https://doi.org/10.1016/j.reactfunctpolym.2020.104501>.
- (6) Tsoi, K. M.; Macparland, S. A.; Ma, X. Z.; Spetzler, V. N.; Echeverri, J.; Ouyang, B.; Fadel, S. M.; Sykes, E. A.; Goldaracena, N.; Kathis, J. M.; Conneely, J. B.; Alman, B. A.; Selzner, M.; Ostrowski, M. A.; Adeyi, O. A.; Zilman, A.; McGilvray, I. D.; Chan, W. C. W. Mechanism of Hard-Nanomaterial Clearance by the Liver. *Nat. Mater.* **2016**, *15* (11), 1212–1221. <https://doi.org/10.1038/nmat4718>.
- (7) Allen, T. M.; Cullis, P. R. Drug Delivery Systems: Entering the Mainstream. *Science* **2004**, *303* (5665), 1818–1822. <https://doi.org/10.1126/science.1095833>.
- (8) Aied, A.; Greiser, U.; Pandit, A.; Wang, W. Polymer Gene Delivery: Overcoming the Obstacles. *Drug Discov. Today* **2013**, *18* (21–22), 1090–1098. <https://doi.org/10.1016/j.drudis.2013.06.014>.
- (9) Green, J. J.; Langer, R.; Anderson, D. G. A Combinatorial Polymer Library Approach Yields Insight into Nonviral Gene Delivery. *Acc. Chem. Res.* **2008**, *41* (6), 749–759. <https://doi.org/10.1021/ar7002336>.
- (10) Stenström, P.; Manzanares, D.; Zhang, Y.; Ceña, V.; Malkoch, M. Evaluation of Amino-Functional Polyester Dendrimers Based on Bis-MPA as Nonviral Vectors for siRNA Delivery. *Molecules* **2018**, *23* (8), 2028. <https://doi.org/10.3390/molecules23082028>.
- (11) Kim, J.-H.; Park, K.; Nam, H. Y.; Lee, S.; Kim, K.; Kwon, I. C. Polymers for Bioimaging. *Prog. Polym. Sci.* **2007**, *32* (8–9), 1031–1053. <https://doi.org/10.1016/j.progpolymsci.2007.05.016>.
- (12) Ding, C.; Cheng, W.; Sun, Y.; Wang, X. Novel Fungus-Fe₃O₄ Bio-Nanocomposites as High Performance Adsorbents for the Removal of Radionuclides. *J. Hazard. Mater.* **2015**, *295*, 127–137. <https://doi.org/10.1016/j.jhazmat.2015.04.032>.
- (13) Braeken, Y.; Cheruku, S.; Ethirajan, A.; Maes, W. Conjugated Polymer Nanoparticles for Bioimaging. *Materials* **2017**, *10* (12), 1420. <https://doi.org/10.3390/ma10121420>.

- (14) Hong, G.; Zou, Y.; Antaris, A. L.; Diao, S.; Wu, D.; Cheng, K.; Zhang, X.; Chen, C.; Liu, B.; He, Y.; Wu, J. Z.; Yuan, J.; Zhang, B.; Tao, Z.; Fukunaga, C.; Dai, H. Ultrafast Fluorescence Imaging in Vivo with Conjugated Polymer Fluorophores in the Second Near-Infrared Window. *Nat. Commun.* **2014**, *5*.
<https://doi.org/10.1038/ncomms5206>.
- (15) Zhou, Y.; Fang, A.; Wang, F.; Li, H.; Jin, Q.; Huang, L.; Fu, C.; Zeng, J.; Jin, Z.; Song, X. Core-Shell Lipid-Polymer Nanoparticles as a Promising Ocular Drug Delivery System to Treat Glaucoma. *Chin. Chem. Lett.* **2020**, *31* (2), 494–500.
<https://doi.org/10.1016/j.ccllet.2019.04.048>.
- (16) Ihre, H.; Hult, A.; Fréchet, J. M. J.; Gitsov, I. Double-Stage Convergent Approach for the Synthesis of Functionalized Dendritic Aliphatic Polyesters Based on 2,2-Bis(Hydroxymethyl)Propionic Acid. *Macromolecules* **1998**, *31* (13), 4061–4068.
<https://doi.org/10.1021/ma9718762>.
- (17) Movellan, J.; Urbán, P.; Moles, E.; de la Fuente, J. M.; Sierra, T.; Serrano, J. L.; Fernández-Busquets, X. Amphiphilic Dendritic Derivatives as Nanocarriers for the Targeted Delivery of Antimalarial Drugs. *Biomaterials* **2014**, *35* (27), 7940–7950.
<https://doi.org/10.1016/j.biomaterials.2014.05.061>.
- (18) Stenström, P.; Hjorth, E.; Zhang, Y.; Andrén, O. C. J.; Guette-Marquet, S.; Schultzberg, M.; Malkoch, M. Synthesis and in Vitro Evaluation of Monodisperse Amino-Functional Polyester Dendrimers with Rapid Degradability and Antibacterial Properties. *Biomacromolecules* **2017**, *18* (12), 4323–4330.
<https://doi.org/10.1021/acs.biomac.7b01364>.
- (19) McNelles, S. A.; Knight, S. D.; Janzen, N.; Valliant, J. F.; Adronov, A. Synthesis, Radiolabeling, and In Vivo Imaging of PEGylated High-Generation Polyester Dendrimers. *Biomacromolecules* **2015**, *16* (9), 3033–3041.
<https://doi.org/10.1021/acs.biomac.5b00911>.
- (20) Gillies, E. R.; Dy, E.; Fréchet, J. M. J.; Szoka, F. C. Biological Evaluation of Polyester Dendrimer: Poly(Ethylene Oxide) “Bow-Tie” Hybrids with Tunable Molecular Weight and Architecture. *Mol. Pharm.* **2005**, *2* (2), 129–138.
<https://doi.org/10.1021/mp049886u>.
- (21) Killops, K. L.; Campos, L. M.; Hawker, C. J. Robust, Efficient, and Orthogonal Synthesis of Dendrimers via Thiol-Ene “Click” Chemistry. *J. Am. Chem. Soc.* **2008**, *130* (15), 5062–5064. <https://doi.org/10.1021/ja8006325>.
- (22) Carlmark, A.; Malmström, E.; Malkoch, M. Dendritic Architectures Based on Bis-MPA: Functional Polymeric Scaffolds for Application-Driven Research. *Chem. Soc. Rev.* **2013**, *42* (13), 5858–5879. <https://doi.org/10.1039/c3cs60101c>.
- (23) Agashe, H. B.; Dutta, T.; Garg, M.; Jain, N. K. Investigations on the Toxicological Profile of Functionalized Fifth-Generation Poly(Propylene Imine) Dendrimer. *J. Pharm. Pharmacol.* **2006**, *58* (11), 1491–1498.
<https://doi.org/10.1211/jpp.58.11.0010>.
- (24) Thiagarajan, G.; Greish, K.; Ghandehari, H. Charge Affects the Oral Toxicity of Poly(Amidoamine) Dendrimers. *Eur. J. Pharm. Biopharm.* **2013**, *84* (2), 330–334.
<https://doi.org/10.1016/j.ejpb.2013.01.019>.

- (25) Janaszewska, A.; Lazniewska, J.; Trzepiński, P.; Marcinkowska, M.; Klajnert-Maculewicz, B. Cytotoxicity of Dendrimers. *Biomolecules* **2019**, *9* (8), 330. <https://doi.org/10.3390/biom9080330>.
- (26) Feliu, N.; Walter, M. V.; Montañez, M. I.; Kunzmann, A.; Hult, A.; Nyström, A.; Malkoch, M.; Fadeel, B. Stability and Biocompatibility of a Library of Polyester Dendrimers in Comparison to Polyamidoamine Dendrimers. *Biomaterials* **2012**, *33* (7), 1970–1981. <https://doi.org/10.1016/j.biomaterials.2011.11.054>.
- (27) Goodwin, A. P.; Lam, S. S.; Fréchet, J. M. J. Rapid, Efficient Synthesis of Heterobifunctional Biodegradable Dendrimers. *J. Am. Chem. Soc.* **2007**, *129* (22), 6994–6995. <https://doi.org/10.1021/ja071530z>.
- (28) Feliu, N.; Walter, M. V.; Montañez, M. I.; Kunzmann, A.; Hult, A.; Nyström, A.; Malkoch, M.; Fadeel, B. Stability and Biocompatibility of a Library of Polyester Dendrimers in Comparison to Polyamidoamine Dendrimers. *Biomaterials* **2012**, *33* (7), 1970–1981. <https://doi.org/10.1016/j.biomaterials.2011.11.054>.
- (29) Huang, D.; Wu, D. Biodegradable Dendrimers for Drug Delivery. *Mater. Sci. Eng. C* **2018**, *90* (March), 713–727. <https://doi.org/10.1016/j.msec.2018.03.002>.
- (30) García-Gallego, S.; Hult, D.; Olsson, J. V.; Malkoch, M. Fluoride-Promoted Esterification with Imidazolide-Activated Compounds: A Modular and Sustainable Approach to Dendrimers. *Angew. Chem. - Int. Ed.* **2015**, *54* (8), 2416–2419. <https://doi.org/10.1002/anie.201411370>.
- (31) Antoni, P.; Robb, M. J.; Campos, L.; Montanez, M.; Hult, A.; Malmström, E.; Malkoch, M.; Hawker, C. J. Pushing the Limits for Thiol-Ene and CuAAC Reactions: Synthesis of a 6th Generation Dendrimer in a Single Day. *Macromolecules* **2010**, *43* (16), 6625–6631. <https://doi.org/10.1021/ma101242u>.
- (32) McNelles, S. A.; Adronov, A. Rapid Synthesis of Functionalized High-Generation Polyester Dendrimers via Strain-Promoted Alkyne-Azide Cycloaddition. *Macromolecules* **2017**, *50* (20), 7993–8001. <https://doi.org/10.1021/acs.macromol.7b01765>.
- (33) Medina, S. H.; El-Sayed, M. E. H. Dendrimers as Carriers for Delivery of Chemotherapeutic Agents. *Chem. Rev.* **2009**, *109* (7), 3141–3157. <https://doi.org/10.1021/cr900174j>.
- (34) McNelles, S. A.; Pantaleo, J. L.; Meichsner, E.; Adronov, A. Strain-Promoted Azide-Alkyne Cycloaddition-Mediated Step-Growth Polymerization. *Macromolecules* **2019**, *52* (19), 7183–7187. <https://doi.org/10.1021/acs.macromol.9b01609>.
- (35) Durán-Lara, E. F.; Marple, J. L.; Giesen, J. A.; Fang, Y.; Jordan, J. H.; Godbey, W. T.; Marican, A.; Santos, L. S.; Grayson, S. M. Investigation of Lysine-Functionalized Dendrimers as Dichlorvos Detoxification Agents. *Biomacromolecules* **2015**, *16* (11), 3434–3444. <https://doi.org/10.1021/acs.biomac.5b00657>.
- (36) Zhou, Z.; Cong, M.; Li, M.; Tintaru, A.; Li, J.; Yao, J.; Xia, Y.; Peng, L. Negative Dendritic Effect on Enzymatic Hydrolysis of Dendrimer Conjugates. *Chem. Commun.* **2018**, *54* (47), 5956–5959. <https://doi.org/10.1039/c8cc01221k>.

- (37) Kayahara, E.; Yamada, H.; Yamago, S. Generation of Carbanions through Stibine-Metal and Bismuthine-Metal Exchange Reactions and Its Applications to Precision Synthesis of ω -End-Functionalized Polymers. *Chem. - Eur. J.* **2011**, *17* (19), 5272–5280. <https://doi.org/10.1002/chem.201100265>.
- (38) Cottrell, I. F.; Cowley, A. R.; Croft, L. J.; Hymns, L.; Moloney, M. G.; Nettleton, E. J.; Kirsty Smithies, H.; Thompson, A. L. Acyloxylactonisations Mediated by Lead Tetracarboxylates. *Tetrahedron* **2009**, *65* (12), 2537–2550. <https://doi.org/10.1016/j.tet.2009.01.042>.
- (39) Ramsay, W. J.; Bell, N. A. W.; Qing, Y.; Bayley, H. Single-Molecule Observation of the Intermediates in a Catalytic Cycle. *J. Am. Chem. Soc.* **2018**, *140* (50), 17538–17546. <https://doi.org/10.1021/jacs.8b09282>.
- (40) Mueller, R.; Yang, J.; Duan, C.; Pop, E.; Zhang, L. H.; Huang, T.-B.; Denisenko, A.; Denisko, O. V.; Oniciu, D. C.; Bisgaier, C. L.; Pape, M. E.; Freiman, C. D.; Goetz, B.; Cramer, C. T.; Hopson, K. L.; Dasseux, J.-L. H. Long Hydrocarbon Chain Ether Diols and Ether Diacids That Favorably Alter Lipid Disorders in Vivo. *J. Med. Chem.* **2004**, *47* (21), 5183–5197. <https://doi.org/10.1021/jm0400395>.

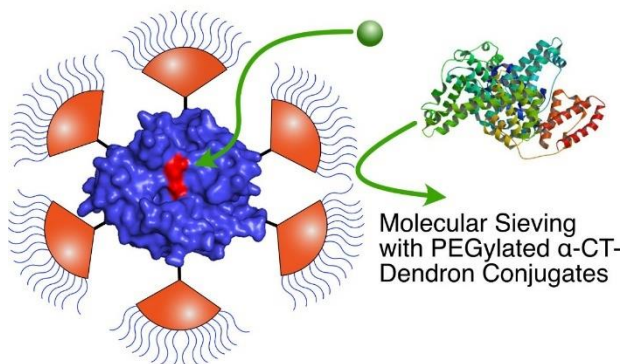
Chapter 3. Molecular Sieving with PEGylated Dendron-Protein

Conjugates

This chapter has been reproduced with permission from Deng, B.; Burns, E.; McNelles, S. A.; Sun, J.; Ortega, J.; Adronov, A. Molecular Sieving with PEGylated Dendron-Protein Conjugates. *Bioconjugate Chemistry* **2023**, *34* (8), 1467–1476. Copyright 2023, American Chemical Society.

This work detailed in this chapter was carried out in collaboration with Evan Burns, Stuart McNelles, Jingyu Sun and Joaquin Ortega. Billy Deng and Evan Burns synthesized and characterized the small molecules and dendrimers. Billy Deng synthesized, characterized, and assayed the dendron-protein conjugates. Jingyu Sun and Joaquin Ortega performed cryo-EM microscopy. Billy Deng, Jingyu Sun, Joaquin Ortega, Stuart McNelles and Alex Adronov prepared the manuscript.

Graphical Abstract:



3.1 Abstract

A series of generation 3–5 dendrons based on a bis(2,2-hydroxymethylpropionic acid) (bis-MPA) scaffold bearing three respective lengths of linear poly(ethylene glycol) at their

periphery and a dibenzocyclooctyne unit at their core was prepared. These dendrons were appended to the surface of azide-decorated α -chymotrypsin (α -CT) via strain-promoted azide–alkyne cycloaddition to yield a library of dendron-protein conjugates. These conjugates were characterized by FT-IR and NMR spectroscopy and were imaged using cryo-electron microscopy. The activity of the PEGylated α -CT-dendron conjugates was investigated using a small molecule (benzoyl-L-tyrosine *p*-nitroanilide) as well as different proteins of different sizes and crystallinities (casein and bovine serum albumin) as substrates. It was found that the activity of the conjugates toward the small molecule was largely retained, while the activity toward the proteins was significantly diminished. Furthermore, the results indicate that for most of the conjugates the PEG length had a more pronounced impact on enzyme activity than the dendron generation. Overall, the highest sieving ratios were found for α -CT-dendron conjugates decorated with G3-PEG₂₀₀₀, G4-PEG₂₀₀₀, and G5-PEG₁₀₀₀, with the latter two structures offering the best combination of sieving ratio and small molecule activity.

3.2 Introduction

Polymer-protein conjugates are versatile therapeutic agents that exhibit unique characteristics relative to their native counterparts, such as polymer shielding of antigenic epitopes and increased protein stability *in vivo*.¹⁻⁶ One of the most common methods of modifying proteins is the grafting of poly(ethylene glycol) (PEG) chains onto the surface of proteins, also known as PEGylation. PEGylated proteins have been found to exhibit lower immunogenicity⁷⁻⁹ and increased half-life, and PEG grafts have also been employed to improve protein solubility in both aqueous and organic media. As such, despite having

begun nearly 50 years ago,^{10,11} PEGylation is still widely considered to be the gold-standard for protein modification. Innovations in utility and architecture continue to be reported, such as controlled and site-specific PEGylation for increasing enzyme stability,^{2,12,13} and protein grafting with PEG-derived, comb-shaped poly[oligo(ethylene glycol)] (pOEGMA) to impart stealth properties while minimizing anti-PEG antigenicity.^{1,14} Hyper-PEGylation with high-density PEG brushes has also been used to prevent protein-surface interactions^{14,15} and even to inhibit phagocytic cell uptake of ovalbumin nanocapsules.¹⁶ In recent years, enzymes grafted with PEG-brushes and combs have been used to selectively block protein-protein interactions while still allowing small molecule substrates to diffuse through to the active site – an effect known as molecular sieving.^{8,17} The seminal work by Gauthier and coworkers showcased this size-based effect with chymotrypsin¹⁸ (CT) and L-asparaginase¹⁹ conjugates, respectively, using pOEGMA comb polymers. The authors noted that sieving efficiency was affected by polymer molecular weight and conformation in solution. Moreover, the conformation of the grafted monolayer in solution depended on its grafting density and the flexibility of the polymer chain, the latter of which was in turn tunable by altering the backbone and sidechain lengths. The comb polymer architecture was further employed by Russell and coworkers using poly(carboxybetaine methacrylate) (PCBMA) grafted to avidin, with similar results.²⁰ The authors therein elegantly demonstrated that sieving activity (as measured through binding kinetics of biotin and biotin-PEG ligands) positively correlated with grafting density on the surface of avidin. In contrast to Gauthier's findings,¹⁸ however, the molecular weight of the grafted PCBMA had only a small influence on sieving activity relative to grafting density. Nonetheless, the

general trend appears to be that a high-density monolayer comprised of polymers that occupy a large hydrodynamic volume correlates with better exclusion of macromolecules. The above work infers that optimizing sieving activity on a protein conjugate is a multifaceted process that cannot simply be achieved through modifying grafting density, architecture, or molecular weight alone. Using a different approach, our group has recently explored molecular sieving in dendritic polymer conjugates, specifically high-generation dendrimer-chymotrypsin (CT) hybrids.²¹ Dendrimers offer excellent control over dispersity and morphology, which we rationalized would ensure a uniform monolayer when grafted onto the enzyme. In our work, CT was conjugated with a library of poly(bis-2,2-(hydroxymethylpropionic acid)) (bis-MPA)-based polyester dendrimers, spanning generations (G) 2-8. When compared to native CT, the two highest generation (G7 and G8) protein-dendrimer conjugates exhibited unhindered activity toward a small molecule substrate, while exhibiting low activity (9% and 4%, respectively) toward the ~60 kDa BSA.²¹ We reported that dendrimer generation positively correlated with hydrodynamic volume, which in turn led to increasingly hindered activity toward the macromolecular substrate. A critical generation (G7) had to be reached before a significant sieving effect was observed. Moreover, all the conjugates showed unaffected activity toward casein (22 kDa) which was likely due to the flexible structure of this substrate, thus allowing it to fit through the interstitial space of the dendrimers.²¹ While all these results have corroborated the fact that dense coverage on the protein surface is necessary, the influence of polymer architecture on sieving activity is still underexplored, given that only a few comb, brush, and dendritic structures have been reported as effective sieving architectures thus far.

Although we have shown that a dendritic scaffold is an effective architecture for sieving, the high dendrimer generations that were required to achieve the desired result are synthetically prohibitive. In addition, the dendritic surface coating is more compact relative to what is achieved with linear polymers,^{22,23} and it is possible that the relatively thin coating will not fully prevent protein-protein interactions. To address these shortcomings, we combined the synthetic ease of using linear polymers with the advantages of dendritic architectures by utilizing low-to-medium generation linear-dendritic hybrid structures (Figure 3.1). This approach allows the use of easily synthesized lower generation dendrons that are surface functionalized with linear PEG chains to achieve a dense coating on the enzyme surface.²⁴⁻²⁶ The linear-dendritic regime can also mitigate poor sieving associated with the lower internal density observed in lower generation dendrons.²¹ Linear PEG is a promising candidate polymer to be introduced at the dendron periphery as it has previously been shown to prevent cell-adhesion and repel protein adsorption,^{15,27-30} but has yet to be used widely in the context of molecular sieving.^{31,32} While it has been found that introduction of multiple PEG chains directly on the protein surface can result in significant loss of activity,^{9,12,33-35} we hypothesized that a dendritic spacer could serve as a buffer against PEG-protein self-association or blockage of the active site.^{36,37} Therefore, in a continued effort to explore optimal architectures for molecular sieving, we herein present a series of α -CT conjugates with bis-MPA dendrons of generations (G) 3-5 with three different PEG chain lengths at their periphery ($M_w = 350$ Da, 1 kDa, 2 kDa, $n = 8, 22, 45$ respectively). We demonstrate the effect of both dendron generation and PEG chain length on the reactivity of α -CT toward both small and large substrates.

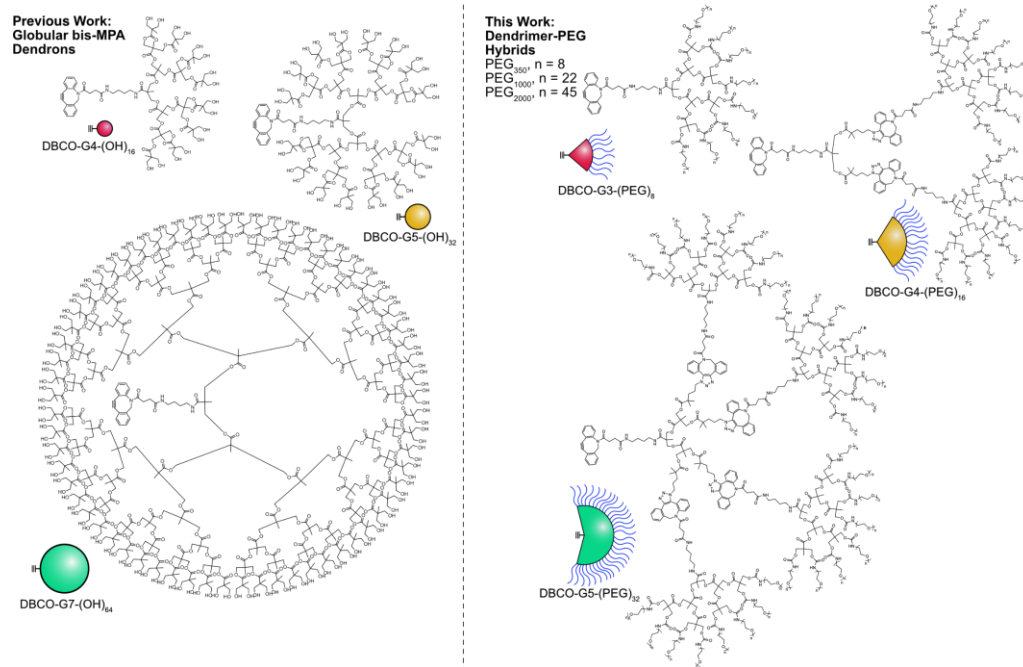
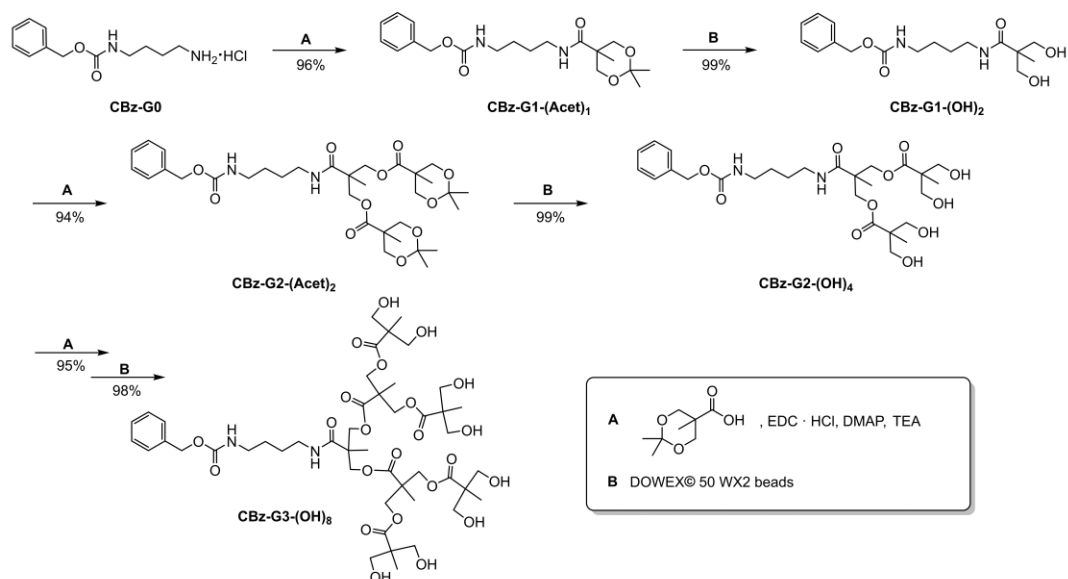


Figure 3.1. Dendritic architectures used for grafting onto proteins for molecular sieving.

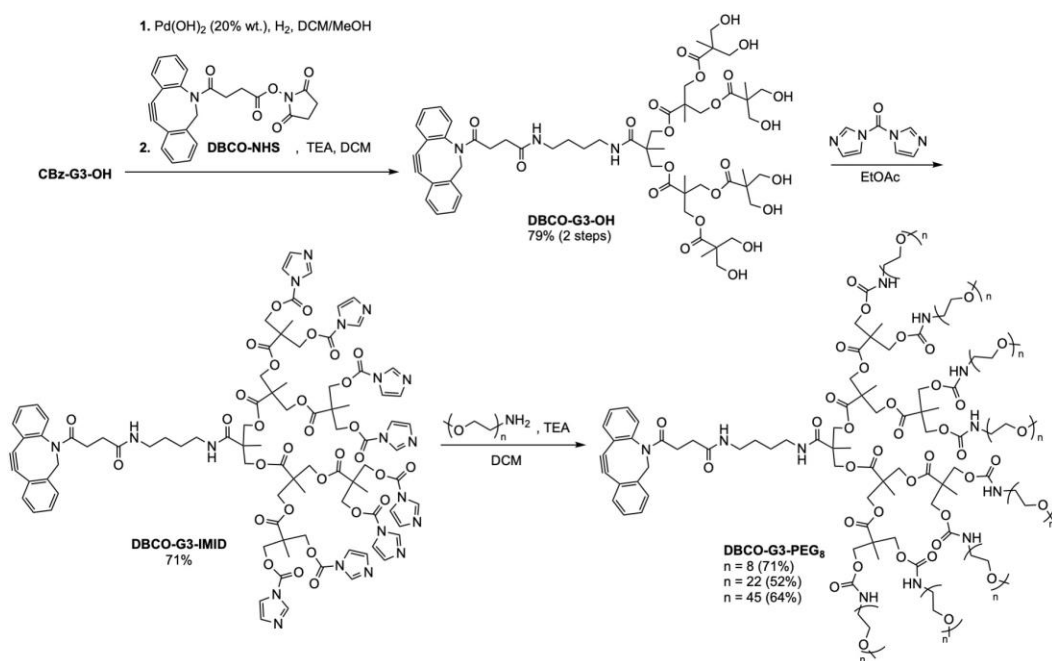
3.3 Results and Discussion

Synthesis of PEGylated Dendrons. The third generation (G3) hydroxyl terminated bis-MPA dendron was prepared via the divergent approach,^{21,38,39} starting with the mono CBZ-protected N-Z-1,4-butanediamine hydrochloride as the core and the acetonide-protected bis-MPA as the building block (Scheme 3.1). All dendrons up to G3 were prepared in good yields (94% or higher) and were characterized by ¹H NMR and ESI-MS (see SI in Chapter 3.5). The benzyl carbamate on **CBz-G3-(OH)**₈ was then removed by hydrogenation using Pd/C to liberate the reactive amine core. The amine core of H₂N-G3-OH was then amidated using DBCO-N-hydroxysuccinimide (DBCO-NHS) to install the reactive cyclooctyne that enables SPAAC reactions (Scheme 3.2). Functionalization of the peripheral hydroxyl groups with PEG chains was accomplished through initial activation using 1,1'-carbonyldiimidazole (CDI) to produce the acylimidazole activated periphery (DBCO-G3-

IMI) followed by amidation using mPEG-NH₂⁴⁰⁻⁴² (Scheme 3.2) to yield the **DBCO-G3-**(PEG_x)₈ (x = 350, 1000, 2000) series of dendrons.



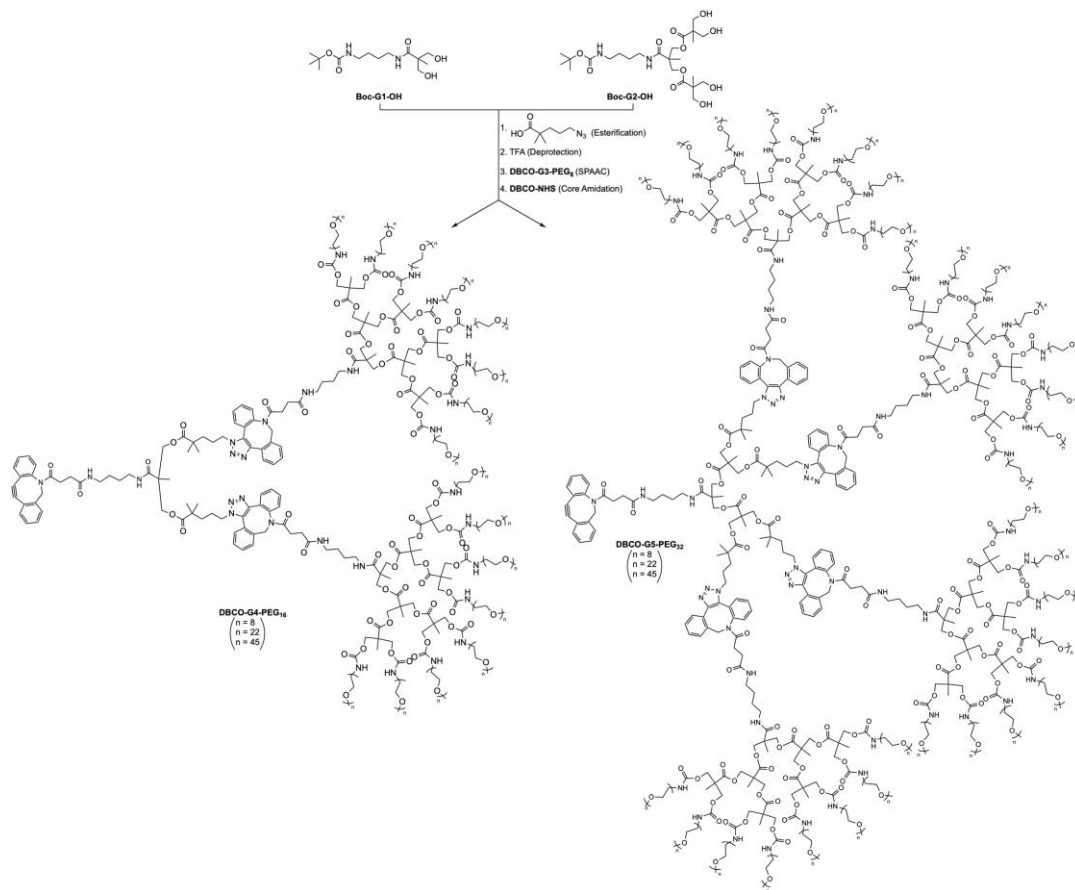
Scheme 3.1. Synthesis of the benzyl carbamate protected G3 dendron **CBz-G3-(OH)**₈.



Scheme 3.2. Synthesis of the SPAAC-reactive PEGylated dendrons, **DBCO-G3-(PEG_x)**₈ (x = 350, 1000, 2000).

It should be noted that the introduction of PEG chains on higher generation dendrons (G4, G5) did not result in quantitative functionalization, especially with the higher molecular weight PEG₁₀₀₀ and PEG₂₀₀₀. Additionally, all attempts at convergent growth of PEGylated G3 using known esterification conditions to access higher generation dendrons were unsuccessful. Having previously shown that the SPAAC reaction allows facile preparation of peripherally-functionalized high generation dendrons,⁴³ we chose to use this approach to prepare our desired G4 and G5 PEGylated dendrons. This required preparation of azide-terminated G1 and G2 “inner” dendrons, which could subsequently be coupled to the **DBCO-G3-(PEG_x)₈** “outer” dendrons to produce the desired G4 and G5 structures. Synthesis of the “inner” dendrons required a slight modification to the synthetic scheme presented above, in which we started with the mono Boc-protected 1,4-butanediamine. Iterative coupling with the acetonide protected bis-MPA anhydride followed by deprotection yielded Boc-G1-(OH)₂ and Boc-G2-(OH)₄. These structures were then esterified with 5-azido-2,2-dimethyl valeric acid, using *N,N,N',N'*-tetramethylchloroformamidinium hexafluoro-phosphate (TCFH) activation as described by Beutner et al.,⁴⁴ to introduce the required terminal azides on these internal dendrons (Scheme 3). The resulting neopentyl ester linkage mimics the bis-MPA dendron backbone and imparts hydrolytic stability to the resulting structure.³⁸ The Boc-G1-(N₃) and Boc-G2-(N₃) structures were then deprotected under acidic conditions to liberate the core amine, and subsequently reacted with DBCO-G3-PEG₈ via SPAAC to cleanly produce the PEGylated G4 and G5 dendrons bearing a single amine at the core. These dendrons were then treated with DBCO-NHS to install the reactive cyclooctyne functionality at the core

(Scheme 3.3). The resulting neopentyl ester linkage mimics the bis-MPA dendron backbone and imparts hydrolytic stability to the resulting structure.³⁸ The Boc-G1-(N₃) and Boc-G2-(N₃) structures were then deprotected under acidic conditions to liberate the core amine, and subsequently reacted with DBCO-G3-PEG₈ via SPAAC to cleanly produce the PEGylated G4 and G5 dendrons bearing a single amine at the core. These dendrons were then treated with DBCO-NHS to install the reactive cyclooctyne functionality at the core (Scheme 3.3). Quantitative conversion from the SPAAC assembly of the G4 and G5 dendrons was easily monitored by infrared (IR) spectroscopy through the disappearance of the azide stretch at ~2100 cm⁻¹ (see SI in Chapter 3.5 for DRIFTS-IR spectra). Additionally, ¹H NMR was used to follow the SPAAC reaction by monitoring the methylene protons adjacent to the amide in DBCO, which shift from a sharp signal at 5.17 ppm to a broad signal at ~6 ppm upon triazole formation (see Figure S3.18). MALDI-TOF-MS was attempted to characterize the PEGylated dendrons but produced extremely weak and broad signals due to poor ionization associated with the abundance and dispersity of the peripheral PEG chains (data not shown).



Scheme 3.3. Synthesis of the G4 and G5 dendrons (**DBCO-G4-(PEG_x)₁₆** and **DBCO-G5-(PEG_x)₃₂**, respectively, x = 350, 1000, or 2000) by convergent SPAAC reaction of G1 and G2 azide-terminated dendrons with **DBCO-G3-(PEG_x)₈**, followed by installation of DBCO at the core.

Synthesis and Characterization of PEGylated α -CT-Dendron Conjugates. Having prepared the PEGylated dendrons with reactive DBCO units at the core, we proceeded to graft these structures to the surface of α -CT, following previously established protocols.²¹ Treatment of the 14 surface lysine residues of α -CT with 2-azidoacetic acid introduced the required azide functionalities on the enzyme to allow SPAAC coupling with the dendrons, while maintaining aqueous solubility. Complete conversion of all the lysines was confirmed by MALDI-TOF-MS (Figure S3.29). Interestingly, catalytic activity of the

azide-decorated enzyme was not significantly altered, showing a slight increase in activity toward the small molecule substrate, BTPNA, relative to the native enzyme (Figures S3.39 and S3.40). The azidified enzyme was then treated with an excess of the DBCO-core dendrons (20-25 mol eq. to α -CT, \sim 1.4-1.8 eq. dendron per azide) to produce a library of nine polymer-protein conjugates (Figure 3.2).

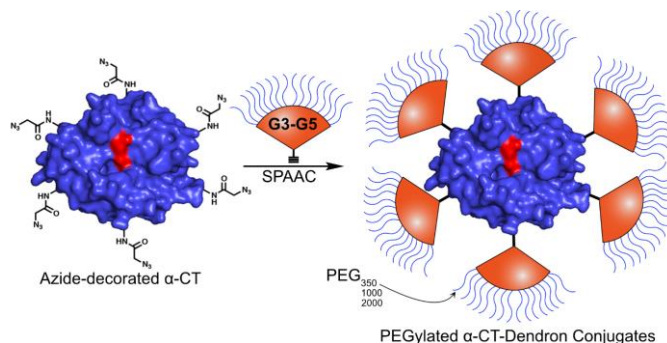


Figure 3.2. Schematic representation depicting the preparation of PEGylated α -CT-dendron conjugates, where the dendron is varied from G3 to G5, and the PEG chain lengths were 350, 1000, and 2000 Da at each dendron generation (a total of 9 different conjugates).

Unreacted dendron and buffer salts were removed by dialyzing against deionized water. Complete conjugation to α -CT was verified via diffuse-reflectance IR spectroscopy (DRIFTS) by the disappearance of the azide signal at \sim 2100 cm^{-1} (Figure 3.3), as well as comparing mass fractions of grafted dendrons to the whole conjugate by quantitative ^1H NMR spectroscopy (qNMR).²¹ The relative integration of the inner ester methylene protons of the conjugate was examined against a sodium formate internal standard (See SI in Chapter 3.5 for details). The measured mass fraction of the dendrons in the overall conjugate by qNMR generally agreed well with theoretical values (Table 3.1). In some instances, such as α -CT-G3-PEG₃₅₀, α -CT-G4-PEG₃₅₀, and α -CT-G4-PEG₂₀₀₀, the measured mass fraction of the dendron is slightly lower than the calculated value, indicating that one of the 14

azides may have been left uncoupled in some fraction of the sample. Overall, the majority of the measured values was in agreement with expectations, indicating that the SPAAC reaction was highly efficient in allowing near complete dendronization of α -CT.

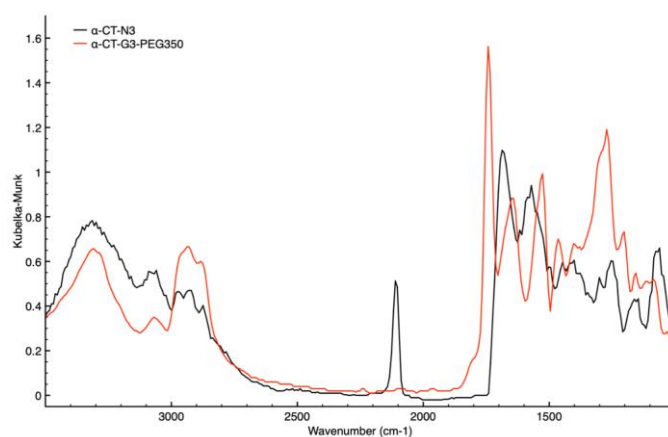


Figure 3.3. DRIFTS IR spectra of α -CT-(N₃)₁₄ (black), and a fully conjugated α -CT-G3-PEG₃₅₀ (red). The azide peak at 2100 cm⁻¹ completely disappears after SPAAC coupling.

Table 3.1. Calculated vs. experimentally measured dendron mass fractions.

Conjugate	Calcd. Dendrimer Mass Fraction (%)	Expt. Dendrimer Mass Fraction (%)
CT-G3-PEG ₃₅₀	66.7	62.7
CT-G3-PEG ₁₀₀₀	81.8	78.0
CT-G3-PEG ₂₀₀₀	89.7	87.0
CT-G4-PEG ₃₅₀	81.8	76.0
CT-G4-PEG ₁₀₀₀	90.5	86.2
CT-G4-PEG ₂₀₀₀	94.7	89.3
CT-G5-PEG ₃₅₀	90.9	90.4
CT-G5-PEG ₁₀₀₀	95.1	93.0
CT-G5-PEG ₂₀₀₀	97.3	98.6

In addition to the FT-IR and NMR measurements, the PEGylated α -CT-dendron conjugates were investigated by cryo-electron microscopy (cryo-EM). As seen in Figure 3.4, it was possible to observe the individual conjugates as discrete spherical structures. Considering that the CT-G5-PEG₂₀₀₀ has a mass of 1,023 kDa, it was clearly visible in the cryo-EM images, exhibiting roughly spherical structures having an average diameter of 19.7 ± 2.8 nm ($n = 20$). Conversely, the CT-G3-PEG₂₀₀₀ structure has a mass of 273 kDa, which is on the lower edge of molecular weights that can be reliably observed with low-dose cryo-EM methods. Nevertheless, it was possible to visualize spherical structures having an average diameter of 6.3 ± 1.1 nm ($n = 20$), roughly one quarter the size of the G5 structures, as expected from the relative molecular weights. Interestingly, both the G3

and G5 structures are relatively monodisperse and do not exhibit significant aggregation, likely a result of extended PEG chains providing steric stabilization in solution.

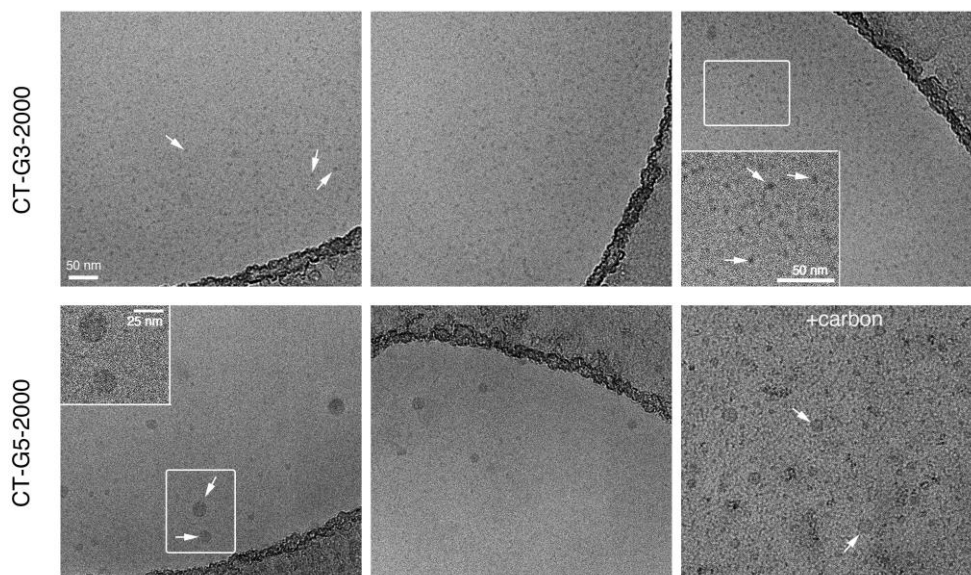


Figure 3.4. Cryo-electron microscopy of CT-G3-PEG₂₀₀₀ (273 kDa) and CT-G5-PEG₂₀₀₀ (1023 kDa). The top three panels show representative cryo-EM images from CT-G3-PEG₂₀₀₀. The inset in the top right picture shows a zoomed view of the area included in the white frame. The arrowheads point to individual CT-G3-PEG₂₀₀₀ dendrons. The bottom panels display three representative cryo-EM images from the CT-G5-PEG₂₀₀₀ sample. In this case, the images on the left and middle panels were taken inside the grid holes. The left panel shows a zoomed view of the two dendrons shown in the image. The right panel shows an image of the carbon area between holes. Given the higher affinity of CT-G3-PEG₂₀₀₀ dendrons towards carbon, this area shows a higher density of dendrons than images inside the holes, but with higher background caused by the continuous carbon layer. Arrowheads point to individual CT-G5-PEG₂₀₀₀ dendrons. The 50 nm scale bar in the top left panel applies to all panels as all images were taken at 80,000 \times magnification.

Small Molecule Assay. Enzymatic activity toward the small molecule substrate, BTpNA, was investigated by performing an assay with the series of PEGylated α -CT-dendron conjugates in tris buffer and DMF. Activity of over 100% of native α -CT in the **G3-PEG₃₅₀**, **G3-PEG₁₀₀₀** and **G4-PEG₃₅₀** conjugates was observed, which is consistent with previous

findings that suggest grafted polymers on the protein promote local hydrophobic interactions between the substrate and the enzyme.^{1,18} Independent studies by Russell⁴⁵ and Ding,⁴⁶ as well as simulations by Drossis et al.¹⁷ have also shown that enzymes grafted with short-chain polymers could surpass the activity of native enzymes, which was postulated to be due to microenvironmental effects that induce pre-concentration of substrates near the active site. Within the series of G3 and G4 PEGylated dendrons, it is clear that increasing PEG chain length causes a decrease in enzyme activity (Figure 3.5), which is reminiscent of what has been reported with directly conjugated PEG- α -CT species;³⁵ direct PEGylation to an enzyme surface is known to lower its activity.^{7,12,13,33,34} In our case, this is likely due to the steric congestion introduced around the enzyme's active site, slowing down the diffusion of the substrate. Interestingly, in the G5 series, there was an observable increase in activity when the PEG chain length increased from PEG₃₅₀ to PEG₁₀₀₀, but then the activity drops dramatically with PEG₂₀₀₀ chains. It is possible that the G5-PEG₁₀₀₀ structure did not undergo quantitative reaction with the enzyme, where only 13 of the 14 available sites may have reacted. This could have provided a pathway for the substrate to access the active site and resulted in the anomalous increase in activity for this structure. In addition, as the dendron generation (and hence the density of PEG chains at the surface) increases, the enzyme activity again decreases. This trend is most clearly observed with the G3-G5 series having PEG₃₅₀ chains at the periphery. Even with PEG₁₀₀₀ and PEG₂₀₀₀, it is clear that activity at G5 is lower than that at G3. Again, this supports the hypothesis that, as the steric congestion at the enzyme periphery increases, it diminishes the ability of substrates to access the enzyme's active site. Control experiments in which

native α -CT was mixed with the appropriate ratio (14 equivalents) of un-conjugated PEGylated dendrons of each generation and PEG length were also performed and showed that there was no impact on enzyme activity when the dendrons were not attached (Figure 3.5).

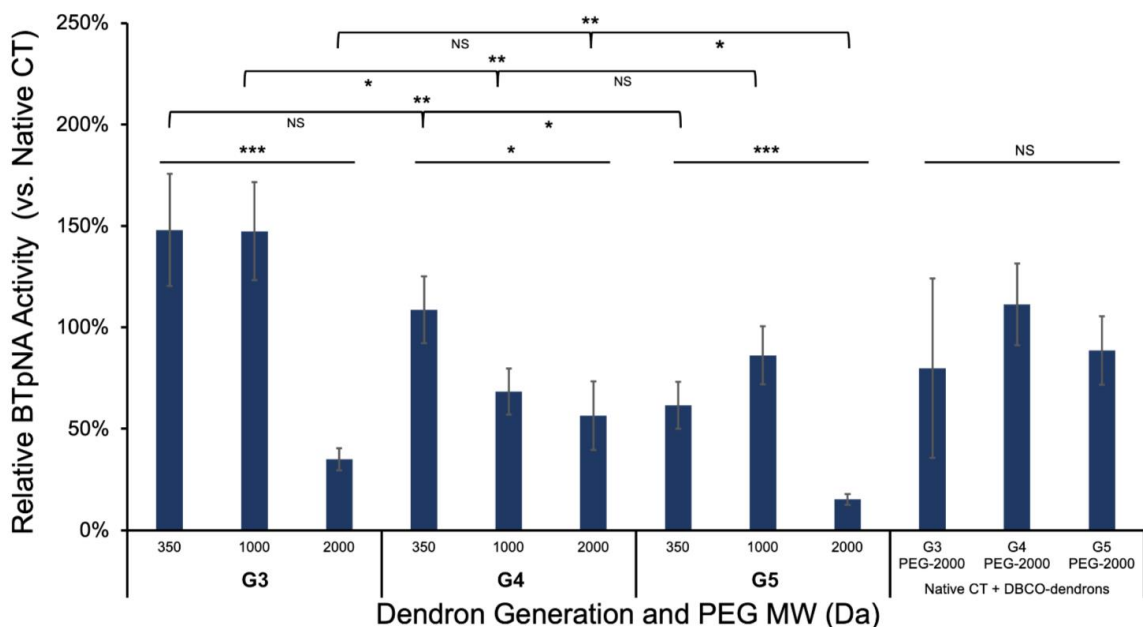


Figure 3.5. Relative activity of the PEGylated α -CT conjugates (G3-G5) toward BTpNA versus native chymotrypsin. As well, control data for native α -CT in the presence of un-conjugated G3-G5 PEGylated dendrons is provided. Error bars indicate standard error ($n=3$). One-way ANOVA was performed to determine significance of PEG length and dendron generation on relative activity ($p < 0.001$ (***) , $p < 0.01$ (**), $p < 0.05$ (*), NS = not significant).

Casein and Bovine Serum Albumin (BSA) Assays and Sieving Ratios. Having established the dendronized enzyme's activity toward its small molecule substrate, we investigated activity toward two macromolecular substrates, milk casein (22 kDa) and bovine serum albumin (BSA, 66 kDa). Interestingly, apart from the case of CT-G3-PEG₃₅₀, reactivity toward casein decreased significantly at all generations and PEG lengths when

compared to the native α -CT (Figure 3.6). Consistent with observations with the small molecule substrate, it is clear that the PEGylated dendron periphery impedes casein's ability to access the enzyme's active site. Additionally, as the dendron generation increased, the enzyme activity generally decreased. In the conjugates bearing PEG₂₀₀₀ chains, activity toward casein was very similar, regardless of generation, indicating that the steric congestion at the enzyme's surface was high enough to impede reactivity even at the third generation. Upon increasing PEG length within any one generation, enzyme activity decreased dramatically, especially with PEG₂₀₀₀ chains. Unsurprisingly, with the more rigid and larger BSA, activity also decreased with all conjugates. Consistent with our previous findings, activity toward BSA was much lower than that toward casein. BSA is large and crystalline while casein is small, amorphous, and much more flexible, allowing it to intercalate through the PEG layer more effectively. For G3 and G4, activity toward BSA dropped dramatically when PEG₂₀₀₀ chains were appended to the dendron periphery. With G5 dendrons, the activity was extremely low and within error for all PEG lengths.

Comparison of enzyme activity toward small and large substrates allows calculation of the sieving ratio, which, in our case, is defined as the measured activity toward BTPNA divided by the activity toward the protein (casein or BSA). Figure 3.6B shows the sieving ratios of all the conjugates with respect to both casein and BSA. In the case of casein, although the sieving ratios are small for all the conjugates studied, it is clear that as the PEG chain length increases, the sieving ratio increases. In fact, the dendron generation does not seem to play any role in dictating sieving with these conjugates. The only anomaly is the G5-PEG₂₀₀₀ conjugate, which shows the lowest sieving ratio of all the structures. This

observation stems from the fact that the G5-PEG₂₀₀₀ structure is so sterically congested that it impedes reactivity for both casein and the small molecule substrate, BTPNA. Since activity toward both substrates is similarly low, the ratio is also low. In the case of BSA, the pattern of sieving ratios is somewhat different. For the G3 and G4 conjugates, there was no significant difference between structures bearing PEG₃₅₀ and PEG₁₀₀₀ chains.

However, a large increase in sieving ratio was observed for the PEG₂₀₀₀ analogs because activity toward BSA is almost completely eliminated with these structures (Figure 3.6A). For the G5 series of conjugates, the sieving ratios for G5-PEG₃₅₀ and G5-PEG₁₀₀₀ were significantly higher than the analogous structures at the lower generations, again because of the highly congested polymer shell present within these conjugates. However, similarly to the situation with casein, the sieving ratio for G5-PEG₂₀₀₀ dropped dramatically because this structure had significantly reduced activity to both the large protein and the small molecule. It should be noted that, although large sieving ratios toward BSA were observed with several of the conjugates, this metric is of limited utility when the activity toward the small molecule is diminished. A high sieving ratio is only useful in cases where the small molecule activity is preserved relative to the native enzyme. Based on these results, it seems that the G4-PEG₂₀₀₀ and G5-PEG₁₀₀₀ conjugates offer the best combination of sieving ratio and small molecule activity. Control experiments in which native α -CT was mixed with the appropriate ratio (14 equivalents) of un-conjugated PEGylated dendrons of each generation and PEG length again indicated no impact on enzyme activity toward the protein substrates, which translated to a lack of any sieving (Figure 3.6).

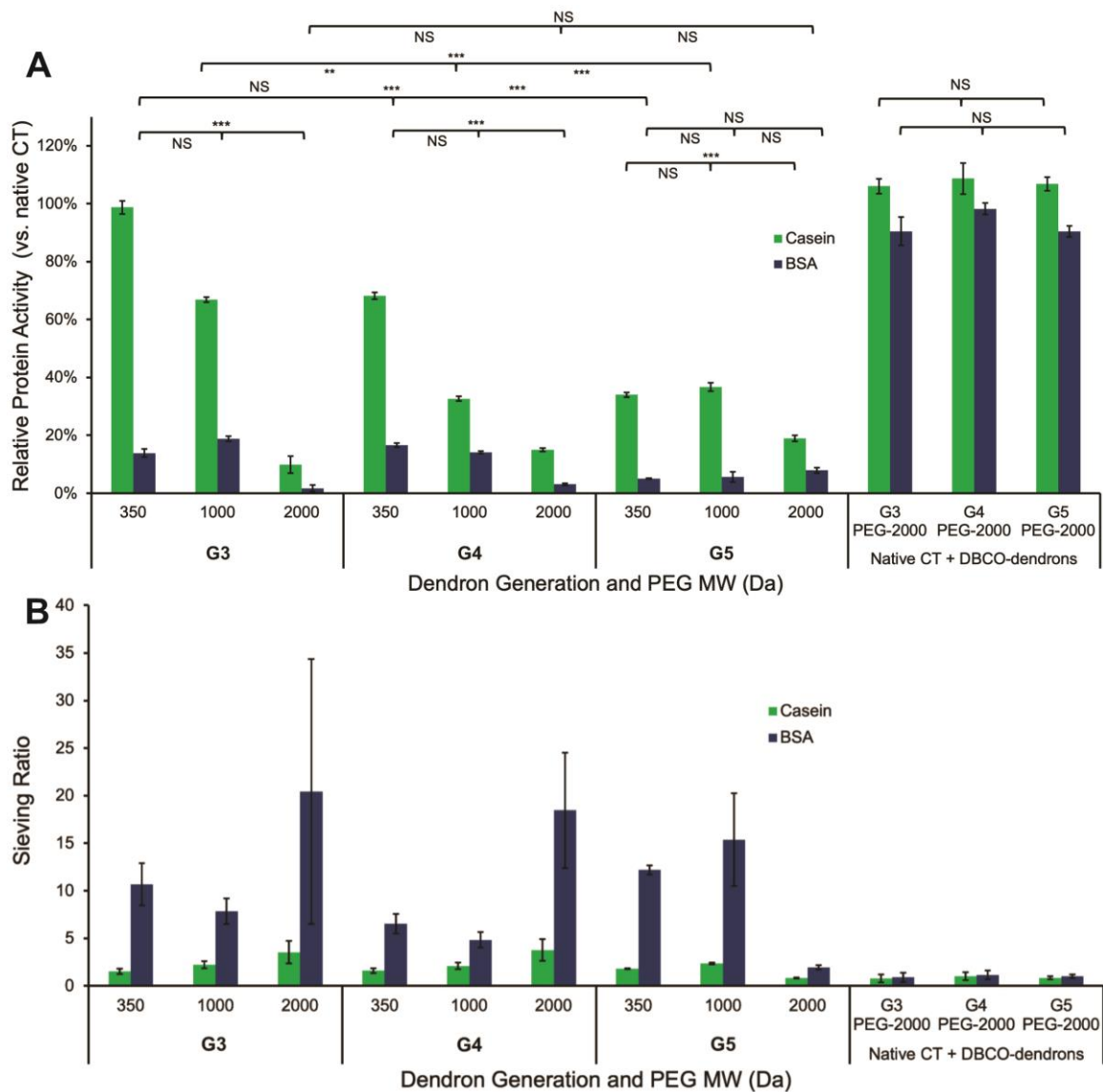


Figure 3.6. (A) Relative activity of the G3-G5 PEGylated conjugates toward casein and BSA. One-way ANOVA was performed to determine significance of PEG length and dendron generation on relative activity ($p < 0.001$ (***) , $p < 0.01$ (**), $p < 0.05$ (*), NS = not significant). (B) Sieving ratios for the G3-G5 PEGylated conjugates, expressed as a ratio of activity toward BTPNA and the respective proteins (casein and BSA). For both (A) and (B), control data from mixtures of the native α -CT in the presence of un-conjugated G3-G5 PEGylated dendrons are provided.

3.4 Conclusion

We have prepared a series of PEGylated α -CT-dendron conjugates of generation 3, 4, and 5, bearing 8, 16, and 32 linear PEG chains, respectively. The PEG chains also varied in length, with 8, 22, and 45 repeat units (350, 1000, and 2000 Da, respectively). The SPAAC reactions between azide-decorated α -CT and the dendrons bearing a DBCO unit at their core proceeded with high efficiency, allowing production of the desired conjugates in good yield. Relative to native α -chymotrypsin, activity of these conjugates toward a small substrate (BTpNA) was retained when low generation dendrons and low molecular weight PEG chains were attached (G3-PEG₃₅₀, G3-PEG₁₀₀, G4-PEG₃₅₀), while the other conjugates had lower activity, likely because of steric congestion around the active site. Decreased activity toward casein and BSA was also observed, though the effect was more pronounced for BSA on account of its larger size and higher crystallinity. In general, as the dendron generation and PEG length increased, the activity of the conjugate decreased. The ratio of activity toward BTpNA and the macromolecules, also referred to as the sieving ratio, was observed to be highest for the G3-PEG₂₀₀₀, G4-PEG₂₀₀₀, and G5-PEG₁₀₀₀ conjugates. Interestingly, not all the structures that had low activity toward the macromolecules exhibited high sieving ratios.

3.5 Supporting Information

Cryo-Electron Microscopy (cryo-EM) Methods. Sample vitrification was performed using a Vitrobot Mark IV (Thermo Fisher Scientific). Holey carbon grids (C-Flat 2/2-3Cu-T) were washed with chloroform for 2 hours and glow discharge in air at 10 mA for 15 seconds before the sample was applied. For both the CT-G3-PEG₂₀₀₀ and CT-G5-PEG₂₀₀₀,

a volume of 3.6 μL of the sample was applied to the grids. The grids were then blotted with filter paper (Standard Vitrobot Filter Paper, $\text{\O}55/20\text{mm}$, Grade 595) once for 3 sec, using a blot force +1 and a drain time of 0.5 seconds, before they were plunged into liquid ethane at ~ -190 $^{\circ}\text{C}$. The blotting camera in the Vitrobot was set at 25°C and 100% relative humidity. Grids were loaded into the Tecnai F20 electron microscope operated at 200 kV at the Facility for Electron Microscopy Research (FEMR) at McGill using a Gatan 626 single tilt side entry cryo-holder. This holder maintained the sample at -180 $^{\circ}\text{C}$ during imaging. The data acquisition was performed using SerialEM software,⁴⁷ and images were recorded with a TVIPS XF416 CMOS camera. All images were collected at a magnification of 80,000x, which produced images with a calibrated pixel size of 1.358 \AA . The total dose and defocus used to collect the images were ~ 30 $\text{e}^{-}/\text{\AA}^2$ and -5 μm , respectively. Measurements of particle size were done using Photoshop tools to measure the diameter of the dendrons in pixels. The number of pixels was multiplied by the image sampling (1.358 $\text{\AA}/\text{px}$). Average and standard deviation calculations were performed in Microsoft Excel.

Synthetic Procedures

General Procedure 1: Synthesis of G1-G3 bis-MPA Dendrimers

Prepared according to literature procedures.²¹ A round bottom flask was equipped with a magnetic stir bar and charged with bis-MPA acetonide (synthesized according to previous procedures)²¹ (4 eq. per dendron OH), EDC (2 eq. per dendron OH), and DCM. The mixture was stirred at room temperature for 30 min. Separately, 1 eq. of either *N*-Z-1,4-butanediamine hydrochloride (G0), CBz-, or Boc-G_x-(OH)_y and DMAP (0.25 eq. per dendron OH) were dissolved in pyridine and were then added to the mixture followed by

2 eq. per -OH of TEA. The reaction mixture was left stirring overnight at which point it was quenched with 1 mL of water and allowed to stir for 1 h. The crude mixture was diluted with 50 mL of DCM and then washed with 1M H₃PO₄ (3 x 50 mL), 10% Na₂CO₃ (3 x 50 mL), and brine (1 x 50 mL). The organic layer was dried with MgSO₄, filtered, then concentrated by rotary evaporation. The crude material was purified by flash chromatography using a 40 g silica flash column with 10-60% acetone in hexanes and monitored at 205 nm. Fractions containing product were combined, concentrated by rotary evaporation, and dried under vacuum to afford CBz- or Boc-G_{x+1}-(acet)_y as a clear viscous oil.

General Procedure 2: Deprotection of Acetonide-Periphery Dendrons

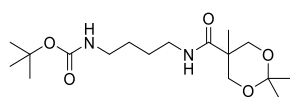
A round bottom flask was equipped with a magnetic stir bar and charged with 1 eq. of CBz- or Boc-G_x-(acet)_y, MeOH, and DOWEX® 50WX2 beads. This was left stirring at room temperature until completion, as monitored by TLC and/or ESI-MS. The mixture was vacuum filtered and rinsed with MeOH to recover the catalyst, and the solution was concentrated by rotary evaporation, followed by drying *in vacuo* to afford Boc-G_x-(OH)_{2y} as a viscous pale-yellow oil.

General Procedure 3: PEGylation of DBCO-G3 Dendrons

A round bottom flask was equipped with a magnetic stir bar and charged with 1 eq. of DBCO-G3-(IMI)₈, 1.5 eq./imidazole of mPEG-NH₂, 2 eq./imidazole of TEA, and DCM. The reaction mixture was left stirring overnight at room temperature. The next day, the solvent was removed by rotary evaporation under mild heating (< 37°C) and the crude

material was dissolved in ~2 mL of deionized water and purified by dialysis overnight using either 3.5 kDa or 12 kDa MWCO dialysis tubing. Dialysis water was changed twice over the span of a 24 h period and the solution was then lyophilized overnight to afford the product.

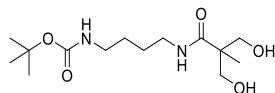
Boc-G1-(acet)₁



A round bottom flask was equipped with a magnetic stir bar and charged with bis-MPA-acetonide (1.33 g, 7.65 mmol), EDC (733 mg, 3.82 mmol), and DCM (15 mL). This was left stirring at room temperature for 30 min at which point *N*-Boc-1,4-butanediamine (360 mg, 1.91 mmol) and TEA (800 μ L, 5.74 mmol) were added. The mixture was left stirring overnight. The following day the reaction mixture was quenched with 500 μ L of water and stirred for 1 h. The mixture was then diluted with 40 mL of DCM and washed with 1M H_3PO_4 (3 x 40 mL), 10% Na_2CO_3 (3 x 40 mL), and brine (1 x 40 mL). The organic layer was dried with MgSO_4 , filtered, and then concentrated by rotary evaporation. The crude material was purified by flash chromatography using a 40 g silica flash column with 10-60% acetone in hexanes (loaded in DCM) and monitored at 205 nm. Fractions containing product were combined, concentrated by rotary evaporation and dried under vacuum to afford the product as a clear oil (607 mg, 92%). ^1H NMR (600 MHz; CDCl_3): δ 7.09 (s, 1H), 4.58 (s, 1H), 3.90 (d, $J = 12.4$ Hz, 2H) 3.76 (d, $J = 12.4$ Hz, 2H), 3.32 (q, $J = 6.3$ Hz,

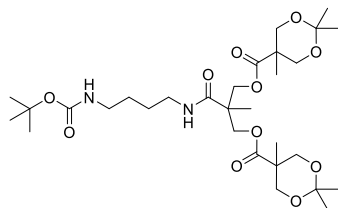
2H), 3.14 (d, $J = 5.6$ Hz, 2H), 1.59-1.53 (m, 4H), 1.47 (s, 3H), 1.40-1.39 (m, 12H), 1.00 (s, 3H). MS (ESI⁺) m/z calc'd for C₁₇H₃₂N₂O₅ [M+H]⁺ = 345.23, found [M+H]⁺ 345.2

Boc-G1-(OH)₂



Following General Procedure 2, a round bottom flask was equipped with a magnetic stir bar and charged with Boc-G1-(acet)₁ (500 mg, 1.45 mmol), DOWEX® beads (750 mg), and MeOH (50 mL). The reaction was stirred at room temperature for 4 hs. The mixture was vacuum filtered, and the solution was concentrated by rotary evaporation, then dried under vacuum to afford the product as a clear oil (439 mg, 99%). ¹H NMR (600 MHz; MeOD): δ 3.63 (q, $J = 13.5$ Hz, 4H), 3.22 (t, $J = 6.7$ Hz, 2H), 3.04 (t, $J = 6.7$ Hz, 2H), 1.53-1.43 (m, 13H), 1.11 (s, 3H). MS (ESI⁺) m/z calc'd for C₁₄H₂₈N₂O₅ [M+H]⁺ = 305.20, found [M+H]⁺ 305.2.

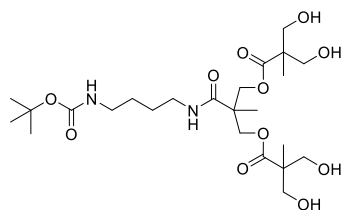
Boc-G2-(acet)₂



Following General Procedure 1, a round bottom flask was equipped with a magnetic stir bar and charged with bis-MPA-acetonide (686 mg, 3.94 mmol), EDC (378 mg, 1.97 mmol), and DCM (2 mL). This was left stirring at room temperature for 30 min. Separately, Boc-

G1-(OH)₂ (150 mg, 0.49 mmol), and DMAP (30 mg, 0.25 mmol), were dissolved in pyridine (1.3 mL) and were then added to the mixture followed by TEA (293 μL, 1.97 mmol). The reaction mixture was left stirring overnight at which point it was quenched with 350 μL of water and stirred for 1 h. The mixture was then diluted with 40 mL of DCM and washed with 1M H₃PO₄ (3 x 40 mL), 10% Na₂CO₃ (3 x 40 mL), and brine (1 x 40 mL). The organic layer was dried with MgSO₄, filtered, and then concentrated by rotary evaporation. The crude material was purified by flash chromatography using a 12 g silica flash column with 10-60% acetone in hexanes (loaded in DCM) and monitored at 205 nm. Fractions containing product were combined, concentrated by rotary evaporation and dried under vacuum to afford the product as a clear oil (290 mg, 95%). ¹H NMR (600 MHz; CDCl₃): δ 6.53 (s, 1H), 4.67 (s, 1H), 4.36 (d, *J* = 11.2 Hz, 2H), 4.29 (d, *J* = 11.2 Hz, 2H), 4.17 (d, *J* = 11.9 Hz, 4H), 3.66 (d, *J* = 11.9 Hz, 4H), 3.26 (q, *J* = 6.3 Hz, 2H), 3.13-3.10 (m, 2H), 1.53-1.49 (m, 4H), 1.44 (m, 15H), 1.37 (s, 6H), 1.28 (s, 3H), 1.12 (s, 6H). MS (ESI⁺) *m/z* calc'd for C₃₀H₅₂N₂O₁₁ [M+Na]⁺ = 639.35, found [M+Na]⁺ 639.3.

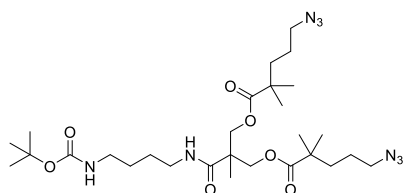
Boc-G2-(OH)₄



Following General Procedure 2, a round bottom flask was equipped with a magnetic stir bar and charged with Boc-G2-(acet)₂ (280 mg, 0.45 mmol), DOWEX® beads (420 mg), and MeOH (15 mL). The reaction was stirred at room temperature for 4 hs. The mixture

was vacuum filtered, and the solution was concentrated by rotary evaporation, then dried under vacuum to afford the product as a clear oil (241 mg, 99%). ^1H NMR (600 MHz; MeOD): δ 4.26 (q, $J = 9.8$ Hz, 4H), 3.69 (d, $J = 10.9$ Hz, 4H), 3.60 (d, $J = 10.9$ Hz, 4H), 3.21 (q, $J = 6.3$ Hz, 2H), 3.05 (t, $J = 6.8$ Hz, 2H), 1.55-1.43 (m, 13H), 1.27 (s, 3H), 1.15 (s, 6H). MS (ESI⁺) m/z calc'd for $\text{C}_{24}\text{H}_{44}\text{N}_2\text{O}_{11}$ $[\text{M}+\text{H}]^+ = 537.29$, found $[\text{M}+\text{H}]^+ 537.2$.

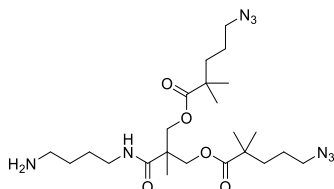
Boc-G1-(N₃)₂



An oven dried round bottom flask was equipped with a magnetic stir bar, purged under vacuum and backfilled with nitrogen three times before addition of 5-azido-2,2-dimethylpentanoic acid (synthesized according to previous procedures)³⁸ (225 mg, 1.31 mmol), NMI (370 μL , 4.60 mmol), dry MeCN (1 mL), and *N,N,N',N'*-tetramethylchloroformamidinium hexafluorophosphate (TCFH) (369 mg, 1.31 mmol). This was left to stir for 10 min at room temperature at which point a solution of Boc-G1-(OH)₂ (100 mg, 0.33 mmol) in 500 μL of dry MeCN was added. The mixture was left stirring at room temperature for 30 min at which point it was quenched with 100 μL of water and stirred for another 5 min. The reaction mixture was then diluted with 40 mL of EtOAc and washed with water (3 x 60 mL), 1M H₃PO₄ (3 x 60 mL), 10% Na₂CO₃ (3 x 60 mL), and brine (1 x 60 mL). The organic layers were then dried with MgSO₄, filtered, and concentrated under rotary evaporation. The crude material was then purified using a 12 g

silica flash column with 5-60% acetone in hexanes (loaded in DCM) and monitored at 205 nm. Fractions containing product were combined, concentrated by rotary evaporation and dried under vacuum to afford the product as a yellow oil. (142 mg, 71%). ^1H NMR (600 MHz; CDCl_3): δ 6.20 (s, 1H), 4.63 (s, 1H), 4.23-4.19 (m, 4H), 3.30-3.26 (m, 6H), 3.13 (d, $J = 5.9$ Hz, 2H), 1.60-1.56 (m, 4H), 1.54-1.49 (m, 8H), 1.44 (s, 9H), 1.25 (s, 3H), 1.18 (s, 12H). ^{13}C NMR (150 MHz; CDCl_3): δ 176.8, 172.1, 79.3, 66.4, 51.7, 46.4, 42.2, 39.9, 39.4, 37.5, 28.4, 27.7, 26.5, 25.1, 24.6, 18.0. HRMS (ESI $^+$) m/z calc'd for $\text{C}_{28}\text{H}_{50}\text{N}_8\text{O}_7$ $[\text{M}+\text{H}]^+$ = 611.3875, found $[\text{M}+\text{H}]^+$ 611.3871.

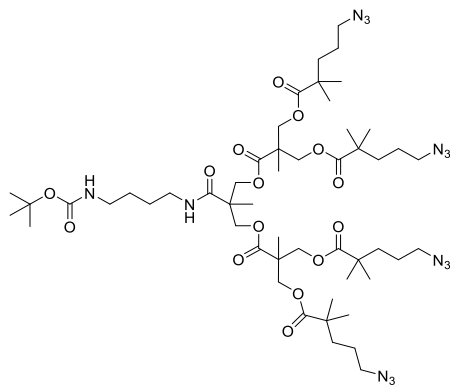
NH₂-G1-(N₃)₂



A round bottom flask was equipped with a magnetic stir bar and charged with Boc-G1-(N₃)₂ (43 mg, 0.07 mmol) and DCM (2 mL). TFA (1 mL) was added dropwise, and the reaction was stirred at room temperature for 1 h at which point it was diluted with 10 mL of DCM and brought to pH ~14 by adding saturated KOH dropwise. The aqueous layer was extracted with DCM (6 x 20 mL) and the organic layers were washed with brine (1 x 20 mL), dried with MgSO_4 , filtered, then concentrated under rotary evaporation. The product was dried under vacuum to afford a yellow oil (20 mg, 56%). ^1H NMR (600 MHz; CDCl_3): δ 6.68 (s, 1H), 4.20 (q, $J = 9.2$ Hz, 4H), 3.28-3.25 (m, 6H), 2.74 (t, $J = 6.2$ Hz, 2H), 1.59-1.49 (m, 12H), 1.24 (s, 3H), 1.24 (RNH₃ $^+$, s, 3H; overlapping with s at 1.24),

1.18 (s, 12H). ^{13}C NMR (151 MHz, CDCl_3) δ 176.79, 171.98, 77.21, 77.00, 76.79, 66.34, 51.65, 46.34, 42.20, 41.47, 39.63, 37.48, 30.62, 29.67, 27.00, 25.08, 24.57, 18.04. HRMS (ESI $^+$) m/z calc'd for $\text{C}_{23}\text{H}_{42}\text{N}_8\text{O}_5$ $[\text{M}+\text{H}]^+ = 511.3351$, found $[\text{M}+\text{H}]^+ 511.3361$.

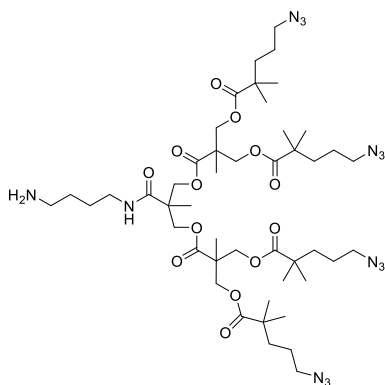
Boc-G2-(N₃)₄



An oven dried round bottom flask was equipped with a magnetic stir bar, purged under vacuum and backfilled with nitrogen three times before addition of 5-azido-2,2-dimethylpentanoic acid (498 mg, 2.91 mmol), NMI (811 μL , 10.2 mmol), dry MeCN (1 mL), and TCFH (816 mg, 2.91 mmol). This was left to stir for 10 min at room temperature at which point a solution of Boc-G2-(OH)₂ (195 mg, 0.36 mmol) in 500 μL of dry MeCN was added. The mixture was left stirring at room temperature for 30 min at which point it was quenched with 200 μL of water and stirred for another 5 min. The reaction mixture was then diluted with 40 mL of EtOAc and washed with water (3 x 60 mL), 1M H_3PO_4 (3 x 60 mL), 10% Na_2CO_3 (3 x 60 mL), and brine (1 x 60 mL). The organic layers were then dried with MgSO_4 , filtered, and concentrated under rotary evaporation. The crude material was then purified using a 12 g silica flash column with 5-60% acetone in hexanes (loaded in DCM) and monitored at 205 nm. Fractions containing product were combined,

concentrated by rotary evaporation and dried under vacuum to afford the product as a yellow oil (344 mg, 82%). ^1H NMR (600 MHz; CDCl_3): δ 6.36 (s, 1H), 4.85 (s, 1H), 4.24-4.13 (m, 12H), 3.29-3.24 (m, 10H), 3.12 (d, $J = 6.1$ Hz, 2H), 1.58-1.48 (m, 20H), 1.42 (s, 9H), 1.25 (s, 9H), 1.16 (s, 24H). ^{13}C NMR (151 MHz, CDCl_3) δ 176.8, 171.8, 171.4, 79.1, 67.2, 65.0, 51.6, 46.7, 46.3, 42.2, 40.0, 39.6, 37.4, 30.9, 28.4, 27.6, 26.6, 25.0, 24.6, 17.7. HRMS (ESI $^+$) m/z calc'd for $\text{C}_{52}\text{H}_{88}\text{N}_{14}\text{O}_{15}$ $[\text{M}+\text{H}]^+ = 1149.6626$, found $[\text{M}+\text{H}]^+ 1149.6618$.

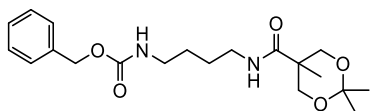
NH₂-G2-(N₃)₄



A round bottom flask was equipped with a magnetic stir bar and charged with Boc-G2-(N₃)₂ (90 mg, 0.08 mmol) and DCM (2 mL). TFA (1 mL) was added dropwise, and the reaction was stirred at room temperature for 1 h at which point it was diluted with 10 mL of DCM and brought to pH ~14 by adding saturated KOH dropwise. The aqueous layer was extracted with DCM (6 x 20 mL) and the organic layers were washed with brine (1 x 20 mL), dried with MgSO_4 , filtered, then concentrated under rotary evaporation. The product was dried under vacuum to afford a yellow oil (60 mg, 73%). ^1H NMR (600 MHz; CDCl_3): δ 6.90 (t, $J = 5.4$ Hz, 1H), 4.26-4.13 (m, 12H), 3.29-3.25 (m, 10H), 2.75 (t, $J = 6.6$

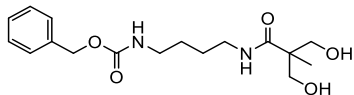
Hz, 2H), 1.61-1.49 (m, 20H), 1.26 (s, 9H), 1.17 (s, 24H). ^{13}C NMR (150 MHz; CDCl_3): δ 176.7, 171.9, 171.3, 67.3, 65.1, 51.6, 46.7, 42.2, 41.6, 39.8, 37.4, 27.0, 25.1, 24.6, 17.8. HRMS (ESI⁺) m/z calc'd for $\text{C}_{47}\text{H}_{80}\text{N}_{14}\text{O}_{13}$ $[\text{M}+\text{H}]^+ = 1049.6102$, found $[\text{M}+\text{H}]^+ 1049.6104$.

Cbz-G1-(acet)₁



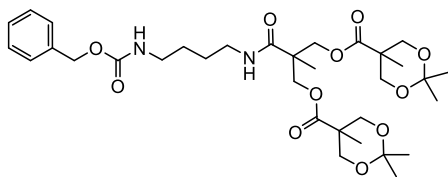
Following General Procedure 1, a round bottom flask was equipped with a magnetic stir bar and charged with bis-MPA-acetonide (1.32 g, 7.61 mmol), EDC (729 mg, 3.80 mmol) and DCM (6.3 mL). This was left stirring at room temperature for 30 min at which point *N*-Z-1,4-butanediamine HCl (820 mg, 3.17 mmol) and TEA (1.6 mL, 11.10 mmol) were added. The mixture was left stirring overnight. The following day the reaction mixture was diluted with 50 mL of DCM and washed with 1M H_3PO_4 (3 x 50 mL), 10% Na_2CO_3 (3 x 50 mL), and brine (1 x 50 mL). The organic layer was dried with MgSO_4 , filtered, and then concentrated by rotary evaporation. The crude material was purified by flash chromatography using a 40 g silica flash column with 10-60% acetone in hexanes (loaded in DCM) and monitored at 205 nm. Fractions containing product were combined, concentrated by rotary evaporation and dried under vacuum to afford the product as a clear oil (1.151 g, 96%). ^1H NMR (600 MHz; CDCl_3): δ 7.33-7.28 (m, 5H), 7.09 (s, 1H), 5.06 (s, 2H), 4.82 (s, 1H) 3.87 (d, $J = 12.16$ Hz, 2H), 3.73 (d, $J = 12.28$ Hz, 2H), 3.30-3.20 (m, 4H), 1.58-1.54 (m, 4H), 1.45 (s, 3H), 1.39 (s, 3H), 0.97 (s, 3H). HRMS (ESI⁺) m/z calc'd for $\text{C}_{20}\text{H}_{30}\text{N}_2\text{O}_5$ $[\text{M}+\text{Na}]^+ = 401.2047$, found $[\text{M}+\text{Na}]^+ 401.2051$.

Cbz-G1-(OH)₂



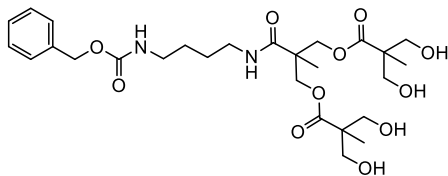
Following General Procedure 2, Cbz-G1-(acet)₁ (745 mg, 1.97 mmol) was dissolved in 110 mL of MeOH followed by the addition of DOWEX® beads (1 scoop, ~1.12 g) and stirred for 3 h. (Yield: 666 mg, 99%). ¹H NMR (600 MHz; MeOD): δ 7.34-7.27 (m, 5H), 5.09 (s, 2H), 3.65 (d, *J* = 10.94 Hz, 2H), 3.60 (d, *J* = 10.94 Hz, 2H), 3.22-3.12 (m, 4H), 1.53-1.49 (m, 4H), 1.09 (s, 3H). HRMS (ESI⁺) *m/z* calc'd for C₁₇H₂₆N₂O₅ [M+Na]⁺ = 361.1734, found [M+Na]⁺ 361.1736.

Cbz-G2-(acet)₂



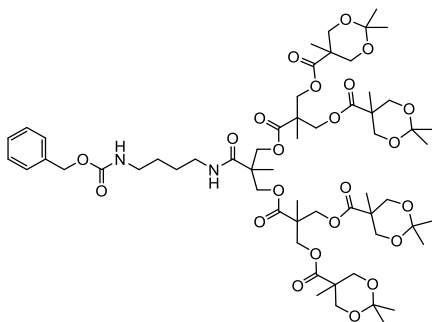
Following General Procedure 1, bis-MPA-acetonide (3.292 g, 18.9 mmol) and EDC (1.813 g, 9.46 mmol) were dissolved in 5.6 mL of DCM followed by addition of Cbz-G1-(OH)₂ (**3**) (800 mg, 2.36 mmol), DMAP (144 mg, 1.18 mmol) and TEA (1.3 mL, 9.46 mmol), in 3.8 mL of pyridine. (Yield: 1.445 g, 94%). ¹H NMR (600 MHz; CDCl₃): δ 7.35-7.28 (m, 5H), 6.50 (s, 1H), 5.07 (s, 2H), 4.93 (s, 1H), 4.33 (d, *J* = 11.25 Hz, 2H), 4.26 (d, *J* = 11.26 Hz, 2H), 4.14 (d, *J* = 11.90 Hz, 4H), 3.63-3.61 (m, 4H), 3.26-3.15 (m, 4H), 1.52-1.47 (m, 4H), 1.39 (s, 6H), 1.32 (s, 6H), 1.23 (s, 3H), 1.07 (s, 6H). HRMS (ESI⁺) *m/z* calc'd for C₃₃H₅₀N₂O₁₁ [M+Na]⁺ = 673.3313, found [M+Na]⁺ 361.3316.

Cbz-G2-(OH)₄



Following General Procedure 2, Cbz-G2-(acet)₂ (1.654 g, 2.54 mmol) was dissolved in 145 mL of MeOH followed by the addition of DOWEX® (4 scoops, ~6.25 g) and stirred for 3 h. (Yield: 1.448 g, 99%). ¹H NMR (600 MHz; MeOD): δ 7.37-7.30 (m, 5H), 5.06 (s, 2H), 4.28-4.22 (m, 4H), 3.68 (d, *J* = 10.84 Hz, 4H), 3.59 (d, *J* = 10.87 Hz, 4H), 3.23-3.11 (m, 4H), 1.56-1.48 (m, 4H), 1.27 (s, 3H), 1.15 (s, 6H). HRMS (ESI⁺) *m/z* calc'd for C₂₇H₄₂N₂O₁₁ [M+Na]⁺ = 593.2687, found [M+Na]⁺ 593.2693.

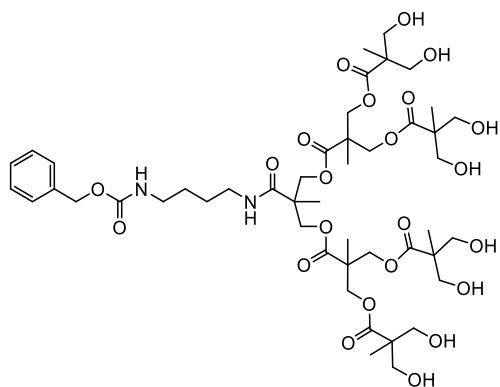
Cbz-G3-(acet)₄



Following General Procedure 1, bis-MPA-acetonide (5.662 g, 32.5 mmol) and EDC (3.118 g, 16.3 mmol) were dissolved in 7 mL of DCM, followed by addition of Cbz-G2-(OH)₄ (**5**) (1.16 g, 2.03 mmol), DMAP (248 mg, 2.03 mmol) and TEA (2.3 mL, 16.3 mmol), in 4.7 mL of pyridine. (Yield: 2.306 g, 95%). ¹H NMR (600 MHz; CDCl₃): δ 7.33-7.27 (m, 5H), 6.37 (s, 1H), 5.39 (s, 1H), 5.06 (s, 2H), 4.33-4.17 (m, 12H), 4.13-4.09 (m, 8H), 3.61-3.56

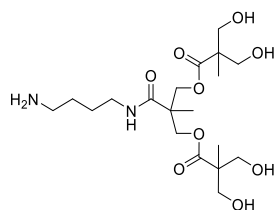
(m, 8H), 3.28-3.17 (m, 4H), 1.56-1.50 (m, 4H), 1.37 (s, 12H), 1.30 (s, 12H), 1.23-1.21 (m, 9H), 1.08 (s, 12H). HRMS (ESI⁺) *m/z* calc'd for C₅₉H₉₀N₂O₂₃ [M+H]⁺ = 1195.6007, found [M+H]⁺ 1195.6015.

Cbz-G3-(OH)₈



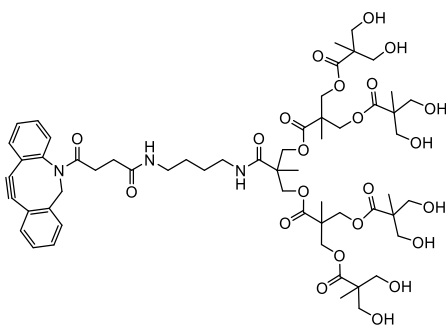
Following General Procedure 2, Cbz-G3-(acet)₄ (870 mg, 0.73 mmol) was dissolved in 330 mL of MeOH followed by the addition of DOWEX beads (5 scoops, ~8.7 g) and stirred for 3 h. (Yield: 745 mg, 98%). ¹H NMR (600 MHz; MeOD): δ 7.38-7.27 (m, 5H), 5.07 (s, 2H), 4.31-4.21 (m, 12H), 3.68-3.66 (m, 8H), 3.57-3.60 (m, 8H), 3.23-3.13 (m, 4H), 1.57-1.49 (m, 4H), 1.29-1.27 (m, 9H), 1.15 (s, 12H). HRMS (ESI⁺) *m/z* calc'd for C₄₇H₇₄N₂O₂₃ [M+H]⁺ = 1035.4755, found [M+H]⁺ 1035.4767.

NH₂-G3-(OH)₈



A round bottom flask was equipped with a magnetic stir bar and charged with Cbz-G3-(OH)₈ (1.00 g, 0.97 mmol), Pd(OH)₂/C (100 mg, 10 wt.%), and a solution of 1:1 DCM:MeOH (10 mL). The reaction vessel was purged under vacuum and backfilled with hydrogen gas three times and was then left stirring at room temperature overnight under a hydrogen balloon. The next day the reaction was filtered over a 0.22 μm PTFE filter, concentrated by rotary evaporation, and then dried under vacuum overnight to afford NH₂-G3-(OH)₈ as a white sticky solid (840 mg, 97%). ¹H NMR (600 MHz; MeOD): δ 4.30-4.22 (m, 12H), 3.69-3.67 (m, 8H), 3.60-3.58 (m, 8H), 3.23 (t, *J* = 7.1 Hz, 2H), 2.85 (t, *J* = 7.4 Hz, 2H), 1.61-1.58 (m, 4H), 1.30 (s, 9H), 1.14 (s, 12H). MS (ESI⁺) *m/z* calc'd for C₃₉H₆₈N₂O₂₁ [M+H]⁺ = 901.44, found [M+H]⁺ 901.4.

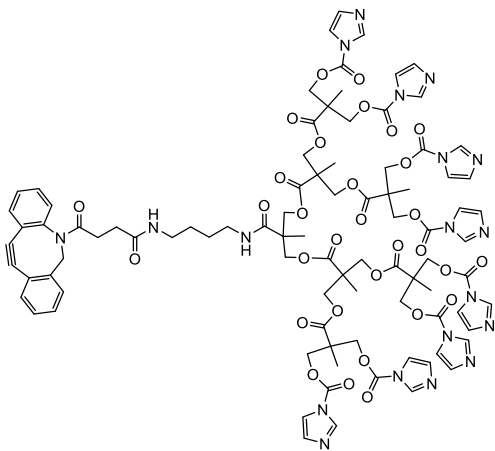
DBCO-G3-(OH)₈ (prepared according to literature procedures⁴⁸).



A round bottom flask was equipped with a magnetic stir bar and charged with NH₂-G3-(OH)₈ (230 mg, 0.26 mmol), and MeOH (2 mL). To this, DBCO-NHS (98 mg, 0.24 mmol) dissolved in DCM (1 mL), was added, followed by TEA (53 μL, 0.38 mmol). The reaction mixture was stirred at room temperature for 1.5 h and then concentrated by rotary evaporation. The crude residue was dissolved in 2 mL of 1:1 DMSO:H₂O and purified by

reverse phase flash chromatography with 5-100% MeCN in H₂O and monitored at 205 nm. Fractions containing product were combined, and MeCN was removed by rotary evaporation. The remaining water was lyophilized over two nights to give DBCO-G3-(OH)₈ as a white powder (233 mg, 81%). ¹H NMR (600 MHz; MeOD): δ 7.65 (d, *J* = 7.4 Hz, 1H), 7.61-7.59 (m, 1H), 7.48-7.45 (m, 3H), 7.38-7.32 (m, 2H), 7.26-7.25 (m, 1H), 5.13 (d, *J* = 14.1 Hz, 1H), 4.30-4.22 (m, 12H), 3.71 (d, *J* = 14.1 Hz, 1H), 3.67-3.66 (m, 8H), 3.59-3.57 (m, 8H), 3.18 (t, *J* = 7.1 Hz, 2H), 3.10-3.05 (m, 2H), 2.72-2.66 (m, 1H), 2.37-2.31 (m, 1H), 2.19-2.14 (m, 1H), 2.01-1.96 (m, 1H), 1.50-1.45 (m, 2H), 1.42-1.38 (m, 2H), 1.28 (s, 9H), 1.14 (s, 12H). MS (ESI⁺) *m/z* calc'd for C₅₈H₈₁N₃O₂₃ [M+Na]⁺ = 1210.52, found [M+H]⁺ 1210.5.

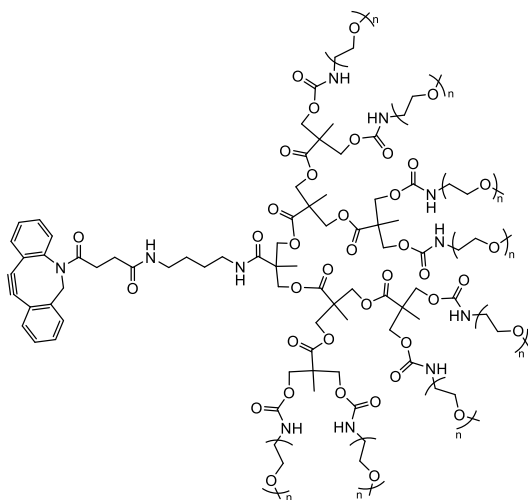
Synthesis of DBCO-G3-(IMI)₈



A round bottom flask was equipped with a magnetic stir bar and charged with DBCO-G3-(OH)₈ (230 mg, 0.19 mmol) and dry MeCN (2 mL). To this, CDI (1.255 g, 7.74 mmol) dissolved in dry MeCN (8 mL) was added in one portion. The reaction mixture was stirred overnight at room temperature at which point white solids precipitated out of solution. The

mixture was cooled to 0 °C and filtered by vacuum filtration and washed with a 50 mL solution of 1:1 ether/hexanes. The solid was then dried under vacuum to afford DBCO-G3-(IMI)₈ as a cream-coloured powder (268 mg, 71%). ¹H NMR (600 MHz; DMSO-*d*₆): δ 8.24 (s, 8H), 7.73 (t, *J* = 5.3 Hz, 1H), 7.68-7.61 (m, 2H), 7.55 (s, 8H), 7.49-7.42 (m, 2H), 7.38-7.28 (m, 3H), 7.03 (s, 8H), 5.01 (d, *J* = 14.1 Hz, 1H), 4.59-4.54 (m, 16H), 4.21 (s, 8H), 4.08-4.01 (m, 4H), 3.60 (d, *J* = 14.0 Hz, 1H), 2.98-2.88 (m, 4H), 2.59-2.55 (m, 1H), 2.24-2.18 (m, 1H), 1.99-1.94 (m, 1H), 1.79-1.74 (m, 1H), 1.32-1.24 (m, 16H), 1.10 (s, 9H). MS (ESI⁺) *m/z* calc'd for C₉₀H₉₇N₁₉O₃₁ [M+Na]⁺ = 1962.65, found [M+H]⁺ 1962.7.

DBCO-G3-(PEG₃₅₀)₈



Following General Procedure 3, DBCO-G3-(IMI)₈ (80 mg, 0.04 mmol), PEG₃₅₀-NH₂ (190 mg, 0.50 mmol), and TEA (105 μL, 0.74 mmol) were dissolved in DCM (2 mL). The mixture was purified using 3.5 kDa MWCO dialysis tubing and the product was afforded as a dark yellow oil. (131 mg, 71%). ¹H NMR (600 MHz; CDCl₃): δ 7.65 (d, *J* = 5.3 Hz, 1H), 7.52-7.49 (m, 1H), 7.39-7.30 (m, 5H), 7.16-7.10 (m, 1H), 6.75 (s, 1H), 6.60 (s, 1H),

5.54 (br. s, 8H), 5.13 (d, $J = 13.9$ Hz, 1H), 4.25-4.12 (m, 28H), 3.75-3.53 (m, 240H), 3.37 (s, 24H), 3.32 (s, 16H), 3.20-3.08 (m, 4H), 2.78-2.70 (m, 1H), 2.45-2.35 (m, 1H), 2.22-2.16 (m, 1H), 2.04-1.99 (m, 1H), 1.25-1.08 (m, 25H).

DBCO-G3-(PEG₁₀₀₀)₈

Following General Procedure 3, DBCO-G3-(IMI)₈ (30 mg, 0.016 mmol), PEG1000-NH₂ (186 mg, 0.19 mmol), and TEA (39 μ L, 0.28 mmol) were dissolved in DCM (2 mL). The mixture was purified using 12 kDa MWCO dialysis tubing and the product was afforded as a white powder. (75 mg, 52%). ¹H NMR (600 MHz; CDCl₃): δ 7.66 (d, $J = 5.3$ Hz, 1H), 7.49-7.47 (m, 1H), 7.40-7.30 (m, 5H), 7.17-7.11 (m, 1H), 6.88 (s, 1H), 6.78 (s, 1H), 5.50 (d, $J = 120.6$ Hz, 8H), 5.13 (d, $J = 13.9$ Hz, 1H), 4.26-4.12 (m, 28H), 3.77-3.53 (m, 720H), 3.38 (s, 24H), 3.33 (s, 16H), 3.22-3.10 (m, 4H), 2.78-2.70 (m, 1H), 2.45-2.35 (m, 1H), 2.22-2.16 (m, 1H), 2.04-1.99 (m, 1H), 1.31-1.09 (m, 25H).

DBCO-G3-(PEG₂₀₀₀)₈

Following General Procedure 3, DBCO-G3-(IMI)₈ (33 mg, 0.017 mmol), PEG2000-NH₂ (411 mg, 0.20 mmol), and TEA (43 μ L, 0.31 mmol) were dissolved in DCM (2 mL). The mixture was purified using 12 kDa MWCO dialysis tubing and the product was afforded as a white powder. (190 mg, 64%). ¹H NMR (600 MHz; CDCl₃): δ 7.66-7.64 (m, 1H), 7.52-7.49 (m, 1H), 7.39-7.30 (m, 5H), 7.16-7.10 (m, 1H), 6.88 (s, 1H), 6.77 (s, 1H), 5.68-5.43 (m, 8H), 5.13 (d, $J = 13.9$ Hz, 1H), 4.30-4.11 (m, 28H), 3.76-3.51 (m, 1520H), 3.38 (s,

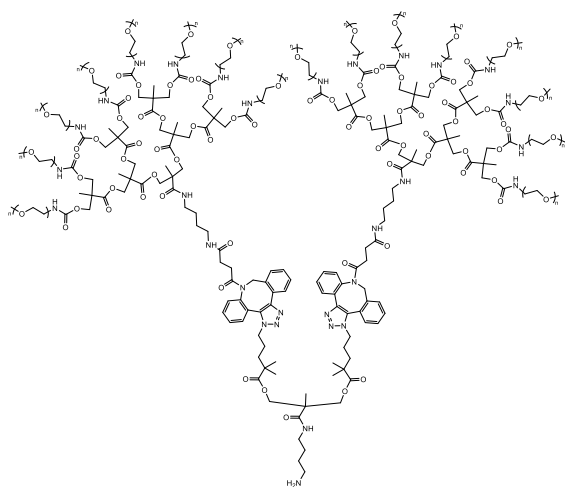
24H), 3.32 (s, 16H), 3.20-3.09 (m, 4H), 2.78-2.70 (m, 1H), 2.45-2.35 (m, 1H), 2.22-2.16 (m, 1H), 2.04-1.99 (m, 1H), 1.31-1.13 (m, 25H).

General Procedure 4: Synthesis of G4 and 5 Dendrons

A round bottom flask was equipped with a magnetic stir bar and charged with 1 eq. of $\text{H}_2\text{N-G}_x(\text{N}_3)_y$ dissolved in DCM. A 1 eq. per azide solution of DBCO-G3-(PEG_n)₈ in DCM was added to the mixture in 100 μL aliquots. The reaction was left to stir at room temperature for 20 minutes after every addition of an aliquot and monitored by FTIR to observe the disappearance of the azide peak at $\sim 2100\text{ cm}^{-1}$. At full disappearance of the azide signal, the solvent was removed by rotary evaporation and the mixture was dissolved in $\sim 1\text{ mL}$ of deionized water and purified by dialysis using either 12 kDa or 100 kDa MWCO dialysis tubing. Dendrimers dialyzed with 12 kDa tubing were dialyzed overnight and water was changed twice. Dendrimers dialyzed with 100 kDa tubing were dialyzed for $\sim 24\text{ h}$ and the water was changed thrice. After dialysis the solution was lyophilized overnight to afford the $\text{NH}_2\text{-G}_x(\text{PEG}_n)_y$.

To amidate the amine core with DBCO (i.e., to make DBCO-G_x-(PEG_n)_y), a round bottom flask was equipped with a magnetic stir bar and charged with $\text{H}_2\text{N-G}_x(\text{PEG})_y$ (1 eq.), DCM, DBCO-NHS (10 eq.) and TEA (12 eq.). The reaction mixture was left stirring at room temperature overnight. The next day the solvent was concentrated by rotary evaporation and the crude material was directly purified using a 12 g flash column with a gradient of 1-2% MeOH in DCM to elute all small molecules (monitored at 254 nm), followed by isocratic elution with 20% MeOH in DCM until the dendrimer was fully eluted (monitored at 205 nm). Fractions containing dendrimer were collected, concentrated *in*

vacuo and passed through a neutral alumina plug to remove residual DBCO-containing small molecules. The plug was then flushed with 100% MeOH to elute the dendrimer. The collected fractions were dried *in vacuo* and then lyophilized overnight to afford the product, **DBCO-G_x-(PEG_n)_y**.



NH₂-G4-(PEG₃₅₀)₁₆

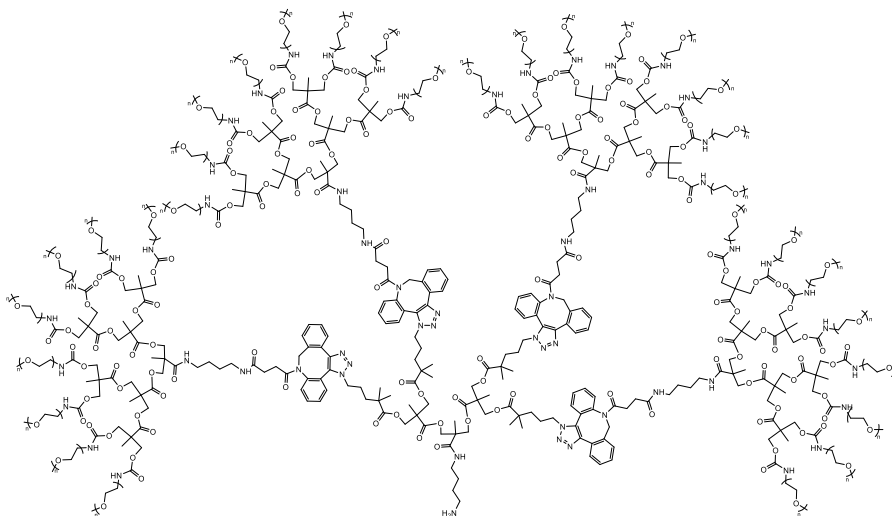
Following General Procedure 2, NH₂-G1-(N₃)₂ (9 mg, 0.018 mmol) was dissolved in 100 μ L of DCM. A solution of DBCO-G3-(PEG₃₅₀)₈ (157 mg, 0.035 mmol) in DCM (3 mL) was added in 100 μ L aliquots until complete disappearance of the azide peak was observed and reaction was deemed finished. The mixture was purified using 12 kDa MWCO dialysis tubing and the product was obtained as a sticky orange oil (87 mg, 52%). ¹H NMR (600 MHz; CDCl₃): δ 7.64-7.02 (m, 20H), 6.03 (dd, J = 46.8, 12.9 Hz, 2H), 5.66-5.35 (m, 16H), 4.26-4.11 (m, 64H), 3.76-3.54 (m, 480H), 3.37 (s, 48H), 3.32 (s, 32H), 3.21-3.09 (m, 12H), 1.47-1.10 (m, 85H).

NH₂-G4-(PEG₁₀₀₀)₁₆

Following General Procedure 2, $\text{NH}_2\text{-G1-(N}_3)_2$ (5 mg, 0.010 mmol) was dissolved in 100 μL of DCM. A solution of $\text{DBCO-G3-(PEG1000)}_8$ (184 mg, 0.020 mmol) in DCM (3 mL) was added in 100 μL aliquots until complete disappearance of the azide peak was observed and reaction was deemed finished. The mixture was purified using 100 kDa MWCO dialysis tubing and the product was obtained as a flaky pale orange powder (46 mg, 24%). $^1\text{H NMR}$ (600 MHz; CDCl_3): δ 7.62-7.03 (m, 20H), 6.09-5.97 (m, 2H), 5.59-5.34 (m, 16H), 4.26-4.12 (m, 64H), 3.76-3.51 (m, 1440H), 3.37 (s, 48H), 3.32 (s, 32H), 3.25-3.14 (m, 12H), 1.30-1.12 (m, 85H).

$\text{NH}_2\text{-G4-(PEG2000)}_{16}$

Following General Procedure 2, $\text{NH}_2\text{-G1-(N}_3)_2$ (3 mg, 0.006 mmol) was dissolved in 100 μL of DCM. A solution of $\text{DBCO-G3-(PEG2000)}_8$ (206 mg, 0.012 mmol) in DCM (3 mL) was added in 100 μL aliquots until complete disappearance of the azide peak was observed and reaction was deemed finished. The mixture was purified using 100 kDa MWCO dialysis tubing and the product was obtained as a white powder (31 mg, 15%). $^1\text{H NMR}$ (600 MHz; CDCl_3): δ 7.59-7.02 (m, 20H), 6.10-5.97 (m, 2H), 5.68-5.47 (m, 16H), 4.36-4.11 (m, 64H), 3.76-3.51 (m, 3040H), 3.38 (s, 48H), 3.33 (s, 32H), 3.27-3.16 (m, 12H), 1.30-1.10 (m, 85H).



NH₂-G5-(PEG₃₅₀)₃₂

Following General Procedure 2, NH₂-G2-(N₃)₄ (15 mg, 0.014 mmol) was dissolved in 100 μ L of DCM. A solution of DBCO-G3-(PEG₃₅₀)₈ (255 mg, 0.057 mmol) in DCM (3 mL) was added in 100 μ L aliquots until complete disappearance of the azide peak was observed and reaction was deemed finished. The mixture was purified using 12 kDa MWCO dialysis tubing and the product was obtained as a sticky orange oil (172 mg, 64%). ¹H NMR (600 MHz; CDCl₃): δ 7.60-7.03 (m, 40H), 6.05-5.97 (m, 4H), 5.62-5.33 (m, 32H), 4.40-4.12 (m, 132H), 3.75-3.54 (m, 960H), 3.37 (s, 96H), 3.32 (s, 64H), 3.20-3.08 (m, 20H), 1.45-1.09 (m, 169H).

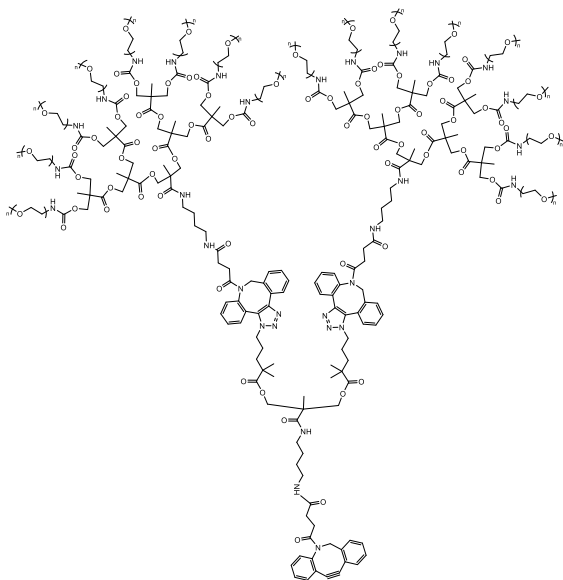
NH₂-G5-(PEG₁₀₀₀)₃₂

Following General Procedure 2, NH₂-G2-(N₃)₄ (8 mg, 0.008 mmol) was dissolved in 100 μ L of DCM. A solution of DBCO-G3-(PEG₁₀₀₀)₈ (287 mg, 0.031 mmol) in DCM (3 mL) was added in 100 μ L aliquots until complete disappearance of the azide peak was observed and reaction was deemed finished. The mixture was purified using 100 kDa MWCO dialysis tubing and the product was obtained as an orange oil (62 mg, 21%). ¹H NMR (600

MHz; CDCl₃): δ 7.61-7.03 (m, 40H), 6.06-5.97 (m, 4H), 5.64-5.31 (m, 32H), 4.40-4.16 (m, 132H), 3.75-3.52 (m, 2280H), 3.37 (s, 96H), 3.32 (s, 64H), 3.25-3.11 (m, 20H), 1.47-1.08 (m, 169H).

NH₂-G5-(PEG₂₀₀₀)₃₂

Following General Procedure 4, NH₂-G2-(N₃)₄ (3 mg, 0.003 mmol) was dissolved in 100 μ L of DCM. A solution of DBCO-G3-(PEG1000)₈ (200 mg, 0.014 mmol) in DCM (3 mL) was added in 100 μ L aliquots until complete disappearance of the azide peak was observed and reaction was deemed finished. The mixture was purified using 100 kDa MWCO dialysis tubing and the product was obtained as a white powder (46 mg, 23%). ¹H NMR (600 MHz; CDCl₃): δ 7.60-7.03 (m, 40H), 6.06-5.95 (m, 4H), 5.72-5.30 (m, 32H), 4.38-4.18 (m, 132H), 3.75-3.50 (m, 6080H), 3.36 (s, 96H), 3.31 (s, 64H), 3.19-3.10 (m, 20H), 1.44-1.08 (m, 169H).



DBCO-G4-(PEG₃₅₀)₁₆

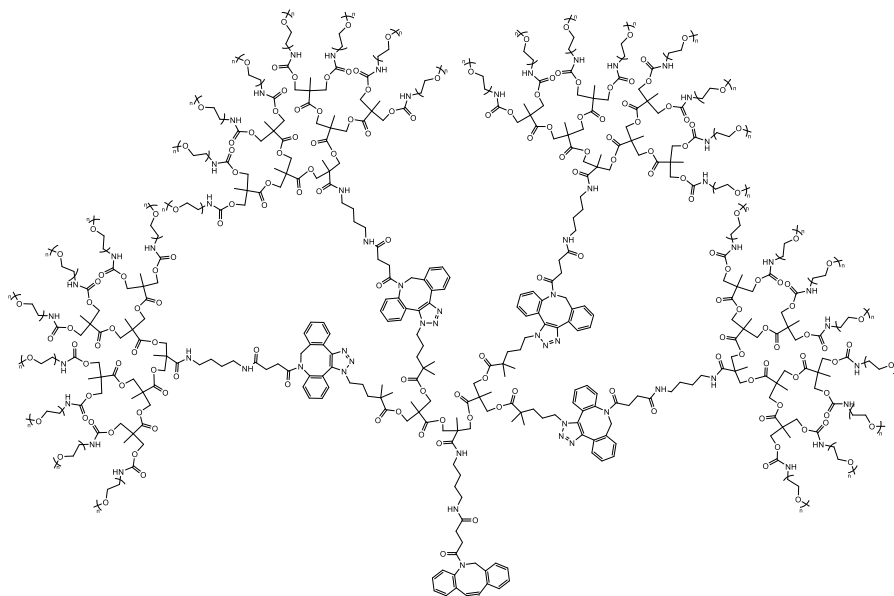
Following General Procedure 4, NH₂-G4-(PEG₃₅₀)₁₆ (83 mg, 0.009 mmol) and DBCO-NHS (35 mg, 0.088 mmol) were dissolved in 1 mL of DCM, followed by addition of TEA (34 μL, 0.25 mmol). The product was obtained as a sticky orange oil (71 mg, 83%).

DBCO-G4-(PEG₁₀₀₀)₁₆

Following General Procedure 4, NH₂-G4-(PEG₁₀₀₀)₁₆ (63 mg, 0.003 mmol) and DBCO-NHS (13 mg, 0.033 mmol) were dissolved in 1 mL of DCM, followed by addition of TEA (13 μL, 0.091 mmol). The product was obtained as an off-white to orange oil (47 mg, 73%).

DBCO-G4-(PEG₂₀₀₀)₁₆

Following General Procedure 4, NH₂-G4-(PEG₂₀₀₀)₁₆ (41 mg, 0.001 mmol) and DBCO-NHS (5 mg, 0.011 mmol) were dissolved in 1 mL of DCM, followed by addition of TEA (2 μL, 0.014 mmol). The product was obtained as a white powder (25 mg, 61%).



DBCO-G5-(PEG₃₅₀)₃₂

Following General Procedure 3, NH₂-G5-(PEG₃₅₀)₃₂ (71 mg, 0.004 mmol) and DBCO-NHS (15 mg, 0.038 mmol) were dissolved in 1 mL of DCM, followed by addition of TEA (6.3 μL, 0.045 mmol). The product was obtained as a sticky orange oil (58 mg, 81%).

DBCO-G5-(PEG₁₀₀₀)₃₂

Following General Procedure 3, NH₂-G5-(PEG₁₀₀₀)₃₂ (37 mg, 0.001 mmol) and DBCO-NHS (4 mg, 0.010 mmol) were dissolved in 1 mL of DCM, followed by addition of TEA (1.6 μL, 0.012 mmol). The product was obtained as a sticky orange oil (26 mg, 70%).

DBCO-G5-(PEG₂₀₀₀)₃₂

Following General Procedure 3, NH₂-G5-(PEG₂₀₀₀)₃₂ (46 mg, 0.0006 mmol) and DBCO-NHS (3 mg, 0.0065 mmol) were dissolved in 1 mL of DCM, followed by addition of TEA (1.1 μL, 0.008 mmol). The product was obtained as a white powder (19 mg, 41%).

Synthesis of azide-CT and CT-dendron Conjugates

Azide-CT was synthesized from modified procedures.²¹ 2-Azidoacetic acid (51 mg, 0.5 mmol) and *N*-hydroxysuccinimide (348 mg, 3.03 mmol) were dissolved in 450 μL of 0.1 M phosphate buffer (pH 8). Separately, EDC · HCl (290 mg, 4.53 mmol) was dissolved in 300 μL of 0.1 M phosphate buffer and added to the reaction mixture. The solution was stirred under ambient conditions for 1.5 hours and then directly added to a solution of α-chymotrypsin (270 mg) dissolved in 8 mL of 0.1 M phosphate buffer (pH 8). The reaction mixture was then stirred at 4 °C in a fridge for overnight, at which point the pH was adjusted back to ~ 8 via dropwise addition of 2 M KOH, then left to stir for an additional hour at 4 °C. The reaction mixture was then dialyzed in 12 kDa tubing against deionized water.

Changing water 3 times over 24 hours then lyophilized, giving CT-N₃ as a fluffy white powder. (173 mg, 62%)

General Procedure 5: Preparation of CT-Dendron Conjugates

A 20 mL scintillation vial was equipped with a magnetic stir bar and charged with approximately 20-28 eq. (i.e., 1.4-2 eq. per azide) of DBCO-G_x-(PEG_n)_y dissolved in 400-800 μL of 0.1 M pH 8 phosphate buffer. Separately, 1 eq. of azide functionalized α-chymotrypsin was dissolved in 400-800 μL of 0.1 M pH 8 phosphate buffer. The dendron solution was added to the protein solution and stirred for overnight at 4 °C. The mixture was then directly dialyzed using 50-1000 kDa MWCO tubing for 2 days against deionized water. Water was changed 3 times. The solution was then lyophilized overnight to afford the conjugate as a white solid.

CT-G3-(PEG₃₅₀)₈

Using general procedure 5, DBCO-G3-(PEG₃₅₀)₈ (23.2 mg, 0.0058 mmol) was dissolved in 400 uL of 0.1 M phosphate buffer and added to a solution of CT-N₃ (8.1 mg, 0.00029 mmol) in 400 uL of 0.1 M phosphate buffer. The conjugate was dialyzed in 12 kDa MWCO tubing and isolated as a fluffy white powder (16 mg, 67%).

CT-G3-(PEG₁₀₀₀)₈

Using general procedure 5, DBCO-G3-(PEG₁₀₀₀)₈ (90 mg, 0.01 mmol) was dissolved in 1000 uL of 0.1 M phosphate buffer and added to a solution of α-CT-N₃ (14 mg, 0.0004

mmol) in 500 uL of 0.1 M phosphate buffer. The conjugate was dialyzed in 50 kDa MWCO tubing and isolated as a fluffy white powder (54 mg, 71%).

CT-G3-(PEG₂₀₀₀)₈

Using general procedure 5, DBCO-G3-(PEG₂₀₀₀)₈ (88 mg, 0.005 mmol) was dissolved in 2000 uL of 0.1 M phosphate buffer and added to a solution of α -CT-N₃ (5 mg, 0.0002 mmol) in 500 uL of 0.1 M phosphate buffer. The conjugate was dialyzed in 50 kDa MWCO tubing and isolated as a fluffy white powder (22 mg, 44%).

CT-G4-(PEG₃₅₀)₁₆

Using general procedure 5, DBCO-G4-(PEG₃₅₀)₁₆ (54 mg, 0.006 mmol) was dissolved in 2000 uL of 0.1 M phosphate buffer and added to a solution of α -CT-N₃ (6 mg, 0.0002 mmol) in 500 uL of 0.1 M phosphate buffer. The conjugate was dialyzed in 100 kDa MWCO tubing and isolated as a fluffy white powder (15 mg, 45%).

CT-G4-(PEG₁₀₀₀)₁₆

Using general procedure 5, DBCO-G4-(PEG₁₀₀₀)₁₆ (57 mg, 0.003 mmol) was dissolved in 2000 uL of 0.1 M phosphate buffer and added to a solution of α -CT-N₃ (2.9 mg, 0.00010 mmol) in 500 uL of 0.1 M phosphate buffer. The conjugate was dialyzed in 100 kDa MWCO tubing and isolated as a fluffy white powder (27 mg, 84%).

CT-G4-(PEG₂₀₀₀)₁₆

Using general procedure 5, DBCO-G4-(PEG₂₀₀₀)₁₆ (60 mg, 0.0017 mmol) was dissolved in 2000 uL of 0.1 M phosphate buffer and added to a solution of α -CT-N₃ (1.7 mg, 6.07 x

10^{-5} mmol) in 500 uL of 0.1 M phosphate buffer. The conjugate was dialyzed in 300 kDa MWCO tubing and isolated as a fluffy white powder (24 mg, 75%).

CT-G5-(PEG₃₅₀)₃₂

Using general procedure 5, DBCO-G5-(PEG₃₅₀)₃₂ (118 mg, 0.006 mmol) was dissolved in 2000 uL of 0.1 M phosphate buffer and added to a solution of α -CT-N₃ (8 mg, 0.0003 mmol) in 500 uL of 0.1 M phosphate buffer. The conjugate was dialyzed in 300 kDa MWCO tubing and isolated as a fluffy white powder (34 mg, 37%).

CT-G5-(PEG₁₀₀₀)₃₂

Using general procedure 5, DBCO-G5-(PEG₁₀₀₀)₃₂ (152 mg, 0.004 mmol) was dissolved in 2000 uL of 0.1 M phosphate buffer and added to a solution of α -CT-N₃ (5 mg, 0.0002 mmol) in 500 uL of 0.1 M phosphate buffer. The conjugate was dialyzed in 500 kDa MWCO tubing and isolated as a fluffy white powder (59 mg, 58%).

CT-G5-(PEG₂₀₀₀)₃₂

Using general procedure 5, DBCO-G4-(PEG₂₀₀₀)₃₂ (50.8 mg, 0.0007 mmol) was dissolved in 2000 uL of 0.1 M phosphate buffer and added to a solution of α -CT-N₃ (1 mg, 3.57×10^{-5} mmol) in 500 uL of 0.1 M phosphate buffer. The conjugate was dialyzed in 1000 kDa MWCO tubing and isolated as a fluffy white powder (33 mg, 89%).

NMR Spectra of Synthesized Compounds

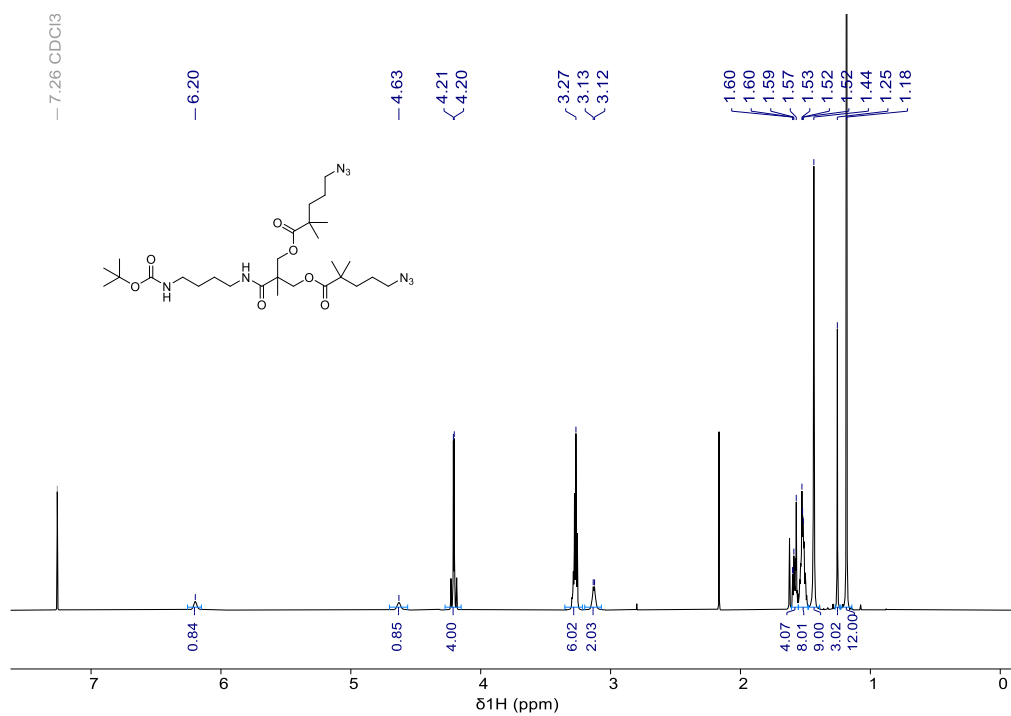


Figure S3.1. ¹H NMR of Boc-G1-(N₃)₂

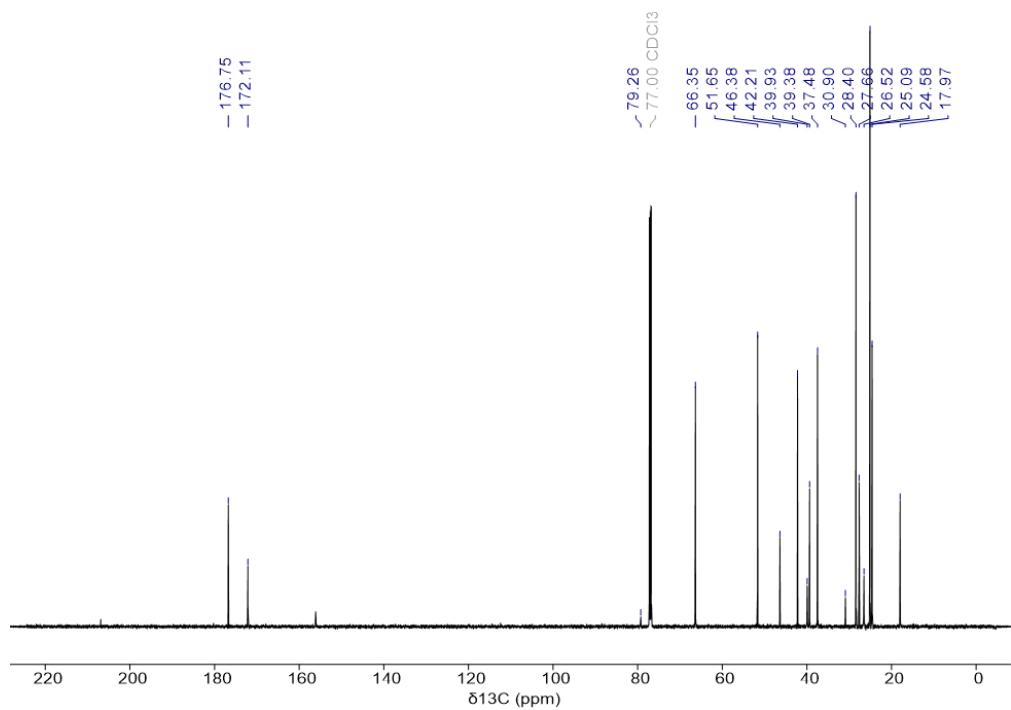


Figure S3.2. ¹³C NMR of Boc-G1-(N₃)₂

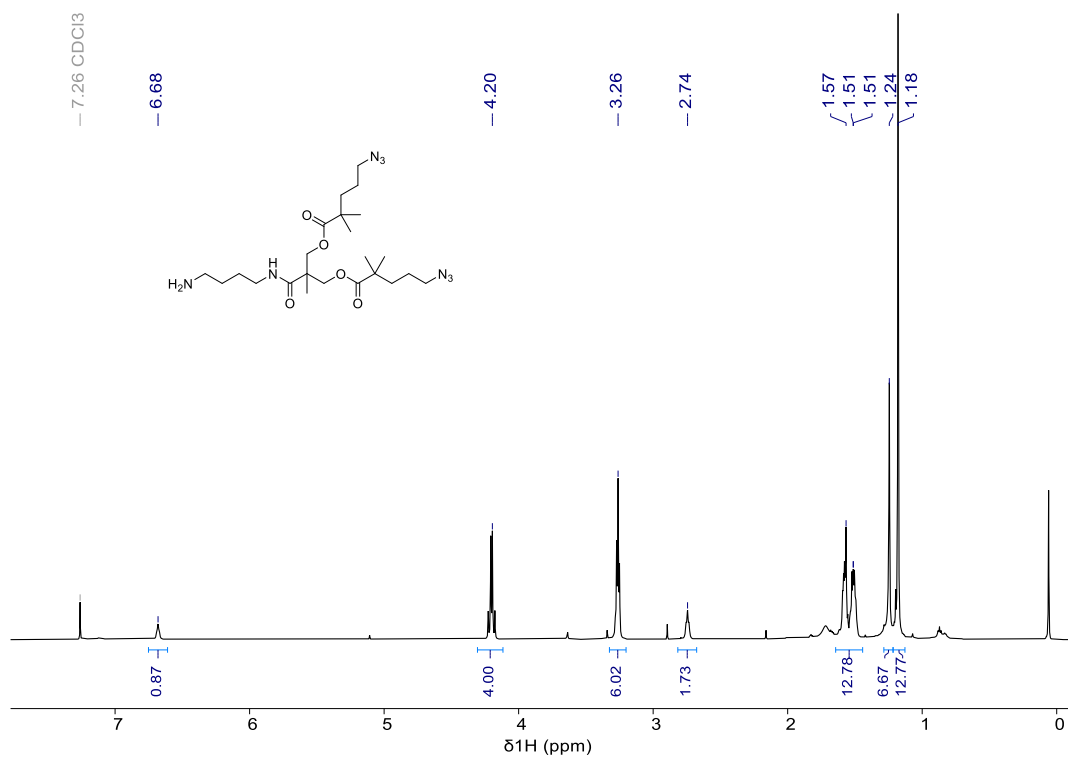


Figure S3.3. $^1\text{H NMR}$ of $\text{NH}_2\text{-G1-(N}_3)_2$

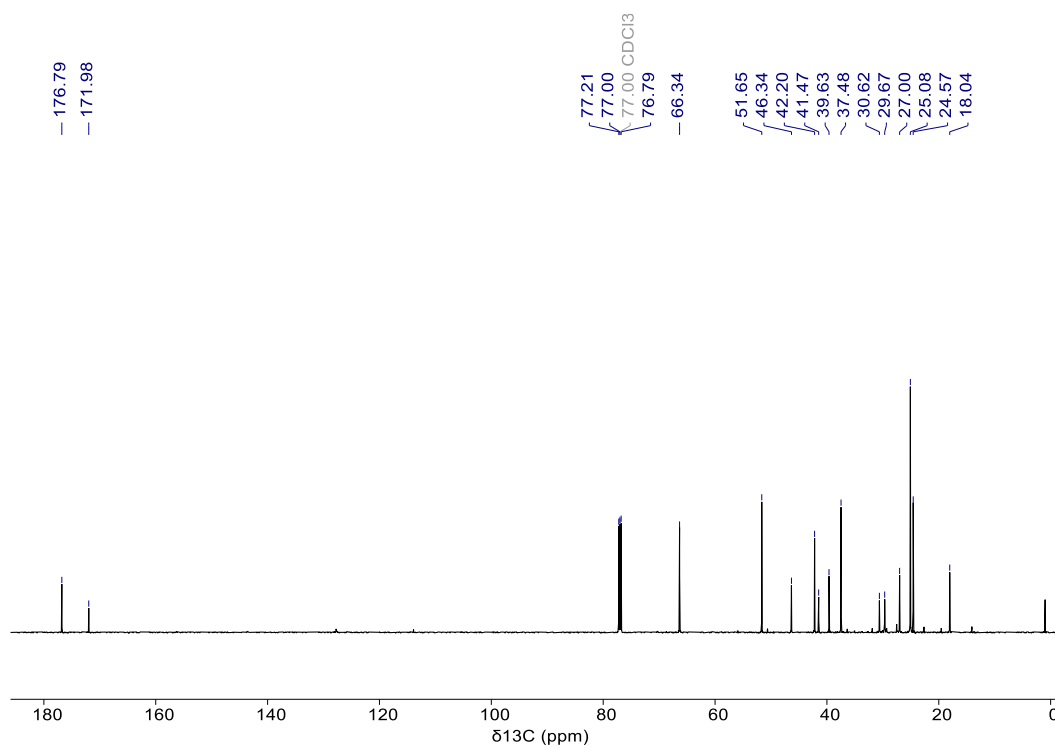


Figure S3.4. $^{13}\text{C NMR}$ of $\text{NH}_2\text{-G1-(N}_3)_2$

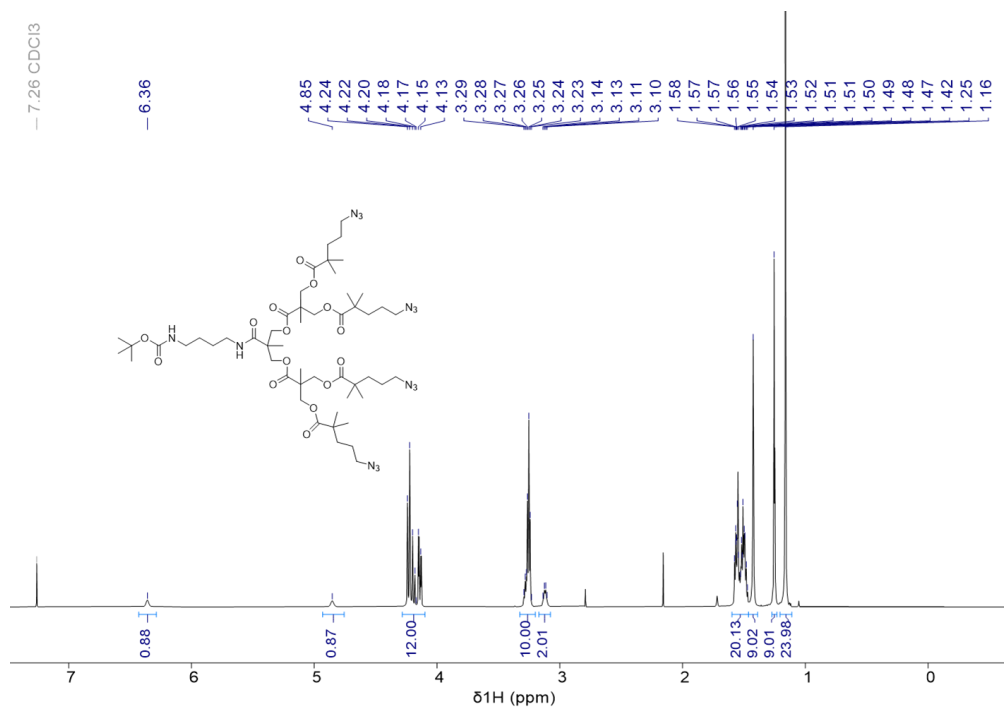


Figure S3.5. ¹H NMR of Boc-G2-(N₃)₄

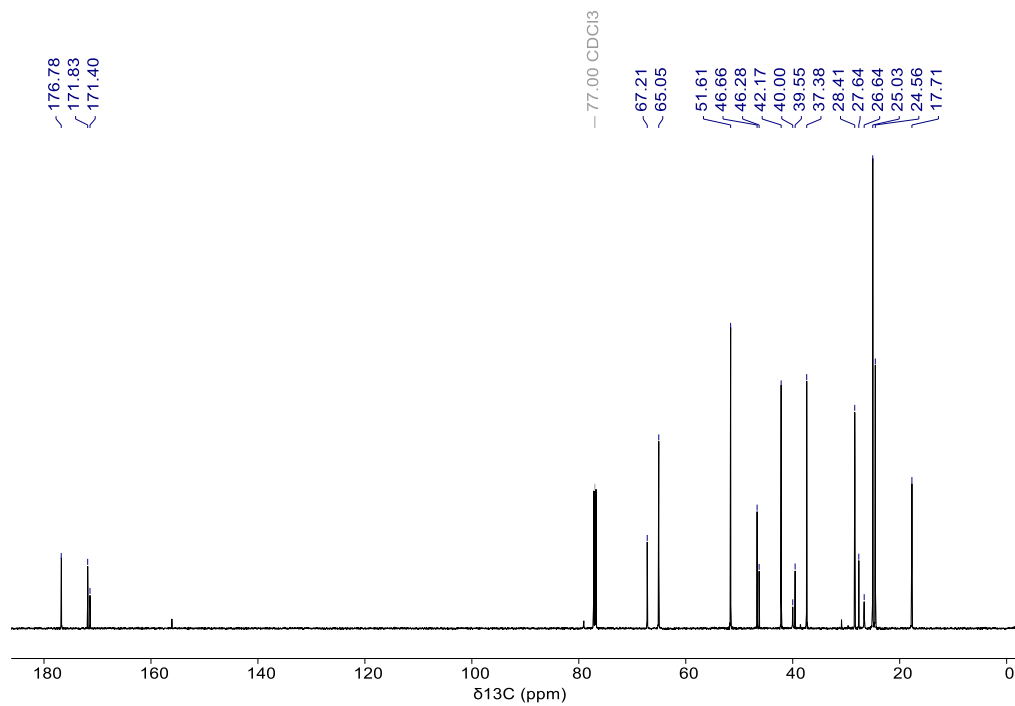


Figure S3.6. ¹³C NMR of Boc-G2-(N₃)₄

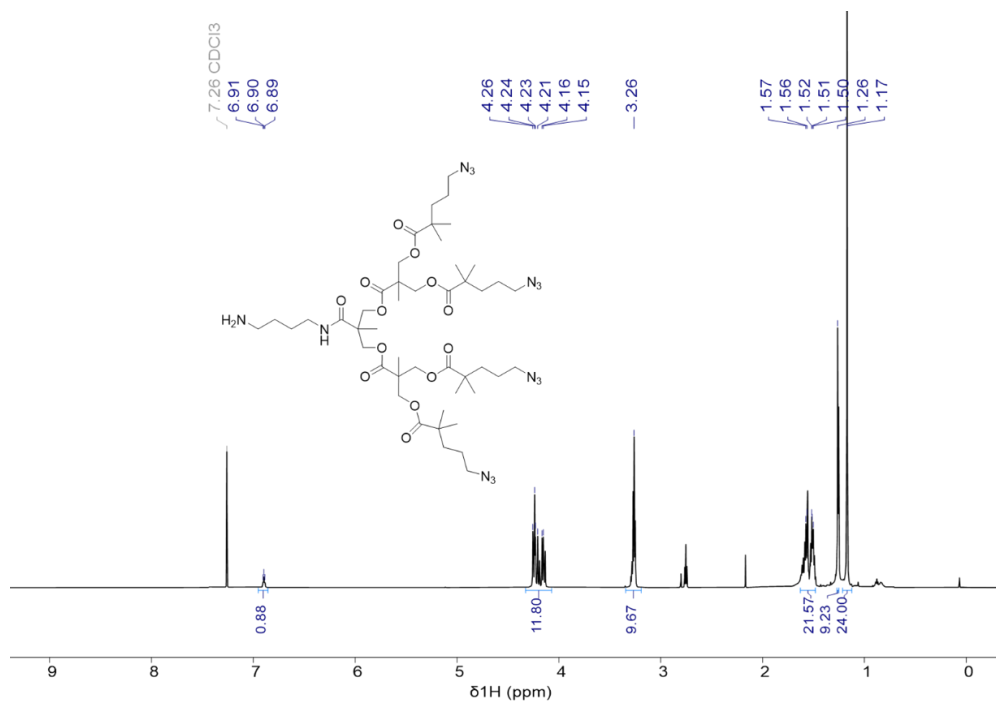


Figure S3.7. $^1\text{H NMR}$ of $\text{NH}_2\text{-G2-(N}_3)_4$

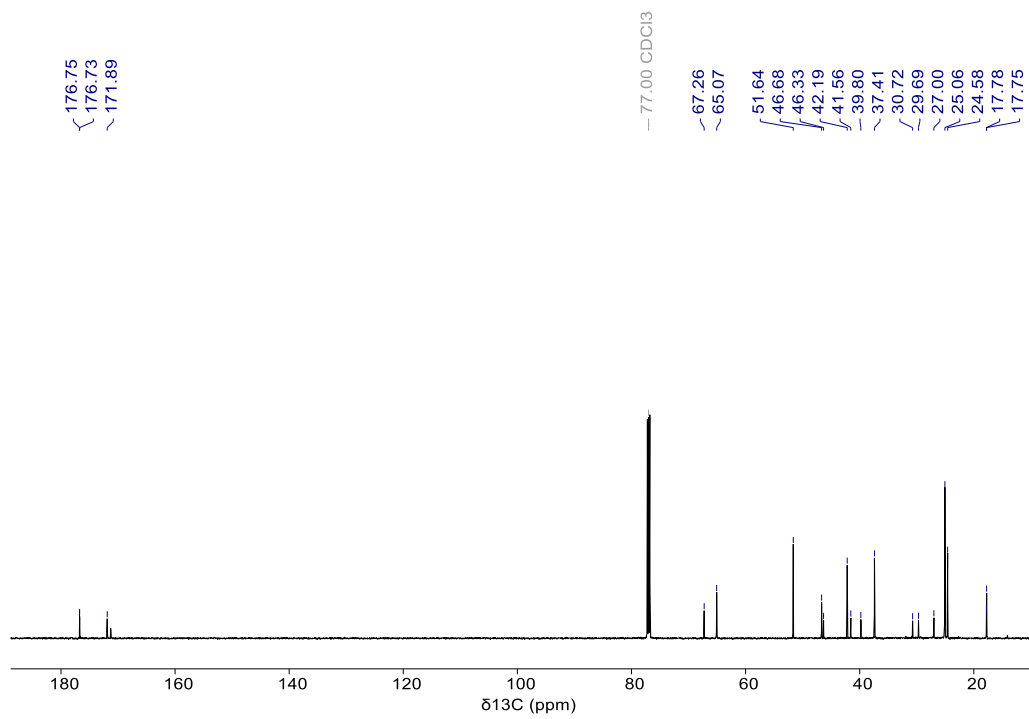


Figure S3.8. $^{13}\text{C NMR}$ of $\text{NH}_2\text{-G2-(N}_3)_4$

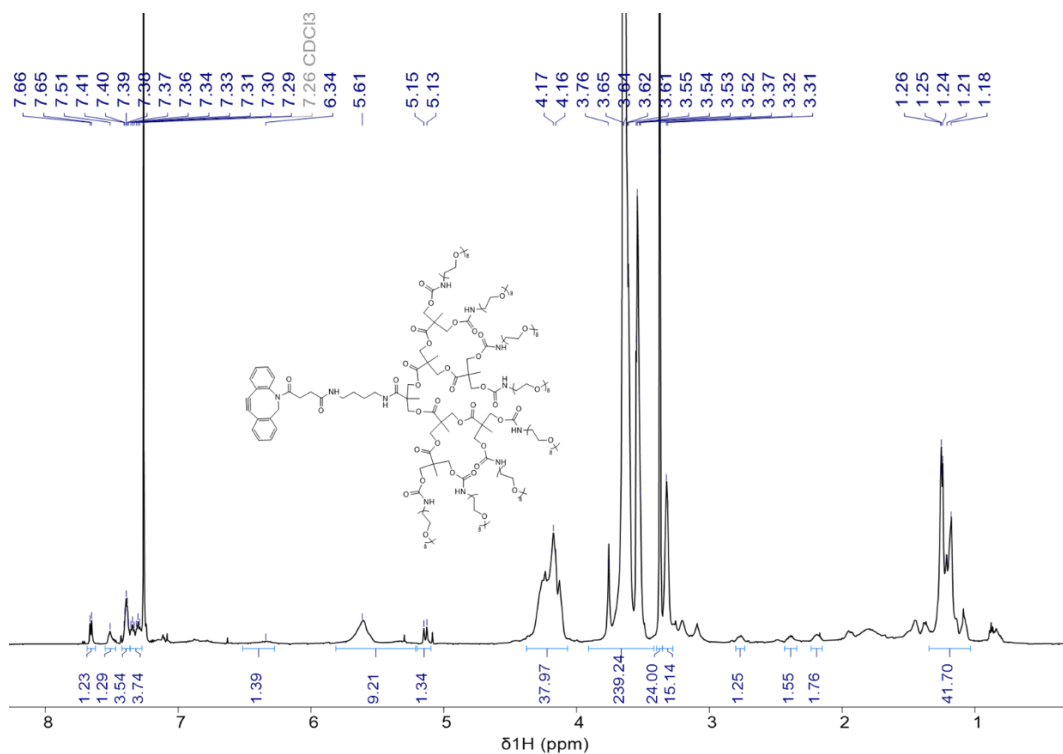


Figure S3.9. ¹H NMR of DBCO-G3-(PEG₃₅₀)₈.

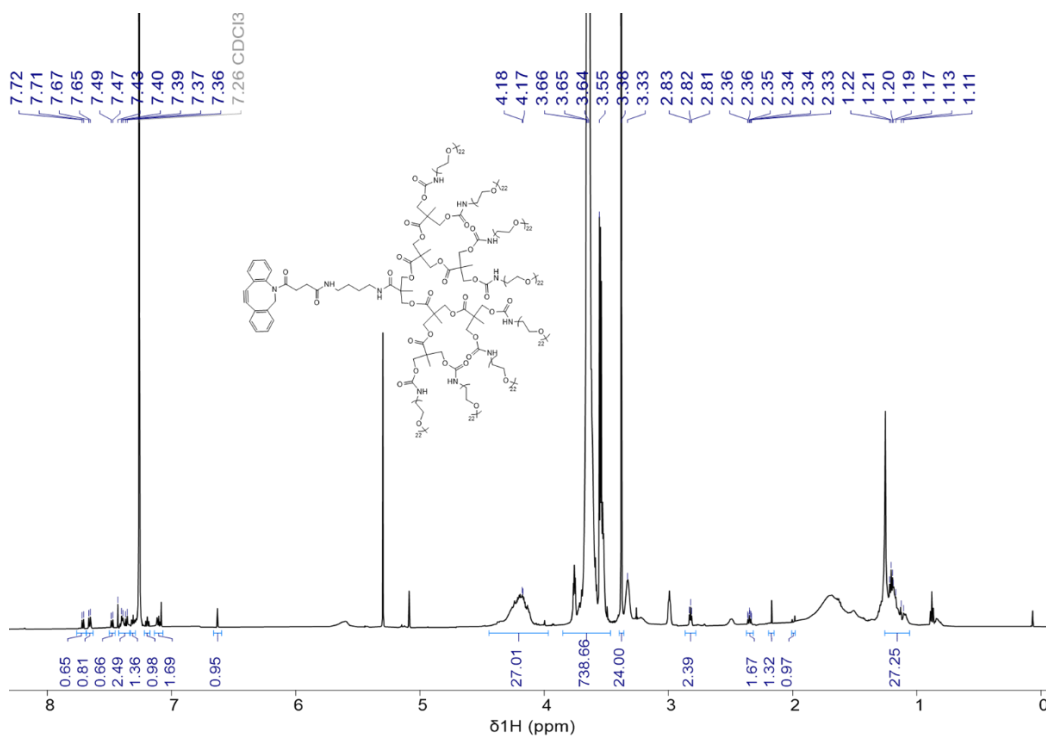


Figure S3.10. ¹H NMR of DBCO-G3-(PEG₁₀₀₀)₈

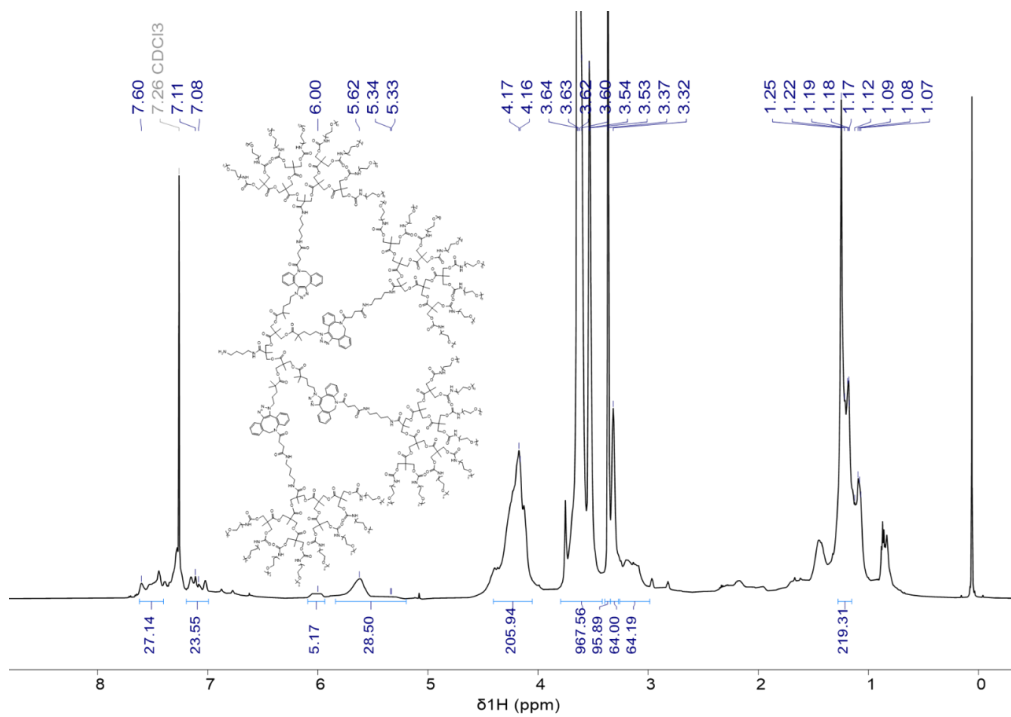


Figure S3.15. ^1H NMR of $\text{NH}_2\text{-G5-(PEG}_{350})_{32}$

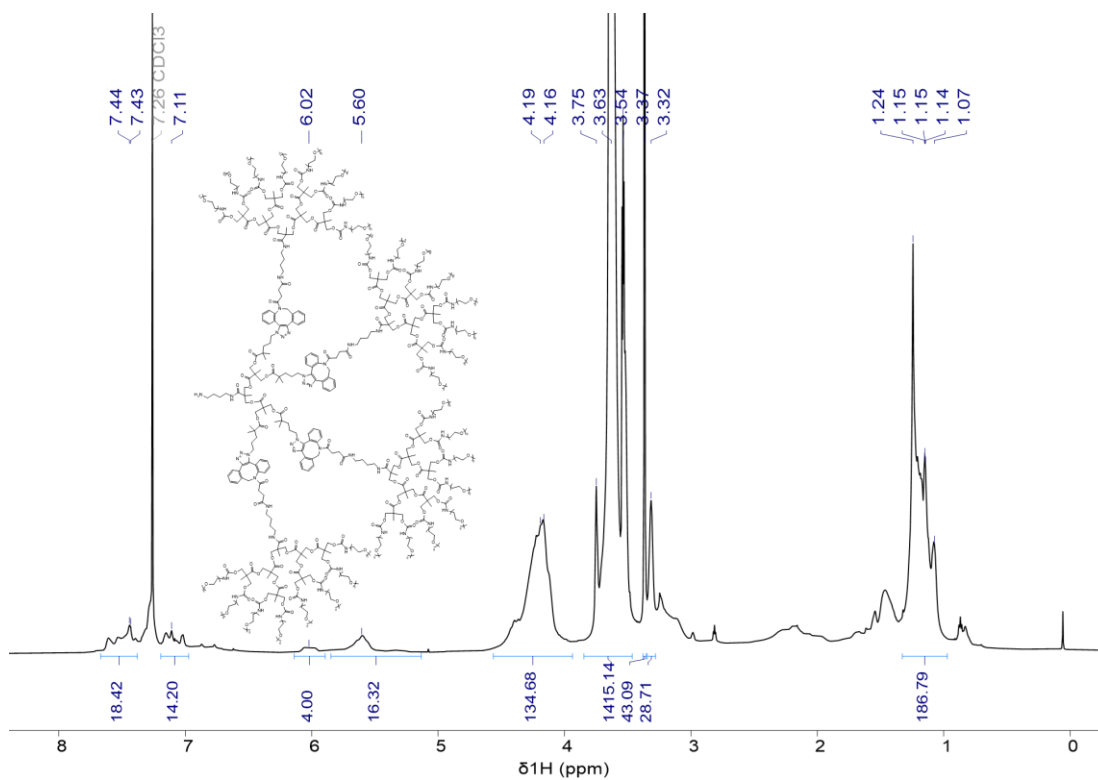


Figure S3.16. ^1H NMR of $\text{NH}_2\text{-G5-(PEG}_{1000})_{32}$

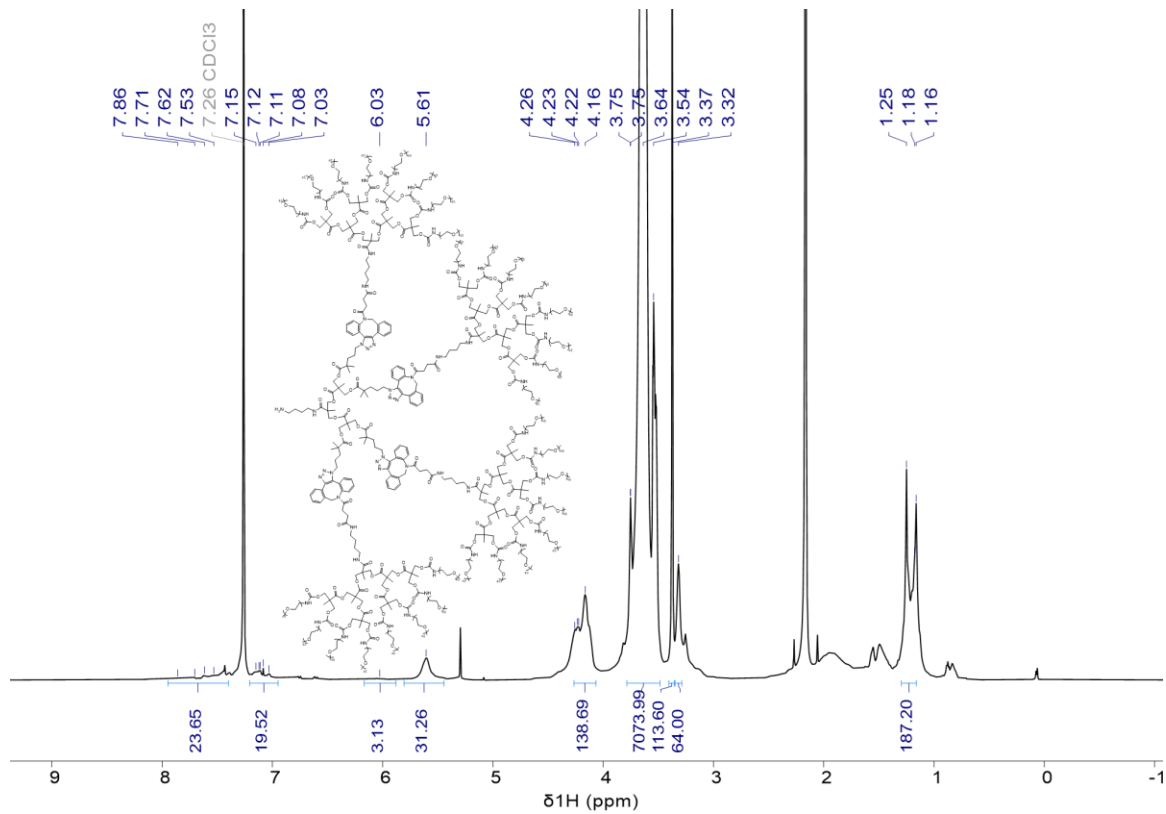


Figure S3.17. ^1H NMR of $\text{NH}_2\text{-G5-(PEG}_{2000}\text{)}_{32}$

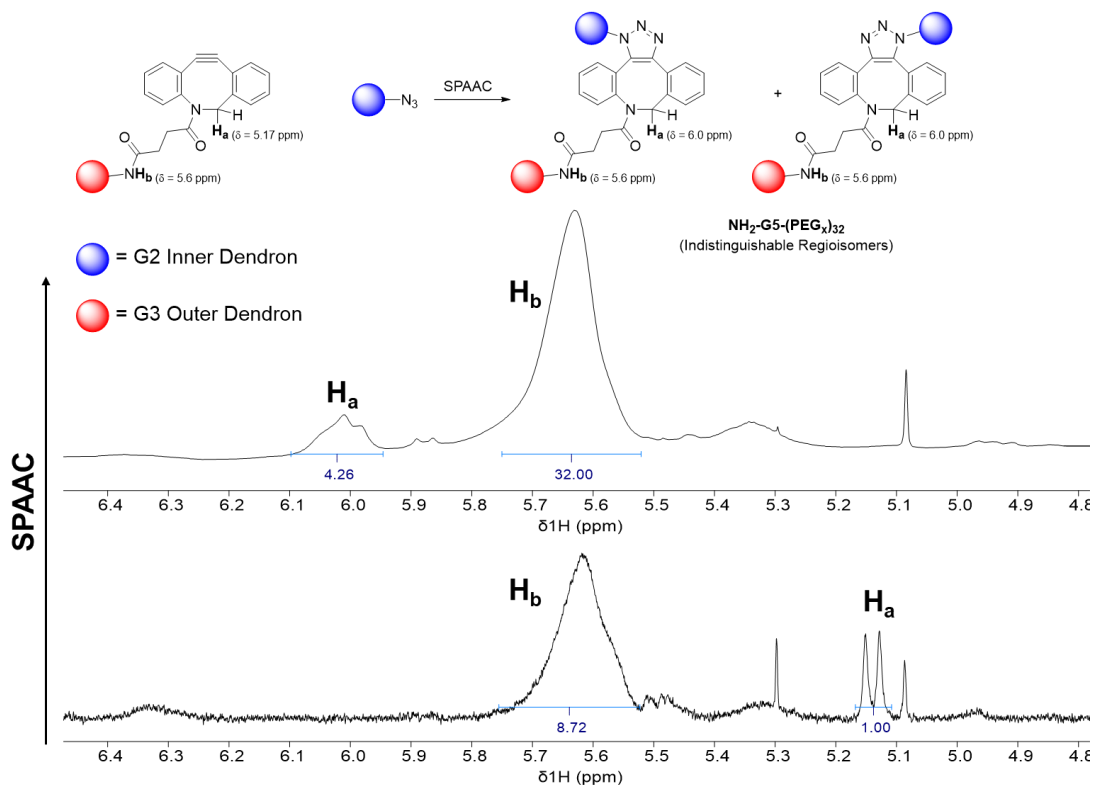


Figure S3.18. Monitoring ^1H NMR spectra of DBCO-G3-(PEG_x)₈ (bottom spectrum) undergoing SPAAC to form NH₂-G5-(PEG)₃₂ (top spectrum) with critical integral values illustrating complete PEGylation.

Determination of Degree of Protein Conjugation by ^1H qNMR

Quantitative ^1H NMR spectra were recorded on either a Bruker NEO 600 or NEO 700 Spectrometer. A known mass of conjugate was dissolved in 500 μL of D₂O containing 5 mg/mL sodium formate (HCOONa, i.e., 2.5 mg) as the internal standard. The experiment was run with an RF pulse of 90° and a relaxation time of 30 seconds between pulses at 64 scans. The dendrimer signal at 4.2 ppm was integrated with the assumption of 1 molar equivalent of dendron, which allowed for the determination of the relative molar ratio of HCOONa to dendron, which was then compared to the initial weighed mass of the dendron to determine the mass fraction.

Calculating Degree of Conjugation of α -CT-N₃ using DBCO-G3-(PEG₂₀₀₀)₈

Calculations are done according to previous procedures.²¹ Assume 1 eq. dendron, integrating the HCOONa singlet at 8.44 ppm against dendron ester α -methylene at 4.22 ppm.

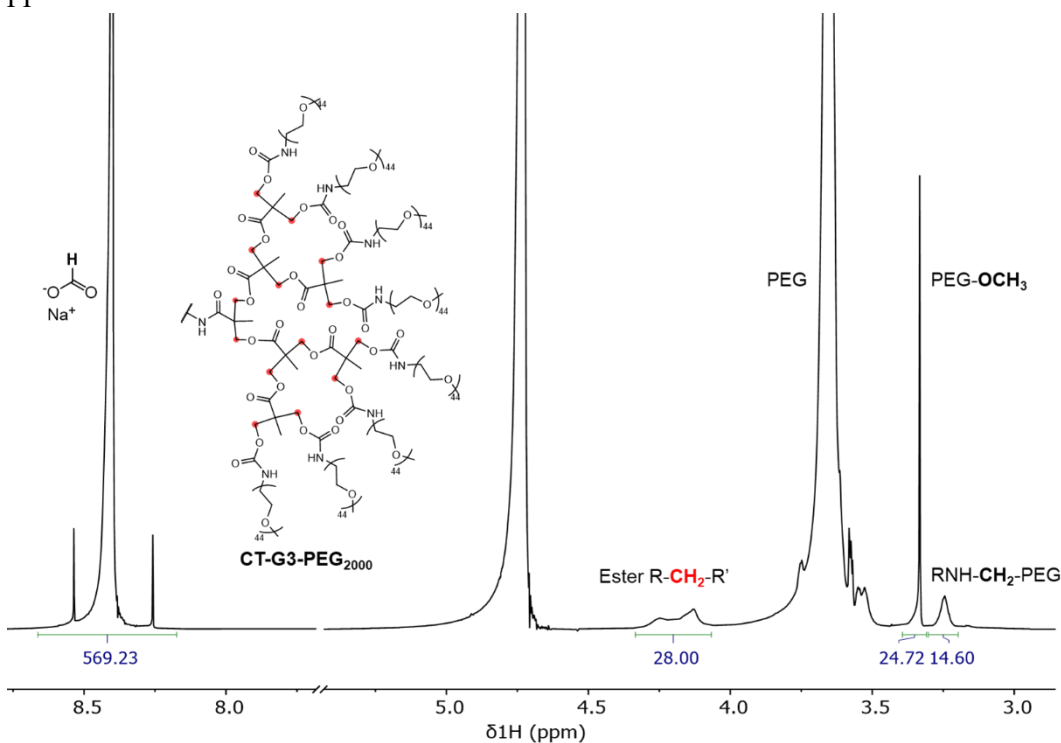


Figure S3.19. ¹H qNMR of CT-G3-PEG₂₀₀₀. The ester multiplet at 4.22 ppm is highlighted red in the inset structure. Correspondingly, the same multiplet integrates to 56 in CT-G4 and 112 in CT-G5.

$$\text{Molar ratio of HCOONa to dendrimer} = \frac{\text{Int}_{\delta\text{H}(8.44 \text{ ppm})} = 569}{\text{Int}_{\delta\text{H}(4.2 \text{ ppm})} = 1}$$

$$N_{\text{HCOONa}} = \frac{m_{\text{HCOONa}}}{MW_{\text{HCOONa}}}$$

$$= \frac{0.0025 \text{ g}}{68.01 \text{ g mol}^{-1}} = 3.676 \times 10^{-5} \text{ mol}$$

$$N_{\text{Dendrimer}} = \frac{3.676 \times 10^{-5} \text{ mol}}{569} = 6.460 \times 10^{-8} \text{ mol}$$

$$m_{\text{Dendrimer}} = 6.460 \times 10^{-8} \text{ mol} \times 17500 \text{ g mol}^{-1} = 1.13 \text{ mg}$$

1.13 mg of dendrimer was conjugated to the enzyme. Given that 1.30 mg of conjugate was initially added:

$$\text{Experimental dendrimer mass \%} = \frac{1.13 \text{ mg}}{1.30 \text{ mg}} \times 100 = \mathbf{87.0\%}$$

Theoretical dendrimer mass % of dendrimer (assuming full conjugation of 14 eq. of dendrimer per CT) is calculated as follows:

$$MW_{\text{conjugate}} = 273,000 \text{ g/mol}$$

$$14 \times MW_{\text{Dendron}} = 245,000 \text{ g/mol}$$

$$\text{Calculated dendrimer mass \%} = \frac{245000 \text{ g/mol}}{273000 \text{ g/mol}} \times 100\% = \mathbf{89.7\%}$$

Mass % of a single conjugated dendron is calculated as follows:

$$\begin{aligned} \text{Mass \% (dendron)} &= \frac{MW_{\text{Dendron}}}{MW_{\text{Conjugate}} - MW_{\text{CT}}} \\ &= \frac{17500 \text{ g mol}^{-1}}{273000 \text{ g mol}^{-1} - 28000 \text{ g mol}^{-1}} \times 100\% = \mathbf{7.14\%} \end{aligned}$$

Therefore, since the difference between the experimental and theoretical dendrimer mass % ($\Delta = 2.7\%$) is within the calculated mass % of a single dendron, the average conjugate is assumed to have 14 dendrons functionalized to it.

Table S3.1. Mass fraction of dendron-protein conjugates.

Conjugate	Calculated Conjugate MW (g/mol)	Calcd. Dendrimer Mass Fraction (%)^a	Expt. Dendrimer Mass Fraction (%)^b	Calcd. Mass Fraction (%) of 1 dendron
CT-G3-PEG₃₅₀	84000	66.7	65.0	4.76
CT-G3-PEG₁₀₀₀	154000	81.8	75.1	5.84
CT-G3-PEG₂₀₀₀	273000	89.7	91.4	6.41

CT-G4- PEG₃₅₀	154000	81.8	76.0	5.84
CT-G4- PEG₁₀₀₀	294000	90.5	86.2	6.46
CT-G4- PEG₂₀₀₀	525252	94.7	89.3	6.76
CT-G5- PEG₃₅₀	306670	90.9	90.4	6.49
CT-G5- PEG₁₀₀₀	568960	95.1	93.0	6.79
CT-G5- PEG₂₀₀₀	1022882	97.3	98.6	6.95

^aInterpreted as the ratio of MW of 14 dendrons and MW of the conjugate. ^bObtained from ¹H NMR. Relative integration of dendritic ester CH₂ (4.22 ppm) vs. the sodium formate (HCOONa, 8.44 ppm) internal standard.

Quantitative NMR for Determining Dendrimer Conjugation to CT

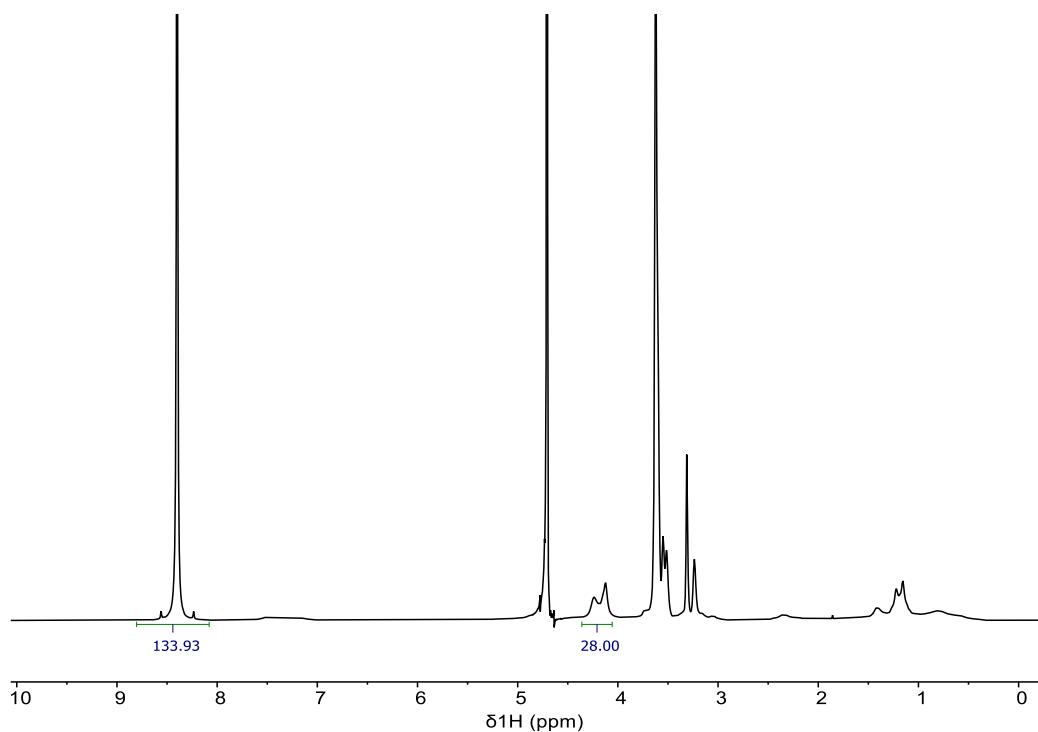


Figure S3.20. ¹H NMR spectrum for quantitation of dendron mass fraction of CT-G3-PEG₃₅₀.

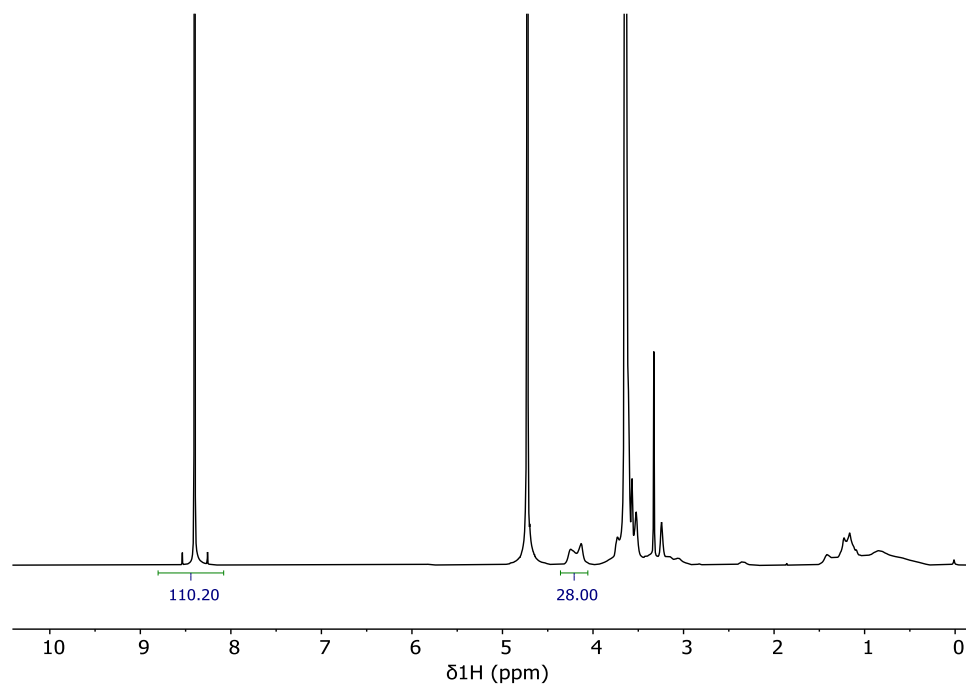


Figure S3.21. ¹H NMR spectrum for quantitation of dendron mass fraction of CT-G3-PEG₁₀₀₀.

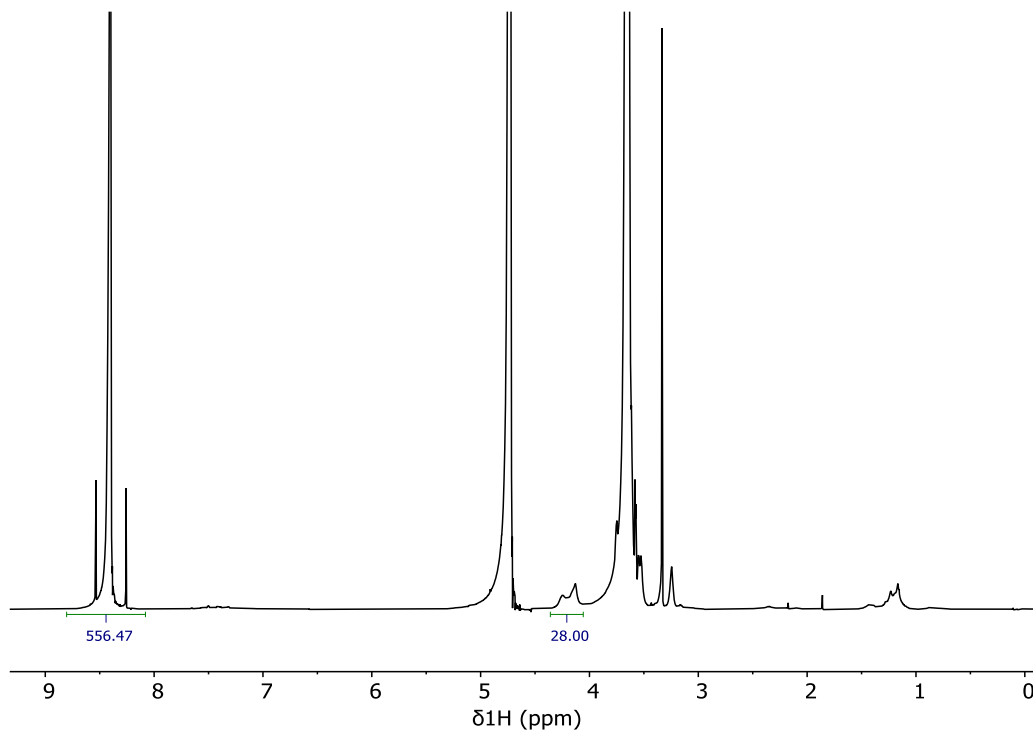


Figure S3.22. ¹H NMR spectrum for quantitation of dendron mass fraction of CT-G3-PEG₂₀₀₀.

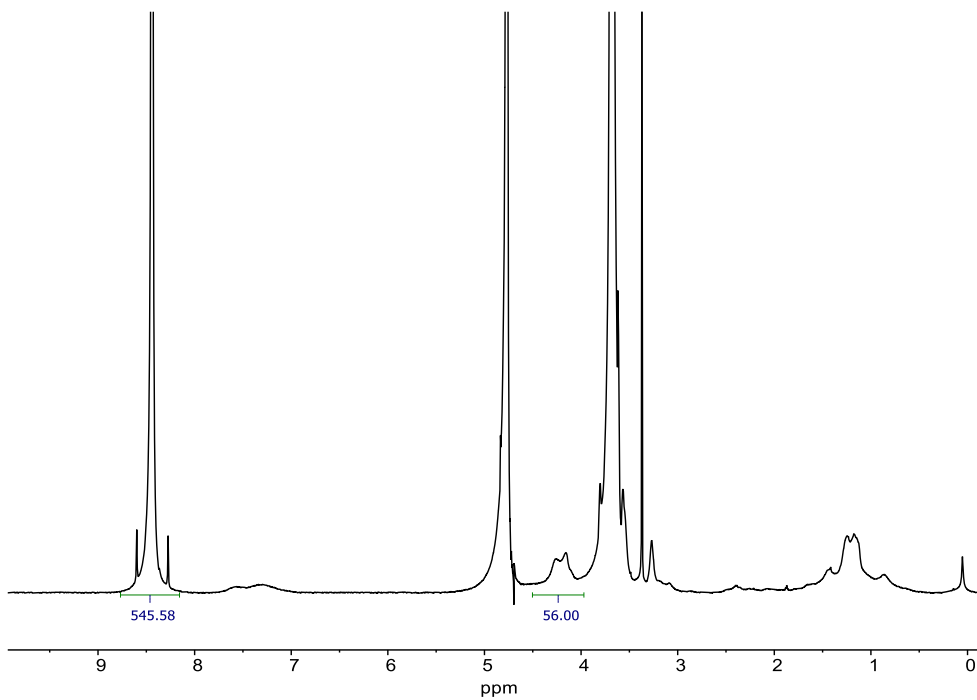


Figure S3.23. ^1H NMR spectrum for quantitation of dendron mass fraction of CT-G4-PEG₃₅₀.

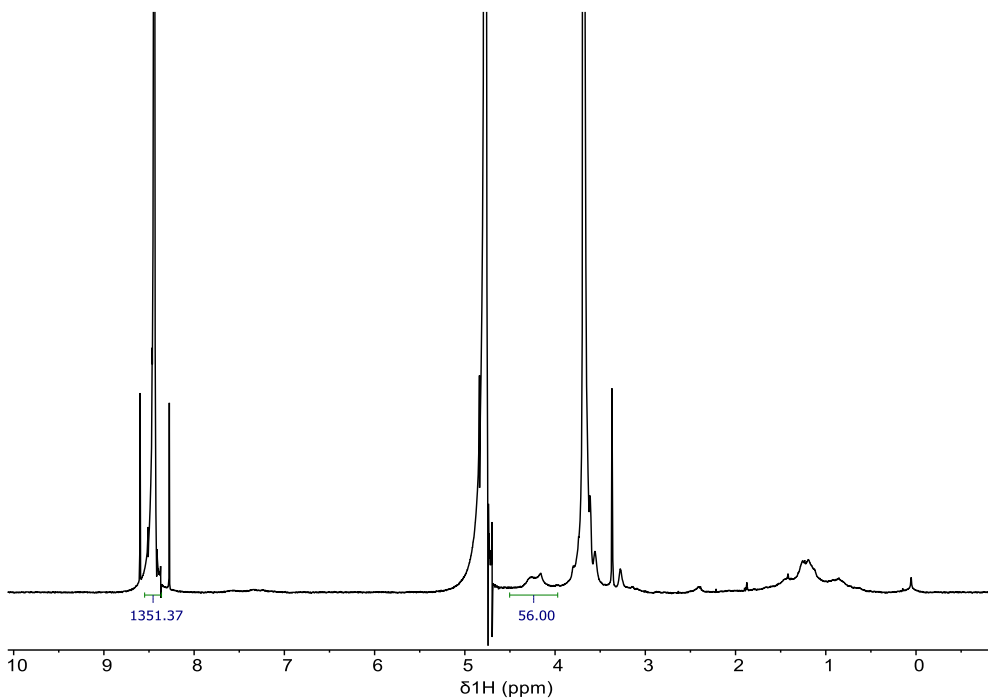


Figure S3.24. ^1H NMR spectrum for quantitation of dendron mass fraction of CT-G4-PEG₁₀₀₀.

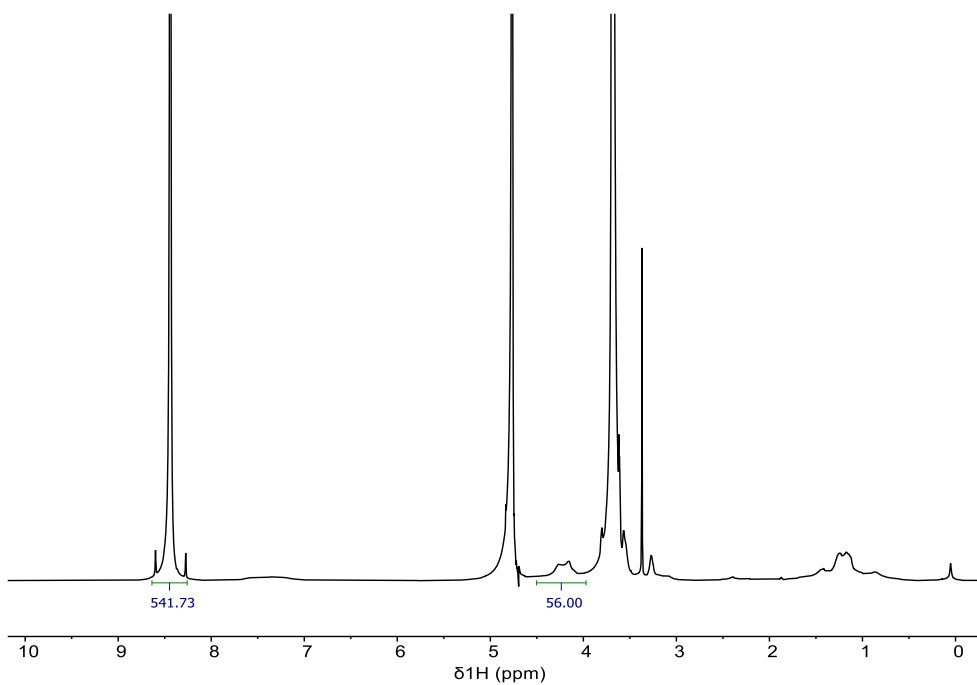


Figure S3.25. ¹H NMR spectrum for quantitation of dendron mass fraction of CT-G4-PEG₂₀₀₀.

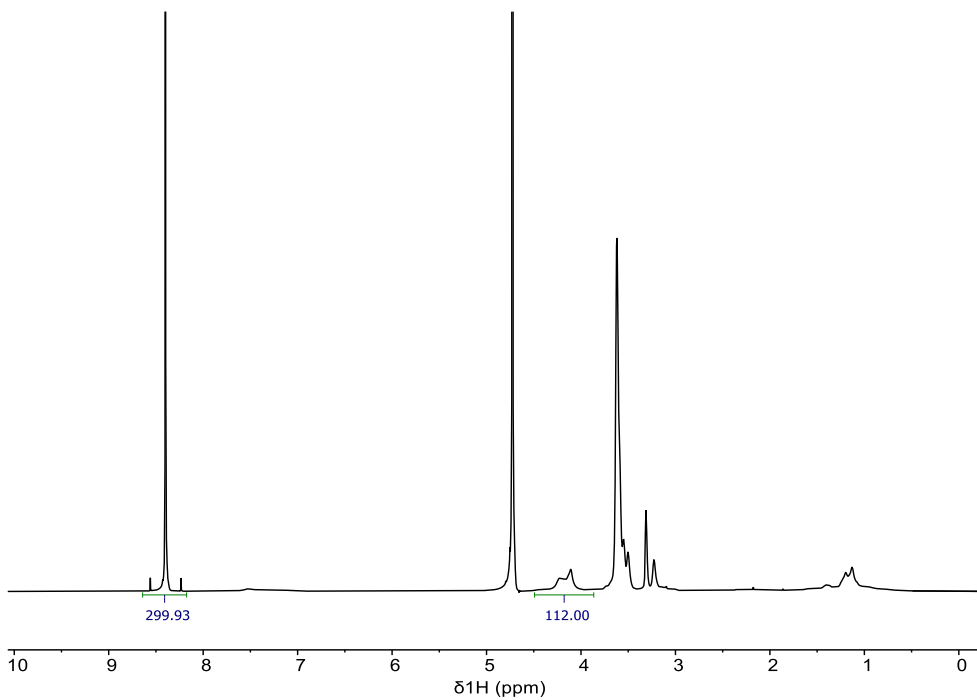


Figure S3.26. ¹H NMR spectrum for quantitation of dendron mass fraction of CT-G5-PEG₃₅₀.

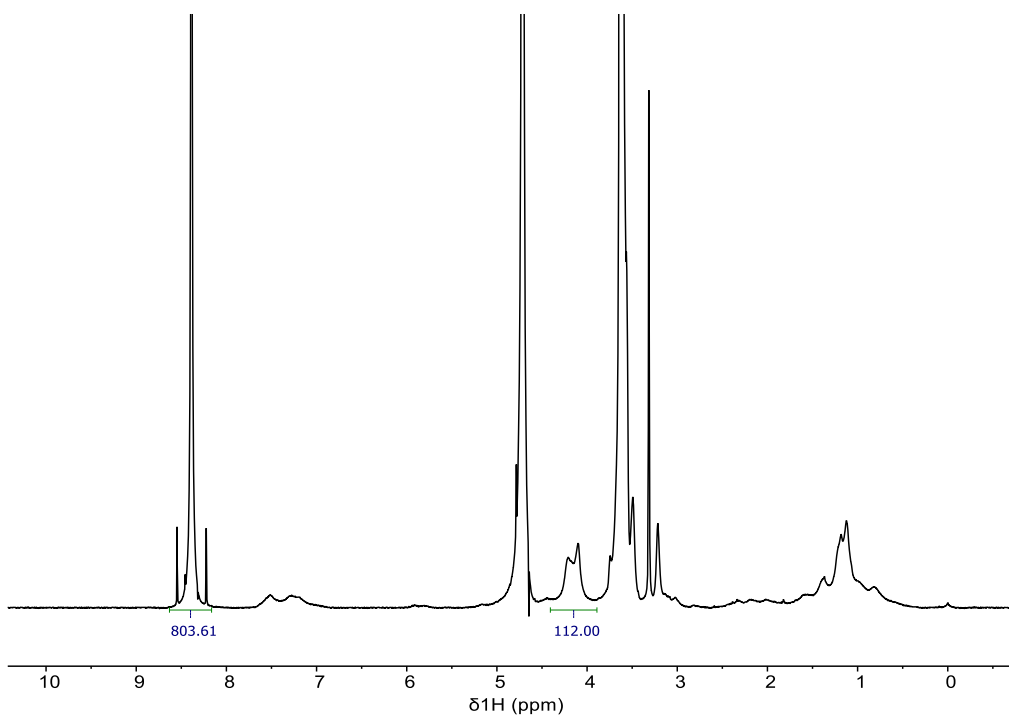


Figure S3.27. ¹H NMR spectrum for quantitation of dendron mass fraction of CT-G5-PEG₁₀₀₀.

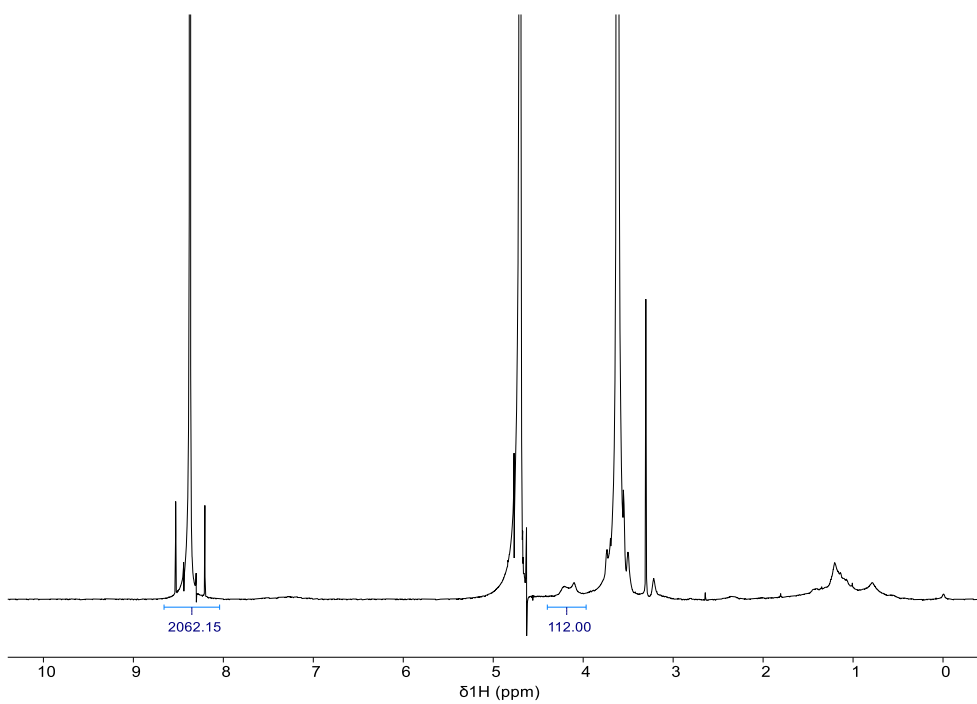


Figure S3.28. ¹H NMR spectrum for quantitation of dendron mass fraction of CT-G5-PEG₂₀₀₀.

MALDI-TOF Spectra of Functionalized CT

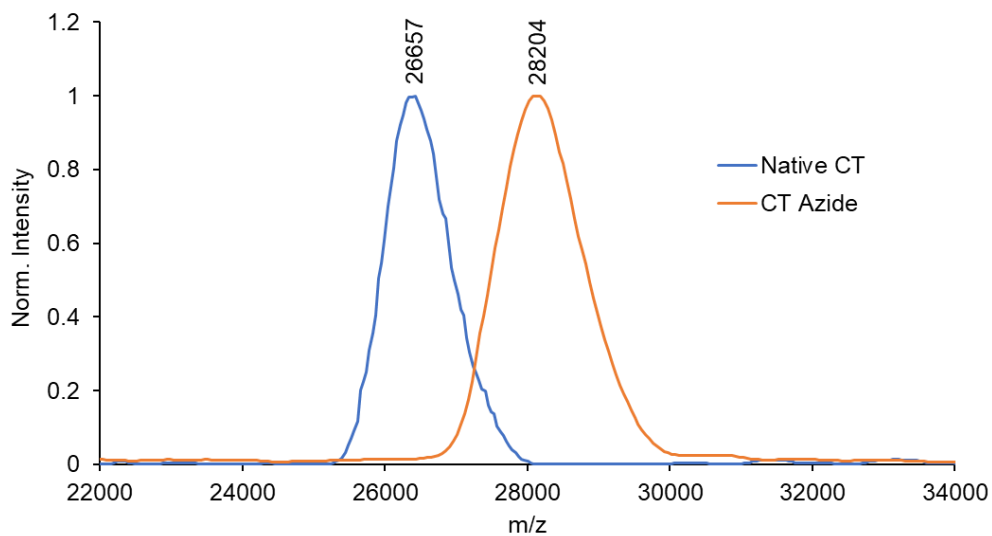


Figure S3.29. MALDI-TOF Spectra of Native CT and CT functionalized with 14 azides. Expected mass increase = 1.4 kDa.

DRIFTS-IR Spectra of Dendrimer-CT Conjugates

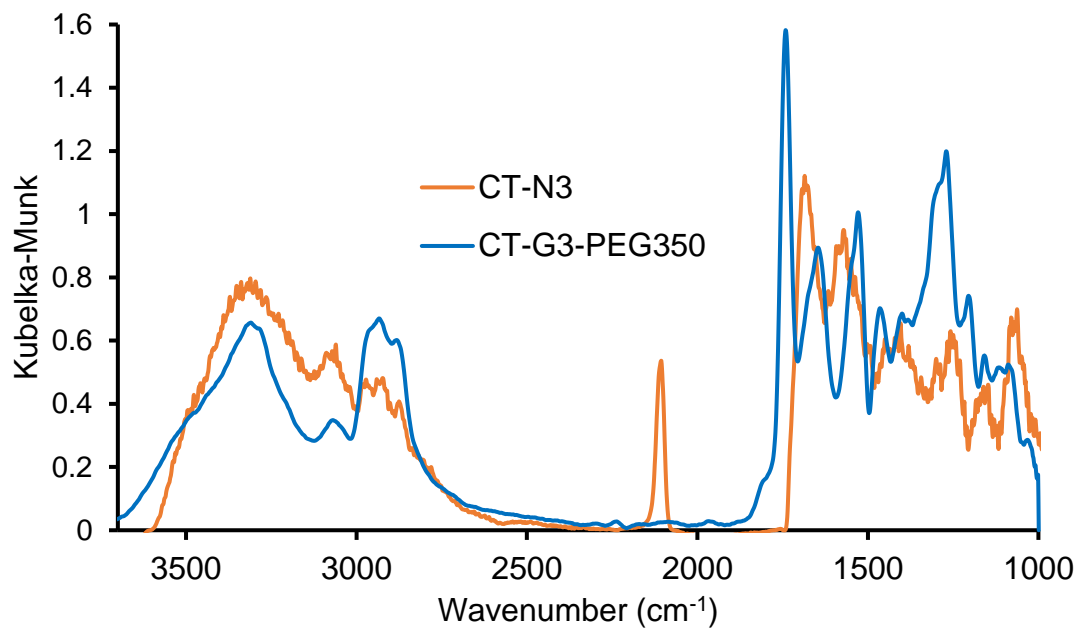


Figure S3.30. DRIFTS FTIR Spectrum of CT-G3-PEG₃₅₀.

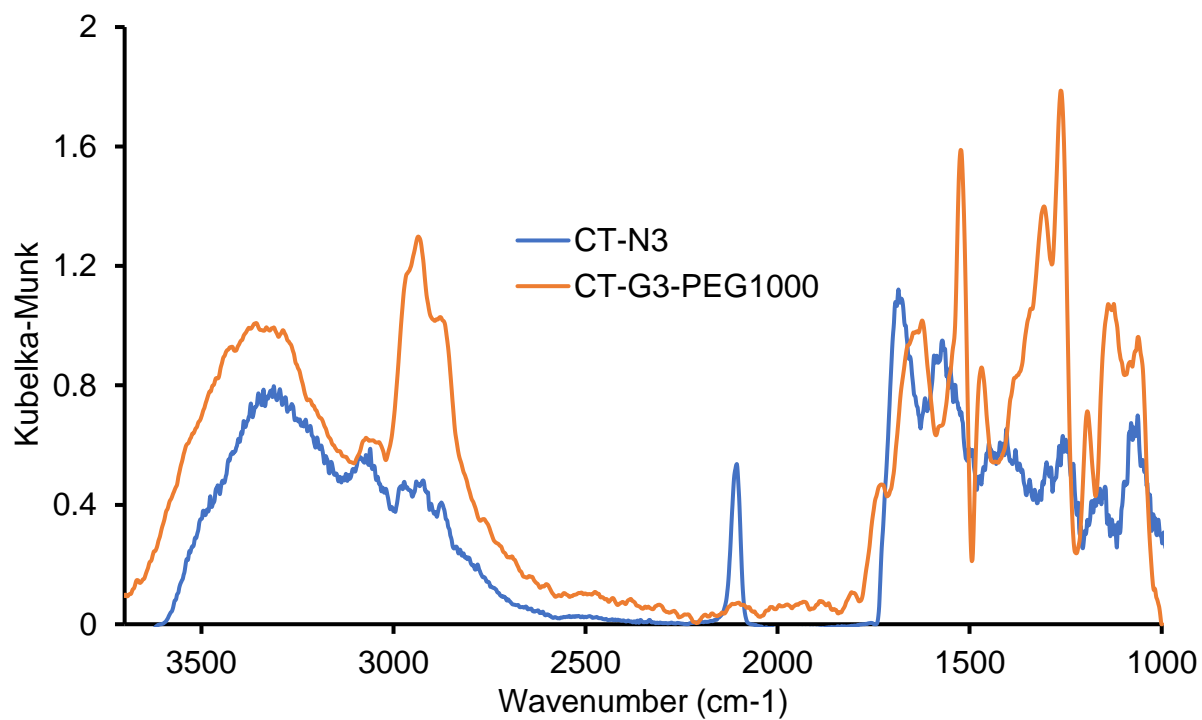


Figure S3.31. DRIFTS FTIR Spectrum of CT-G3-PEG₁₀₀₀.

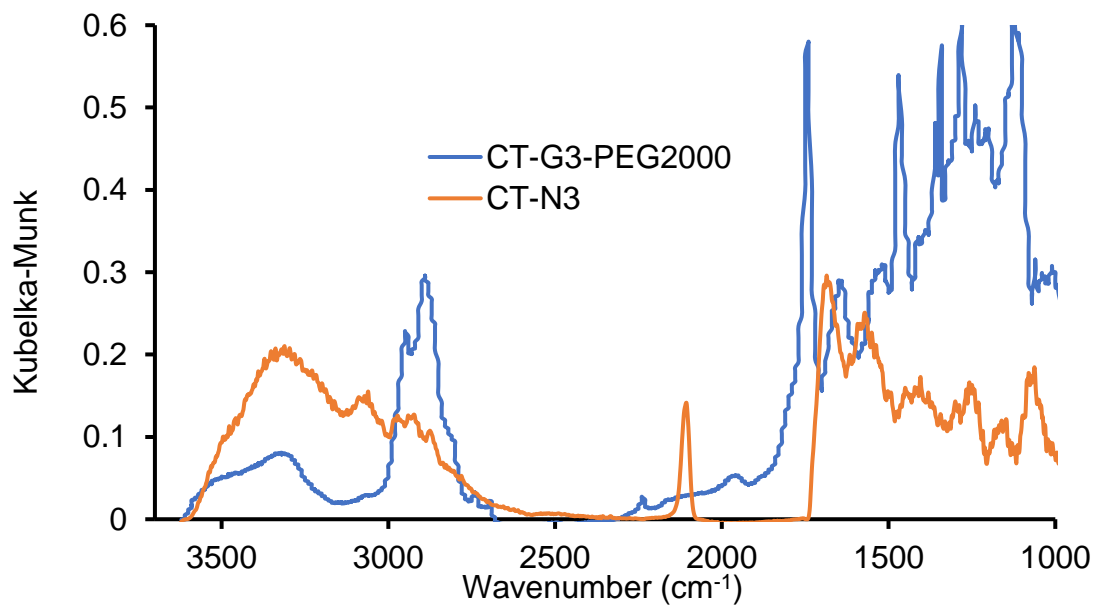


Figure S3.32. DRIFTS FTIR Spectrum of CT-G3-PEG₂₀₀₀.

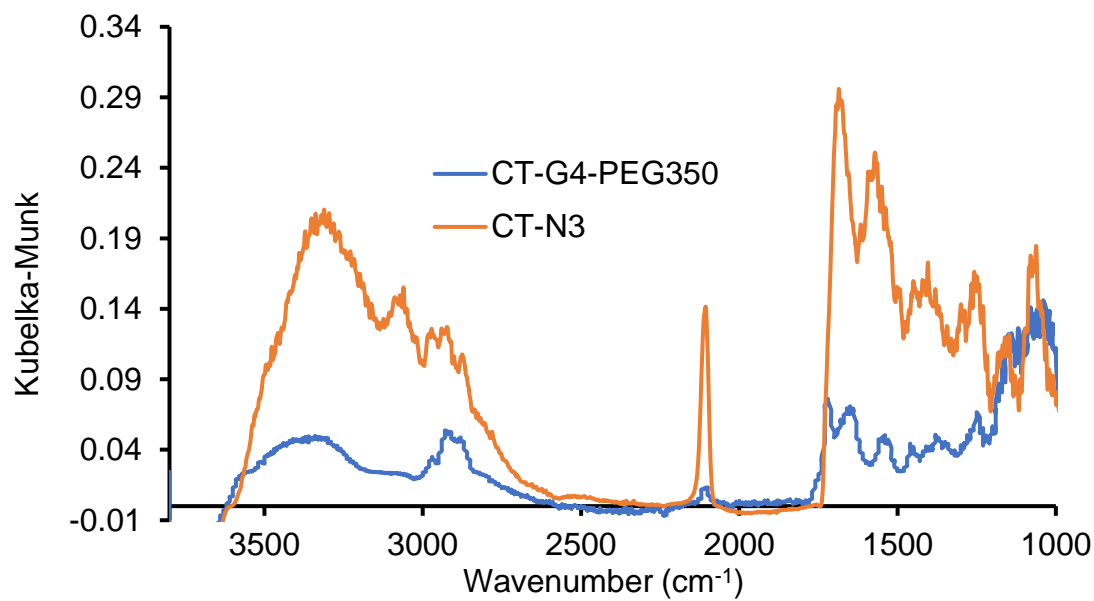


Figure S3.33. DRIFTS FTIR Spectrum of CT-G4-PEG₃₅₀.

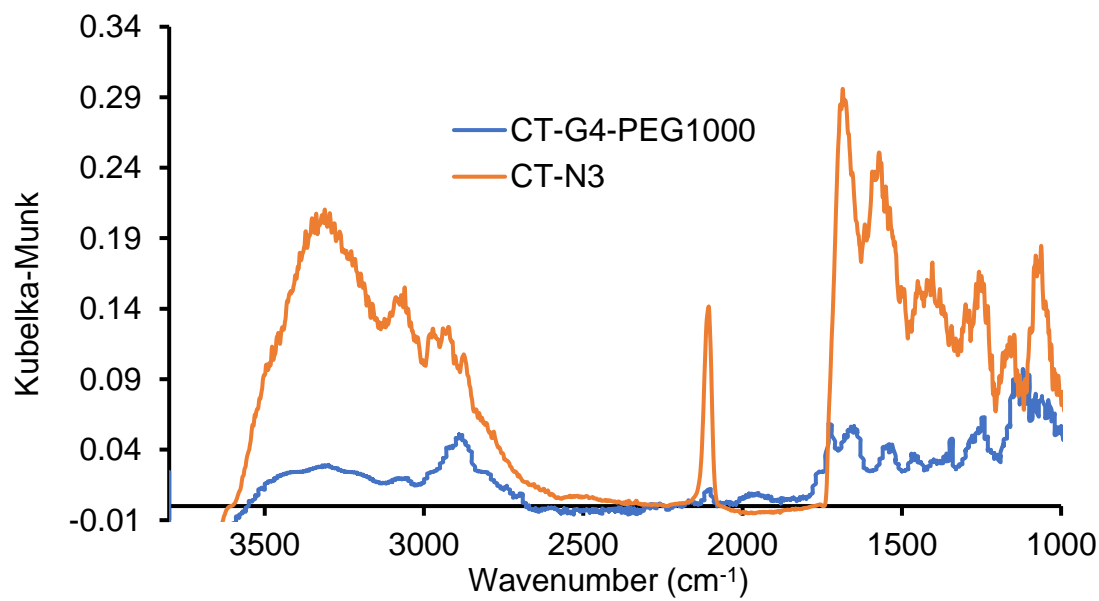


Figure S3.34. DRIFTS FTIR Spectrum of CT-G4-PEG₁₀₀₀.

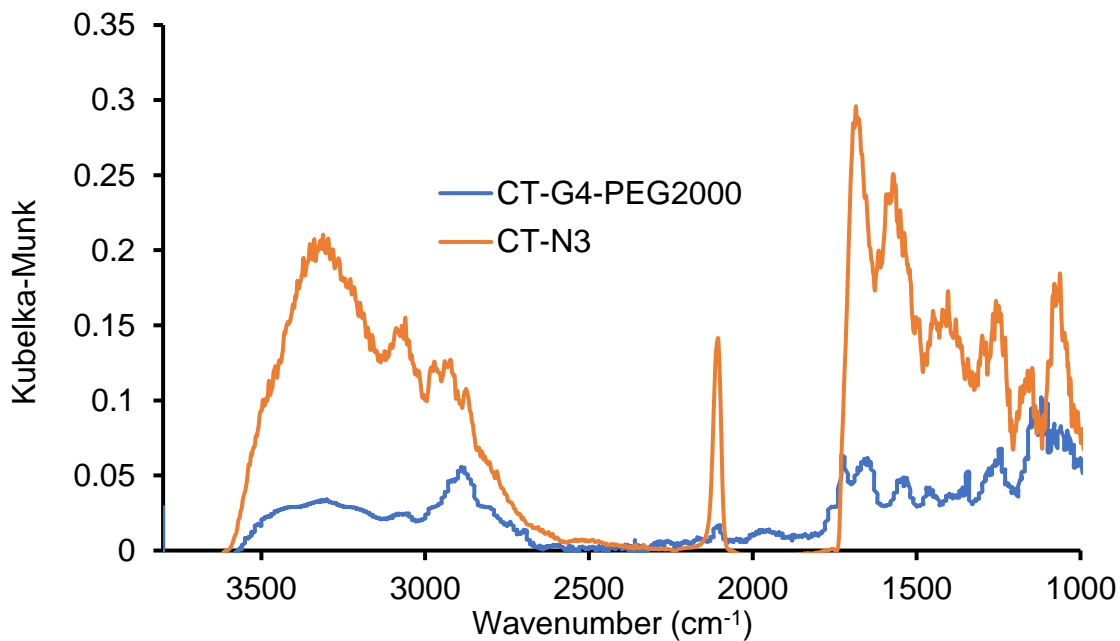


Figure S3.35. DRIFTS FTIR Spectrum of CT-G4-PEG₂₀₀₀.

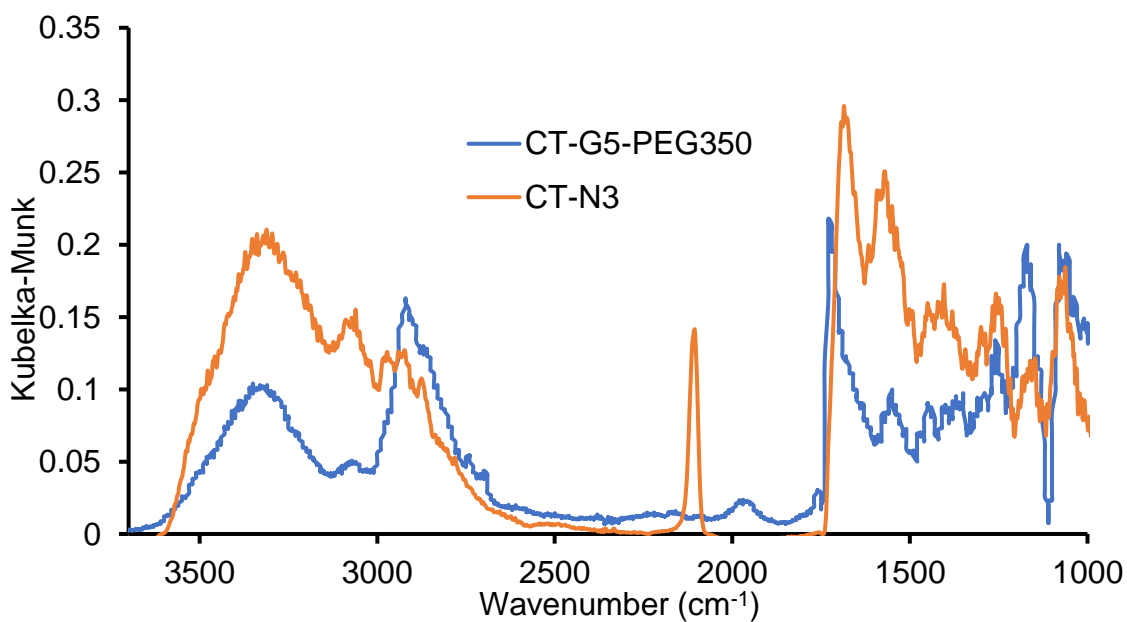


Figure S3.36. DRIFTS FTIR Spectrum of CT-G5-PEG₃₅₀.

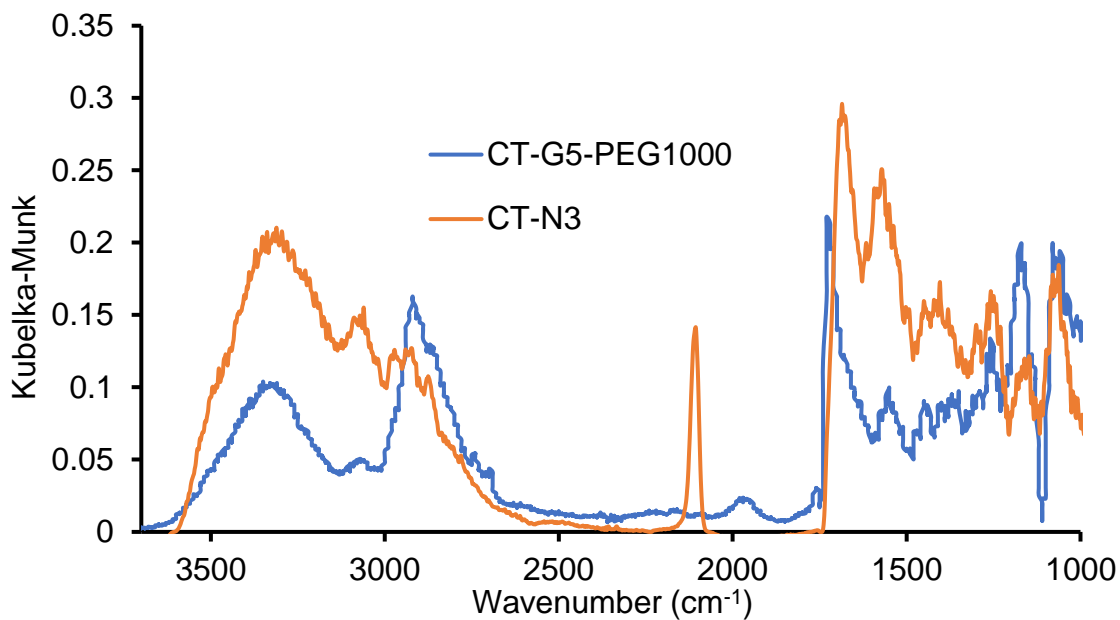


Figure S3.37. DRIFTS FTIR Spectrum of CT-G5-PEG₁₀₀₀.

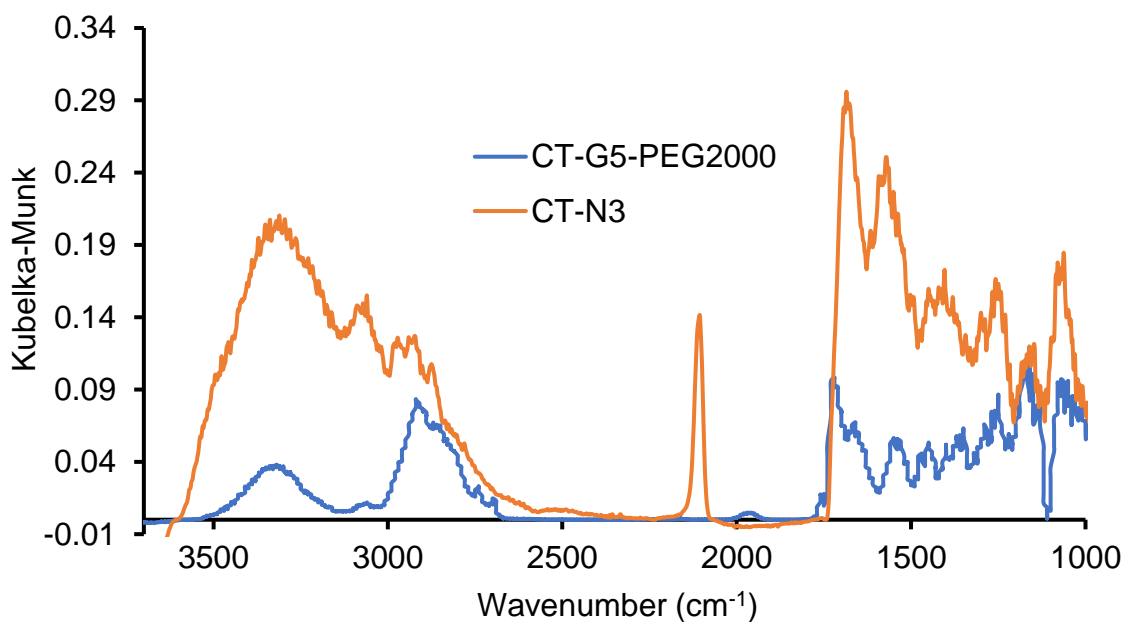


Figure S3.38. DRIFTS FTIR Spectrum of CT-G5-PEG₂₀₀₀.

BTpNA Assay

The assays were performed in triplicate according to modified previous procedures.²¹ UV-absorbance readings were taken on a Biotek Cytation5™ plate reader ($\lambda_{\text{abs}} = 412 \text{ nm}$). A

stock solution of native α -chymotrypsin (CT), azide-CT, or CT-dendrimer conjugate was prepared in 0.1 M tris buffer (pH 8) with an absorbance of approximately 0.5 AU, which allowed for the calculation of the precise concentration of enzyme in solution (see Table S2). 200 μ L of this solution was added to a 96-well plate and incubated at 37 $^{\circ}$ C for 3 minutes. Separately, a stock solution of BTpNA was prepared at 1 mg/mL in DMF. 50 μ L of this solution was added to the well at the 3-minute incubation mark, and the absorbance at 412 nm was measured every 4 s or 5 s for 1 min (depending on the number of wells measured simultaneously). The activity of the enzyme was interpreted from the initial slope of the absorbance line from $t=0$ to $t=30$ s, wherein the linear absorption was observed. Base absorbance at 412 nm measured at $t=0$ was subtracted from the absorbance over time plots to normalize the absorbance to 0 at 412 nm at $t=0$. Following the above procedures, three separate control experiments were run ($n=3$) using the same native CT (0.5 AU, 200 μ L) spiked with 14 mol equivalents of DBCO-G3-PEG₂₀₀₀, DBCO-G3-PEG₂₀₀₀, and DBCO-G3-PEG₂₀₀₀, respectively, to monitor the enzyme activity towards BTpNA in the presence of polymers.

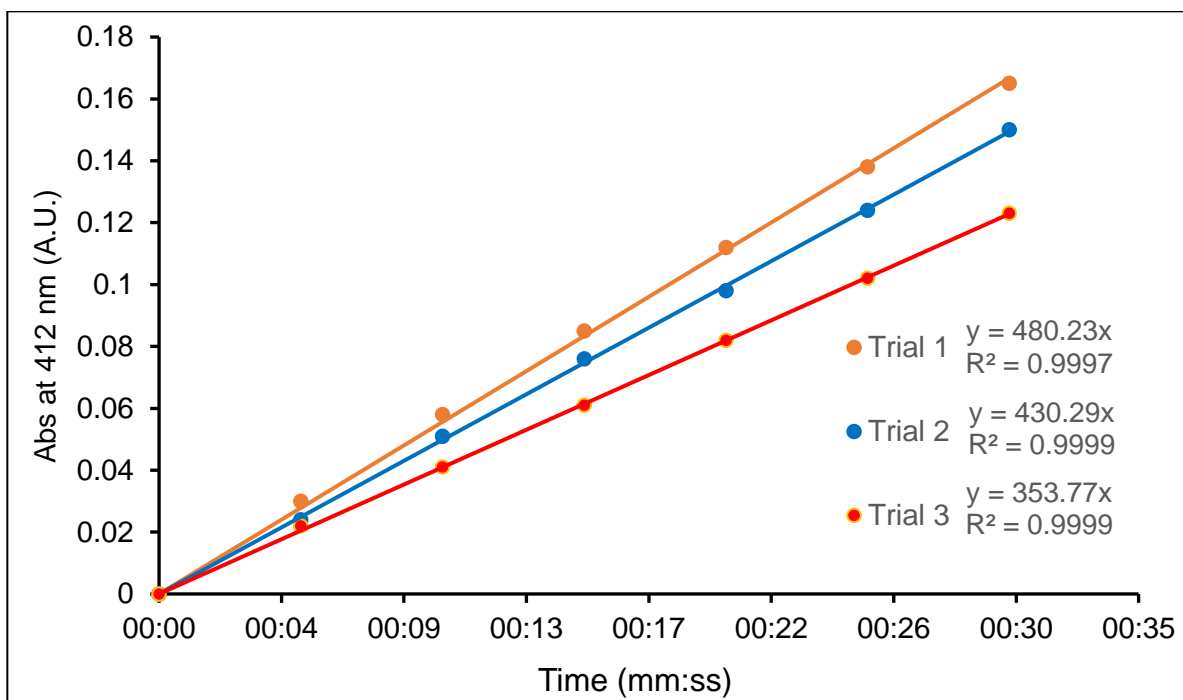


Figure S3.39. Absorbance over time of BTpNA cleavage by Native CT.

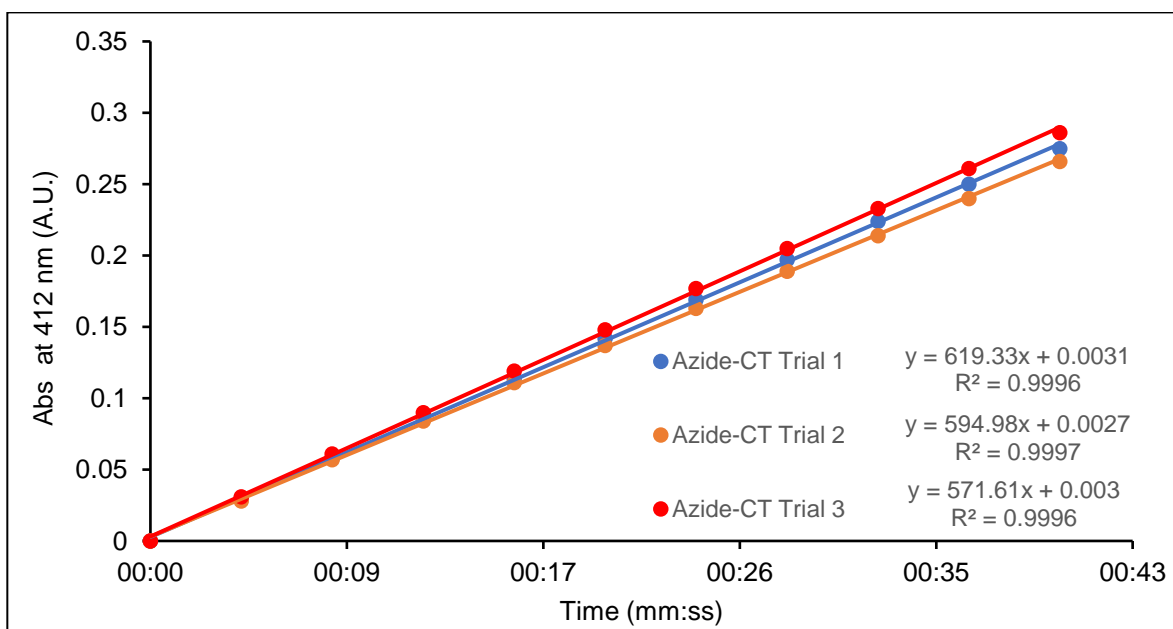


Figure S3.40. Absorbance over time of BTpNA cleavage by Azide-CT.

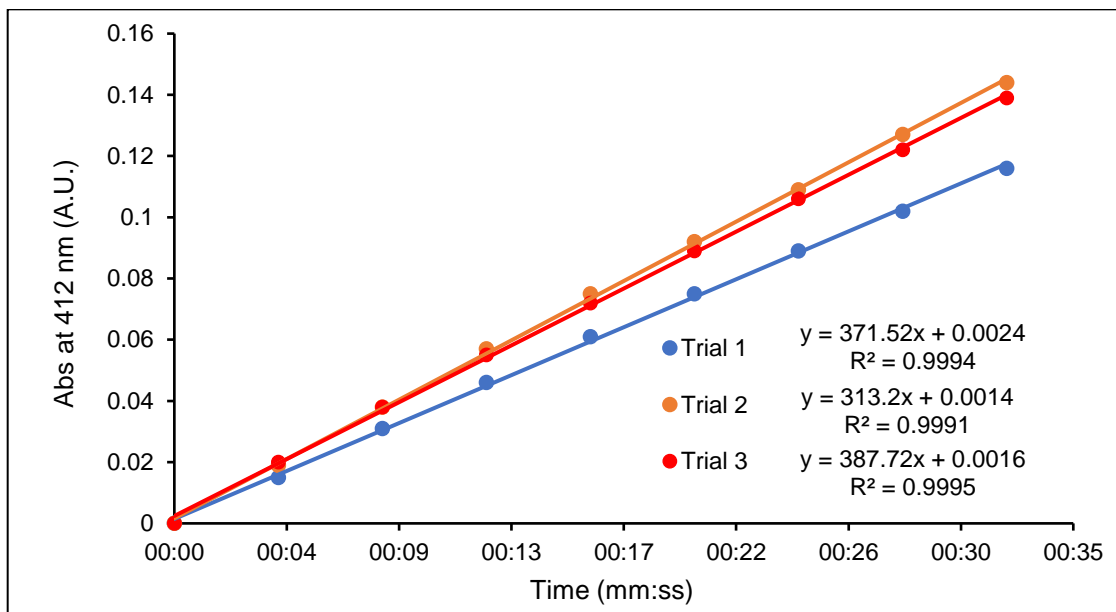


Figure S3.41. Absorbance over time of BTpNA cleavage by CT-G3-PEG₃₅₀.

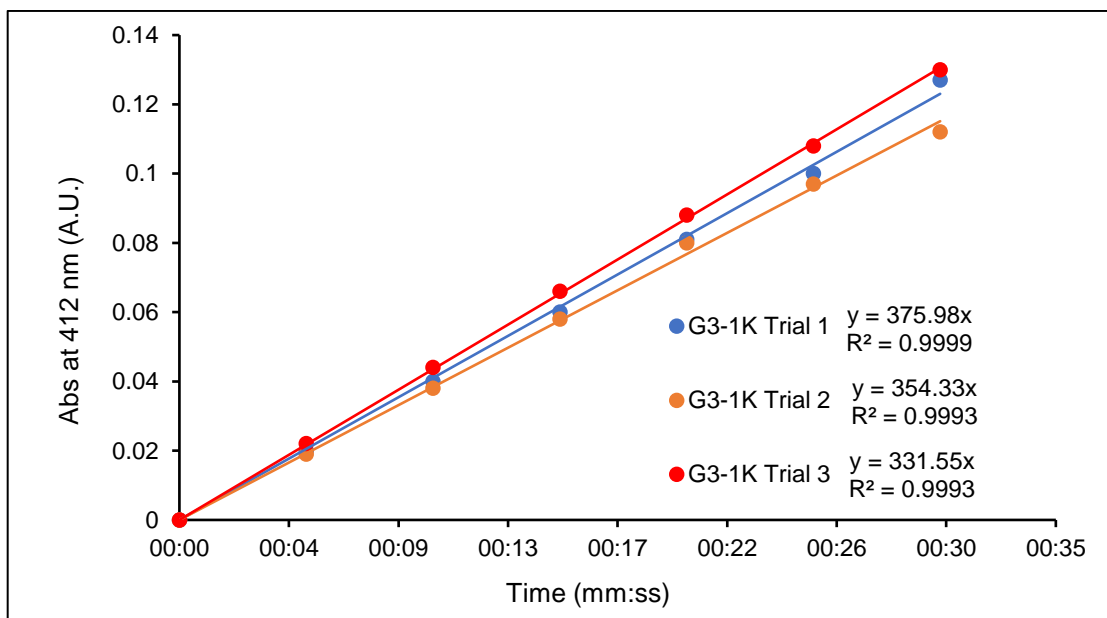


Figure S3.42. Absorbance over time of BTpNA cleavage by CT-G3-PEG₁₀₀₀.

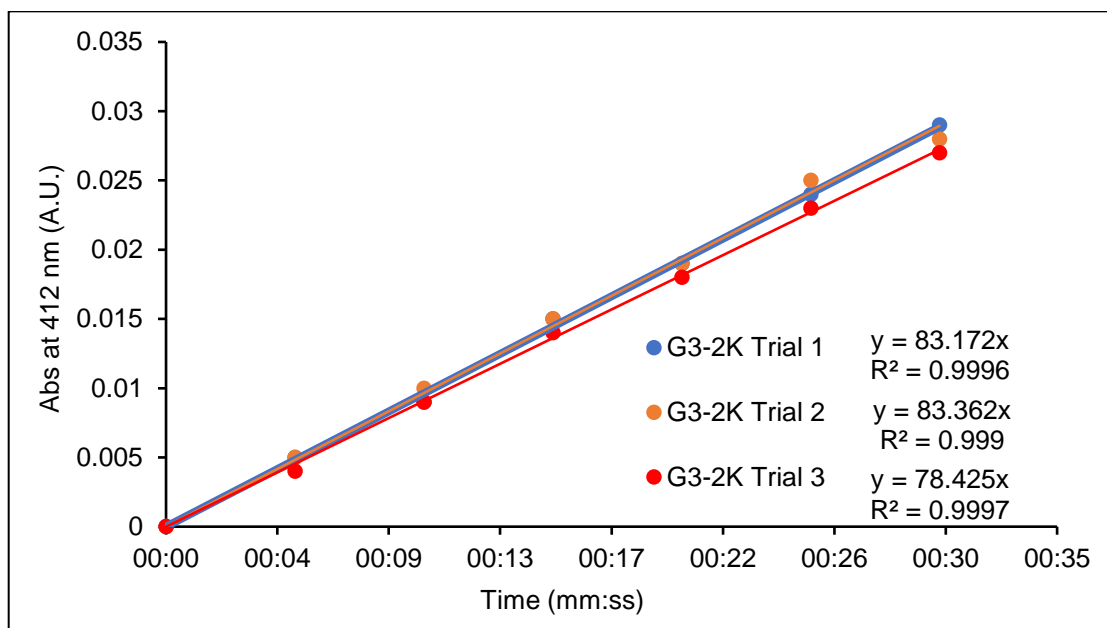


Figure S3.43. Absorbance over time of BTPNA cleavage by CT-G3-PEG₂₀₀₀.

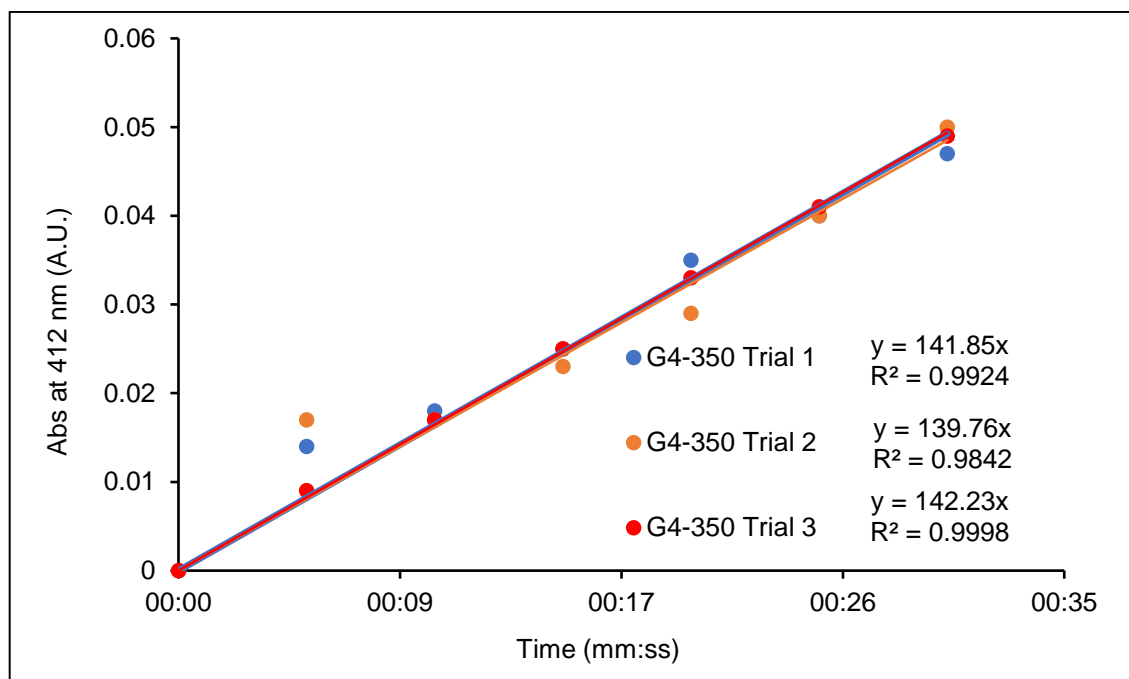


Figure S3.44. Absorbance over time of BTPNA cleavage by CT-G4-PEG₃₅₀.

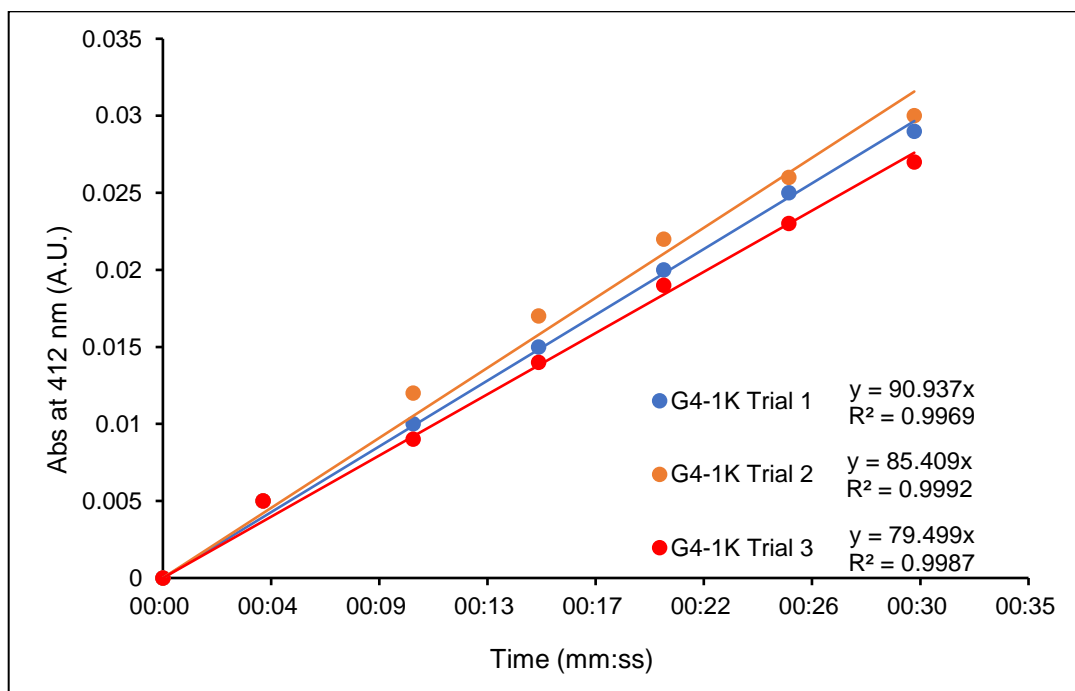


Figure S3.45. Absorbance over time of BTPNA cleavage by CT-G4-PEG₁₀₀₀.

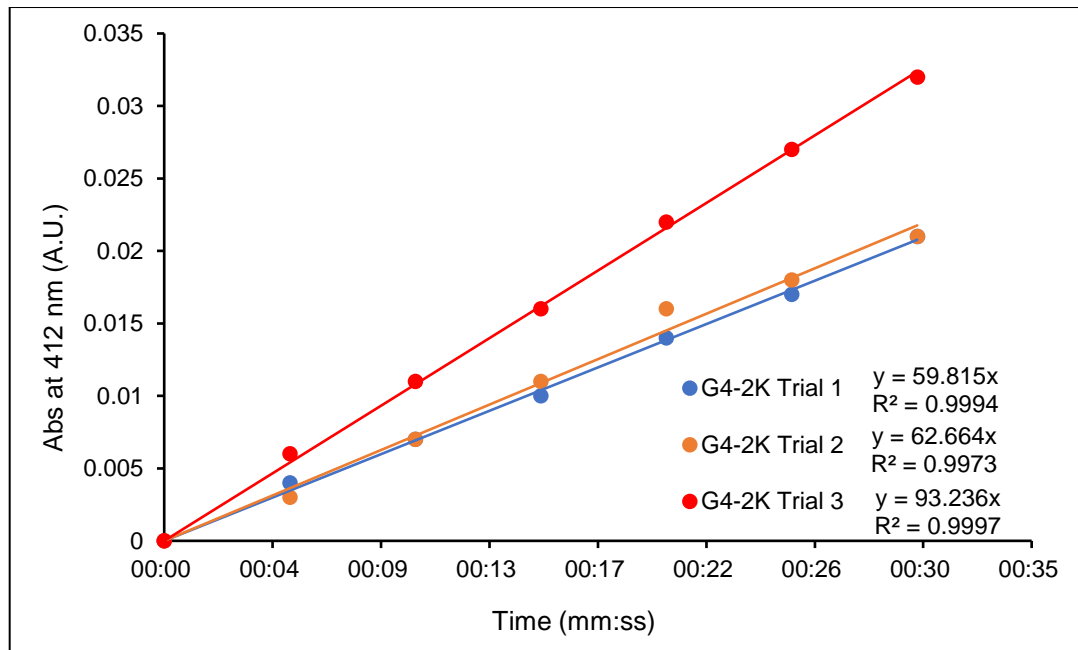


Figure S3.46. Absorbance over time of BTPNA cleavage by CT-G4-PEG₂₀₀₀.

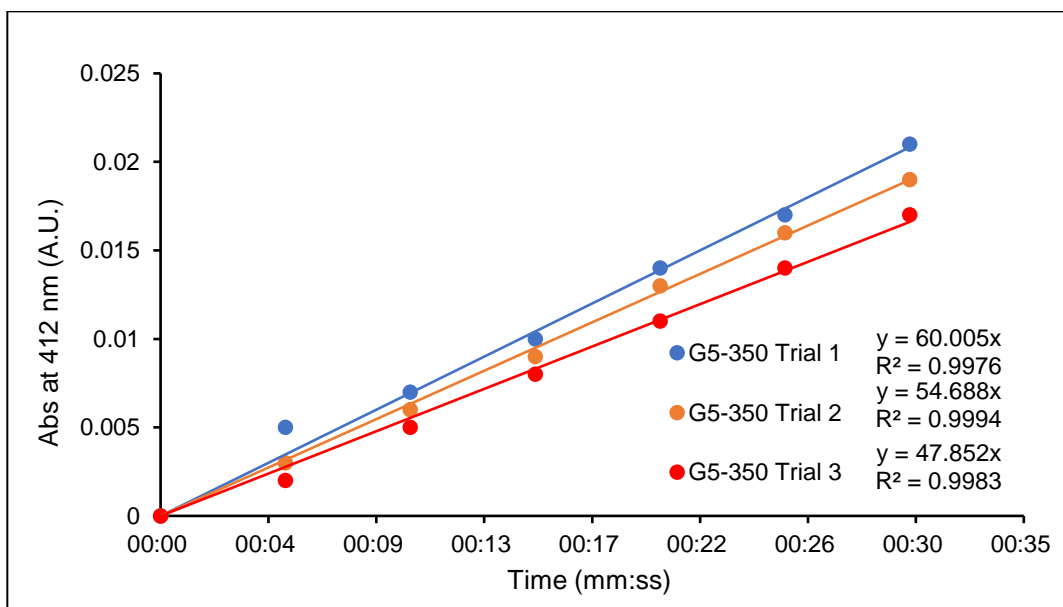


Figure S3.47. Absorbance over time of BTpNA cleavage by CT-G5-PEG₃₅₀.

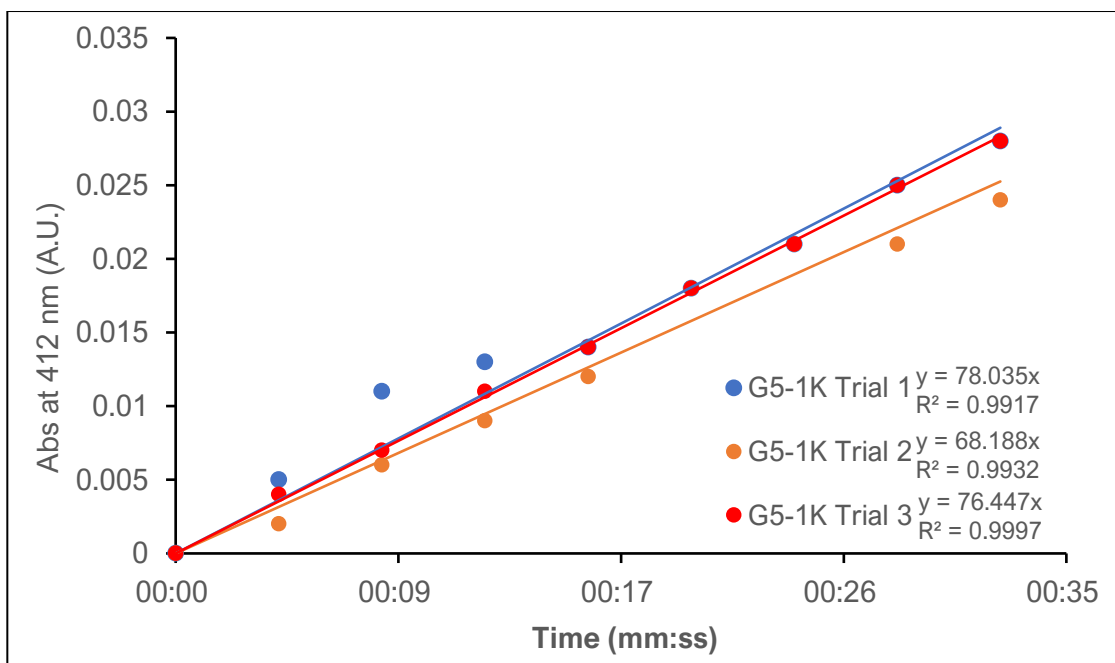


Figure S3.48. Absorbance over time of BTpNA cleavage by CT-G5-PEG₁₀₀₀.

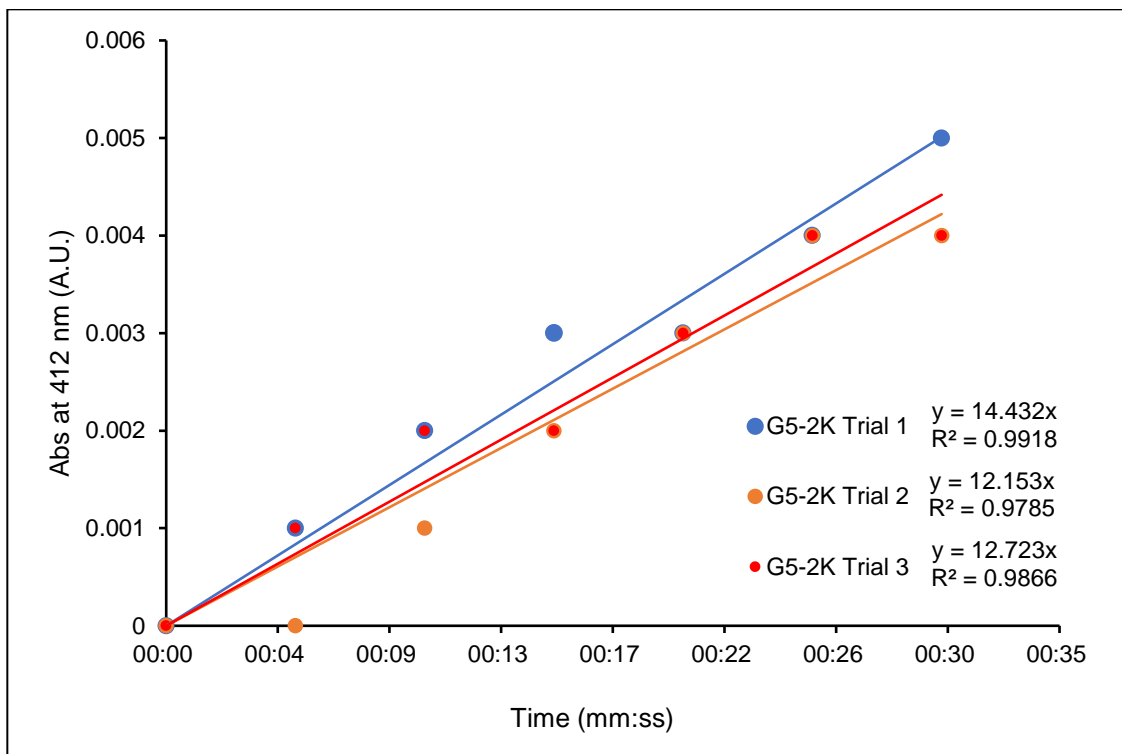


Figure S3.49. Absorbance over time of BTPNA cleavage by CT-G5-PEG₂₀₀₀.

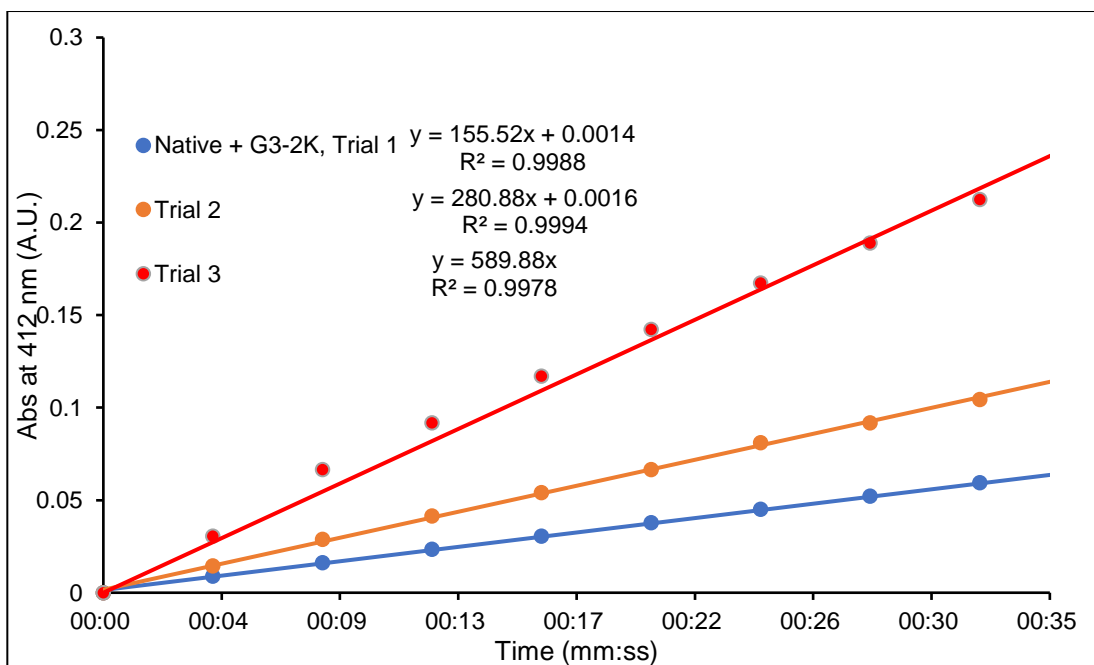


Figure S3.50. Absorbance over time of BTPNA cleavage by Native CT + DBCO-G3-(PEG₂₀₀₀)₈.

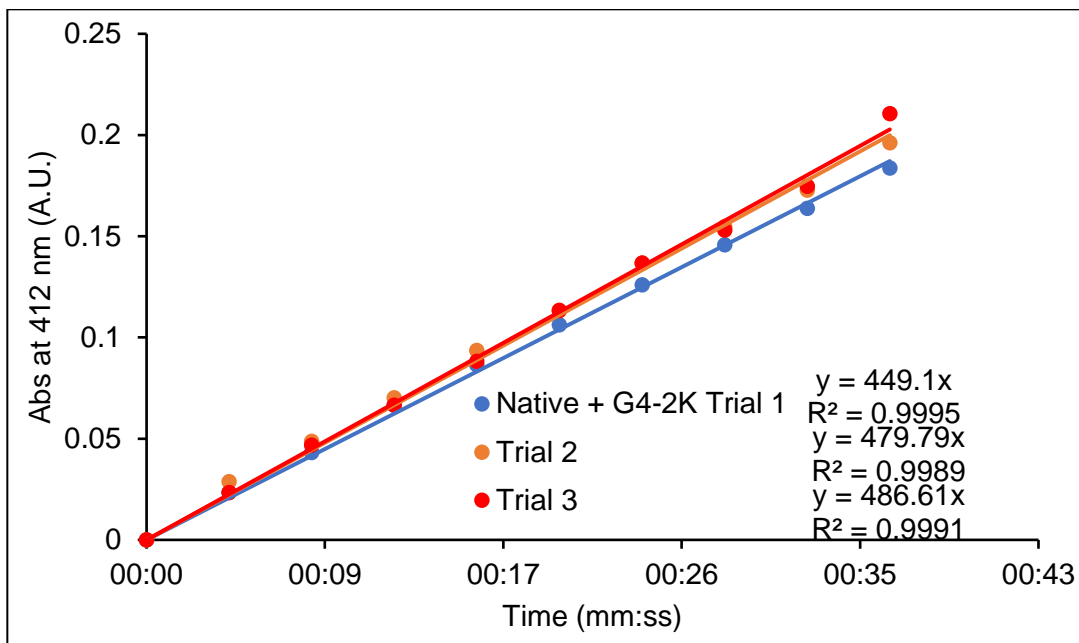


Figure S3.51. Absorbance over time of BTpNA cleavage by Native CT + DBCO-G4-(PEG₂₀₀₀)₁₆.

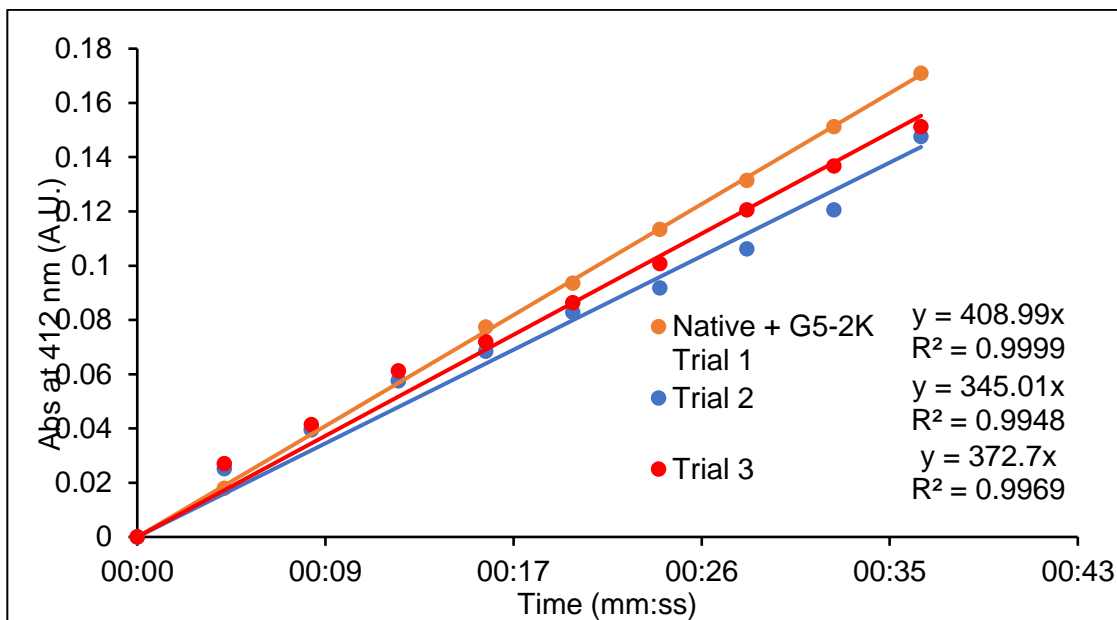


Figure S3.52. Absorbance over time of BTpNA cleavage by Native CT + DBCO-G5-(PEG₂₀₀₀)₃₂.

BSA and Casein Digestion Assays

The activity of CT and CT-dendron conjugates towards casein and BSA was determined according to previous procedures ($n=3$). 700 μL of a 10 mg/mL suspension of milk casein or BSA in 0.1 M Tris buffer (pH 8) was prepared and equilibrated at 37 °C for 1 min with vigorous stirring. Separately, a stock solution of either α -CT or α -CT-dendrimer conjugate was dissolved in the same buffer solution to an absorbance at 280 nm of approximately 0.5 AU to precisely determine the concentration of the conjugates (see Table S2). 100 μL of this stock was then added to the protein substrate suspensions and was left to stir at 37 °C for 20 min, at which point the reaction was quenched for 20 s by the addition of 200 μL of 50% trichloroacetic acid (TCA; w/v) in water ($V_{\text{total}} = 1000 \mu\text{L}$). The precipitated protein was then pelleted by centrifugation at 4 °C at 10000 g for 10 min. 600 μL of the supernatant was transferred to a low-volume 1 cm path length quartz cuvette and the absorbance was measured at 280 nm using the Cary WinUV Simple Reads application.

The following control experiments were performed. To account for residual precipitation of the protein substrates, **Control 1** ($n=3$), denoted as A_{blank} , was run with conditions as described above but with the addition of 100 μL of tris buffer instead of the CT conjugate. **Control 2** ($n=3$), denoted as A_{conj} , was performed with the addition of 800 μL of tris buffer instead of protein substrate to quantify conjugate precipitation with TCA. **Control 3** ($n=3$), denoted as A_{TCA} , was performed with 800 μL buffer and 200 μL of 50% TCA to measure residual absorbance of the solution. Activity of the dendron- α -CT conjugates, denoted as “Corrected A_{protein} ”, was interpreted as the absorbance at 280 nm (1) subtracted A_{blank} and A_{conj} (mean of 3 trials) and added A_{TCA} , and (2) has been corrected for protein concentration vs. the native α -CT to reflect equivalent per molar activity. For (2), determination of the

molar absorbance of the CT-conjugates was reported previously.²¹ The table below shows the protein concentration of the conjugate solutions.

Following the above procedures, two separate control experiments were run ($n=3$) using native CT (0.5 AU, 100 μ L) spiked with 14 mol equivalents of DBCO-G3-PEG₂₀₀₀, DBCO-G3-PEG₂₀₀₀, and DBCO-G3-PEG₂₀₀₀, respectively ($n=3$), and added 700 μ L BSA and 200 μ L 50% TCA, to monitor the enzyme activity in the presence of polymers.

Table S 3.2. Concentration of protein-dendrimer conjugates for preparing digestion assays.

Species	Base ϵ (CT) @280 nm	# DBCO triazine s	ϵ from DBCOs in a 14x conjugate	Total ϵ (cm-1 M-1)	Measur -ed AU	Protein conc (M)	conc (μM)	Relative Conc. To Native CT
CT-G3-350	52400	1	40600	93000	0.50741	5.456E-06	5.45602	0.5730
CT-G3-1K	52400	1	40600	93000	0.50446	5.424E-06	5.42430	0.5697
CT-G3-2K	52400	1	40600	93000	0.49227	5.293E-06	5.29323	0.5559
CT-G4-350	52400	3	121800	174200	0.51205	2.939E-06	2.93944	0.3087
CT-G4-1K	52400	3	121800	174200	0.49162	2.822E-06	2.82216	0.2964
CT-G4-2K	52400	3	121800	174200	0.50171	2.880E-06	2.88008	0.3025
CT-G5-350	52400	5	203000	255400	0.50882	1.992E-06	1.99225	0.2092
CT-G5-1K	52400	5	203000	255400	0.49699	1.946E-06	1.94593	0.2044

CT-G5-2K	52400	5	203000	255400	0.51052	1.999E-06	1.99890	0.2099
Native CT	52400	0	0	52400	0.49891	9.521E-06	9.52118	1.0000
Azide CT	52400	0	0	52400	0.50721	9.680E-06	9.67958	1.0166

Table S3.3. Summarized data for BTPNA assay.

Species	Initial Slopes	Concentration Adjusted slopes	Avg. slope	Activity Relative to Native CT	Std. Dev.
CT-G3-PEG350	313.2	546.56	623.83	1.4803	0.2764
	387.72	676.6			
	371.52	648.33			
CT-G3-PEG1000	375.98	659.95	621.29	1.4742	0.2413
	354.33	621.95			
	331.55	581.96			
CT-G3-PEG2000	83.172	149.61	146.87	0.3485	0.0540
	83.362	149.95			
	78.425	141.07			
CT-G4-PEG350	141.85	459.47	457.73	1.0861	0.1645
	139.76	452.7			
	142.33	461.02			
CT-G4-PEG1000	90.937	306.8	287.72	0.6827	0.1129
	85.409	288.15			
	79.499	268.21			
CT-G4-PEG2000	59.815	197.74	237.71	0.5641	0.1685
	62.664	207.16			
	93.236	308.23			
CT-G5-PEG350	60.005	286.77	258.94	0.6144	0.1157
	54.688	261.36			
	47.852	228.69			
CT-G5-PEG1000	78.035	381.82	363.17	0.8617	0.1440
	68.188	333.64			
	76.447	374.05			
CT-G5-PEG2000	14.432	70.614	64.11	0.1521	0.0268

	12.153	59.463			
	12.723	62.252			
Azide CT	619.33	609.22	585.59	1.3895	19.1648
	594.98	585.26			
	571.61	562.28			
Native CT	480.23	480.23	421.43	1.0000	52.0058
	430.29	430.29			
	353.77	353.77			
Native CT + DBCO-G3- (PEG2000)₈	155.52	155.52	338.49	0.8032	0.4422
	280.87	280.87			
	579.08	579.08			
Native CT + DBCO-G4- (PEG2000)₁₆	449.10	449.10	471.83	1.1196	0.2011
	479.79	479.79			
	486.61	486.61			
Native CT + DBCO-G5- (PEG2000)₃₂	408.99	408.99	375.57	0.8912	0.1688
	345.01	345.01			
	372.70	372.70			

Table S3.4. Summarized data for casein digestion assay.

Generation	PEG Mw	A _{casein} (280) Raw	Raw Average	Corrected A _{casein} (280)	Casein activity rel. to CT	SD (relative activity)	Sieving Ratio (casein)	SR SD
G3	350	1.0761	1.0682	1.4249	0.98723	0.022	1.4994	0.282
		1.0398						
		1.0887						
	1000	0.80355	0.80117	0.96525	0.66878	0.009	2.2044	0.3618
		0.80349						
		0.79648						
2000	0.36345	0.32929	0.14243	0.09868	0.030	3.5316	1.2021	
	0.28123							
	0.34319							
G4	350	0.57395	0.58205	0.98452	0.68213	0.012	1.5923	0.2427
		0.59622						
		0.57598						
	1000	0.41245	0.42221	0.47045	0.32596	0.008	2.0945	0.3502
		0.42432						
		0.42987						

	2000	0.32519	0.3185	0.21642	0.14995	0.006	3.7616	1.1343
		0.3138						
		0.31652						
G5	350	0.34357	0.35427	0.49029	0.3397	0.008	1.8087	0.0467
		0.35886						
		0.36037						
	1000	0.37515	0.37518	0.52985	0.36711	0.015	2.3474	0.0984
		0.38542						
		0.36498						
	2000	0.30092	0.31015	0.27387	0.18975	0.010	0.8017	0.0415
		0.30458						
		0.32496						
Native CT		1.7218	1.718	1.4433	1	1.000	-	-
		1.7149						
		1.7173						
Native CT + G3-PEG2000		1.6442	1.6527	1.53076	1.0606	0.026	0.75	0.41736
		1.6776						
		1.6363						
Native CT + G4-PEG2000		1.7704	1.6825	1.56873	1.0869	0.054	1.02	0.4157
		1.6362						
		1.6409						
Native CT + G5-PEG2000		1.67	1.6560333	1.54248	1.0687	0.023	0.83	0.159
		1.6223						
		1.6758						

Table S3.5. Summarized data for BSA digestion assay.

Generation	PEG Mw	Acasein (280) Raw	Raw Average	Corrected ABSA (280)	BSA activity rel. to CT	SD (relative activity)	Sieving Ratio (BSA)	SR SD
G3	350	0.14726	0.149870	0.1446	0.14005	0.0136	10.6678	2.2445
		0.14312						
		0.15923						
	1000	0.17017	0.178393	0.19629	0.19011	0.00916	7.8272	1.3351
		0.17817						
		0.18684						
	2000	0.06677	0.075293	0.01778	0.01722	0.01143	20.4302	13.9300
		0.07057						
		0.08854						

G4	350	0.14201	0.14688 7	0.17323	0.1677 7	0.00744	6.5342	1.0310
		0.15373						
		0.14492						
	1000	0.14013	0.14183 7	0.14766	0.1430 1	0.00445	4.8185	0.8106
		0.1439						
		0.14148						
	2000	0.07678	0.07796 7	0.03182	0.0308 2	0.00419	18.470 8	6.0631
		0.07753						
		0.07959						
G5	350	0.07678	0.07796 7	0.05251	0.0508 5	0.00199	12.195 2	0.4907
		0.07753						
		0.07959						
	1000	0.10067	0.09414 3	0.05845	0.0566 1	0.01793	15.363 7	4.8717
		0.09618						
		0.08558						
	2000	0.09629	0.08524 0	0.08231	0.0797 2	0.00972	1.9261	0.2350
		0.07718						
		0.08225						
Native CT		1.1382	1.1322	1.0422	1.0000	0.0213	-	-
Continued on next page.								...

	1.1439	1.0428	0.9431	0.9050	0.0490	0.89	0.4909
	1.1145						
Native CT + DBCO-G3-(PEG2000)₈	1.0941	1.1238	1.0241	0.9827	0.0146	1.14	0.4569
	1.0022						
	1.0321						
Native CT + DBCO-G4- (PEG2000)₁₆	1.1210	1.0420	0.9424	0.9043	0.0159	0.98	0.1870
	1.1255						
	1.1248						
Native CT + DBCO-G5-(PEG2000)₃₂	1.0368	1.0420	0.9424	0.9043	0.0159	0.98	0.1870
	1.0496						
	1.0397						

3.6 References

- (1) Ozer, I.; Tomak, A.; Zareie, H. M.; Baran, Y.; Bulmus, V. Effect of Molecular Architecture on Cell Interactions and Stealth Properties of PEG. *Biomacromolecules* **2017**, *18* (9), 2699–2710. <https://doi.org/10.1021/acs.biomac.7b00443>.
- (2) Chen, C.; Ng, D. Y. W.; Weil, T. Polymer Bioconjugates: Modern Design Concepts toward Precision Hybrid Materials. *Prog. Polym. Sci.* **2020**, *105*, 101241. <https://doi.org/10.1016/j.progpolymsci.2020.101241>.
- (3) Pasut, G. Polymers for Protein Conjugation. *Polymers* **2014**, *6* (1), 160–178. <https://doi.org/10.3390/polym6010160>.
- (4) Liechty, W. B.; Kryscio, D. R.; Slaughter, B. V.; Peppas, N. A. Polymers for Drug Delivery Systems. *Annu. Rev. Chem. Biomol. Eng.* **2010**, *1* (1), 149–173. <https://doi.org/10.1146/annurev-chembioeng-073009-100847>.
- (5) Ekladius, I.; Colson, Y. L.; Grinstaff, M. W. Polymer–Drug Conjugate Therapeutics: Advances, Insights and Prospects. *Nat. Rev. Drug Discov.* **2019**, *18* (4), 273–294. <https://doi.org/10.1038/s41573-018-0005-0>.
- (6) Pelegri-Oday, E. M.; Lin, E. W.; Maynard, H. D. Therapeutic Protein-Polymer Conjugates: Advancing beyond Pegylation. *J. Am. Chem. Soc.* **2014**, *136* (41), 14323–14332. <https://doi.org/10.1021/ja504390x>.
- (7) Gupta, V.; Bhavanasi, S.; Quadir, M.; Singh, K.; Ghosh, G.; Vasamreddy, K.; Ghosh, A.; Siahaan, T. J.; Banerjee, S.; Banerjee, S. K. Protein PEGylation for Cancer Therapy: Bench to Bedside. *J. Cell Commun. Signal.* **2019**, *13* (3), 319–330. <https://doi.org/10.1007/s12079-018-0492-0>.
- (8) Kaupbayeva, B.; Russell, A. J. Polymer-Enhanced Biomacromolecules. *Prog. Polym. Sci.* **2020**, *101*, 101194. <https://doi.org/10.1016/j.progpolymsci.2019.101194>.
- (9) Caliceti, P.; Veronese, F. M. Pharmacokinetic and Biodistribution Properties of Poly(Ethylene Glycol)-Protein Conjugates. *Adv. Drug Deliv. Rev.* **2003**, *55* (10), 1261–1277. [https://doi.org/10.1016/S0169-409X\(03\)00108-X](https://doi.org/10.1016/S0169-409X(03)00108-X).
- (10) Milton Harris, J.; Chess, R. B. Effect of Pegylation on Pharmaceuticals. *Nat. Rev. Drug Discov.* **2003**, *2* (3), 214–221. <https://doi.org/10.1038/nrd1033>.
- (11) Davis, F. F.; Abuchowski, A.; van Es, T.; Palczuk, N. C.; Chen, R.; Savoca, K.; Wieder, K. Enzyme-Polyethylene Glycol Adducts: Modified Enzymes with Unique Properties. In *Enzyme Engineering*; Springer US: Boston, MA, 1978; pp 169–173. https://doi.org/10.1007/978-1-4684-6985-1_35.
- (12) Pasut, G.; Veronese, F. M. State of the Art in PEGylation: The Great Versatility Achieved after Forty Years of Research. *J. Controlled Release* **2012**, *161* (2), 461–472. <https://doi.org/10.1016/j.jconrel.2011.10.037>.
- (13) Schulz, J. D.; Patt, M.; Basler, S.; Kries, H.; Hilvert, D.; Gauthier, M. A.; Leroux, J. C. Site-Specific Polymer Conjugation Stabilizes Therapeutic Enzymes in the Gastrointestinal Tract. *Adv. Mater.* **2016**, *28* (7), 1455–1460. <https://doi.org/10.1002/adma.201504797>.

- (14) Joh, D. Y.; Zimmers, Z.; Avlani, M.; Heggstad, J. T.; Aydin, H. B.; Ganson, N.; Kumar, S.; Fontes, C. M.; Achar, R. K.; Hershfield, M. S.; Hucknall, A. M.; Chilkoti, A. Architectural Modification of Conformal PEG-Bottlebrush Coatings Minimizes Anti-PEG Antigenicity While Preserving Stealth Properties. *Adv. Healthc. Mater.* **2019**, *8* (8), 1–13. <https://doi.org/10.1002/adhm.201801177>.
- (15) Zdyrko, B.; Klep, V.; Luzinov, I. Synthesis and Surface Morphology of High-Density Poly(Ethylene Glycol) Grafted Layers. *Langmuir* **2003**, *19* (24), 10179–10187. <https://doi.org/10.1021/la034974r>.
- (16) Li, M.; Jiang, S.; Simon, J.; Paßlick, D.; Frey, M. L.; Wagner, M.; Mailander, V.; Crespy, D.; Landfester, K. Brush Conformation of Polyethylene Glycol Determines the Stealth Effect of Nanocarriers in the Low Protein Adsorption Regime. *Nano Lett.* **2021**, *21* (4), 1591–1598. <https://doi.org/10.1021/acs.nanolett.0c03756>.
- (17) Drossis, N.; Gauthier, M. A.; de Haan, H. W. Elucidating the Mechanisms of the Molecular Sieving Phenomenon Created by Comb-Shaped Polymers Grafted to a Protein – a Simulation Study. *Mater. Today Chem.* **2022**, *24*, 100861. <https://doi.org/10.1016/j.mtchem.2022.100861>.
- (18) Liu, M.; Tirino, P.; Radivojevic, M.; Phillips, D. J.; Gibson, M. I.; Leroux, J. C.; Gauthier, M. A. Molecular Sieving on the Surface of a Protein Provides Protection without Loss of Activity. *Adv. Funct. Mater.* **2013**, *23* (16), 2007–2015. <https://doi.org/10.1002/adfm.201202227>.
- (19) Liu, M.; Leroux, J. C.; Gauthier, M. A. Conformation-Function Relationships for the Comb-Shaped Polymer pOEGMA. *Prog. Polym. Sci.* **2015**, *48*, 111–121. <https://doi.org/10.1016/j.progpolymsci.2015.03.001>.
- (20) Kaupbayeva, B.; Murata, H.; Lucas, A.; Matyjaszewski, K.; Minden, J. S.; Russell, A. J. Molecular Sieving on the Surface of a Nano-Armored Protein. *Biomacromolecules* **2019**, *20* (3), 1235–1245. <https://doi.org/10.1021/acs.biomac.8b01651>.
- (21) McNelles, S. A.; Marando, V. M.; Adronov, A. Globular Polymer Grafts Require a Critical Size for Efficient Molecular Sieving of Enzyme Substrates. *Angew. Chem. - Int. Ed.* **2019**, *58* (25), 8448–8453. <https://doi.org/10.1002/anie.201902864>.
- (22) Astruc, D.; Boisselier, E.; Ornelas, C. Dendrimers Designed for Functions: From Physical, Photophysical, and Supramolecular Properties to Applications in Sensing, Catalysis, Molecular Electronics, Photonics, and Nanomedicine. *Chem. Rev.* **2010**, *110* (4), 1857–1959. <https://doi.org/10.1021/cr900327d>.
- (23) Durán-Lara, E. F.; Marple, J. L.; Giesen, J. A.; Fang, Y.; Jordan, J. H.; Godbey, W. T.; Marican, A.; Santos, L. S.; Grayson, S. M. Investigation of Lysine-Functionalized Dendrimers as Dichlorvos Detoxification Agents. *Biomacromolecules* **2015**, *16* (11), 3434–3444. <https://doi.org/10.1021/acs.biomac.5b00657>.
- (24) Carlmark, A.; Hawker, C.; Hult, A.; Malkoch, M. New Methodologies in the Construction of Dendritic Materials. *Chem. Soc. Rev.* **2009**, *38* (2), 352–362. <https://doi.org/10.1039/b711745k>.
- (25) Twibanire, J. D.; K. Amour; Grindley, T. B. Polyester Dendrimers. *Polymers* **2012**, *4* (1), 794–879. <https://doi.org/10.3390/polym4010794>.

- (26) Jansen, J. F. G. A.; de Brabander-van den Berg, E. M. M.; Meijer, E. W. Encapsulation of Guest Molecules into a Dendritic Box. *Science* **1994**, *266* (5188), 1226–1229. <https://doi.org/10.1126/science.266.5188.1226>.
- (27) Zdyrko, B.; Varshney, S. K.; Luzinov, I. Effect of Molecular Weight on Synthesis and Surface Morphology of High-Density Poly(Ethylene Glycol) Grafted Layers. *Langmuir* **2004**, *20* (16), 6727–6735. <https://doi.org/10.1021/la049359h>.
- (28) Tessmar, J. K.; Göpferich, A. M. Customized PEG-Derived Copolymers for Tissue-Engineering Applications. *Macromol. Biosci.* **2007**, *7* (1), 23–39. <https://doi.org/10.1002/mabi.200600096>.
- (29) Blümmel, J.; Perschmann, N.; Aydin, D.; Drinjakovic, J.; Surrey, T.; Lopez-Garcia, M.; Kessler, H.; Spatz, J. P. Protein Repellent Properties of Covalently Attached PEG Coatings on Nanostructured SiO₂-Based Interfaces. *Biomaterials* **2007**, *28* (32), 4739–4747. <https://doi.org/10.1016/j.biomaterials.2007.07.038>.
- (30) Erkoc, P.; Ulucan-Karnak, F. Nanotechnology-Based Antimicrobial and Antiviral Surface Coating Strategies. *Prosthesis* **2021**, *3* (1), 25–52. <https://doi.org/10.3390/prosthesis3010005>.
- (31) Sofia, S. J.; Premnath, V.; Merrill, E. W. Poly(Ethylene Oxide) Grafted to Silicon Surfaces: Grafting Density and Protein Adsorption. *Macromolecules* **1998**, *31* (15), 5059–5070. <https://doi.org/10.1021/ma971016l>.
- (32) Szleifer, I. Protein Adsorption on Surfaces with Grafted Polymers: A Theoretical Approach. *Biophys. J.* **1997**, *72* (2 I), 595–612. [https://doi.org/10.1016/S0006-3495\(97\)78698-3](https://doi.org/10.1016/S0006-3495(97)78698-3).
- (33) Rodríguez-Martínez, J. A.; Solá, R. J.; Castillo, B.; Cintrón-Colón, H. R.; Rivera-Rivera, I.; Barletta, G.; Griebenow, K. Stabilization of α -Chymotrypsin upon PEGylation Correlates with Reduced Structural Dynamics. *Biotechnol. Bioeng.* **2008**, *101* (6), 1142–1149. <https://doi.org/10.1002/bit.22014>.
- (34) Zaghmi, A.; Mendez-Villuendas, E.; Greschner, A. A.; Liu, J. Y.; de Haan, H. W.; Gauthier, M. A. Mechanisms of Activity Loss for a Multi-PEGylated Protein by Experiment and Simulation. *Mater. Today Chem.* **2019**, *12*, 121–131. <https://doi.org/10.1016/j.mtchem.2018.12.007>.
- (35) Rodríguez-Martínez, J. A.; Rivera-Rivera, I.; Solá, R. J.; Griebenow, K. Enzymatic Activity and Thermal Stability of PEG- α -Chymotrypsin Conjugates. *Biotechnol. Lett.* **2009**, *31* (6), 883–887. <https://doi.org/10.1007/s10529-009-9947-y>.
- (36) Le Cœur, C.; Combet, S.; Carrot, G.; Busch, P.; Teixeira, J.; Longeville, S. Conformation of the Poly(Ethylene Glycol) Chains in DiPEGylated Hemoglobin Specifically Probed by SANS: Correlation with PEG Length and in Vivo Efficiency. *Langmuir* **2015**, *31* (30), 8402–8410. <https://doi.org/10.1021/acs.langmuir.5b01121>.
- (37) Munasinghe, A.; Mathavan, A.; Mathavan, A.; Lin, P.; Colina, C. M. Molecular Insight into the Protein-Polymer Interactions in N-Terminal PEGylated Bovine Serum Albumin. *J. Phys. Chem. B* **2019**, *123* (25), 5196–5205. <https://doi.org/10.1021/acs.jpcc.8b12268>.
- (38) Deng, B.; McNelles, S. A.; Da-Ré, G.; Marando, V. M.; Ros, S.; Stöver, H. D. H.; Adronov, A. Neopentyl Esters as Robust Linkers for Introducing Functionality to

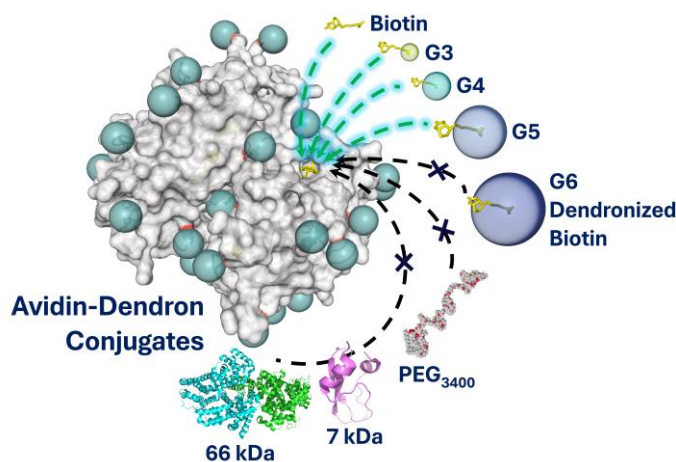
- Bis-MPA Dendrimers. *Macromolecules* **2022**, *55* (1), 270–275.
<https://doi.org/10.1021/acs.macromol.1c01974>.
- (39) Ihre, H.; Hult, A.; Fréchet, J. M. J.; Gitsov, I. Double-Stage Convergent Approach for the Synthesis of Functionalized Dendritic Aliphatic Polyesters Based on 2,2-Bis(Hydroxymethyl)Propionic Acid. *Macromolecules* **1998**, *31* (13), 4061–4068.
<https://doi.org/10.1021/ma9718762>.
- (40) Goswami, L. N.; Houston, Z. H.; Sarma, S. J.; Jalisatgi, S. S.; Hawthorne, M. F. Efficient Synthesis of Diverse Heterobifunctionalized Clickable Oligo(Ethylene Glycol) Linkers: Potential Applications in Bioconjugation and Targeted Drug Delivery. *Org. Biomol. Chem.* **2013**, *11* (7), 1116–1126.
<https://doi.org/10.1039/c2ob26968f>.
- (41) Hattori, T.; Tsubone, A.; Sawama, Y.; Monguchi, Y.; Sajiki, H. Systematic Evaluation of the Palladium-Catalyzed Hydrogenation under Flow Conditions. *Tetrahedron* **2014**, *70* (32), 4790–4798. <https://doi.org/10.1016/j.tet.2014.05.038>.
- (42) González-Fernández, D.; Torneiro, M.; Lazzari, M. Some Guidelines for the Synthesis and Melting Characterization of Azide Poly(Ethylene Glycol) Derivatives. *Polymers* **2020**, *12* (6), 1269. <https://doi.org/10.3390/polym12061269>.
- (43) McNelles, S. A.; Adronov, A. Rapid Synthesis of Functionalized High-Generation Polyester Dendrimers via Strain-Promoted Alkyne-Azide Cycloaddition. *Macromolecules* **2017**, *50* (20), 7993–8001.
<https://doi.org/10.1021/acs.macromol.7b01765>.
- (44) Beutner, G. L.; Young, I. S.; Davies, M. L.; Hickey, M. R.; Park, H.; Stevens, J. M.; Ye, Q. TCFH-NMI: Direct Access to N-Acyl Imidazoliums for Challenging Amide Bond Formations. *Org. Lett.* **2018**, *20* (14), 4218–4222.
<https://doi.org/10.1021/acs.orglett.8b01591>.
- (45) Baker, S. L.; Munasinghe, A.; Murata, H.; Lin, P.; Matyjaszewski, K.; Colina, C. M.; Russell, A. J. Intramolecular Interactions of Conjugated Polymers Mimic Molecular Chaperones to Stabilize Protein-Polymer Conjugates. *Biomacromolecules* **2018**, *19* (9), 3798–3813.
<https://doi.org/10.1021/acs.biomac.8b00927>.
- (46) Ding, Z.; Chen, G.; Hoffman, A. S. Unusual Properties of Thermally Sensitive Oligomer-Enzyme Conjugates of Poly(N-Isopropylacrylamide)-Trypsin. *J. Biomed. Mater. Res.* **1998**, *39* (3), 498–505. [https://doi.org/10.1002/\(SICI\)1097-4636\(19980305\)39:3<498::AID-JBM22>3.0.CO;2-5](https://doi.org/10.1002/(SICI)1097-4636(19980305)39:3<498::AID-JBM22>3.0.CO;2-5).
- (47) Schorb, M.; Haberbosch, I.; Hagen, W. J. H.; Schwab, Y.; Mastronarde, D. N. Software Tools for Automated Transmission Electron Microscopy. *Nat. Methods* **2019**, *16* (6), 471–477. <https://doi.org/10.1038/s41592-019-0396-9>.
- (48) Parrott, M. C.; Rahima Benhabbour, S.; Saab, C.; Lemon, J. A.; Parker, S.; Valliant, J. F.; Adronov, A. Synthesis, Radiolabeling, and Bio-Imaging of High-Generation Polyester Dendrimers. *J. Am. Chem. Soc.* **2009**, *131* (8), 2906–2916.
<https://doi.org/10.1021/ja8078175>.

Chapter 4. Dendrimer-Mediated Molecular Sieving on Avidin

This chapter has been reproduced with permission from Deng, B.; McNelles, S. A.; Sun, J.; Ortega, J.; Adronov, A. Dendrimer-Mediated Molecular Sieving on Avidin. *Biomacromolecules* **2025**, *26* (2), 1320–1334. Copyright © 2025 American Chemical Society.

This work detailed in this chapter was carried out in collaboration with Stuart McNelles, Jingyu Sun and Joaquin Ortega. Billy Deng and Stuart McNelles synthesized and characterized the dendrimers. Billy Deng synthesized, characterized, and assayed the dendrimer-avidin conjugates. Jingyu Sun and Joaquin Ortega performed cryo-EM microscopy. Billy Deng, Jingyu Sun, Joaquin Ortega, and Alex Adronov prepared the manuscript.

Graphical Abstract:



4.1 Abstract

Decoration of proteins and enzymes with well-defined polymeric structures allows precise decoration of protein surfaces, enabling controlled modulation of activity. Here, the impact of dendronization on the interaction between avidin and biotin was investigated. A series of generation 3-7 bis-(2,2-hydroxymethyl)propionic acid (bis-MPA) dendrons were coupled to either biotin or avidin to yield a library of dendronized avidin and biotin structures. The thermodynamics of binding each biotinylated generation to a library of avidin conjugates was probed with isothermal titration calorimetry (ITC). Dissociation constants of high-generation biotin-dendrons (G5 and G6) with higher-generation avidin-dendron conjugates (Av-G6) increased from $\sim 10^{-15}$ M (for the native structures) to $\sim 10^{-6}$ M, and binding was found to be weaker than that of the Avidin-HABA complex. Avidin-G5 and Avidin-G6 were highly size-selective for biotinylated ligands; both prevented binding of aprotinin (6.9 kDa), bovine serum albumin (BSA), and PEG₃₄₀₀, while forming fractional complexes with smaller biotinylated dendrons.

4.2 Introduction

The modification of protein surfaces through polymer functionalization has attracted significant attention as it can affect properties such as in-vivo stability, activity, and circulation half-life while decreasing immunogenicity.¹⁻⁶ The past decade has seen an increasing interest in controlling protein-ligand interactions through surface modification.⁷⁻¹³ In particular, the use of PEG-based brushes to decorate protein surfaces in high density has allowed discrimination between potential ligands according to their size.^{7,8} This concept, where small molecules penetrate the polymer shell while larger

molecules are rejected, known as “molecular sieving,” was pioneered through the seminal work of Gauthier and co-workers.⁷ In this work, polymer conjugates of both chymotrypsin and L-asparaginase were decorated with poly[oligo(ethylene glycol) methacrylate] (POEGMA) comb polymers, and it was shown that the activity of conjugates to small substrates (BTpNA and L-asparagine) was unaffected, while reactivity toward proteins and recognition by antibodies was dramatically reduced.⁸ This work identified critical characteristics of the polymer shell, such as globular morphology, high degree of branching, and dense surface grafting. Additionally, Russell and co-workers showed that poly(carboxybetaine methacrylate) (pCBMA), polymerized from the surface of avidin results in “nano armor” that shields the protein from binding to ligand derivatives (biotinylated compounds) of different size.¹³ These studies clearly demonstrated that grafting density directly impacts avidin-biotin binding kinetics, which was used as a proxy for sieving. Although this work showed only a small effect of polymer molecular weight on sieving efficiency, the general trend that a high-density polymeric monolayer on the protein surface imparts size selectivity to substrates was reinforced. Recently, we showed that a dendritic shell is also effective in molecular sieving when the dendrimer reaches a critical size. It was found that attachment of G7 and G8 dendrimers at the surface lysine residues of chymotrypsin resulted in a significantly lower activity toward large, rigid proteins (e.g., BSA), while retaining unhindered activity toward small substrates.¹¹ Furthermore, we showed that lower generation surface-PEGylated dendrimers could also achieve efficient sieving.¹²

Inspired by the work of Russel and co-workers, we aimed to determine if dendritic macromolecules could also impart sieving effects in the strong avidin-biotin binding interaction. Avidin, a tetrameric glycoprotein composed of identical, eight-stranded beta-barrel subunits,¹⁴ binds to biotin with high specificity and exceptionally strong affinity ($K_d \sim 10^{-15}$ M).¹⁵ This system has seen ubiquitous use in biochemistry and protein engineering^{16,17} and recently in the context of molecular sieving.^{13,18} Although Russell and coworkers¹³ elegantly quantified the kinetics of the sieving effect in pCBMA-decorated avidin, it is still unclear how the grafted polymers influence binding stoichiometry, complex formation, and what are the limits in molecular size for which sieving can be achieved.

In this work, we demonstrate molecular sieving using a series of structurally well-defined dendritic conjugates of both avidin and biotin. We investigate the impact of dendrimer attachment on the morphology and flexibility of the protein and its substrate, as these characteristics have been found to influence sieving effectiveness.¹¹ To do so, G3-G7 polyester dendrons were conjugated to both biotin and avidin, where 10 surface lysines per monomeric unit (40 total for the tetrameric structure) were derivatized. We demonstrate the dynamic impact of dendron generation on binding efficiency as well as the stoichiometry of the biotin-avidin complex (Figure 4.1). By mixing-and-matching dendronized avidin-biotin pairs with different dendron size, it is possible to not only prevent the binding interaction, but also to enable differential binding without using mutants and/or biotin mimics.^{19,20}

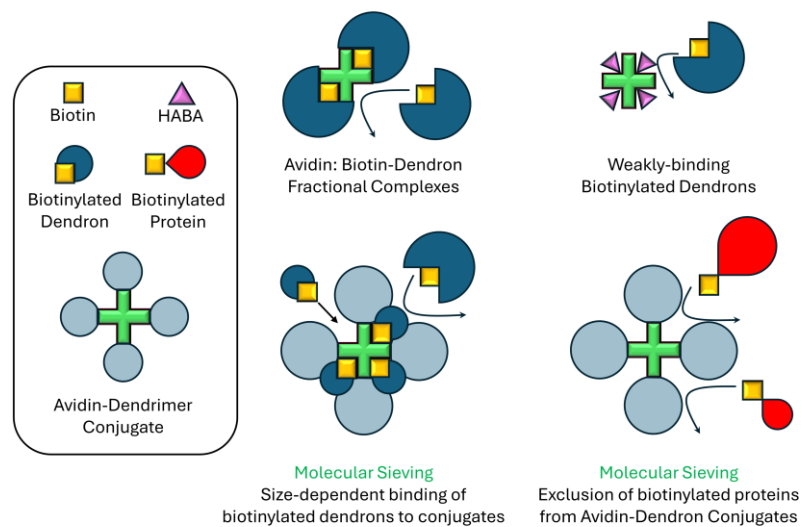
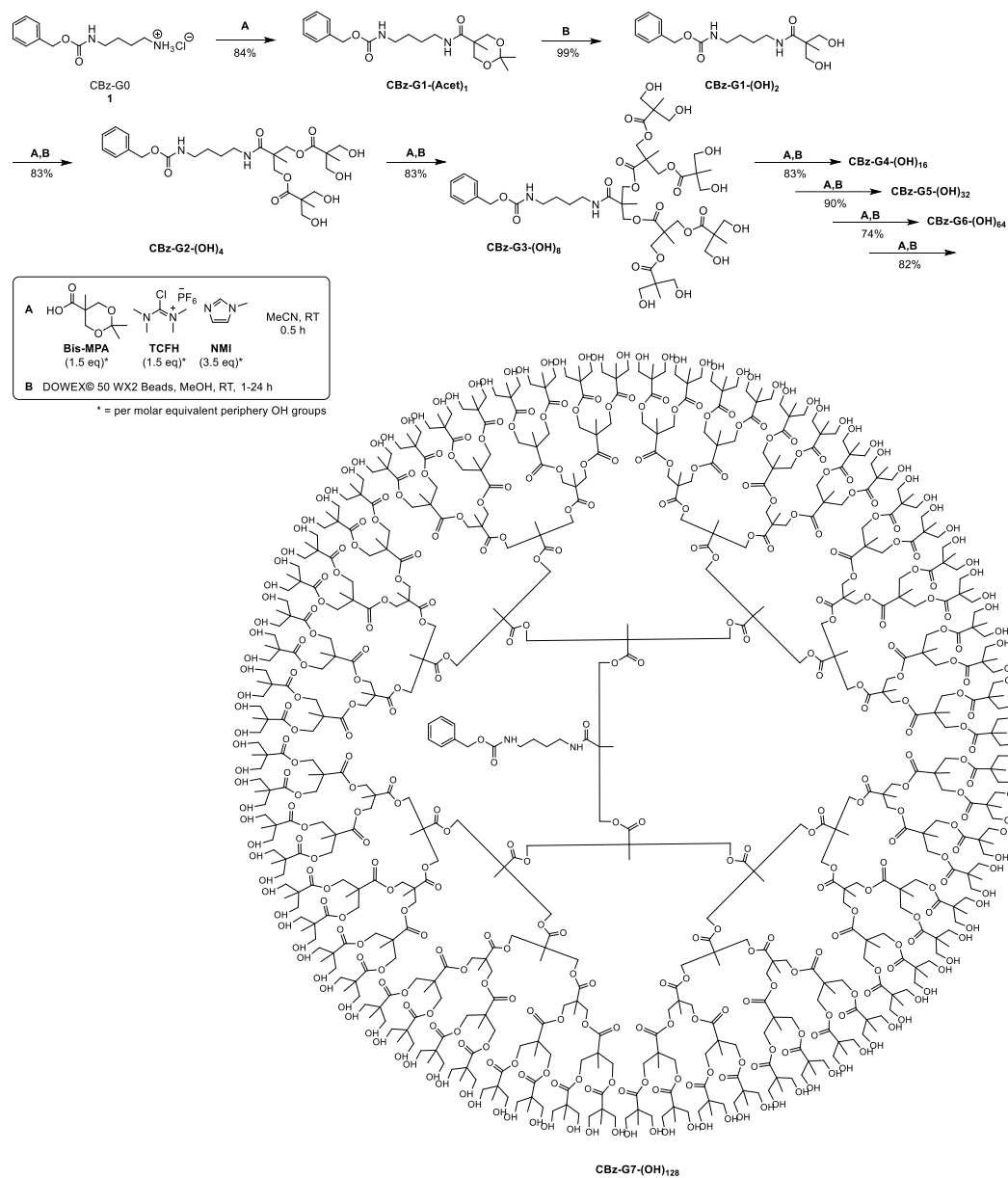


Figure 4.1. Schematic representation of dendron generation-controlled sieving processes involving avidin-dendron conjugates interacting with biotin, dendronized biotin, and biotinylated proteins. Structures are not drawn to scale – size discrepancy between ligands are illustrated by differently sized cartoons.

4.3 Results and Discussion

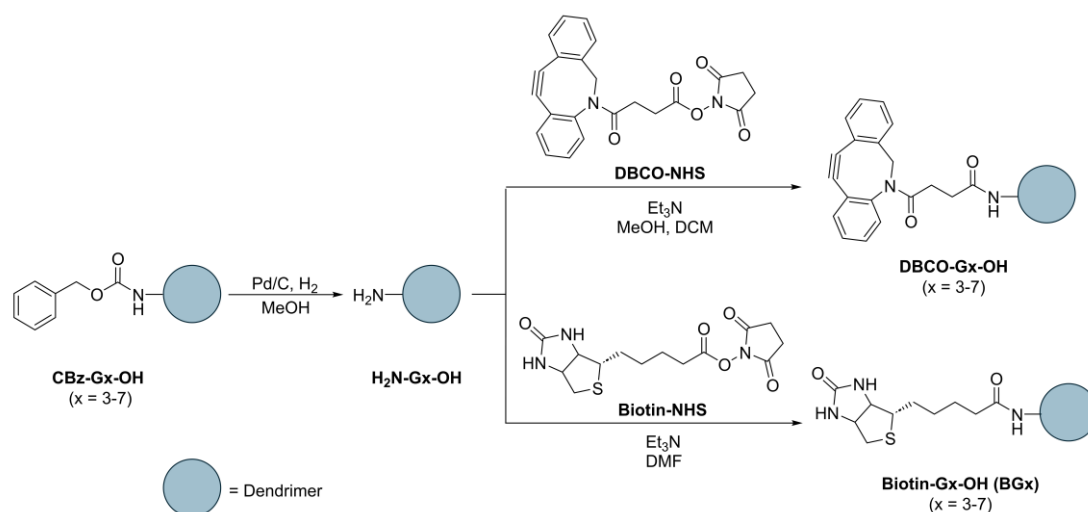
Synthesis of DBCO- and Biotin-core Polyester Dendrons. G3-G7 dendrons were prepared following a previously reported convergent strategy *via* N,N,N',N' -tetramethylchloroformamidinium hexafluorophosphate (TCFH) – N-methylimidazole (NMI) mediated coupling.^{11,21,22} Aside from being scalable to gram quantities, we found the TCFH-NMI method to be a more rapid esterification relative to other methods used for dendrimer growth.^{21,23,24} Starting from the mono benzyl carbamate (CBz) protected diamine (**1**), we employed a stepwise iterative process of dendrimer growth with acetonide-protected bis-MPA as the monomer, followed by acidic deprotection of the dendrimer periphery to expose the hydroxyl groups. This two-step process was repeated to produce the desired dendrons in good yield (Scheme 4.1).



Scheme 4.1. Iterative synthesis of benzyl carbamate-protected polyester dendrons up to the 7th generation, **CBz-G7-(OH)₁₂₈**. Structures of G4, 5, 6 dendrons bearing 16, 32, and 64 hydroxyl groups at the periphery, respectively, are omitted for clarity.

The CBz-core was removed at the desired generation of hydroxyl-periphery dendrons *via* catalytic hydrogenation, followed by amidation with biotin-NHS²⁵ to yield the core-biotinylated dendrons (**BG_x**; x = 3-7). The analogous DBCO-core G3-7 dendrons (**DBCO-**

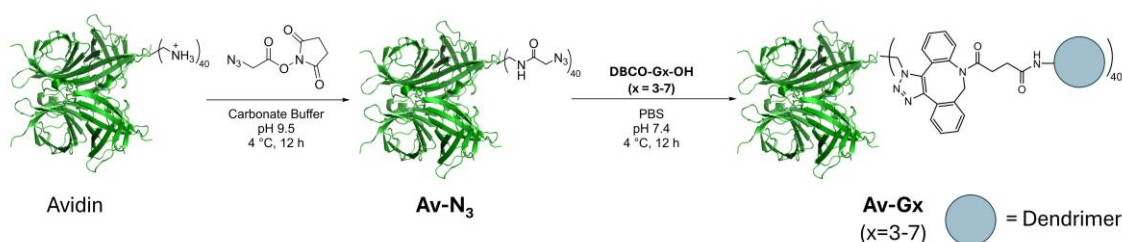
G_x; x = 3-7) were synthesized in the same manner but instead using DBCO-NHS as the amidation partner (Scheme 4.2). Detailed synthetic procedures and spectroscopic data for the dendrons (¹H NMR, ¹³C NMR, ESI, MALDI-TOF) are provided in the Supporting Information in Chapter 4.5.



Scheme 4.2. Core functionalization of bis-MPA-based polyester dendrons.

Synthesis and Characterization of Dendronized Avidin. We next proceeded to graft the DBCO-core dendrons onto the surface of native avidin *via* the strain-promoted azide-alkyne cycloaddition (SPAAC) reaction. As was done previously with chymotrypsin,^{11,12} we initially attempted to exhaustively install azides on the surface lysines in a one-pot procedure by forming the NHS ester of 2-azidoacetic acid via EDC-promoted esterification, followed by amidation of the avidin lysines. This led to incomplete functionalization and poor yield, which was due to the relatively high pI of avidin, a result of the abundant lysine

residues ($n = 40$ in avidin tetramer).^{13,26} When the amidation was performed in neutral phosphate buffered saline (PBS) or mildly basic buffer (pH 8.5), the highly cationic surface coupled sluggishly to the NHS-ester and was hindered by hydrolysis of the ester and rearrangement of intermediates into urea side-products.^{27,28} Conversely, addition of isolated azidoacetyl-NHS²⁹ directly to avidin in a carbonate-bicarbonate buffer (pH 9.5), resulted in complete amidation to yield azide-functionalized avidin, **Av-N₃** (Scheme 4.3).



Scheme 4.3. Synthesis of avidin azide (**Av-N₃**) and Avidin-dendron conjugates (**Av-Gx**) from native avidin.

The crude protein was purified *via* size-exclusion chromatography (SEC) and centrifugal filtration. Complete functionalization of the surface lysines was confirmed *via* fluorescamine assay,³⁰ which indicated the absence of primary amines. The increase in molecular weight from avidin to **Av-N₃** was determined by MALDI-TOF MS (Figure S4.15), and avidin content in the purified protein solids was quantified by UV-Vis spectroscopy (by measuring absorption at 280 nm, A_{280}). Both techniques indicated that the desired decoration of the avidin surface was accomplished. The G3-G7 dendrons functionalized with DBCO at their core (**DBCO-Gx-OH**; $x = 3-7$) were then coupled to **Av-N₃** *via* SPAAC to yield the dendronized avidin at the various generations, **Av-Gx** ($x = 3-7$) (Scheme 4.3). Through prior doping studies,¹¹ we validated that FT-IR can detect

minute quantities of residual azides if the SPAAC reaction does not go to completion. We therefore monitored the SPAAC reaction *via* FT-IR to determine the complete disappearance of the azide signal at $\sim 2100\text{ cm}^{-1}$ (Figure 4.2A). Upon completion, crude products were purified by dialysis and centrifugal filtration and quantified by bicinchoninic acid (BCA) assay. The degree of conjugation was also confirmed through the BCA assay by relating protein concentration to mass percent of avidin in the conjugate (see Supporting Information for calculations). Both analyses indicated quantitative dendronization of peripheral lysines on avidin. Native PAGE was then used to qualitatively assess the relative molecular weight of the avidin conjugates (Figure 4.2B). Consistent with FT-IR, we found no traces of **Av-N₃** in any of the conjugate samples. As expected, residual charges on avidin resulted in lower R_f values and overestimated molecular weights relative to the standards in the molecular weight ladder (calculated molecular weights for the conjugates are provided in Table 4.1).^{31,32} Based on the PAGE results, we observed a steady increase in molecular weight of the avidin-dendron conjugates with increasing dendron generation. It should be noted that native avidin does not migrate through the gel under normal polarity due to its significant cationic character under these conditions (Figure 4.2B).

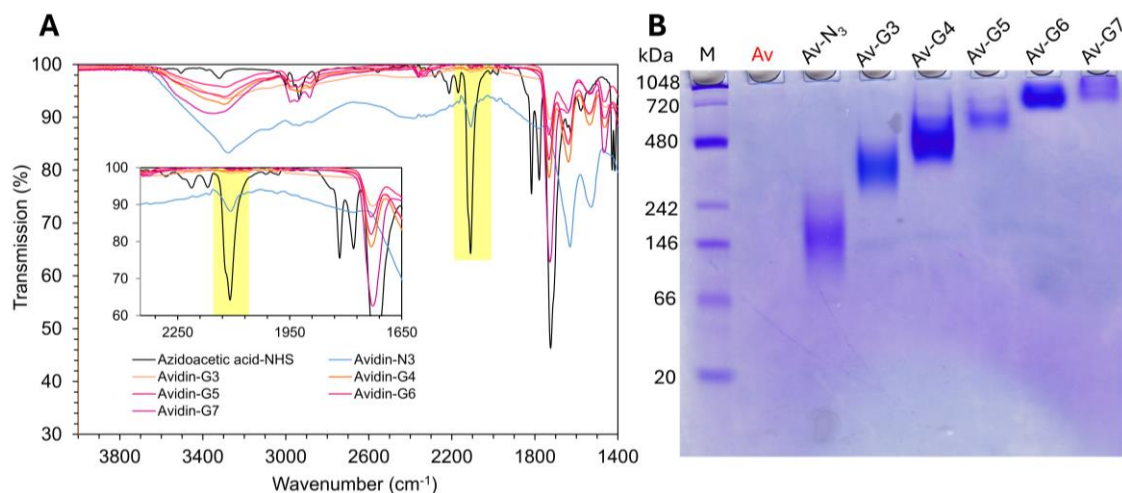


Figure 4.2. A) Stacked FT-IR spectra of azidoacetic acid NHS ester, avidin- N_3 , and **Av-G x** conjugates showing complete consumption of azides post SPAAC. Inset shows highlighted azide signal centered at $\sim 2110\text{ cm}^{-1}$. B) Native PAGE (6%) of avidin-dendron conjugates. From left to right: Ladder (NativeMark), avidin, avidin azide (**Av-N $_3$**) and avidin-dendron conjugates (**Av-G x** , $x = 3-7$; lanes 4-8). PAGE was run in pH 8.3 tris-glycine buffer and stained with Coomassie R250. Native avidin was immobile under these conditions.

Circular dichroism (CD) spectroscopy was used to probe the secondary structure of avidin-dendron conjugates (Figure 4.3).³³ It was found that **Av-G3** to **Av-G7** retained a positive CD band at $\sim 228\text{ nm}$, characteristic of β -sheets in avidin and specifically from exciton contributions from Trp70, Trp97, and Trp110 (from the adjoining comonomer) in the biotin binding pocket of avidin.³⁴⁻³⁶ There is a slight hypsochromic shift from native avidin to **avidin-N $_3$** ($\lambda_{\text{max}} = 227\text{ nm}$) which does not change further upon SPAAC reaction. Interestingly, there is a strong change in the λ_{max} band intensity of the conjugates, but a clear trend relative to dendron generation could not be ascertained. **Av-G3**, **G5** and **G7** led to a decrease in intensity relative to native avidin, while the opposite was observed for **Av-G4** and **Av-G6**. Although the DLS and binding experiments (*vide infra*) did not indicate signs of tetramer dissociation or conjugate denaturation, CD suggests distortions to the

avidin structure, possibly from hydrogen bonding interactions between the hydroxyl periphery of the dendrons and residues within the binding pocket or the backbone of the β -barrels. The variation in band intensity is likely attributed to perturbations of exciton coupling between tryptophan residues within the biotin binding pocket.³⁶

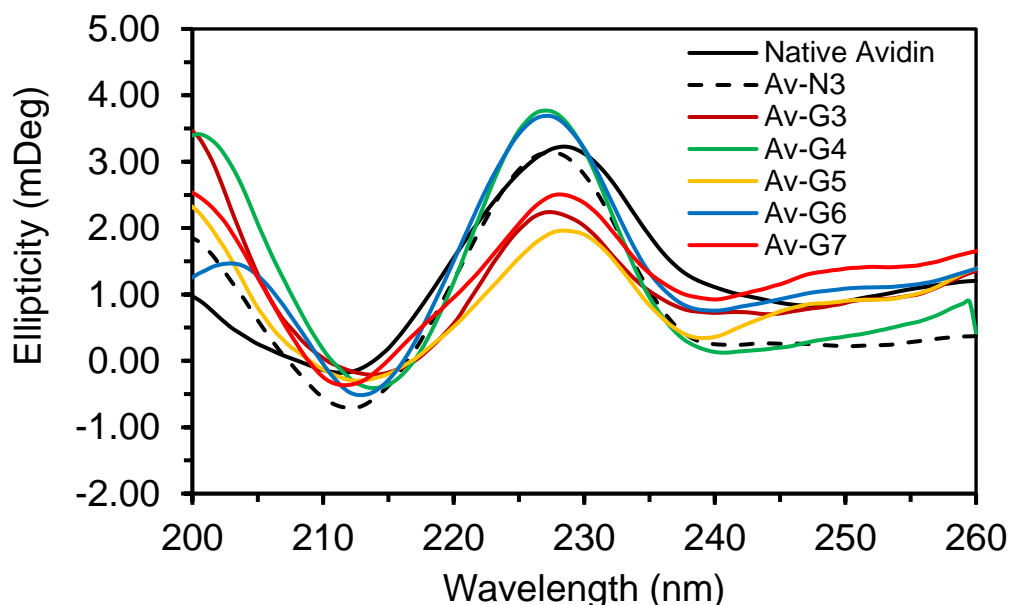


Figure 4.3. Circular Dichroism spectra of avidin-dendron conjugates (0.2 mg/mL) in 10 mM PBS.

DLS was used to investigate the relationship between dendron generation and the overall conjugate size. In PBS (10 mM, pH 7.4), native avidin was found to have a hydrodynamic diameter D_h (Z-avg) of ~ 8 nm. Upon functionalization with dendrons, D_h increases (Table 4.1) with dendron generation up to 16 nm for **Av-G7** (Figure 4.4, see Figure S4.16 for particle size distribution plots). Assuming a globular structure,³⁷ these size measurements are in good agreement with previous DLS experiments conducted on native avidin and DBCO-core globular dendrons, respectively.^{11,13} As expected, D_h of the conjugates increased non-linearly with dendron generation and molecular weight as the

dendritic shell is not rigid and can collapse on the protein surface (Figure 4.4). Despite our best efforts, we were unable to measure the precise size of **Av-G3**, as it formed large aggregates in the micrometer scale, as shown in Figure S4.16 by presence of multimodal peaks. This is likely due to the relatively low aqueous solubility of the free dendron **DBCO-G3-OH**. The poor aqueous solubility of **Av-G3** precluded its use in binding studies.

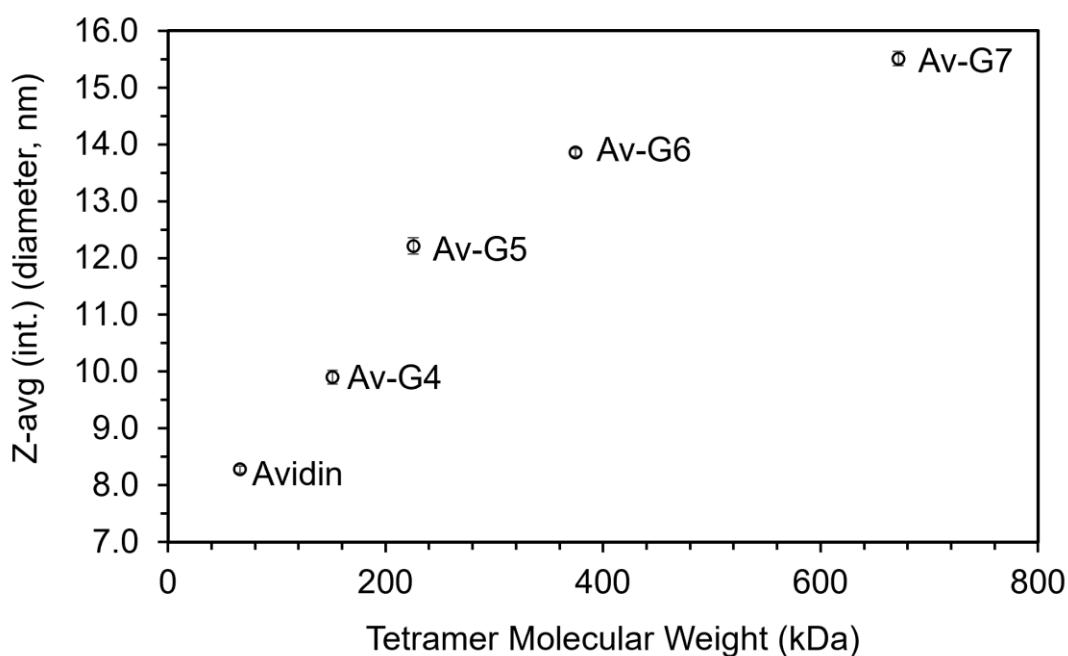


Figure 4.4. Z-average diameter versus molecular weight of avidin-dendron conjugates. Error bars represent standard deviation.

Table 4.1. Intensity weighted hydrodynamic diameter (Z-avg d) of avidin-dendron conjugates.

Avidin Conjugate	Molecular Weight (kDa)	Z-avg d (nm) ($n=5$)	SD (nm)	PDI	PDI SD
Native	66.0	8.30	0.060	0.243	0.011
Av-G4	151	9.91	0.120	0.136	0.010
Av-G5	226	12.2	0.144	0.240	0.009
Av-G6	375	13.9	0.064	0.102	0.012

Av-G7	676	15.5	0.123	0.336	0.025
-------	-----	------	-------	-------	-------

Characterization of the dendronized avidins by Cryo-EM. Cryo-electron microscopy (cryo-EM) was used to visualize the dendronized avidin structures. At each generation of dendronized avidin, it was possible to observe highly uniform spherical structures within the TEM images, with sizes that increased with dendron generation (Figure 4.5). On average, the observed spherical particles had diameters of 6.17 ± 0.15 nm, 11.04 ± 0.49 nm, and 12.18 ± 0.31 nm for G4, G5, and G6 ($n = 3$), respectively, which agree well with DLS measurements (Table 4.1). The slightly smaller diameter observed compared to DLS is likely due to the hydration shell that forms around the dendron periphery in solution, thus increasing the D_h measured by DLS. Images from the G7 sample showed a heterogeneous mixture of particles (Figure 4.5D) with smaller particles (Figure 4.5E) and large vesicle-like particles (Figure 4.5F), indicating the possibility of some higher-order assembly/aggregation.

To gain additional structural details of the dendronized avidins, we collected a large dataset from the G6 sample. We used these images to obtain two-dimensional averages of the particles observed in this sample. Approximately half a million particles were selected (Figure 4.5G, left panel) and extracted from the electron micrographs before they were subjected to the 2D classification, alignment and averaging. The obtained 2D class averages (Figure 4.5G, right panel) revealed that the G6 particles are comprised of a central core density, where the avidin tetramer is located, and this density is surrounded by seven or eight spherical densities of 2.84 ± 0.2 nm ($n = 3$) diameter that represent the linked

dendrons. The position of the dendron spheres relative to the central avidin density was highly variable and changed on spacing and distance. Consequently, generating a high-resolution three-dimensional cryo-EM structure from these 2D averages was not possible.

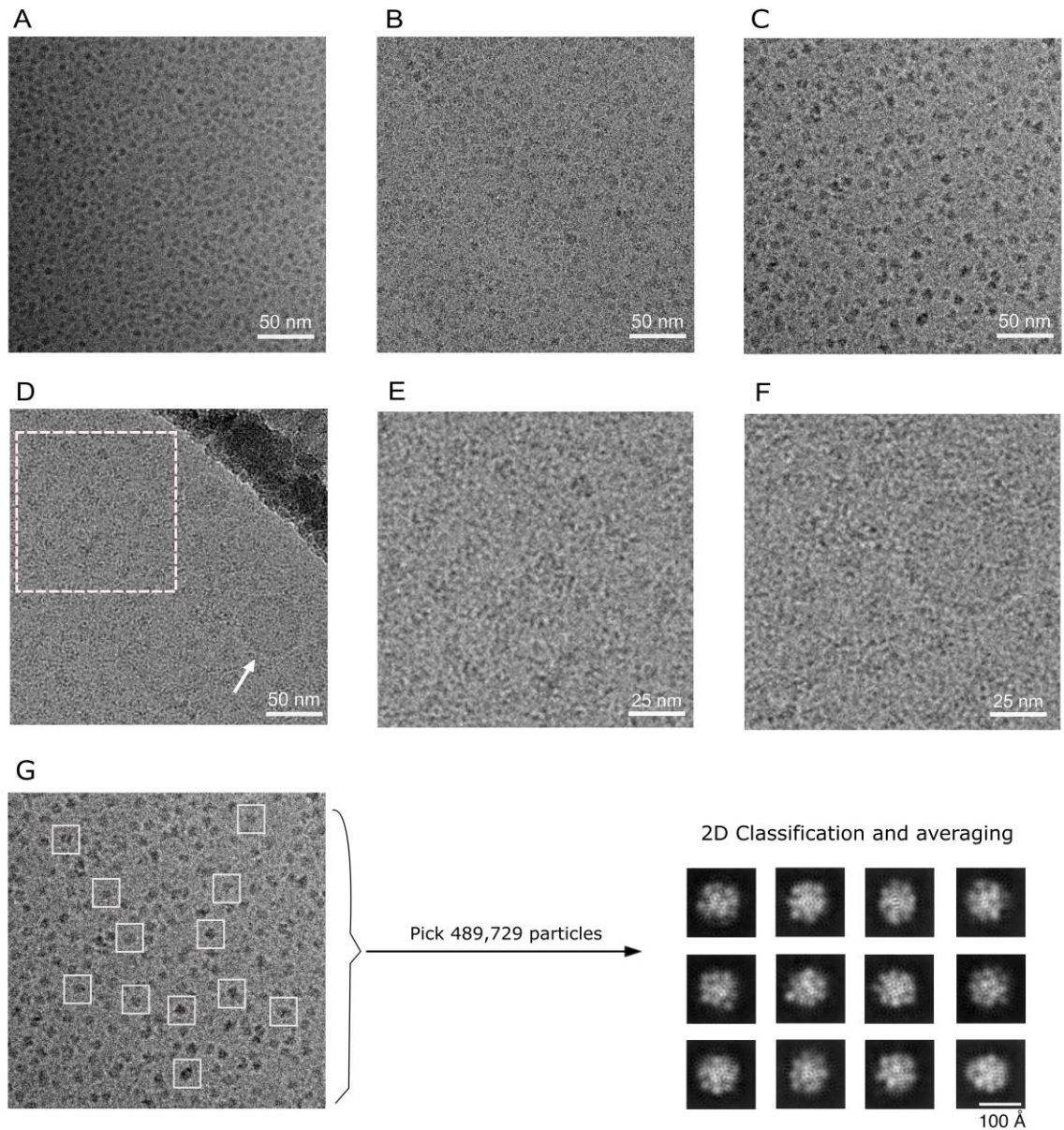


Figure 4.5. Cryo-EM analysis of Av-G4, Av-G5, Av-G6, and Av-G7. Panels (A) to (D) show representative cryo-electron micrographs obtained for the Av-G4, G5, G6 and G7

samples. (E) Zoomed-in view of the framed area in panel (D) shows the small particles in the G7 sample. (F) Zoomed-in view of the vesicle-like particle in panel (D) indicated with a white arrow as a representative example of the vesicles also observed in the G7 sample. (G) Single particle analysis of the G6 sample. About half a million particles were selected and extracted from the electron micrographs (left panel) and subjected to 2D classification and averaging. The right panel shows a few selected 2D class averages for the G6 sample.

Binding of Dendronized Biotin to Native Avidin. Isothermal titration calorimetry (ITC) was used to investigate the binding of biotin and **BGx** to native avidin (Figure 4.6a-f). The extremely strong binding interaction characteristic of the biotin:avidin complex is evident in Figure 4.6a from the steep slope at the equivalence point and $\Delta H_{\text{binding}}$ (-23.7 kcal/mol, Table 4.2), which was in good agreement with previous findings.^{15,38-41} In general, the binding isotherms also show that increasing the dendron generation attached to biotin results in increased K_d values (*i.e.*, weaker binding). This agrees with literature findings that high molecular weight biotinylated ligands,^{20,42} such as biotinylated DNA,⁴³ will typically lead to weaker association with avidin due to steric bulk, slow kinetics, and/or a poor fit within the binding pocket(s).

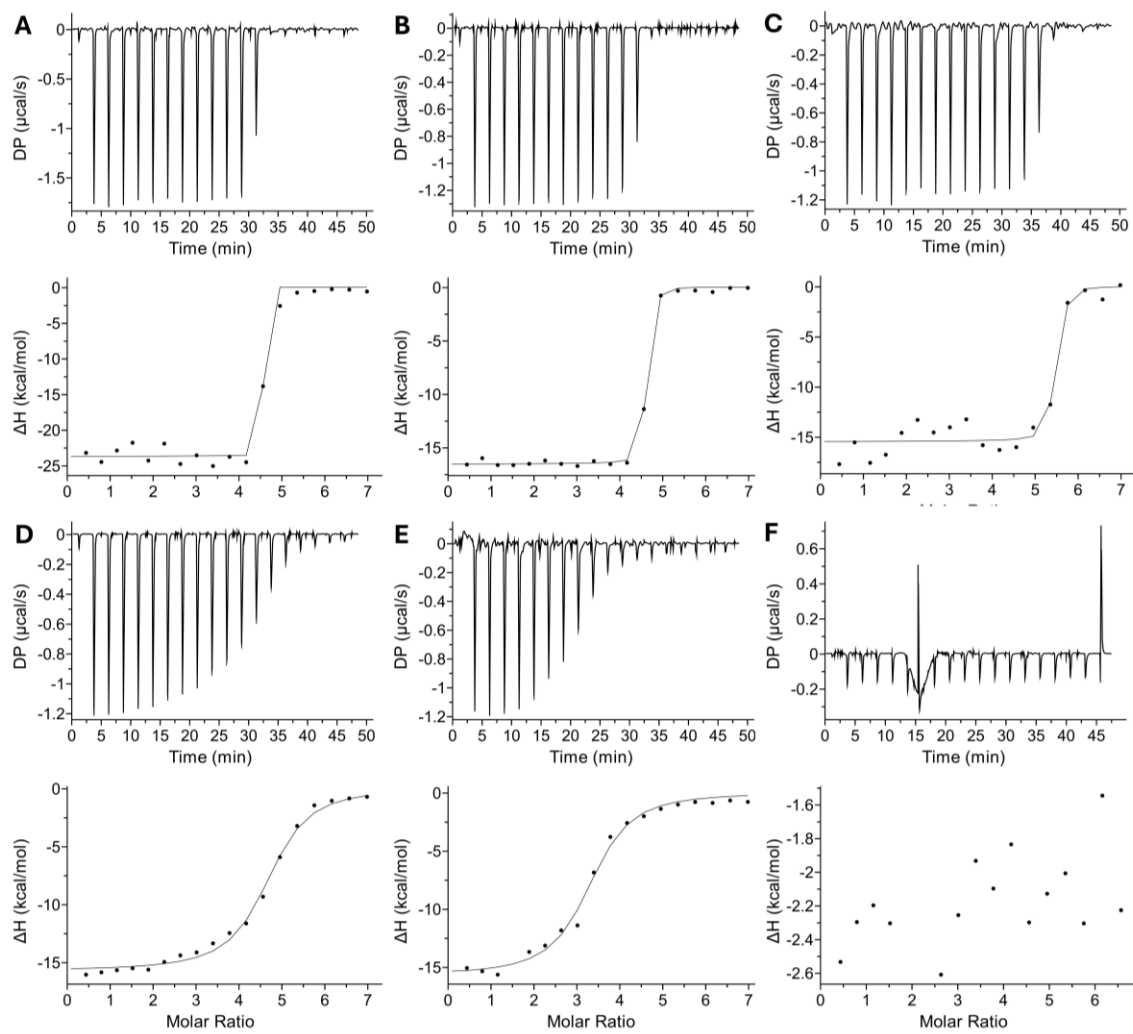


Figure 4.6. Binding of biotin and **BG_x** ($x = 3-7$) to native avidin measured by ITC. (A) Biotin, (B) **BG₃**, (C) **BG₄**, (D) **BG₅**, (E) **BG₆**, (F) **BG₇**. From the top: Row 1: Raw heats evolved from binding for titrants A-C; Row 2: Corresponding enthalpy derived from integrated heats. Rows 3-4: Raw heat evolved and corresponding enthalpy, respectively, for titrants D-F.

Table 4.2. Tabulated ITC titration data for binding of dendronized biotin (**BGx**) to native avidin.

Titrant	Bound Sites per avidin tetramer (N)	K_d (M)	ΔG (kcal/mol)	ΔH (kcal/mol)	-TΔS (kcal/mol)
Biotin	4.39	1.00E-15	-20.5	-23.7	3.26
Biotin-G3	4.45	7.59E-09	-11.1	-16.6	5.53
Biotin-G4	4.24	1.20E-08	-10.8	-14.8	3.99
Biotin-G5	4.54	5.31E-07	-8.56	-15.7	7.16
Biotin-G6	3.20	7.79E-07	-8.34	-15.7	7.38
Biotin-G7 ^a	n.b.	-	-	-	-

^a Thermograms fit the non-binding model. Parameters were not calculated; n.b. = no binding.

More specifically, the ITC data shows that the strength of the avidin-biotin interaction drops significantly upon attachment of the third-generation dendron to biotin (**BG3**), with K_d increasing by a factor of 10⁶ from biotin:avidin (Table 4.2). In general, K_d continues to increase with dendron generation from **BG4** to **BG6** (Table 4.2), however, after **BG3** the increase in K_d is relatively modest (Table 4.2 and Figure 4.7). This indicates that the weakening in biotin binding is affected to the largest extent by amidation of the valeric acid on biotin with the dendron, and marginally by dendron generation. Considering that a significant contributor to the avidin-biotin binding strength is the closure of the loop connecting β3 to β4, *i.e.*, the L3,4 loop, upon the insertion of biotin within the avidin binding pocket, any disruption to the ability of the L3,4 loop to close will significantly increase K_d.^{14,44,45} In fact, previous studies have shown that mutant proteins not having the L3,4 loop exhibit a decrease in the avidin-biotin association constant by a factor of 10⁶, exactly matching our observations.^{46,47} Furthermore, the interaction of 5'-biotinylated

DNA, having lengths between 100 and 5000 base pairs, with streptavidin-coated polystyrene particles was found to also exhibit a binding constant that was approximately six orders of magnitude lower than the streptavidin-biotin interaction.⁴³ It is likely that, in the case of dendronized biotin, the G3 dendron is large enough to sterically impede the L3,4 loop from closing, and the higher generation dendrons result in similar steric hindrance. Enthalpy of binding (ΔH) correspondingly decreases in magnitude to -16.6 kcal/mol with **BG3** and plateaus with increasing dendron generation (Table 4.2). Entropically, the difference between binding biotin and any of the dendronized biotin conjugates is minimal, as biotin binding causes displacement of water molecules present in the active site.^{44,45,47} This displacement occurs to the same extent irrespective of the dendron generation bound to biotin, so the $|T\Delta S|$ value is similar in all cases.

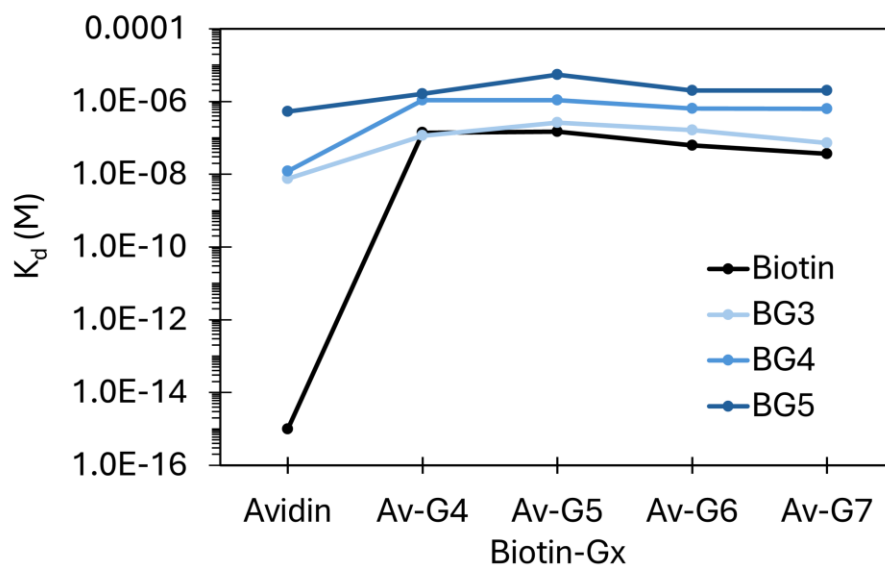


Figure 4.7. Equilibrium dissociation constants (K_d) of **BGx** binding to **Av-Gx** as measured by ITC.

The number of bound sites on an avidin tetramer (N) was also affected by biotin dendronization. The lower generation structures, **BG3**, **BG4**, and **BG5** (having molecular weights of 1.1, 2.0, and 3.9 kDa, respectively) all formed the expected 4:1 ligand:protein complexes with avidin (Table 4.2 and Figure 4.8). However, we found that **BG6** (7.6 kDa) exclusively formed a 3:1 complex, even though the vacant site maintained its ability to bind small ligands, as confirmed by complexation with 2-(4-hydroxyphenylazo)benzoic acid (HABA) and displacement of the Avidin:HABA:**BG6** complex with biotin (Figure S4.26).⁴⁸ This data indicates that there is a sharp cut-off in binding stoichiometry with increasing dendron generation from **BG5** to **BG6**. The structural similarity of these two ligands implies that it can only be their molecular weight (or hydrodynamic diameter) that is responsible for the difference in binding stoichiometry, rather than other factors such as morphology and chemical composition.^{49,50} The combination of significantly increased K_d to within the realm of reversibility in binding, and the steric repulsion of the dendritic ligands prevents binding at the fourth site when **BG6** is used. Furthermore, the largest dendronized structure we examined, **BG7** (15 kDa), did not exhibit any detectable binding to native avidin due to complete site isolation of the core (Figure 4.6F), which is characteristic of high generation dendrimers.⁵¹⁻⁵⁵ We therefore proceeded to use **BG6** as the largest dendritic ligand in subsequent binding studies of dendronized avidin conjugates.

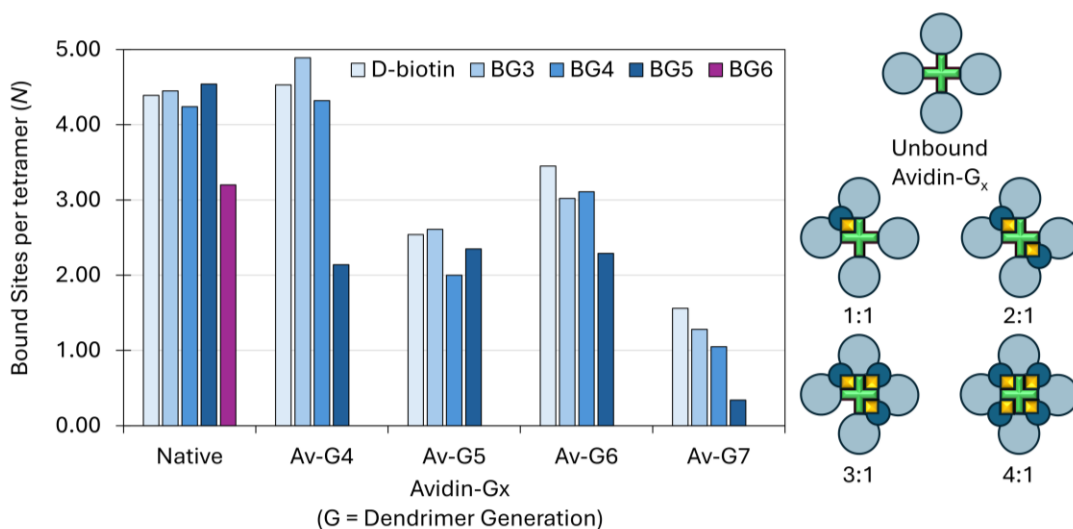


Figure 4.8. Left: Binding stoichiometry between biotin, **BG_x** and avidin and **Av-G_x**. Right: schematic representation of **BG_x : Av-G_x** complexes. Illustrations of conjugates are not to scale.

Binding of Dendronized Biotin to Dendronized Avidin. We next investigated binding of the avidin conjugates (**Av-G_x**, $x = 4-7$) with the series of dendronized biotin derivatives. Analogous to the case of native avidin, the interaction of each dendronized avidin with the series of biotin derivatives (**BG3** to **BG5**) exhibits a pattern of increasing K_d with increasing biotin dendron generation (Figure 4.7 and Table 4.3). However, the decrease in binding strength with each generation is relatively small compared to the initial jump in binding strength from native avidin-biotin. This is consistent with results reported by Russell and co-workers, who found that biotin binding was not significantly affected by increasing molecular weight of polymer chains attached to the avidin surface.¹³ The K_d values observed for **BG5** with **Av-G5** to **Av-G7** were similar to that of HABA ($K_d \sim 10^{-6}$ M).³⁶ These relatively weak binding interactions were confirmed through a series of

competitive binding experiments *via* ITC using the HABA complex of **Av-G6** as the titrand. It was found that **BG5** could not displace HABA from **Av-G6**, while biotin could partially perform the displacement (Figure S4.21). As a control, the same competitive binding experiments were conducted using the HABA complex of native avidin and we found that **BG3-BG6** were all able to displace HABA (Figure S4.20, Table S4.10-S4.11).

Table 4.3. Binding and thermodynamic parameters for binding of **BGx** by **Av-Gx**.

Titrand	Titrant	Bound Sites per avidin tetramer (N)	K_d (M)	ΔH (kcal/mol)	ΔG (kcal/mol)	-TΔS (kcal/mol)
Av-G4	Biotin	4.53	1.39E-07	-20.8	-9.36	11.5
	BG3	4.89	1.15E-07	-13.7	-9.47	4.20
	BG4	4.32	1.08E-06	-11.7	-8.14	3.59
	BG5	2.14	1.61E-06	-15.4	-7.91	7.47
	BG6 ^a	n.b.	-	-	-	-
Av-G5	Biotin	2.54	1.48E-07	-20.8	-9.32	11.5
	BG3	2.61	2.64E-07	-13.2	-8.98	4.23
	BG4	2.00	1.08E-06	-10.2	-8.15	2.04
	BG5	2.35	5.51E-06	-17.0	-7.18	9.81
	BG6 ^a	n.b.	-	-	-	-
Av-G6	Biotin	3.45	6.22E-08	-21.9	-9.84	12.1
	BG3	3.02	1.63E-07	-14.9	-9.27	5.63
	BG4	3.11	6.35E-07	-11.6	-8.46	3.18
	BG5	2.29	2.01E-06	-15.1	-7.77	7.34
	BG6	n.d.	-	-	-	-
Av-G7	Biotin	1.56	3.64E-08	-23.0	-10.2	12.8
	BG3	1.28	7.23E-08	-16.4	-9.75	6.65
	BG4	1.05	6.31E-07	-15.3	-8.46	6.85
	BG5 ^b	0.341 ^b	1.99E-06 ^b	-36.7 ^b	-7.78 ^b	28.9 ^b
	BG6 ^a	n.b.	-	-	-	-

^aNon-binding: parameters were not calculated; n.b. = no binding. ^b Due to low binding, there is significant baseline interference (see Supporting Information for thermograms).

As with native avidin, we investigated the stoichiometry between **Av-G_x** and biotin ligands (*i.e.*, biotin and **BG_x**). The conjugate with the smallest dendrons, **Av-G₄**, was found to form 4:1 complexes with biotin, **BG₃**, and **BG₄**, while only forming a 2:1 complex with **BG₅** (Figure 4.8 and Table 4.3). Considering that the binding sites are distributed as two pairs at opposite ends of the avidin tetramer,⁵⁶ we speculate that dendron-dendron interactions between the dendronized ligand and the dendrons on the protein surface can impede binding. Specifically, there is likely an additive size-exclusion effect where **BG₅** in the bound site and grafted G₄ in close proximity to the neighbouring vacant site together hinder binding at this vacant site. In contrast to native avidin, **BG₆** was completely excluded from **Av-G₄** to **Av-G₇** (Figure 4.8). Titration of **BG₆** against the smallest conjugate species, **Av-G₄**, even at elevated temperature (37 °C), did not result in any observable binding (Figure S4.23). We expected that the increase in size of the dendritic shell on avidin with growing dendron generation would exacerbate the exclusion of **BG_x** ligands. Indeed, **Av-G₅** forms exclusively 2:1 complexes with **BG₃** to **BG₅** (Figure 4.8), with ligand occupancy likely at opposite ends of avidin. However, biotin also formed a 2:1 complex, which may indicate an interference of the G₅ dendron on the protein surface with the biotin binding sites, particularly when one biotin binding site of each pair is occupied. This is consistent with the CD spectrum of **Av-G₅** (Figure 4.3) which shows a decreased β -sheet character relative to avidin. We speculate that the tertiary structure of **Av-G₅** is distorted upon conjugation to the dendrons such that only two sites are receptive toward binding. This observation indicates a negative cooperative effect (Figure 4.9), similar to what was observed in the 3:1 complex formed between **BG₆** and avidin; the tight binding

of biotin or **BGx** to one of the **Av-G5** binding sites induces conformational changes that propagate across the conjugate, rendering the binding of additional ligands to the vacant sites unfavourable (Figure 4.9). It is worthy to note that negative binding cooperativity in (strept)avidin has been documented, particularly in the case of larger biotinylated ligands.^{50,57} It has been reported that the first 3 biotin binding events result in larger structural changes to the protein compared to the final one,^{56,58} which is consistent with our findings, particularly with 1:1 and 3:1 complexes (e.g., native avidin : **BG6**). In the case of **Av-G5**, the dendritic layer likely exerts structural changes to avidin (as seen in CD) and the initial two binding events inhibit further binding regardless of ligand size, thus indicating that this negative cooperative effect is also exacerbated by the grafted dendrons. Interestingly, **Av-G6** was trivalent while binding biotin, **BG3** and **BG4** and divalent when binding **BG5**. This increased binding to **Av-G6** versus **Av-G5** may be attributed to an increased distance of the G6 surface dendrons from the avidin surface relative to G5, the latter of which has been shown to adopt a more ellipsoid conformation and “flatten” onto the surface of other molecules.⁵⁹ Finally, investigation of **Av-G7** showed that biotin, **BG3**, and **BG4** all form roughly 1:1 complexes, while an average of 0.3 molecules of **BG5** were bound to each tetramer (Figure 4.8), thus indicating that the combined steric hindrance and negative cooperative effects imparted by G7 surface dendrons and the guest dendron inhibit further binding. Note that the β -sheet character of the conjugates as measured by CD correlates to their binding stoichiometry, in that **Av-G4** and **Av-G6** had an increase in β -sheet character relative to avidin and are also higher in binding versus their higher-generation counterparts (*i.e.*, **Av-G5** and **Av-G7**, respectively). Our findings reveal that,

counterintuitively, the stoichiometry of binding of biotin is nonlinear versus the size of the grafted dendron, and molecular sieving with multivalent conjugates is much more nuanced than that of monovalent systems. Specifically, in addition to steric effects, one must consider dynamic structural changes stemming from the grafting polymer layer and binding events, which can further change the stoichiometry of the conjugate.

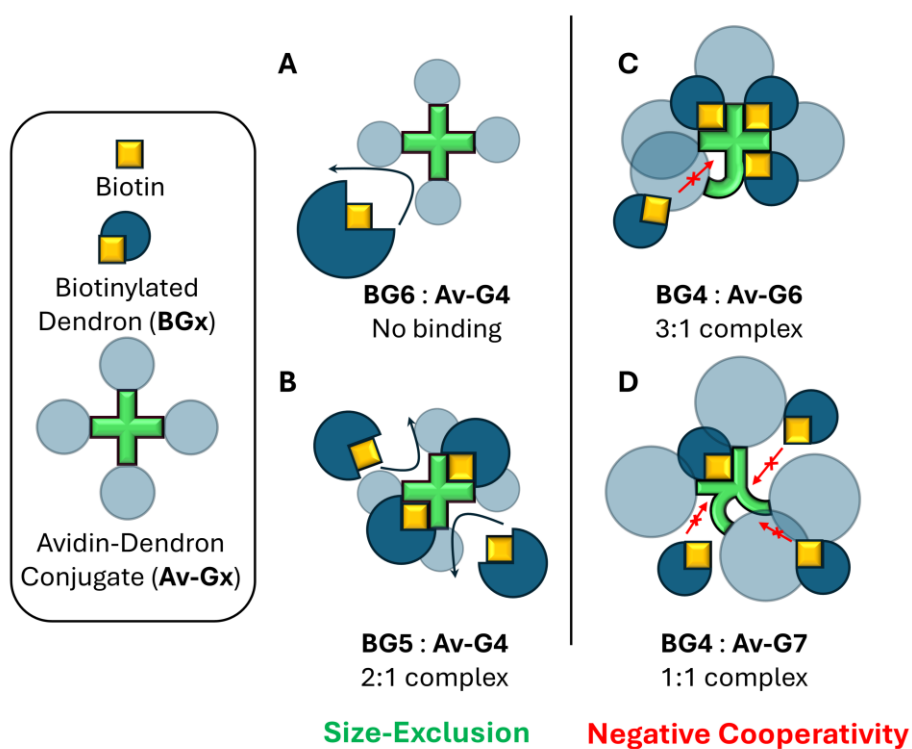


Figure 4.9. A comparison of size-exclusion effects (left) and negatively cooperative effects (right) in avidin-dendron conjugates. A. Grafted dendrons (light blue spheres) on **Av-G4** exclude the access of **BG6** (dark blue spheres) to the binding sites. B. **Av-G4** preferentially binds two molecules of **BG5** at opposing binding sites, which then act as an additional steric barrier to exclude **BG5** from further binding. C. **BG4** binds three subunits of **Av-G6** and distorts the remaining site, inhibiting further binding. D. **BG5** binds an already compromised **Av-G7**, further distorts the vacant subunits, preventing further binding. Structures are not drawn to scale – size discrepancy between ligands are illustrated by differently sized cartoons.

Binding of Non-dendrimer Biotinylated Ligands to Av-Gx.

The molecular weight of the biotin-functionalized dendrons approximately doubles with each generation from ~1.1 kDa (**BG3**) to 15 kDa (**BG7**). While **BG3-BG5** represent the weight range of oligopeptides or very small proteins, the G6 and G7 dendrons have hydrodynamic diameters (D_h) that roughly correspond to small or mid-size proteins ($D_h \sim 3-4$ nm, Table 4).⁶⁰ Considering that **BG6** was the smallest biotin conjugate to be completely excluded from all **Av-Gx** structures, its size corresponds to the size of a biotinylated protein that will be unable to bind any of the avidin conjugates. Conversely, **BG5** was able to bind to all **Av-Gx** conjugates, so its size should correspond to the maximum size of a protein that will exhibit some degree of binding. We hypothesized that these bounds could serve as an estimate for the interstitial space, i , between grafted dendrons on avidin. To test these bounds ($1.95 < i \leq 3.21$ nm, Figure 4.10), aprotinin (~6.9 kDa, $D_{h(\min)} = 2.7$ nm) was used as a globular protein similar to **BG6** (7.7 kDa) in molecular weight and morphology.⁶¹ Biotinylated BSA (~66 kDa, $D_h \sim 7$ nm) was used as a negative control as it is not expected to bind to **Av-Gx** due to its large size and rigidity.⁶⁰ Unsurprisingly, although biotinylated BSA binds to native avidin, its titration against dendronized avidin did not result in observable binding (Figure S4.22). Similar studies using biotinylated aprotinin demonstrated that it too can bind native avidin (Figure 4.9C), but exhibited no binding, even to **Av-G4**, which represents the least sterically hindered conjugate (Figure 4.9D, Figure 4.38), thereby validating our established boundaries for the interstitial space between the dendrons. Lastly, to test whether a morphologically irregular ligand would penetrate the dendritic shell, the biotinylated ligand 1,2-distearoyl-sn-

glycero-3-phosphoethanolamine-N-[biotinyl(polyethylene glycol), DSPE-PEG₃₄₀₀-biotin, was investigated. This PEGylated ligand was chosen because PEG exhibits a random-coil configuration and relatively high flexibility in aqueous solution, which has been shown to enhance diffusion through the surface dendron layer.¹¹ Although this structure likely forms micelles (DLS indicated a $D_h = 52\text{-}53$ nm, see Figure S4.17) it is able to bind native avidin at all four sites, while exhibiting no binding to **Av-G4** (Table S4.7 and Figure S4.22). All of these examples indicate that the dendronized avidin structure represents an effective molecular sieving system having a cutoff within the proposed bounds.

Table 4.4. Molecular weight and hydrodynamic diameters of hydroxyl (OH)-periphery dendrons

Compound	MW (kDa)	Hydrodynamic Radius (D_h nm)
Biotin	0.244	-
G3-(OH) ₈	1.13	0.640 ^a
G4-(OH) ₁₆	2.06	1.12 ^a
G5-(OH) ₃₂	3.91	1.95^a
G6-(OH) ₆₄	7.65	3.21^b
G7-(OH) ₁₂₈	15.1	4.50 ^b
G8-(OH) ₂₅₆	30.0	5.96 ^b

^a Interpolated from 3rd order polynomial regression of reported D_h for G6-G8 dendrons ($r^2 = 1.00$).

^b Previously reported volume-average D_h .¹¹ Highlighted values indicate our proposed bounds for interstitial space between dendrons grafted onto avidin.

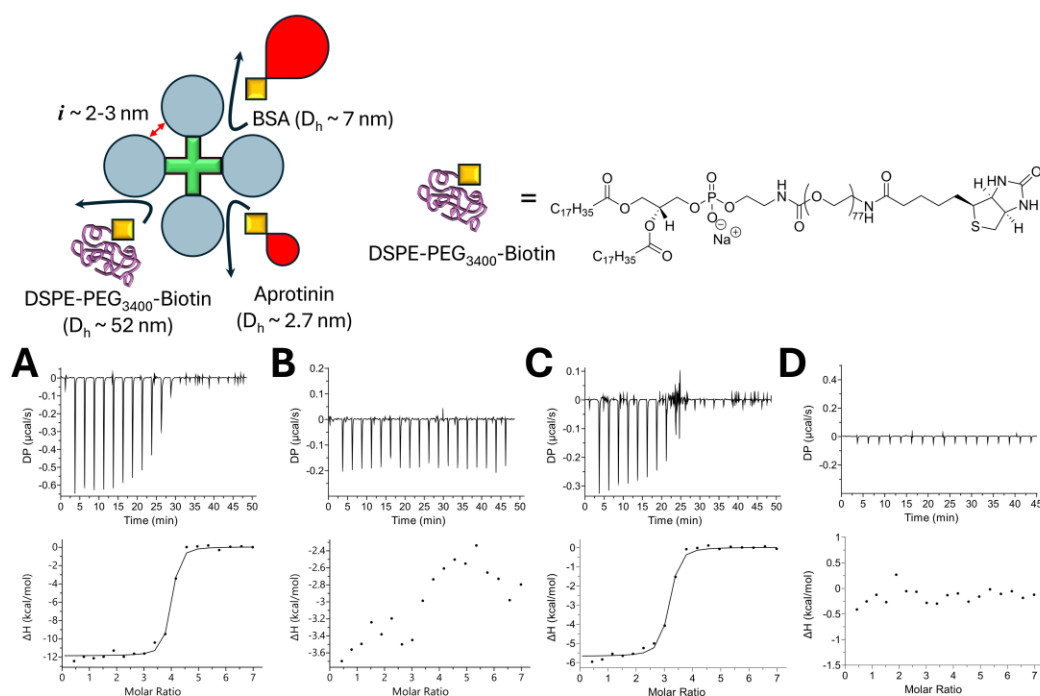


Figure 4.10. Top: Schematic representation of interstitial space between grafted dendrons in Av-Gx and sieving of various biotinylated ligands. Structures are not drawn to scale. Bottom: Binding of two small biotinylated ligands, aprotinin and PEG₃₄₀₀, to avidin and Av-G4 measured by ITC. **A.** native avidin : PEG₃₄₀₀. **B.** Av-G4 : PEG₃₄₀₀. **C.** native avidin : aprotinin. **D.** Av-G4 : aprotinin.

The exclusion of non-dendronized ligands indicates that the observed molecular sieving with Av-Gx is not specific to polymeric ligands that entangle or hydrogen bond with one another,⁶² but is rather a general phenomenon driven by steric interactions and size exclusion. We have shown that the size limits for penetration of the diffusional barrier on a protein surface can be empirically defined using controlled grafting of uniform polymer and ligand architectures. We were also able to modulate the binding of biotinylated ligands below a 10 kDa threshold, which can potentially expand the selectivity of avidin-biotin-based systems used for ligand purification.¹⁸ The diverse binding

stoichiometries observed in this work, as imparted by both dendron conjugation and dendronization of the biotin ligand, allow tailoring of the system to a wide range of applications that require precise valency without making genetic modifications to (strept)avidin-producing organisms.^{50,63–65}

4.4 Conclusion

We have synthesized and characterized a series of polyester dendron-avidin conjugates that exhibit a molecular sieving effect controllable within the sub-10 kDa range of ligands. Through systematic ITC studies using biotin-core dendrons of different generations, we found that the interstitial space between the grafted dendrons on the avidin surface can be limited to 2-3 nm and completely excludes ligands above 7 kDa. Our work shows a specific molecular weight cut-off within a polymer-protein conjugate. Beyond the molecular sieving effect, we also show evidence for a negatively cooperative effect on avidin upon large dendron conjugation that controls the sequential binding of biotin and biotinylated ligands, which is consistent with previous work. Avidin and avidin-dendron conjugates were both found to selectively form fractional complexes with biotin-dendrons and their binding stoichiometries were tunable by altering dendron generations on both biotin and avidin. Increasing the dendron generation on biotin also correlated to weaker binding to avidin and avidin-dendron conjugates. This work not only provides a new example of molecular sieving through functionalization of proteins with well-defined, highly branched macromolecules, but also demonstrates the ability to tune the strength and stoichiometry of the avidin-biotin interaction, which may have important applications in manufacturing protein-ligand nano-assemblies and multivalent avidin sensors.

4.5 Supporting Information

General Procedure 1: Synthesis of CBz-core G2-G7 Acetonide-Periphery Dendrimers

Under a nitrogen atmosphere, an oven-dried round bottom flask was charged with a magnetic stir bar, CBz-G_x-(OH)₂^x (1 eq.), acetonide-protected bis-MPA (1.5 eq. per dendrimer periphery OH), NMI (3.5 eq. per dendrimer periphery OH), and acetonitrile (1.25 mL per mmol acetonide-protected bis-MPA). The mixture was stirred at room temperature for 10 minutes until fully dissolved. TCFH (1.5 eq. per dendrimer periphery OH) was added in a single portion. The reaction mixture was allowed to stir for 20 minutes (reaction is exothermic upon addition of TCFH) and was monitored by TLC (40% acetone in hexanes, stained with PMA). Upon completion, the crude mixture was diluted in ten volume equivalents of ethyl acetate and washed with dH₂O and brine. The organic layer was dried with MgSO₄ and concentrated by rotary evaporation. For G3-5 dendrimers, the crude material was purified by flash chromatography using a gradient of 0-40% acetone in hexanes and monitored at 215 nm. Fractions containing product were combined, concentrated by rotary evaporation, and dried under vacuum to afford CBz-G_{x+1}-(acet)₂^x as a clear viscous oil. Reactions containing G6 and G7 dendrimers were purified by SEC chromatography using Sephadex LH-20 as the stationary phase and methanol as the eluent.

General Procedure 2: Synthesis of OH-Periphery Dendrimers

Adapted from previous procedures.¹² A round bottom flask was charged with a magnetic stir bar, CBz-G_x-(acet)₂^{x-1} (1 eq.), MeOH (~50 mL per mmol dendrimer periphery acetonide), and catalytic amounts of DOWEX® 50WX2 DVB-supported sulfonic acid

resin. The reaction was allowed to stir at room temperature until completion as monitored by TLC (40% acetone in hexanes, stained with PMA), ESI-MS and/or ^1H NMR. The mixture was vacuum filtered, and the resin was rinsed with MeOH. The solution was concentrated by rotary evaporation and dried *in vacuo* to afford CBZ-G_x-(OH)₂^x.

CBZ-G1-Acet

An oven-dried 100 mL round bottom flask was charged with a magnetic stir bar, 1,1-carbonyldiimidazole (11.28 g, 70 mmol), and ethyl acetate (30 mL). The CDI suspension was stirred rapidly at 50 °C while acetonide-protected bis-MPA (12.72 g, 73 mmol) was added in small portions over two minutes. The reaction was allowed to stir at 50 °C for 30 minutes with a bleed needle attached to allow for the venting of CO₂. *N*-Z-1,4-butanediamine hydrochloride (9.0 g, 35 mmol) and TEA (17 mL, 122 mmol) were added, and the reaction was allowed to stir for 3 h at 50 °C. The reaction was cooled to room temperature and diluted with ethyl acetate (120 mL). The organic phase was washed with H₃PO₄ (1 M, 3 x 30 mL), Na₂CO₃ (1 M, 3 x 30 mL) and brine (1 x 30 mL) and dried over MgSO₄. The crude mixture was concentrated using a rotary evaporator and purified using a 120 g silica Sorbtech EZ Flash column with 10-40% acetone in hexanes (loaded in DCM) and monitored at 205 nm. Fractions containing the product were combined, concentrated by rotary evaporation, and dried under vacuum to afford the CBZ-G1-Acet as a white waxy solid (Yield = 11.1 g, 84%). ^1H NMR (600 MHz, CDCl₃) δ 7.35 (d, J = 4.4 Hz, 4H), 7.33 – 7.27 (m, 1H), 7.10 (br s, 1H), 5.09 (s, 2H), 4.85 (s, 1H), 3.90 (d, J = 12.0 Hz, 2H), 3.76

(d, $J = 12.5$ Hz, 2H), 3.42 – 3.18 (m, 4H), 1.47 (s, 3H), 1.41 (s, 3H), 1.00 (s, 3H). Spectral data matches previously reported in literature.¹²

Cbz-G1-(OH)₂

Following General Procedure 2, Cbz-G1-Acet (745 mg, 1.97 mmol) was dissolved in 110 mL of MeOH followed by the addition of DOWEX® resin (1 scoop, ~1 g) and was allowed to stir for 3 h. (Yield: 666 mg, 99%). ¹H NMR (600 MHz, MeOD): δ 7.34-7.27 (m, 5H), 5.09 (s, 2H), 3.65 (d, $J = 10.94$ Hz, 2H), 3.60 (d, $J = 10.94$ Hz, 2H), 3.22-3.12 (m, 4H), 1.53-1.49 (m, 4H), 1.09 (s, 3H). Spectral data matches previously reported in literature.¹²

Cbz-G2-(acet)₂

Following General Procedure 1, acetonide-protected bis-MPA (4.17 g, 23.95 mmol) and CBz-G1-(OH)₂ (2.70 g, 7.98 mmol) were suspended in dry ACN (20 mL), followed by addition of NMI (4.5 mL, 56 mmol). Upon complete dissolution, TCFH (6.72 g, 23.95 mmol) was added in a single portion and the reaction was allowed to stir for 20 minutes. The reaction was diluted in 200 mL of ethyl acetate and washed with dH₂O (6 x 40 mL) and brine (1 x 40 mL). The organic layer was dried with MgSO₄ and concentrated by rotary evaporation. The crude material was purified by flash chromatography using a gradient of 0-40% acetone in hexanes and monitored at 215 nm. Fractions containing product were concentrated by rotary evaporation and dried under vacuum to afford CBz-G2-(acet)₂ as a clear viscous oil (Yield: 4.4 g, 84%). ¹H NMR (600 MHz, CDCl₃): δ 7.35-7.28 (m, 5H), 6.50 (s, 1H), 5.07 (s, 2H), 4.93 (s, 1H), 4.33 (d, $J = 11.25$ Hz, 2H), 4.26 (d, $J = 11.26$ Hz, 2H), 4.14 (d, $J = 11.90$ Hz, 4H), 3.63-3.61 (m, 4H), 3.26-3.15 (m, 4H), 1.52-1.47 (m, 4H),

1.39 (s, 6H), 1.32 (s, 6H), 1.23 (s, 3H), 1.07 (s, 6H). Spectral data matches previously reported in literature.¹²

Cbz-G2-(OH)₄

Following General Procedure 2, Cbz-G2-(acet)₂ (4.0 g, 6.15 mmol) was dissolved in 500 mL of MeOH followed by the addition of DOWEX® (4 scoops, ~4 g) and was allowed to stir for 3 h. (Yield: 3.5 g, 99%). ¹H NMR (600 MHz, MeOD): δ 7.37-7.30 (m, 5H), 5.06 (s, 2H), 4.28-4.22 (m, 4H), 3.68 (d, *J* = 10.84 Hz, 4H), 3.59 (d, *J* = 10.87 Hz, 4H), 3.23-3.11 (m, 4H), 1.56-1.48 (m, 4H), 1.27 (s, 3H), 1.15 (s, 6H). Spectral data matches previously reported in literature.¹²

Cbz-G3-(acet)₄

Following General Procedure 1, acetonide-protected bis-MPA (5.79 g, 33.2 mmol) and CBz-G2-(OH)₄ (3.16 g, 5.54 mmol) were suspended in 27 mL of dry ACN, followed by addition of NMI (6.18 mL, 77.5 mmol). Upon complete dissolution, TCFH (9.32 g, 33.22 mmol) was added in a single portion and the reaction was allowed to stir for 20 minutes. The reaction was diluted in 270 mL of ethyl acetate and washed with dH₂O (6 x 60 mL) and brine (1 x 60 mL). The organic layer was dried with MgSO₄ and concentrated by rotary evaporation. The crude material was purified by flash chromatography using a gradient of 0-40% acetone in hexanes and monitored at 215 nm. Fractions containing product were concentrated by rotary evaporation and dried under vacuum to afford Cbz-G3-(acet)₄ as a clear viscous oil (Yield: 5.58 g, 84%). ¹H NMR (600 MHz, CDCl₃): δ 7.33-7.27 (m, 5H), 6.37 (br s, 1H), 5.39 (br s, 1H), 5.06 (s, 2H), 4.33-4.17 (m, 12H), 4.13-4.09 (m, 8H), 3.61-

3.56 (m, 8H), 3.28-3.17 (m, 4H), 1.56-1.50 (m, 4H), 1.37 (s, 12H), 1.30 (s, 12H), 1.23-1.21 (m, 9H), 1.08 (s, 12H). Spectral data matches previously reported in literature.¹²

Cbz-G3-(OH)₈

Following General Procedure 2, Cbz-G3-(acet)₄ (1.52 g, 1.27 mmol) was dissolved in 600 mL of MeOH followed by the addition of DOWEX resin (3 scoops, ~3 g) and was allowed to stir for 3 h. (Yield: 1.3 g, 99%). ¹H NMR (600 MHz, MeOD): δ 7.38-7.27 (m, 5H), 5.07 (s, 2H), 4.31-4.21 (m, 12H), 3.68-3.66 (m, 8H), 3.57-3.60 (m, 8H), 3.23-3.13 (m, 4H), 1.57-1.49 (m, 4H), 1.29-1.27 (m, 9H), 1.15 (s, 12H). Spectral data matches previously reported in literature.¹²

CBz-G4-(Acet)₈

Following General Procedure 1, acetonide-protected bis-MPA (982 mg, 5.63 mmol) and CBz-G3-(OH)₈ (486 mg, 0.47 mmol) were suspended in 4.7 mL of dry ACN, followed by addition of NMI (1.05 mL, 13.2 mmol). Upon complete dissolution, TCFH (1.58 g, 5.63 mmol) was added in a single portion and the reaction was allowed to stir for 20 minutes. The reaction was diluted in 50 mL of ethyl acetate and washed with dH₂O (6 x 10 mL) and brine (1 x 10 mL). The organic layer was dried with MgSO₄ and concentrated by rotary evaporation. The crude material was purified by flash chromatography using a gradient of 0-40% acetone in hexanes and monitored at 215 nm. Fractions containing product were concentrated by rotary evaporation and dried under vacuum to afford CBz-G4-(acet)₈ as a white foam (Yield: 910 mg, 85%). ¹H NMR (600 MHz, CDCl₃) δ 7.38 – 7.28 (m, 5H), 6.46 (t, *J* = 5.9 Hz, 1H), 5.35 (t, *J* = 6.1 Hz, 1H), 5.07 (s, 2H), 4.37 – 4.19 (m, 28H), 4.13 (d, *J*

= 13.1 Hz, 16H), 3.61 (dd, $J = 11.7, 2.4$ Hz, 16H), 3.36 – 3.08 (m, 4H), 1.57 – 1.50 (m, 4H), 1.40 (s, 24H), 1.34 (s, 21H), 1.30 – 1.22 (m, 21H), 1.12 (s, 24H). ^{13}C NMR (151 MHz, CDCl_3) δ 173.73, 173.71, 173.68, 172.09, 172.05, 171.66, 171.47, 156.69, 136.85, 128.62, 128.30, 128.20, 98.26, 67.52, 66.66, 66.11, 66.06, 65.83, 65.78, 64.97, 64.96, 53.57, 47.00, 46.89, 46.51, 42.20, 40.69, 39.67, 27.51, 26.97, 25.47, 25.45, 25.43, 22.09, 22.08, 22.06, 18.63, 17.83, 17.68. MS (ESI⁺) m/z calc'd for $\text{C}_{111}\text{H}_{170}\text{N}_2\text{O}_{47}$ $[\text{M}+\text{H}]^+ = 2285.11$, found $[\text{M}+\text{H}]^+ 2285.11$, $[\text{M}+\text{H}+\text{NH}_4]^{2+} = 1151.57$.

CBz-G4-(OH)₁₆

Following General Procedure 2, Cbz-G4-(acet)₈ (2 g, 0.88 mmol) was dissolved in 400 mL of MeOH followed by the addition of DOWEX resin (2 scoops, ~2 g) and was allowed to stir for 3 h. (Yield: 1.68 g, 98%). ^1H NMR (600 MHz, MeOD) δ 7.48 – 7.24 (m, 5H), 5.07 (s, 2H), 4.52 – 4.06 (m, 28H), 3.72 – 3.63 (m, 16H), 3.60 (d, $J = 10.9$ Hz, 16H), 3.24 (t, $J = 6.8$ Hz, 2H), 3.15 (t, $J = 6.5$ Hz, 2H), 1.64 – 1.48 (m, 4H), 1.36 – 1.27 (m, 21H), 1.15 (s, 24H). ^{13}C NMR (151 MHz, MeOD) δ 175.94, 174.28, 173.81, 173.35, 158.91, 138.46, 129.50, 128.98, 128.84, 68.32, 67.38, 67.09, 66.17, 65.98, 65.85, 51.81, 48.09, 47.95, 47.68, 41.46, 40.56, 28.38, 27.83, 18.33, 18.19, 18.13, 17.36. MS (ESI⁺) m/z calc'd for $\text{C}_{87}\text{H}_{138}\text{N}_2\text{O}_{47}$ $[\text{M}+\text{H}]^+ = 1963.85$, found $[\text{M}+\text{Na}]^+ = 1985.84$.

CBz-G5-(Acet)₁₆

Following General Procedure 1, acetonide-protected bis-MPA (2.25 g, 12.9 mmol) and CBz-G4-(OH)₁₆ (1.06 g, 0.54 mmol) were suspended in 17 mL of dry ACN, followed by addition of NMI (2.4 mL, 30.4 mmol). Upon complete dissolution, TCFH (3.62 g, 12.9

mmol) was added in a single portion and the reaction was allowed to stir for 20 minutes. The reaction was diluted in 170 mL of ethyl acetate and washed with dH₂O (6 x 40 mL) and brine (1 x 40 mL). The organic layer was dried with MgSO₄ and concentrated by rotary evaporation. The crude material was purified by flash chromatography using a gradient of 0-40% acetone in hexanes and monitored at 215 nm. Fractions containing product were concentrated by rotary evaporation and dried under vacuum to afford CBz-G5-(acet)₁₆ as a white foam (Yield: 2.21 g, 91%). ¹H NMR (600 MHz, CDCl₃) δ 7.33 (s, 5H), 5.50 (br s, 1H), 5.06 (s, 2H), 4.42 – 4.18 (m, 60H), 4.13 (d, *J* = 11.7 Hz, 32H), 3.61 (dd, *J* = 11.6, 2.5 Hz, 32H), 3.39 – 3.01 (m, 4H), 1.55 – 1.49 (m, 4H), 1.40 (s, 48H), 1.33 (s, 48H), 1.29 – 1.24 (m, 45H), 1.12 (s, 48H). ¹³C NMR (151 MHz, CDCl₃) δ 207.1, 173.7, 172.0, 171.7, 171.5, 136.9, 128.6, 128.3, 128.2, 98.2, 66.1, 65.5, 64.9, 47.0, 46.8, 42.2, 38.8, 31.1, 25.5, 22.1, 18.6, 17.8, 17.6, 17.6. MS (ESI⁺) *m/z* calc'd for C₂₁₅H₃₃₀N₂O₉₅ [M+H]⁺ = 4463.12, found [M+2K]²⁺ = 2270.54, [M+Na+K]²⁺ = 2262.03, [M+H+K]²⁺ = 2251.05.

CBz-G5-(OH)₃₂

Following General Procedure 2, Cbz-G5-(acet)₁₆ (2.95 g, 0.66 mmol) was dissolved in 600 mL of MeOH followed by the addition of DOWEX resin (1 scoop, ~1 g) and was allowed to stir for 12 h. (Yield: 2.5 g, 99%). ¹H NMR (600 MHz, MeOD) δ 7.45 – 7.23 (m, 5H), 5.08 (s, 0H), 4.41 – 4.20 (m, 12H), 3.72 – 3.63 (m, 6H), 3.61 (d, *J* = 10.8 Hz, 6H), 3.26 (d, *J* = 4.4 Hz, 2H), 3.17 (d, *J* = 6.8 Hz, 2H), 1.56 (s, 4H), 1.15 (s, 48H). ¹³C NMR (151 MHz, CDCl₃) δ 173.79, 172.50, 156.56, 136.71, 128.61, 128.26, 128.21, 98.41, 66.72, 66.50, 66.29, 66.24, 53.55, 46.75, 42.37, 40.72, 39.33, 31.03, 27.31, 26.76, 26.48, 20.99, 18.41,

17.90. MS (ESI⁺) *m/z* calc'd for C₁₆₇H₂₆₆N₂O₉₅ [M+H]⁺ = 3822.62, found [M+2Na]²⁺ = 1933.80, [M+3Na]³⁺ = 1296.86.

CBz-G6-(Acet)₃₂

Following General Procedure 1, acetonide-protected bis-MPA (3.20 g, 18.4 mmol) and CBz-G5-(OH)₃₂ (1.46 g, 0.38 mmol) were suspended in 14 mL of dry ACN, followed by addition of NMI (3.42 mL, 42.92 mmol). Upon complete dissolution, TCFH (5.16 g, 18.4 mmol) was added in a single portion and the reaction was allowed to stir for 20 minutes. The reaction was diluted in 140 mL of ethyl acetate and washed with dH₂O (6 x 30 mL) and brine (1 x 30 mL). The organic layer was dried with MgSO₄ and concentrated by rotary evaporation. The crude material was redissolved in MeOH (1 mL) and purified by SEC chromatography using Sephadex LH-20 as the stationary phase and methanol as the eluent. Fractions containing product were concentrated by rotary evaporation and dried under vacuum to afford CBz-G6-(acet)₃₂ as a white foam (Yield: 2.52 g, 75%). ¹H NMR (600 MHz, CDCl₃) δ 7.36 – 7.31 (m, 5H), 6.67 (br s, 1H), 5.67 (br s, 1H), 5.07 (s, 2H), 4.42 – 4.22 (m, 124H), 4.15 (d, *J* = 11.7 Hz, 64H), 3.63 (dd, *J* = 11.6, 2.9 Hz, 64H), 3.36 – 3.08 (m, 4H), 1.42 (s, 96H), 1.36 (s, 96H), 1.32 – 1.26 (m, 96H), 1.15 (s, 96H). ¹³C NMR (151 MHz, CDCl₃) δ 173.60, 171.98, 171.57, 171.35, 128.61, 128.21, 98.20, 66.08, 66.02, 65.95, 65.28, 64.83, 46.95, 46.93, 46.88, 46.77, 42.16, 25.35, 22.24, 18.65, 17.88, 17.70, 17.50. MS (ESI⁺) *m/z* calc'd for C₄₂₃H₆₅₀N₂O₁₉₂ [M+H]⁺ = 8834.14, found [M+3H]³⁺ = 2945.40.

CBz-G6-(OH)₆₄

Following General Procedure 2, Cbz-G6-(acet)₃₂ (2.0 g, 0.45 mmol) was dissolved in 600 mL of MeOH followed by the addition of DOWEX resin (3 scoops, ~3 g) and was allowed to stir for 3 h. (Yield: 1.30 mg, 99%). ¹H NMR (600 MHz, MeOD) δ 7.48 – 7.19 (m, 5H), 5.08 (d, *J* = 6.1 Hz, 2H), 4.44 – 4.19 (m, 124H), 3.77 – 3.57 (m, 124H), 3.29 – 3.23 (m, 2H), 3.21 – 3.13 (m, 2H), 1.57 (s, 1H), 1.40 – 1.26 (m, 93H), 1.15 (s, 96H). ¹³C NMR (151 MHz, MeOD) δ 176.23, 175.95, 173.83, 173.60, 173.46, 173.32, 173.24, 66.18, 65.88, 51.80, 51.77, 49.85, 48.07, 47.94, 38.88, 18.39, 18.01, 17.45, 17.31, 17.23.

CBz-G7-(Acet)₆₄

Following General Procedure 1, acetonide-protected bis-MPA (923 mg, 5.30 mmol) and CBz-G6-(OH)₆₄ (417 mg, 55.2 μmol) were suspended in 7 mL of dry ACN, followed by addition of NMI (1.0 mL, 12.4 mmol). Upon complete dissolution, TCFH (1.49, 5.30 mmol) was added in a single portion and the reaction was allowed to stir for 20 minutes. The reaction was diluted in 70 mL of ethyl acetate and washed with dH₂O (6 x 15 mL) and brine (1 x 20 mL). The organic layer was dried with MgSO₄ and concentrated by rotary evaporation. The crude material was redissolved in MeOH (1 mL) and purified by SEC chromatography using Sephadex LH-20 as the stationary phase and methanol as the eluent. Fractions containing product were concentrated by rotary evaporation and dried under vacuum to afford CBz-G6-(acet)₃₂ as a white foam (Yield: 804 mg, 83%). ¹H NMR (600 MHz, CDCl₃) δ 6.70 (br s, 1H), 5.74 (br s, 1H), 5.02 (s, 2H) 4.51 – 4.17 (m, 124H), 4.11 (d, *J* = 11.7 Hz, 128H), 3.62 (d, *J* = 11.7, 128H), 3.36 – 3.08 (m, 4H), 1.39 (s, 192H), 1.32 (s, 192H), 1.29 – 1.22 (m, 192H), 1.09 (s, 192H). ¹³C NMR (151 MHz, CDCl₃) δ 173.67,

172.04, 98.21, 66.06, 66.01, 65.21, 64.83, 42.16, 38.76, 31.08, 25.42, 22.17, 18.60, 17.87, 17.69.

CBz-G7-(OH)₁₂₈

Following General Procedure 2, Cbz-G7-(acet)₆₄ (100 mg, 5.7 μ mol) was dissolved in 20 mL of MeOH followed by the addition of DOWEX resin (1 scoops, \sim 0.5 g) and was allowed to stir for 4. (Yield: 85 mg, 99%). ¹H NMR (600 MHz, MeOD) δ 7.48 – 7.19 (m, 5H), 5.08 (d, J = 6.1 Hz, 2H), 4.44 – 4.19 (m, 124H), 3.77 – 3.57 (m, 124H), 3.29 – 3.23 (m, 2H), 3.21 – 3.13 (m, 2H), 1.57 (s, 1H), 1.40 – 1.26 (m, 93H), 1.15 (s, 96H). ¹³C NMR (151 MHz, MeOD) δ 176.23, 175.95, 173.83, 173.60, 173.46, 173.32, 173.24, 66.18, 65.88, 51.80, 51.77, 49.85, 48.07, 47.94, 38.88, 18.39, 18.01, 17.45, 17.31, 17.23.

Synthesis of Biotin- and DBCO-core Bis-MPA Dendrimers

General Procedure 3: Synthesis of H₂N-core OH-periphery Dendrimers

Adapted from previous literature procedures.¹¹ A round bottom flask was charged with a magnetic stir bar, Cbz-G_x-(OH)_y, 10 % Pd(OH)₂/C (10 wt. % of dendrimer), and a solution of 1:1 DCM:MeOH. The reaction vessel was purged under vacuum and backfilled with hydrogen gas three times and was allowed to stir overnight at room temperature under a hydrogen atmosphere. The solution was filtered over a 0.45 μ m PTFE membrane, concentrated by rotary evaporation, and dried *in vacuo* to afford H₂N-G_x-(OH)_y as a white waxy foam.

H₂N-G3-(OH)₈

Prepared according to literature procedures.¹¹ (Yield = 1.2 g, 99%). ¹H NMR (600 MHz, MeOD) δ 4.35 – 4.04 (m, 1H), 3.68 – 3.60 (m, 8H), 3.55 (dd, J = 10.9, 0.9 Hz, 8H), 3.25 – 3.15 (m, 2H), 2.96 (t, J = 7.2 Hz, 2H), 1.76 – 1.51 (m, 4H), 1.29 – 1.23 (m, 9H), 1.15 – 0.95 (s, 12H).

H₂N-G4-(OH)₁₆

Prepared according to literature procedures.¹¹ (Yield = 1 g, 97%) ¹H NMR (600 MHz, MeOD) δ 4.45 – 4.10 (m, 28H), 3.71 – 3.65 (m, 16H), 3.60 (d, J = 10.8 Hz, 16H), 3.28 – 3.25 (m, 2H, overlapped with MeOD), 3.01 (t, J = 7.4 Hz, 2H), 1.67 (m, 4H), 1.34 (s, 3H), 1.32 (s, 6H), 1.30 (d, J = 1.5 Hz, 12H), 1.15 (s, 24H).

H₂N-G5-(OH)₃₂

Prepared according to literature procedures.¹¹ (Yield = 822 mg, 98%) ¹H NMR (600 MHz, MeOD): δ 4.39-4.24 (m, 60H), 3.68 (dd, J = 10.8, 3.9, 32H), 3.61 (d, J = 10.8, 32H), 3.28 (d, J = 7.3, 2H, overlapped with MeOD), 3.04 (t, J = 7.5, 2H), 1.69 (m, 4H), 1.38 (s, 3H), 1.35 (s, 6H), 1.32 (d, J = 5.8, 36H), 1.16 (s, 48H).

H₂N-G6-(OH)₆₄

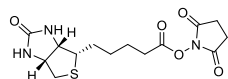
Prepared according to literature procedures.¹¹ (Yield = 605 mg, 99%) ¹H NMR (600 MHz, MeOD): δ 4.42-4.20 (m, 124H), 3.69 (dd, J = 10.9, 4.2, 64H), 3.61 (d, J = 10.9, 64H), 1.40-1.28 (m, 93H), 1.16 (s, 96H).

H₂N-G7-(OH)₁₂₈

Prepared according to literature procedures.¹¹ (Yield = 382 mg, 99%) ¹H NMR (600 MHz, MeOD): δ 4.45-4.20 (m, 252H), 3.69 (dd, J = 10.8, 4.6, 128H), 3.62 (d, J = 10.9, 128H), 1.39-1.28 (m, 188H), 1.16 (s, 192H)

A round-bottom flask was charged with a magnetic stir bar, H₂N-G_x-(OH)_y, anhydrous DMF, Et₃N and biotin-NHS. The reaction was allowed to stir under a nitrogen atmosphere for overnight. DMF was removed *in vacuo* and the crude mixture was redissolved in MeOH and purified by SEC using Sephadex LH-20 as the stationary phase and MeOH as the eluent.

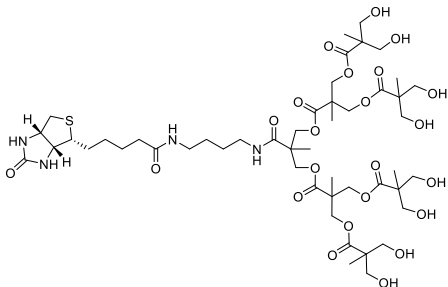
Biotin-NHS



General Procedure 4: Synthesis of Biotin-G_x-(OH) Dendrimers

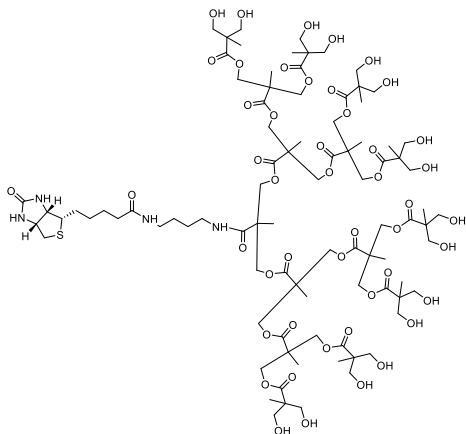
Adapted from previous procedures.²⁵ A flame-dried 25 mL Schlenk flask was charged with a magnetic stir bar, Biotin (250 mg, 1.02 mmol), *N*-hydroxysuccinimide (130 mg, 1.13 mmol), and dry DMF (8.5 mL). The mixture was allowed to stir for 0.5 h at 30 °C before DCC (275 mg, 1.33 mmol) was added in a single portion. The reaction was allowed to stir for overnight at room temperature. The mixture was filtered through celite and DMF was removed *in vacuo*. The residue was triturated with diethyl ether and biotin-NHS was afforded as a white powder (Yield = 340 mg, 97%). ¹H NMR (600 MHz, DMSO): δ 6.39 (d, J = 35.1, 2H), 4.30 (dd, J = 7.6, 5.1, 1H), 4.15 (ddd, J = 7.3, 4.8, 2.1, 1H), 3.10 (ddd, J = 8.1, 6.3, 4.6, 1H), 2.82 (dd, J = 11.1, 5.9, 5H), 2.67 (t, J = 7.5, 2H), 2.58 (d, J = 12.6, 1H), 1.64 (tt, J = 12.8, 6.5, 3H), 1.53-1.47 (m, 1H), 1.42 (tq, J = 14.4, 7.1, 2H).

Biotin-G3-(OH)₈ (BG3)



Following General Procedure 4, NH₂-G3-(OH)₈ (248 mg, 275 μmol) was dissolved in DMF (0.5 mL). Biotin-NHS (113 mg, 330.2 μmol, 1.2 eq.) and triethylamine (58 μL, 303 μmol, 1.5 eq.) was added and the reaction was allowed to stir overnight under nitrogen. *Note:* Biotin-G3 is well below fractionation range for Sephadex LH-20 and was purified instead using reverse-phase column chromatography. DMF was removed *in vacuo* and the crude was solubilized in a mixture of 1:1 H₂O:DMSO (1 mL) and purified *via* C18 flash chromatography using 0-60% acetonitrile in water over 20 column volumes. Acetonitrile was removed *in vacuo* and the aqueous fractions were lyophilized to yield a white foam. (Yield = 160 mg, 52%) ¹H NMR (500 MHz, MeOD) δ 4.50 (ddt, *J* = 8.3, 5.2, 1.6 Hz, 1H), 4.34 – 4.20 (m, 13H), 3.68 (ddd, *J* = 10.8, 2.0, 1.2 Hz, 8H), 3.62 – 3.56 (m, 8H), 3.21 (dt, *J* = 8.9, 6.6 Hz, 4H), 2.97 – 2.89 (m, 1H), 2.71 (d, *J* = 12.8 Hz, 1H), 2.21 (t, *J* = 7.4 Hz, 2H), 1.80 – 1.40 (m, 11H), 1.30 (s, 9H), 1.15 (s, 12H). ¹³C NMR (151 MHz, MeOD) δ 176.1, 176.0, 175.6, 174.4, 173.8, 166.1, 68.2, 66.4, 66.3, 65.9, 63.4, 63.3, 61.6, 57.0, 51.9, 48.0, 47.7, 41.1, 40.6, 40.0, 37.8, 36.9, 35.8, 33.8, 29.9, 29.8, 29.6, 29.5, 27.9, 27.9, 26.9, 26.2, 18.3, 18.2, 17.3. MS (ESI⁺) *m/z* calc'd for C₄₉H₈₂N₄O₂₃S [M+H]⁺ = 1128.26, found [M+H]⁺ = 1128.3.

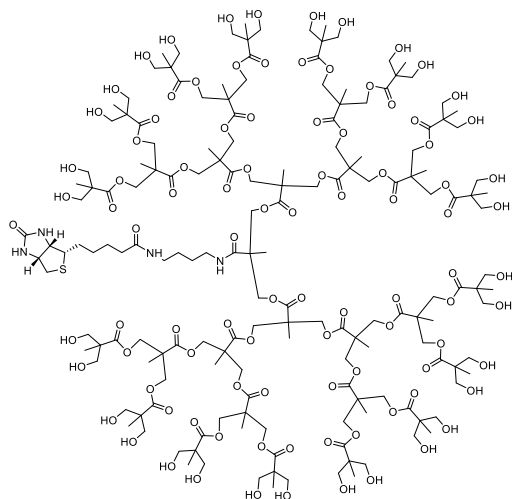
Biotin-G4-(OH)₁₆ (BG4)



Following General Procedure 4, NH₂-G4-(OH)₁₆ (111 mg, 61 μmol) was dissolved in DMF (0.6 mL). Biotin-NHS (25 mg, 73 μmol, 1.2 eq.) and triethylamine (13 μL, 91 μmol, 1.5 eq.) was added and the reaction was allowed to stir overnight under nitrogen. DMF was removed *in vacuo* and the crude was solubilized in MeOH (1 mL) and purified *via* SEC using Sephadex LH-20 and MeOH as eluent. Fractions containing product were pooled and dried *in vacuo* to yield a white foam. (Yield = 110 mg, 88%) ¹H NMR (700 MHz, MeOD): δ 4.50 (dd, J = 7.7, 4.7, 1H), 4.33-4.31 (m, 19H), 4.27-4.25 (m, 11H), 3.68 (dd, J = 10.8, 3.9, 17H), 3.60 (d, J = 10.9, 16H), 3.26-3.20 (m, 4H), 2.94 (dd, J = 12.7, 5.0, 1H), 2.71 (d, J = 12.7, 1H), 2.21 (quintet, J = 7.3, 2H), 1.77-1.71 (m, 1H), 1.71-1.60 (m, 3H), 1.59-1.54 (m, 4H), 1.45 (quintet, J = 7.7, 2H), 1.34 (s, 3H), 1.31 (s, 6H), 1.30 (s, 12H), 1.15 (s, 24H). ¹³C NMR (176 MHz, MeOD): δ 176.02, 175.94, 174.3, 173.8, 173.3, 166.1, 71.6, 68.3, 67.1, 66.2, 65.9, 63.4, 61.6, 57.0, 51.8, 48.11, 47.97, 47.7, 41.1, 40.5, 40.0, 36.9, 29.8, 29.5, 27.99, 27.93, 26.9, 18.35, 18.22, 18.16, 17.4. MALDI: *m/z* calc'd for C₈₉H₁₄₆N₄O₄₇S

$[M+H]^+ = 2055.89$, found $[M+Na]^+ = 2077.88$, $[M+2Na]^{2+} = 1050.43$, $[M+H+Na]^{2+} = 1039.94$.

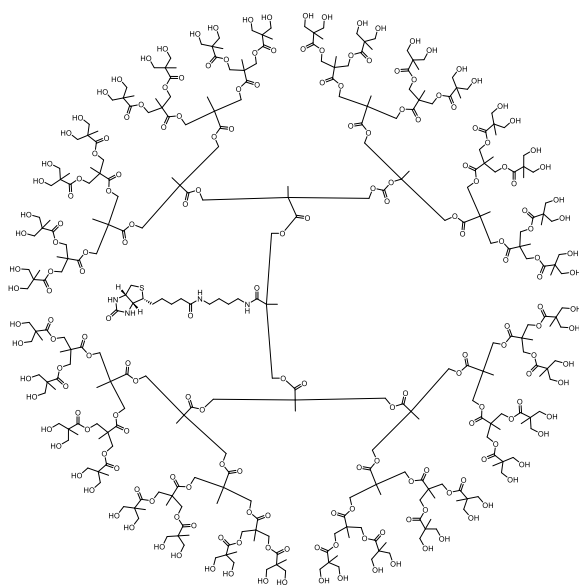
Biotin-G5-(OH)₃₂ (BG5)



Following General Procedure 4, NH₂-G5-(OH)₃₂ (172 mg, 47 μmol) was dissolved in DMF (0.5 mL). Biotin-NHS (19 mg, 56 μmol, 1.2 eq.) and triethylamine (10 μL, 70 μmol, 1.5 eq.) was added and the reaction was allowed to stir overnight under nitrogen. DMF was removed *in vacuo* and the crude was solubilized in MeOH (0.5 mL) and purified *via* SEC using Sephadex LH-20 and MeOH as eluent. Fractions containing product were pooled and dried *in vacuo* to yield a white foam. (Yield = 149 mg, 81%) ¹H NMR (700 MHz, MeOD): δ 4.51 (dd, J = 7.8, 4.9, 1H), 4.33 (d, J = 10.7, 42H), 4.26 (dd, J = 11.0, 2.5, 18H), 3.68 (dd, J = 10.9, 4.0, 32H), 3.61 (d, J = 10.9, 32H), 3.26 (t, J = 6.7, 2H), 3.21 (dd, J = 8.8, 4.8, 2H), 2.95 (dd, J = 12.8, 5.0, 1H), 2.72 (d, J = 12.7, 1H), 2.25-2.19 (m, 2H), 1.75 (td, J = 14.1, 7.6, 1H), 1.71-1.60 (m, 3H), 1.60-1.55 (m, 4H), 1.45 (quintet, J = 7.7, 2H), 1.37 (s, 3H), 1.35 (s, 6H), 1.32 (s, 12H), 1.31 (s, 24H), 1.16 (s, 48H). ¹³C NMR (176 MHz, MeOD): δ

175.9, 174.2, 173.8, 173.33, 173.23, 166.1, 68.6, 67.3, 67.0, 66.2, 65.9, 63.4, 61.7, 57.0, 51.8, 48.09, 47.95, 47.77, 41.1, 40.6, 40.1, 36.9, 29.9, 29.5, 28.06, 27.98, 26.9, 18.42, 18.25, 17.4. MS (ESI⁺): m/z calc'd for C₁₆₉H₂₇₄N₄O₉₅S [M+H]⁺ = 3915.05, found [M+ACN+2H]²⁺ = 1978.81, [M+2Na]²⁺ = 1050.43, [M+3Na]³⁺ = 1327.54.

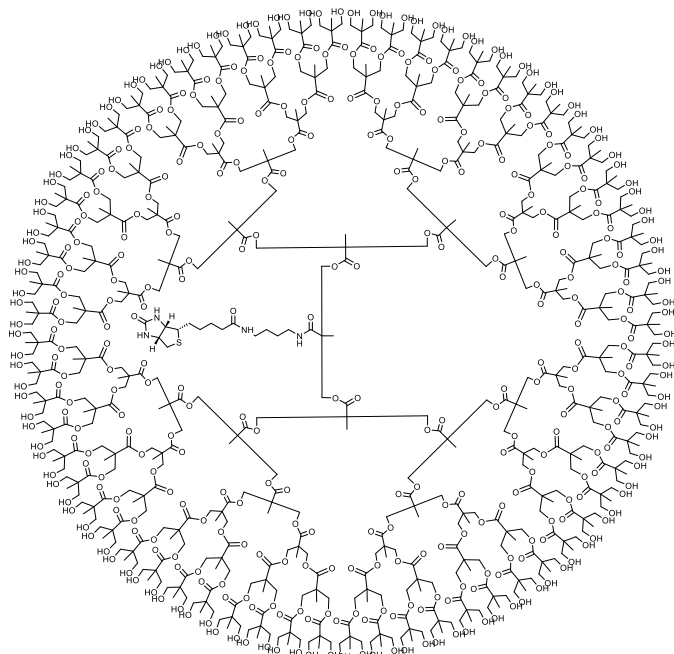
Biotin-G6-(OH)₆₄ (BG6)



Following General Procedure 4, NH₂-G6-(OH)₆₄ (100 mg, 14 μmol) was dissolved in DMF (0.5 mL). Biotin-NHS (6 mg, 16 μmol, 1.2 eq.) and triethylamine (3 μL, 20 μmol, 1.5 eq.) was added and the reaction was allowed to stir for 3 h under nitrogen. DMF was removed *in vacuo* and the crude was solubilized in MeOH (0.5 mL) and purified *via* SEC using Sephadex LH-20 and MeOH as eluent. Fractions containing product were pooled and dried *in vacuo* to yield a white foam. (Yield = 77 mg, 75%) ¹H NMR (700 MHz, MeOD): δ 5.00 (s, 1H), 4.58 (s, 1H), 4.52 (dd, J = 7.9, 4.9, 1H), 4.38-4.32 (m, 89H), 4.27 (d, J = 11.1, 35H), 3.68 (dd, J = 10.9, 4.3, 64H), 3.62 (d, J = 10.9, 64H), 3.27-3.21 (m, 4H), 2.96 (dd, J = 12.7,

4.9, 1H), 2.73 (d, J = 12.7, 1H), 2.23 (t, J = 6.9, 2H), 1.76 (tt, J = 13.7, 7.0, 1H), 1.70-1.61 (m, 2H), 1.61-1.53 (m, 4H), 1.46 (dt, J = 15.0, 7.4, 2H), 1.41 (s, 3H), 1.37 (s, 6H), 1.36 (s, 12H), 1.34 (s, 24H), 1.32 (s, 48H), 1.16 (s, 96H). ¹³C NMR (176 MHz, MeOD): δ 176.0, 174.1, 173.9, 173.34, 173.24, 166.0, 69.1, 67.22, 67.09, 66.96, 66.2, 65.9, 63.4, 61.7, 57.0, 51.8, 48.08, 47.95, 41.1, 40.7, 40.2, 37.0, 29.9, 29.6, 28.14, 28.09, 27.0, 18.52, 18.40, 18.35, 17.5. MS (ESI⁺): *m/z* calc'd for C₃₂₉H₅₃₀N₄O₁₉₂S [M+H]⁺ = 7646.76, [M+ACN+H]⁺ = 7687.79, [M+H+2Na]³⁺ = 2564.25, found [M+ACN+H]⁺ = 7687.52, [M+H+2Na]³⁺ = 2563.18.

Biotin-G7-(OH)₁₂₈ (BG7)



Following General Procedure 4, NH₂-G7-(OH)₁₂₈ (200 mg, 14 μmol) was dissolved in DMF (0.5 mL). Biotin-NHS (6 mg, 16 μmol, 1.2 eq.) and triethylamine (3 μL, 20 μmol, 1.5 eq.) was added and the reaction was allowed to stir for 3 h under nitrogen. DMF was

removed *in vacuo* and the crude was solubilized in MeOH (0.5 mL) and purified *via* SEC using Sephadex LH-20 and MeOH as eluent. Fractions containing product were pooled and dried *in vacuo* to yield a white foam. (Yield = 164 mg, 81%) ^1H NMR (600 MHz, MeOD) δ 4.46 – 4.17 (m, 252H), 3.69 (dd, J = 10.9, 3.9 Hz, 128H), 3.62 (d, J = 10.9 Hz, 128H), 3.29 – 3.21 (m, 4H), 2.98 (q, J = 8.1 Hz, 1H), 2.75 (d, J = 12.6 Hz, 1H), 2.25 (br. s, 2H) 1.83 – 1.54 (m, 13H), 1.39 – 1.32 (m, 189H), 1.17 (s, 192H). ^{13}C NMR (176 MHz, CDCl_3) δ 173.5, 172.0, 171.6, 171.5, 98.2, 66.0, 66.0, 65.1, 65.0, 64.8, 46.9, 46.7, 42.1, 25.3, 22.3, 18.7, 17.9, 17.7. MS (MALDI): m/z calc'd for $\text{C}_{649}\text{H}_{1042}\text{N}_4\text{O}_{383}\text{S}$ $[\text{M}+2\text{DMSO}+\text{H}]^+ = 15218$, found $[\text{M}+2\text{DMSO}+\text{H}]^+ = 15211$.

General Procedure 5: Synthesis of DBCO-Gx-(OH) Dendrimers

DBCO-NHS

Prepared according to previous procedures.²¹ (Yield = 1.2 g, 74%). ^1H NMR (600 MHz, CDCl_3) δ 7.69 (d, J = 7.6 Hz, 1H), 7.44 – 7.34 (m, 5H), 7.31 (td, J = 7.6, 1.3 Hz, 1H), 7.26 (m, 1H, overlapped with CDCl_3), 5.18 (d, J = 13.9 Hz, 1H), 3.69 (d, J = 13.9 Hz, 1H), 2.98 (dt, J = 17.6, 7.7 Hz, 1H), 2.86 – 2.74 (m, 5H), 2.64 (ddd, J = 17.6, 7.8, 5.4 Hz, 1H), 2.08 (ddd, J = 16.9, 7.9, 5.5 Hz, 1H).

DBCO-G3-(OH)₈

Prepared according to previous procedures (Yield = 150 mg, 49%).¹¹ ^1H NMR (700 MHz, MeOD): δ 7.65 (d, J = 7.5, 1H), 7.61-7.60 (m, 1H), 7.48-7.45 (m, 3H), 7.35 (dtd, J = 25.2, 7.5, 1.2, 2H), 7.25 (dd, J = 7.5, 1.2, 1H), 5.13 (d, J = 14.1, 1H), 4.30-4.22 (m, 12H), 3.71 (d, J = 14.1, 1H), 3.68-3.57 (m, 16H), 3.19-3.17 (m, 2H), 3.07 (td, J = 6.9, 4.0, 2H), 2.72-

2.67 (m, 1H), 2.34 (dt, $J = 15.2, 7.5$, 1H), 2.19-2.15 (m, 1H), 1.98 (dt, $J = 16.6, 6.8$, 1H), 1.50-1.46 (m, 2H), 1.42-1.39 (m, 2H), 1.28 (s, 9H), 1.14 (s, 12H).

DBCO-G4-(OH)₁₆

Prepared according to previous procedures (Yield = 301 mg, 60%).¹¹ ¹H NMR (500 MHz, MeOD) δ 7.76 – 7.61 (m, 2H), 7.49 (d, $J = 7.1$ Hz, 3H), 7.42 – 7.32 (m, 2H), 7.28 (d, $J = 7.7$ Hz, 1H), 5.16 (d, $J = 14.0$ Hz, 1H), 4.41 – 4.19 (m, 28H), 3.73 (d, $J = 14.0$ Hz, 1H), 3.69 (dd, $J = 10.8, 2.7$ Hz, 16H), 3.62 (d, $J = 10.8$ Hz, 16H), 2.77 – 2.68 (m, 1H), 2.39 – 2.31 (m, 1H), 2.19 (dt, $J = 14.6, 7.3$ Hz, 1H), 2.05 – 1.95 (m, 1H), 1.57 – 1.40 (m, 4H), 1.36 – 1.30 (m, 21H), 1.17 (s, 24H).

DBCO-G5-(OH)₃₂

Prepared according to previous procedures (Yield = 820 mg, 82%).¹¹ ¹H NMR (700 MHz, MEOD): δ 7.73-7.02 (m, 8H), 5.15-5.10 (m, 1H), 5.04-5.03 (m, 2H), 4.32-4.25 (m, 60H), 3.69-3.60 (m, 64H), 3.21-3.21 (m, 2H), 3.08-3.08 (m, 1H), 2.71 (s, 1H), 2.35-2.33 (m, 1H), 2.17 (s, 1H), 2.00-1.96 (m, 1H), 1.57-1.42 (m, 4H), 1.32 (d, $J = 38.5$, 45H), 1.15 (s, 48H).

DBCO-G6-(OH)₆₄

Prepared according to previous procedures (Yield = 165 mg, 65%).¹¹ ¹H NMR (600 MHz, MeOD) δ 7.71 – 7.60 (m, 2H), 7.54 – 7.44 (m, 3H), 7.42 – 7.31 (m, 2H), 7.27 (dd, $J = 7.4, 1.5$ Hz, 1H), 5.15 (d, $J = 14.4$ Hz, 2H), 4.42 – 4.21 (m, 124H), 3.73 (d, $J = 14.4$ Hz, 2H), 3.68 (dd, $J = 10.9, 3.6$ Hz, 64H), 3.61 (d, $J = 10.9$ Hz, 64H), 3.23 (s, 2H), 3.09 (d, $J = 3.7$ Hz, 2H), 2.73 (dt, $J = 15.6, 7.5$ Hz, 1H), 2.36 (dt, $J = 15.0, 7.4$ Hz, 1H), 2.23 – 2.11 (m,

1H), 1.99 (dt, $J = 16.6, 6.8$ Hz, 1H), 1.50 (d, $J = 7.7$ Hz, 2H), 1.37 – 1.29 (m, 93H), 1.16 (s, 96H).

DBCO-G7-(OH)₁₂₈

Prepared according to previous procedures (Yield = 144 mg, 92%).¹¹ ¹H NMR (700 MHz, MeOD): δ 8.02-7.29 (m, 8H), 5.16 (s, 1H), 4.37 (d, $J = 161.0, 177$ H), 4.28 (s, 75H), 3.68 (s, 129H), 3.63 (s, 128H), 3.25 (s, 2H), 3.08 (s, 2H), 2.75 (s, 1H), 2.35 (s, 1H), 2.20 (s, 1H), 2.00 (s, 1H), 1.33 (s, 193H), 1.16 (s, 192H).

Synthesis of Avidin-N₃ and Avidin-Dendrimer Conjugates

Avidin-N₃

Native avidin from chicken egg was purchased from Lee BioSolutions (MO, USA) as a lyophilized solid and used without further purification. A 5 mL Eppendorf tube was charged with native avidin (60 mg, 36 μ mol lysine eq.) and sodium carbonate buffer (6 mL, 0.1 M, pH 9.5). Azidoacetyl-N-hydroxysuccinimide (54 mg, 273 μ mol) was added in a single portion and the reaction was allowed to mix *via* a rotating apparatus for 2 h at room temperature. The reaction mixture was adjusted to pH 9.5 and was allowed to mix for 12 h at 4 °C. The reaction was filtered over a 0.45 μ m polyethersulfone (PES) filter and purified and buffer exchanged to PBS (10 mM, pH 7.4) *via* HiTrap™ Desalting columns. Avidin-N₃ was stored as a solution in PBS (10 mM, pH 7.4) at 4 °C (5.5 mg/mL, 9 mL PBS, yield = 82%).

General Procedure: Preparation of Avidin-Dendrimer Conjugates

A 5 mL Eppendorf tube was charged with 1.5-1.6 eq. per azide (*i.e.*, 60-64 eq. per avidin- N_3 tetramer) of DBCO- G_x -(OH) $_{(2^x)}$ and PBS (10 mM, pH 7.4). Separately, 1 eq. of avidin- N_3 was dissolved in PBS (10 mM, pH 7.4). The dendrimer solution was added to the avidin solution and reaction was allowed to mix for 12 h at 4 °C. Upon disappearance of the azide signal by FT-IR, the reaction was dialyzed using 12-50 kDa MWCO tubing against PBS (10 mM, pH 7.4).

Av-G3

Using General Procedure, DBCO-G3-(OH) $_8$ (6 mg, 5.2 μ mol) was added in a single portion to a solution of Av- N_3 (1 mL, 5.5 mg/mL). The reaction was dialyzed for 2 days using 12 kDa MWCO tubing against PBS (10 mM, pH 7.4) and additionally desalted *via* 1 x HiTrap desalting column (5 mL). Av-G3 was stored as a solution in PBS at 4 °C (1.6 mg, 16%).

Av-G4

Using General Procedure, DBCO-G4-(OH) $_{16}$ (11 mg, 5.2 μ mol) was added in a single portion to a solution of Av- N_3 (1 mL, 5.5 mg/mL). The reaction was dialyzed for 2 days using 50 kDa MWCO tubing against PBS (10 mM, pH 7.4). Av-G4 was stored as a solution in PBS at 4 °C (Yield = 2.6 mg, 20%)

Av-G5

Using General Procedure, DBCO-G5-(OH) $_{32}$ (17 mg, 14 μ mol) was added in a single portion to a solution of Av- N_3 (1 mL, 5.5 mg/mL). The reaction was dialyzed for 2 days

using 50 kDa MWCO tubing against PBS (10 mM, pH 7.4). Av-G5 was stored as a solution in PBS at 4 °C (Yield = 4.5 mg, 24%).

Av-G6

Using General Procedure, DBCO-G6-(OH)₆₄ (112 mg, 15 μmol) was added in a single portion to a solution of Av-N₃ (2.4 mL, 5.5 mg/mL). The reaction was dialyzed overnight using 100 kDa MWCO tubing against PBS (10 mM, pH 7.4) and concentrated *via* spin column (100 kDa MWCO). Av-G6 was stored as a solution in PBS at 4 °C (Yield = 42 mg, 61%).

Av-G7

Using General Procedure, DBCO-G7-(OH)₁₂₈ (123 mg, 10.6 μmol) was added in a single portion to a solution of Av-N₃ (2.5 mL, 5.5 mg/mL). The reaction was dialyzed overnight using 100 kDa MWCO tubing against PBS (10 mM, pH 7.4) and concentrated *via* spin column (100 kDa MWCO). Av-G6 was stored as a solution in PBS at 4 °C (Yield = 72 mg, 59%).

Synthesis of Biotinylated Aprotinin

Adapted from previous procedures.¹³ Aprotinin from bovine lung was purchased from Sigma Aldrich as a crystalline solid and used without further purification. A 2 mL Eppendorf tube was charged with aprotinin (661 μg) and sodium phosphate buffer (132 μL, pH 8.5). Biotin-NHS (350 μg, 1.0 μmol) was added as a solution in DMSO (20 μL). The reaction was allowed to mix using a tube rotator (Fisherbrand) for 2 h at room temperature

followed by 12 h at 4 °C. The reaction was dialyzed overnight using 3.5 kDa MWCO tubing against PBS (10 mM, pH 7.4). Protein content was verified by BCA assay and degree of biotinylation was characterized by fluorescamine assay. Biotinylated aprotinin was stored as a solution in PBS (Biotin molecules per protein = 4.2, Yield = 517 μ g, 68%).

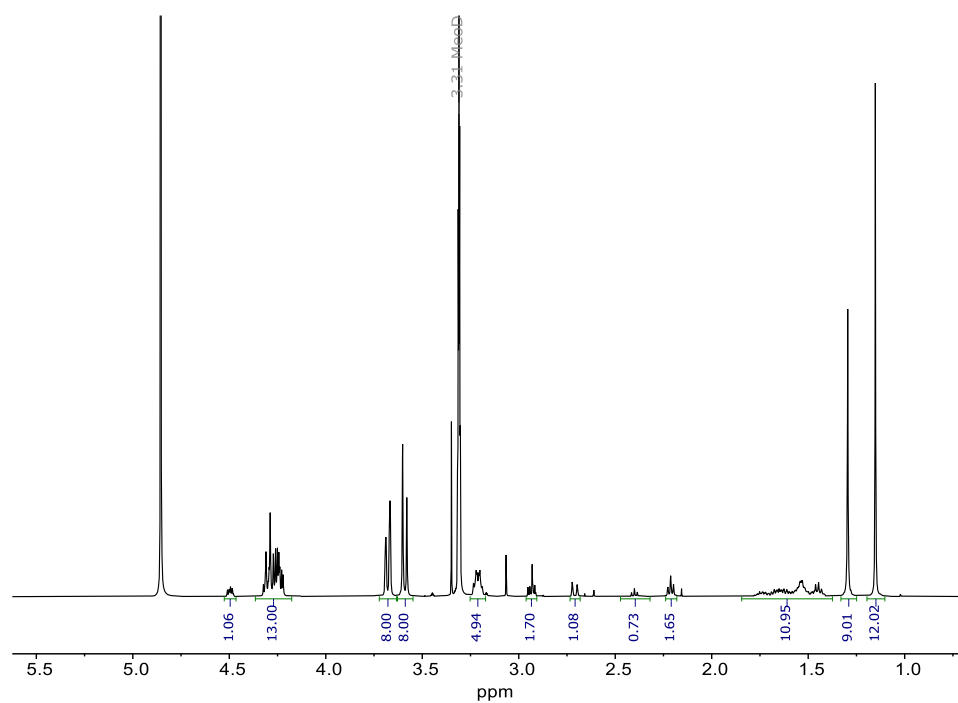


Figure S4.1. ^1H NMR spectrum of **BG3**.

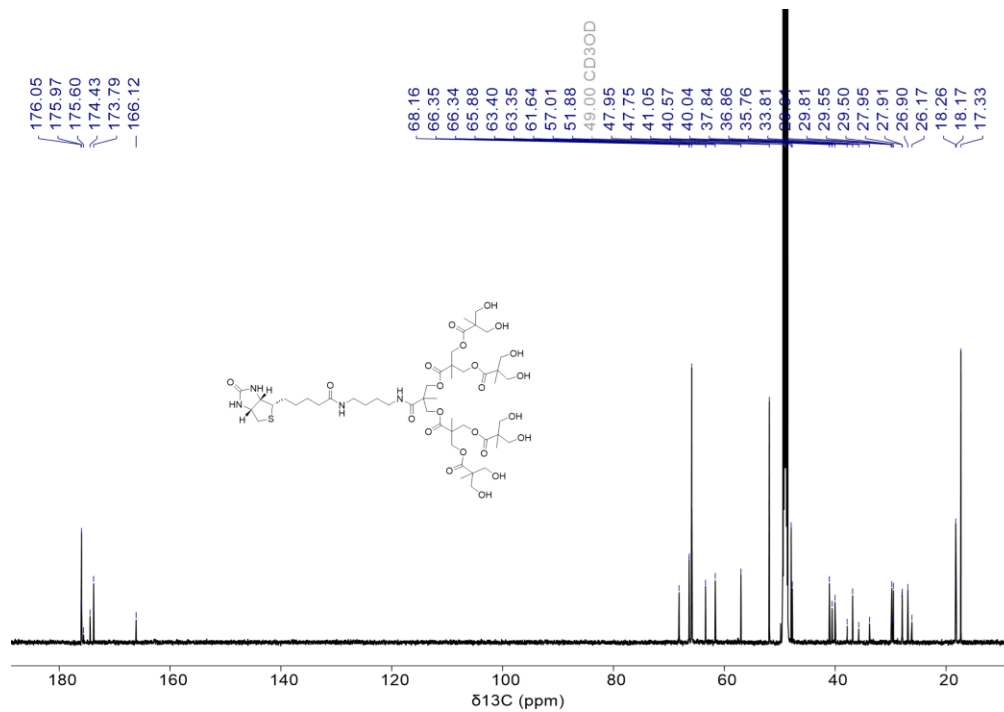


Figure S4.2. ^{13}C NMR spectrum of BG3.

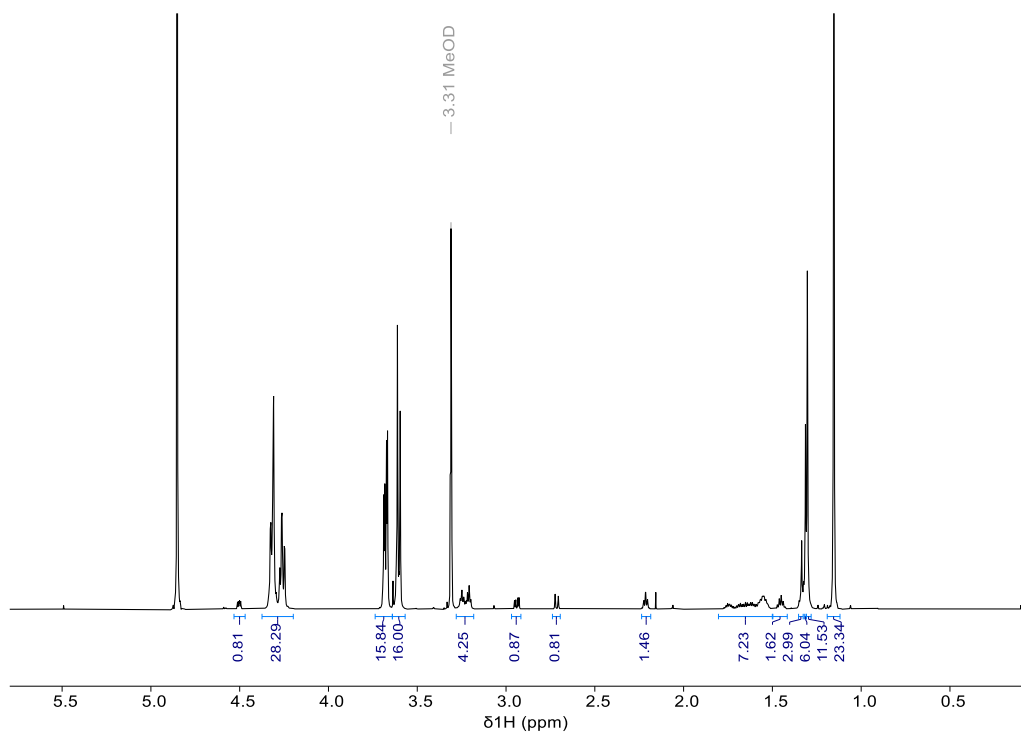


Figure S4.3. ^1H NMR spectrum of BG4.

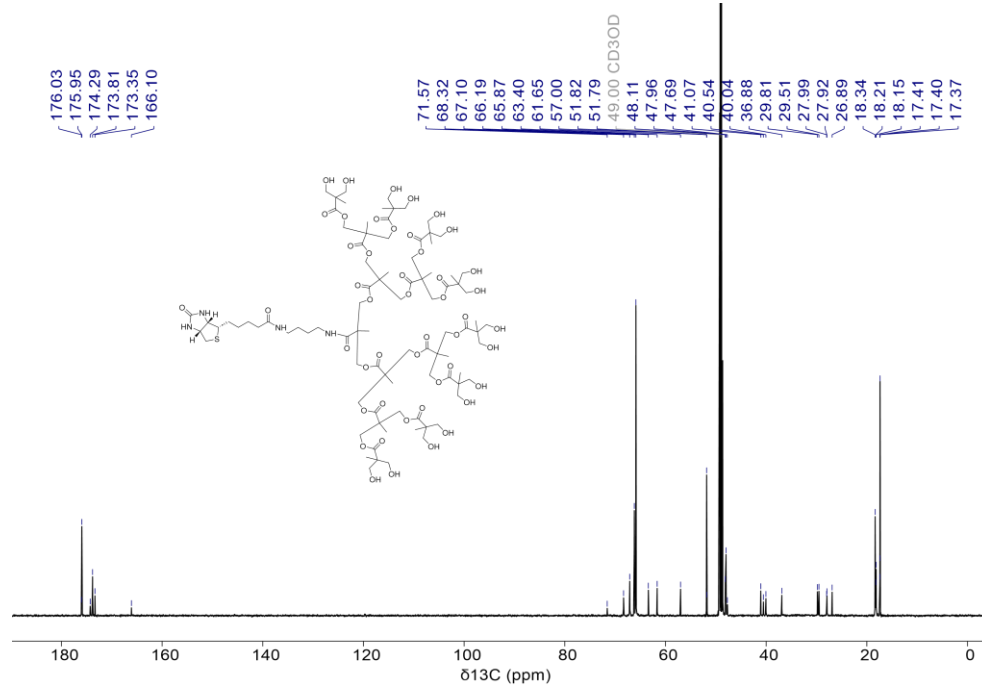


Figure S4.4. ^{13}C NMR spectrum of BG4.

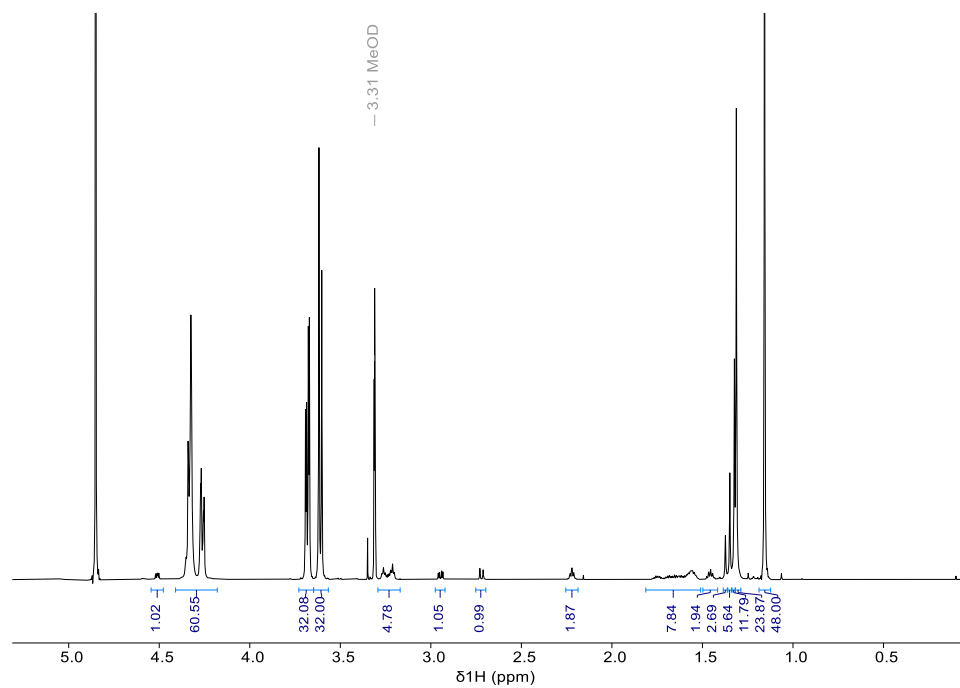


Figure S4.5. ^1H NMR spectrum of BG5.

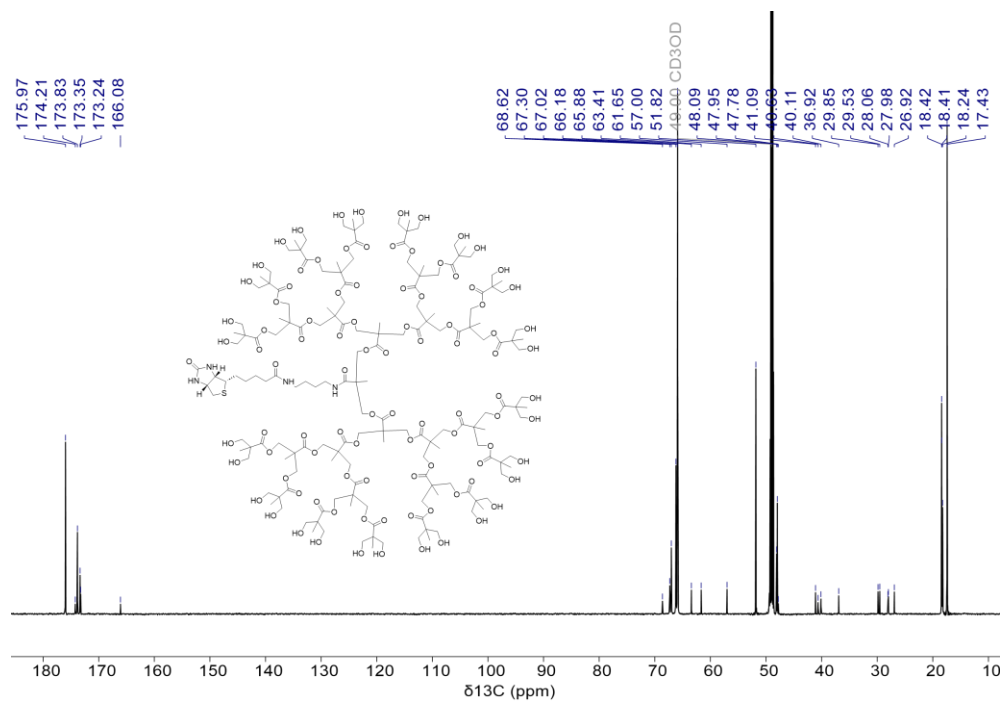


Figure S4.6. ^{13}C NMR spectrum of BG5.

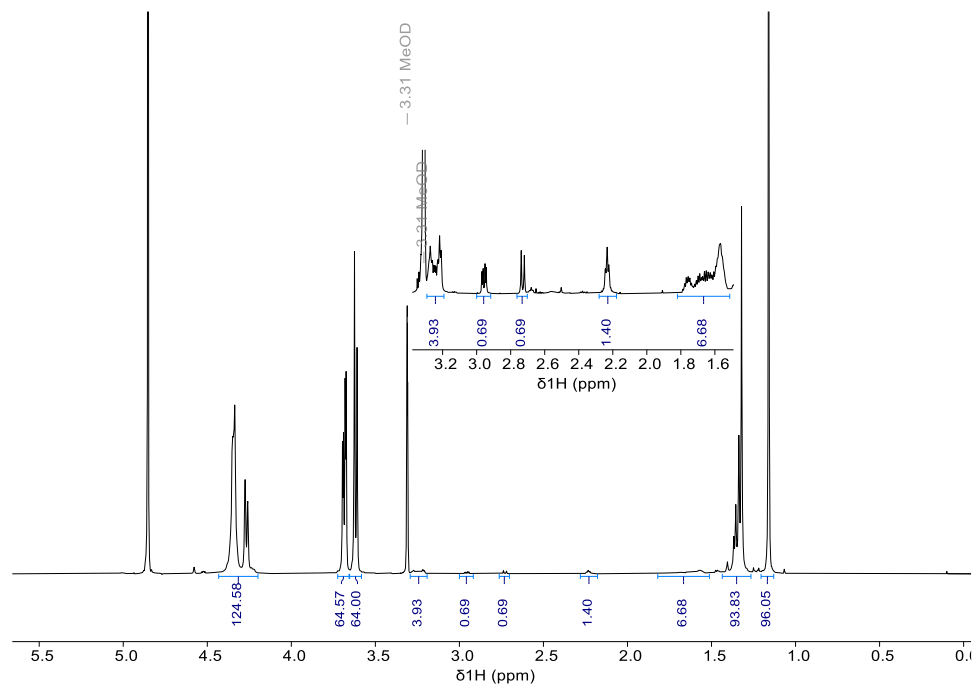


Figure S4.7. ^1H NMR spectrum of BG6.

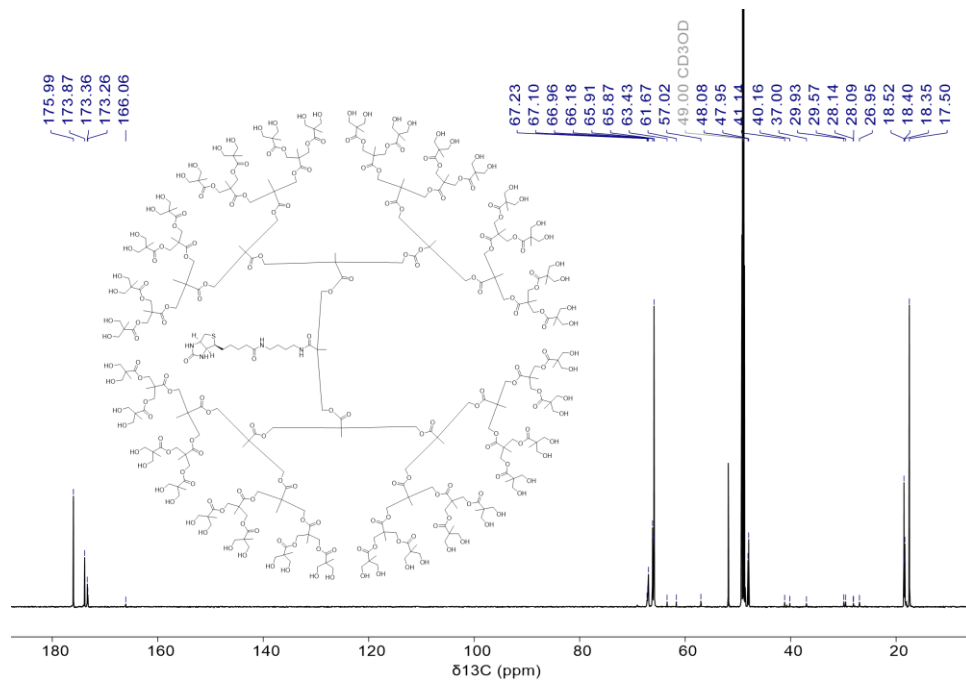


Figure S4.8. ^{13}C NMR spectrum of BG6.

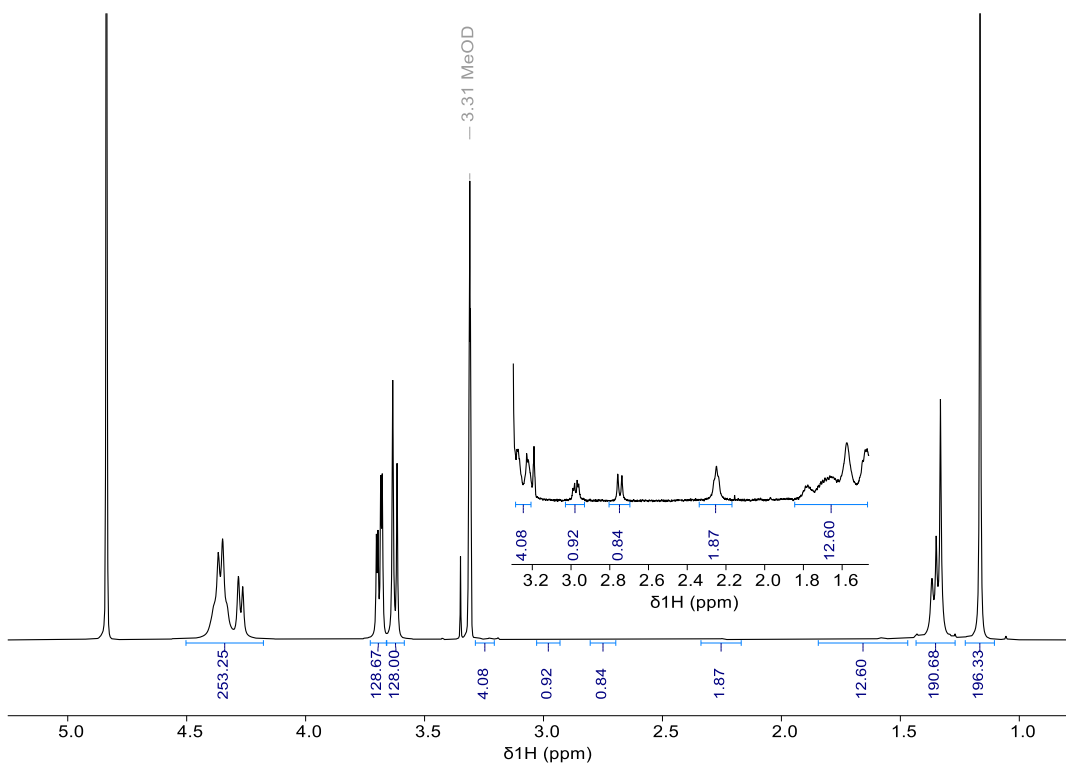


Figure S4.9. ^1H NMR spectrum of BG7.

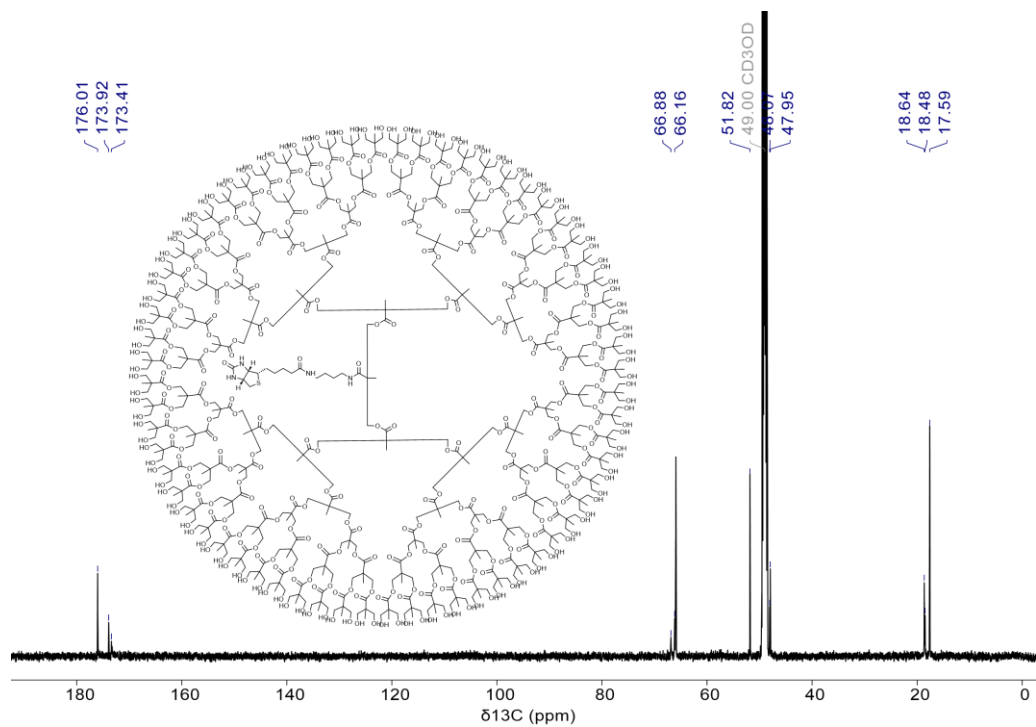


Figure S4.10. ^{13}C NMR spectrum of BG7.

ESI and MALDI-TOF Spectra

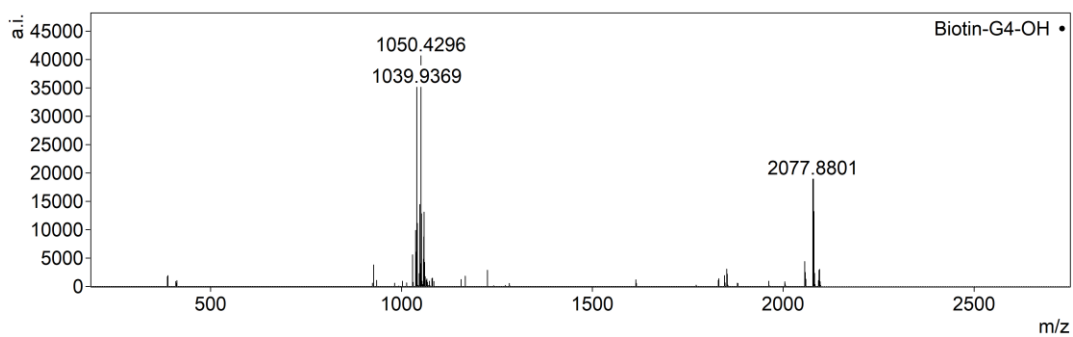


Figure S4.11. ESI $^+$ MS spectrum of biotin-G4-OH.

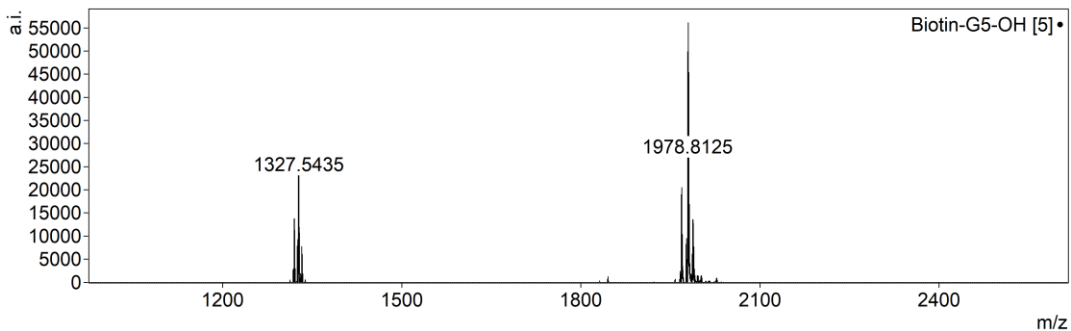


Figure S4.12. ESI⁺ MS spectrum of biotin-G5-OH.

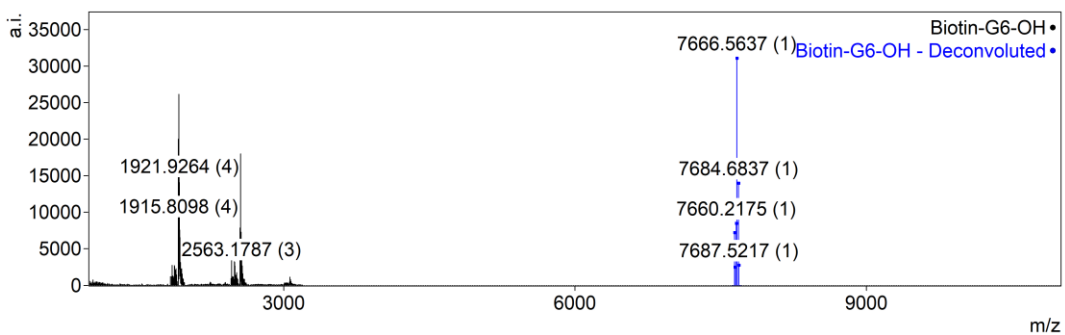


Figure S4.13. Deconvoluted ESI⁺ MS spectrum of biotin-G6-OH.

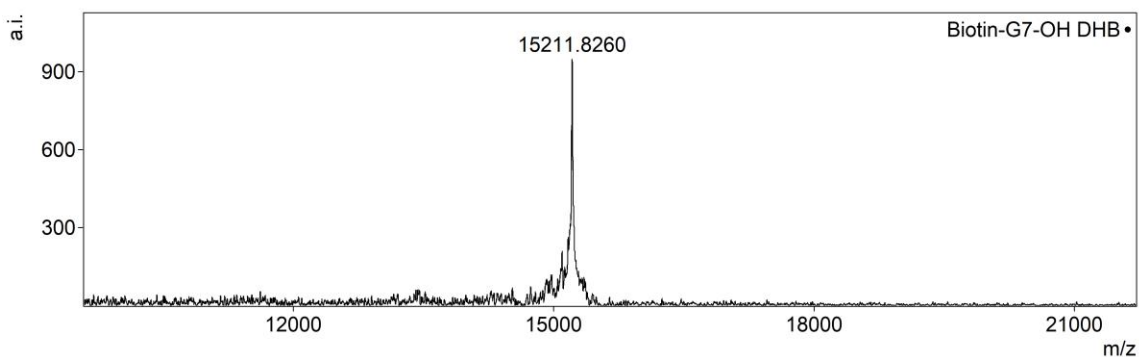


Figure S4.14. MALDI MS spectrum of biotin-G7-OH (matrix = 2,5-Dihydroxybenzoic acid (DHB)).

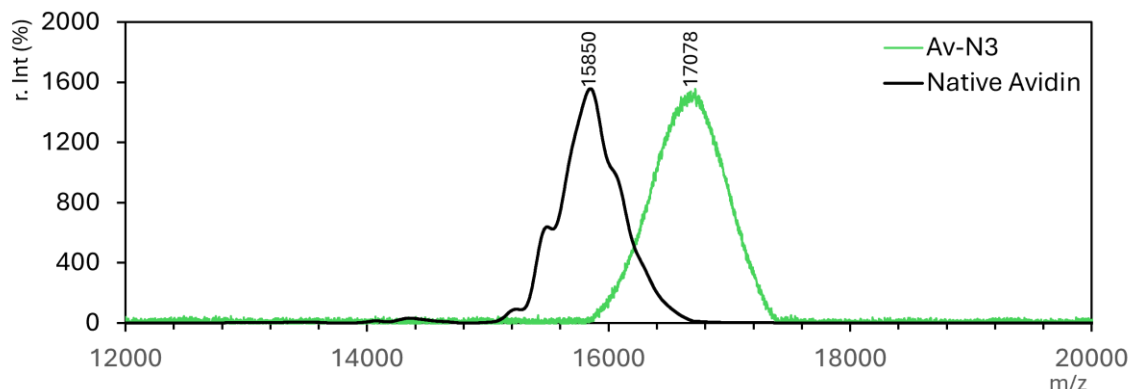


Figure S4.15. MALDI MS spectrum of Avidin and avidin-azide (Av-N₃) monomer. 10 azide groups (MW = 84) correspond to an expected mass increase of 840 per avidin monomer (15-16 kDa).

Dynamic Light Scattering (DLS)

DLS data was collected on a Malvern Zetasizer Nano ZS instrument. Native avidin and avidin conjugates (1.0 mg/mL) were dissolved in PBS (10 mM, pH 7.4) and filtered through a 0.22 μm PES membrane prior to measurement. The hydrodynamic diameter (D_h) of the samples was measured five times (15 accumulated scans per measurement) at 25 $^{\circ}\text{C}$ using a backscatter angle of 173 $^{\circ}$. Reported distribution values are Z-average intensities.

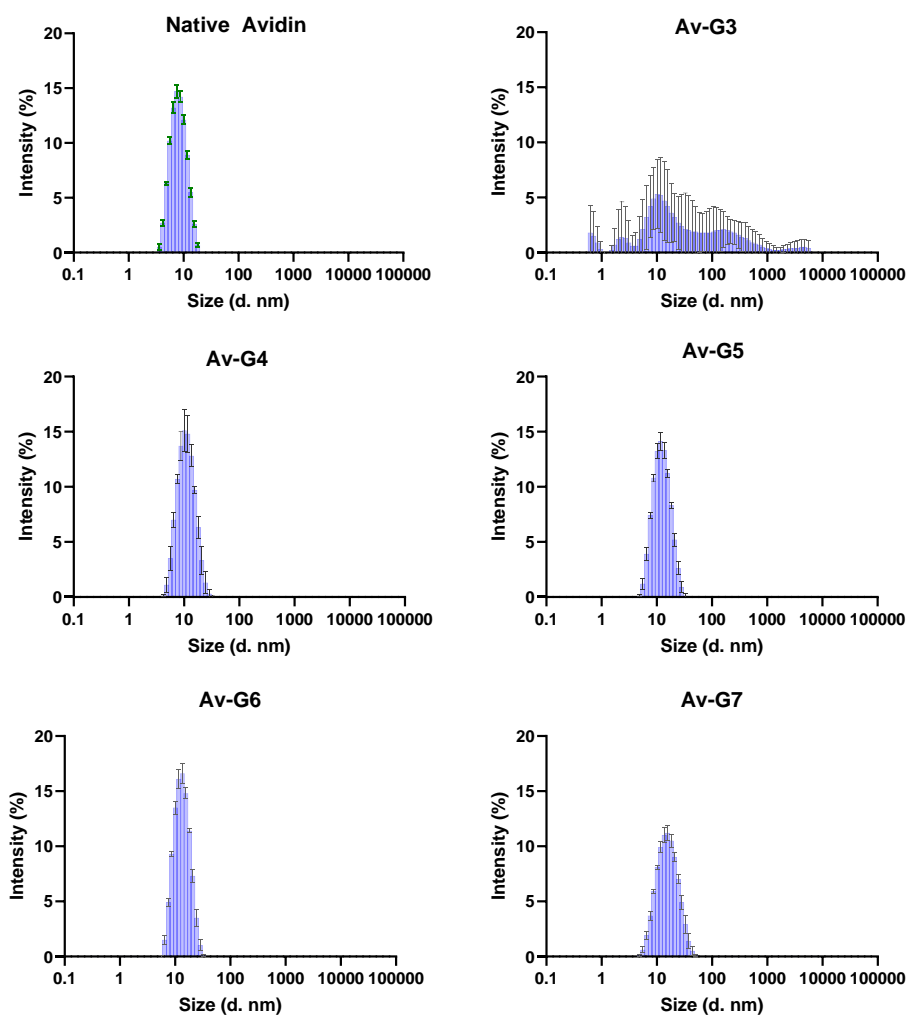


Figure S4.16. Particle size distribution of avidin-dendrimer conjugates by intensity distribution (Z-average)

Table S4.1. Hydrodynamic diameters (D_h) of biotin and hydroxyl periphery dendrimers.

Dendrimer	MW (kDa)	Dendrimer D_h (nm)
Biotin	0.244	-
G3-(OH) ₈	1.13	0.64 ^a
G4-(OH) ₁₆	2.06	1.12 ^a
G5-(OH) ₃₂	3.91	1.95^a
G6-(OH) ₆₄	7.65	3.21^b
G7-(OH) ₁₂₈	15.1	4.50 ^b
G8-(OH) ₂₅₆	30.0	5.96 ^b

^a Interpolated from 3rd order polynomial regression analysis of G6-G8 dendrimers ($r^2 = 1.00$). ^b Volume-average hydrodynamic diameter of dendrimers have been reported previously.¹¹

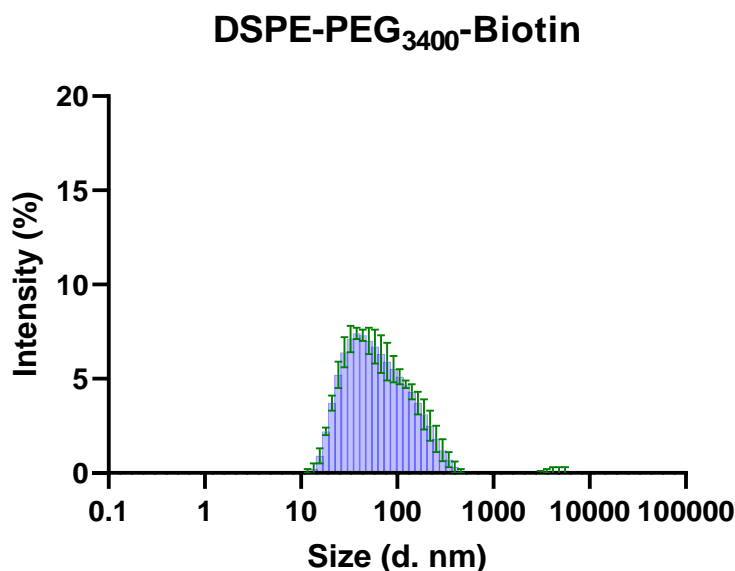


Figure S4.17. Particle size distribution of DSPE-PEG₃₄₀₀-biotin (Z-average). Measured Z-average (n = 5; diameter) = 52.8 nm, PDI = 0.292.

Circular Dichroism (CD) Spectroscopy

CD spectra were recorded on a JASCO J-1100 spectrophotometer (JASCO Corp., Japan) at 25 ± 0.2 °C. All measurements were performed using a low-volume rectangular quartz cell of 1 cm optical pathlength containing 400 μ L of sample. Avidin and avidin-dendrimer conjugates (0.15 mg) were dissolved in 10 mM pH 7.4 PBS and filtered through a 0.22 μ m PES membrane prior to measurement. Each spectrum represents the average of five trials of five accumulated scans per cycle. Each spectrum was obtained by collecting data at scan speed of 200 nm min⁻¹ and at a bandwidth of 1 nm. CD traces of avidin-conjugates were corrected for baseline by subtracting the spectra of PBS. Ellipticity (Θ) values were reported in units of millidegrees.

Fluorescamine Assay

Fluorescamine assay was used to determine extent of azidofication of native avidin to yield **Av-N₃**. A standard curve comprised of nine avidin standards (0-400 $\mu\text{g/mL}$) was constructed using pH 8.5 100 mM sodium phosphate buffer. To each well in a 96-well black microplate was added 80 μL of standard, 80 μL buffer, and 40 μL of 3 mg/mL fluorescamine in acetonitrile. Wells were allowed to incubate at room temperature in the dark for 10 minutes. Fluorescence intensities were measured at $\lambda_{\text{ex}} = 390 \text{ nm}$, $\lambda_{\text{em}} = 470 \text{ nm}$ with 10 nm bandwidths on a Biotek Cytation5TM plate reader.

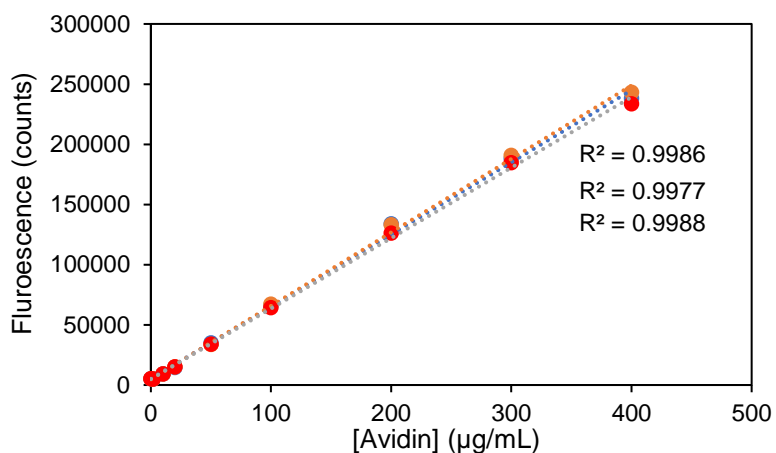


Figure S4.18. Fluorescence standard curves ($n = 3$) constructed from native avidin.

Native PAGE

A native gel (6%) was run in a Mini-PROTEAN Tetra Cell from Bio-Rad. NativeMarkTM Unstained Protein Standard by Invitrogen was purchased from Thermo Fisher Scientific. 5 μL of NovexTM Tris-Glycine Native Sample Buffer (2X) (Thermo Fisher Scientific) was added to a 15 μL 1X tris-glycine (pH 8.3) solution of either Avidin (15 μg), **Av-N₃**

(15 µg), **Av-G3** (18 µg eq. avidin), **Av-G3** (18 µg eq. avidin), **Av-G4** (14 µg eq. avidin), **Av-G5** (16 µg eq. avidin), **Av-G6** (18 µg eq. avidin), or **Av-G7** (15 µg eq. avidin). 8 µL of the ladder and 20 µL of conjugate samples were respectively loaded into each lane. Native PAGE was performed in non-denaturing, pH 8.3 tris-glycine buffer (1X) in 4 °C, under normal polarity at 100 V, 30 mA for 1.5 h. Gels were stained using Coomassie Brilliant Blue R250 for 15 minutes and destained overnight.

Bicinchoninic Acid (BCA) Assay

BCA assay of avidin and avidin-dendrimer conjugates were performed using a QuantiPro™ BCA Assay Kit from Sigma Aldrich. All proteins were dissolved in PBS (10 mM, pH 7.4) and mixed in a 1:1 ratio to a BCA reagent/CuSO₄ solution (prepared according to supplier instructions) and incubated at 60 °C for 1 hour. Sample was allowed to cool to room temperature (15 minutes), following which absorbance at 562 nm for all the samples was recorded using UV-VIS spectroscopy within a 10-minute window. UV-VIS data was plotted and interpolated using GraphPad Prism 9.

Quantification of Dendrimer Conjugation to Avidin by BCA method

A known amount of avidin-conjugate ($n = 3$) in a solution of PBS (1 mL, 10 mM, pH 7.4) was measured against a standard curve (second-order regression) constructed from native avidin. Number of conjugated dendrimers and average avidin wt. % was compared to the theoretical values (Table S2-6) and conjugation was deemed complete if experimental avidin wt. % was $\pm 1\%$ from upper/lower bounds. Avidin contains 9 lysines plus 1 *N*-terminal amine per subunit; all conjugates were found to be within $\pm 1\%$ of bounds. Note

that the accuracy might be affected by the presence of grafted dendrons, which may shield surface peptide residues from complex formation.

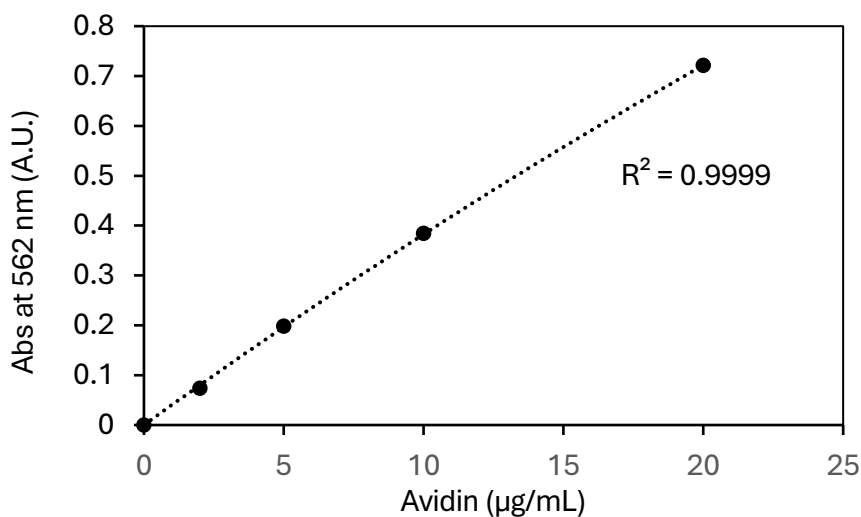


Figure S4.19. BCA assay constructed using native avidin standards.

Sample calculation using Av-G5:

$$\text{Theoretical Av(wt. \%)} = \frac{MW \text{ Native avidin}}{MW \text{ Av-G5}} \times 100 \% = \frac{66 \text{ kDa}}{226 \text{ kDa}} \times 100 \% = 29\%$$

A solution of **Av-G5** (52.7 µg lyophilized solids dissolved in 1 mL PBS) was measured in triplicates against an avidin standard curve to yield an average A.U. corresponding to 15.56 ± 0.46 µg/mL avidin. Therefore:

$$\text{Measured Av(wt. \%)} = \frac{\text{Mass measured avidin}}{\text{Mass Av-G5 weighed}} \times 100 \% = \frac{15.56}{52.7} \times 100 \% = 29.5\%; \text{ conjugation}$$

was deemed complete *i.e.*, there are 40 **DBCO-G5-OH** grafted onto the avidin tetramer.

Note: protein conjugates that were stored in PBS after the purification process were buffer exchanged with dH₂O using a HiTrap desalting column (Sephadex G25), lyophilized, weighed out and quantified *via* BCA assay as described.

Table S4.2. Expected weight percent (Wt. %) of avidin (Av) in **Av-G3** conjugate with increasing degrees of dendrimer conjugation.

# of Grafted DBCO-G3	Total G3 MW (KDa)	Conjugate MW (monomer) (kDa) ^a	Conjugate MW (tetramer) (kDa)	Avidin (wt. %) in Conjugate, lower bound ^b	Avidin (wt. %) in Conjugate; upper bound ^c
0	0.00	16.7	66.6	100%	100%
1	1.19	17.8	71.4	93%	97%
2	2.38	19.0	76.1	88%	91%
3	3.56	20.2	80.9	82%	85%
4	4.75	21.4	85.6	78%	81%
5	5.94	22.6	90.4	74%	76%
6	7.13	23.8	95.1	70%	73%
7	8.32	25.0	99.9	67%	69%
8	9.51	26.2	105	64%	66%
9	10.7	27.4	109	61%	63%
10	11.9	28.5	114	58%	60%

^a Calculated as MW(Avidin) + MW(Dendrimer) * Number of dendrimers on conjugate) .

^b Assuming a 66 kDa native tetramer. Assuming a 69 kDa native tetramer.

Table S4.3. Expected weight percent (Wt. %) of avidin (Av) in **Av-G4** conjugate with increasing degrees of conjugation.

# of Grafted DBCO-G4	Total G4 MW (KDa)	Conjugate MW (monomer) (kDa) ^a	Conjugate MW (tetramer) (kDa)	Avidin (wt. %) in Conjugate, lower bound ^b	Avidin (wt. %) in Conjugate; upper bound ^c
0	0.00	16.7	66.6	100%	100%
1	2.12	18.8	75.1	89%	92%
2	4.23	20.9	83.6	80%	83%
3	6.35	23.0	92.0	72%	75%
4	8.47	25.1	100	66%	69%

5	10.6	27.2	109	61%	63%
6	12.7	29.4	117	57%	59%
7	14.8	31.5	126	53%	55%
8	16.9	33.6	134	50%	51%
9	19.1	35.7	143	47%	48%
10	21.2	37.8	151	44%	46%

^a Calculated as MW(Avidin) + MW(Dendrimer) * Number of dendrimers on conjugate).

^b Assuming a 66 kDa native tetramer. ^c Assuming a 69 kDa native tetramer.

Table S4.4. Expected weight percent (Wt. %) of avidin (Av) in **Av-G5** conjugate with increasing degrees of dendrimer conjugation.

# of Grafted DBCO-G5	Total G5 MW (KDa)	Conjugate MW (monomer) (kDa) ^a	Conjugate MW (tetramer) (kDa)	Avidin (wt. %) in Conjugate, lower bound ^b	Avidin (wt. %) in Conjugate; upper bound ^c
0	0.00	16.7	66.6	100%	100%
1	3.98	20.6	82.5	81%	84%
2	7.95	24.6	98.4	68%	70%
3	11.9	28.6	114	58%	60%
4	15.9	32.6	130	51%	53%
5	19.9	36.5	146	46%	47%
6	23.9	40.5	162	41%	43%
7	27.8	44.5	178	37%	39%
8	31.8	48.5	194	34%	36%
9	35.8	52.4	210	32%	33%
10	39.8	56.4	226	30%	31%

^a Calculated as MW(Avidin) + MW(Dendrimer) * Number of dendrimers on conjugate).

^b Assuming a 66 kDa native tetramer. ^c Assuming a 69 kDa native tetramer.

Table S4.5. Expected weight percent (Wt. %) of avidin (Av) in **Av-G6** conjugate with increasing degrees of dendrimer conjugation.

# of Grafted DBCO-G6	Total G6 MW (KDa)	Conjugate MW (monomer) (kDa) ^a	Conjugate MW (tetramer) (kDa)	Avidin (wt. %) in Conjugate, lower bound ^b	Avidin (wt. %) in Conjugate; upper bound ^c
0	0.00	16.7	66.6	100%	100%
1	7.71	20.6	97.4	68%	71%
2	15.4	24.6	128	52%	54%

3	23.1	28.6	159	42%	43%
4	30.8	32.6	190	35%	36%
5	38.5	36.5	221	30%	31%
6	46.2	40.5	252	26%	27%
7	53.9	44.5	282	24%	24%
8	61.7	48.5	313	21%	22%
9	69.4	52.4	344	19%	20%
10	77.1	56.4	375	18%	18%

^a Calculated as MW(Avidin) + MW(Dendrimer) * Number of dendrimers on conjugate).

^b Assuming a 66 kDa native tetramer. ^c Assuming a 69 kDa native tetramer.

Table S4.6. Expected weight percent (Wt. %) of avidin (Av) in **Av-G7** conjugate with increasing degrees of dendrimer conjugation.

# of Grafted DBCO-G7	Total G7 MW (KDa)	Conjugate MW (monomer) (kDa) ^a	Conjugate MW (tetramer) (kDa)	Avidin (wt. %) in Conjugate, lower bound ^b	Avidin (wt. %) in Conjugate; upper bound ^c
0	0.00	16.7	66.6	100%	100%
1	15.1	31.8	127.1	52%	54%
2	30.2	46.9	188	36%	37%
3	45.4	62.0	248	27%	28%
4	60.5	77.1	309	22%	22%
5	75.6	92.3	369	18%	19%
6	90.7	107.4	430	16%	16%
7	106	122.5	490	14%	14%
8	121	137.6	551	12%	13%
9	136	152.8	611	11%	11%
10	151	167.9	672	10%	10%

^a Calculated as MW(Avidin) + MW(Dendrimer) * Number of dendrimers on conjugate).

^b Assuming a 66 kDa native tetramer. ^c Assuming a 69 kDa native tetramer.

Isothermal Titration Calorimetry (ITC)

Apo avidin binding: ITC experiments were performed on a MicroCal PEAQ-ITC instrument (Malvern Instruments Ltd., UK). Biotinylated BSA (8-16 average biotin/BSA) was purchased from Sigma Aldrich and used without further purification. DSPE-PEG₃₄₀₀-

biotin ($MW_{\text{avg}} = 4417$, 98% purity) was purchased from BroadPharm (San Diego, CA) and used without purification. Unless otherwise specified, biotin, dendronized biotin (**BGx**), PEG-biotin, or biotinylated protein(s) were used as titrant and avidin, avidin-azide or avidin-dendrimer conjugate was used as titrand. $[\text{avidin}]_{\text{tetramer}} = 5.5 \mu\text{M}$, $[\text{Biotin}]$, $[\text{BGx}]$, $[\text{biotinylated protein}] = 200 \mu\text{M}$. All binding experiments were performed in PBS (10 mM, pH 7.4) at 25.0 °C versus a reference cell containing distilled water with a supplied reference power of 41.9 μW (10 $\mu\text{cal/s}$). Unless specified otherwise, injection method for each titration was as follows: 300 μL of titrand was equilibrated at 25.0 °C for 120 s. An initial injection (0.5 μL) of titrant was followed by 18 injections (2.0 μL) each spaced 150 seconds apart while stirring at 750 rpm. Heat evolved from the initial injection was excluded from analysis. Three control experiments were performed wherein (1) Cell containing 10 mM PBS was titrated with Biotin, (2) Cell containing native avidin was titrated with 10 mM PBS, and (3) Cell containing 10 mM PBS was titrated with 10 mM PBS. Heats from control experiments were subtracted from experimental data. Thermodynamic parameters were fitted to the isotherms based on a single binding site model using Malvern's analytical software.

HABA-displacement experiments: 10 equivalents of HABA per avidin protomer was added to either avidin or **Av-G6** and the resulting HABA-avidin solutions were allowed to equilibrate at room temperature for three hours prior to ITC experiments. $[\text{HABA:avidin}]_{\text{tetramer}} = 5.5 \mu\text{M}$, $[\text{Biotin}]$ or $[\text{BGx}] = 200 \mu\text{M}$. Thermodynamic parameters were fitted to the isotherms based on a competitive binding model using Malvern's analytical software. HABA was arbitrarily chosen to be the weak ligand in the fitting model,

using experimental K_D values of biotin/biotin-dendrimer conjugates from apo avidin binding experiments described above.

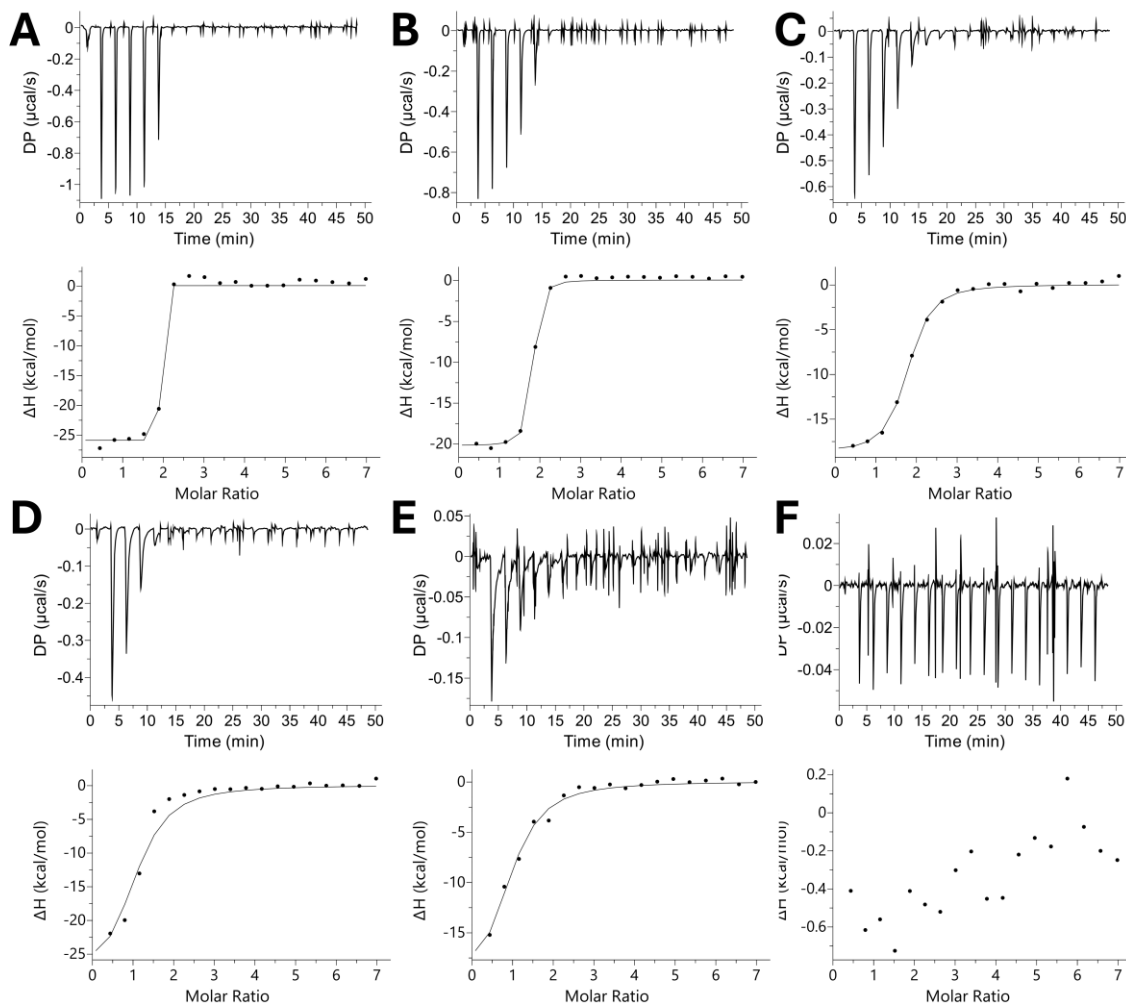


Figure S4.20. Competitive binding of biotin and **BG x** ($x = 3-7$) to native avidin-HABA measured by ITC. (A) Biotin, (B) **BG3**, (C) **BG4**, (D) **BG5**, (E) **BG6**, (F) **BG7**. From the top: Row 1: Raw heats evolved from binding for titrants A-C; Row 2: Corresponding enthalpy derived from integrated heats. Rows 3-4: Raw heat evolved and corresponding enthalpy, respectively, for titrants D-F.

Table S4.7. ITC Binding and thermodynamic parameters of DSPE-PEG₃₄₀₀-biotin : avidin and **Av-G4**.

Avidin-G _x	N (sites)	K _D (M)	ΔH (kcal/mol)	ΔG (kcal/mol)	-TΔS (kcal/mol)	Red. Chi-Sqr. (kcal/mol) ²
Avidin	3.81	2.37E-08	-11.9	-10.4	1.48	0.148
Av-G4	n.b. ^a	-	-	-	-	-

^a Non-binding; parameters were not calculated; n.b. = no binding.

Table S4.8. ITC Binding and thermodynamic parameters of BSA-biotin (8-16 average biotin group per protein) : avidin and **Av-G6**.

Avidin-G _x	N (sites)	K _D (M)	ΔH (kcal/mol)	ΔG (kcal/mol)	-TΔS (kcal/mol)	Red. Chi-Sqr. (kcal/mol) ²
Avidin	2.3	4.82E-07	-6.29	-8.62	-2.33	4.80E-02
Avidin-G6	n.b. ^a	-	-	-	-	-

^a Non-binding; parameters were not calculated; n.b. = no binding.

Table S4.9. ITC Binding and thermodynamic parameters of Aprotinin-biotin (4.2 average biotins per protein) : avidin, **Av-N₃**, and **Av-G4** to **Av-G6**.

Avidin-G _x	N (sites)	K _D (M)	ΔH (kcal/mol)	ΔG (kcal/mol)	-TΔS (kcal/mol)	Red. Chi-Sqr. (kcal/mol) ²
Avidin	3.00 ± 0.021 ^a	4.68E-08	-5.69	-10	-4.32	2.70E-02
Av-N ₃	3.00 ± 0.104 ^a	2.65E-06	-5.00	-7.61	-2.61	7.40E-03
Av-G4	n.b. ^b	-	-	-	-	-
Av-G5	n.b. ^b	-	-	-	-	-
Av-G6	n.b. ^b	-	-	-	-	-

^a Measurement error included to differentiate between identical values. ^b Non-binding; parameters were not calculated; n.b. = no binding.

Table S4.10. Competitive binding of biotin and **BG_x** (x = 3-7) to native avidin-HABA measured by ITC, tabulated data.

Titra nt	N (sites)	K _D (M)	ΔH (kcal/mol)	ΔG (kcal/mol)	-TΔS (kcal/mol)	Red. Chi-Sqr. (kcal/mol) ²
----------	-----------	--------------------	---------------	---------------	-----------------	---------------------------------------

Biotin	1.80	1.00E-15	-25.9	-20.5	5.48	0.725
BG3	1.65	2.42E-08	-20.3	-10.4	9.87	0.172
BG4	1.66	2.73E-07	-18.9	-8.96	9.91	0.154
BG5	1.04	1.96E-07	-23.5	-9.16	14.3	0.214
BG6	0.87	1.35E-06	-21.9	-8.01	13.9	0.251
BG7	<i>n.b.^a</i>	-	-	-	-	-

^bNon-binding; parameters were not calculated; *n.b.* = no binding.

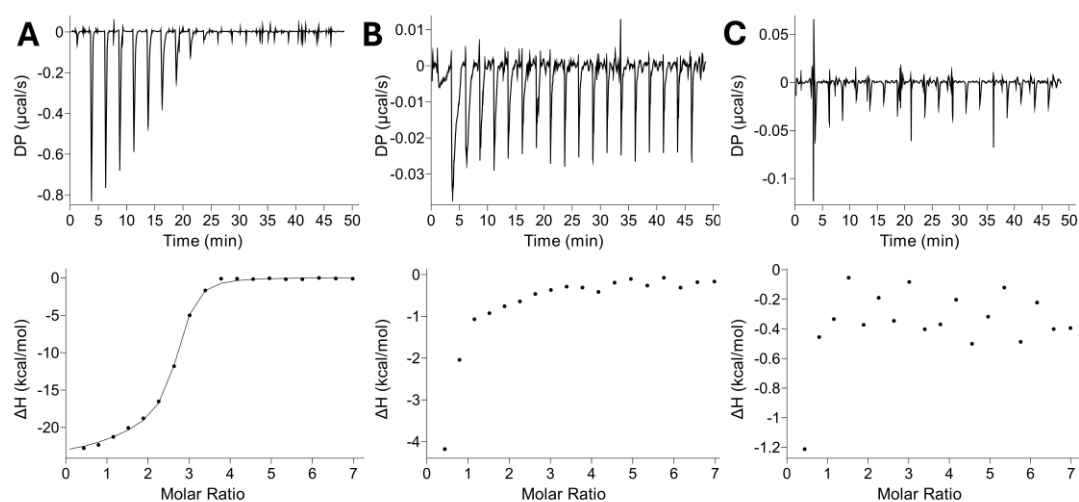


Figure S4.21. Competitive binding of (A) Biotin, (B) **BG5** and (C) **BG6** to Av-G6-HABA measured by ITC. (C) was used as a negative control as **BG6** was found to not bind Av-G6.

Table S4.11. Tabulated data of competitive binding of Biotin, **BG5** and **BG6** to Av-G6-HABA.

Titra nt	N (sites)	K _D (M)	ΔH (kcal/mol)	ΔG (kcal/mol)	-TΔS (kcal/mol)	Red. Chi-Sqr. (kcal/mol) ²
Biotin	2.47	1.71E-07	-22.2	-9.24	12.9	0.373
BG5	<i>n.b.^a</i>	-	-	-	-	-
BG6	<i>n.b.^a</i>	-	-	-	-	-

^bNon-binding; parameters were not calculated; *n.b.* = no binding.

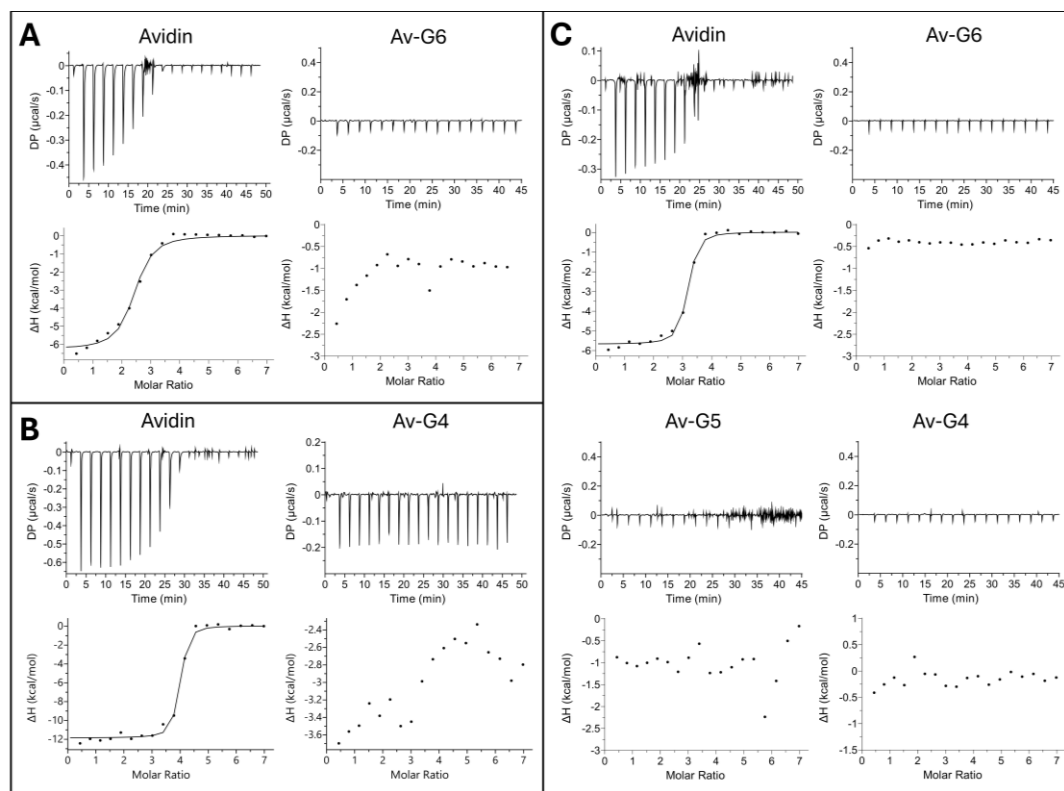


Figure S4.22. Binding of biotinylated BSA, aprotinin, and PEG₃₄₀₀ to avidin and select Av-Gx species as measured by ITC. **A.** BSA. **B.** DSPE-PEG₃₄₀₀. **C.** Aprotinin.

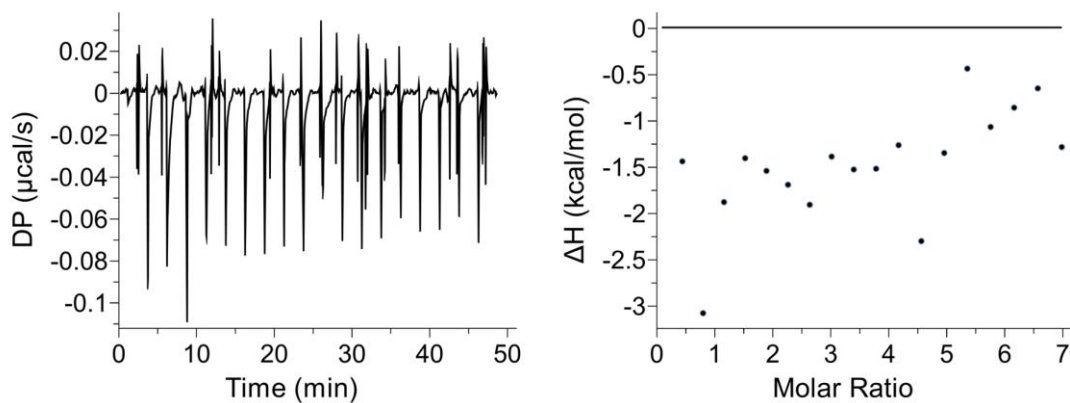


Figure S4.23. Titration of BG6 to Av-G4 at 37 °C as measured by ITC. Left: raw heat. Right: enthalpy derived from raw heats. The line at 0 kcal/mol is a line of best fit when a “binding” model is forced upon the data in order to calculate thermodynamic parameters (see Table S12).

Table S4.12. Titration of **BG6** to **Av-G4** at 37 °C, tabulated data.

Titrant	N (sites)	K_D (M)	ΔH (kcal/mol)	ΔG (kcal/mol)	-TΔS (kcal/mol)	Red. Chi-Sqr. (kcal/mol)²
BG6	0.0018 ± 3.9E6 ^a	3.43E-04 ^a	0.011 ^a	-4.73 ^a	-4.74 ^a	3.05 ^a

^a Calculations are based on a *forced* binding model.

Quantification of Avidin Binding by HABA Assay

HABA assays were performed using a modified procedure from Green.⁶⁶ A known amount of avidin or avidin conjugate (**Av-Gx**), as quantified prior by BCA assay, along with 10 eq. per tetramer of HABA was dissolved in PBS (10 mM, pH 7.4). Biotin or **BGx** (80 μM, PBS) was added in aliquots to the solution containing the avidin-HABA complex and the decrease in absorbance ($\lambda_{\text{ex}} = 500 \text{ nm}$, $\epsilon_{500} = 35000 \text{ M}^{-1} \text{ cm}^{-1}$) after each aliquot was measured either using a Cary 5000 Spectrometer or a Biotek Cytation5TM plate reader. Absorbance values were normalized for pathlength and dilution. *Quenching Experiments.* For select **Av-Gx** species, **BGx** was titrated as described above; upon reaching plateau in absorbance or upon exceeding 4:1 **BGx** : Avidin ratio, biotin (80 μM) was instead added to the solution until absorbance values plateaued.

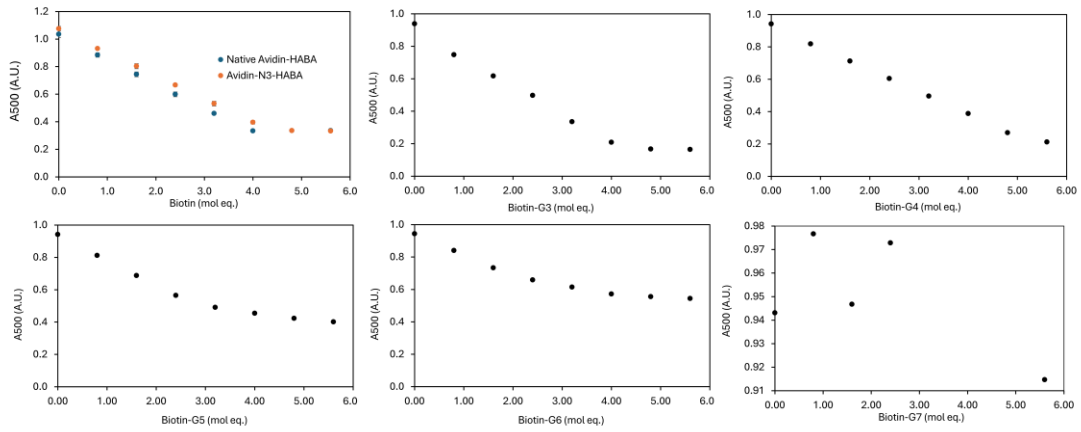


Figure S4.24. Titration of Avidin-HABA complex (PBS) with **BGx** (PBS).

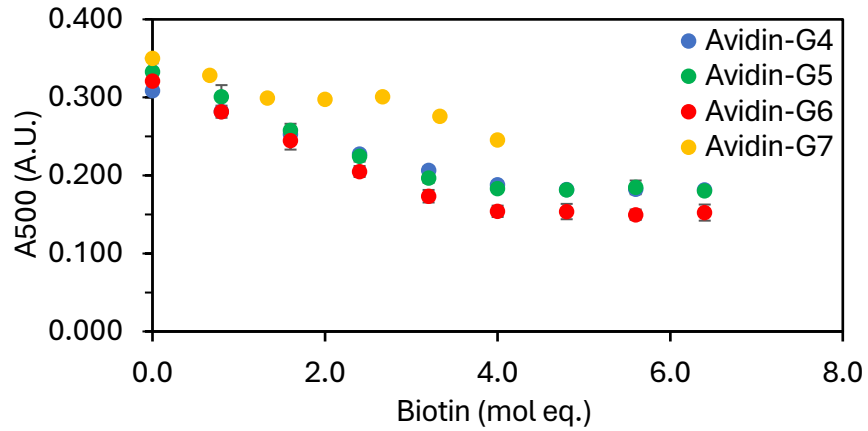


Figure S4.25. Titration of **Av-Gx + HABA** with biotin.

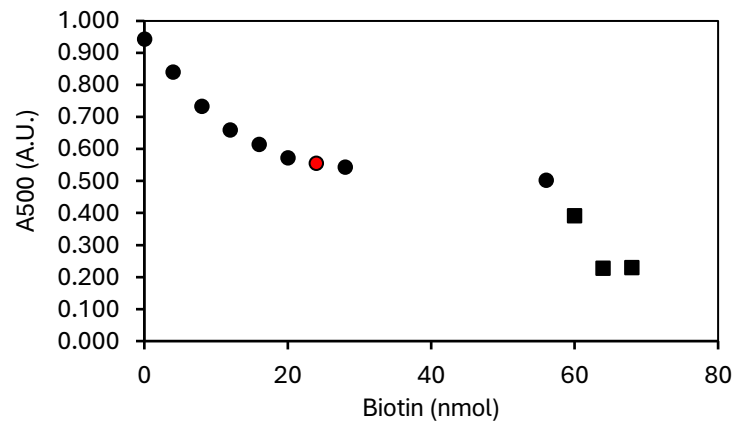


Figure S4.26. Quenching of Native Avidin-HABA with **BG6** and Biotin. Native avidin (~0.45 mg, 22-24 nmol eq. monomer) complexed with 10 eq. per monomer of HABA was titrated with 4 nmol aliquots of **BG6** (circles), followed by biotin (squares). Red circle denotes calculated equivalence point. An additional 28 nmol (7 aliquot equivalents) of **BG6** was added after equivalence point, before biotin (12 nmol, 4 aliquot equivalents).

4.6 References

- (1) Gupta, V.; Bhavanasi, S.; Quadir, M.; Singh, K.; Ghosh, G.; Vasamreddy, K.; Ghosh, A.; Siahaan, T. J.; Banerjee, S.; Banerjee, S. K. Protein PEGylation for Cancer Therapy: Bench to Bedside. *J. Cell Commun. Signal.* **2019**, *13* (3), 319–330. <https://doi.org/10.1007/s12079-018-0492-0>.
- (2) Pelegri-Oday, E. M.; Lin, E. W.; Maynard, H. D. Therapeutic Protein-Polymer Conjugates: Advancing beyond Pegylation. *J. Am. Chem. Soc.* **2014**, *136* (41), 14323–14332. <https://doi.org/10.1021/ja504390x>.
- (3) Kiran, P.; Khan, A.; Neekhra, S.; Pallod, S.; Srivastava, R. Nanohybrids as Protein-Polymer Conjugate Multimodal Therapeutics. *Front. Med. Technol.* **2021**, *3*, 676025. <https://doi.org/10.3389/fmedt.2021.676025>.
- (4) Chen, C.; Ng, D. Y. W.; Weil, T. Polymer Bioconjugates: Modern Design Concepts toward Precision Hybrid Materials. *Prog. Polym. Sci.* **2020**, *105*, 101241. <https://doi.org/10.1016/j.progpolymsci.2020.101241>.
- (5) Zhao, W.; Liu, F.; Chen, Y.; Bai, J.; Gao, W. Synthesis of Well-Defined Protein-Polymer Conjugates for Biomedicine. *Polymer* **2015**, *66*, A1–A10. <https://doi.org/10.1016/j.polymer.2015.03.054>.
- (6) Schulz, J. D.; Patt, M.; Basler, S.; Kries, H.; Hilvert, D.; Gauthier, M. A.; Leroux, J. C. Site-Specific Polymer Conjugation Stabilizes Therapeutic Enzymes in the Gastrointestinal Tract. *Adv. Mater.* **2016**, *28* (7), 1455–1460. <https://doi.org/10.1002/adma.201504797>.
- (7) Liu, M.; Tirino, P.; Radivojevic, M.; Phillips, D. J.; Gibson, M. I.; Leroux, J. C.; Gauthier, M. A. Molecular Sieving on the Surface of a Protein Provides Protection without Loss of Activity. *Adv. Funct. Mater.* **2013**, *23* (16), 2007–2015. <https://doi.org/10.1002/adfm.201202227>.
- (8) Liu, M.; Leroux, J. C.; Gauthier, M. A. Conformation-Function Relationships for the Comb-Shaped Polymer pOEGMA. *Prog. Polym. Sci.* **2015**, *48*, 111–121. <https://doi.org/10.1016/j.progpolymsci.2015.03.001>.
- (9) Kaupbayeva, B.; Murata, H.; Rule, G. S.; Matyjaszewski, K.; Russell, A. J. Rational Control of Protein-Protein Interactions with Protein-ATRP-Generated Protease-Sensitive Polymer Cages. *Biomacromolecules* **2022**, *23* (9), 3831–3846. <https://doi.org/10.1021/acs.biomac.2c00679>.
- (10) Kaupbayeva, B.; Boye, S.; Munasinghe, A.; Murata, H.; Matyjaszewski, K.; Lederer, A.; Colina, C. M.; Russell, A. J. Molecular Dynamics-Guided Design of a Functional Protein-ATRP Conjugate That Eliminates Protein-Protein Interactions. *Bioconjug. Chem.* **2021**, *32* (4), 821–832. <https://doi.org/10.1021/acs.bioconjchem.1c00098>.
- (11) McNelles, S. A.; Marando, V. M.; Adronov, A. Globular Polymer Grafts Require a Critical Size for Efficient Molecular Sieving of Enzyme Substrates. *Angew. Chem. - Int. Ed.* **2019**, *58* (25), 8448–8453. <https://doi.org/10.1002/anie.201902864>.
- (12) Deng, B.; Burns, E.; McNelles, S. A.; Sun, J.; Ortega, J.; Adronov, A. Molecular Sieving with PEGylated Dendron-Protein Conjugates. *Bioconjug. Chem.* **2023**, *34* (8), 1467–1476. <https://doi.org/10.1021/acs.bioconjchem.3c00237>.

- (13) Kaupbayeva, B.; Murata, H.; Lucas, A.; Matyjaszewski, K.; Minden, J. S.; Russell, A. J. Molecular Sieving on the Surface of a Nano-Armored Protein. *Biomacromolecules* **2019**, *20* (3), 1235–1245. <https://doi.org/10.1021/acs.biomac.8b01651>.
- (14) Livnah, O.; Bayer, E. A.; Wilchek, M.; Sussman, J. L. Three-Dimensional Structures of Avidin and the Avidin-Biotin Complex. *Proc. Natl. Acad. Sci.* **1993**, *90* (11), 5076–5080. <https://doi.org/10.1073/pnas.90.11.5076>.
- (15) Green, N. Thermodynamics of the Binding of Biotin and Some Analogues by Avidin. *Biochem. J.* **1966**, *101* (3), 774–780. <https://doi.org/10.1042/bj1010774>.
- (16) Jain, A.; Cheng, K. The Principles and Applications of Avidin-Based Nanoparticles in Drug Delivery and Diagnosis. *J. Controlled Release* **2017**, *245*, 27–40. <https://doi.org/10.1016/j.jconrel.2016.11.016>.
- (17) Jain, A.; Barve, A.; Zhao, Z.; Jin, W.; Cheng, K. Comparison of Avidin, Neutravidin, and Streptavidin as Nanocarriers for Efficient siRNA Delivery. *Mol. Pharm.* **2017**, *14* (5), 1517–1527. <https://doi.org/10.1021/acs.molpharmaceut.6b00933>.
- (18) Wilson, A. L.; Kaupbayeva, B.; Murata, H.; Cummings, C.; Russell, A. J.; Minden, J. S. Utilization of the Polymer Sieving Effect for the Removal of the Small Molecule Biotin-CDM. *ACS Appl. Polym. Mater.* **2019**, *1* (11), 2897–2906. <https://doi.org/10.1021/acsapm.9b00611>.
- (19) Yamaguchi, S.; Ohashi, N.; Minamihata, K.; Nagamune, T. Photodegradable Avidin-Biotinylated Polymer Conjugate Hydrogels for Cell Manipulation. *Biomater. Sci.* **2021**, *9* (19), 6416–6424. <https://doi.org/10.1039/D1BM00585E>.
- (20) Alina, T. B.; Nash, V. A.; Spiller, K. L. Effects of Biotin-Avidin Interactions on Hydrogel Swelling. *Front. Chem.* **2020**, *8*. <https://doi.org/10.3389/fchem.2020.593422>.
- (21) McNelles, S. A.; Adronov, A. Rapid Synthesis of Functionalized High-Generation Polyester Dendrimers via Strain-Promoted Alkyne-Azide Cycloaddition. *Macromolecules* **2017**, *50* (20), 7993–8001. <https://doi.org/10.1021/acs.macromol.7b01765>.
- (22) Beutner, G. L.; Young, I. S.; Davies, M. L.; Hickey, M. R.; Park, H.; Stevens, J. M.; Ye, Q. TCFH-NMI: Direct Access to N-Acyl Imidazoliums for Challenging Amide Bond Formations. *Org. Lett.* **2018**, *20* (14), 4218–4222. <https://doi.org/10.1021/acs.orglett.8b01591>.
- (23) García-Gallego, S.; Hult, D.; Olsson, J. V.; Malkoch, M. Fluoride-Promoted Esterification with Imidazolide-Activated Compounds: A Modular and Sustainable Approach to Dendrimers. *Angew. Chem. - Int. Ed.* **2015**, *54* (8), 2416–2419. <https://doi.org/10.1002/anie.201411370>.
- (24) Deng, B.; McNelles, S. A.; Da-Ré, G.; Marando, V. M.; Ros, S.; Stöver, H. D. H.; Adronov, A. Neopentyl Esters as Robust Linkers for Introducing Functionality to Bis-MPA Dendrimers. *Macromolecules* **2022**, *55* (1), 270–275. <https://doi.org/10.1021/acs.macromol.1c01974>.
- (25) Ratel, M.; Provencher-Girard, A.; Zhao, S. S.; Breault-Turcot, J.; Labrecque-Carbonneau, J.; Branca, M.; Pelletier, J. N.; Schmitzer, A. R.; Masson, J.-F.

- Imidazolium-Based Ionic Liquid Surfaces for Biosensing. *Anal. Chem.* **2013**, *85* (12), 5770–5777. <https://doi.org/10.1021/ac400386z>.
- (26) Green, N. M. Avidin. In *Advances in Protein Chemistry*; Elsevier, 1975; Vol. 29, pp 85–133. [https://doi.org/10.1016/S0065-3233\(08\)60411-8](https://doi.org/10.1016/S0065-3233(08)60411-8).
- (27) Vashist, S. K. Comparison of 1-Ethyl-3-(3-Dimethylaminopropyl) Carbodiimide Based Strategies to Crosslink Antibodies on Amine-Functionalized Platforms for Immunodiagnostic Applications. *Diagnostics* **2012**, *2* (3), 23–33. <https://doi.org/10.3390/diagnostics2030023>.
- (28) Wang, C.; Yan, Q.; Liu, H.-B.; Zhou, X.-H.; Xiao, S.-J. Different EDC/NHS Activation Mechanisms between PAA and PMAA Brushes and the Following Amidation Reactions. *Langmuir* **2011**, *27* (19), 12058–12068. <https://doi.org/10.1021/la202267p>.
- (29) Thamban Chandrika, N.; Green, K. D.; Houghton, J. L.; Garneau-Tsodikova, S. Synthesis and Biological Activity of Mono- and Di- *N*-Acylated Aminoglycosides. *ACS Med. Chem. Lett.* **2015**, *6* (11), 1134–1139. <https://doi.org/10.1021/acsmchemlett.5b00255>.
- (30) Udenfriend, S.; Stein, S.; Böhlen, P.; Dairman, W.; Leimgruber, W.; Weigele, M. Fluorescamine: A Reagent for Assay of Amino Acids, Peptides, Proteins, and Primary Amines in the Picomole Range. *Science* **1972**, *178* (4063), 871–872. <https://doi.org/10.1126/science.178.4063.871>.
- (31) Zheng, C. Y.; Ma, G.; Su, Z. Native PAGE Eliminates the Problem of PEG-SDS Interaction in SDS-PAGE and Provides an Alternative to HPLC in Characterization of Protein PEGylation. *Electrophoresis* **2007**, *28* (16), 2801–2807. <https://doi.org/10.1002/elps.200600807>.
- (32) Woodson, S. A.; Koculi, E. Analysis of RNA Folding by Native Polyacrylamide Gel Electrophoresis. *Methods Enzymol.* **2009**, *469*, 189–208. [https://doi.org/10.1016/S0076-6879\(09\)69009-1](https://doi.org/10.1016/S0076-6879(09)69009-1).
- (33) Greenfield, N. J. Using Circular Dichroism Spectra to Estimate Protein Secondary Structure. *Nat. Protoc.* **2006**, *1* (6), 2876–2890. <https://doi.org/10.1038/nprot.2006.202>.
- (34) Green, N.; Melamed, M. Optical Rotatory Dispersion, Circular Dichroism and Far-Ultraviolet Spectra of Avidin and Streptavidin. *Biochem. J.* **1966**, *100* (3), 614–621. <https://doi.org/10.1042/bj1000614>.
- (35) Zsila, F. Novel Circular Dichroism Spectroscopic Approach for Detection of Ligand Binding of Proteins: Avidin as Example. *Anal. Biochem.* **2009**, *391* (2), 154–156. <https://doi.org/10.1016/j.ab.2009.05.014>.
- (36) Zsila, F. Aromatic Side-chain Cluster of Biotin Binding Site of Avidin Allows Circular Dichroism Spectroscopic Investigation of Its Ligand Binding Properties. *J. Mol. Recognit.* **2011**, *24* (6), 995–1006. <https://doi.org/10.1002/jmr.1147>.
- (37) Ascenzi, P.; Bocedi, A.; Bolognesi, M.; Spallarossa, A.; Coletta, M.; De Cristofaro, R.; Menegatti, E. The Bovine Basic Pancreatic Trypsin Inhibitor (Kunitz Inhibitor): A Milestone Protein. *Curr. Protein Pept. Sci.* **2003**, *4* (3), 231–251. <https://doi.org/10.2174/1389203033487180>.

- (38) General, I. J.; Dragomirova, R.; Meirovitch, H. The Absolute Free Energy of Binding of Avidin/Biotin Revisited. *J. Phys. Chem. B* **2012**, *116* (23), 6628–6636. <https://doi.org/10.1021/jp212276m>.
- (39) Taskinen, B.; Zmurko, J.; Ojanen, M.; Kukkurainen, S.; Parthiban, M.; Määttä, J. A. E.; Leppiniemi, J.; Jänis, J.; Parikka, M.; Turpeinen, H.; Rämetsä, M.; Pesu, M.; Johnson, M. S.; Kulomaa, M. S.; Airene, T. T.; Hytönen, V. P. Zebavidin - An Avidin-Like Protein from Zebrafish. *PLoS ONE* **2013**, *8* (10), e77207. <https://doi.org/10.1371/journal.pone.0077207>.
- (40) Delgadillo, R. F.; Mueser, T. C.; Zaleta-Rivera, K.; Carnes, K. A.; González-Valdez, J.; Parkhurst, L. J. Detailed Characterization of the Solution Kinetics and Thermodynamics of Biotin, Biocytin and HABA Binding to Avidin and Streptavidin. *PLOS ONE* **2019**, *14* (2), e0204194. <https://doi.org/10.1371/journal.pone.0204194>.
- (41) Swamy, M. J. Thermodynamic Analysis of Biotin Binding to Avidin. A High Sensitivity Titration Calorimetric Study. *Biochem. Mol. Biol. Int.* **1995**, *36* (1), 219–225.
- (42) Finn, F. M.; Hofmann, K. H. [37] Synthesis of Biotinyl Derivatives of Peptide Hormones and Other Biological Materials. In *Methods in Enzymology*; Elsevier, 1985; Vol. 109, pp 418–445. [https://doi.org/10.1016/0076-6879\(85\)09107-8](https://doi.org/10.1016/0076-6879(85)09107-8).
- (43) Huang, S.-C.; Stump, M. D.; Weiss, R.; Caldwell, K. D. Binding of Biotinylated DNA to Streptavidin-Coated Polystyrene Latex: Effects of Chain Length and Particle Size. *Anal. Biochem.* **1996**, *237* (1), 115–122. <https://doi.org/10.1006/abio.1996.0208>.
- (44) Pazy, Y.; Kulik, T.; Bayer, E. A.; Wilchek, M.; Livnah, O. Ligand Exchange between Proteins: EXCHANGE OF BIOTIN AND BIOTIN DERIVATIVES BETWEEN AVIDIN AND STREPTAVIDIN *. *J. Biol. Chem.* **2002**, *277* (34), 30892–30900. <https://doi.org/10.1074/jbc.M202874200>.
- (45) Chivers, C. E.; Koner, A. L.; Lowe, E. D.; Howarth, M. How the Biotin–Streptavidin Interaction Was Made Even Stronger: Investigation via Crystallography and a Chimaeric Tetramer. *Biochem. J.* **2011**, *435* (Pt 1), 55–63. <https://doi.org/10.1042/BJ20101593>.
- (46) Chu, V.; Stayton, P. S.; Freitag, S.; Le Trong, I.; Stenkamp, R. E. Thermodynamic and Structural Consequences of Flexible Loop Deletion by Circular Permutation in the Streptavidin-Biotin System. *Protein Sci.* **1998**, *7* (4), 848–859. <https://doi.org/10.1002/pro.5560070403>.
- (47) DeChancie, J.; Houk, K. N. The Origins of Femtomolar Protein–Ligand Binding: Hydrogen-Bond Cooperativity and Desolvation Energetics in the Biotin–(Strept)Avidin Binding Site. *J. Am. Chem. Soc.* **2007**, *129* (17), 5419–5429. <https://doi.org/10.1021/ja066950n>.
- (48) Green, N. Spectrophotometric Determination of Avidin and Biotin. *Methods Enzymol.* **1970**, *18*, 418–424. <https://doi.org/10.1042/bj0940023c>.
- (49) Ke, S.; Wright, J. C.; Kwon, G. S. Intermolecular Interaction of Avidin and PEGylated Biotin. *Bioconjug. Chem.* **2007**, *18* (6), 2109–2114. <https://doi.org/10.1021/bc700204k>.

- (50) Fairhead, M.; Krndija, D.; Lowe, E. D.; Howarth, M. Plug-and-Play Pairing via Defined Divalent Streptavidins. *J. Mol. Biol.* **2014**, *426* (1), 199–214. <https://doi.org/10.1016/j.jmb.2013.09.016>.
- (51) Freeman, A. W.; Koene, S. C.; Malenfant, P. R. L.; Thompson, M. E.; Fréchet, J. M. J. Dendrimer-Containing Light-Emitting Diodes: Toward Site-Isolation of Chromophores. *J. Am. Chem. Soc.* **2000**, *122* (49), 12385–12386. <https://doi.org/10.1021/ja001356d>.
- (52) Fréchet, J. M. J. Dendrimers and Supramolecular Chemistry. *Proc. Natl. Acad. Sci.* **2002**, *99* (8), 4782–4787. <https://doi.org/10.1073/pnas.082013899>.
- (53) Abd-El-Aziz, A. S.; Abdelghani, A. A.; Wagner, B. D.; Bissessur, R. Advances in Light-Emitting Dendrimers. *Macromol. Rapid Commun.* **2019**, *40* (1), 58–61. <https://doi.org/10.1002/marc.201800711>.
- (54) Hecht, S.; Fréchet, J. M. J. Dendritic Encapsulation of Function: Applying Nature's Site Isolation Principle from Biomimetics to Materials Science. *Angew. Chem. Int. Ed.* **2001**, *40* (1), 74–91. [https://doi.org/10.1002/1521-3773\(20010105\)40:1<74::AID-ANIE74>3.0.CO;2-C](https://doi.org/10.1002/1521-3773(20010105)40:1<74::AID-ANIE74>3.0.CO;2-C).
- (55) Parrott, M. C.; Rahima Benhabbour, S.; Saab, C.; Lemon, J. A.; Parker, S.; Valliant, J. F.; Adronov, A. Synthesis, Radiolabeling, and Bio-Imaging of High-Generation Polyester Dendrimers. *J. Am. Chem. Soc.* **2009**, *131* (8), 2906–2916. <https://doi.org/10.1021/ja8078175>.
- (56) Waner, M. J.; Hiznay, J. M.; Mustovich, A. T.; Patton, W.; Ponyik, C.; Mascotti, D. P. Streptavidin Cooperative Allosterism upon Binding Biotin Observed by Differential Changes in Intrinsic Fluorescence. *Biochem. Biophys. Rep.* **2019**, *17*, 127–131. <https://doi.org/10.1016/j.bbrep.2018.12.011>.
- (57) Loosli, A.; Rusbandi, U. E.; Gradinaru, J.; Bernauer, K.; Schlaepfer, C. W.; Meyer, M.; Mazurek, S.; Novic, M.; Ward, T. R. (Strept)Avidin as Host for Biotinylated Coordination Complexes: Stability, Chiral Discrimination, and Cooperativity. *Inorg. Chem.* **2006**, *45* (2), 660–668. <https://doi.org/10.1021/ic051405t>.
- (58) Waner, M. J.; Ellis, G.; Graeca, M.; Ieraci, N.; Morell, C.; Murphy, A.; Mascotti, D. P. Avidin Cooperative Allosterism upon Binding Biotin Observed by Differential Changes in Intrinsic Fluorescence. *Biochem. Biophys. Rep.* **2023**, *36*, 101554. <https://doi.org/10.1016/j.bbrep.2023.101554>.
- (59) Ballauff, M.; Likos, C. N. Dendrimers in Solution: Insight from Theory and Simulation. *Angew. Chem. Int. Ed.* **2004**, *43* (23), 2998–3020. <https://doi.org/10.1002/anie.200300602>.
- (60) Erickson, H. P. Size and Shape of Protein Molecules at the Nanometer Level Determined by Sedimentation, Gel Filtration, and Electron Microscopy. *Biol. Proced. Online* **2009**, *11* (1), 32–51. <https://doi.org/10.1007/s12575-009-9008-x>.
- (61) Talmard, C.; Guilloureau, L.; Coppel, Y.; Mazarguil, H.; Faller, P. Amyloid-Beta Peptide Forms Monomeric Complexes With CuII and ZnII Prior to Aggregation. *ChemBioChem* **2007**, *8* (2), 163–165. <https://doi.org/10.1002/cbic.200600319>.
- (62) Sheveleva, N. N.; Komolkin, A. V.; Markelov, D. A. Influence of the Chemical Structure on the Mechanical Relaxation of Dendrimers. *Polymers* **2023**, *15* (4), 833. <https://doi.org/10.3390/polym15040833>.

- (63) Lim, K. H.; Huang, H.; Pralle, A.; Park, S. Stable, High-Affinity Streptavidin Monomer for Protein Labeling and Monovalent Biotin Detection. *Biotechnol. Bioeng.* **2013**, *110* (1), 57–67. <https://doi.org/10.1002/bit.24605>.
- (64) Laitinen, O. H.; Nordlund, H. R.; Hytönen, V. P.; Uotila, S. T. H.; Marttila, A. T.; Savolainen, J.; Airene, K. J.; Livnah, O.; Bayer, E. A.; Wilchek, M.; Kulomaa, M. S. Rational Design of an Active Avidin Monomer *. *J. Biol. Chem.* **2003**, *278* (6), 4010–4014. <https://doi.org/10.1074/jbc.M205844200>.
- (65) Leppiniemi, J.; Määttä, J. A. E.; Hammaren, H.; Soikkeli, M.; Laitaoja, M.; Jänis, J.; Kulomaa, M. S.; Hytönen, V. P. Bifunctional Avidin with Covalently Modifiable Ligand Binding Site. *PLoS ONE* **2011**, *6* (1), e16576. <https://doi.org/10.1371/journal.pone.0016576>.
- (66) Green, N. Spectrophotometric Determination of Avidin and Biotin. *Methods Enzymol.* **1970**, *18*, 418–424. <https://doi.org/10.1042/bj0940023c>.

Chapter 5. Conclusions and Future Work

5.1 Conclusion

This thesis focused on the development of dendrimers and dendrimer-protein conjugates for use in molecular sieving. In Chapter 2, three neopentyl carboxylic acid precursors, terminated with alkene, alkyne and azide functionalities, respectively, were used to functionalize hydroxyl periphery dendrimers up to the fifth generation. Subsequent click reactions – *i.e.*, thiol-ene, CuAAC, and SPAAC, respectively – with the corresponding dendrimer peripheries progressed to completion by NMR and MALDI, thereby showing that α -neopentyl groups do not negatively affect surface reactivity. G5 neopentyl and valeryl ammonium dendrimers were respectively derived from their azide dendrimers, and it was found that the neopentyl species exhibited superior resistance to hydrolysis compared to their linear counterparts across different pHs over a month. The neopentyl species was also stable when exposed to an esterase over 8 days. Overall, these findings lend support to using neopentyl groups in dendrimers to improve peripheral stability in aqueous environments while minimally changing their overall reactivity and solubility.

In chapter 3, we incorporated neopentyl ester linkages into the construction of complex dendritic architectures for molecular sieving. G1 and G2 “inner” dendrons were furnished with neopentyl azides at their periphery. G3 “outer” dendrons with a PEGylated periphery were correspondingly furnished with a DBCO at their core, which then allowed the convergence of both outer and inner components *via* SPAAC to yield a library of high generation linear-dendritic hybrids. We grafted the dendritic structures onto an azide-

modified chymotrypsin *via* SPAAC and investigated the conjugates' activity toward a small molecule (BTpNA), a small protein (casein), and a large protein (BSA). When the conjugates were grafted with low-generation dendrons with short PEG chains (PEG₃₅₀), they exhibited either increased or comparable relative activity toward BTpNA. Activity toward BSA was reduced to below 20% in all conjugates, while activity toward casein decreased with increasing dendron generation and PEG length. We found that G3 and G5 dendrons with long PEG chains (PEG₂₀₀₀) drastically reduced catalytic activity toward all substrates, but CT with G4-PEG₂₀₀₀ grafts retained good activity toward BTpNA while still excluding protein substrates. Within the scope of polymers investigated in this study, we deemed CT grafted with G4-PEG₂₀₀₀ and G5-PEG₁₀₀₀ exhibited the most optimal sieving behaviour – which is marked by a high activity toward a small substrate and low activity toward large substrates. This study shows that molecular sieving with dendritic PEG architectures is governed by size of the polymer and different chain conformations stemming from different PEG lengths. The outer periphery *i.e.*, the PEG layer is implied to play a strong role in mediating catalytic activity.

In chapter 4, we explored the molecular sieving effect in avidin mediated by high generation dendrimers based on bis-MPA. Avidin was conjugated at lysine residues with low (G3) to high generation (G7) dendrimers with a hydroxyl periphery. Through HABA displacement assays and ITC, we showed that a series of G3-G7 dendronized biotin ligands, ranging from 1-15 kDa and representing a size range from oligopeptides to medium-sized proteins, are selectively excluded from one or more of the four binding pockets of the avidin-dendrimer conjugates depending on dendron generation. The remaining vacant

binding pocket(s) are selective for smaller biotinylated targets than those already bound. We also demonstrated that the smallest conjugate in this work – Avdin-G4, has an exclusion limit of less than 3 nm, as tested by ITC experiments using aprotinin and the G6 dendron, both of which have a hydrodynamic diameter of 3 nm or less. We showed that dendrimer-protein conjugates can exhibit diverse binding stoichiometries that stem from the molecular sieving effect. Furthermore, protein conformation can be changed by dendrimer conjugation, as shown by CD, leading to altered binding strength and stoichiometry. This work indicates that dendrimer conjugation to multimeric proteins is a possible method to modulate binding.

5.2 Future Work

We have shown that dendrimer conjugation introduces properties to the conjugate that are not easily accessible using other polymers, such as total exclusion of substrates below a particular molecular weight cut-off. A clear, immediate continuation of this work would be to investigate dendrimer-mediated sieving in therapeutically relevant species such as asparaginase and uricase. As others have shown, polymer-bound proteins dubbed “caged proteins” can serve as scavengers for small molecules, which is a straightforward application for molecular sieving. The next step in this direction is to utilize dendrimers for the “caging” of the proteins to the same effect. In this case, the dendrimer-protein conjugates can be expected to have different MWCOs based on dendron generation, thereby becoming modular scrubbers in multi-staged purification.

Dendrimers themselves have therapeutic applications stemming from their unique architecture, which might positively overlap with a sieving system on a protein. The most

obvious application is the small molecule encapsulation in the dendrimer backbone for drug delivery. In combining the principles of molecular sieving with small molecule encapsulation, one could envision a caged catalytic system, where a prodrug diffused within the dendrimer could interact with the grafted enzyme as a substrate, and then be released into bulk solvent as the active drug. This manner of small molecule activation could enable access to very interesting systems, such as *in vivo* release of fluorophores from pro-fluorophores.

Finally, the dendrimer peripheries tested in my work were chemically innocuous. These peripheries can be augmented with diverse functionalities such as those outlined in chapter 2, which could complement molecular sieving conjugates.